STRATIGRAPHIC ARCHITECTURE, DEPOSITIONAL PROCESSES AND RESERVOIR IMPLICATIONS OF THE BASIN FLOOR TO SLOPE TRANSITION, NEOPROTEROZOIC WINDERMERE TURBIDITE SYSTEM, CANADA

Lilian Leomer Navarro Ugueto

Thesis submitted to the
Faculty of Graduate and Postdoctoral Studies
in partial fulfillment of the requirements
for the PhD degree in Earth Sciences

Ottawa-Carleton Geoscience Centre and
Department of Earth Science, Faculty of Science
University of Ottawa

Thèse soumise à
Faculté des etudes supérieures et postdoctorales Université d'Ottawa
en vue d'obtention du doctorate en Sciences de la Terre

Centre Géoscientifique d'Ottawa-Carleton et
Département des sciences de la Terre et de l'environnement, Faculté des sciences
Université d'Ottawa
Ottawa, Canada

Members of the Dissertation Committee

Dr. Stephen Hubbard
University of Calgary

Dr. André Desrochers
University of Ottawa & Ottawa-Carleton Geoscience Centre

Dr. Donald Cummins
University of Ottawa & Ottawa-Carleton Geoscience Centre

Dr. Quentin Gall
University of Ottawa & Ottawa-Carleton Geoscience Centre

Supervisor

Dr. R. W.(Bill) C. Arnott
University of Ottawa & Ottawa-Carleton Geoscience Centre

ABSTRACT

Deep-water strata of the Neoproterozoic Kaza Group and Isaac Formation (Cariboo Group) in the southern Canadian Cordillera (B.C.) were deposited in a passive-margin basin during the break-up of supercontinent Rodinia. At the Castle Creek and Mount Quanstrom study areas, a remarkably continuous stratigraphic interval throughout these units preserves a record of basin-floor overlain by strata deposited in the lowermost part of the slope. Although similar stratal intervals have been described from ancient and modern deep-marine settings, they still remain poorly understood.

Three main stratal units are recognized within the study areas. The lower unit consists of three channel-lobe systems formed in the basin floor to slope transition. Uniquely, siliciclastic-dominated strata here consist of a variety of small- and few large-scale scour elements, indicating transport bypass along the channel-lobe transition zone, in addition to detached or attached depositional lobes composed mostly of distributary channels, fine-grained deposits, and uncommon splays, and a rare slope leveed channel complex. The middle unit is a siliciclastic-dominated succession of stacked, km-scale mass-transport deposits (i.e. debrites and slides), which indicates the more frequent emplacement of increasingly larger mass failures on a prograding slope, and are overlain by fine-grained, splay deposits that are successively overlain by channel, ponded and fine-grained deposits. In contrast, the upper unit is a mixed siliciclastic-carbonate slope succession of the first Isaac carbonate, a regional marker horizon that comprises mostly carbonate-rich and siliciclastic-rich fine-grained strata intercalated with channel and gully complexes that are mostly filled with coarser-grained strata.

Abrupt changes in facies trends, stratal stacking patterns and depositional styles throughout these units are largely linked to long-term changes in relative sea level and its control on sediment supply, namely sediment caliber, volume and mineralogy. Notably, in the upper unit, small-scale changes in sediment source and supply are related to shorter sea-level variations superimposed on the long-term eustatic change.

RÉSUMÉ

Les dépôts d'eau profonde d'âge Néoprotérozoïque du groupe Kaza et de la formation Isaac (groupe Cariboo) du sud de la cordillère canadienne ont été déposés dans un bassin de marge passive lors du démantèlement du supercontinent Rodinia. Aux sites d'études de Castle Creek et du mont Quanstrom, grâce à une continuité stratigraphique remarquable, la présence de ces unités sur un intervalle stratigraphique d'une continuité remarquable, permet l'étude détaillée d'une séquence sédimentaire allant de dépôts de plancher de bassin océanique jusqu'à ceux de la base de la pente continentale. Malgré que des dépôts sédimentaires de milieux marins profonds similaires aient été décrits auparavant, tant dans les archives sédimentaires que dans le moderne, ces systèmes sédimentaires demeurent mal compris.

Trois unités stratigraphiques principales ont été identifiées dans la région d'étude. L'unité inférieure est formée de trois systèmes de lobes de chenal formés par la transition entre les dépôts de plancher océanique et de pente continentale. Particulièrement, ces dépôts à dominance silico-clastique, sont constitués d'une variété d'affouillements de petite taille ainsi que de quelques-uns de grande taille marquant une zone de non-déposition le long de la zone de transition entre le chenal et le lobe et de lobes dépositionnels ("reliés" ou "non reliés") composés surtout de chenaux distributifs, de dépôts à grains fins et de rares dépôts d'épandage et de complexe de levées de chenal de pente continentale. L'unité médiane est une succession dominée par des dépôts silico-clastiques formés d'un empilement de dépôts de transport de masse (ex.: débrite et glissement) d'échelle kilométrique indiquant la formation plus fréquente de mouvement de masse de taille croissante associé à la progradation de la pente continentale. Ces dépôts gravitaires sont surmontés par des dépôts d'épandage à grains fins qui sont à leurs tout surmontés par des dépôts de chenaux "avec retenues' (anglais: "ponded"), eux aussi à grains fins. Par opposition, l'unité supérieure est une succession sédimentaire de dépôts de pente mixtes (silico-clastiques et carbonatés) de la formation carbonatée Isaac représentant un marqueur stratigraphique régional constitué surtout de dépôts carbonatés et silico-clastiques à grains fins intercalés avec des complexes de chenaux et de ravins remplis essentiellement de sédiments plus grossiers.

Des changements abrupts dans les tendances de facies, les patrons d'empilement des dépôts et les styles dépositionnels des unités étudiées sont grandement liés aux changements

à long terme du niveau marin relatif et de son influence sur l'apport sédimentaire, en particulier sur la taille des grains, le volume et la minéralogie. Notamment, dans l'unité supérieure, de petits changements dans la source et l'approvisionnement sédimentaires sont reliés aux changements à court terme du niveau marin, eux-mêmes modulés par les changements eustatiques à plus long terme.

To my son Mathis

ACKNOWLEDGEMENTS

First and foremost, I am grateful to my supervisor Dr. Bill Arnott for his limitless support and enthusiasm. I really appreciated for standing by me on the most difficult times of my PhD and life. Thanks for taking your precious time and patience in reviewing the countless pages of the good, the bad and the ugly ideas that I have pondered during all these years regarding the fascinating and intricate succession from the Kaza-Isaac transition interval to the first Isaac carbonate. Thanks to your wife Siobhan for the help and advice about child rearing.

I also would like to acknowledge the initial guidance of Dr. Gerry Ross, who co-founded with Dr. Arnott the Windermere Consortium. Thanks for sharing your passion and wisdom regarding the Windermere rocks across the Canadian Cordillera.

This project was provided by The Windermere Consortium, which is an industry and government supported research program directed by Dr. Arnott. Past and present sponsors of the Windermere Consortium include Natural Sciences and Engineering Council of Canada, Husky Energy, Apache, Statoil, BP, Anadarko, Canadian Natural Resource Ltd., Chevron, ConocoPhillips, Devon, Nexen, and Shell.

Thanks for financial awards, grants and aids I have received during all these years, particularly to AGR Insurance Brokers Scholarship 2012, Brian Rust Memorial Graduate Scholarship 2011, R. Dana Russell Memorial Grant 2008 (AAPG Grants-In-Aid Foundation), University of Ottawa Financial Aid Bursary and CUPE Financial Aids.

Special thanks to the Departments of Earth Science of UO and Carleton, and Ottawa-Carleton Geoscience Centre. Thanks a million Hélène De Gouffe and Lisa Murphy for all the administrative help throughout the years. Merci Dr. Simone Dumas pour traduire l'abstract ou résumé de la présent thèse. My deepest respects to Prof. Andre Lalonde and Brad Simms, two brilliant people from this Department who left this physical world too soon. We missed you greatly.

My thanks to the Laboratories of UO: Tara Kell aided with the XRF training; George Mrazek for preparing the thin sections and tolerating my use of the crusher and pulverizer of the sample preparation lab; Wendy Abdy, Paul Middlestead and Patricia Wickham (G.G. Hatch Isotope Laboratories) for helping me to prepare the samples and process the isotope analyses, and Prof. Andre Desroche, Gilles St-Jean and Glenn Poirier for allowing to try the brand-new (but uncalibrated) cathodoluminescence equipment.

I would like to recognize and thank to all of the Windy crew for greatly assisting or even just giving me a hand during my several field seasons at Castle Creek and one week at Mount Quanstrom, especially Lindsay Coffin, David Lowe, Jordan Clark, Gilliam Cramm, Carley Cramm, Jonathan Rocheleau, Dave Anthony, and Steven Gould. I am grateful to Zishann Khan, Mike Tilston, Viktor

Terlaky, Mark Smith, Omar Al-Mufti, Leena Davis, Natasha Popovic, Gerry Dumouchel, Katrina Angus, Derrick Midwinter, and Anika Bergen for those fruitful Windy discussion sessions on Friday's afternoons.

A big thank you to all undergrad, grad students and post docs of UO who have shared an office space or just have a word with me at the Marion, Macdonald and FSS buildings. Thanks for your genuine friendship to Tea Laurila, Melanie Cousineau, Fedora González, Pascale St-Germaine, and Ben Moulton.

A very special thanks to the McKirdy family: Liz, Brian, Karen and Ross for taking care of all the field logistics and as always providing natural and delicious food supplies.

I thank my husband Herbert Fournier for your encouragement and support. You were a strong shoulder to lean on during the most challenging times of this project. Gracias por aceptarme tal cual y llenarme de amor incondicional y paz.

I owe every challenge and every accomplishment to mi familia back home, mi mami Ilda Margarita Ugueto Marcano y mi hermano Freddy Alberto Navarro Ugueto. Gracias por las firmes palabras de ánimo y aliento desde las distancias.

In special memory to my father Freddy Navarro Morot, whose inadvertent departure I informally found out during the end of this project. Ahora te encuentras, allí donde la lejanía se abraza y las palabras se disuelven. Descansa en paz, papá.

I dedicate this work to my son, Mathis. Our tears and laughs are blended through all of these pages. Aquí, llegué vestida de colores con telas de poesía, sueños e ilusiones, pasaron los años y la frías realidades me carcomieron hasta la epidermis. Aprendí a resguardarme, a mantener en lo más profundo el poco aliento almacenado. Hasta que una pequeña luz apareció, poco a poco fue creciendo, me arropó de amor, inspiración y alegría. Es tu rostro iluminado acurrucado en mi regazo que me han enseñado a respirar cada día como el primer día y cada noche como la primera noche.

A PhD project is a unique travel adventure. Some students have gotten first-class tickets with all the amenities, good nobility titles, praises, and approvals, whereas other students we ought to travel on the back of the plane. Sometimes, on our way, we need to make few stops here and there, help to change tires, take uncertain routes, follow the wrong directions, take another bus, and/or just walk. We might have had gotten some bruises during the travel. Drinking vast amount of humour, curiosity, perseverance, and tolerance to the pounding criticism is indispensable. Everybody will finally arrive at the same place, but at different times. All the roads lead to the promise land of knowledge. The luggage becomes then enriched in life experiences of incommensurable dimensions and values, carrying a modest and minute knowledge of one or many subjects or unlimited awareness of what remains to be explored. LN

TABLE OF CONTENT

LIST OF FIGURES

LIST OF TABLES

Chapter 1

INTRODUCTION

1.1 Thesis Rationale

Over the past decades, most studies of ancient and modern deep-sea fan systems have focused on slope channels and basin-floor fans (see extensive reviews of Posamentier and Kolla, 2003; Posamentier and Walker, 2006), in part because many modern examples have been proven to host significant hydrocarbon reserves (e.g. in the Gulf of Mexico, offshore Brazil, west Africa, Red and Arabian Sea, and northern South China Sea). In many of the modern systems, significant changes in stratal lithology, geometry and architecture have been noted across the transition from continental slope to adjacent deep ocean sea floor, including channel and channel-levee complexes, large scours, patchy sediment waves, mass-transport complexes, and lobe complexes with shallow, low-sinuosity channels and splays (Piper and Normark, 1983; Normark and Piper, 1985; Palanques et al., 1995; Torres et al., 1997; Wynn, 2000; Ercilla et al., 2002; Wynn et al., 2002; Bonnel et al., 2005; Posamentier and Walker, 2006; Macdonald, 2010; Macdonald et al., 2011). However, most observations on these modern slope-fan transition regions are based on seafloor imaging and seismic data that generally lack small-scale (bed-scale) sedimentological detail, which is essential for understanding the formative depositional processes. For that reason, high-resolution outcrop-based studies are crucial.

Many ancient deep-water systems have been reported in the literature, but the spatial and temporal distribution of facies and architectural elements in the slope-basin floor transition interval of these systems still remain poorly understood. On the basis of tectonic setting, ancient slope-to-basin transitions can be arranged in four groups (Fig. 1.1): (i) those from foreland basins; (ii) those from transtensional basins; (iii) those from intracratonic basins; and (iv) those from passive margin basins. In general, those outcrops from foreland, transtensional and intracratonic basins are commonly 1000-3000 m wide, 100-500 m thick and dominated by siltstone and fine-grained sandstone, with the exception of the Ainsa, Grès d'Annot, Mount Messenger/Urenei, Tres Pasos and Cingöz formations, in which coarse-grained sandstone to conglomerate are common. In contrast, outcrops from passive-margin settings are considerable larger, being tens of kilometres wide and over 500 m thick, and importantly made up of a wide range of grain-size, commonly from conglomerate to mudstone.

This dissertation focused on well-exposed and continuous section of transition from basin-floor strata in the uppermost Kaza Group to slope deposits in the Isaac Formation (lowermost Cariboo Group) in the Windermere turbidite system. The analyses of facies and general sedimentologic features, stratal architectural and stratigraphic evolution through this bathymetric, but more importantly sedimentological transition are documented in detail in subsequent chapters. These data, then, can serve as an analogue for similar deep-water systems, especially where lithological data are absent, and seismic imaging is the only input for building reservoir models. Moreover, strata investigated in this thesis record a changeover

from siliciclastic- to carbonate-dominated sedimentation in the Windermere turbidite system, and therein the opportunity to compare and contrast patterns and styles of sedimentation.

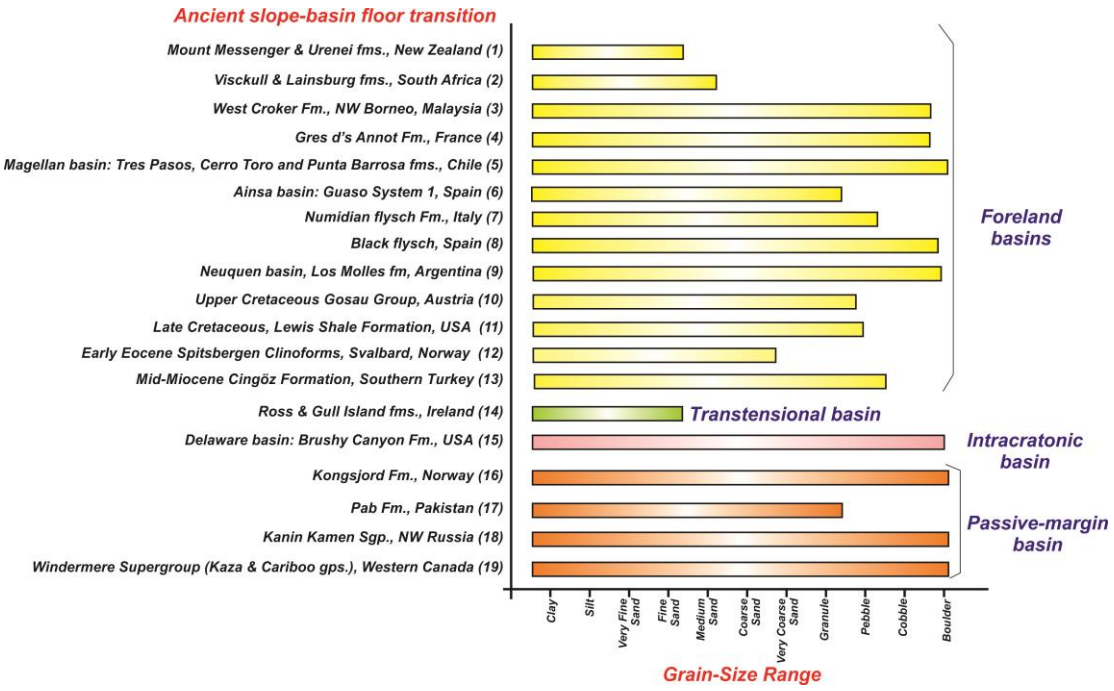

(1) Late Miocene Mount Messenger and Urenui formations, New Zealand (Browne et al., 2000; Coleman et al., 2000; Browne and Slatt, 2002; King and Browne, 2002; Arnot et al., 2007; King et al., 2007a; King et al., 2007b); (2) Permian-Triassic Skoorsteenberg Formation and correlative Laingsburg Formation, Karoo basin, South Africa (Sullivan et al., 2000; Johnson et al., 2001; Hodgson et al., 2006; Fildani et al., 2009b; Tankard et al., 2009; Wild et al., 2009; Flint et al., 2011); (3) Paleogene West Crocker Formation, Northwest Borneo, Malaysia (Crevello et al., 2007a, b); (4) Eocene-Oligocene Gres d'Annot Formation, French Alps (Sinclair and Tomasso, 2002; Joseph and Lomas, 2004; Etienne et al., 2013); (5) Cretaceous Punta Barrosa, Cerro Toro and Tres Pasos formations, Magallanes basin, Chile (Fildani et al., 2009a, and references therein; Romans et al., 2009; Hubbard et al., 2010; Romans et al., 2011); (6) Eocene Hecho Group, Ainsa Basin, Spain (Pickering and Bayliss, 2009, and references therein); (7) Oligo-Miocene Numidian flysch, Italy (Johansson et al., 1998); (8) Albian Black flysch, Spain (Bravo and Robles, 1995; Vicente Bravo and Robles, 1995); (9) Early Jurassic Los Molles Formation, Neuquen basin, Argentina (Tudor, 2014); (10) Upper Cretaceous Gosau Group, Austria (Ortner, 2007; Paton et al., 2007; Wagreich et al., 2011; Hofer et al., 2013); (11) Late Cretaceous, Lewis Shale Formation, USA (Pyles and Slatt, 2000; Pyles and Slatt, 2007; Pyles et al., 2011); (12) Early Eocene Spitsbergen Clinoforms, Svalbard, Norway (Mellere et al., 2002; and references therein; Crabaugh and Steel, 2004; Johannessen and Steel, 2005; Clark and Steel, 2006); (13) Mid-Miocene Cingöz Formation in Southern Turkey (Satur et al., 2000; Kostrewa, 2004; Satur et al., 2005); (14) Late Carboniferous, Ross and Gull Island formations, Ireland (Collinson et al., 1991; Martinsen et al., 2000; Lien et al., 2003; Martinsen et al., 2003; Lien et al., 2007; Pyles, 2007, 2008; Pyles and Jennette, 2009; Pyles et al., 2011); (15) Permian Brushy Canyon Formation, USA (Beaubouef et al., 1999; Gardner and Borer, 2000; Gardner et al., 2003; Rossen and Beaubouef, 2007); (16) Late Precambrian Kongsjord Formation, NE Finnmark, Norway (Pickering, 1983); (17) Upper Maastrichtian Pab Formation, Pakistan (Eschard et al., 2003); (18) Neoproterozoic Kanin Kamen Supergroup, NW Russia (Roberts et al., 2004); (19) Neoproterozoic upper Kaza and lower Cariboo groups (Isaac Formation), Windermere Supergroup, Canada (This study).

Figure 1.1. Comparison of grain-size spectrum and tectonic setting of ancient deep-water systems with reported exposures of the slope to basin floor transition.

1.2 Geologic Background

1.2.1 Geological setting of Windermere basin

The Windermere Supergroup (WSG) crops out extensively in the Cordillera of western North America and is widely thought to record a major episode of continental rifting and following drift associated with the breakup of the supercontinent Rodinia (Figs. 1.2-1.3), and the opening of the paleo-Pacific (Panthalassa) Ocean between Gondwana and western Laurentia (Gabrielse, 1972; Ross, 1991; Sears and Price, 2000). Although the original geometry of the Laurentian margin has been overprinted and modified by post-rift tectonic activity, palinspastic reconstructions of different segments of the Cordillera reflect a recognizable, albeit modified, asymmetric zig-zag shape of the margin (Levy and Christie-Blick, 1989; Christie-Blick et al., 1995; Eyles and Januszczak, 2004; Lund, 2008). Different conjugate counterparts to this margin have been suggested and include Antarctica, Australia, China, and Siberia (Monger and Price, 1979; Monger et al., 1982; Eisbacher, 1985; Moores, 1991; Karlstrom et al., 2000; Sears and Price, 2000; Rogers and Santosh, 2003; Sears and Price, 2003; Li et al., 2008).

To date, no consensus has yet been reached regarding the paleocontinental configuration during Windermere deposition. Some authors (Bond et al., 1984; Colpron et al., 2002; Fanning and Link, 2004) suggest the WSG in the southern Canadian Cordillera was deposited in Neoproterozoic intracontinental rift basins formed during one or multiple (at least two) rifting events, prior to the actual establishment of a Paleozoic passive margin. These authors argue that although

Rodinian rifting began during the Cryogenian, approximately 750-723 Ma (Ross et al., 1995; Monger and Price, 2002; Eyles and Januszczak, 2004), it was a second, younger rifting during the Ediacaran, at about 555-600 Ma (Bond et al., 1984), that eventually opened the new ocean (Sears and Price, 2002).

Alternatively, many other authors (Gabrielse, 1972; Monger and Price, 1979; Ross and Murphy, 1988; Ross, 1991; Hein and McMechan, 1994; Ross et al., 1995; Dalrymple and Narbonne, 1996; MacNaughton et al., 2000; Monger and Price, 2002; Ross and Arnott, 2007; Lund, 2008) suggest that deposition of only the lower part of the WSG was confined to isolated basins formed during early Neoproterozoic rifting, and that much of the WSG accumulated subsequently during continental drift and growth of a tectonically-stable (passive-margin) basin at the end of the Precambrian. This basin was later subjected to a second rifting event that in western Canada culminated in the formation of the passive-margin Western Canada Sedimentary Basin (Dalziel, 1991; Ross, 1991; Lund, 2008; Figs. 1.2-1.4).

This model, linking a post-rift Windermere sedimentation with a stable basin evolution, is widely accepted and supported by numerous observations, including general trend in sediment grain size and paleocurrent data (Ross and Arnott, 2007), configuration of the Windermere basin, the considerable thickness (~9 km) and spatial expanse of the km-scale, continuously upward-shoaling WSG turbidite system (Gabrielse, 1972; Eisbacher, 1985; Ross, 1991; Ross and Arnott, 2007), regional continuity of at least one of three major stratigraphic markers throughout the basin (e.g. Ediacaran Old Fort Point Formation; Ross, 1991; Smith, 2009; Smith et al., 2014a), uniformity of provenance (source composition and ages), long duration of

Windermere deposition, and absence of volcanics. The top of the WSG is marked by a regionally-extensive unconformity at the base of the Paleozoic sequence deposited in a passive margin (Ross and Bowring, 1990; Ross et al., 1991; Lemieux et al., 2007; Ross and Arnott, 2007). Dalziel (2014) suggested that during the Early Cambrian, a major marine transgression and radiation of metazoan life occurred, whilst Laurentian became isolated by the development of a major deep-oceanic gateway between the already well-established paleo-Pacific Ocean and the opening Iapetus Ocean basin.

1.2.2 Regional Stratigraphy of the Windermere Supergroup

According to the general model for Neoproterozoic rift-to-drift passive-margin sedimentation (Aitken, 1969; Ross and Murphy, 1988; Teitz and Mountjoy, 1988; Ross, 1991; Hein and McMechan, 1994; Lickorish and Simony, 1995; Colpron et al., 2002; Ross and Arnott, 2007), two well-defined tectonostratigraphic sequences are recognized in the WSG: syn-rift and overlying post-rift (Fig. 1.5a,b).

The basal *syn-rift sequence* is up to 2.5 km thick, and consists of glaciogenic diamictites and conglomerates of the Toby Formation intercalated with tholeiitic volcanic rocks of the Irene Formation, which are deposited during the rifting and extension of the Rodinia supercontinent (Aalto, 1971; Ross et al., 1995). The ages of the syn-rift sequence are still poorly constrained, but direct ages from basement rocks in the Canadian Cordillera and indirect ages from correlative units of the Toby and Irene formations in British Columbia and western United States range from 684 to 717 Ma.

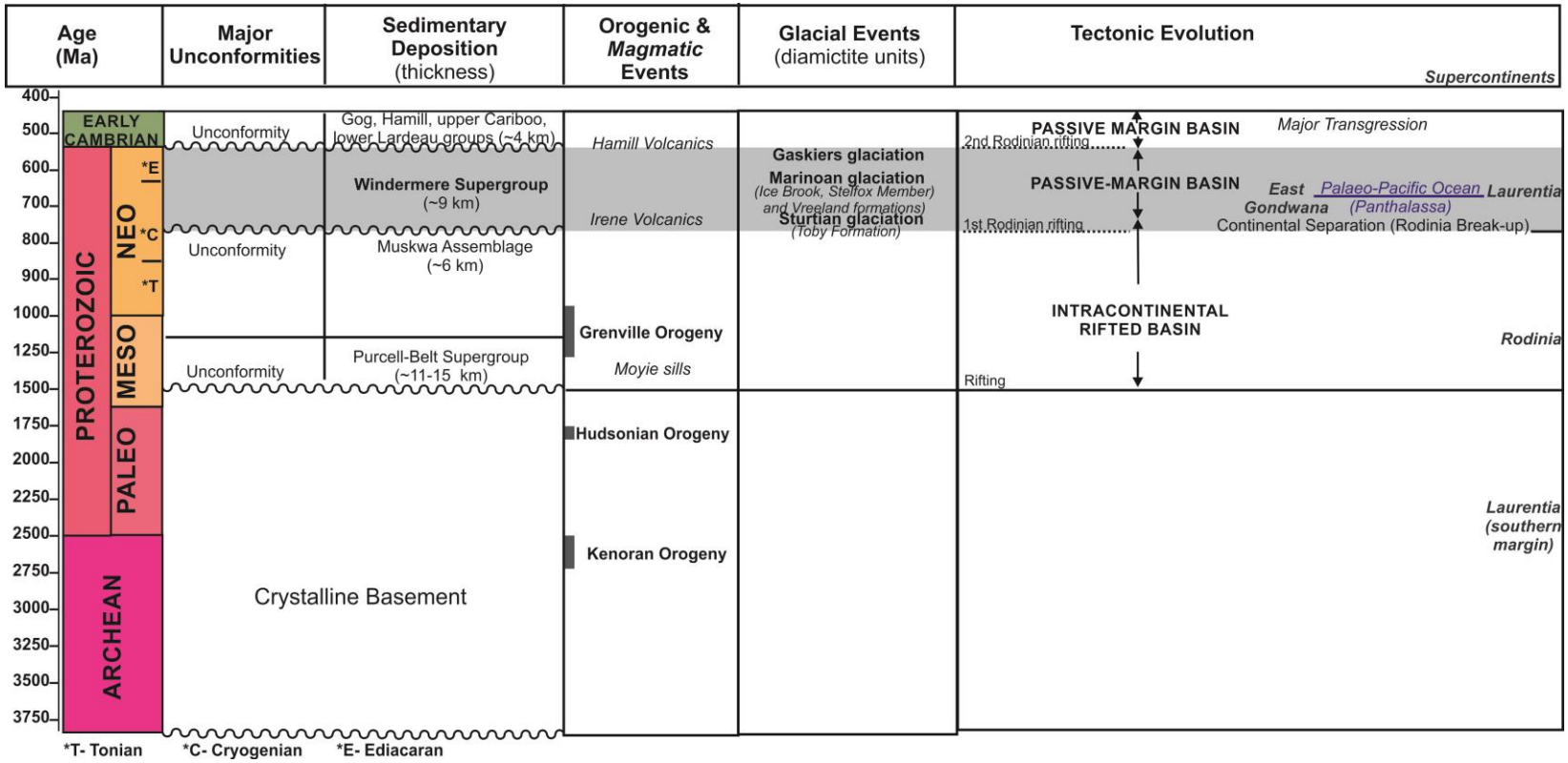

Figure 1.2 Stratigraphic and tectonic settings in the southern Canadian Cordillera during the Archean, Proterozoic and Early Cambrian. Windermere Supergroup is highlighted. See text for details and references.

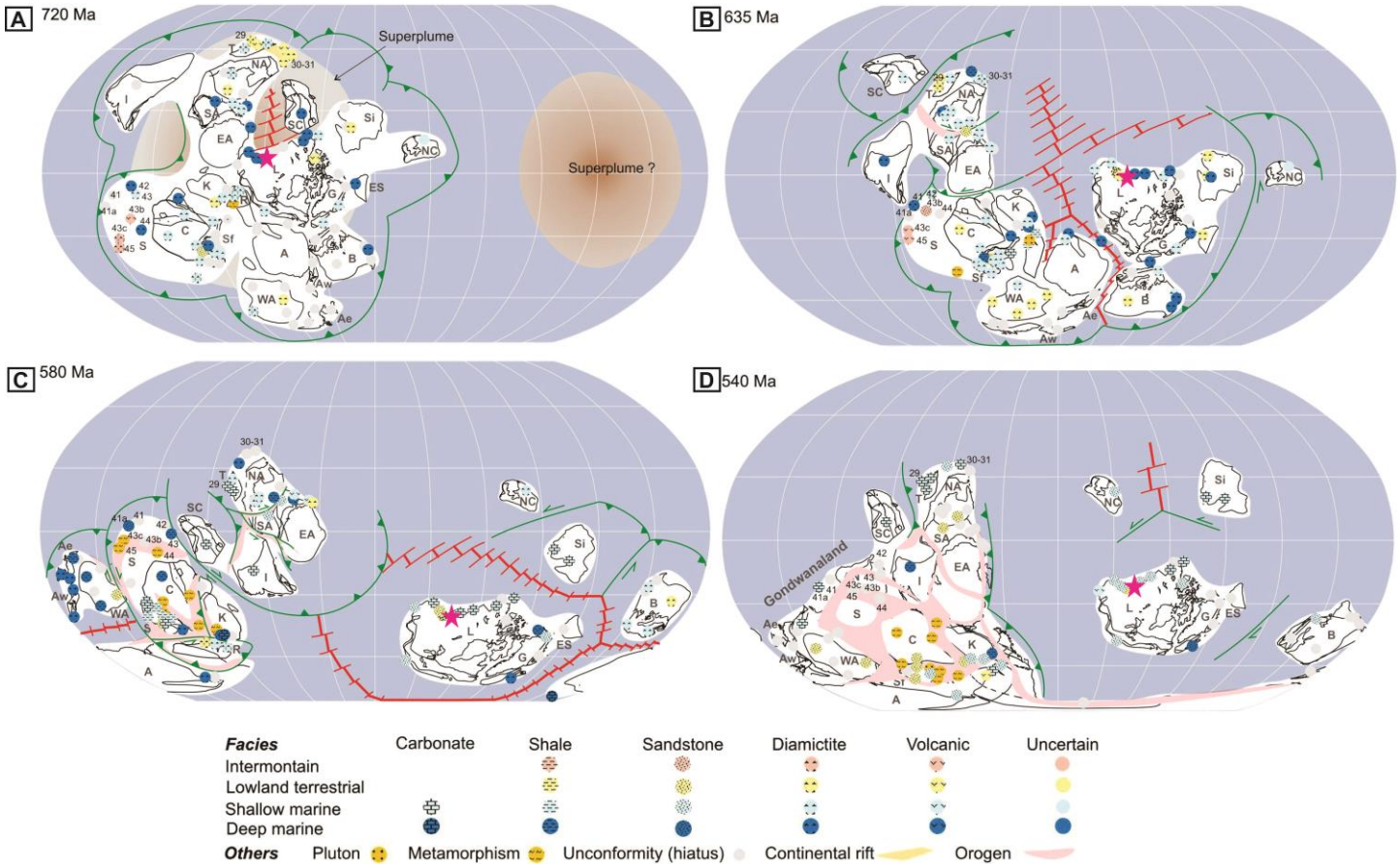

Figure 1.3. Global reconstructions during the Neoproterozoic according to Li et al. (2013) at different time-slices: (A) 720 Ma, illustrating the beginning of the breakup of the lower-latitude Rodinia supercontinent and Sturtian glaciation; (B) 635 Ma, showing the continuation of the Rodinia breakup and the Marinoan glaciation; (C) 580 Ma, featuring the end of the Rodinia breakup and Gaskiers glaciation. (D) 540 Ma, illustration the formation of Gondwanaland assemblage.

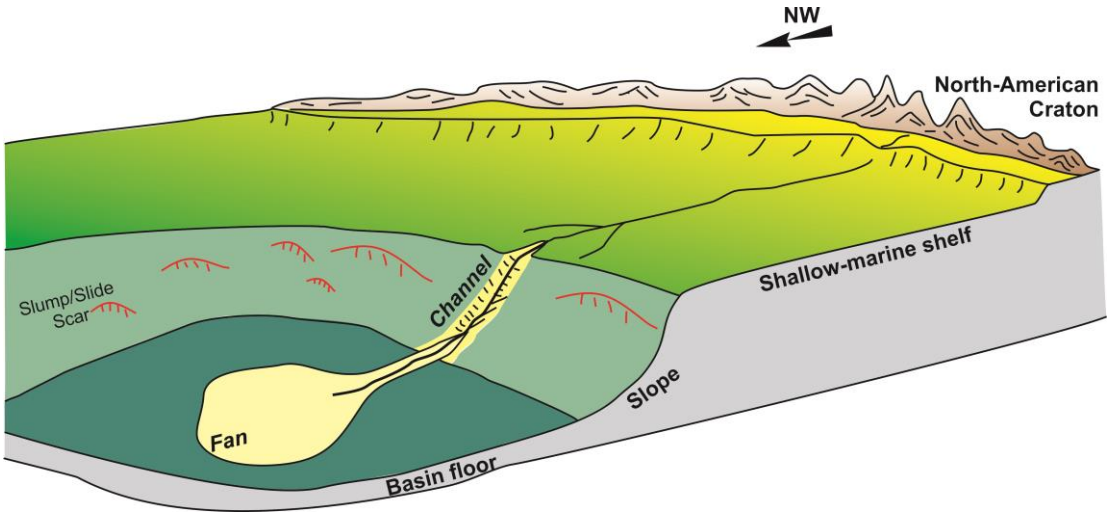

Figure 1.4 Schematic illustration of the Windermere sedimentary basin along the western Laurentian margin during the Neoproterozoic (modified from Smith, 2009). Based on detrital zircon data, the primary sediment source for the Windermere turbidite system is interpreted to be granitic crystalline basement rocks located in southern Alberta and the northwestern United States (Ross and Bowring, 1990).

Basement rocks overlain unconformably by the WSG provide local maximum depositional ages of the WSG, and include 736± 23 Ma U-Pb zircon ages from outliers of the Malton Gneiss Complex (McDonough and Parrish, 1991), 740 ± 36 Ma U-Pb zircon ages from gneisses in the Monashee Complex (Parrish and Scammell, 1988; Sevigny et al., 1990) and 728 ± 8 Ma U-Pb zircon ages from gneiss in the Deserters Range (Evenchick et al., 1984). Indirect dating from interpreted correlatives of the Irene volcanics is variable, including U-Pb zircon age of 689 ± 4.6 Ma from the Gataga Volcanics, northern British Columbia (Ferri, 1999), 684 ± 4 and 685 ± 7 U-Pb zircon ages from mafic rocks of the Golden Cup Member of the Edwardsburg Formation in central Idaho (Lund et al., 2003) and 717 ± 4 U-Pb detrital zircon ages

from the Bannock Volcanic Member of the Pocatello Formation in southeastern Idaho. Indirect age constraints for the correlatives of Toby Formation are sparse, including U-Pb detrital zircon ages of 709 ± 5 Ma from diamictons of the Scout Mountain Member of the Pocatello Formation in southeastern Idaho (Fanning and Link, 2004).

The overlying *post-rift sequence* is approximately 5 km thick, and is composed of coarse-grained sandstone-rich turbidites intercalated with mudstone and minor carbonate intervals (Ross et al., 1995). In the Canadian Cordillera, the stratigraphic nomenclature varies depending on geographical locations: Kaza and Cariboo groups in the Cariboo Mountains, the Horsethief Creek Group in the Purcell Mountains, and the Miette Group in the western Rocky Mountains of Alberta. All these units are interpreted to form a continuous and correlative, upward-shoaling, sedimentary succession deposited in a thermally subsiding deep-water basin (Ross et al., 1995). In the Cariboo Mountains, sandstone-rich turbidites of the Kaza Group represent basin-floor deposits, overlain conformably by slope turbidites of the Isaac Formation (lower Cariboo Group), and then capped by shallow-marine strata of the Cunningham and Yankee Belle formations of the middle-upper Cariboo Group (Hein and McMechan, 1994; Arnott, 2007; McMechan, 2015).

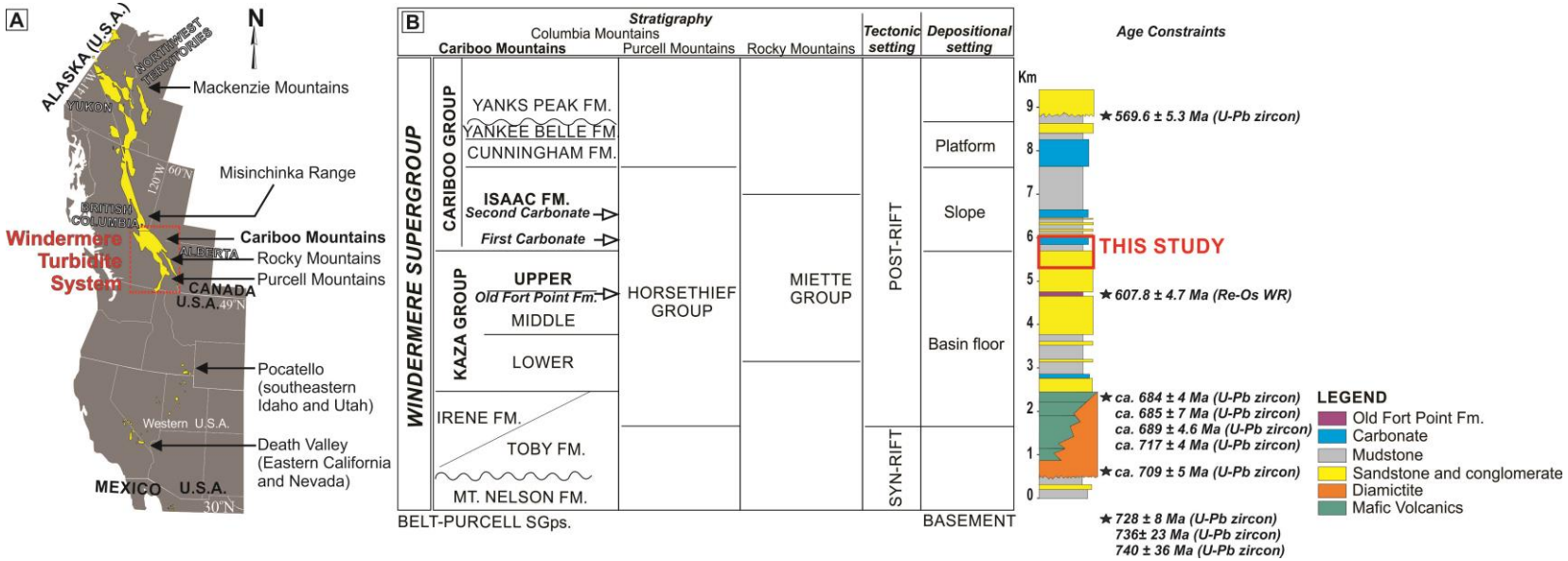

Figure 1.5 Regional geology and stratigraphy of Windermere Supergroup (WSG) and corresponding Windermere turbidite system. (A) Distribution of WSG strata in western North America (modified from Ross et al., 1991), highlighting the areal extent of the turbidite system in the Cariboo Mountains, southern Canadian Cordillera. (B) General stratigraphic column for WSG in the southern Canadian Cordillera (modified from Ross et al., 1995). Rift and post-rift sequences, lithostratigraphic units, tectonic setting, and paleogeographic environments are shown. See text for references on direct and correlative ages.

Age constraints within the post-rift WSG sequence are lacking, except for a single date of 607.8 ± 4.7 Ma Re-Os ages from organic-rich mudstone of the Old Fort Point Formation, a distinctive regionally-extensive unit separating the Middle and Upper Kaza groups (Kendall et al., 2004; Kendall et al., 2009). The minimum timing of WSG sedimentation is provided by U-Pb zircon age of 569.6 ± 5.3 Ma from felsic volcanic rocks of the Hamill Group, which is equivalent to the Yanks Peak Formation (Upper Cariboo Group). These rocks unconformably overlie the WSG (Colpron et al., 2002), and are interpreted to be associated with the second Rodinian rifting event during the Early Cambrian (Fig. 1.2).

1.3 Windermere Turbidite System: Geological setting and Stratigraphy

Deep-marine strata of the WSG basin, also known as the Windermere turbidite system, are well exposed throughout the southern Canadian Cordillera, extending from the Purcell Mountains in the south to the Cariboo Mountains in the north (for locations, see Fig. 1.5a). Here, the Windermere unconformably overlies the Belt-Purcell Supergroup, and in turn is overlain unconformably by Lower Cambrian strata of the Hamill Group (Fig. 1.5b). In addition, the up to 9 km thick Windermere sedimentary pile shows a consistent northwestward change from upper-slope canyon to slope and base-of-slope deposits to basin floor strata (Eisbacher, 1985; Ross, 1991). Moreover, regional paleocurrent data also indicate general transport toward the northwest (Ross, 1991; see Fig. 1.5).

Currently, the Windermere turbidite system is on the order of 35,000 km^2 (Ross and Arnott, 2007), but based on palinspastically restored, it is estimated to be at

least 80,000 km^2 (Ross and Murphy, 1988; Ross, 1991), and therefore, this system is comparable in size to modern passive-margin turbidite systems like the Amazon and Mississippi fans. Based on radiometric dates of the post-rift WSG, the Windermere Turbidite System (plus the overlying Neoproterozoic platformal succession of the Hamill Group) was active for no more than 231 My, but most probably between 113 and 154 My, and during which a succession of up to approximately 7000-8000 m thick of sediment accumulated.

1.3.1 Windermere Turbidite System in the Cariboo Mountains

Deep-water strata of WSG crop out extensively in the Cariboo Mountains (Fig. 1.5), which are located in the northernmost part of the Columbia Mountains, south east-central British Columbia. The Cariboo Mountains are located within the Omineca Belt or Superterrane (Gabrielse, 1991), and are bounded by the Fraser River to the east and the Quesnel Highlands to the west. They contain major mid-Jurassic, regional (kilometre-scale), northwest-trending folds, like the Premier Anticlinorium and Isaac Lake Synclinorium, which then are extensively cross-cut by younger dextral strike-slip fault systems (Campbell, 1973; Murphy, 1987b; Murphy et al., 1995; Reid et al., 2002). Structural style and metamorphic grade change markedly along the Cariboo Mountains (Campbell, 1973; Murphy, 1987a; Reid et al., 2002). In the northern Cariboo Mountains, open to isoclinal, upright to overturned folds are common, and rocks were metamorphosed to greenschist facies (Murphy, 1987a; Reid et al., 2002). In the southern Cariboo Mountains, on the other hand, tight to nearly

isoclinal and overturned folds and strata were affected by higher metamorphic grades in the amphibolite facies (Reid et al., 2002).

In the Cariboo Mountains, the WSG consists mostly of two stratigraphic units, the Kaza and Cariboo groups (Figure 1.5b). The Kaza Group is about 2-4 km thick and comprises sandstone interbedded with conglomerate, siltstone and local carbonate-rich intervals (see Campbell, 1973; Pell and Simony, 1982; Murphy and Rees, 1983; Murphy, 1987a; Pell and Simony, 1987; Ross and Murphy, 1988; Ross et al., 1995; Ross and Arnott, 2007).

The Kaza Group is divided into three stratigraphic sub-units: lower, middle and upper. The lower sub-unit is mudstone-dominated, whereas the middle and upper sub-units are sandstone-dominated and separated by a distinctive and regionally-extensive stratigraphic marker termed the Old Fort Point Formation (Ross and Murphy, 1988; Ross, 1991; Ross et al., 1995; Smith, 2009; Smith et al., 2014a, b). This regional marker consists of a tripartite succession of purple-coloured siltstone that grades upward into rhythmic limestone-siltstone, which in turn is overlain sharply by organic-rich mudstone, in turn overlain by an heterolithic interval of conglomerate, sandstone, siltstone–mudstone and limestone (Smith, 2009; Smith et al., 2014a, b). The Kaza Group is interpreted to represent basin-floor deposition along the passive margin of Neoproterozoic Laurentia (Ross, 1991). The Old Fort Point marker unit represents a major transgressive event and associated highstand deposition related to a post-glacial eustatic rise (Ross and Murphy, 1988; Ross et al., 1995; Smith, 2009; Smith et al., 2014a, b).

The Cariboo Group conformably overlies the Kaza Group and is up to 5 km thick in the Cariboo Mountains, thinning eastward along the western limit of the Rocky Mountain Trench. In the Cariboo Mountains, it has been subdivided into four stratigraphic units (from oldest to youngest): Isaac, Cunningham, Yankee Belle and Yanks Peak formations (for details, see Campbell, 1973; Gabrielse, 1991; Hein and McMechan, 1994).

The Isaac Formation is about 2.5 km thick and consists predominantly of mudstone interbedded with up to 100 m thick, sandstone and conglomerate intervals, in addition to two important regionally-extensive, up to 150-200 m thick, carbonate-rich intervals, informally termed the first/lower and second/upper Isaac carbonates. The Cunningham Formation reaches a maximum thickness of about 550 m in the northern Cariboo Mountains and is typically composed of limestone with minor siliciclastic mudstone and sandstone (Rowe, 2003).The Yankee Belle Formation is up to 900 m thick and consists of rhythmically alternating limestone, siltstone and shale that grade upward into sandstone and shale, whereas the Yanks Peak Formation is up to 800 m and is a quartz-rich sandstone unit. The Isaac Formation is interpreted to represent deposition on the continental slope of Laurentia. The overlying Cunningham, Yankee Belle and Yanks Peaks formations were deposited mostly in upper-slope and then shallow-marine shelf environments (Ross and Murphy, 1988).

The full Kaza-Isaac succession represents a several km-thick, upward-shallowing succession formed by the progradation of the Laurentia continental margin into the proto-Pacific ocean (Ross, 1991; Ross et al., 1995).

1.4 Study areas

In this study, strata between the uppermost Kaza Group and Isaac Formation (lowermost Cariboo Group) were examined in two remote localities near the headwaters of the Castle Creek and Rausch rivers; both major tributaries of the Fraser River. The Castle Creek area was the principal and most intensively examined outcrop site due to outcrop quality and accessibility (Fig. 1.5), whereas the Mount Quanstrom area was ancillary. At both sites, the rapid retreat of glaciers during <100 years (Beedle et al., 2009; Maurer et al., 2012; Beedle et al., 2014) has resulted in exposed outcrops with minimal cover (see Figs 1.6-1.8).

Moreover, both studied areas occur in the western part of the Premier Anticlinorium of the Omineca crystalline belt, which comprises large (kilometre-scale) southwest-verging to overturned folds that dip steeply to moderately toward the northwest (Murphy, 1987a; Murphy, 1987b; Ross and Ferguson, 2003). Strata at Castle Creek and Mount Quanstrom are exposed on the overturned limbs of southwest-verging anticlines (Figs. 1.7), and accordingly strata in Castle Creek are almost vertical, but dipping at about 80-85^{o} at Mount Quanstrom.

Structural elements are complex and formed by at least four major deformational episodes of folding, which are associated with variously oriented faults, planar foliations, lineations, joints, cleavages, and high-angle crenulations (Murphy and Rees, 1983; Murphy, 1987a; Murphy, 1987b; Reid et al., 2002). The broad upright folds at Castle Creek and Mount Quanstrom are associated with the second deformational event (Murphy, 1987a; Reid et al., 2002).

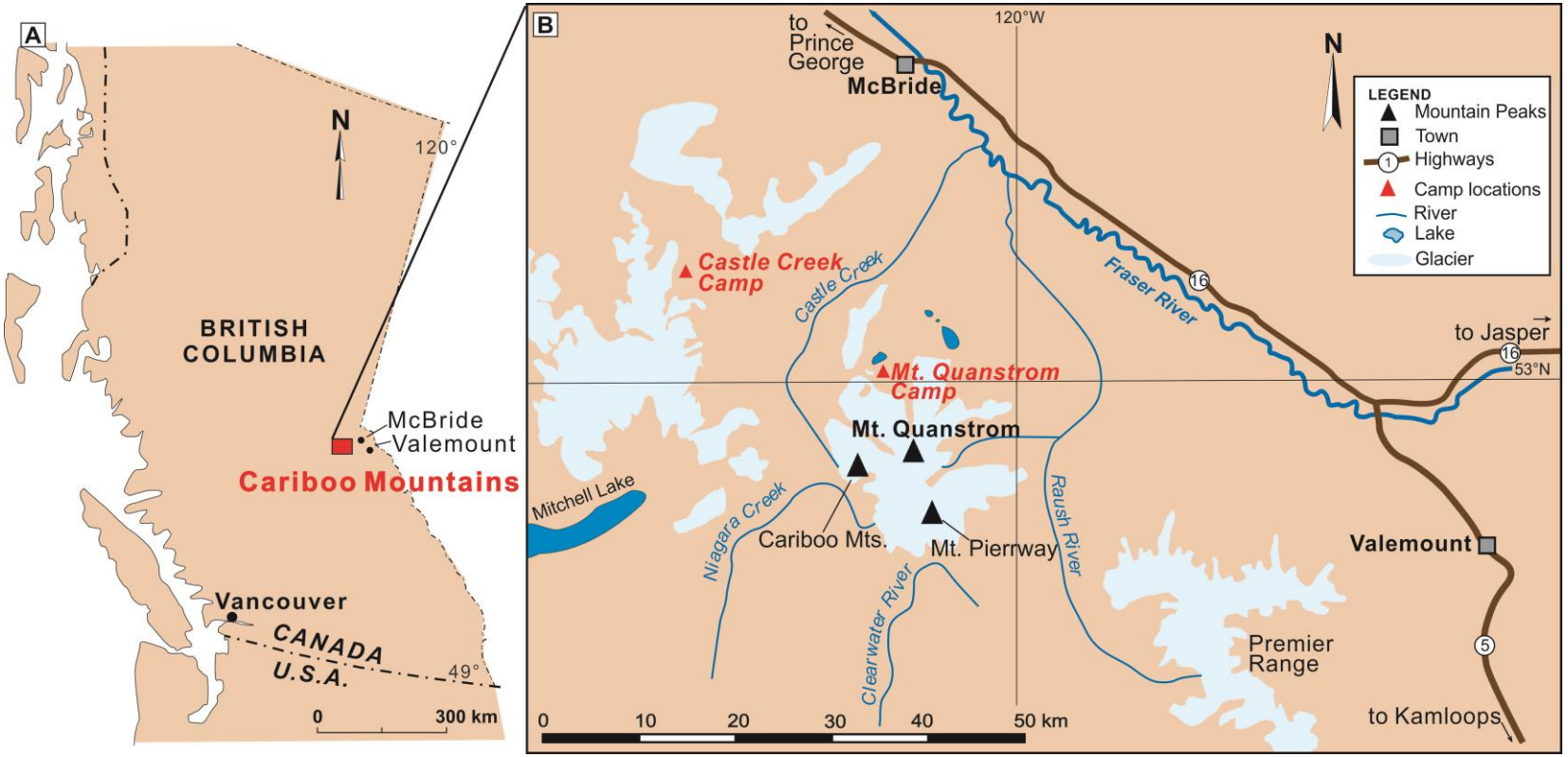

Figure 1.6 Location of the Castle Creek and Mount Quanstrom study areas, Cariboo Mountains, southern Canadian Cordillera. It is shown in relation to: (A) map of western Canada (modified from Ross and Murphy, 1988); (B) map of the Cariboo Mountains (modified from http://www.colwest.ca).

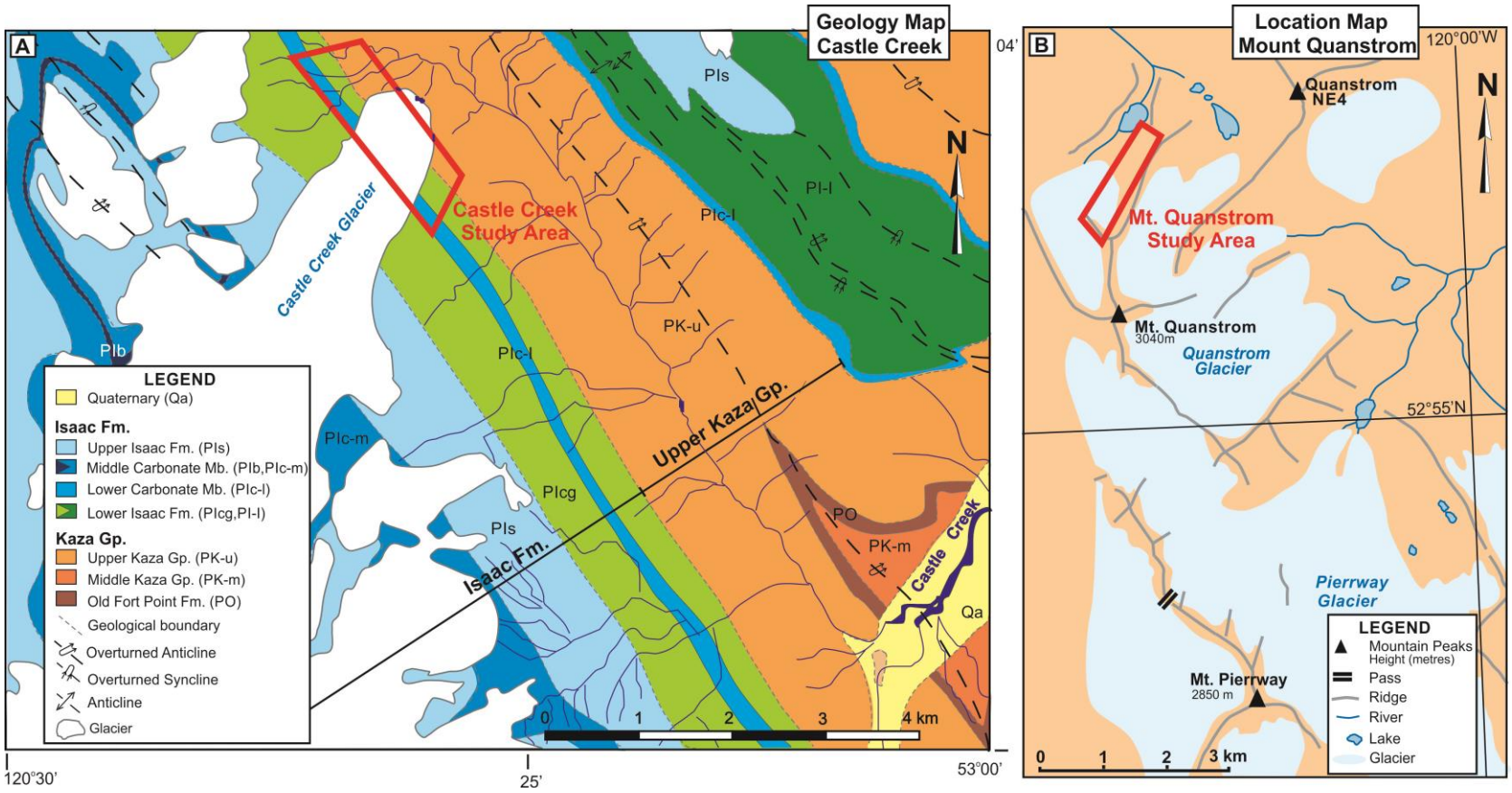

Figure 1.7 Maps of the Castle Creek and Mount Quanstrom study areas in the Cariboo Mountains. (A) regional geology map of Castle Creek (Modified from Ross and Ferguson, 2003, extract of 93H/1 Eddy map-sheet); and (B) surficial map of the Mount Quanstrom (Modified from Government of Canada, 2006, extract of 93A/16 Mount Wider map-sheet). Study areas are enclosed in red polygons.

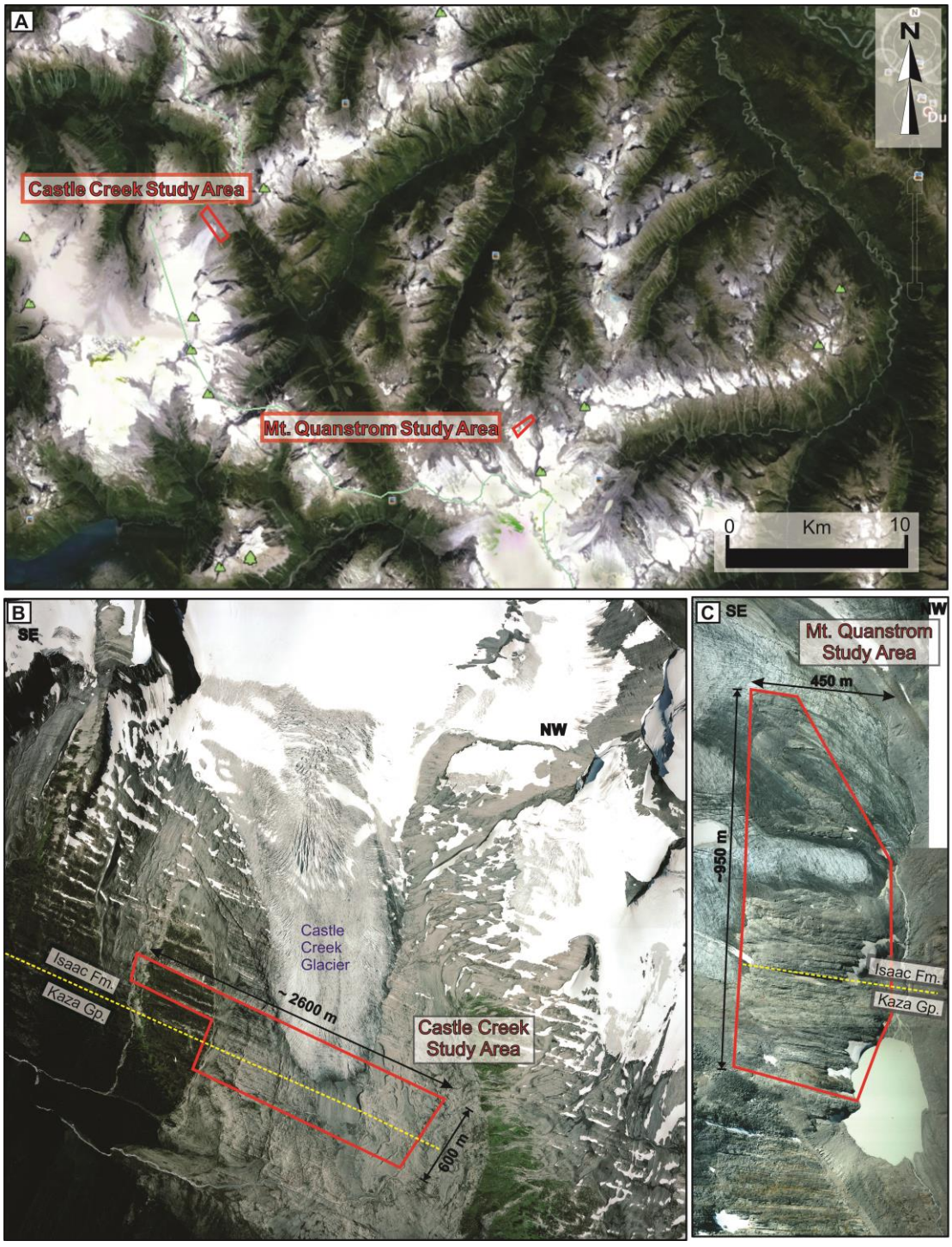

Figure 1.8 Satellite and aerial photographs of the study areas in the Cariboo Mountains. (A) Satellite image of the Cariboo Mountains, showing locations of the study areas (Earth, 2014); (B) Airphotos of the Castle Creek study area (UNBC, 2008); and (C) Photomosaic of airphotos of the Mt. Quanstrom. The interval studied in this work is demarcated by red box, and the contact between these stratigraphic units is indicated by yellow line.

Moreover, episodes of metamorphism have altered the rocks to sub-greenschist and greenschist facies (very low- to low-grade metamorphism; see Murphy, 1987a); however primary sedimentary textures and structures are generally well-preserved.

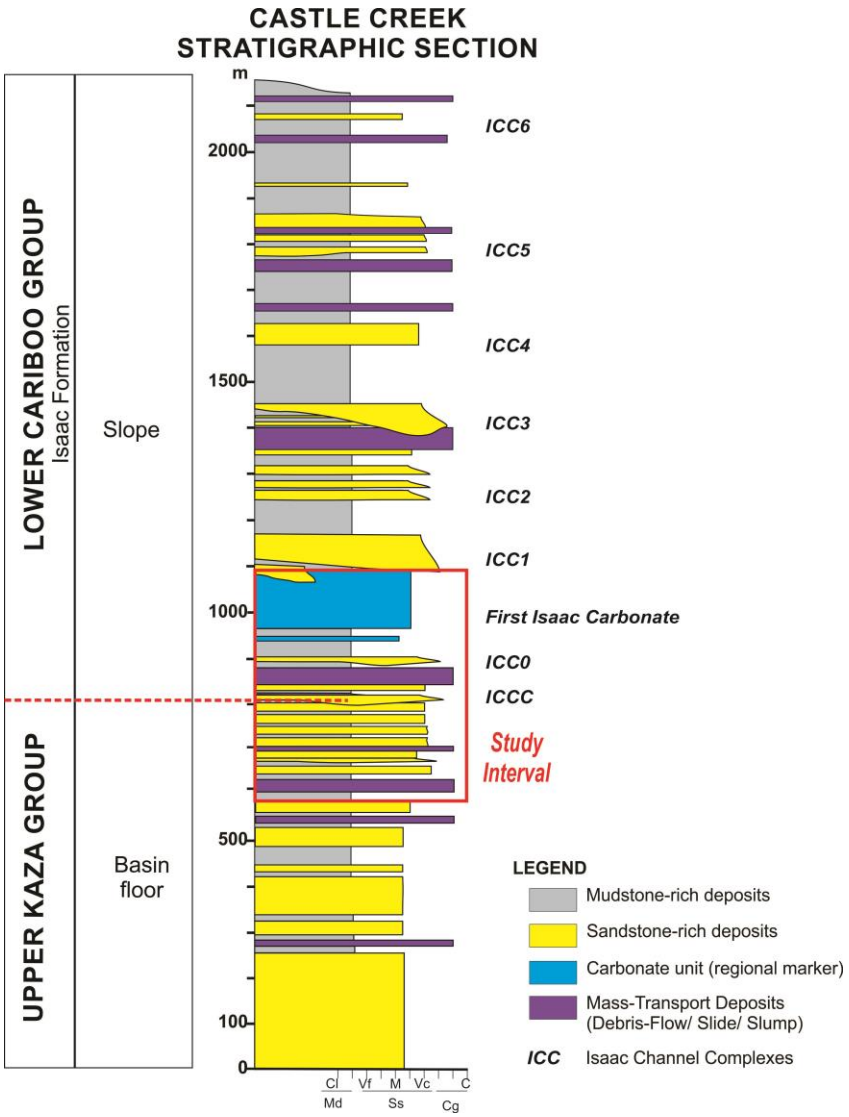

Figure 1.9 Generalized stratigraphy of the Castle Creek (principal) study area. (modified from Ross and Arnott, 2007). The red box indicates the interval studied in this work.

The studied interval is interpreted to represent a change from basin-floor to base of continental slope sedimentation (Ross and Arnott, 2007). At Castle Creek, the interval consists of an approximately 225 m thick, sandstone-dominated succession of uppermost Kaza Group that is overlain by about 375 m thick, mudstone-dominated strata of the lowermost Isaac Formation, including the first Isaac carbonate member (Fig. 1.9). At Mount Quanstrom, the interval includes about 300 m-thick of the uppermost Kaza Group, and an overlying almost 650 m-thick, partly-exposed succession of the lowermost Isaac Formation, including the first Isaac carbonate.

1.5 Previous Works

Over the past fifty years, a number of regional mapping and structural geology studies have been conducted in the Cariboo Mountains (Aitken, 1969; Campbell, 1973; Murphy and Rees, 1983; Murphy, 1987a; Murphy, 1987b; Ross and Murphy, 1988; Gabrielse, 1991; Gabrielse and Campbell, 1991; Hein and McMechan, 1994; Reid et al., 2002; Ross and Ferguson, 2003). However, it has only been during the last decade that research studies, including this one, have increasingly focused on understanding the sedimentology, stratigraphy, architecture and geochemistry of Windermere deep-water strata. Most of these more current studies are part of the Windermere Consortium, an academia-, industry- and government- funded research effort based at the University of Ottawa.

At Mt. Quanstrom, little geological research has been conducted, such as structural studies of Campbell (1973); and Ferguson and Simony (1991), and

sedimentological analyses of basin-floor deposits of the Middle Kaza by van Hees (2008); and Terlaky (2014). Hitherto, no detailed work has been done on rocks at the transition of the uppermost Kaza Group and overlying Isaac Formation, which is the primary focus of this study. Owing to its ease of access and moderate topography, the Castle Creek study area has been the most intensively studied. In the lower part of the outcrops, basin-floor strata of the upper Kaza Group have been studied by Meyer (2004); Longuépée et al. (2007a, 2007b); Meyer and Ross (2007); Privett (2008); Rocheleau (2011); Al-Mufti (2013); English (2013); Terlaky (2014); Terlaky and Arnott (2014); and Terlaky et al. (2016). Likewise, slope deposits of the overlying Isaac Formation have been investigated by Laurin (2005); Leclair and Arnott (2005); Marion (2005); Navarro (2006); Altosaar (2007); Gammon and Arnott (2007); Gammon et al. (2007); Navarro et al. (2007b, 2007a); O'Byrne et al. (2007); Schwarz and Arnott (2007); Mussa-Caleca (2008); Buckley et al. (2009); Anthony (2010); Buckley et al. (2010); Arnott et al. (2011); Davis (2011); Khan et al. (2011); Khan and Arnott (2011); Dumouchel (2012); Khan (2012); and Dumouchel (2015).

Additionally, the Old Fort Point Formation, which separates the Middle and Upper Kaza groups, and also represents the most regionally-extensive stratigraphic marker in the WSG, was studied in various localities of the southern Canadian Cordillera by Smith (2009); Smith et al. (2011); and Smith et al. (2014a); Smith et al. (2014b).

1.6 Thesis Aims

This thesis utilizes outcrop data to develop a detailed understanding of not only facies and stratal architectural elements, but also how those elements are interrelated temporally and spatially within the transition from basin-floor-fan to slope-channel deposition (from upper Kaza Group to Isaac Formation). This thesis appraises the sedimentary context and development of this transitional interval by utilizing three different approaches or scales of observation: (i) grain to bed (mm- to m-scale), stratal-element scale (hundreds to thousands of metres), and (iii) outcrop- or regional-scale (several kilometres). This thesis aims to:

1. Identify and document lithofacies, significant bounding surfaces, and stratal architectural elements in the channel-lobe transition zone (CLTZ) throughout the transition between the upper Kaza and Cariboo groups and above in order to develop an evolutionary model of a deep-water transitional system, which currently are poorly understood in the deep-water literature;
2. Establish the internal distribution of lithofacies and stratal elements within lower slope deposits of the Isaac Formation and to interpret the development of these deposits through time.
3. Determine the sedimentological, stratigraphic and architectural characteristics of the first Isaac carbonate (FIC), a major regional stratigraphic marker in the Isaac Formation. In addition, the origin of changes in sediment composition and supply to the deep-water Windermere basin are investigated.

4. Evaluate and interpret the geological factors that control the long-term evolution and spatial configuration of stratal elements that make up a continental slope to oceanic basin-floor transition. These data are then compared with other modern and ancient deep-water turbidite systems to better recognize and document a suite of common lithological attributes and stratal elements and identify consistent stratal patterns and geometries.

1.7 Thesis Organization

This Ph.D. thesis is organized into five main chapters, and is a combination of thesis monograms and a series of articles. Chapter 2 reviews different types of gravity flows and related deposits in deep-water settings, with emphasis on those deposits that are recognized in the study areas. Chapters 3 to 5 are prepared each as separate (but extended-version) papers, which are intended for further modification and publication in peer-reviewed journals in the future. Chapters 3 and 4 focus solely on the Castle Creek study area, whereas Chapter 5 is a synthesis of data collected largely at the Castle Creek area, but also including the Mt. Quanstrom study area.

Chapter 3 is an expanded version of a manuscript in preparation for submission to *Sedimentology*, titled "Stratigraphic Architecture of An Ancient Deep-Marine Channel-Lobe Transition Zone, Kaza-Isaac Transition, Windermere Turbidite System, Cariboo Mountains, B.C." The co-author of this publication is Dr. R.W. (Bill) C. Arnott.

Chapter 4 is an expanded version of a manuscript in preparation for submission to *Journal of Marine and Petroleum Geology*, titled "Stratal Architecture

And Evolution Of A Slope Mass-Transport Complex And Overlying Deep-Water Deposits, Lower Isaac Formation, Windermere Turbidite Group, Canada." The co-author of this publication is Dr. R.W. (Bill) C. Arnott.

Chapter 5 is an expanded version of a manuscript in preparation for submission to *AAPG Bulletin*, titled "Stratal Architecture, Origin And Allocyclic Control On Deposition in Slope Channels versus Gullies In An Ancient Mixed Siliciclastic-Carbonate Slope System, Neoproterozoic Isaac Formation, Southeastern Canadian Cordillera." The co-author of the publication is Dr. R.W. (Bill) C. Arnott.

Chapter 6 corresponds to the Discussion and Future Works, in which a summarized stratigraphic analysis of a basin floor-slope transition in the Windermere Turbidite System is presented.

Additional data including sample location, maps and airphotos, geochemical data, petrographic analyses, and gamma-ray logs are presented in the various appendices located at the end of the dissertation.

1.8 Statement of Authorship and Contribution

Chapter 3 is based on fieldwork in the Castle Creek study area that was carried out by the author, with assistance from Jordan Clark, and Lindsay Coffin, with additional support of Carley Crann, Zishan Khann, Jonathan Rocheleau, Dave Anthony and Steven Gould. Lori Meyer in her MSc thesis previously conducted fieldwork in the studied section of the uppermost Kaza Group, which at that time was referred as the upper Upper Kaza Group (see Meyer, 2004; Meyer and Ross, 2007), but none of her data or interpretations were used in this thesis. All figures were

prepared by the author, unless original sources are referenced. The initial manuscript for the chapter was written by the author and later revised through discussion with Dr. Arnott.

Chapter 4 is based principally on fieldwork in the Castle Creek study area carried out by the author, with assistance in the field from Jordan Clark, Lindsay Coffin, Carley Crann, and Steven Gould. All figures were prepared by the author, except where indicated. No detailed sedimentological or stratigraphic work had previously been conducted exhaustively within the study area, except for a part of the BSc thesis research by Kenny Wallace, who studied the thick distinctive debrite and part of the slide complex (also studied here), which crops out a short distance of Isaac Channel 0 (see lower debris flow deposit or LDF of Wallace, 2004). In Wallace's work, the debrite was only studied on the southeast outcrops of the Castle Creek area, whereas in our study mapped and analyzed it on both areas, Castle Creek South and North. All figures were drawn by the author, except where specified. The initial manuscript of the chapter was written by the author and later discussed and reviewed with Dr. Arnott.

Chapter 5 is based principally on fieldwork in the Castle Creek study area that was carried out by the author with field assistance by Jordan Clark, and Drs. Paul Gammon and R. W. (Bill) C. Arnott. Fieldwork at the Mt. Quanstrom study area was carried out by the author with assistance from Lindsay Coffin and Dave Lowe. Dr. Gerald M. Ross (formerly of the GSC) previously measured and sampled across part of the first Isaac carbonate (FIC, see Ross, 2003), from which previously unpublished carbon isotope analyses is presented in this study (see Appendix E). Dr. Paul

Gammon conducted preliminary fieldwork in the FIC (Gammon and Arnott, 2007), including petrography/geochemistry of one calcidebrite (here termed calcidebrite 2), but except for general observations none of these data was used in this thesis. All figures were drawn by the author, except where indicated. This study is the first detailed documentation of the sedimentology and stratigraphy of the FIC in both study areas. The initial manuscript of the chapter was written by the author and subsequent revised through discussion with Dr. Arnott.

Appendix G includes most of the field dataset obtained from the Mt. Quanstrom study area by the author with great assistance from Lindsay Coffin and David Lowe. No detailed sedimentological or stratigraphic work had previously been conducted here. Stratal units recognized in Mt. Quanstrom are compared with equivalent units at the Castle Creek study area (included in Chapters 3 and 4). All figures were sketched by the author.

1.9 References

Aalto, K. R., 1971, Glacial marine sedimentation and stratigraphy of the Toby Conglomerate (Upper Proterozoic), southeastern British Columbia, northwestern Idaho and northeastern Washington: Canadian Journal of Earth Sciences, v. 8, p. 753-787.

Aitken, J., 1969, Documentation of the sub-Cambrian unconformity, Rocky Mountains main ranges, Alberta: Canadian Journal of Earth Sciences, v. 6, p. 193-200.

Al-Mufti, O., 2013, Dune or Dune-Like Cross-Stratification in Deep-Marine Sandstones of the Neoproterozoic Windermere Supergroup, Cariboo Mountains, British Columbia, Canada: Unpublished B.Sc. thesis thesis, University of Ottawa, 59 p.

Altosaar, A., 2007, Stratigraphic architecture and sedimentology of interstratified splay, levee and channel deposits, Isaac Formation (Windermere Supergroup), southern Canadian Cordillera: BSc Thesis thesis, University of Ottawa, Ottawa, Ontario.

Anthony, D., 2010, Isaac Channel 1 – siliciclastic lowstand channel deposits following highstand carbonate production.: BSc Thesis thesis, University of Ottawa.

Arnot, M. J., P. R. King, G. H. Browne, and K. Helle, 2007, Channelized, innermost, basin-floor-fan morphologies, Mount Messenger Formation, Waikiekie south beach and inland, New Zealand, *in* T. H. Nilsen, R. D. Shew, G. S. Steffens, and J. R. J. Studlick, eds., Atlas of deep-water outcrops, v. Chapter 63, AAPG studies in geology 56, p. 249-256.

Arnott, R. W. C., 2007, Stratal architecture and origin of lateral accretion deposits (LADs) and conterminuous inner-bank levee deposits in a base-of-slope sinuous channel, lower Isaac Formation (Neoproterozoic), East-Central British Columbia, Canada: Marine and Petroleum Geology, v. 24, p. 515-528.

Arnott, R. W. C., K. Wallace, and J. Laurin, 2011, Stratal architecture and temporal evolution of a passive margin mass-transport deposit, Neoproterozoic Isaac Formation, Cariboo Mountains, British Columbia, Canada, *in* R. C. Shipp, P. Weimer, and H. W. Posamentier, eds., Mass-Transport Deposits in Deepwater Settings, v. SEPM Special Publication, SEPM, p. 221-234.

Beaubouef, R. T., C. Rossen, F. B. Zelt, M. D. Sullivan, D. C. Mohig, and D. C. Jennette, 1999, Deep-water sandstones, Brushy Canyon formation, West Texas, Field Guide for AAPG Hedberg Field Research Conference, v. vol. 40, AAPG Continuing Education Course Note Series, p. 48.

Beedle, M. J., B. Menounos, B. H. Luckman, and R. Wheate, 2009, Annual push moraines as climate proxy: Geophysical Research Letters, v. 36, p. L20501.

Beedle, M. J., B. Menounos, and R. Wheate, 2014, An evaluation of mass-balance methods applied to Castle Creek Glacier, British Columbia, Canada: Journal of Glaciology, v. 60, p. 262-276.

Bond, G. C., P. A. Nickeson, and M. A. Kominz, 1984, Breakup of a supercontinent between 625 Ma and 555 Ma: new evidence and implications for continental histories: Earth and Planetary Science Letters, v. 70, p. 325-345.

Bonnel, C., B. Dennielou, L. Droz, T. Mulder, and S. Berné, 2005, Architecture and depositional pattern of the Rhône Neofan and recent gravity activity in the Gulf of Lions (western Mediterranean): Marine and Petroleum Geology, v. 22, p. 827-843.

Bravo, J. C. V., and S. Robles, 1995, Large-scale mesotopographic bedforms from the Albian Black Flysch, northern Spain: characterization, setting and comparison with recent analogues, *in* K. T. Pickering, R. N. Hiscott, N. H. Kenyon, F. Ricci Lucchi, and R. D. A. Smith, eds., Atlas of Deep Water Environments: Architectural style in turbidite systems: Dordrecht, Springer Netherlands, p. 216-226.

Browne, G. H., and R. M. Slatt, 2002, Outcrop and Behind-Outcrop Characterization of a Late Miocene Slope Fan System, Mt. Messenger Formation, New Zealand: AAPG Bulletin, v. 86, p. 841-862.

Browne, G. H., R. M. Slatt, and P. R. King, 2000, Contrasting styles of basin-floor fan and slope fan deposition: Mount Messenger Formation, New Zealand, *in* A. H. Bouma, and C. G. Stone, eds., Fine-grained turbidite systems, v. AAPG Memoir 72/SEPM Special Publication 68, p. 143-152.

Buckley, S., E. Schwarz, V. Terlaky, J. Howell, and R. Arnott, 2009, Terrestrial laser scanning combined with photogrammetry for digital outcrop modelling: ISPRS Congress 2009, p. 75-80.

Buckley, S. J., E. Schwarz, V. Terlaky, J. A. Howell, and R. Arnott, 2010, Combining aerial photogrammetry and terrestrial lidar for reservoir analog modeling: Photogrammetric Engineering & Remote Sensing, v. 76, p. 953-963.

Campbell, R., 1973, Structural cross-section and tectonic model of the southeastern Canadian Cordillera: Canadian Journal of Earth Sciences, v. 10, p. 1607-1620.

Christie-Blick, N., I. A. Dyson, and C. Von Der Borch, 1995, Sequence stratigraphy and the interpretation of Neoproterozoic Earth history: Precambrian Research, v. 73, p. 3-26.

Clark, B. E., and R. J. Steel, 2006, Eocene turbidite-population statistics from shelf edge to basin floor, Spitsbergen, Svalbard: Journal of Sedimentary Research, v. 76, p. 903-918.

Coleman, J. L., G. H. Browne, P. R. King, R. M. Slatt, R. J. Spang, E. T. Williams, and G. R. Clemenceau, 2000, The inter-relationships of scales of

heterogeneity in subsurface, deep-water E&P projects — lessons learned from the Mount Messenger Formation (Miocene), Taranaki Basin, New Zealand, *in* P. Weimer, R. M. Slatt, J. Coleman, N. C. Rosen, H. Nelson, A. H. Bouma, M. J. Styzen, and D. T. Lawrence, eds., Deep-water reservoirs of the world, Deep-water reservoirs of the world: Gulf Coast Section SEPM 20th Annual Research Conference, p. 263–283. CD-ROM.

Collinson, J. D., O. Martinsen, B. Bakken, and A. Kloster, 1991, Early fill of the Western Irish Namurian Basin: a complex relationship between turbidites and deltas: Basin Research, v. 3, p. 223-242.

Colpron, M., J. M. Logan, and J. K. Mortensen, 2002, U-Pb zircon age constraint for late Neoproterozoic rifting and initiation of the lower Paleozoic passive margin of western Laurentia: Canadian Journal of Earth Sciences, v. 39, p. 133-143.

Crabaugh, J. P., and R. J. Steel, 2004, Basin-floor fans of the Central Tertiary Basin, Spitsbergen; relationship of basin-floor sand-bodies to prograding clinoforms in a structurally active basin, *in* S. A. Lomas, and P. Joseph, eds., Confined Turbidite Systems, v. Special Publication 222: London, Geological Society, p. 187–228.

Crevello, P. D., H. D. Johnson, F. Tongkul, and M. R. Wells, 2007a, Channel-lobe and Leveed-Channel Complexes, Taman Bukit Sepanggar, Northwest Borneo, *in* T. H. Nilsen, R. D. Shew, G. S. Steffens, and J. R. J. Studlick, eds., Atlas of Deep-Water Outcrops, v. AAPG Studies in Geology Volume 56, p. 57-60.

Crevello, P. D., H. D. Johnson, F. Tongkul, and M. R. Wells, 2007b, Lobe, channel-lobe, and Channel Deposits, Lok Kawi, Northwest Borneo, *in* T. H. Nilsen, R. D. Shew, G. S. Steffens, and J. R. J. Studlick, eds., Atlas of Deep-Water Outcrops, v. AAPG Studies in Geology Volume 56, p. 64-66.

Dalrymple, R., and G. Narbonne, 1996, Continental slope sedimentation in the Sheepbed Formation (Neoproterozoic, Windermere Supergroup), Mackenzie Mountains, NWT: Canadian Journal of Earth Sciences, v. 33, p. 848-862.

Dalziel, I. W., 1991, Pacific margins of Laurentia and East Antarctica-Australia as a conjugate rift pair: Evidence and implications for an Eocambrian supercontinent: Geology, v. 19, p. 598-601.

Dalziel, I. W., 2014, Cambrian transgression and radiation linked to an Iapetus-Pacific oceanic connection?: Geology, v. 42, p. 979-982.

Davis, L., 2011, Architecture of deep-marine interchannel deposits: Isaac Formation, Windermere Supergroup (Neoproterozoic), Southern Canadian Cordillera: M.Sc. Thesis thesis, University of Ottawa, Ottawa, 174 p.

Dumouchel, I. G., 2012, Effects of relative sea-level change on the stratigraphic architecture of a passive margin deep-marine channel fill complex, Windermere Supergroup, British Columbia, Canada.: BSc Thesis thesis, University of Ottawa, 59 p.

Dumouchel, I. G., 2015, Stratigraphic Architecture and Depositional History of laterally-accreted channel fills in the Lower Isaac Formation, Windermere Supergroup, British Columbia, Canada, University of Ottawa, Ottawa, 108 p.

Earth, G., 2014, Satellite airphoto Cariboo Mountains.

Eisbacher, G., 1985, Late Proterozoic rifting, glacial sedimentation, and sedimentary cycles in the light of Windermere deposition, western Canada: Palaeogeography, Palaeoclimatology, Palaeoecology, v. 51, p. 231-254.

English, M., 2013, Lateral Facies Changes in Matrix-rich Sandstones, Upper Kaza Group,
Windermere Supergroup, Cariboo Mountains, British Columbia, Canada: BSc Thesis thesis, University of Ottawa, 61 p.

Ercilla, G., R. B. Wynn, B. Alonso, and J. Baraza, 2002, Initiation and evolution of turbidity current sediment waves in the Magdalena turbidite system: Marine Geology, v. 192, p. 153-169.

Eschard, R., E. Albouy, R. Deschamps, T. Euzen, and A. Ayub, 2003, Downstream evolution of turbiditic channel complexes in the Pab Range outcrops (Maastrichtian, Pakistan): Marine and Petroleum Geology, v. 20, p. 691-710.

Etienne, S., T. Mulder, P. Razin, M. Bez, G. Désaubliaux, R. Joussiaume, and E. Tournadour, 2013, Proximal to distal turbiditic sheet-sand heterogeneities: Characteristics of associated internal channels. Examples from the Trois Evêchés area, Eocene-Oligocene Annot Sandstones (Grès d'Annot), SE France: Marine and Petroleum Geology, v. 41, p. 117-133.

Evenchick, C. A., R. R. Parrish, and H. Gabrielse, 1984, Precambrian gneiss and late Proterozoic sedimentation in north-central British Columbia: Geology, v. 12, p. 233-237.

Eyles, N., and N. Januszczak, 2004, 'Zipper-rift': a tectonic model for Neoproterozoic glaciations during the breakup of Rodinia after 750 Ma: Earth-Science Reviews, v. 65, p. 1-73.

Fanning, C. M., and P. K. Link, 2004, U-Pb SHRIMP ages of Neoproterozoic (Sturtian) glaciogenic Pocatello Formation, southeastern Idaho: Geology, v. 32, p. 881-884.

Ferguson, C. A., and P. S. Simony, 1991, Preliminary report on structural evolution and stratigraphic correlations, northern Cariboo Mountains, British Columbia: Current Research, v. Part A, Geological Survey of Canada, p. 103-110.

Ferri, F., 1999, Devono-Mississippian felsic volcanism along the western edge of the Cassiar Terrane, north-central British Columbia (NTS 93N, 94C and 94D): Geological Fieldwork, p. 2000-1.

Fildani, A., S. M. Hubbard, and B. W. Romans, 2009a, Stratigraphic evolution of deep-water architecture: examples of controls on depositional styles from the Magallanes basin, southern Chile, Outcrop Atlas and Field Guide for SEPM Research Conference, v. SEPM Field Trip Guidebook Volume 10, SEPM Society for Sedimentary Geology, p. 73.

Fildani, A., A. Weislogel, N. J. Drinkwater, T. McHargue, A. Tankard, J. Wooden, D. Hodgson, and S. Flint, 2009b, U-Pb zircon ages from the southwestern Karoo Basin, South Africa—Implications for the Permian-Triassic boundary: Geology, v. 37, p. 719-722.

Flint, S., D. Hodgson, A. Sprague, R. Brunt, W. Van der Merwe, J. Figueiredo, A. Prélat, D. Box, C. Di Celma, and J. Kavanagh, 2011, Depositional architecture and sequence stratigraphy of the Karoo basin floor to shelf edge succession, Laingsburg depocentre, South Africa: Marine and Petroleum Geology, v. 28, p. 658-674.

Gabrielse, H., 1972, Younger Precambrian of the Canadian Cordillera: American Journal of Science, v. 272, p. 521-536.

Gabrielse, H., 1991, Late Paleozoic and Mesozoic terrane interactions in north-central British Columbia: Canadian Journal of Earth Sciences, v. 28, p. 947-957.

Gabrielse, H., and R. Campbell, 1991, Upper Proterozoic assemblages: Geology of the Cordilleran Orogen in Canada. Edited by H. Gabrielse and CJ Yorath. Geological Survey of Canada, Geology of Canada, p. 125-150.

Gammon, P. R., and R. W. C. Arnott, 2007, Source control over calciturbidite facies distributions in the Lower Isaac Carbonate, Windermere Supergroup, Canada, AAPG Annual Convention and Exhibition. Abstracts.: Long Beach, California, AAPG Search and Discover Article #90063.

Gammon, P. R., R. W. C. Arnott, and G. M. Ross, 2007, Architectural relationships between channels, levees, and debris flows: Channel 6, Castle Creek South, Lower Isaac Formation, Windermere Supergroup, B.C., Canada, *in* T. H. Nilsen, R. D. Shew, G. S. Steffens, and J. R. J. Studlick, eds., Atlas of Deep-Water Outcrops, AAPG Studies in Geology 56, p. 102-105.

Gardner, M. H., and J. M. Borer, 2000, Submarine channel architecture along a slope to basin profile, Brushy Canyon Formation, West Texas: Special Publication SEPM, v. 68, p. 195-214.

Gardner, M. H., J. M. Borer, J. J. Melick, N. Mavilla, M. Dechesne, and R. N. Wagerle, 2003, Stratigraphic process-response model for submarine channels and related features from studies of Permian Brushy Canyon outcrops, West Texas: Marine and Petroleum Geology, v. 20, p. 757-787.

Government of Canada, 2006, Topographic Map Sheet 93A/16, Mount Winde (1:50,000): Natural Resources Canada, Earth Sciences Sector, Canada Centre for Mapping and Earth Observation.

Hein, F., and M. McMechan, 1994, Proterozoic and Lower Cambrian strata of the western Canada sedimentary basin: GD Mossop and I. Shetsen (comps.). Geological Atlas of the Western Canada Sedimentary Basin. Canadian Society of Petroleum Geologists and Alberta Research Council, p. 57-67.

Hodgson, D. M., S. S. Flint, D. Hodgetts, N. J. Drinkwater, E. P. Johannessen, and S. M. Luthi, 2006, Stratigraphic Evolution of Fine-Grained Submarine Fan Systems, Tanqua Depocenter, Karoo Basin, South Africa: Journal of Sedimentary Research, v. 76, p. 20-40.

Hofer, G., M. Wagreich, and S. Neuhuber, 2013, Geochemistry of fine-grained sediments of the upper Cretaceous to Paleogene Gosau Group (Austria, Slovakia): Implications for paleoenvironmental and provenance studies: Geoscience Frontiers, v. 4, p. 449-468.

Hubbard, S. M., A. Fildani, B. W. Romans, J. A. Covault, and T. R. McHargue, 2010, High-relief slope clinoform development: insights from outcrop, Magallanes Basin, Chile: Journal of Sedimentary Research, v. 80, p. 357-375.

Johannessen, E. P., and R. J. Steel, 2005, Shelf-margin clinoforms and prediction of deepwater sands: Basin Research, v. 17, p. 521-550.

Johansson, M., N. E. Braakenburg, D. A. Stow, and J.-C. Faugères, 1998, Deep-water massive sands: facies, processes and channel geometry in the Numidian Flysch, Sicily: Sedimentary Geology, v. 115, p. 233-265.

Johnson, S. D., S. Flint, D. Hinds, and H. De Ville Wickens, 2001, Anatomy, geometry and sequence stratigraphy of basin floor to slope turbidite systems, Tanqua Karoo, South Africa: Sedimentology, v. 48, p. 987-1023.

Joseph, P., and S. A. Lomas, 2004, Deep-water sedimentation in the Alpine Foreland Basin of SE France: new perspectives on the Gres d'Annot and related system: an introduction, *in* P. Joseph, and S. A. Lomas, eds., Deep Water Sedimetation in the Alpine Basin of SE France. New perspectives on the Grès d'Annot and related systems., v. Special Publication 221: London, Geological Society, p. 1-16.

Karlstrom, K. E., S. A. Bowring, C. M. Dehler, A. H. Knoll, S. M. Porter, D. J. Des Marais, A. B. Weil, Z. D. Sharp, J. W. Geissman, and M. B. Elrick, 2000, Chuar Group of the Grand Canyon: Record of breakup of Rodinia, associated change in the global carbon cycle, and ecosystem expansion by 740 Ma: Geology, v. 28, p. 619-622.

Kendall, B., R. A. Creaser, and D. Selby, 2009, 187Re-187Os geochronology of Precambrian organic-rich sedimentary rocks: Geological Society, London, Special Publications, v. 326, p. 85-107.

Kendall, B. S., R. A. Creaser, G. M. Ross, and D. Selby, 2004, Constraints on the timing of Marinoan "Snowball Earth" glaciation by 187 Re–187Os dating of a Neoproterozoic, post-glacial black shale in Western Canada: Earth and Planetary Science Letters, v. 222, p. 729-740.

Khan, Z., 2012, Origin and architecture of deep-water levee deposits: Insight from the ancient rock record and experiments: PhD Thesis thesis, University of Ottawa, Ottawa, Ontario, 300 p.

Khan, Z. A., B. Arnott, and A. Pugin, 2011, An alternative model of producing topography in the crest region of deep-water levees: AAPG bulletin, v. 95, p. 2085-2106.

Khan, Z. A., and R. W. C. Arnott, 2011, Stratal attributes and evolution of asymmetric inner- and outer-bend levee deposits associated with an ancient deep-water channel-levee complex within the Isaac Formation, southern Canada: Marine and Petroleum Geology, v. 28, p. 824-842.

King, P. R., and G. H. Browne, 2002, Miocene Slope to basin-floor sequences exposed in North Taranaki, New Zealand: A two-day field guide prepared for the New Zealand Petroleum Conference.: 2002 New Zealand Petroleum Conference Proceedings.

King, P. R., G. H. Browne, M. J. Arnot, and M. P. Crundwell, 2007a, A 2-D, oblique-dip outcrop transect through a third-order, progradational, deep-water clastic succession, Urenui–Mount Messenger Formations, New Zealand, *in* T. H. Nilsen, R. D. Shew, G. S. Steffens, and J. R. J. Studlick, eds., Atlas of deep-water outcrops, v. CD-ROM, AAPG Studies in Geology 56, p. 42 p.

King, P. R., G. H. Browne, M. J. Arnot, R. M. Slatt, K. Helle, and I. Stromsoyen, 2007b, An overview of the Miocene Mount Messenger-Urenui Formations, New Zealand : a 2-D, oblique-dip outcrop transect through an entire third-order, progradational, deep-water clastic succession., *in* T. H. Nilsen, R. D. Shew, G. S. Steffens, and J. R. J. Studlick, eds., Atlas of deep-water outcrops., v. Chapter 60, AAPG studies in geology 56. , p. 238-240.

Kostrewa, R., 2004, Internal architecture, geometry and reservoir characterisation of depositional lobes in outcrop and subsurface: examples from S-Turkey and the North Sea.: Unpublished Ph.D. thesis, Eberhard Karls University of Tübingen, 177 p.

Laurin, J., 2005, Depositional history and sequence stratigraphic context of a Neoproterozoic mass transport deposit, Isaac Formation, east-central B.C.: BSc Thesis thesis, University of Ottawa, Ottawa, Ontario, 88 p.

Leclair, S., and R. W. C. Arnott, 2005, Parallel lamination formed by high-density turbidity currents: Journal of Sedimentary Research, v. 75, p. 1-5.

Lemieux, Y., R. Thompson, P. Erdmer, A. Simonetti, and R. Creaser, 2007, Detrital zircon geochronology and provenance of Late Proterozoic and mid-Paleozoic successions outboard of the miogeocline, southeastern Canadian Cordillera: Canadian Journal of Earth Sciences, v. 44, p. 1675-1693.

Levy, M., and N. Christie-Blick, 1989, Pre-Mesozoic palinspastic reconstruction of the eastern Great Basin (western United States): Science, v. 245, p. 1454-1462.

Li, Z.-X., S. Bogdanova, A. S. Collins, A. Davidson, B. De Waele, R. Ernst, I. C. Fitzsimons, R. Fuck, D. Gladkochub, and J. Jacobs, 2008, Assembly, configuration, and break-up history of Rodinia: a synthesis: Precambrian research, v. 160, p. 179-210.

Li, Z.-X., D. A. D. Evans, and G. P. Halverson, 2013, Neoproterozoic glaciations in a revised global palaeogeography from the breakup of Rodinia to the assembly of Gondwanaland: Sedimentary Geology, v. 294, p. 219-232.

Lickorish, W. H., and P. S. Simony, 1995, Evidence for late rifting of the Cordilleran margin outlined by stratigraphic division of the Lower Cambrian Gog Group, Rocky Mountain Main Ranges, British Columbia and Alberta: Canadian Journal of Earth Sciences, v. 32, p. 860-874.

Lien, T., O. J. Martinsen, and R. Walker, 2007, An Overview of the Ross Formation, Shannon Basin, Western Ireland, *in* T. H. Nilsen, R. D. Shew, G. S. Steffens, and J. R. J. Studlick, eds., Atlas of Deep-Water Outcrops, AAPG Studies in Geology Volume 56, p. 192-195.

Lien, T., R. G. Walker, and O. J. Martinsen, 2003, Turbidites in the Upper Carboniferous Ross Formation, western Ireland: reconstruction of a channel and spillover system: Sedimentology, v. 50, p. 113-148.

Longuépée, H., V. Terlaky, and R. W. C. Arnott, 2007a, Detailed architecture of a basin-floor sheetlike deposit: Neoproterozoic Upper Kaza Group, British Columbia, Canada.: AAPG Annual Convention and Exhibition.

Longuépée, H., V. Terlaky, and R. W. C. Arnott, 2007b, Detailed architecture of deep-water sheet sand and associated fine-grained sediments: example from the Upper Kaza Group, British Columbia: CSPG CSEG Convention.

Lund, K., 2008, Geometry of the Neoproterozoic and Paleozoic rift margin of western Laurentia: Implications for mineral deposit settings: Geosphere, v. 4, p. 429-444.

Lund, K., J. N. Aleinikoff, K. V. Evans, and C. M. Fanning, 2003, SHRIMP U-Pb geochronology of Neoproterozoic Windermere Supergroup, central Idaho:

Implications for rifting of western Laurentia and synchroneity of Sturtian glacial deposits: Geological Society of America Bulletin, v. 115, p. 349-372.

Macdonald, H., 2010, Flutes, megaflutes and erosional bedforms: a reappraisal of their dynamics, University of Leeds, 254 p.

Macdonald, H., R. B. Wynn, V. A. I. Huvenne, J. Peakall, D. G. Masson, P. P. E. Weaver, and S. D. McPhail, 2011, New insights into the morphology, fill, and remarkable longevity (>0.2 m.y.) of modern deep-water erosional scours along the northeast Atlantic margin: Geosphere, v. 7, p. 845-867.

MacNaughton, R. B., G. M. Narbonne, and R. W. Dalrymple, 2000, Neoproterozoic slope deposits, Mackenzie Mountains, northwestern Canada: implications for passive-margin development and Ediacaran faunal ecology: Canadian Journal of Earth Sciences, v. 37, p. 997-1020.

Marion, C., 2005, Architecture and sedimentology of a channel and slide complex in the Neoproterozoic Isaac Formation, British Columbia: BSc Thesis thesis, University of Ottawa, Ottawa, Ontario.

Martinsen, O. J., T. Lien, and R. G. Walker, 2000, Upper Carboniferous deep water sediments, western Ireland: Analogues for passive margin turbidite plays: Deep-water reservoirs of the world: Gulf Coast Section SEPM Foundation, Twentieth Annual Research Conference, p. 533-555.

Martinsen, O. J., T. Lien, R. G. Walker, and J. D. Collinson, 2003, Facies and sequential organisation of a mudstone-dominated slope and basin floor succession: the Gull Island Formation, Shannon Basin, Western Ireland: Marine and Petroleum Geology, v. 20, p. 789-807.

Maurer, M. K., B. Menounos, B. H. Luckman, G. Osborn, J. J. Clague, M. J. Beedle, R. Smith, and N. Atkinson, 2012, Late Holocene glacier expansion in the Cariboo and northern Rocky Mountains, British Columbia, Canada: Quaternary Science Reviews, v. 51, p. 71-80.

McDonough, M. R., and R. R. Parrish, 1991, Proterozoic gneisses of the Malton Complex, near Valemount, British Columbia: U-Pb ages and Nd isotopic signatures: Canadian Journal of Earth Sciences, v. 28, p. 1202-1216.

McMechan, M. E., 2015, The Neoproterozoic succession of the central Rocky Mountains, Canada: Bulletin of Canadian Petroleum Geology, v. 63, p. 243-273.

Mellere, D., P. Plink-Björklund, and R. Steel, 2002, Anatomy of shelf deltas at the edge of a prograding Eocene shelf margin, Spitsbergen: Sedimentology, v. 49, p. 1181-1206.

Meyer, L., 2004, Internal architecture of an ancient deep-water, passive margin, basin-floor fan system, Upper Kaza Group, Windermere Supergroup, Castle Creek, British Columbia: M.Sc. Thesis thesis, Univeristy of Calgary, Calgary, Alberta, 175 p.

Meyer, L., and G. M. Ross, 2007, Channelized lobe and sheet sandstones of the Upper Kaza Group basin-floor turbidite system, British Columbia, Canada, *in* T. H. Nilsen, R. D. Shew, G. S. Steffens, and J. R. J. Studlick, eds., Atlas of deep-water outcrops, v. Studies in Geology 56, AAPG, p. 22.

Monger, J., and R. Price, 1979, Geodynamic evolution of the Canadian Cordillera-progress and problems: Canadian Journal of Earth Sciences, v. 16, p. 770-791.

Monger, J., and R. Price, 2002, The Canadian Cordillera: geology and tectonic evolution: CSEG Recorder, v. 27, p. 17-36.

Monger, J., R. Price, and D. Tempelman-Kluit, 1982, Tectonic accretion and the origin of the two major metamorphic and plutonic welts in the Canadian Cordillera: Geology, v. 10, p. 70-75.

Moores, E., 1991, Southwest US-East Antarctic (SWEAT) connection: a hypothesis: Geology, v. 19, p. 425-428.

Murphy, D., 1987a, Kaza Group, eastern Wells Gray Park, British Columbia: Current research, part A. Geological Survey of Canada, Paper, p. 735-742.

Murphy, D., and C. Rees, 1983, Structural transition and stratigraphy in the Cariboo Mountains, British Columbia: Geol. Surv. Pap. Can, p. 245-252.

Murphy, D. C., 1987b, Suprastructure/infrastructure transition, east-central Cariboo Mountains, British Columbia: geometry, kinematics and tectonic implications: Journal of Structural Geology, v. 9, p. 13-29.

Murphy, D. C., P. van der Heyden, R. R. Parrish, D. Klepacki, W. McMillan, L. Struik, and J. Gabites, 1995, New geochronological constraints on Jurassic deformation of the western edge of North America, southeastern Canadian Cordillera: Geological Society of America Special Papers, v. 299, p. 159-172.

Mussa-Caleca, M., 2008, Architecture and depositional history of a Neoproterozoic deep-water slope channel complex in a passive margin setting: Isaac Formation, Windermere Supergroup, southern Canadian Cordillera.: M.Sc. Thesis thesis, University of Ottawa, Ottawa, Ontario.

Navarro, L., 2006, Depositional Architecture and Evolution of deep-water base-of-slope and slope channel complexes in a passive-margin setting: Isaac Formation, Windermere Supergroup (Neoproterozoic), Southern Canadian Cordillera: M.Sc.Thesis thesis, University of Ottawa, Ottawa, 272 p.

Navarro, L., Z. Khan, and R. W. C. Arnott, 2007a, Architecture of a deep-water channel-levee complex: Channel 3, Castle Creek South, Isaac Formation, Windermere Supergroup, Bristish Columbia, Canada, *in* T. H. Nilsen, R. D. Shew, G. S. Steffens, and J. R. J. Studlick, eds., Atlas of Deep-Water Outcrops, AAPG Studies in Geology 56, p. 93-96.

Navarro, L., Z. Khan, and R. W. C. Arnott, 2007b, Depositional architecture and evolution of a deep-marine channel-levee complex: Isaac Formation (Windermere Supergroup), Southern Canadian Cordillera., *in* T. H. Nilsen, R. D. Shew, G. S. Steffens, and J. R. J. Studlik, eds., Atlas of Deep-water Outcrops., v. CD-ROM: Tulsa, AAPG Studies in Geology 56, CD-ROM, p. 22.

Normark, W. R., and D. J. W. Piper, 1985, Navy Fan, Pacific Ocean, *in* A. H. Bouma, W. R. Normark, and N. E. Barnes, eds., Submarine fans and related turbidite systems: New York, Springer-Verlag, p. 87-94.

O'Byrne, C. J., M. D. Barton, G. S. Steffens, C. Pirmez, and H. Buergisser, 2007, Architecture of a laterally migrating channel complex - Isaac Formation, Windermere Supergroup, British Columbia, Canada, *in* T. H. Nilsen, R. D. Shew, G. S. Steffens, and J. R. J. Studlick, eds., Atlas of deep-water outcrops, v. CD-ROM: Tulsa, AAPG, p. 11 p.

Ortner, H., 2007, Styles of soft-sediment deformation on top of a growing fold system in the Gosau Group at Muttekopf, Northern Calcareous Alps, Austria: slumping versus tectonic deformation: Sedimentary Geology, v. 196, p. 99-118.

Palanques, A., N. H. Kenyon, B. Alonso, and A. Limonov, 1995, Erosional and depositional patterns in the Valencia Channel Mouth: an example of a modern channel-lobe transition zone: Marine Geophysical Researches, v. 17, p. 503-517.

Parrish, R., and R. Scammell, 1988, The age of the Mount Copeland syenite gneiss and its metamorphic zircons, Monashee complex, southeastern British Columbia: Radiogenic age and isotopic studies: Report, v. 2, p. 88-2.

Paton, D., M. Carr, B. Trudgill, H. Ortner, and D. A. Medwedeff, 2007, Alpine-scale 3D geospatial modeling: Applying new techniques to old problems: Geosphere, v. 3, p. 527-549.

Pell, J., and P. Simony, 1982, Hadrynian Horsethief Creek Group/Kaza Group correlations in the southern Cariboo Mountains, British Columbia: Current Research, Part A, Geological Survey of Canada Paper, v. 82, p. 305-308.

Pell, J., and P. Simony, 1987, New correlations of Hadrynian strata, south-central British Columbia: Canadian Journal of Earth Sciences, v. 24, p. 302-313.

Pickering, K. T., 1983, Transitional submarine fan deposits from the late Precambrian Kongsijord Formation submarine fan, NE Finnmark, N. Norway: Sedimentology, v. 30, p. 18I-199.

Pickering, K. T., and N. J. Bayliss, 2009, Deconvolving tectono-climatic signals in deep-marine siliciclastics, Eocene Ainsa basin, Spanish Pyrenees: Seesaw tectonics versus eustasy: Geology, v. 37, p. 203-206.

Piper, D. J. W., and W. R. Normark, 1983, Turbidite depositional patterns and flow characteristics, Navy Submarine Fan, California Borderland: Sedimentology, v. 30, p. 681-694.

Posamentier, H. W., and V. Kolla, 2003, Seismic geomorphology and stratigraphy of depositional elements in deep-water settings: Journal of Sedimentary Research, v. 73, p. 367–388.

Posamentier, H. W., and R. G. Walker, 2006, Deep-water turbidites and submarine fans: SEPM Special Publication, v. 84, p. 397–520.

Privett, K., 2008, Architecture and depositional history of a Neoproterozoic depositional lobe in a passive margin setting, Lower Kaza Group, Windermere Supergroup, southern Canadian Cordillera: BSc Thesis thesis, University of Ottawa, Ottawa, 68 p.

Pyles, D. R., 2007, Architectural Elements in a Ponded Submarine Fan, Ross Sandstone, Ireland, *in* T. H. Nilsen, R. D. Shew, G. S. Steffens, and J. R. J.

Studlick, eds., Atlas of Deep-Water Outcrops., AAPG Studies in Geology Volume 56, p. 206-209.

Pyles, D. R., 2008, Multiscale stratigraphic analysis of a structurally confined submarine fan: Carboniferous Ross Sandstone, Ireland: AAPG Bulletin, v. 92, p. 557-587.

Pyles, D. R., and D. C. Jennette, 2009, Geometry and architectural associations of co-genetic debrite–turbidite beds in basin-margin strata, Carboniferous Ross Sandstone (Ireland): Applications to reservoirs located on the margins of structurally confined submarine fans: Marine and Petroleum Geology, v. 26, p. 1974–1996.

Pyles, D. R., and R. M. Slatt, 2000, A high-frequency sequence stratigraphic framework for shallow through deep-water deposits of the Lewis Shale and Fox Hills Sandstone, Great Divide and Washakie basins, Wyoming: Deep Water Reservoirs of the World, p. 836-861.

Pyles, D. R., and R. M. Slatt, 2007, Stratigraphic evolution of the upper cretaceous Lewis Shale, Southern Wyoming: applications to understanding shelf to base-of-slope changes in stratigraphic architecture of mud-dominated, progradational depositional systems, *in* T. H. Nilsen, R. D. Shew, G. S. Steffens, and J. R. J. Studlick, eds., Atlas of Deepwater Outcrops, AAPG Studies in Geology 56,CD-ROM,, p. 19 p.

Pyles, D. R., J. P. M. Syvitski, and R. M. Slatt, 2011, Defining the concept of stratigraphic grade and applying it to stratal (reservoir) architecture and evolution of the slope-to-basin profile: An outcrop perspective: Marine and Petroleum Geology, v. 28, p. 675-697.

Reid, L., P. Simony, and G. Ross, 2002, Dextral strike-slip faulting in the Cariboo Mountains, British Columbia: a natural example of wrench tectonics in relation to Cordilleran tectonics: Canadian Journal of Earth Sciences, v. 39, p. 953-970.

Roberts, D., A. Siedlecka, and V. G. Olovyanishnikov, 2004, Neoproterozoic, passive-margin, sedimentary systems of the Kanin Peninsula, and northern and central Timan, NW Russia: Geological Society, London, Memoirs, v. 30, p. 5-17.

Rocheleau, J., 2011, Depositional architecture of a near-slope turbidite succession: Upper Kaza Group, Windermerer Supergroup, Castle Creek, British Columbia, Canada: M.Sc. thesis, University of Ottawa, Ottawa, 94 p.

Rogers, J. J., and M. Santosh, 2003, Supercontinents in Earth history: Gondwana Research, v. 6, p. 357-368.

Romans, B. W., A. Fildani, S. M. Hubbard, J. A. Covault, J. C. Fosdick, and S. A. Graham, 2011, Evolution of deep-water stratigraphic architecture, Magallanes Basin, Chile: Marine and Petroleum Geology, v. 28, p. 612-628.

Romans, B. W., S. M. Hubbard, and S. A. Graham, 2009, Stratigraphic evolution of an outcropping continental slope system, Tres Pasos Formation at Cerro Divisadero, Chile: Sedimentology, v. 56, p. 737–764.

Ross, G., R. Parrish, M. Villeneuve, and S. Bowring, 1991, Geophysics and geochronology of the crystalline basement of the Alberta Basin, western Canada: Canadian Journal of Earth Sciences, v. 28, p. 512-522.

Ross, G. M., 1991, Tectonic setting of the Windermere Supergroup revisited: Geology, v. 19, p. 1125-1128.

Ross, G. M., 2003, Slope Carbonate deposition in the Neoproterozoic Windermere turbidite system (Western Canada) significance in basin analysis, Slope Conference, Submarine Slope Systems: processes, products and predictions. Abstracts.: Liverpool, p. 71.

Ross, G. M., and R. W. C. Arnott, 2007, Regional geology of the Windermere Supergroup, southern Canadian Cordillera and stratigraphic setting of the Castle Creek study area, Canada, *in* T. H. Nilsen, R. D. Shew, G. S. Steffens, and J. R. J. Studlick, eds., Atlas of deep-water outcrops, v. 56, AAPG Studies in Geology, CD-ROM, p. 16.

Ross, G. M., J. D. Bloch, and H. R. Krouse, 1995, Neoproterozoic strata of the southern Canada Cordillera and the isotopic evolution of seawater sulfate: Precambriam Research, v. 73, p. 71-99.

Ross, G. M., and S. A. Bowring, 1990, Detrital zircon geochronology of the Windermere Supergroup and the tectonic assembly of the southern Canadian Cordillera: The Journal of Geology, p. 879-893.

Ross, G. M., and C. A. Ferguson, 2003, Geology and structure cross-sections, Eddy, British Columbia. Map 1967A, scale 1:50,000: Geol. Surv. Can.

Ross, G. M., and D. C. Murphy, 1988, Transgressive stratigraphy, anoxia, and regional correlations within the late Precambrian Windermere grit of the southern Canadian Cordillera: Geology, v. 16, p. 139-143.

Rossen, C., and R. T. Beaubouef, 2007, Overview: Examples of Slope to Basin Floor Reservoir Architecture, Brushy, Canyon Formation, Texas, USA, *in* T. H. Nilsen, R. D. Shew, G. S. Steffens, and J. R. J. Studlick, eds., Atlas of Deep-Water Outcrops, v. AAPG Studies in Geology Volume 56, p. 425-428.

Rowe, C. E., 2003, The Cunningham formation: a ramp to platform carbonate in the terminal proterozoic of the Cariboo Mountains, British Columbia: MSc Thesis thesis, University of Calgary, 121 p.

Satur, N., A. Hurst, B. T. Cronin, G. Kelling, and K. Gürbüz, 2000, Sand body geometry in a sand-rich, deep-water clastic system, Miocene Cingöz Formation of southern Turkey: Marine and Petroleum Geology, v. 17, p. 239-252.

Satur, N., G. Kelling, B. T. Cronin, A. Hurst, and K. Gürbüz, 2005, Sedimentary architecture of a canyon-style fairway feeding a deep-water clastic system, the Miocene Cingöz Formation, southern Turkey: significance for reservoir characterisation and modelling: Sedimentary Geology, v. 173, p. 91-119.

Schwarz, E., and R. W. C. Arnott, 2007, Anatomy and evolution of a slope channel-complex set (Neoproterozoic Isaac Formation, Windermere Supergroup, southern Canadian Cordillera); implications for reservoir characterization: Journal of Sedimentary Research, v. 77, p. 89-109.

Sears, J., and R. Price, 2002, The hypothetical Mesoproterozoic supercontinent Columbia: implications of the Siberian-west Laurentian connection: Gondwana Research, v. 5, p. 35-39.

Sears, J. W., and R. A. Price, 2000, New look at the Siberian connection: no SWEAT: Geology, v. 28, p. 423-426.

Sears, J. W., and R. A. Price, 2003, Tightening the Siberian connection to western Laurentia: Geological Society of America Bulletin, v. 115, p. 943-953.

Sevigny, J., R. Parrish, R. Donelick, and E. Ghent, 1990, Northern Monashee Mountains, Omineca crystalline belt, British Columbia: Timing of metamorphism, anatexis, and tectonic denudation: Geology, v. 18, p. 103-106.

Sinclair, H., and M. Tomasso, 2002, Depositional evolution of confined turbidite basins: Journal of Sedimentary Research, v. 72, p. 451-456.

Smith, M., R. Arnott, and G. Ross, 2014a, The Old Fort Point Formation: Redefinition and formal subdivision of a distinctive stratigraphic marker in the Neoproterozoic Windermere Supergroup, southern Canadian Cordillera: Bulletin of Canadian Petroleum Geology, v. 62, p. 1-13.

Smith, M., R. Arnott, and G. Ross, 2014b, Physical and geochemical controls on sedimentation along an ancient continental margin: The deep-marine Old Fort Point Formation (Ediacaran), southern Canadian Cordillera: Bulletin of Canadian Petroleum Geology, v. 62, p. 14-36.

Smith, M. D., 2009, Stratigraphic and Geochemical Evolution of the Old Fort Point Formation, Southern Canadian Cordillera: The deep-marine perspective of Ediacaran Post-Glacial Environmental Change: PhD Thesis thesis, University of Ottawa, Ottawa, 430 p.

Smith, M. D., E. Arnaud, R. Arnott, and G. M. Ross, 2011, The record of Neoproterozoic glaciations in the Windermere Supergroup, southern Canadian Cordillera: Geological Society, London, Memoirs, v. 36, p. 413-424.

Sullivan, M. D., G. N. Jensen, F. J. Goulding, D. C. Jennette, J. L. Foreman, and D. Stern, 2000, Architectural analysis of deepwater outcrops: Implications for exploration and production of the Diana Sub-basin, western Gulf of Mexico, *in* P. Weimer, R. M. Slatt, A. H. Bouma, and D. T. Lawrence, eds., Deepwater reservoirs of the world, GCSSEPM Foundation, p. 1010-1032.

Tankard, A., H. Welsink, P. Aukes, R. Newton, and E. Stettler, 2009, Tectonic evolution of the Cape and Karoo basins of South Africa: Marine and Petroleum Geology, v. 26, p. 1379-1412.

Teitz, M., and E. Mountjoy, 1988, The late Proterozoic Yellowhead carbonate platform west of Jasper, Alberta.

Terlaky, V., 2014, Sedimentology, Stratigraphy, Architecture and Origin of deep-water, basin-floor deposits: Middle and Upper Kaza Group, Windermere Supergroup, B.C., Canada: Ph.D. thesis, University of Ottawa, Ottawa, 213 p.

Terlaky, V., and R. W. C. Arnott, 2014, Matrix-rich and associated matrix-poor sandstones: Avulsion splays in slope and basin-floor strata: Sedimentology, v. 61, p. 1175-1197.

Terlaky, V., J. Rocheleau, and R. W. C. Arnott, 2016, Stratal composition and stratigraphic organization of stratal elements in an ancient deep-marine basin-floor succession, Neoproterozoic Windermere Supergroup, British Columbia, Canada: Sedimentology, v. 63, p. 136-175.

Torres, J., L. Droz, B. Savoye, E. Terentieva, P. Cochonat, N. H. Kenyon, and M. Canals, 1997, Deep-sea avulsion and morphosedimentary evolution of the Rhône Fan Valley and Neofan during the Late Quaternary (north-western Mediterranean Sea): Sedimentology, v. 44, p. 457-477.

Tudor, E. P., 2014, Facies Variability in deep-water channel-to-lobe transition zone: Jurassic Los Molles Formation, Neuquen Basin Argentina: Unpublished thesis, University of Texas, Austin, Texas, 76 p. p.

UNBC, W. C. C. N. a., 2008, Airphoto Castle Creek Glacier.

van Hees, G., 2008, Detailed architecture and sedimentology of sheetlike turbidites sandstones: Middle Kaza Group, Windermere Supergroup, Mt. Quanstrom: BSc Thesis thesis, University of Ottawa, Ottawa, Ontario, 77 p.

Vicente Bravo, J. C., and S. Robles, 1995, Large-scale mesotopographic bedforms from the Albian Black Flysch, northern Spain: characterization, setting and comparison with recent analogues, *in* K. T. Pickering, R. N. Hiscott, N. H. Kenyon, F. R. Lucchi, and R. D. A. Smith, eds., Atlas of deep water environments: Architectural style in turbidite systems: London, Chapman and Hall, p. 216-226.

Wagreich, M., T. Ilickovic, A. Popovic, C. Porpaczy, J. Steinbrener, and G. Wessely, 2011, Biostratigraphy and sedimentology of Campanian deep-water sections (Nierental Formation, Gosau Group) in Lower Austria: Austrian Journal of Earth Sciences, v. 104, p. 108-121.

Wallace, K., 2004, Architecture and Sedimentology of Two Submarine Debris Flow Deposits in the Neoproterozoic Isaac Formation, East-Central British Columbia: B.Sc. Thesis thesis, University of Ottawa, Ottawa, Canada, 133 p.

Wild, R., S. S. Flint, and D. M. Hodgson, 2009, Stratigraphic evolution of the upper slope and shelf edge in the Karoo Basin, South Africa: Basin Research, v. 21, p. 502-527.

Wynn, R. B., 2000, Turbidity current processes and deposits on the Northwest African Margin: Ph.D. thesis, University of Southampton, 281 p.

Wynn, R. B., N. H. Kenyon, D. G. Masson, D. A. V. Stow, and P. P. E. Weaver, 2002, Characterization and recognition of deep-water channel-lobe transition zones: AAPG Bulletin, v. 86, p. 1441–1462.

Chapter 2

DEEP-WATER PROCESSES AND ASSOCIATED DEPOSITS

2.1 Introduction

This chapter provides a general overview of deep-water processes and associated deposits, including historical background and classifications. This will be useful in later chapters where for the first time, a detailed sedimentological and architectural analysis of the rocks between the uppermost Kaza Group and the lowermost Isaac Formation will be presented.

2.2 Deep-water sedimentation: Historical background

Historically, evidence that large quantities of sediment were transported into deep-water environments (>200 m deep, see Fig. 2.1) by various subaqueous gravity-driven flows began to appear in the literature at the end of 19th century. After Dana (1863) and Davidson (1887) reported the existence of submarine canyons, which were steep-sided valleys that extend over hundreds of kilometers off the coast and were incised in the continental slope (Shepard and Dill, 1966), Forel (1885) recognized, for first time, sediment-laden currents moving through these impressive geomorphic features. Later, Milne (1897) reported the breaking of submarine telegraph cables off the coasts of Brazil and Mexico, and Smith (1902) proposed that ocean currents were the principal agent for transporting sand away from the shore and

then through submarine canyons. Davis (1934) and Daly (1936) suggested that strong offshore bottom currents, induced by ocean waves, were most likely responsible for the formation of submarine canyons and, to a certain extent, cable breaking.

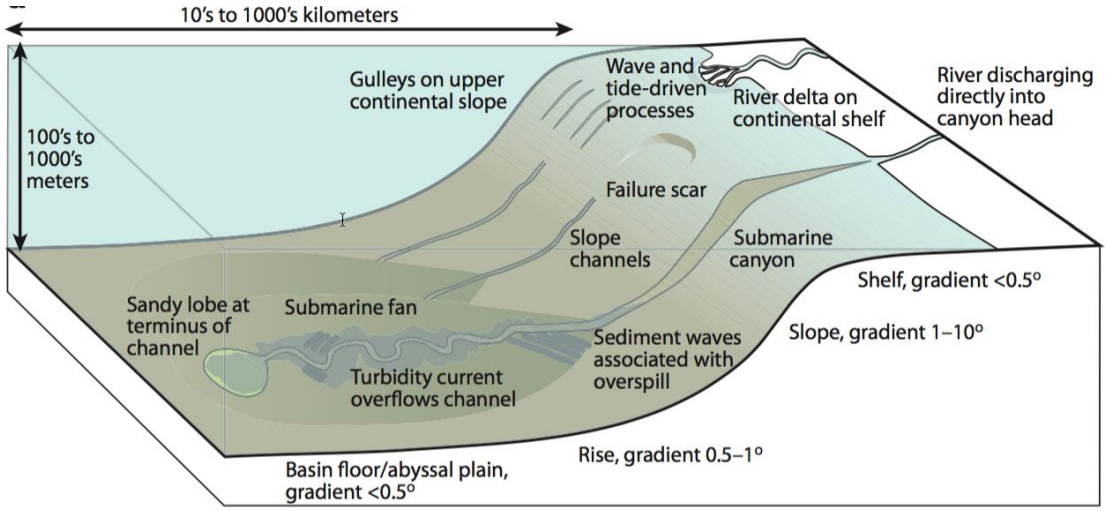

Figure 2.1. Schematic showing the shelf and deep-water physiographic provinces. The shelf is directly linked to the deepest water regions through submarine canyons and slope channels. On the basin floor, which physiographically include part of the continental rise and abyssal plain, submarine fans are formed and represent the largest geomorphic features on the surface of the Earth. Other common features include levees that border the channels, sediment waves, gullies, and lobes (From Meiburg and Kneller, 2010).

Johnson (1938) introduced the term "turbidity current" for turbid flows driven by the weight of their own suspended sediment, and began to hypothesize about the role of submarine turbidity currents in the formation of the canyons (Fig. 2.1). After flowing through the canyons, turbidity currents were considered to flow down the continental slope (Kuenen, 1938; Bramlette and Bradley, 1940), and then out onto the

deep ocean floor where the suspended sediment was eventually deposited and depositional fans were built up (Kuenen, 1951).

Nevertheless, the most direct link between the submarine cable breaks, a submarine turbidity current, and a large earthquake event occurred on the Grand Banks of Newfoundland in 1929 (Heezen and Ewing, 1952). The earthquake resulted in submarine landslides that during movement downslope were transformed into mudflows and then turbidity currents. A series of submarine cables were broken downslope from numerous successive slumps, slides and related turbidity currents (Piper et al., 1999). Based on the timing and distance of the cable breaks, the frontal part of the turbidity currents travelled for at least 4 h (most likely, about 11 h), reached velocities of at least 19 m/s on a gradient of only 0.25^{o}, and formed a sediment deposit of more than 150 km^3 (Piper and Aksu, 1987; Piper, 1988; Hughes Clarke, 1990; Piper et al., 1999). Thus, the 1929 Grand Banks earthquake was an important natural event that demonstrated the magnitude and intriguing nature of what have become known as sediment gravity flows, sparking the avid interest in the scientific community.

Owing to their powerful and destructive nature, direct monitoring of natural submarine gravity-driven flows is challenging (e.g. Khripounoff et al., 2003), and as a consequence much of our current understanding of the mechanistic basis of these flows comes from key laboratory experiments and numerical models (e.g. Middleton and Hampton, 1973; Garcia and Parker, 1993; Middleton, 1993; Parsons and Garcıa, 1998; Mulder and Alexander, 2001; Leclair and Arnott, 2005; Baas et al., 2011;

Sylvester et al., 2011), scientific reasoning based on observations in the modern and ancient deep-marine sedimentary record (e.g. Bouma, 1962; Lowe, 1982; Mutti, 1992; Kneller and McCaffrey, 2003), and high-resolution seismic and oceanographic images (e.g. Wynn et al., 2002; Posamentier and Walker, 2006; Macdonald et al., 2011; McHargue et al., 2011).

In addition to scientific interest in submarine gravity-driven flows and their related deposits, economic interest, in particular the hydrocarbon industry, but also submarine geohazards and tsunami researches, have collectively elevated the attention to study the deep-marine sedimentary realm (Heezen and Ewing, 1952; Prior and Coleman, 1982; Hampton et al., 1996; Todorovska et al., 2002; Trifunac and Todorovska, 2002; Khripounoff et al., 2003; Zakeri et al., 2008).

2.3 Sediment gravity flows and related deposits

Sediment gravity flows are turbid mixtures of sediment particles and fluid that are propelled by gravity. In contrast to rivers, where the fluid moves the particles, sediment gravity flows are produced where gravity acts upon a density difference between a volume of sediment particles suspended in a fluid and the surrounding ambient fluid (typically seawater). These flows (e.g. turbidity currents) are principally responsible for transporting sand and coarser sediment from the continental shelf into deep marine environment, and they build up the world's largest sediment accumulations called submarine fans. Many sandstone-rich submarine fan and channel deposits host economically important hydrocarbon reservoirs, for example in the Gulf of Mexico, offshore Brazil, North Sea, Indonesia, and West Africa (Slatt and

Weimer, 1999; Posamentier and Kolla, 2003; Weimer and Slatt, 2004; Posamentier and Walker, 2006; Weimer and Pettingill, 2007), or mineral resources, including gold deposits in Australia and Canada (Haynes, 1986; Keppie et al., 1986; Ramsay et al., 1998).

A large spectrum of classification schemes and terminologies for sediment gravity flows have been proposed (e.g. Bagnold, 1962; Bouma, 1962; Dott, 1963; Middleton and Hampton, 1973; Lowe, 1979; Lowe, 1982; Massari, 1984; Postma, 1986; Guibaudo, 1992; Mutti, 1992; Middleton, 1993; Kneller, 1995; Kneller and Branney, 1995; Pickering et al., 1995; Shanmugam, 1997, 2000; Mulder and Alexander, 2001; Shanmugam, 2002; Gani, 2004; Haughton et al., 2009; Mutti et al., 2009; Talling et al., 2012); however the most widely used are those that fundamentally combined field description, flow rheology or properties, and sediment-support mechanisms (Fig. 2.2), including Bouma (1962), Lowe (1982), Mutti (1992), and Mulder and Alexander (2001). In this thesis, most deposits related to gravity-driven sediment flows are classified into two major categories: mass-transport deposits and turbidites.

2.3.1 Mass movements and related deposits

The terms mass-transport deposit and mass-transport complex (MTD and MTC, respectively) have been extensively used to describe a seismically-imaged sedimentary body with chaotic internal reflection, which are interpreted to be the deposit of mass movements, such as slides, slumps or debris flows (Weimer, 1989, 1990). More recently, these terms have become more widely accepted, and often

interchangeably used in both seismic (e.g. Posamentier and Kolla, 2003; Moscardelli et al., 2006; Posamentier and Walker, 2006; Bull et al., 2009; Frey-Martínez, 2010) and outcrop-based studies (e.g. Lucente and Pini, 2003; Pickering and Corregidor, 2005; Ogata, 2010; Pini et al., 2012). Shipp et al. (2011) presented one of the most extensive and state-of-the-art compilations of studies related to MTD/MTCs in a deep-water setting. Simplistically, a MTD corresponds to the sedimentary accumulation of a single mass-wasting event, whereas a MTC consists of an amalgamation of two or more MTD.

2.3.1.1 Submarine slide

Submarine slides or landslides are the result from the failure of semi-consolidated to consolidated sediments that move as a coherent mass downslope under gravitational forces. Typically, the slide mass glides over a planar basal shear surface or detachment surface, resulting in little or no internal deformation (Stow, 1986; Shanmugam et al., 1995). Since the shear forces are mostly concentrated along a discrete basal plane, original (i.e. pre-slide) stratal layering, textures and fabrics are preserved but only disrupted by minor faulting and lesser folding.

Submarine slides encompass a wide variety of dimensional scales, ranging from local movement of meter-scale blocks to the displacement of kilometer-scale masses over hundreds of kilometers (e.g., Figs. 2.3A-D; Canals et al., 2004). Numerous triggering factors have been invoked to cause slope failure and include (1) high sedimentation rates, (2) sudden loading, (3) loading and crust flexure, (4) methane hydrate destabilization (5) weak layers or diagenetic fronts, (6)

oversteepening of the slope, (7) erosion at the base of the slope, (8) seismic events and loading due to earthquakes, (9) sea-level changes, (10) human activities affecting the seafloor, amongst many others (see extensive reviews in Locat and Lee, 2002; Canals et al., 2004).

In an idealized model, a submarine landslide can be subdivided longitudinally into different domains or regions that exhibit different stress regimes and related deformation mechanisms (see Figs. 2.3D and 2.4): (1) a headwall or extensional domain including headwall scarps and extensional ridges and blocks; (2) a translational domain comprising the main slide body; and (3) a toe or compressional domain composed of pressure ridges and thrust and fold systems (for characterisation and analysis of external geometry and internal distribution of deformational structures, and key kinematic indicators, see Frey-Martínez et al., 2006; Bull et al., 2009; and references therein).

Slide deposits vary in size with thickness in the order of tens to hundreds of meters, and lengths and widths ranging from few meters to several hundreds of kilometers. Overall, slide complexes are characterized internally by numerous chaotically-arranged sediment masses bounded by basal and internal shear or detachment surfaces along which relative motion has occurred. Based on high-resolution images from modern 3D seismic, the basal shear surface of a slide (or slide complex) is irregular or uneven, often with lineations (Posamentier and Kolla, 2003; Bull et al., 2009).

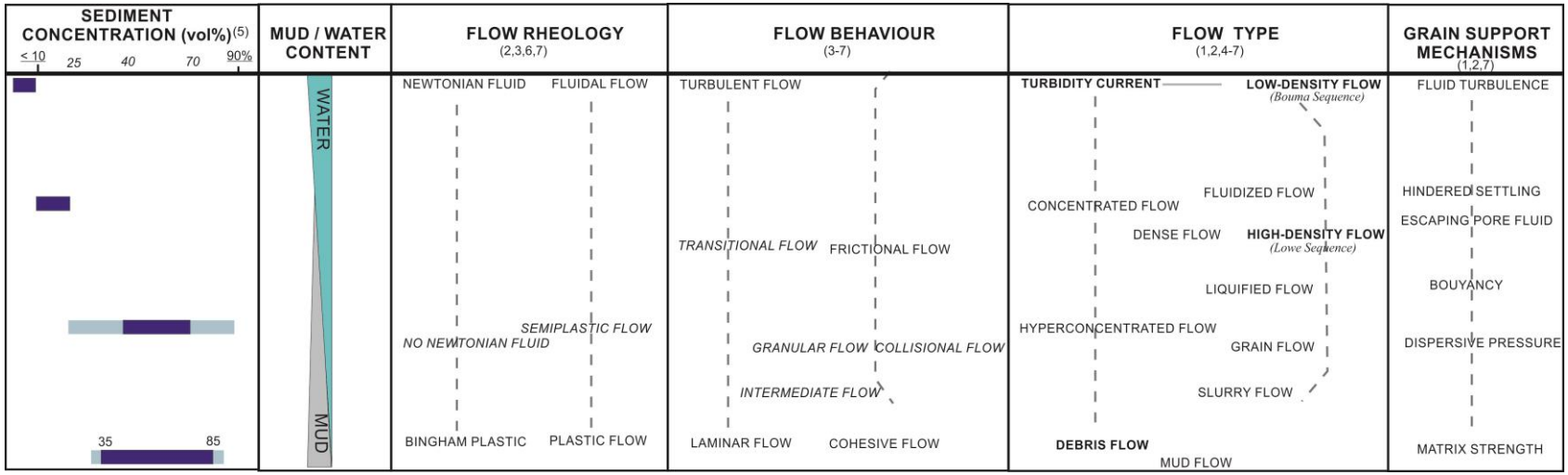

Figure 2.2. General classification of subaqueous sediment gravity or density flows. It shows different classifications of gravity flows according based on flow rheology, flow behaviour and grain-support mechanisms. Based on (1) Middleton and Hampton (1973), (2) Lowe (1982), (3) Shanmugan (2000), (4) Lowe and Guy (2000), (5) Mulder and Alexander (2001), (6) Dagnustpa (2003), and (7) Gani (2004).

In addition to shear surfaces and zones, internal deformational structures within the slide deposits include listric normal faults, recumbent folds, thrusts, boudinage and stacked blocks (Alves et al., 2003; Lucente and Pini, 2003; Alves, 2010; Ogata et al., 2012; Pini et al., 2012; Alves et al., 2014; Alves, 2015).

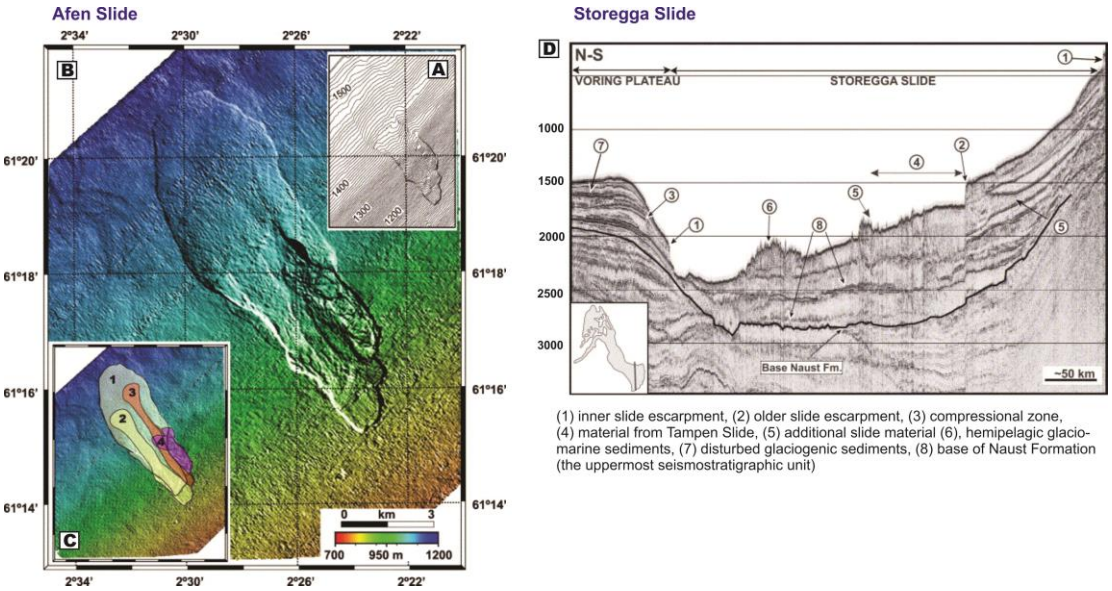

Figure 2.3. Examples of two well-studied submarine slides: Afen and Storegga Slides. (A) Detailed bathymetry and (B,C) Uninterpreted and interpreted acoustic images of the Afen Slide from the Faeroe-Shetland Channel at 87 km NW of the Shetlands Islands, illustrating four failure phases from 1-oldest to 4-youngest (from Bulat, 2003; Wilson et al., 2003; modified by Canals et al., 2004). (D) Seismic reflection profile across the giant Storegga Slide located off Norway, showing internal configuration (Canals et al., 2004; Haflidason et al., 2004). See location on lower left inset. Vertical scale in ms TWTT.

During the last few decades, geophysical studies based on side-scan images, multi-beam morpho-bathymetry, high-resolution 2D and 3D seismic datasets have been able to detail the external geometry, dimensions, and nature of the basal surface of many modern slides (e.g. Trincardi and Normark, 1989; Canals et al., 2004; Frey-

Martínez et al., 2006; Moscardelli et al., 2006; Bull et al., 2009). On the other hand, ancient slide and related mass-transport deposits provide information on the deformational structures within the slide (e.g. Ineson, 1985; Pickering, 1987; Martinsen and Bakken, 1990; Macdonald et al., 1993; Pini, 1999; Lucente and Pini, 2003; Pickering and Corregidor, 2005; Mutti et al., 2006; Callot et al., 2008; Armitage et al., 2009; and Sharman et al., 2015), although commonly the outcrop exposures are limited and widely spaced (with the exception of ancient slides presented by Sharman et al., 2015). In this thesis, two different submarine slide deposits have been described from the Isaac Formation: Isaac slide 1 and Isaac slide 2 (see chapters 3 and 4, respectively, for detailed description and interpretation).

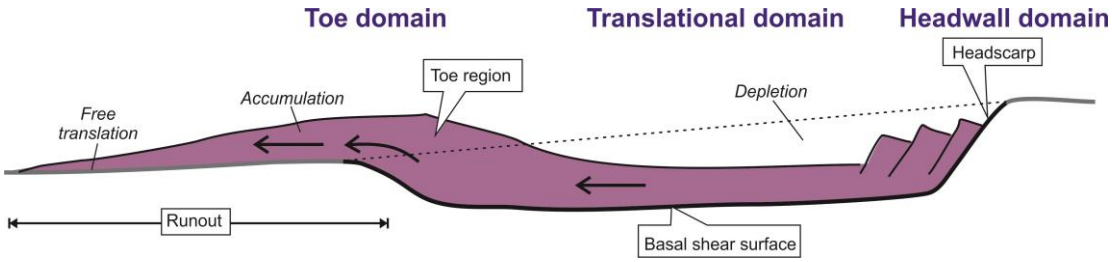

Figure 2.4. Simplified schematic representation of a submarine slide, illustrating the three deformational domains: headwall, translational and toe (Frey-Martínez et al., 2006). This type of submarine slide is a termed frontally-emergent slide because the slide ramps out of the original basal shear surface.

2.3.1.2 Submarine debris flows

Submarine debris flows are downslope-moving, plastic flows of particles suspended in a cohesive matrix consisting typically of mud (silt and clay) and water

(Fig. 2.5). The strength imparted to the sediment dispersion is provided by the electrostatic attraction of adjacent clay mineral particles and the formation of a particulate network. Based on experimental data, clay content as low as 2-5% is considered to be sufficient to induce cohesive behaviors in flows (Middleton and Hampton, 1973; Hampton, 1975). In addition to cohesive strength, buoyancy (Middleton and Hampton, 1973; Hampton, 1979), excess pore pressure (Iverson, 1997; Major and Iverson, 1999), and dispersive pressure (Naylor, 1980) might aid also in particle suspension.

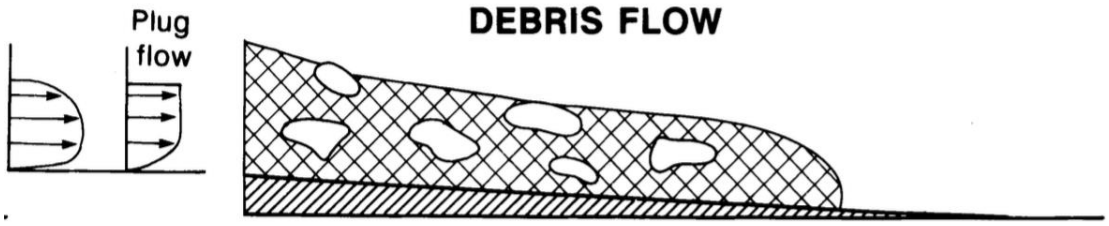

Figure 2.5. Schematic diagram of a debris flows and idealized velocity profiles (Mulder and Alexander, 2001).

In natural settings and laboratory experiments, debris flows are capable of travelling long distances (Takahashi, 1991; Iverson, 1997; Major and Iverson, 1999) – a phenomenon attributed to a trapped basal ("lubricating") layer of water on which the debris flow hydroplanes (Iverson, 1997; Mohrig et al., 1998; Major and Iverson, 1999; Mohrig et al., 1999; Elverhoi et al., 2000; Harbitz et al., 2003; Mohrig and Marr, 2003; Ilstad et al., 2004). Additionally, sustained high internal pore-fluid pressure has also been suggested to help decrease the cohesive strength of sediment-

water mixtures, and thereby enhance debris-flow mobility (Hampton, 1979; Major, 1997; Major and Iverson, 1999; Major, 2000).

Debris flow deposition occurs ‘en masse’ as the entire flow comes to rest. Their deposits, commonly termed debrites, exhibit a diverse range of dimensions, varying from centimeters and up to hundreds of meters in thickness and up to tens of kilometers in width (Fig. 2.6; Posamentier and Kolla, 2003). The base of most debrites is generally flat, but in most cases marked locally by a variety of long grooves or scours (Posamentier and Kolla, 2003; Moscardelli et al., 2006; Posamentier and Walker, 2006) and striations (Gee et al., 2005; Gee et al., 2006; Gee et al., 2007). Classically, debrites consist of pebbly mudstone or matrix-supported conglomerate with a dark coloured poorly-sorted matrix in which sand and coarser grains are dispersed – imparting a “starry night” appearance to the deposit.

Submarine debrites have been widely recognized and described from modern settings (e.g. Shanmugam et al., 1994; Laberg and Vorren, 1995; Gee et al., 2001; Posamentier and Kolla, 2003; Normark et al., 2004; Posamentier and Walker, 2006; Talling et al., 2007) and ancient (e.g. Naylor, 1981; Postma, 1984; Sohn, 2000; Wallace, 2004; Pickering and Corregidor, 2005; Laurin et al., 2007; Burg et al., 2008; Lund, 2008; Strachan, 2008) sedimentary records. Debrites in this study includes predominantly matrix-rich debrites in both the upper Kaza Group (e.g. D1-D5 in chapter 3) and Isaac Formation (e.g. Isaac D1 in chapter 4), and a rare clast-rich debrite (e.g. cD1 in chapter 3). In addition, several calcidebrites (i.e. carbonate-rich debris-flow deposits) are recognized in the first Isaac carbonate (chapter 5).

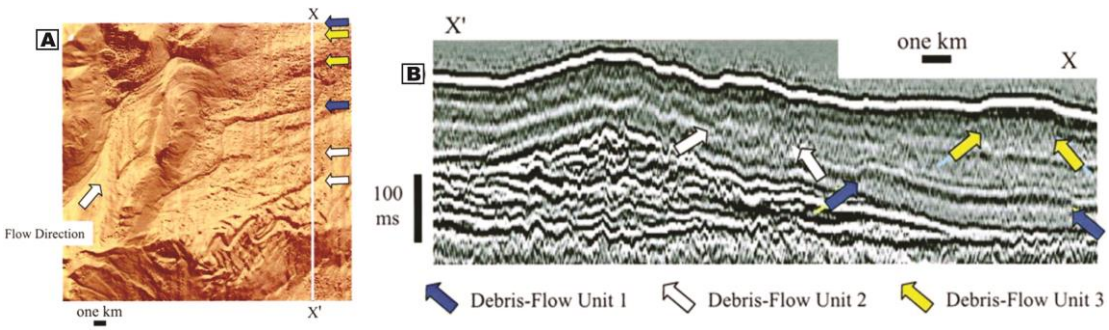

Figure 2.6. Example of submarine debris flows, offshore eastern Borneo, Kalimantan, Indonesia. (A- sea-floor map and B-seismic profile), highlighting three distinct stacked debris-flow units (Posamentier and Kolla, 2003). Note their chaotic seismic reflections that contrast the parallel reflections elsewhere.

2.3.2 Turbidity currents and related deposits

Turbidity currents are gravity-driven sediment flows in which the sediment particles are supported principally by the upward component of fluid turbulence (Middleton and Hampton, 1973; Middleton, 1993). Gravity acts on the density contrast between the turbid plume and ambient fluid, allowing the plume to flow, typically downslope for up to several hundred of kilometers (Mulder and Alexander, 2001). Although rare, observations of natural turbidity currents have been made (see comprehensive review by Talling et al., 2013), for example, in the Bute Inlet (fjord) in British Columbia, Canada (Prior et al., 1987), in Zaire-Congo submarine valley (Khripounoff et al., 2003) and in Monterrey and Hueneme submarine canyons offshore California, USA (Inman et al., 1976; Paull et al., 2002; Xu et al., 2004; Paull et al., 2005; Paull et al., 2013). Results from the Californian examples show that these

turbidity currents are supercritical (i.e. flows with Froude number exceeding unity), and generally start quickly, gain speed as they travel downslope and attain their maximum velocity rapidly (<10 min), and then progressively die out.

Numerous laboratory experiments and numerical computer models have attempted to simulate the sediment transport dynamics in turbidity currents (e.g. Bagnold, 1962; Middleton, 1967; Garcia and Parker, 1991; Middleton, 1993; Zeng and Lowe, 1997a, b; Kneller and Buckee, 2000; Baas and Best, 2002; Alves et al., 2003; Leclair and Arnott, 2005; Huang et al., 2008; Hu and Cao, 2009; Sequeiros et al., 2009; Islam and Imran, 2010; Parsons et al., 2010; Sequeiros et al., 2010; Xu, 2010; Tilston et al., 2015). Since sediment-driven experimental turbidity currents have short life span and have implicated serious measurement challenges, many experiments turbidity currents are carried out using saline solutions (e.g. Garcia and Parker, 1993; Sequeiros et al., 2009; Parsons et al., 2010; Sequeiros et al., 2010). Poorly understood, however, is how analogous the turbidity currents generated in laboratory experiments are to natural sediment-driven flows, and as a result interpretations supported by these experimental data should be considered carefully. Nevertheless, after measuring and normalizing velocity profiles of natural turbidity currents from the canyons of offshore California, Xu (2010) suggested that laboratory experiments whose spatial and time scale are two to three orders of magnitude smaller, represented field data fairly well.

In general, turbidity currents can be subdivided longitudinally into three parts: head or front, body and tail (Fig. 2.7). The head has an overhanging nose that

corresponds to the height of the streamwise velocity maximum, and is formed in response to frictional forces along the lower and upper boundaries of the flow. The head area is typically thicker and moves slower than the rest of the flow (Komar, 1972), allowing the faster moving body to continuously feed sediment into the head and maintain the density contrast of the current.

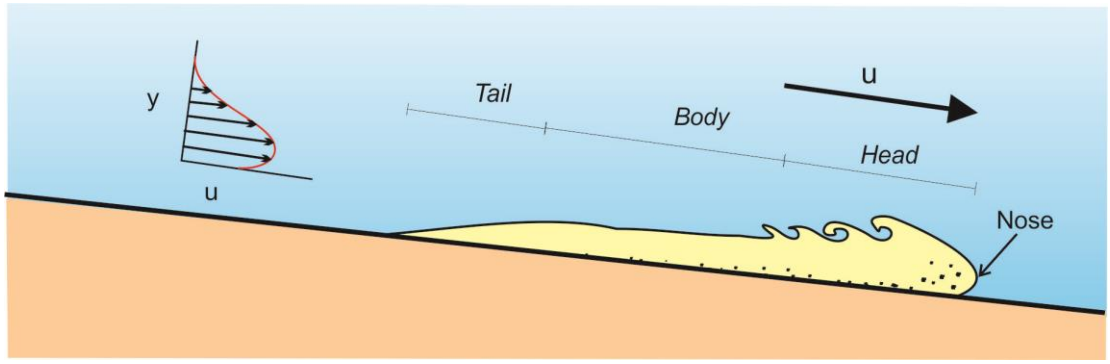

Figure 2.7. Downslope development of a moving turbidity current. The flow head accelerates downslope, commonly eroding the substrate in the process. These sediments become incorporated into the flow, which in turn in turn increase the density contrast between the flow and the ambient fluid. Behind the head is the thinner but faster flowing body, which continuous feeds sediment to the head. The tail is a dilute suspension that trails behind the main flow.

Turbidites are the deposits of turbidity currents and range in thickness from a few millimeters to several meters, and extend for a few meters to hundreds of kilometers. Based on his seminal work from the Eocene-Oligocene Annot Sandstone in France, Bouma (1962) was the first to describe the idealized vertical succession of that what now become termed a classical or Bouma turbidite. An ideal Bouma sequence comprises five divisions or intervals – the T_a to T_e divisions (Fig. 2.8A). The T_a division consists of massive to graded, structureless, coarse- to medium-

grained sandstone that overlies a sharp, commonly erosional basal surface ornamented with local flue and tool marks. Deposition of the T_a division is generally interpreted to be the result of direct sediment suspension fallout with negligible bedload transport (Arnott and Hand, 1989). The overlying T_b division consists of planar-laminated medium to fine sandstone, and indicates reduced rates of sediment fallout and more prolonged bed-load transport. The T_c division comprises small-scale ripple cross-laminated, fine- to very fine-grained sandstone, formed by migrating current ripples. The T_d division is composed of interlaminated siltstone-mudstone couplets formed by suspension fallout interspersed with episodes of traction transport. The T_e division includes homogenous, structureless mudstone, deposited by suspension settling.

Following the pioneering work of Bouma (1962), Lowe (1976) noted that most of the sand of the deep-marine sedimentary record consists not of the classical turbidites, but instead simple graded sandstone. Based on theoretical evaluation and field observation of thick, structureless sandstone and conglomerate beds in flysch sequences, Lowe argued that these strata could not have been deposited by a simple turbulent suspension, but instead were deposited by flows, termed density-modified grain flows, in which dispersive pressure played a major role in particle support. Later, Lowe (1979) expanded the mechanisms for particle support to include, in addition to turbulence and dispersive pressure, hindered settling, upward escaping fluid, buoyancy, and matrix strength (Lowe, 1979; Lowe, 1982; Postma et al., 1988; for detailed definition and terminology, see Middleton, 1993; and Mulder and

Alexander, 2001), which would allow these dense, frictional flows to suspend coarser grained sediment, including coarse sand to gravel (Fig. 2.9). Lowe then proposed that these deposits be termed high-density turbidity currents –a term originally proposed by Kuenen (1951).

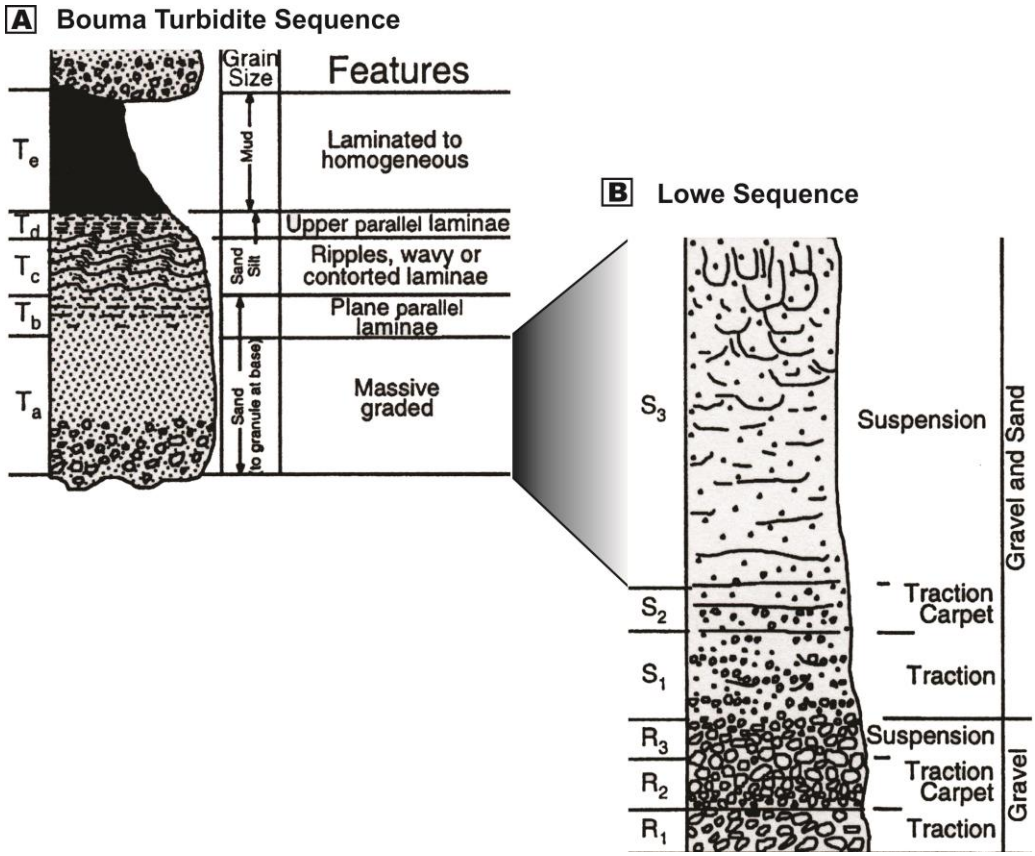

Figure 2.8. Classical sequences utilized to describe and interpret low- and high-density flow deposits. (A) A complete Bouma turbidite sequence (Bouma, 1962) interpreted to the deposit of a low-density turbidity current; and (B) Lowe Sequence deposited from a high-density turbidity currents (Lowe, 1982).

Following the work of Lowe (1982, 1979, 1976), it is now accepted that turbidity currents can be classified as low- and high-concentration, or similar, but

more commonly, low- and high- density turbidity flows. Low-density turbidity flows are taken to be flows with sediment concentration less than the Bagnold limit of 9% volume sediment concentration (Mulder and Alexander, 2001), and in which the sediment is suspended largely or wholly supported by fluid turbulence. In contrast, flows with sediment concentrations from 10 to 25 vol% (concentrated) and higher (hyperconcentrated) correspond to high-density turbidity currents.

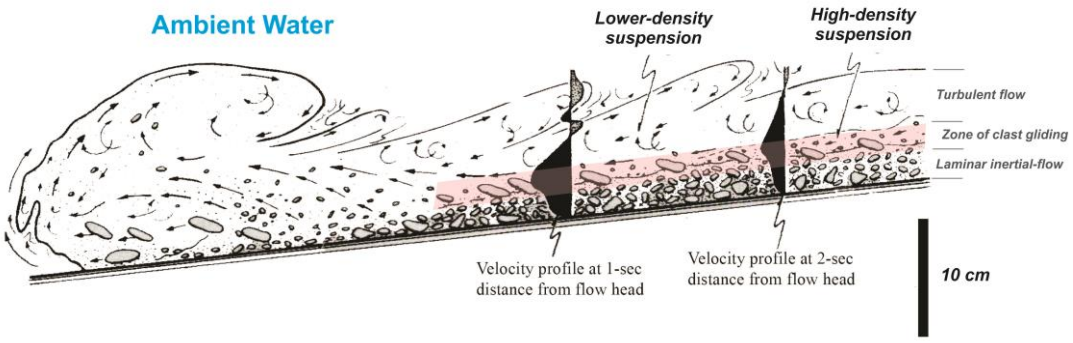

Figure 2.9. Schematic illustration of an experimental high-density turbidity current (from Postma et al., 1988). The current is flowing down a 25° slope and head velocity is 108 cm/sec. High particle concentration in the lower part of the flow results in extensive grain-to-grain interaction (dispersive pressure) and an upward flux of pore fluid –owing to the high sediment concentration, flow conditions are interpreted to be laminar. Lower sediment concentration in the upper part of the flow results in turbulent flow condition and extensive mixing with the ambient fluid. Note that mudstone intraclasts become concentrated along the rheological interface (highlighted pinkish zone) between the lower and upper parts of the flow.

Lowe (1982) interpreted that classical turbidites to be the deposits of low-density turbidity currents, and the T_a division should be disregarded as being deposited by such currents. He instead proposed a new classification scheme to describe the deposits of coarse-grained sandy and gravelly, high-density turbidity

currents (Fig. 2.9). The classification scheme, now is called a Lowe Sequence (Fig. 2.8), consists of six idealized units, which stratigraphically upward are R_1 to R_3 and S_1 to S_3. R_1 is made up of the coarsest conglomerate at the base of the bed and exhibits parallel- or cross-lamination, indicating traction deposition. R_2 consists of inversely-graded conglomerate, representing deposition from traction carpets, where grain-to-grain collision (dispersive pressure) is the dominant support mechanism. R_3 represents suspension deposition of gravel. As flow conditions progressively wane, gravel deposition becomes replaced by sand deposition. S_1 corresponds to bed load transport of coarse sand and finer gravel and generally exhibits planar lamination and cross-stratification. S_2 involves traction carpet sedimentation of coarse sand to finer gravel. S_3, which is the equivalent to the Ta Bouma division, comprises massive to graded beds with occasional dish structures and pipes, and represents rapid suspension deposition of fine to coarse sand.

Over the few past decades, turbidites have been exhaustively studied in both modern and ancient systems (e.g. Bouma, 1962; Lowe, 1982; Allen, 1991; Pickering et al., 1995; Pirmez et al., 1997; Wynn, 2000; Posamentier and Kolla, 2003; Sylvester and Lowe, 2004; Gervais et al., 2006; Navarro, 2006; Posamentier and Walker, 2006; Arnott, 2007b; Arnott, 2007a; Deptuck et al., 2007; Navarro et al., 2007; Schwarz and Arnott, 2007; Sylvester, 2007; Jegou et al., 2008; Prélat et al., 2009; Romans et al., 2009; Khan and Arnott, 2011; Prélat and Hodgson, 2013; Pyles et al., 2014; Smith et al., 2014; Hofstra et al., 2015). In this work, turbidites have been documented from a wide variety of deep-water settings across the slope and basin-floor (see chapters 3

to 5). Notably, calciturbidites (i.e. carbonate-rich turbidites that exhibit complete or incomplete Bouma or Lowe sequences) are documented in the first Isaac carbonate (chapter 5).

2.3.3 Flow transformation from slide to debris flow to turbidity current

Once initiated, a submarine slide may begin to change or transform (see Fig. 2.10), which in part is controlled by a combination of the mechanical attributes of the sliding mass and intensity of the forcing mechanism(s) (Martinsen, 1994; Shanmugam et al., 1995; Mulder and Alexander, 2001). During movement, if internal deformation increases significantly, the slide may evolve into a slump, in which the mass now moves along an upward-concave basal detachment surface coincident with the development of a wide range of internal deformational structures with evident contortion and rotation. Additionally, the ingestion and mixing of ambient water into the mass, significantly promotes internal disruption and disaggregation, eventually leading to complete disaggregation and the development of a debris flow (Stow, 1986). With continued movement, shear and resultant destabilization of the boundaries of the debris flow results in the progressive, albeit slow, mixing and ingestion of ambient fluid. Eventually, mixing of ambient fluid and consequent expansion of the flow overcomes (internal) cohesive strength causing particles to now become independently suspended in a now fluidal particle-fluid mixture. At this point, fluid turbulence has become the primary sediment supporting mechanism, and accordingly the debris flow becomes a turbidity current.

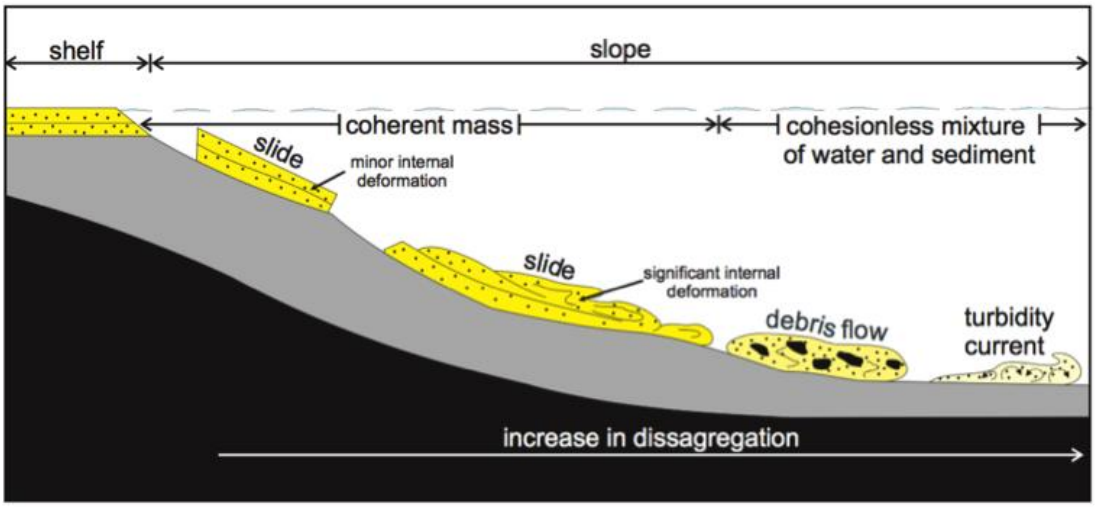

Figure 2.10. Schematic diagram illustrating the typical downslope evolution or transformation of sediment gravity flows, from a slide to debris flow and finally a turbidity current. (From Shanmugam et al., 1994; Shanmugam et al., 1995; modified by Khan, 2012).

2.4 References

Allen, J. R. L., 1991, The Bouma division A and the possible duration of turbidity currents: Journal of Sedimentary Petrology, v. 61, p. 291-295.

Alves, T. M., 2010, 3D Seismic examples of differential compaction in mass-transport deposits and their effect on post-failure strata: Marine Geology, v. 271, p. 212-224.

Alves, T. M., 2015, Submarine slide blocks and associated soft-sediment deformation in deep-water basins: A review: Marine and Petroleum Geology, v. 67, p. 262-285.

Alves, T. M., R. L. Gawthorpe, D. W. Hunt, and J. H. Monteiro, 2003, Cenozoic tectono-sedimentary evolution of the western Iberian margin: Marine Geology, v. 195, p. 75-108.

Alves, T. M., M. Strasser, and G. F. Moore, 2014, Erosional features as indicators of thrust fault activity (Nankai Trough, Japan): Marine Geology, v. 356, p. 5-18.

Armitage, D. A., B. W. Romans, J. A. Covault, and S. A. Graham, 2009, The influence of mass-transport-deposit surface topography on the evolution of turbidite architecture: the Sierra Contreras, Tres Pasos formation (Cretaceous), southern Chile: Journal of Sedimentary Research, v. 79, p. 287-301.

Arnott, R. W. C., 2007a, Stratal architecture and origin of lateral accretion deposits (LADs) and conterminuous inner-bank levee deposits in a base-of-slope sinuous channel, lower Isaac Formation (Neoproterozoic), East-Central British Columbia, Canada: Marine and Petroleum Geology, v. 24, p. 515-528.

Arnott, R. W. C., 2007b, Stratigraphic architecture and depositional processes of a proximal crevasse splay and genetically related, sinuous channel fill, Isaac Formation, British Columbia, Canada, *in* T. H. Nilsen, R. D. Shew, G. S. Steffens, and J. R. J. Studlick, eds., Atlas of deep-water outcrops, AAPG Studies in Geology 56, p. 12 p.

Arnott, R. W. C., and B. M. Hand, 1989, Bedforms, primary structures, and grain fabric in the presence of suspended sediment rain: Journal of Sedimentary Petrology, v. 59, p. 1062-1069.

Baas, J. H., and J. L. Best, 2002, Turbulence modulation in clay-rich sediment-laden flows and some implications for sediment deposition: Journal of Sedimentary Research, v. 72, p. 336-340.

Baas, J. H., J. L. Best, and J. Peakall, 2011, Depositional processes, bedform development and hybrid bed formation in rapidly decelerated cohesive (mud–sand) sediment flows: Sedimentology, v. 58, p. 1953-1987.

Bagnold, R. A., 1962, Auto-suspension of transported sediment: turbidity currents: Proc. Roy. Soc. London, Ser. A, v. 265, p. 315-319.

Bouma, A. H., 1962, Sedimentology of some Flysch Deposits. A graphic approach to facies interpretation: Amsterdam, Elsevier.

Bramlette, N. M., and W. H. Bradley, 1940, Geology and biology of North Atlantic deepsea cores, part I., US Geol. Surv. Prof. Pap. 196A, p. 1-34.

Bulat, J., 2003, Imaging the Afen Slide From Commercial 3D Seismic — Methodology and Comparisons With High-Resolution Data, *in* J. Locat, J. Mienert, and L. Boisvert, eds., Submarine Mass Movements and Their

Consequences: Advances in Natural and Technological Hazards Research, v. 19, Springer Netherlands, p. 205-213.

Bull, S., J. Cartwright, and M. Huuse, 2009, A review of kinematic indicators from mass-transport complexes using 3D seismic data: Marine and Petroleum Geology, v. 26, p. 1132-1151.

Burg, J. P., D. Bernoulli, J. Smit, A. Dolati, and A. Bahroudi, 2008, A giant catastrophic mud- and- debris flow in the Miocene Makran: Terra Nova, v. 20, p. 188-193.

Callot, P., T. Sempere, F. Odonne, and E. Robert, 2008, Giant submarine collapse of a carbonate platform at the Turonian–Coniacian transition: the Ayabacas Formation, southern Peru: Basin Research, v. 20, p. 333-357.

Canals, M., G. Lastras, R. Urgeles, J. L. Casamor, J. Mienert, A. Cattaneo, M. De Batist, H. Haflidason, Y. Imbo, J. S. Laberg, J. Locat, D. Long, O. Longva, D. G. Masson, N. Sultan, F. Trincardi, and P. Bryn, 2004, Slope failure dynamics and impacts from seafloor and shallow sub-seafloor geophysical data: case studies from the COSTA project: Marine Geology, v. 213, p. 9-72.

Daly, R. A., 1936, Origin of submarine canyons.: Am. J. Sci., v. 5, p. 401-420.

Dana, J. D., 1863, Manual of Geology: Philadelphia, 798 p.

Davidson, G., 1887, Submarine valley of on the Pacific Coast of the United States: Calif. Acad. Sci. Bull., v. 2, p. 265-268.

Davis, W. M., 1934, Submarine mock valleys: Geogr. Rev., v. 24, p. 297-308.

Deptuck, M. E., D. J. W. Piper, B. Savoye, and A. Gervais, 2007, Dimensions and architecture of late Pleistocene submarine lobes off the northern margin of East Corsica: Sedimentology, p. 1-32.

Dott, R. H. J., 1963, Dynamics of subaqueous gravity depositional processes: AAPG Bulletin, v. 47.

Elverhoi, A., C. B. Harbitz, P. Dimakis, D. Mohrig, and G. P. JeffMarr, 2000, On the dynamics of subaqueous debris flows: Oceanography, v. 13, p. 109.

Forel, F. A., 1885, Les ravins sous-lacustres des fleuves glaciaires.: C. R. Acad. Sci., v. 101, p. 725-728.

Frey-Martínez, J., 2010, 3D Seismic Interpretation of Mass Transport Deposits: Implications for Basin Analysis and Geohazard Evaluation, *in* D. Mosher, R. C. Shipp, L. Moscardelli, J. Chaytor, C. P. Baxter, H. Lee, and R. Urgeles, eds., Submarine Mass Movements and Their Consequences: Advances in Natural and Technological Hazards Research, v. 28, Springer Netherlands, p. 553-568.

Frey-Martínez, J., J. Cartwright, and D. James, 2006, Frontally confined versus frontally emergent submarine landslides: A 3D seismic characterisation: Marine and Petroleum Geology, v. 23, p. 585-604.

Gani, M. R., 2004, From Turbid to Lucid: A Straightforward Approach to Sediment Gravity Flows and Their Deposits.: The Sedimentary Record, SEPM, v. 2, p. 4-8.

Garcia, M., and G. Parker, 1991, Entrainment of bed sediment into suspension: Journal of Hydraulic Engineering, v. 117, p. 414-435.

Garcia, M., and G. Parker, 1993, Experiments on the entrainment of sediment into suspension by a dense bottom current: Journal of Geophysical Research: Oceans (1978–2012), v. 98, p. 4793-4807.

Gee, M. J., D. G. Masson, A. B. Watts, and N. C. Mitchell, 2001, Passage of debris flows and turbidity currents through a topographic constriction: seafloor erosion and deflection of flow pathways: Sedimentology, v. 48, p. 1389-1409.

Gee, M. J. R., R. L. Gawthorpe, and J. S. Friedmann, 2005, Giant striations at the base of a submarine landslide: Marine Geology, v. 214, p. 287-294.

Gee, M. J. R., R. L. Gawthorpe, and S. J. Friedmann, 2006, Triggering and Evolution of a Giant Submarine Landslide, Offshore Angola, Revealed by 3D Seismic Stratigraphy and Geomorphology: Journal of Sedimentary Research, v. 76, p. 9-19.

Gee, M. J. R., H. S. Uy, J. Warren, C. K. Morley, and J. J. Lambiase, 2007, The Brunei slide: A giant submarine landslide on the North West Borneo Margin revealed by 3D seismic data: Marine Geology, v. 246, p. 9-23.

Gervais, A., B. Savoye, T. Mulder, and E. Gonthier, 2006, Sandy modern turbidite lobes: A new insight from high resolution seismic data: Marine and Petroleum Geology, v. 23, p. 485-502.

Guibaudo, G., 1992, Subaqueous sediment gravity flow deposits: practical criteria for their field description and classification. Sedimentology: Sedimentology, v. 39, p. 423-454.

Haflidason, H., H. P. Sejrup, A. Nygård, J. Mienert, P. Bryn, R. Lien, C. F. Forsberg, K. Berg, and D. Masson, 2004, The Storegga Slide: architecture, geometry and slide development: Marine Geology, v. 213, p. 201-234.

Hampton, M., 1975, Competence of fine-grained debris flows: Journal of Sedimentary Research, v. 45, p. 834-844.

Hampton, M. A., 1979, Buoyancy in debris flows: Journal of Sedimentary Research, v. 49, p. 753-758.

Hampton, M. A., H. J. Lee, and J. Locat, 1996, Submarine landslides: Reviews of geophysics, v. 34, p. 33-59.

Harbitz, C. B., G. Parker, A. Elverhøi, J. G. Marr, D. Mohrig, and P. A. Harff, 2003, Hydroplaning of subaqueous debris flows and glide blocks: Analytical solutions and discussion: Journal of Geophysical Research: Solid Earth (1978–2012), v. 108.

Haughton, P., C. Davis, W. McCaffrey, and S. Barker, 2009, Hybrid sediment gravity flow deposits–classification, origin and significance: Marine and Petroleum Geology, v. 26, p. 1900-1918.

Haynes, S. J., 1986, Geology and chemistry of turbidite-hosted gold deposits, greenschist facies, eastern Nova Scotia: Turbidite-hosted gold deposits. Edited by JD Keppie, RW Boyle, and SJ Haynes. Geologial Association of Canada, Special Paper, v. 32, p. 161-178.

Heezen, B. C., and M. Ewing, 1952, Turbidity currents and submarine slumps and the 1929 Grand Banks earthquake: Am. J. Sci., v. 250, p. 849-873.

Hofstra, M., D. M. Hodgson, J. Peakall, and S. S. Flint, 2015, Giant scour-fills in ancient channel-lobe transition zones: Formative processes and depositional architecture: Sedimentary Geology, v. 329, p. 98-114.

Hu, P., and Z. Cao, 2009, Fully coupled mathematical modeling of turbidity currents over erodible bed: Advances in Water Resources, v. 32, p. 1-15.

Huang, H., J. Imran, and C. Pirmez, 2008, Numerical study of turbidity currents with sudden-release and sustained-inflow mechanisms: Journal of Hydraulic Engineering, v. 134, p. 1199-1209.

Hughes Clarke, J. E., 1990, Late stage slope failure in the wake of the 1929 Grand Banks earthquake. : Geo-Marine Letters, v. 10, p. 69-80.

Ilstad, T., F. V. De Blasio, A. Elverhøi, C. B. Harbitz, L. Engvik, O. Longva, and J. G. Marr, 2004, On the frontal dynamics and morphology of submarine debris flows: Marine Geology, v. 213, p. 481-497.

Ineson, J., 1985, Submarine glide blocks from the Lower Cretaceous of the Antarctic Peninsula: Sedimentology, v. 32, p. 659-670.

Inman, D. L., C. E. Nordstrom, and R. E. Flick, 1976, Currents in submarine canyons: an air-sea-land interaction: Annual Review of Fluid Mechanics, v. 8, p. 275-310.

Islam, M. A., and J. Imran, 2010, Vertical structure of continuous release saline and turbidity currents: Journal of Geophysical Research: Oceans (1978–2012), v. 115.

Iverson, R. M., 1997, The physics of debris flows: Reviews of geophysics, v. 35, p. 245-296.

Jegou, I., B. Savoye, C. Pirmez, and L. Droz, 2008, Channel-mouth lobe complex of the recent Amazon Fan: The missing piece: Marine Geology, v. 252, p. 62–77.

Johnson, D., 1938, The origin of submarine canyons.: Journal of Geomorphology, v. 1.

Keppie, J. D., R. W. Boyle, and S. J. Haynes, 1986, Turbidite-hosted gold deposits, v. 32, St. John's, Nfld., Canada: Geological Association of Canada.

Khan, Z., 2012, Origin and architecture of deep-water levee deposits: Insight from the ancient rock record and experiments: PhD Thesis thesis, University of Ottawa, Ottawa, Ontario, 300 p.

Khan, Z. A., and R. W. C. Arnott, 2011, Stratal attributes and evolution of asymmetric inner- and outer-bend levee deposits associated with an ancient deep-water channel-levee complex within the Isaac Formation, southern Canada: Marine and Petroleum Geology, v. 28, p. 824-842.

Khripounoff, A., A. Vangriesheim, N. Babonneau, P. Crassous, B. Dennielou, and B. Savoye, 2003, Direct observation of intense turbidity current activity in the Zaire submarine valley at 4000 m water depth: Marine Geology, v. 194, p. 151-158.

Kneller, B., 1995, Beyond the turbidite paradigm: physical models for deposition of turbidites and their implications for reservoir prediction: Special Publication Geological Society of London, v. 94, p. 31-31.

Kneller, B., and C. Buckee, 2000, The structure and fluid mechanics of turbidity currents: a review of some recent studies and their geological implications: Sedimentology, v. 47, p. 62-94.

Kneller, B. C., and M. J. Branney, 1995, Sustained high-density turbidity currents and the deposition of thick massive sands: Sedimentology, v. 42, p. 607-616.

Kneller, B. C., and W. D. McCaffrey, 2003, The interpretation of vertical sequences in turbidite beds: the influence of longitudinal flow structure: Journal of Sedimentary Research, v. 73, p. 706-713.

Komar, P. D., 1972, Relative significance of head and body spill from a channelized turbidity current: Geological Society of America Bulletin, v. 83, p. 1151-1156.

Kuenen, P. H., 1938, Density currents in connection with the problem of submarine canyons: Geol. Mag., v. 75, p. 241-249.

Kuenen, P. H., 1951, Properties of turbidity currents of high density, *in* L. J. Hough, ed., Turbidity currents and the transportation of coarse sediments to deep water v. 2, SEPM Spec. Publ. 2, p. 14-33.

Laberg, J., and T. Vorren, 1995, Late Weichselian submarine debris flow deposits on the Bear Island Trough mouth fan: Marine Geology, v. 127, p. 45-72.

Laurin, J., K. Wallace, R. W. C. Arnott, and E. Schwarz, 2007, Stratigraphic anatomy and depositional history of a mass transport complex (MTC), Isaac Formation,

Windermere Supergroup, Canada, *in* T. H. Nilsen, R. D. Shew, G. S. Steffens, and J. R. J. Studlick, eds., Atlas of deep-water outcrops, AAPG Studies in Geology 56, p. 119-122.

Leclair, S., and R. W. C. Arnott, 2005, Parallel lamination formed by high-density turbidity currents: Journal of Sedimentary Research, v. 75, p. 1-5.

Locat, J., and H. J. Lee, 2002, Submarine landslides: advances and challenges: Canadian Geotechnical Journal, v. 39, p. 193-212.

Lowe, D. R., 1976, Grain flow and grain flow deposits: Journal of Sedimentary Research, v. 46, p. 188-199.

Lowe, D. R., 1979, Sediment gravity flows: their classification and some problems of application to natural flows and deposits, v. SEPM Special Publication No 27, p. 75-82.

Lowe, D. R., 1982, Sediment gravity flows: II. Depositional models with special reference to the deposits of high-density turbidity currents: Journal of Sedimentary Petrology, v. 52, p. 279-297.

Lucente, C. C., and G. A. Pini, 2003, Anatomy and emplacement mechanism of a large submarine slide within a Miocene foredeep in the northern Apennines, Italy: A field perspective: American Journal of Science, v. 303, p. 565-602.

Lund, K., 2008, Geometry of the Neoproterozoic and Paleozoic rift margin of western Laurentia: Implications for mineral deposit settings: Geosphere, v. 4, p. 429-444.

Macdonald, D. I., A. C. Moncrieff, and P. J. Butterworth, 1993, Giant slide deposits from a Mesozoic fore-arc basin, Alexander Island, Antarctica: Geology, v. 21, p. 1047-1050.

Macdonald, H., R. B. Wynn, V. A. I. Huvenne, J. Peakall, D. G. Masson, P. P. E. Weaver, and S. D. McPhail, 2011, New insights into the morphology, fill, and remarkable longevity (>0.2 m.y.) of modern deep-water erosional scours along the northeast Atlantic margin: Geosphere, v. 7, p. 845-867.

Major, J. J., 1997, Depositional processes in large-scale debris-flow experiments: The Journal of Geology, v. 105, p. 345-366.

Major, J. J., 2000, Gravity-driven consolidation of granular slurries--implications for debris-flow deposition and deposit characteristics: Journal of Sedimentary Research, v. 70, p. 64-83.

Major, J. J., and R. M. Iverson, 1999, Debris-flow deposition: effects of pore-fluid pressure and friction concentrated at flow margins: Geological Society of America Bulletin, v. 111, p. 1424-1434.

Martinsen, O. J., 1994, Mass movements., *in* A. Maltman, ed., The Geological Deformation of Sediments.: London, Chapman & Hall, p. 127-165.

Martinsen, O. J., and B. Bakken, 1990, Extensional and compressional zones in slumps and slides in the Namurian of County Clare, Ireland: Journal of the Geological Society, v. 147, p. 153-164.

Massari, F., 1984, Resedimented conglomerates of a Miocene fandelta complex, Southern Alps, Italy, *in* E. H. Koster, and R. J. Steel, eds., Sedimentology of Gravels and Conglomerates, v. 10, Can. Soc. Petrol. Geol. Mem., p. 259-278.

McHargue, T., M. J. Pyrcz, M. D. Sullivan, J. D. Clark, A. Fildani, B. W. Romans, J. A. Covault, M. Levy, H. W. Posamentier, and N. J. Drinkwater, 2011, Architecture of turbidite channel systems on the continental slope: Patterns and predictions: Marine and Petroleum Geology, v. 28, p. 728-743.

Meiburg, E., and B. Kneller, 2010, Turbidity currents and their deposits: Annual Review of Fluid Mechanics, v. 42, p. 135-156.

Middleton, G. V., 1967, Experiments on density and turbidity currents: III. Deposition of sediment: Canadian Journal of Earth Sciences, v. 4, p. 475-505.

Middleton, G. V., 1993, Sediment deposition from turbidity currents.: Annu. Rev. Earth Planet. Sci., v. 21, p. 89-114.

Middleton, G. V., and M. A. Hampton, 1973, Sediment gravity flows: mechanics of flow and deposition, *in* G. V. Middleton, and A. H. Bouma, eds., Turbidites and Deep Water Sedimentation. : Los Angeles, Short Course Notes, No 1, SEPM (Pacific Section), p. 1-38.

Milne, J., 1897, Sub-Oceanic Changes: Geogr. J., v. 10, p. 259-285.

Mohrig, D., C. Ellis, G. Parker, K. X. Whipple, and M. Hondzo, 1998, Hydroplaning of subaqueous debris flows: Geological Society of America Bulletin, v. 110, p. 387-394.

Mohrig, D., A. Elverhøi, and G. Parker, 1999, Experiments on the relative mobility of muddy subaqueous and subaerial debris flows, and their capacity to remobilize antecedent deposits: Marine Geology, v. 154, p. 117-129.

Mohrig, D., and J. G. Marr, 2003, Constraining the efficiency of turbidity current generation from submarine debris flows and slides using laboratory experiments: Marine and Petroleum Geology, v. 20, p. 883-899.

Moscardelli, L., L. Wood, and P. Mann, 2006, Mass-transport complexes and associated processes in the offshore area of Trinidad and Venezuela: AAPG Bulletin, v. 90, p. 1059-1088.

Mulder, T., and J. Alexander, 2001, The physical character of subaqueous density flows and their deposits: Sedimentology, v. 48, p. 269-299.

Mutti, E., 1992, Turbidite sandstones: Milan: Agip, Istituto di geologia, Università di Parma, 275 p.

Mutti, E., D. Bernoulli, F. R. Lucchi, and R. Tinterri, 2009, Turbidites and turbidity cur rents from Alpine ‘flysch’to the exploration of continental margins: Sedimentology, v. 56, p. 267-318.

Mutti, E., M. Carminatti, J. L. P. Moreira, and A. A. Grassi, 2006, Chaotic deposits: examples from the Brazilian offshore and from outcrop studies in the Spanish Pyrenees and Northern Apennines, Italy., AAPG. Annual meeting, Houston, 9–12 April.

Navarro, L., 2006, Depositional Architecture and Evolution of deep-water base-of-slope and slope channel complexes in a passive-margin setting: Isaac Formation, Windermere Supergroup (Neoproterozoic), Southern Canadian Cordillera: M.Sc.Thesis thesis, University of Ottawa, Ottawa, 272 p.

Navarro, L., Z. Khan, and R. W. C. Arnott, 2007, Depositional architecture and evolution of a deep-marine channel-levee complex: Isaac Formation (Windermere Supergroup), Southern Canadian Cordillera., *in* T. H. Nilsen, R. D. Shew, G. S. Steffens, and J. R. J. Studlik, eds., Atlas of Deep-water

Outcrops., v. CD-ROM: Tulsa, AAPG Studies in Geology 56, CD-ROM, p. 22.

Naylor, M. A., 1980, The origin of inverse grading in muddy debris flow deposits--a review: Journal of Sedimentary Research, v. 50, p. 1111-1116.

Naylor, M. A., 1981, Debris flow (olistostromes) and slumping on a distal passive continental margin: The Palombini limestone–shale sequence of the northern Apennines: Sedimentology, v. 28, p. 837-852.

Normark, W. R., M. McGann, and R. Sliter, 2004, Age of Palos Verdes submarine debris avalanche, southern California: Marine Geology, v. 203, p. 247-259.

Ogata, K., 2010, Mass Transport Complexes in Structurally contreolled basins: The Epiligurian Specchio Unit (Northern Appeninnes, Italy): Ph.D. Thesis thesis, University of Parma, Parma, 476 p.

Ogata, K., R. Tinterri, G. A. Pini, and E. Mutti, 2012, The Specchio Unit (Northern Apennines, Italy): An Ancient Mass Transport Complex Originated from Near-Coastal Areas in an Intra-Slope Setting, *in* Y. Yamada, K. Kawamura, K. Ikehara, Y. Ogawa, R. Urgeles, D. Mosher, J. Chaytor, and M. Strasser, eds., Submarine mass movements and their consequences: 5th International Symposium, Springer, p. 595-605.

Parsons, D. R., J. Peakall, A. E. Aksu, R. D. Flood, R. N. Hiscott, Ş. Beşiktepe, and D. Mouland, 2010, Gravity-driven flow in a submarine channel bend: direct field evidence of helical flow reversal: Geology, v. 38, p. 1063-1066.

Parsons, J. D., and M. H. Garcıa, 1998, Similarity of gravity current fronts: Physics of Fluids, v. 10, p. 3209-3213.

Paull, C., W. Ussler, H. Greene, R. Keaten, P. Mitts, and J. Barry, 2002, Caught in the act: the 20 December 2001 gravity flow event in Monterey Canyon: Geo-Marine Letters, v. 22, p. 227-232.

Paull, C. K., D. W. Caress, E. Lundsten, R. Gwiazda, K. Anderson, M. McGann, J. Conrad, B. Edwards, and E. J. Sumner, 2013, Anatomy of the La Jolla Submarine Canyon system; offshore southern California: Marine Geology, v. 335, p. 16-34.

Paull, C. K., P. Mitts, W. Ussler, R. Keaten, and H. G. Greene, 2005, Trail of sand in upper Monterey Canyon: offshore California: Geological Society of America Bulletin, v. 117, p. 1134-1145.

Pickering, K. T., 1987, Wet-sediment deformation in the Upper Ordovician Point Leamington Formation: an active thrust-imbricate system during sedimentation, Notre Dame Bay, north-central Newfoundland: Geological Society, London, Special Publications, v. 29, p. 213-239.

Pickering, K. T., J. D. Clark, R. D. A. Smith, R. N. Hiscott, F. R. Lucchi, and N. H. Kenyon, 1995, Architectural element analysis of turbidite systems, and selected topical problems for sand-prone deep-water systems, Atlas of deep water environments, Springer, p. 1-10.

Pickering, K. T., and J. Corregidor, 2005, Mass-transport Complexes (MTCs) and tectonic control on basin-floor submarine fans, Middle Eocene, South Spanish Pyrenees: Journal of Sedimentary Research, v. 75, p. 761-783.

Pini, G. A., 1999, Tectonosomes and olistostromes in the Argille Scagliose of the Northern Apennines, Italy, v. 335, Geological Society of America, 73 p.

Pini, G. A., K. Ogata, A. Camerlenghi, A. Festa, C. C. Lucente, and G. Codegone, 2012, Sedimentary Mélanges and Fossil Mass- Transport Complexes: A Key for Better Understanding Submarine Mass Movements?, *in* Y. Yamada, K. Kawamura, K. Ikehara, Y. Ogawa, R. Urgeles, D. Mosher, J. Chaytor, and M. Strasser, eds., Submarine mass movements and their consequences: 5th International Symposium, v. Advances in Natural and Technological Hazards Research 31, p. 585-594.

Piper, D. J. W., 1988, Glaciomarine sediments on the continental slope off eastern Canada: Geosci. Can., v. 15, p. 23-28.

Piper, D. J. W., and A. E. Aksu, 1987, The source and origin of the 1929 Grand Banks turbidity current inferred from sediment budgets: Geo-Marine Letters, v. 7, p. 177-182.

Piper, D. J. W., P. Cochonat, and M. L. Morrison, 1999, The sequence of events around the epicentre of the 1929 Grand Banks earthquake: initiation of debris flows and turbidity current inferred from sidescan sonar: Sedimentology, v. 46, p. 79-97.

Pirmez, C., R. N. Hiscott, and J. J. D. Kronen, 1997, Sandy turbidite successions at the base of channel-levee systems of the Amazon Fan revealed by FMS logs and cores: Unraveling the facies architecture of large submarine fans, *in* R. D. Flood, D. J. W. Piper, A. Klaus, and L. C. Peterson, eds., Proceedings of the Ocean Drilling Program, Scientific Results, v. 155, p. 7-33.

Posamentier, H. W., and V. Kolla, 2003, Seismic geomorphology and stratigraphy of depositional elements in deep-water settings: Journal of Sedimentary Research, v. 73, p. 367–388.

Posamentier, H. W., and R. G. Walker, 2006, Deep-water turbidites and submarine fans: SEPM Special Publication, v. 84, p. 397–520.

Postma, G., 1984, Mass-flow conglomerates in a submarine canyon: Abrioja fan-delta, Pliocene, southeast Spain, *in* E. H. Koster, and R. J. Steel, eds., Sedimentology of Gravels and Conglomerates, v. Memoir 10, Canadian Society of Petroleum Geologists, p. 237-258.

Postma, G., 1986, Classification for sediment gravity-flow deposits based on flow conditions during sedimentation: Geology, v. 14, p. 291-294.

Postma, G., W. Nemec, and K. L. Kleinspehn, 1988, Large floating clasts in turbidites: a mechanism for their emplacement: Sedimentary geology, v. 58, p. 47-61.

Prélat, A., and D. M. Hodgson, 2013, The full range of turbidite bed thickness patterns in submarine lobes: controls and implications: Journal of the Geological Society, v. 170, p. 209-214.

Prélat, A., D. M. Hodgson, and S. S. Flint, 2009, Evolution, architecture and hierarchy of distributary deep-water deposits: a high-resolution outcrop investigation from the Permian Karoo Basin, South Africa: Sedimentology, v. 56, p. 2132-2154.

Prior, D. B., B. D. Bornhold, W. J. Wiseman, and D. R. Lowe, 1987, Turbidity current activity in a British Columbia fjord: Science, v. 237, p. 1330-1333.

Prior, D. B., and J. M. Coleman, 1982, Active slides and flows in underconsolidated marine sediments on the slopes of the Mississippi delta, Marine slides and other mass movements, Springer, p. 21-49.

Pyles, D. R., L. J. Strachan, and D. C. Jennette, 2014, Lateral juxtapositions of channel and lobe elements in distributive submarine fans: Three-dimensional outcrop study of the Ross Sandstone and geometric model: Geosphere, v. 10, p. 1104-1122.

Ramsay, W. R. H., F. P. Bierlein, D. C. Arne, and A. H. M. VandenBerg, 1998, Turbidite-hosted gold deposits of Central Victoria, Australia: their regional setting, mineralising styles, and some genetic constraints: Ore Geology Reviews, v. 13, p. 131-151.

Romans, B. W., S. M. Hubbard, and S. A. Graham, 2009, Stratigraphic evolution of an outcropping continental slope system, Tres Pasos Formation at Cerro Divisadero, Chile: Sedimentology, v. 56, p. 737–764.

Schwarz, E., and R. W. C. Arnott, 2007, Anatomy and evolution of a slope channel-complex set (Neoproterozoic Isaac Formation, Windermere Supergroup, southern Canadian Cordillera); implications for reservoir characterization: Journal of Sedimentary Research, v. 77, p. 89-109.

Sequeiros, O. E., H. Naruse, N. Endo, M. H. Garcia, and G. Parker, 2009, Experimental study on self-accelerating turbidity currents: Journal of Geophysical Research: Oceans (1978–2012), v. 114.

Sequeiros, O. E., B. Spinewine, R. T. Beaubouef, T. Sun, M. H. García, and G. Parker, 2010, Characteristics of velocity and excess density profiles of saline underflows and turbidity currents flowing over a mobile bed: Journal of Hydraulic Engineering, v. 136, p. 412-433.

Shanmugam, G., 1997, The Bouma sequence and the turbidite mind set.: Earth-Science Reviews, v. 42, p. 201-229.

Shanmugam, G., 2000, 50 years of the turbidite paradigm (1950s–1990s): deep-water processes and facies models: Marine and Petroleum Geology, v. 17, p. 285-342.

Shanmugam, G., 2002, Ten turbidite myths: Earth-Science Reviews, v. 58, p. 311-341.

Shanmugam, G., R. B. Bloch, S. M. Mitchell, G. W. Beamish, R. J. Hodgkinson, J. E. Damuth, T. Straume, S. E. Syvertsen, and K. E. Shields, 1995, Basin-floor

fans in the North Sea: sequence stratigraphic models vs. sedimentary facies: AAPG bulletin, v. 79, p. 477-511.

Shanmugam, G., L. R. Lehtonen, T. Straume, S. E. Syvertsen, R. J. Hodgkinson, and M. Skibeli, 1994, Slump and debris-flow dominated upper slope facies in the Cretaceous of the Norwegian and northern North seas (61-67 N): implications for sand distribution: AAPG bulletin, v. 78, p. 910-937.

Sharman, G. R., S. A. Graham, L. U. Masalimova, L. E. Shumaker, and P. R. King, 2015, Spatial patterns of deformation and paleoslope estimation within the marginal and central portions of a basin-floor mass-transport deposit, Taranaki Basin, New Zealand: Geosphere, v. 11, p. 266-306.

Shepard, F. P., and R. F. Dill, 1966, Submarine canyons and other sea valleys: Chicago, Rand McNally, 381 p.

Shipp, R. C., P. Weimer, and H. W. Posamentier, 2011, Mass-transport deposits in deepwater settings, v. 96, SEPM Soc for Sed Geology, 527 p.

Slatt, R. M., and P. Weimer, 1999, Turbidite systems. Part 2: Subseismic-scale reservoir characteristics: The Leading Edge, p. 562-567.

Smith, M., R. Arnott, and G. Ross, 2014, Physical and geochemical controls on sedimentation along an ancient continental margin: The deep-marine Old Fort Point Formation (Ediacaran), southern Canadian Cordillera: Bulletin of Canadian Petroleum Geology, v. 62, p. 14-36.

Smith, W. S. T., 1902, The Submarine Valleys of the California Coast.: Science, v. 15, p. 670-672.

Sohn, Y. K., 2000, Depositional processes of submarine debris flows in the Miocene fan deltas, Pohang Basin, SE Korea with special reference to flow transformation: Journal of Sedimentary Research, v. 70, p. 491-503.

Stow, D. A. V., 1986, Deep clastic seas, *in* H. G. Reading, ed., Sedimentary Environments and Facies: Oxford, Blackwell Scientific Publications, p. 399-444.

Strachan, L. J., 2008, Flow transformations in slumps: a case study from the Waitemata Basin, New Zealand: Sedimentology, v. 55, p. 1311-1332.

Sylvester, Z., 2007, Turbidite bed thickness distributions: methods and pitfalls of analysis and modelling: Sedimentology, v. 54, p. 847-870.

Sylvester, Z., and D. R. Lowe, 2004, Textural trends in turbidites and slurry beds from the Oligocene flysch of the East Carpathians, Romania: Sedimentology, v. 51, p. 945-972.

Sylvester, Z., C. Pirmez, and A. Cantelli, 2011, A model of submarine channel-levee evolution based on channel trajectories: Implications for stratigraphic architecture: Marine and Petroleum Geology, v. 28, p. 716-727.

Takahashi, T., 1991, Debris flow, Balkema.

Talling, P., R. Wynn, D. Masson, M. Frenz, B. Cronin, R. Schiebel, A. Akhmetzhanov, S. Dallmeier-Tiessen, S. Benetti, and P. Weaver, 2007, Onset of submarine debris flow deposition far from original giant landslide: Nature, v. 450, p. 541-544.

Talling, P. J., D. G. Masson, E. J. Sumnet, and G. Malgesini, 2012, Subaqueous sediment density flows: Depositional processes and deposit types: Sedimentology, v. 59, p. 1937-2003.

Talling, P. J., C. K. Paull, and D. J. W. Piper, 2013, How are subaqueous sediment density flows triggered, what is their internal structure and how does it evolve? Direct observations from monitoring of active flows: Earth-Science Reviews, v. 125, p. 244-287.

Tilston, M., R. Arnott, C. Rennie, and B. Long, 2015, The influence of grain size on the velocity and sediment concentration profiles and depositional record of turbidity currents: Geology, v. 43, p. 839-842.

Todorovska, M., A. Hayir, and M. Trifunac, 2002, A note on tsunami amplitudes above submarine slides and slumps: Soil Dynamics and Earthquake Engineering, v. 22, p. 129-141.

Trifunac, M. D., and M. I. Todorovska, 2002, A note on differences in tsunami source parameters for submarine slides and earthquakes: Soil Dynamics and Earthquake Engineering, v. 22, p. 143-155.

Trincardi, F., and W. R. Normark, 1989, Pleistocene Suvero slide, Paola basin, southern Italy: Marine and Petroleum Geology, v. 6, p. 324-335.

Wallace, K., 2004, Architecture and Sedimentology of Two Submarine Debris Flow Deposits in the Neoproterozoic Isaac Formation, East-Central British Columbia: B.Sc. Thesis thesis, University of Ottawa, Ottawa, Canada, 133 p.

Weimer, P., 1989, Sequence stratigraphy of the Mississippi Fan (Plio-Pleistocene), Gulf of Mexico: Geo-Marine Letters, v. 9, p. 185-272.

Weimer, P., 1990, Sequence Stratigraphy, Facies Geometries, and Depositional History of the Mississippi Fan, Gulf of Mexico (1): AAPG bulletin, v. 74, p. 425-453.

Weimer, P., and H. W. Pettingill, 2007, Deep-water exploration and production: a global overview, *in* T. Nilsen, R. D. Shew, G. S. Steffens, and J. Studlick, eds., Atlas of deep-water outcrops of the world. AAPG Studies in Geology No. 56, CD-ROM, p. 29 p.

Weimer, P., and R. M. Slatt, 2004, Petroleum systems of deepwater settings.

Wilson, C., D. Long, and J. Bulat, 2003, The Afen Slide—A Multistaged Slope Failure in the Faroeshetland Channel, Submarine Mass Movements and Their Consequences, Springer, p. 317-324.

Wynn, R. B., 2000, Turbidity current processes and deposits on the Northwest African Margin: Ph.D. thesis, University of Southampton, 281 p.

Wynn, R. B., N. H. Kenyon, D. G. Masson, D. A. V. Stow, and P. P. E. Weaver, 2002, Characterization and recognition of deep-water channel-lobe transition zones: AAPG Bulletin, v. 86, p. 1441–1462.

Xu, J., 2010, Normalized velocity profiles of field-measured turbidity currents: Geology, v. 38, p. 563-566.

Xu, J., M. Noble, and L. K. Rosenfeld, 2004, In-situ measurements of velocity structure within turbidity currents: Geophysical Research Letters, v. 31.

Zakeri, A., K. Høeg, and F. Nadim, 2008, Submarine debris flow impact on pipelines—Part I: Experimental investigation: Coastal engineering, v. 55, p. 1209-1218.

Zeng, J., and D. R. Lowe, 1997a, Numerical simulation of turbidity current flow and sedimentation: I. Theory: Sedimentology, v. 44, p. 67-84.

Zeng, J., and D. R. Lowe, 1997b, Numerical simulation of turbidity current flow and sedimentation: II. Results and geological applications: Sedimentology, v. 44, p. 85-104.

Chapter 3

STRATIGRAPHIC ARCHITECTURE OF AN ANCIENT DEEP-MARINE CHANNEL-LOBE TRANSITION ZONE, KAZA-ISAAC TRANSITION AND LOWER ISAAC FORMATION, WINDERMERE TURBIDITE SYSTEM, CARIBOO MOUNTAINS, B.C.

3.1 Introduction

The slope-basin transition typically includes the channel-lobe transition zone or CLTZ (Normark et al., 1979; Mutti and Normark, 1987, 1991), which is the area within any turbidite system that separates well-defined channels from basinward lobes (Fig. 1). Even though, the quality and resolution of modern sea-floor and seismic images from many modern CLTZs have greatly improved during the last decades (e.g. O'Connell et al., 1991; Kenyon and Millington, 1995; Kenyon et al., 1995; Palanques et al., 1995; Morris et al., 1998; Wynn et al., 2002; Bonnel et al., 2005; Duarte et al., 2010; Macdonald et al., 2011), they only provide limited insights into the different constituents across these transition zones. Thus, little is still known about the lithofacies distribution, stratigraphic architecture and evolution within the zone.

It is important to note the term ‘transition zone’ has been variously used in the literature and might be subject to misinterpretation. Some authors have described the CLTZ within upper slope deposits (Romans et al., 2009), or have referred to a

transition zone within basin-margin deposits (Pyles and Jennette, 2009). Similarly, the term has been used to different scales of observations and interpretations. At the large-scale, it represents the region between submarine canyon or channel and genetically-related fan (Mutti and Normark, 1987; Wynn et al., 2002), but at the small-scale, it has been considered to signify the connection area between a discrete channel and its corresponding downstream lobe element (e.g. Gordon, 2014; Pyles et al., 2014). In this study, the deep-water transition zone is considered at the large-scale, which is defined along the continental rise, located between the continental slope and the abyssal plain.

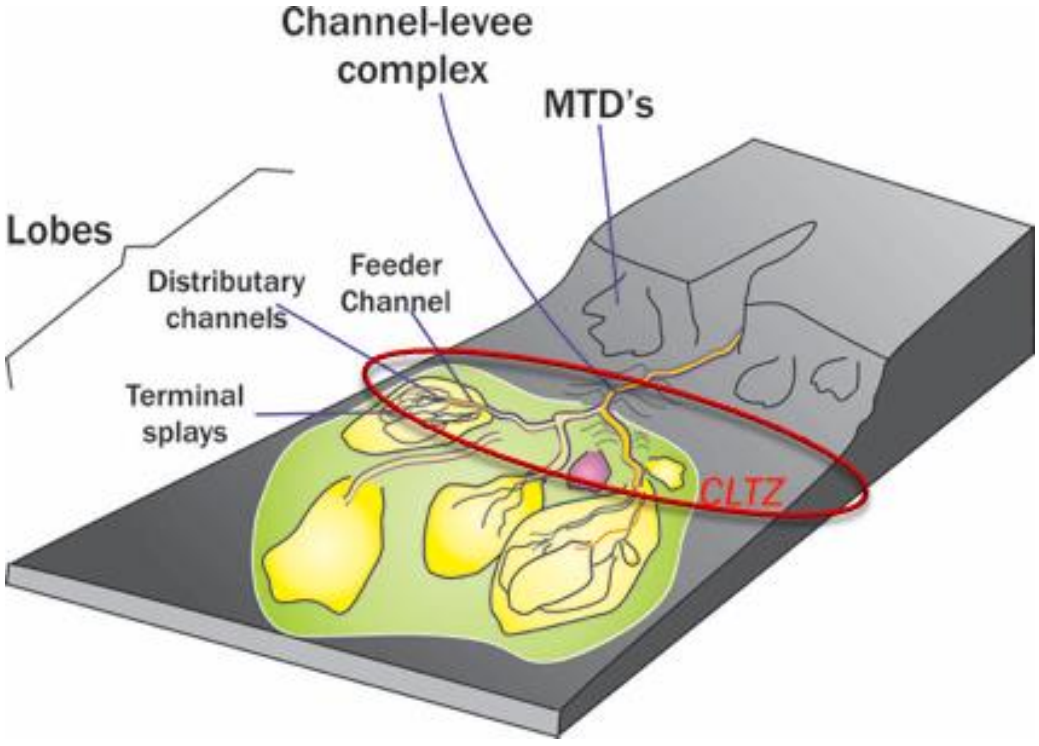

Figure 3.1. Schematic representation of the transition between slope and basin floor settings, showing the channel-lobe transition zone or CLTZ

In many places where the slope-basin floor transition has been reported from the ancient sedimentary record (for instance, Magallanes basin, Chile; Karoo basin, South Africa; Namurian basin, Ireland; Kongsijord Fm., Norway; Cignoz Fm., Turkey; Ainsa basin, Spain; Neuquén basin, Argentina; among many others, for references see Chapter 1), the exposures are scattered and stratigraphic context can be equivocal. Therefore, the identification of the CLTZ in outcrops is challenging (Mutti and Normark, 1991; Wynn et al., 2002). Among deep-water ancient analogues of CLTZ (e.g. Pickering, 1983; Vicente Bravo and Robles, 1991, 1995; Drinkwater and Pickering, 2001; Cornamusini, 2004; Kostrewa, 2004; Thomas, 2011; Gordon, 2014; Pyles et al., 2014; Tudor, 2014; Van der Merwe et al., 2014; Pemberton et al., 2015; this study), the glacially-polished exposures of the Neoproterozoic Windermere Supergroup in the southern Canadian Cordillera certainly provide a unique opportunity to describe and evaluate (at small- and large-scale) the distribution and geometry of major deep-water elements.

Two main stratigraphic units comprise much of the most deep-water strata in the Windermere basin: the Upper Kaza Group (UKG) and the overlying Isaac Formation (IF, lower Cariboo Group), which respectively are interpreted as sheet-like, Dm-thick-sandstone-dominated, basin-floor submarine fan deposits and Dm-thick channelized sandstone bounded by mudstone-dominated toe-to-slope and slope deposits (Ross and Arnott, 2007). This study features the first published detailed stratigraphic architectural analysis along the interval between the KIT and overlying LIF. It aims to describe the vertical and lateral distribution of the constituent architectural elements formed in submarine channel-lobe systems, to establish

depositional styles and architectural patterns that indicate the development or not of the CLTZ, and to determine the links to possible (allo- and/or autocyclic) sedimentological drivers.

3.2 Kaza-Isaac transition interval (KIT) and overlying lowermost Isaac Formation (LIF)

At the Castle Creek study area, an 800 m thick, sandstone-dominated, basin-floor succession of uppermost Kaza Group is conformably overlain by a 1300 m thick, mudstone-dominated slope strata of Isaac Formation, lowermost Cariboo Group (Fig. 3.2, for a stratigraphic review of this study area, see Ross and Arnott, 2007). The contact between these two main lithostratigraphic units is sharp to gradational and regionally mappable, and is recognized by marked increasing in mudstone proportion, appearance of distinctive blue-grey mudstone and calcareous sandstone, and the occurrence of the first or lower Isaac carbonate member (Campbell, 1973; Campbell et al., 1973; Ross and Ferguson, 2003; Ross and Arnott, 2007). Campbell et al. (1973) mentioned that the contact between these two units across the southern Cariboo Mountains is difficult to define in places, and suggested to be generally placed it at the top of the highest coarse-grained 'grit' beds; but here the Kaza-Isaac boundary is distinct at the base of the highest, coarsest and more resistant strata (containing pebble conglomerate).

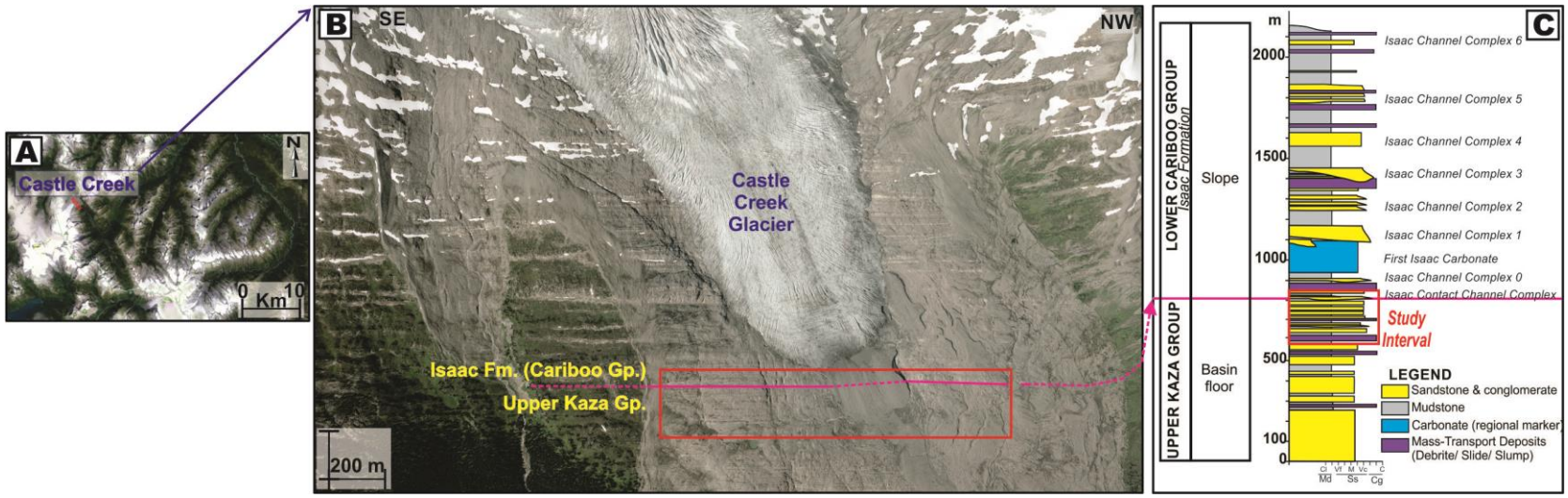

Figure 3.2. Kaza-Isaac transition (KIT) within the Cariboo Mountain regions. (A-B) Location of the KIT in the Castle Creek, principal study area. Red rectangles indicate position of the KIT, which includes the contact between the Upper Kaza Group and overlying Isaac Formation, Lower Cariboo Group. (A- satellite image from Google Earth, 2014; B-aerial photo from Western Canadian Cryospheric Network and UNBC, 2008). (C) Composite stratigraphic column for the Castle Creek area, highlighting the KIT study interval (Modified from Ross and Arnott, 2007). Labels to the right of the column in the Isaac Formation refer to informal names of channel complexes and a regional carbonate marker (see chapter 5).

The studied interval between the Kaza-Isaac transition, or simply KIT, and overlying lowermost Isaac Formation (LIF) is well-exposed and shows exceptional vertical and lateral continuity. This interval is overlain by a thick slope succession of mass-transport complex named Isaac MTC 1 and overlying deposits including Isaac channel complex 0 (see chapter 4), which are then extensively overlain by the First Isaac Carbonate (see chapter 5).

3.3 Data and Methods

This study is mainly focused on a section including the KIT and the LIF at the Castle Creek study area. It is about 290 m thick and can be traced laterally for >1.2 km (Fig. 3.2), in which a detailed analysis of the lithological distribution and internal architecture of turbidite elements was conducted. Additionally, a secondary section (approximately 415 m thick and up to 450 m wide) at the Mount Quanstrom area, situated 20 km east of Castle Creek, was also measured (see Appendix G for aerial photomosaics, logs and correlation panels). Similar stratal elements and lithofacies distribution have been recognized in both areas.

The composition and mineral assemblage of the rocks in the Cariboo Mountains suggested they were subjected to very-low to low grade metamorphic conditions (Murphy and Rees, 1983), in which rocks from Mount Quanstrom have undergone slightly higher metamorphic grade than those in Castle Creek. Nevertheless, in both areas, the outcrop quality is outstanding due to the preservation of primary structures and textures in both coarse- and fine-grained facies. Locally, however, strata are buried by moraine and outwash plain.

The dataset comprises 127 measured vertical sections documenting lithology, grain size, thickness, primary and secondary sedimentary structures and, where possible, paleocurrent direction. In total, 4127 m of stratigraphy at Castle Creek area was measured bed by bed. Based on the almost vertical strata, lithological units, architectural elements, key bounding surfaces and beds are easily walked out along the outcrop and mapped on high-resolution aerial photographs. Location of logs and paleocurrent measurements collected from cross-beds are provided in Fig 3.4A, and also in Appendix B. In addition to field-based data, a total of 55 petrographic and 14 X-ray fluorescence samples were collected, prepared and evaluated (see Appendices C and D).

3.4 Lithofacies

In the study area, nine lithofacies are identified based on grain size, primary physical sedimentary structures, bed thickness, and degree of bed amalgamation. Table 1 summarizes the principal attributes of each lithofacies and its interpreted depositional process, and Figure 3.3 shows representative photos of these facies. The two-dimensionality of the outcrop made difficult to obtain accurate paleocurrent measurements, yet some paleocurrent directions were measured from cross-beds and suggest a general paleoflow toward the Northeast.

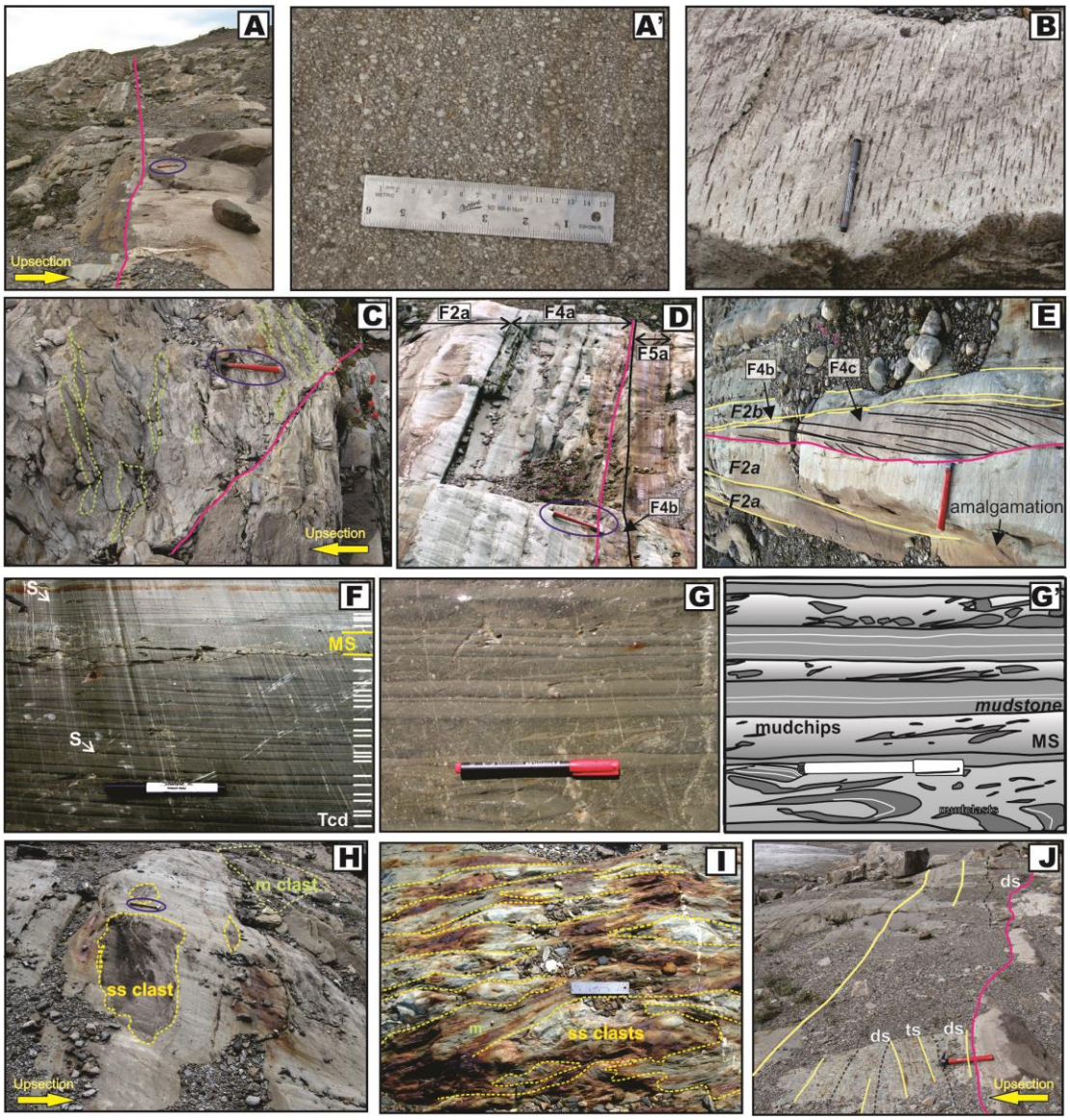

Figure 3.3. Representative lithofacies in the KIT. Erosional surfaces are delineated by bold fuchsia lines. Bedding is highlighted by light yellow lines. (A) Thick-bedded, amalgamated normal-graded conglomerate and very coarse sandstone of IF (F1 and F2a, respectively). (A') Close-up photograph of a pebble conglomerate bed of F1). (B) Brownish carbonate-cemented, dewatering-pipes in thick-bedded coarse sandstone (F2a) of UKG. (C) Thick-bedded mudstone-clast breccia (F3). Clasts (some highlighted by dashed green lines) are dark- to medium-toned grey, unlaminated and tabular, and supported in a matrix of coarse- and very coarse-grained sand. (D) Interval of intercalated, laminated medium-grained sandstone and mudstone tops (F4a), locally overlain by cross-stratified (dune) coarse-grained sandstone (F4b) and brownish-weathered interbedded fine-grained sandstone and mudstone (F5a). (E) Interpreted photograph of long-wavelength bedform unit comprises of planar laminated part (left) that terminate into high-angle dune cross-stratified part (right) in coarse-sandstone (F4c). It erosively overlies F2 beds, and includes at least five sets. Note ripples (F4b) are

capping the whole unit. (F) Glacially-polished, sequence of medium grey, rippled cross-laminated, fine-grained sandstone interbedded with lighter (yellowish) grey, mudstone (Tcd's Bouma divisions, F5a). Few isolated ripples (s) are observed. Locally matrix-rich sandstone (F7) are also intercalated. (G-G') Photograph and corresponding line drawing of dark grey, matrix-rich (muddy) sandstone (F7) intercalated with medium to light grey, sharply graded mudstone beds (Td's Bouma division, facies F5b). F7 are poorly-sorted sandstone containing abundant medium sand-size grains as well as abundant mud-rich matrix. Some matrix-rich sandstone beds have deformed mudstone clasts and chips embedded. (H) Matrix-supported conglomerate (F8a), consisting of outsized, rounded to sub-rounded clasts of carbonate-cemented, coarse-grained sandstone and mudstone, that are embedded in a poorly-sorted mixed matrix that ranges from mud to pebbles. (I) Only observed in the UKG, clast-supported breccia (F8b) is characterized by elongated, 'boudinage-like' clasts of white-to pinkish, coarse-grained sandstone clasts surrounded by brownish-tinted, mudstone layers. (J) Only observed in the IF, chaotic facies here (F9) consist of undeformed grey, thin-bedded, fine-grained turbidites, but with local unusual "blocks" (enclosed in dashed black lines) of thin-bedded turbidites that are tilted and/or disrupted.

Table 3.1. Description and interpretation of lithofacies documented in this study occurring in the KIT and LIF

Lithofacies	*Bed distribution and continuity*	*Description and Sedimentary Structures*	*Bed thickness, bed amalgamation degree and contacts*	*Interpreted Depositional Processes*	*Equivalent to Turbidite divisions*
F1. Thin- to thick-bedded clast-supported conglomerate	Locally observed in UKG, but common in the IF. It occurs mostly in the axial parts of channel fills. Beds can be followed for few hundred meters laterally.	Poorly-sorted, clast-supported conglomerate with common quartz and feldspar clasts (granule to fine pebble); beds in IF are coarser with clasts, up to medium pebble. Matrix is coarse to medium sandstone. Elongate mudstone (rip-up) clasts, up to 27 cm long occur locally. Brown-orange weathered carbonate clasts are rare. Commonly normally graded, consisting of granule to fine pebble conglomerate that grade upward to coarse and very coarse sandstone (Fig. 3.3A,B), however some massive beds are also present. Soft-sediment deformational structures are locally developed, and include basal load structures.	Range from 0.12 to 3.3 m thick. Beds are typically high to partly amalgamated. Sharp, loaded, undulatory or irregular erosive basal contacts are common.	Differential settling or rapid suspension deposition from gravelly to sandy, high-concentration turbidity flows (Lowe, 1982; Mulder and Alexander, 2001). Load structures indicate water-saturated bed conditions due to short recurrence interval between depositional events.	R3 Lowe division
F2. Thin-to thick-bedded sandstone	Principal component in coarse-grained distributary channels, splay elements, and some scour fills in the UKG, and also occur in channel complexes of IF. Beds are traceable laterally for several hundred of meters. It is not uncommon that strata of F2b are comparatively more tabular and laterally continuous than F2a.	F2a. Normally-graded, pink to light brown, coarse to very coarse sandstone, that grade upward to coarse or medium sandstone. Granule and pebble-size (0.3-0.7 cm) clasts are common to abundant at the base of beds, but in some beds clasts are dispersed throughout. Up to 27 cm, boulder-size mudstone intraclasts occur locally. Load and flame structures are common. Dark-brown, dewatering pipes are observed in some UKG beds (Fig. 3.3B). Typical pink to reddish brown sandstone beds in IF are calcareous, containing relatively higher carbonate cement content (up to 30%) than sandstone UKG.	Beds range from 0.01 to 2.7 m. Thicker beds (>1 m) tend to be amalgamated. Sharp or irregular erosive bases, and loaded bases are recognized locally.	Gradual or rapid deposition from sandy high-concentration turbidity flows (Lowe, 1982; Mulder and Alexander, 2001). Dewatering pipes suggest rapid syndepositional upward fluid movement and elutriation in rapidly consolidating, water-saturated sandy and gravelly beds (Lowe and LoPiccolo, 1974; R., 1999).	S3 Lowe or basal Ta Bouma divisions.
		F2b. Normally-graded and massive, green to light-grey, medium to fine sandstone (Fig. 3.3D). Some beds are overlain by (planar-or cross-) laminated fine-grained sandstone and/or thin mudstone layer	Beds are 0.02 and 0.7 m. Sharp- or shallowly-scoured bases, and tops are typically planar.	Deposition from moderate to low-concentration turbidity flows	Incomplete (rarely complete) Bouma sequences: Ta/Tad, Tabd/Tabcd or

					Tacd
F3. Thin- to thick-bedded mudstone-clast breccia	Observed locally in UKG and IF. Beds are poorly stratified and can be laterally traced only over few to tens of meters. F3 is recognized in channelized and scour elements, as well as terminal splays.	Mudstone-clast breccia (Fig. 3.3C) are ungraded, structureless, and clast-supported with more than 25% greyish silty mudstone clasts dispersed through the bed. Clasts are tabular, up to 45 cm in length (boulder size), and oriented sub-parallel to the base of the bed. Internally, clasts are massive, laminated or interstratified with fine-sandstone. Shapes range from angular to subangular, although subrounded to rounded black coloured clasts are observed locally. The poorly-sorted matrix consists of medium sand grains to fine pebbles.	Beds vary from 0.1 to 0.9 m thick, and thick beds are typically amalgamated. In general basal contacts are scoured.	Deposition from very high-concentration to transitional flows between sandy-hyperconcentrated and cohesive (debris) flows (sensu Mulder and Alexander, 2001) with abundant mudstone clasts derived from local or upflow scouring of the muddy substrate.	F3 Mutti Facies
F4. Thin- to thick-bedded stratified (planar- and cross-) sandstone	Much more common in UKG. F4a, occur within scours and distributary channels, whereas F4b are present in distributary channels, terminal splays, and less common in channels of IF. F4c are exclusively observed in distributary channels and rarely within scour deposits. Stratified beds are normally cemented with ferroan calcite, which gives them a distinctive reddish brown to pink colour. However, some F4a does not exhibit calcite cement. F4a,b abruptly overlies facies F1, F2, or a basal erosion surface. F4c locally overlie F2, and occur in lenticular or wedge-shaped units that are traceable discontinuously for a few to hundred of meters laterally.	F4a. Planar-laminated sandstone are composed of well-sorted, coarse- to medium-grained sandstone with dispersed pebble grains in some beds. Stratification is well developed. Laminae are generally normally graded. Occasionally, some beds are overlain by F4b (ripple cross-lamination), and/or mudstone (Fig. 3.3D) F4b. Cross-stratified sandstone consisting of well-sorted fine to very coarse sandstone. Coarser beds also contain dispersed granules and pebbles. Mudstone clasts are uncommon. Typically, cross-stratification occurs as a single set. Based on bed thickness, two types of cross beds are recognized: small- and medium- scale (Fig. 3.3D,E). F4c. Long-wavelength, dune-like bedforms consisting of planar-laminated sandstone that transition (downflow) into high-angle (up to 20^{o}), dune-like cross-stratified sandstone (Fig. 3.3e). They occur as a single set, but multiple	Planar-Laminated beds are 0.01-1.25 cm thick. Bed boundaries are sharp and planar. Beds are locally scoured and loaded. Sets of small-scale (ripple) cross-lamination are typically 2-3 cm thick, whereas sets of medium-scale (dunes) cross-stratification are up to 0.4 m thick. Bed bases are sharp or erosive. They are <1 m thick.	Deposition from high- to moderate-energy, sandy turbidity flows under tractional conditions Small-scale (ripple) cross-laminated sandstone were deposited by low-energy, low-concentration unidirectional. turbidity flows. Medium-scale (dune) cross-stratified sandstone were deposited from similarly low concentration but higher speed sandy turbidity currents. They comprise unit bars formed in a submerged hydraulic jump (Macdonald et al., 2009; Macdonald, 2012; Macdonald et al.,	S1 Lowe division, or Tb (or Tbcd) Bouma division Small-scale (ripple) cross-laminated sandstone correspond to Tc Bouma division, and medium-scale (dune) cross-stratified sandstone correspond to F6 Mutti Facies

		sets (up to five) are locally observed. Sandstone are typically coarse- to medium-grained. F4c are overlain by small-scale cross-laminated sandstone and/or mudstone (F4b and/or F5 respectively).		2013). The planar laminate part form the upflow portion of the unit bar, whereas the dune-like cross-stratified part is on its downflow side.	
F5. Thin-to medium-bedded, interbedded sandstone and mudstone, and mudstone beds	Units of thin- to medium-bedded, interbedded sandstone and mudstone occur in both UKG and IF, however they are thicker in IF. Some stratal units are laterally continuous at outcrop scale (>500 m). In the UKG, these units show distinctive bands of brown to red iron-oxide staining. Fine-grained sheets are commonly composed of F5a, but some are locally interbedded with F5b.	F5a. Units consist of alternating layers of fine-grained sandstone and mudstone (Fig. 3.3D,F). The proportion of sandstone to mudstone varies, but typically mudstone dominates. Occasionally, units exhibit a fining- and thinning-upward trend. Green to olive and light grey, very fine- to fine-grained sandstone are structureless, parallel laminated or small-scale cross-laminated. Even though structureless (massive or normally graded) and parallel laminated sandstone are common, cross-laminated sandstone dominate. Typically, cross-laminated sandstone are a single set thick, although multiple (up to three or four) sets are also observed. Local isolated ripple formsets are also present (Fig. 3.3F). Sandstone-mudstone couplets are commonly capped by a massive or graded layer of grey silty mudstone. Parallel laminations are locally observed. F5b. Mudstone beds, generally sharply overlie coarser sandstone strata (usually F2 and F4), and are composed of unlaminated medium- to dark- grey mudstone (Fig. 3.3G-G') that in general grades upward from silt to clay.	Sandstone-mudstone couplets are 0.1 to 25 cm thick. Sandstone beds range from pinstripe (1 mm) to 18 cm, whereas mudstone beds range from 0.1 to 24 cm thick, with most range between 2 to 10 cm thick. Sandstone have sharp to loaded bases.	F5a. Sandstone-mudstone couplets were deposited by waning fine-grained, low-concentration turbidity flows. Structureless sandstone were deposited by rapid suspension with high sediment fallout and little traction (Arnott and Hand, 1989; Allen, 1991). Planar- and cross-laminated sandstone overlain by graded mudstone suggests traction followed by sediment fallout. Isolated ripple formsets indicate deposition by sediment starved low-concentration turbidity currents. F5b. Silty mudstone beds are interpreted to have been deposited by low-energy traction-plus-fallout processes from waning fine-grained, low-concentration turbidity flows.	Upper divisions of Bouma sequence, including Tcd and/or Tcde. Occasionally Tbcd Uppermost division of Bouma sequence, including Td, Tde, and/or Te
F6. Phosphatic-rich claystone	Exclusively interbedded with thick units of thin-bedded,	Rare, thin layers of hard, medium-grey, massive, calcareous claystone with high	1-2 cm thick	Thin layers of phosphatic-rich claystone were discretely	

	sandstone and mudstone of UKG. They can be traced for up to 300 m.	phosphorus content (13-14%, see Appendix D: Geochemistry), consisting of cryptocrystalline francolite (carbonate fluoroapatite).		deposited from low-concentration turbidity currents that were highly enriched in phosphorus. The source of the phosphorus might be external from shelfal areas within the upwell-related regions. Subsequent to the sudden deposition of the phosphatic-bearing layer, phosphate enrichment and phosphogenesis could have also occurred (Follmi, 1996; Álvaro et al., 2016).	
F7. Matrix-rich sandstone	Matrix-rich (muddy) sandstone occurs mostly in UKG. They are laterally continuous for several hundreds of meters, and exhibit a distinctive smooth weathered surface.	Green coloured, structureless, poorly sorted, medium- to coarse-grained sandstone. Beds are coarse-tail graded or ungraded, and commonly contain floating elongated, platy and tabular, mudstone intraclasts and mudchips. Locally, some intraclasts are folded and disrupted. Individual matrix-rich sandstone are capped by cross- or parallel laminated (clean) fine-sandstone (Figs. 3.3F,G-G') and/or more commonly silty mudstone (F4 and F5b, respectively). Load structures are locally observed. Matrix-rich sandstone beds consistently occur interstratified with thin-bedded, interbedded sandstone and mudstone (F5a; see Figs. 3.3G-G'). Locally, they underlie at the base of thick-bedded coarse-grained sandstone (F2).	Beds are sharp-based, up to 22 cm thick, but commonly 6-14 cm. Thick beds are uncommon, and tend to be amalgamated. Mud fraction in the matrix is up to 50%.	Direct suspension sedimentation with negligible traction from collapsing high-sediment concentration turbidity flow, possibly downflow of an internal hydraulic jump (Leclair and Arnott, 2005). Erosion in the jump formed the common elongated mud clasts and chips, as well as abundant mud matrix in the bed significantly increased flow density. Rapid and voluminous sedimentation downflow rapidly weaken the flow (Hiscott, 1994; Huang et al., 2009a), and deposited matrix-rich sandstone.	
F8. Matrix-supported conglomerate and clast-supported breccia	F8 are recognized in both stratigraphic units, but are more in the IF. Strata of F8a extend and correlate for tens to several hundreds of meters, whereas F8b is observed only in the UKG, has a lenticular geometry and can be traced	F8a. Matrix-supported conglomerate contain polymictic clasts of mudstone, interbedded fine sandstone and mudstone, sandstone, calcareous sandstone and/or carbonates (Fig. 3.3h). Sub-angular to rounded, up to boulder-size clasts (some 2-3 m in diameter) are folded or partially fragmented and chaotically dispersed in a	Matrix-supported conglomerates vary from 0.01 to 16 m thick, but commonly 2.5-3 m. Basal contacts are sharp and planar.	Deposition from submarine (cohesive) debris flows generated by upslope instability, collapse and erosion.	F8a is comparable to F1 Mutti Facies

	for more several hundreds meters laterally, before wedging out toward the SE.	poorly sorted matrix of clay to granule quartz grains. F8a strata commonly are overlain by cross-stratified sandstone (F5b). F8b. Clast-supported breccias are poorly-sorted, mostly monomict and contain up to boulder-sized, angular to subangular intraclasts of medium- to coarse-grained sandstone and mudstone supported in a sheared mudstone matrix with a distinctive foliation (Fig, 3.3I). Clasts are elongated and irregularly lensoid shape, closely-spaced, and aligned sub-parallel to the bed base (Fig. 3.3I). Clasts tend to exhibit boudinage, disruption and fragmentation. They are embedded within reddish to brownish weathered stained matrix of silty mudstone (Fig. 3.3I). The distinct surficial staining of the mudstone matrix caused by oxidation of abundant pyrite crystals is like in surrounding fine-grained strata. Some are overlain by an up to 1 m thick interval of fine-grained turbidites intercalated with matrix-rich sandstone (F5 and F7), and localized lens of structureless coarse-grained sandstone (F2).	Clast-supported breccias are up to 1.8 m thick with common erosive bases.	Deposition from local, highly viscous debris-flow. Lensoid and other irregularly shaped and fragmented intraclasts indicate extensive and intense internal deformation, remoulding, stretching and shearing of semi-lithified competent sandstone beds during gravity-driven downslope movement (Tripsanas et al., 2003), which culminated with the deposition of a clast-supported debris flow.	
F9. Chaotic facies	F9 facies is observed solely in IF, and are correlated for >700 m wide.	F9 is a unit comprising predominantly of undeformed thin-bedded, fine-grained turbidites, but (in the lower part of the strata) locally disturbed by clastic sills and dykes of coarse-grained sandstone. Additionally, few localized deformed “blocks” of interbedded fine-grained sandstone (Fig. 3.3J) and mudstone, or of coarse-grained sandstone are also present. Laterally-discontinuous beds of cross- and planar-laminated sandstone are observed at the top. F9 facies scours into F1 and F2, and is overlain by widespread unit of F5a.	It is up to 13 m thick. Basal contact is scoured.	Submarine slide deposit from the failure of (inner-bend levee) fine-grained deposits along the margins of a slope channel.	

Turbidite divisions from Bouma (1962), Lowe (1982), and Mutti (1992)

3.5 Architectural elements and facies distribution through the interval between the Kaza-Isaac Transition (KIT) and overlying lowermost Isaac Formation (LIF)

At the Castle Creek area, the studied interval is bounded by two distinctive regionally-extensive mass-transport complexes, and consists of a lithologically diverse and stratigraphically complex assemblage that contrasts the markedly more sandstone-rich, sheet-like basin-floor deposits of the underlying upper Kaza Group and laterally-discontinuous, sandstone-filled slope channels encased in fine-grained deposits of the overlying Isaac Formation, lower Cariboo Group (Ross and Arnott, 2007). On the basis of the original definition of Mutti and Normark (1987, 1991), this interval is likely represent the channel-lobe succession within the Windermere turbidite system, separating well-defined channels from well-defined lobes. Numerous examples of the deep-marine basin floor-to-slope transition have been reported from the ancient geological record (see examples and references in the Chapter 1-Introduction), however the strata of the KIT and overlying LIF are unique in its vertical and lateral continuity and architecture. To illustrate the architectural heterogeneity here, major lithofacies, elements and bounding surfaces are shown in Fig. 3.4A-B.

Based on dimensions, facies, and stratal geometries, the transitional succession comprises at least 36 main units that make up six principal or representative stratal elements: (3.5.1) mass-transport deposits (debrites and slide), (3.5.2) channel complexes (plus levee deposits), (3.5.3) scours-and-fill elements,

(3.5.4) distributary channels, (3.5.5) splays, and (3.5.6) mudstone-rich deposits. Moreover, two other important elements have been also recognized associated with some of these principal elements: (3.5.7) crevasse/avulsion splays (3.5.8) bars. Many of these elements are consistent with architectural elements previously documented and interpreted in the underlying UKG strata (Meyer, 2004; Meyer and Ross, 2007; Al-Mufti, 2013; Terlaky, 2014; Terlaky and Arnott, 2014; Terlaky et al., 2016). Each one of stratal elements will be described and interpreted here as follow (see summarized Table 3.2):

3.5.1 Mass-transport deposits

Mass-transport deposits (MTDs) are important in the KIT and LIF in general, as they increase in thickness, and lithological complexity stratigraphically upward (Fig. 3.4). MTDs in the KIT include several debrites and slide deposits (Fig. 3.4). In contrast, MTD in the Isaac Formation (above this study) consist of thick, laterally-continuous slide and slump complexes, as well as debrites (see Chapter 4; and also Ross and Arnott, 2007; Arnott et al., 2011). On the basis of the dominant lithology and internal arrangement, MTDs in the study area are divided in matrix-rich debrites and slide.

3.5.1.1 Matrix-rich debrites

Matrix-rich debrite units occur isolated at various scales and stratigraphic positions in the Castle Creek studied section. They have sharp, planar bases and sheet-like or lenticular geometries (Figs. 3.4, 3.5A-B).

Table 3.2. Distinguishing characteristics of interpretive stratal elements that occur in the KIT and LIF

Stratal Element		***Occurrence***	***Exposed Dimensions (Thickness and width)***	***Basal surface***	***Sedimentary facies***	***Vertical and/or Lateral trends***	***Architectural association and/or stacking patterns***
Mass-transport deposits	Debrites	KIT and LIF	0.6-18 m, few 10s->1200 m	Sharp	F8a	None	-
	Slide deposit (i.e. Slide Complex 1)	KIT	12.5 m, up to 700 m	Locally-steep, scarp surface	F9, typically deformed strata above the basal surface	None	Above the leveed channel complex
Channel complexes	Erosional Channel Complex (i.e. Kaza Channel 1)	KIT	Up to 13 m, only exposed for 60 m	Terraced-like composite surface	Mostly F2a and F3, minor F4b and F5	Subtle vertical and lateral fining and thinning	Vertical stacking
	Slope levee channel complex (i.e. Isaac Contact Channel Complex)	KIT	- Channel Complex: Up to 25 m, >1200 m - Channel Element: Up to 19 m, several 100s m - Mudstone-rich levee deposits: up to 16 m, several 100s m	Composite	-Channels: F1, F2, and less common F3, F4b and F5 -Levee: F5a,b	Channel elements: Little to no upward and/or lateral fining and change in facies, but abrupt lateral thinning and pinch out on the SE margins	Vertically stacked, and lateral offset of channel elements
Scour-and-fill elements	Small isolated scours	KIT and LIF	1-6 m deep and 10s to few 100s m wide	Single or composite	- F2a, F3, F4a,b, and F5. Less common, solely F3, F4b, F5, F1, and F8b	-Little to none vertical and/or lateral changes in facies	-
	Large (amalgamated and isolated) scours	KIT and LIF	Amalgamated: Up to 12.5 m, >600 m Isolated: few cm-<1.9m, >1200 m	Composite	Amalgamated: F1, F2a, and minor F3, F2b, less common F5 and F7 Isolated: Discontinuous layer or lenses of F5, F4, F1, F3, and F5	- Little to none vertical and/or lateral facies changes - Amalgamated: Lateral amalgamation of scour fills -Isolated: Abrupt and discontinuous facies distribution	Overlying mudstone-rich deposits, and intercalated and/or underlying numerous small isolated scours
Distributary channels	Nested distributary channels	KIT	- Individual: <2-3m, and <300 m - Unit (multiple stacked shallow channels): 5-6 m,	Erosive	F2a and F1, and subordinate F2b, F4 and F5	- Little vertical changes in facies, fining and thinning and bed amalgamation, except for the channel tops	Vertical stack and lateral offset

			at least 600 m -Multiple stacked units: up to 35 m >1200 m			-Rapid (over few 10s-100 m) lateral fining, thinning and less bed amalgamation -Wing-like geometries	
	Vertically-stacked distributary channels	KIT and LIF	Up to 5 m, 300-500 m	Sharp to less erosive	F2a, common F2b, F4 and F5a	- Little upward changes in facies and bed fining and thinning, except for the channel tops -Rapid (over few m) lateral bed fining, thinning and facies changes	Vertical stack
Splays		KIT	Individual: 1.5-4 m, 100's m Unit (multiple splays): 9-14m, >1200 m	Sharp	F2a, and minor F2b, and F3. Only at the tops of splays: F5 and F4b	Little to none vertical change in facies and bed thickness - Gradual lateral changes in grain size, facies and bed amalgamation over >1 km	Vertical stack
Mudstone-rich deposits	Type 1 mudstone-rich deposits (sandstone: mudstone ratio <0.3)	KIT and LIF	Up to 12 m, >450 m) to several km	Sharp	F5a,b, rarely F6	-Common gradual vertical and/or lateral bed fining and thinning	Overlying sandstone-rich distributary channels, splays, and/or slope channels
	Type 2 mudstone-rich deposits (sandstone: mudstone ratio 0.3-0.6)	KIT	<0.5 m, few 10s to 100s m	Sharp	F5a, with common interbeds of F2, F4, and/or F7. Uncommon F5b	-No vertical changes in facies -Common lateral bed thinning and fining and increasing in mudstone beds	Lateral change into type 1 mudstone-rich deposits
Crevasse/ avulsion splays		KIT and LIF	0.1-9 m; 300-600 m	Sharp	F7 and F5	-None vertical facies changes -Lateral facies changes into F5	Underlying distributary channels and splays
Bars		KIT	0.1-1 m deep, 10s-100s m wide	Bowl- or spoon-like erosive surfaces	F5c, with common F5a at the top	-Vertical fining. -None lateral facies changes, except for occasional changes in grain size	Discontinuous horizons overlying distributary channels and splays, and rarely scour fills

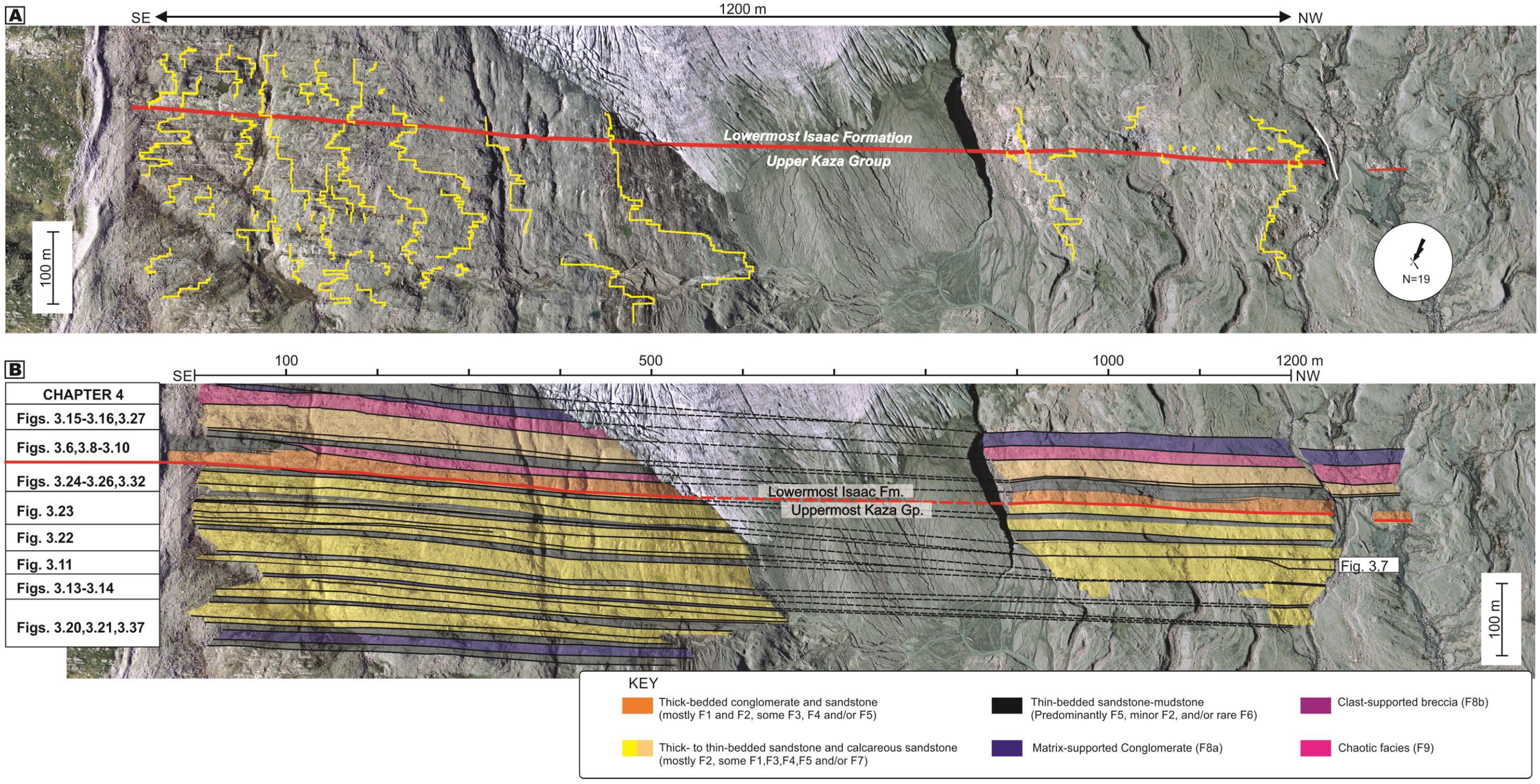

Figure 3.4. Stratigraphic and architectural map of the KIT and LIF in the Castle Creek area. The Kaza-Isaac contact is delineated by a bold red line. (A) Measured section locations and paleoflow rose diagram. (B) Lithofacies distribution. On the left, Figure locations relative to the stratigraphic framework are identified.

Continuation Fig. 3.4.

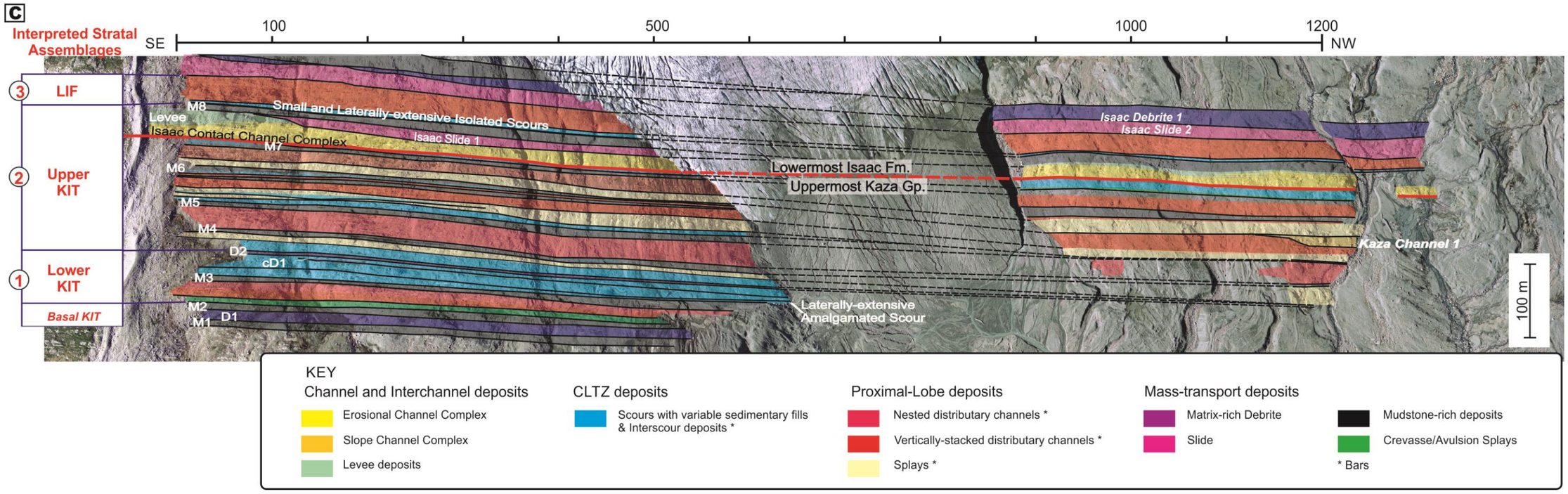

Figure 3.4. (Continued) (C) Architectural elements. Stratigraphically upward, three different stratal assemblages comprising numerous stratal elements are interpreted.

Generally, the most laterally continuous (>1200 m) matrix-rich debrites (e.g. D1-D2 in Fig. 3.4) are the thickest (18 and 3 m, respectively) and contain the largest and most compositionally diverse assemblage of clasts. Few laterally-discontinuous, matrix-rich debrites are mostly narrower (few hundreds of meters) and thinner (up to 0.6 m), and tend to contain few types of mudstone and sandstone clasts.

These matrix-rich debrites consist of poorly-sorted, matrix-supported conglomerate (F8a) with abundant dispersed sand- to pebble-size quartz grains, as well as chaotically-arranged, decimetre- to metre-scale, subangular to rounded clasts and/or stratified blocks of undeformed, folded and/or distorted mudstone, sandstone, thinly interstratified fine-grained sandstone-mudstone, and carbonate-cemented sandstone (Figs. 3.3H, 3.5A-E). Limestone fragments are uncommon. Clasts are dispersed in a structureless, silty mudstone matrix (Fig. 3.5A'). Strata at the top of most matrix-rich debrites exhibit better sorting and less mud matrix. Commonly, they are overlain by planar or cross-laminated sandstone turbidite (F4).

Interpretation

Laterally-continuous matrix-rich debrites are interpreted to be result from deposition of major debris flows that spread across several kilometres, whereas laterally-discontinuous matrix-rich debrites were deposited by much smaller debris flows. The typical rounded shape of the clasts in matrix-rich debrites suggests the remobilization of previously reworked sediments. More importantly, their polymictic composition, which contrast to the general lithological make up of strata in the KIT, indicate more distant upslope sourcing of sediments. Moreover, rare carbonate fragments indicate a shallow marine source. Common planar- and cross-laminated

sandstone that directly overlie these debris-flow deposits or debrites suggest that during movement, these debris flows entrained seawater along their tops, and as a consequence generated a dilute, moderate- to high-speed, turbidity current that reworked the top of the underlying (parent) debrite (Mulder and Alexander, 2001).

3.5.1.2 Slide deposit

At the top of the KIT in the Castle Creek South area, a slide deposit was interpreted (Fig. 3.4), and informally termed Isaac Slide 1.

This slide is up to 12.5 m thick, 500-700 m wide (Fig. 3.6A), and erosively overlies a leveed channel complex (see section 3.5.2.2, including Fig. 3.8). The basal surface is marked by a steep and irregular scar that (Figs. 3.6A,B), which then is overlain by blocks of undeformed thinly-bedded fine-grained sandstone and siltstone, but locally intercalated with centimeter-scale injections (e.g. dykes and sills) of poorly-sorted, coarse-grained sandstone (Fig. 3.6C), and uncommon blocks of disrupted, fine-grained sandstone-siltstone, and coarse-grained sandstone (Fig. 3.6D). The top of the chaotic-block unit is marked by discontinuous, cross- and parallel-laminated sandstone beds (F4a,b).

Interpretation

Isaac Slide 1, at the Castle Creek area, is interpreted to have been formed by local collapse along the margins of highly sinuous channel. Slides associated with localized channel-margin collapse have been identified in both modern (e.g. Sawyer et al., 2007; Dalla Valle and Gamberi, 2010; Gamberi and Rovere, 2011), and ancient (e.g. Pickering and Corregidor, 2005) deep-marine systems.

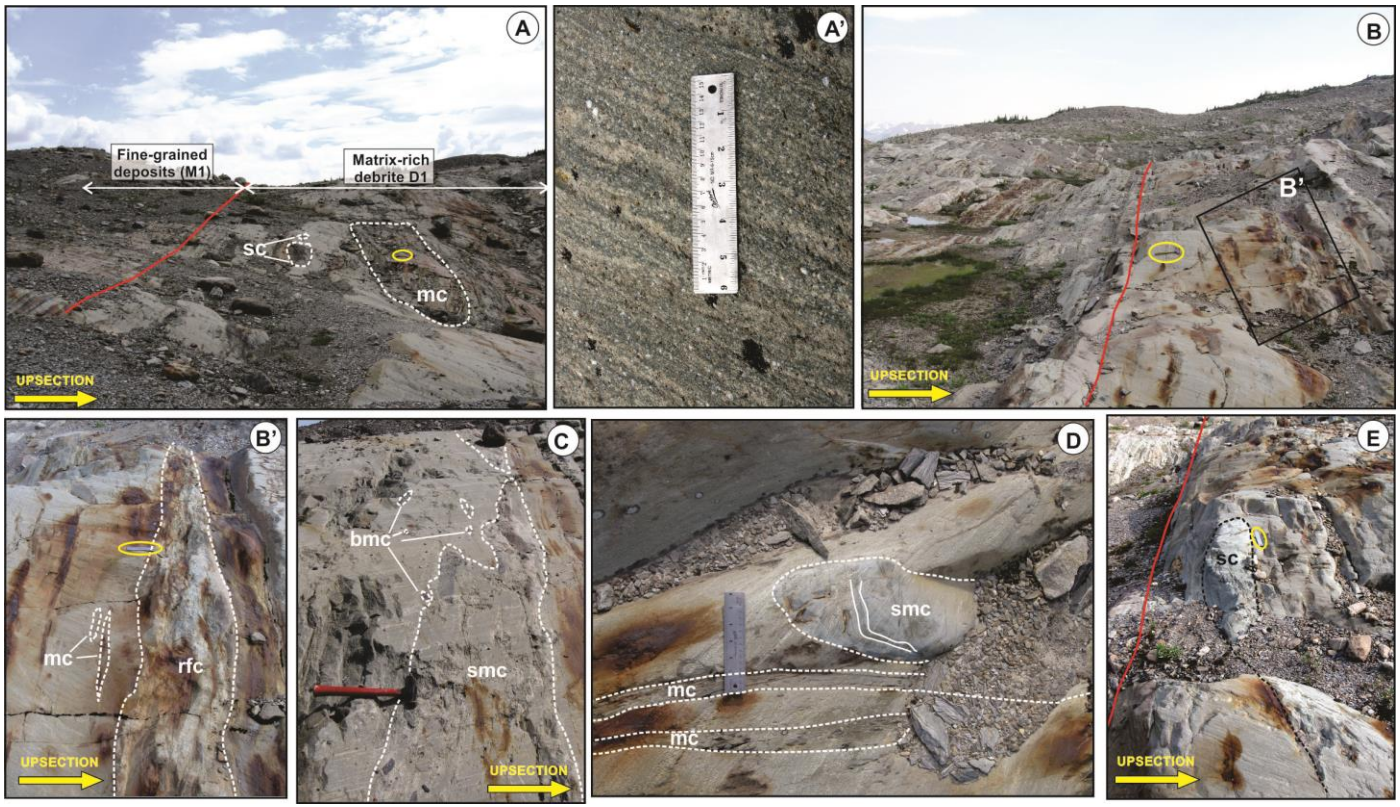

Figure 3.5. Matrix-rich debris-flow deposits in the KIT. Debrite bases are highlighted by red lines. (A) Thick matrix (mud)-rich debrites with meter-sized intraclasts or blocks of mudstone (mc) and carbonate-cemented stratified sandstone (sc), which tend to be subparallel to the base of the debrite. (A') The matrix is extremely poorly-sorted, consisting of abundant dispersed quartz sand and granule (white particles) embedded in a light grey admixture of silt and mud. (B-E) Thick chaotic debris-flow deposit contains tabular mudstone clasts (mc), rounded black mudstone clasts (bmc), and rounded sandstone clasts (rsc). It also has rafted blocks of stratified sandstone and mudstone (rfc in B' and C) that occur at or near its top. Such clasts exhibit internal disaggregation and are presumed to have been rafted along the surface of the flow. Hammer for scale in A-C and 15-cm ruler for scale in A',B',D, E.

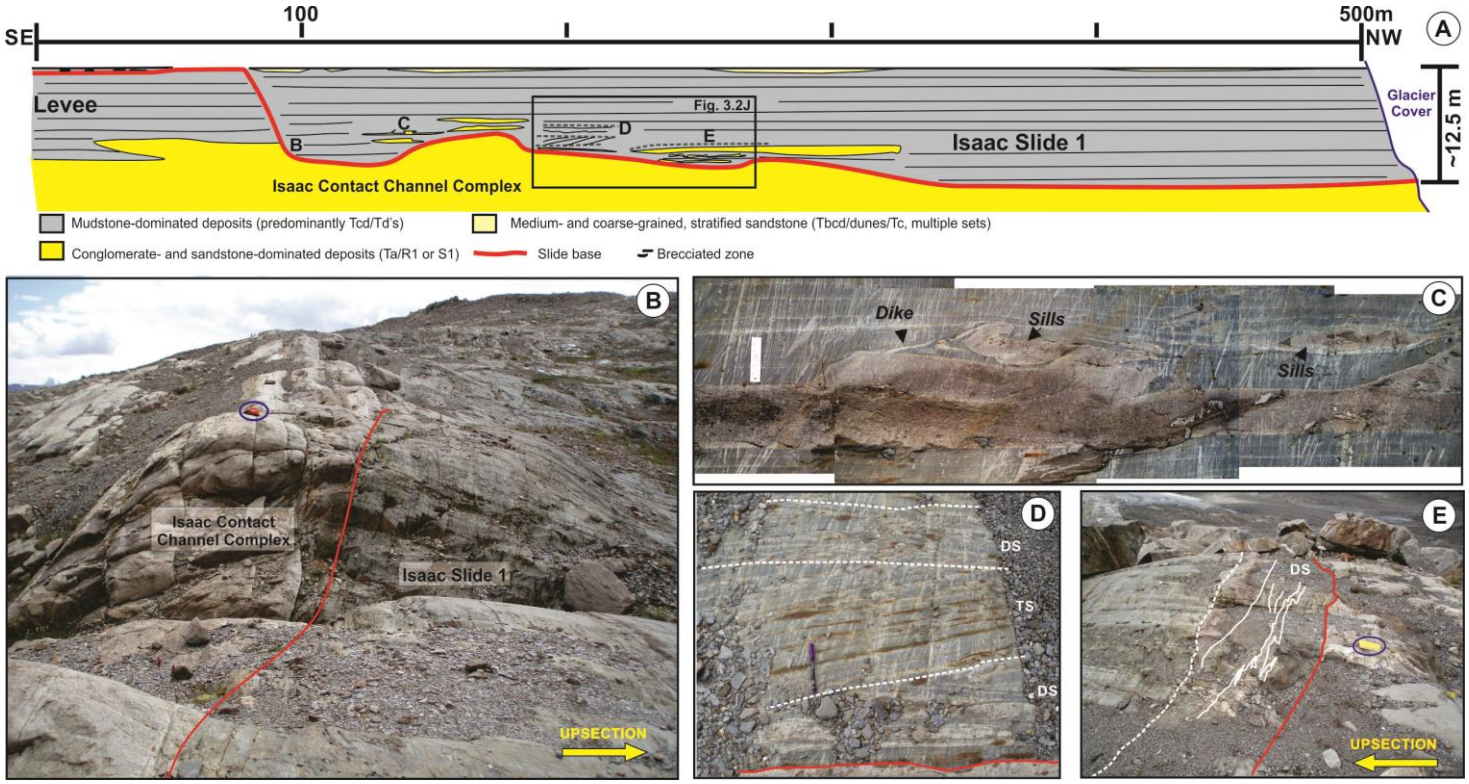

Figure 3.6. Slide deposits in the KIT. Basal slide surface is delineated by bold red lines. (A) Simplified sketch of the Isaac Slide 1. The basal surface of the slide truncates irregularly the top of Isaac Contact Channel (both channel fills and inner-bend levee deposits). The top of the slide is marked by laterally-discontinuous, lenses of stratified sandstone. (B) The slide escarpment is partly discerned in the SE (Backpack top pocket lid is ~30 cm-long). Isaac Slide 1 consists mainly of undeformed, thin-bedded, fine-grained turbidites, except for small-scale irregularities and "blocks" that are observed almost near the escarpment. (C) Cm-scale sandstone intrusions within the slide, including sills and dike of coarse-grained sandstone that laterally intrude within thin-bedded turbidites (Metal ruler is 15.24 cm). (D-E) Localized "blocks" (enclosed by white dashed lines) occur above the slide base. These blocks are composed of disrupted and/ or titled strata (ds and ts). In E, coarse-grained sandstone beds are delineated by thin white lines.

This failure formed a slide scar onto which, thick allocthonous blocks of mud-rich (probably levee) deposits was juxtaposed. Though the slide comprises mostly blocks of undeformed fine-grained strata, localized blocks along its basal surface suggest minor substrate disintegration and deformation during movement. Additionally, coarse-grained sandstone injections are interpreted to be result of the rearrangement of sand grains contained in discrete sand interbeds within the sliding sediment pile. This rearrangement caused pore pressure to rise and sand grains to become fluidized and ultimately remobilized, forming the injections.

With respect to most MTDs in the UKG, the thickness and lateral extension of this slide is considerable; however it is smaller compared to MTDs interpreted on seismic data from offshore Gulf of Mexico, Indonesia and Nigeria (Posamentier and Kolla, 2003; Posamentier and Walker, 2006).

3.5.2 Channel Complexes

On the basis of their stratigraphic location, scale and morphological character, and dominant grain size, two kinds of channel complexes have been identified in the upper KIT: erosional, and leveed.

3.5.2.1 Erosional Channel Complex

Incised into sandstone-rich strata of the UKG is a channel complex, informally termed Kaza Channel 1 (Fig. 3.4). Compared to leveed slope channel complexes (next section 3.5.2.2), Kaza Channel 1 is moderately thinner, up to 13 m thick, and is only exposed at the end of Castle Creek north area for approximately 60

m laterally (Fig. 3.7A-C). The basal of Kaza Channel 1 is mostly flat, but then it rises steeply along the one exposed (SE) margin, wherein localized small sub-horizontal terraces or flat are also observed (Fig. 3.7A-C). Highly amalgamated beds of mudstone-clast breccia (F3) are plastered discontinuously along the surface.

Kaza Channel 1 comprises two vertically-stacked, up to 5 m thick, sandstone-rich channels that are separated by an approximately 0.5 m thick unit of thin-bedded, fine-grained turbidites (F5a).

The channels are filled predominantly of thick- to medium-bedded, amalgamated coarse- to very coarse-grained sandstone (F2a) with common granules at their bases or dispersed throughout the beds, and occasional mudstone layer at their tops (Fig. 3.7C,D1-D5). Where present, mudstone clasts occur at the base or in the middle of beds. Intercalated, ripple and dune cross-laminated sandstone, and/or fine-grained turbidites (F4b and F5a respectively) are also observed. Strata show subtle upward and lateral -fining and -thinning trends, and decrease in bed amalgamation away from the channel axis as fine-grained turbidites become increasingly common.

The top of Kaza Channel 1 is covered by laterally-continuous, up to 3 m thick intervals of thin-bedded, fine-grained turbidites (F5a) with local interbeds of discontinuous, thin- to thick-bedded, coarse-grained sandstone (F2a).

Interpretation

Kaza Channel 1 is interpreted to be a deeply incised, submarine feeder channel (e.g. Gervais et al., 2006; Saller et al., 2008). This unit, informally termed Kaza Channel 1, is considered to be a long-lived conduit for transferring significant sand-rich sediments further downflow to a distributive fan system. There are two

well-exposed examples of feeder channels of the UKG, which have been recognized and described at Castle Creek (Meyer, 2004; Meyer and Ross, 2007; Rocheleau, 2011; Terlaky, 2014).

The deep-scoured (locally terraced) base, localized occurrence of lag deposits (i.e. mudstone-clast breccia) and multiple channels of Kaza Channel 1 provide evidence that it did not result from a single episode of incision and backfill, but instead more complicated history of multiple cut and fill episodes. Initially, the basal erosional surface and overlying mudstone-clast breccias were generated by highly erosive flows passing through a newly activated channel conduit (Fig. 3.8A). The channel was occasionally filled by sand-rich, high-concentration turbulent flows, depositing coarse-grained strata in the lower channel fill (Fig. 3.8B); however, thin-bedded, fine-grained turbidites at the top of the fill suggest that the channel ceased temporarily to be a sediment transport avenue.

The widening of the channel wall occurred during later incisions (Fig. 3.8C), resulting in the formation of channel margin terraces. Patches of mudstone clast-rich breccias were produced during the concentrated erosion along the margin. This is associated to the tendency of the flows to intensely erode and bypass, as they become more focused within the axis of the conduit, most likely in response of increasing flow discharge due to upstream channel maturation (Rocheleau, 2011; Terlaky, 2014).

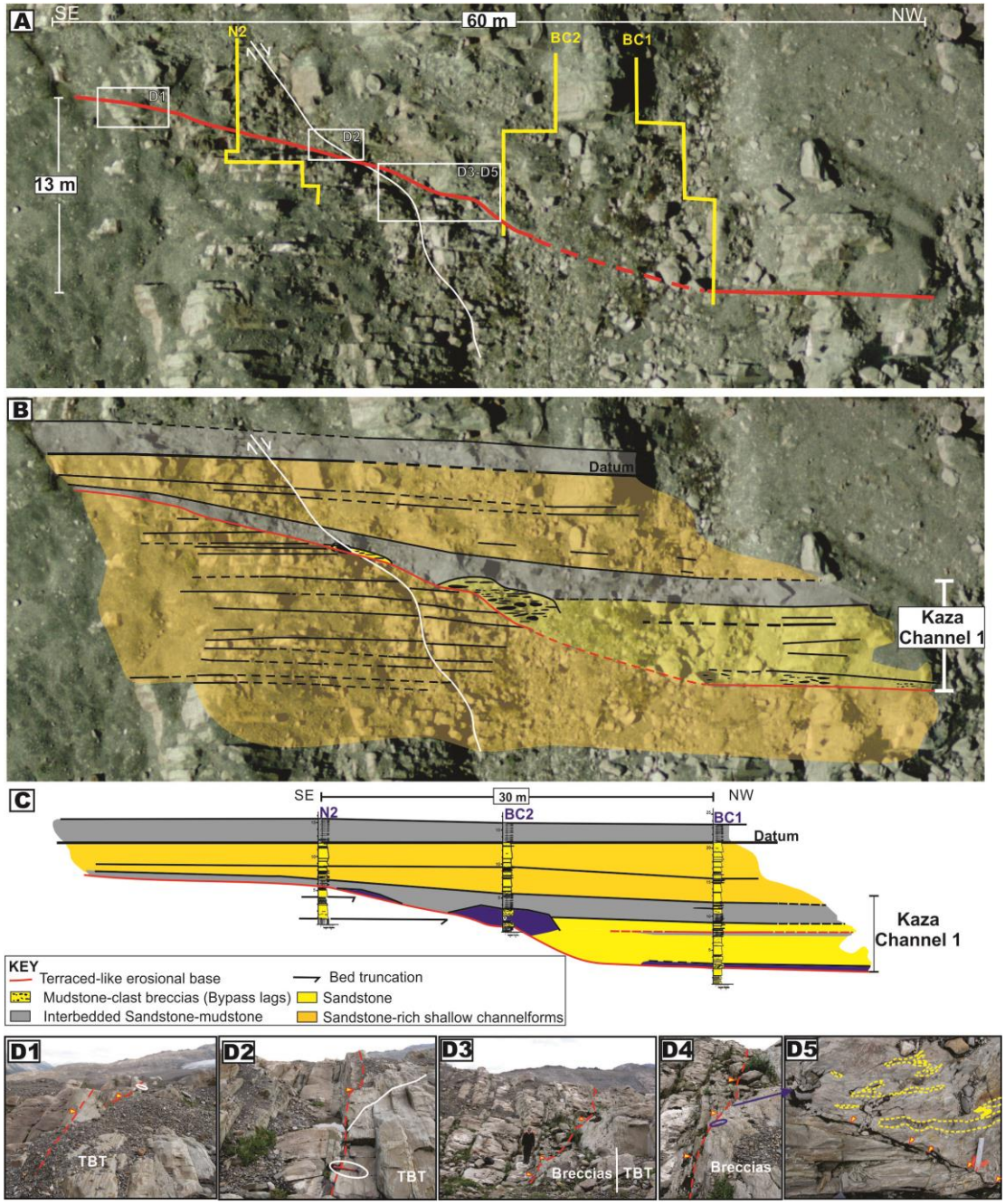

Figure 3.7. Architecture of a basin-floor feeder channel in the KIT. (A) High-resolution airphoto of Kaza Channel 1 (KC1), showing basal erosion surface (thick red line) and location of measured sections. Note fault displacement is negligible (<23 cm). (B,C) Schematic diagram and cross-section of KC1, illustrating several sandstone-rich channel fills separated by thin-bedded turbidites. The master erosion surface deeply truncated into underlying sandstone-rich strata filling distributary channels (yellow pointers in D1-D5). This surface is overlain, in turn, by thin-bedded turbidites (e.g. D1-D2) and mudstone-clast breccia (e.g. D4-D5). In D5, various mudstone clasts are

highlighted with yellow dashed lines. (Hammer for scale in D1-D2, person for scale in D3, and 15 cm-long ruler for scale in D4-D5).

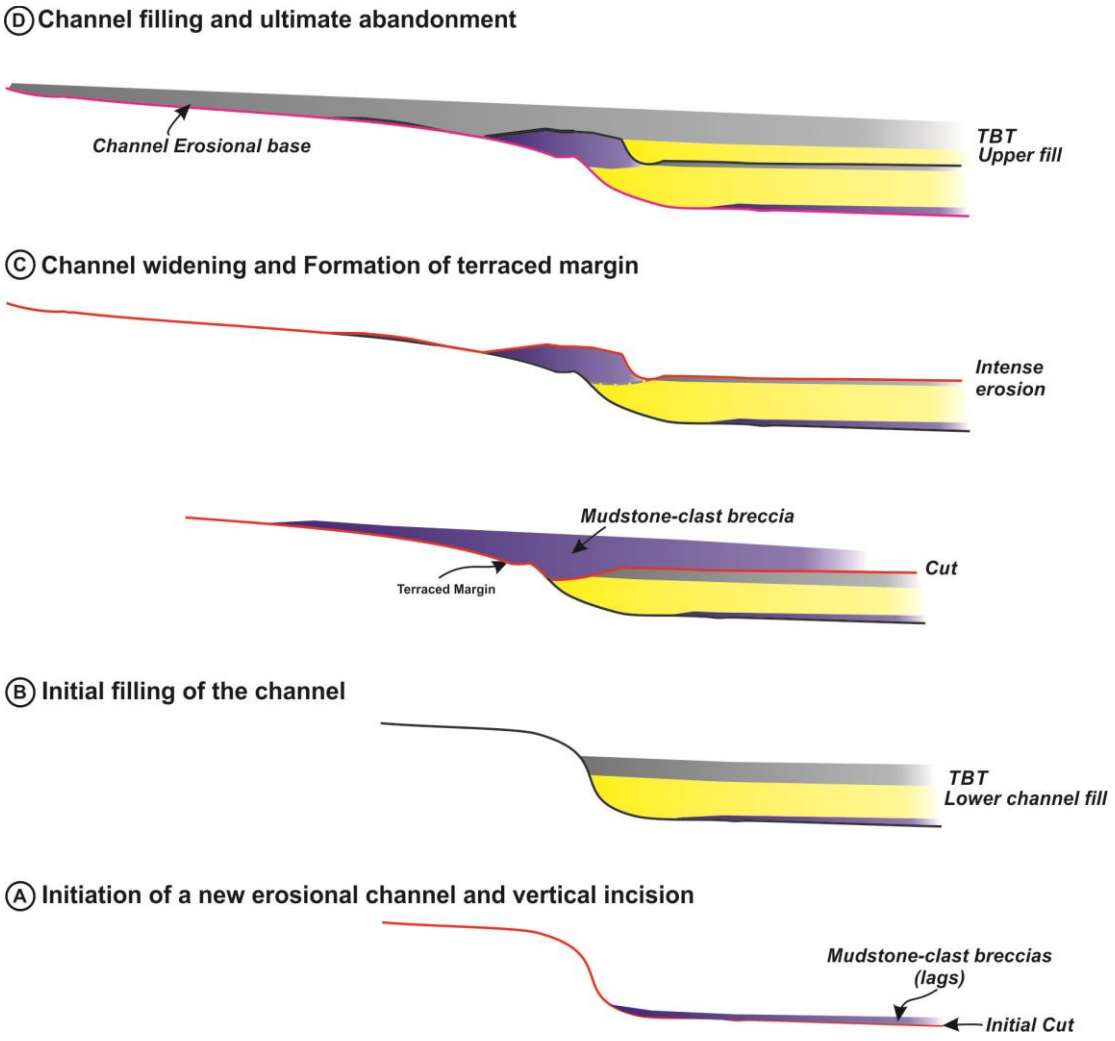

Figure 3.8. Simplified model illustrating the initiation and evolution of basin-floor feeder channel, Kaza Channel 1. See text for explanation.

Subsequently, the channel was almost completely filled by sandstone-rich, high-concentration flows (Fig. 3.8D), which resulted in the deposition of coarse-grained sandstone in the upper fill. The subtle lateral-fining and -thinning trends of channel-margin strata suggest that flows were smaller, muddier and less dense along

their lateral margins (McCaffrey and Kneller, 2001; Kneller, 2003). At the top of Kaza Channel 1, the fine-grained interval (Fig. 3.8D) represents the complete abandonment of the channel, and most probably also a distributive system located downstream.

Compared to the Pleistocene Indonesia fan mapped by Saller et al. (2008), Kaza Channel 1 might be equivalent to those channels with low to moderate sinuosity that cut most proximal lobes (e.g. A-F) in the fan and feed other lobes more basinward.

3.5.2.2 Leveed channel complex

At the contact between the UKG and IF, a distinctive leveed channel complex, informally termed Isaac Contact Channel Complex (or ICCC), is recognized in the Castle Creek study area (Figs. 3.4, 3.9). It is about 25 m thick and crops out across the full width (>1.2 km) and beyond the study area. It overlies crevasse/avulsion splay, scours, and mudstone-rich deposits. It consists of at least three juxtaposed channel elements (sensu McHargue et al., 2011), which laterally offset-stack toward the NW.

The base of ICCC is distinctly planar and horizontal; however the basal surfaces of some channel elements show apparent dip or inclination relative to the main horizontal base. These surfaces are commonly overlain locally by an up to 1 m thick, mudstone-clast breccia layer (F3).

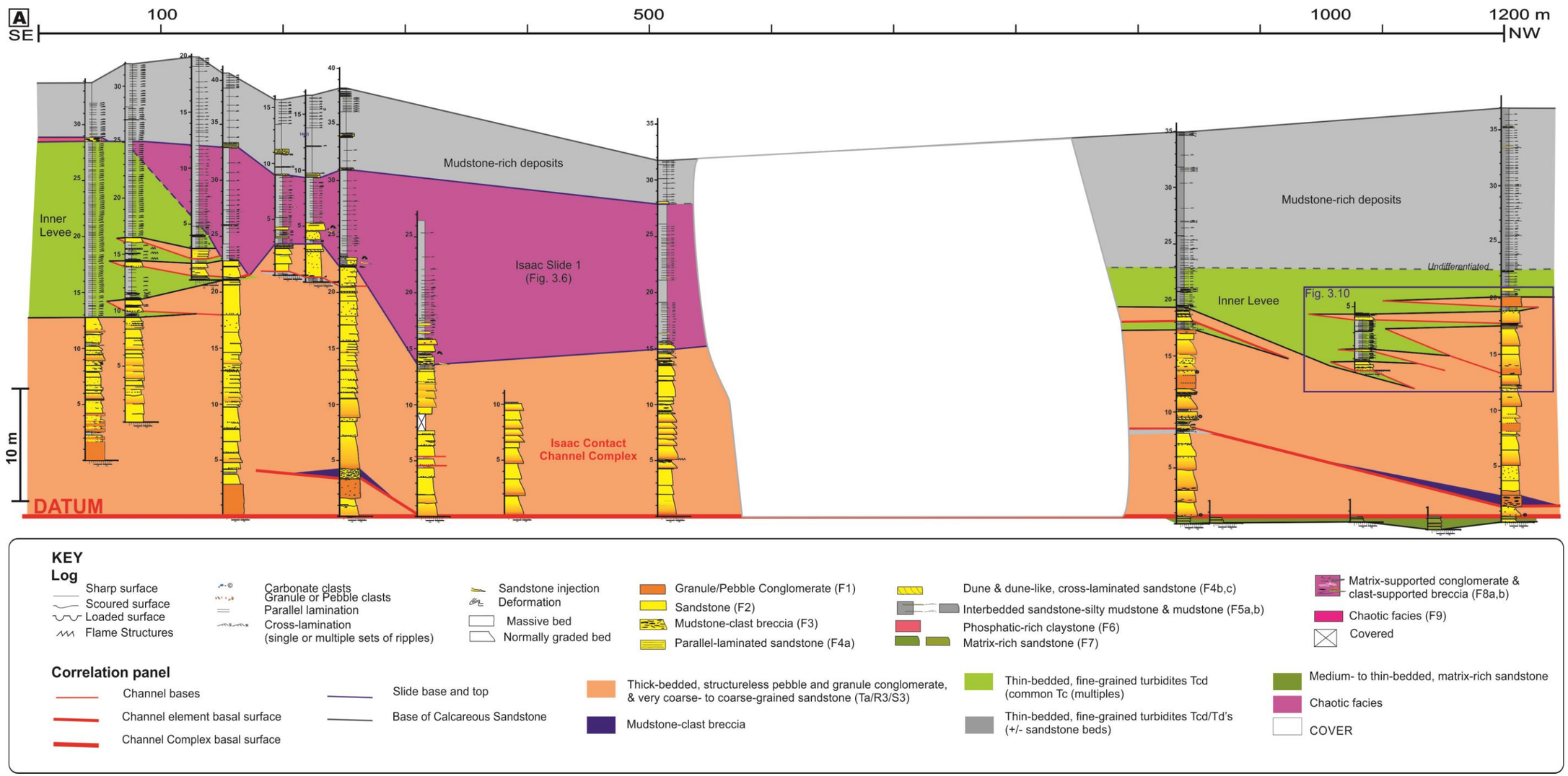

Figure 3.9. Architectural configuration of Isaac Contact Channel and Isaac Slide 1. Interpreted correlation panel, showing the distribution of (A) lithofacies of channels and levee deposits. On the Castle Creek South outcrops, the upper part of the second channel element is locally incised by Isaac slide 1. At the top, fine-grained deposits blanketed the channel complex.

Continuation of Fig. 3.9

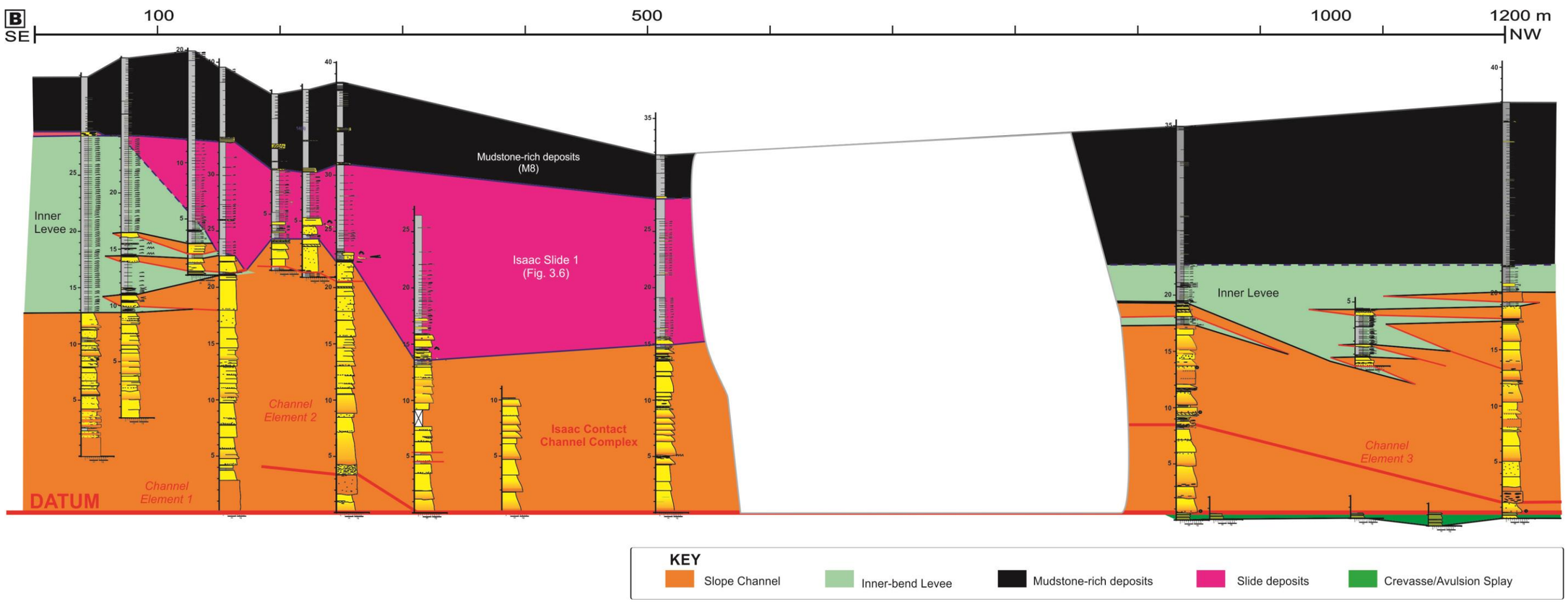

Figure 3.9 (Continued). (B) Architecture of channel and levee deposits. At least three channel elements offset stacked to form this channel complex.

Individually, channel elements are up to 19 m thick and several hundred meters wide, and are composed of numerous flat-based channels filled with coarsest strata than underlying strata of the UKG, including amalgamated, thick-bedded (up to 2.95 m), normally-graded, clast-supported, granule to pebble conglomerate and very coarse- to coarse-grained sandstone with granules at their bases (F1 and F2a, respectively; Figs. 3.3A-A'). Mudstone-clast breccia (F3), cross-bedded sandstone (F4b) and mudstone (F5b) are less common. Bed bases are commonly sharp and erosive. Mineralogically, grains are mostly quartz and feldspar, but distinctively brick-red to orange weathered dispersed carbonate fragments.

Stratigraphically upward, channel elements show negligible to minor change in grain size, facies or composition, with sandstone content exceeding 95%. At the top of the channel elements, however, significant oblique and lateral changes are observed (Fig. 3.10).

Toward their SE channel margins, strata consist of few thin to medium beds of poorly-sorted and ungraded, coarse- or medium-grained sandstone (F2a,b) with dispersed granules, and common cm-scale flame structures and sandstone sills occurring locally along the bed bases. These strata exhibit lateral thinning and become interfingered and abruptly pinch out over very short distances, in less than few tens to a hundred meters, with mudstone-rich levee deposits (Figs. 3.10A-B).

Levee strata consist predominantly of thin-bedded (up to 8 cm, but generally 1–3 cm), fine-grained interstratified sandstone and mudstone (F5a) with multiple (2–6, average 3–4) sets of non-climbing ripple cross-laminated, fine to medium sandstone (Figs. 3.9-3.10). Uncommon, interbeds of medium-bedded massive

sandstone (F2b) are also observed. These strata have low sandstone content, up to 15%, and stack to form a unit up to almost 16 m thick.

In most places, ICCC is capped by an up to few decametre-thick, mudstone-rich sheet-like deposits consisting of thin-bedded, fine-grained strata (F5) with occasional medium-bedded, medium-grained sandstone (F2b and/or F4b). Locally, however, it is overlain by a thick Slide deposit (see previous section 3.5.1.2, Figs. 3.6, 3.9).

Interpretation

Isaac Contact Channel Complex or ICCC shows a lithologically different and more complex architecture than those feeder channels described previously from the Upper Kaza Group (e.g. Rocheleau, 2011; Terlaky, 2014; and also this study, see previous section 3.5.2.1). Conglomerate/sandstone-filled channels of ICCC with adjacent levee deposits are similar in lithofacies and architecture to small laterally-accreted channels with well-developed (inner-bend) leveed deposits (sensu Arnott, 2007; and Dumouchel, 2015). Thus, ICCC is interpreted to result from the lateral migration of a single deep-water sinuous channel.

The basal erosion surface of each channel element, overlain locally by discontinuous, mudstone-clast breccia layers, was generated by high-energy bypassing turbidity currents (Mutti and Normark, 1987). In contrast to many submarine channel-levee models (e.g. Samuel et al., 2003; Mayall et al., 2006; Deptuck et al., 2007; Kolla et al., 2007), these surfaces are not interpreted to be associated with frequent reincision events.

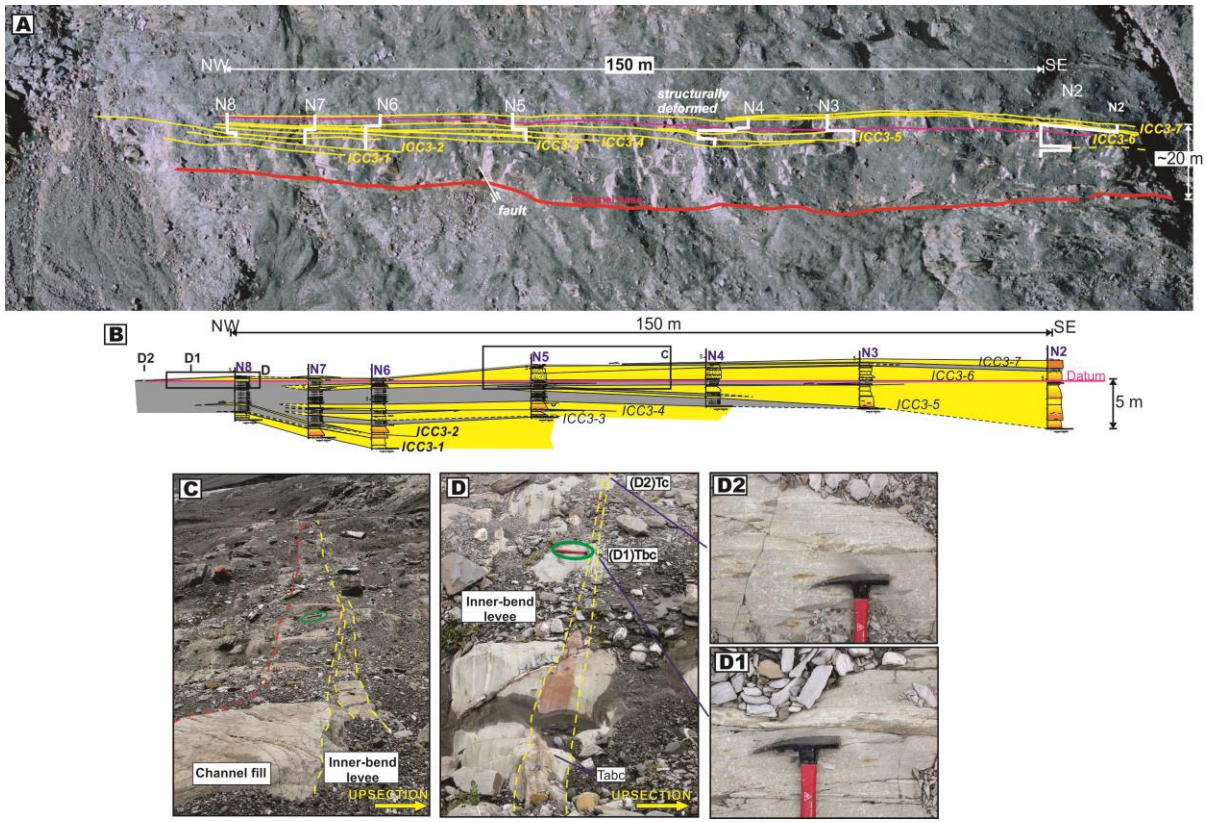

Figure 3.10. Channel-fill and inner-bend levee deposits in the upper channel element of the Isaac Contact Channel Complex. (A) Line drawing of stacked channel-fill deposits, showing how the channel fills are amalgamated (NW side), whereas they change obliquely upward and laterally toward the SE. (B) Detailed cross-section across selected channel fills and coeval SE levee, exhibiting lateral changes from axis to margin to these channels occurring over short distance, < 150 m. (C) Channel-fill strata abruptly pinch out onto the levee. Coarse-grained Ta beds are structureless and highly amalgamated. (15-cm ruler for scale). (D) Detailed photos across a 'finger'-like termination of one channel fill, showing coarse-grained sandstone Tabc bedset become rapidly thinner and grade into medium- and fine-grained strata Tbc and Tc turbidites (D1-D2) over few tens of meters (Hammer for scale).

These surfaces are rather interpreted to resulted by a more continuous lateral migration of the ICCC toward the NW (cf. Sylvester et al., 2011) that was only interrupted temporally by local truncation and emplacement of Isaac Slide 1, resulting from channel-margin failure. The erosional juxtaposition and systematic lateral offset of the channel elements here suggest preferential reoccupation of an older, but underfilled channel conduit (McHargue et al., 2011; Macauley and Hubbard, 2013).

Following the incision of each element, channels were filled by highly density-stratified flows consisting of a concentrated, anomalously coarser-grained lower portion and an overlying fine-grained, diluted upper portion. The highly concentrated lower portion of the flows resulted in the uniform deposition of thick-bedded, coarse-grained strata within the channels (Arnott, 2007). These channels exhibit significant aggradation and lateral confinement. They seem to steeply aggrade as they become more confined along the SE margin by the coeval deposition of fine-grained inner-bend levees formed as a consequence of channel flow overspilling and lower-energy deposition along the upper part of the inner-bend margin. The systematic lateral accretion of these channels suggest recurring changes in flow conditions passing through the channel bends (Arnott, 2007). Dumouchel (2015) suggested an intricate interaction of inertial and pressure forces along the deep-marine sinuous channels walls, influencing the formation of two superimposed cross-channel secondary currents, which caused enhanced erosion on the outer bend side and preferential deposition of coarse-grained sediment along the inner bend.

The final deactivation of ICCC is represented at its top by thin-bedded, fine-grained turbidites of fine-grained sheet-like unit, that are interpreted to be deposited from lower-concentration turbidity flows.

Numerous slope leveed channel complexes have been recognized in the Castle Creek study area (Navarro, 2006; Arnott, 2007; Navarro et al., 2007; O'Byrne et al., 2007; Schwarz and Arnott, 2007; Khan and Arnott, 2011; Dumouchel, 2015), however many of the stratal components, lithological associations and architectural style of Isaac Contact Channel Complex resemble those described from Isaac channels 2 and 5, and Units 14 and Unit 21 (e.g. IC2.2 of Arnott, 2007; and C3.4 of Schwarz and Arnott, 2007; Dumouchel, 2015). Isaac Contact Channel is comparable in size, stacking pattern and architecture to some leveed channels documented from large passive-margin fans, such as Gulf of Mexico (Beaubouef and S.J. Friedmann, 2000; Posamentier and Kolla, 2003; Posamentier and Walker, 2006), Amazon fan (Pirmez et al., 1997; Jegou et al., 2008), and Indus Fan and Niger Delta (Deptuck et al., 2007; Wynn et al., 2007).

3.5.3 Scour-and-fill elements

Scours with variable sedimentary fills are common in the KIT and overlying LIF at both Castle Creek (Figs. 3.4, 3.11-3.16) and Mount Quanstrom study areas (see Appendix G). They differ widely in their width:depth ratio and lithological make up. Based on their dimensions, they can be categorized as: small isolated and large scours, in which the former are significantly more common. Normally, only one side of the erosional features crops out.

3.5.3.1 Small isolated scours

Small scours are typically isolated, as they occur encased or separated by dm- to m-thick, laterally-continuous, mudstone-rich strata of thin-bedded, fine-grained turbidites (F5), and/or thin- to medium-beds of medium-grained sandstone and/or matrix-rich sandstone (F2b and/or F7, respectively). Nevertheless, some isolated scours incise locally into sandstone-rich elements (such as distributary channels, or splays, see next sections 3.5.4 and 3.5.5, respectively). On strike-oriented cross-sections, the erosion surfaces at the base of isolated scours are typically of the order of 1-6 m deep (common <1.9 m), and extend laterally for tens to few hundreds of meters.

They are filled by one or several thick to medium beds of amalgamated, structureless, coarse- to very coarse-grained sandstone (F2a, Figs. 3.12A-D) with local interbeds of mudstone-clast rich breccia, planar- and/or cross-laminated sandstone and mudstone (F3, F4a-b, and F5, respectively). Less commonly, small scour fills are composed solely of mudstone-clast breccia (F3), planar laminated sandstone (F4b, Figs. 3.12G-L), thin-bedded fine-grained turbidites (F5, e.g. Figs. 3.12E-F), granule conglomerate (F1, Figs. 3.13E-G), medium-grained sandstone (F2b), or debrites (F8, Fig. 3.12M). Beds are typically lenticular but in some cases onlap and then terminate along the basal surface. Characteristically, the infill of small isolated scours shows little lithological changes laterally and/or vertically.

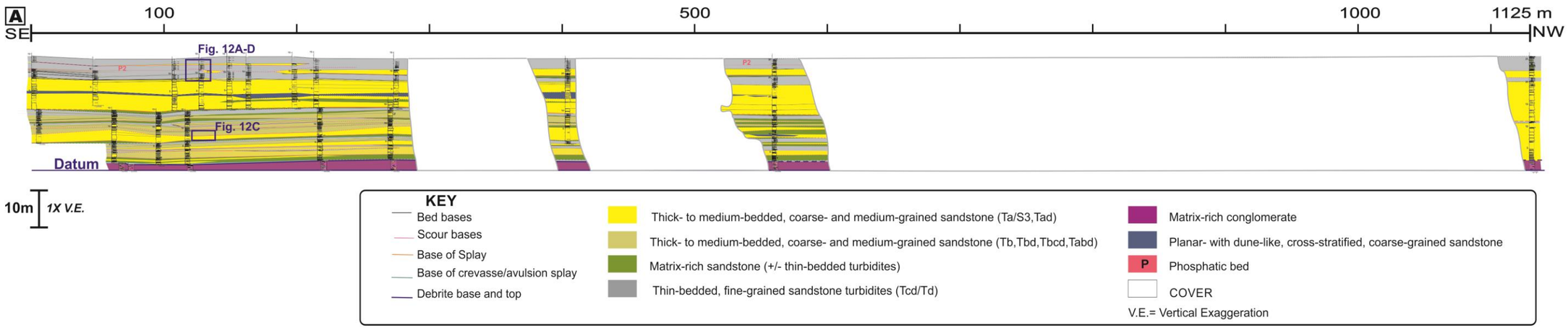

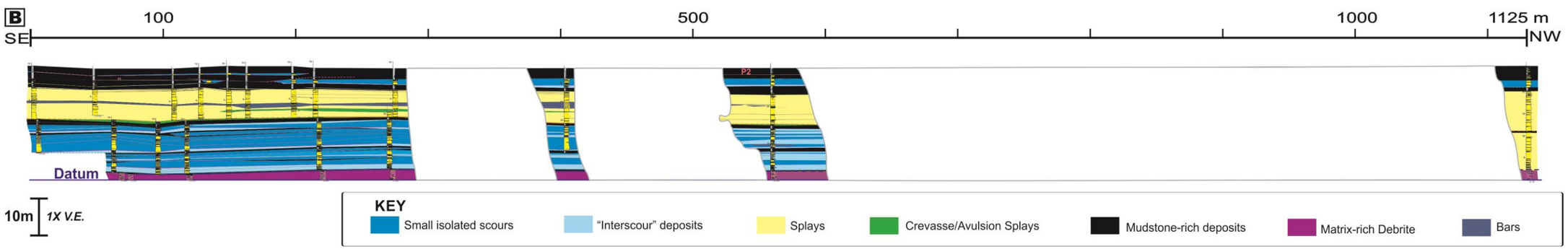

Figure 3.11. Isolated scours in the KIT. Interpreted correlation panel and stratigraphic columns documenting the (A) lithofacies, and (B) architecture of small scour deposits in the KIT. Location of these elements is shown on Fig. 3.3. Scour bases are indicated with fuchsia bold lines. In the lower part of the section, a laterally-extensive, up to 3 m matrix-rich debrite is overlain by an up to 15 m-thick and > 600 m wide unit comprising of numerous small scours. The scours are filled primarily with thick- and medium-bedded, planar-laminated sandstone, and minor structureless coarse-grained sandstone. Locally intercalated between the scours, thin to medium beds of fine-grained turbidites, and matrix-rich sandstone are present. The lower scours are overlain by an up to 9 m thick terminal splays. In the upper part of the section, few small isolated scours are encased within thin-bedded turbidites.

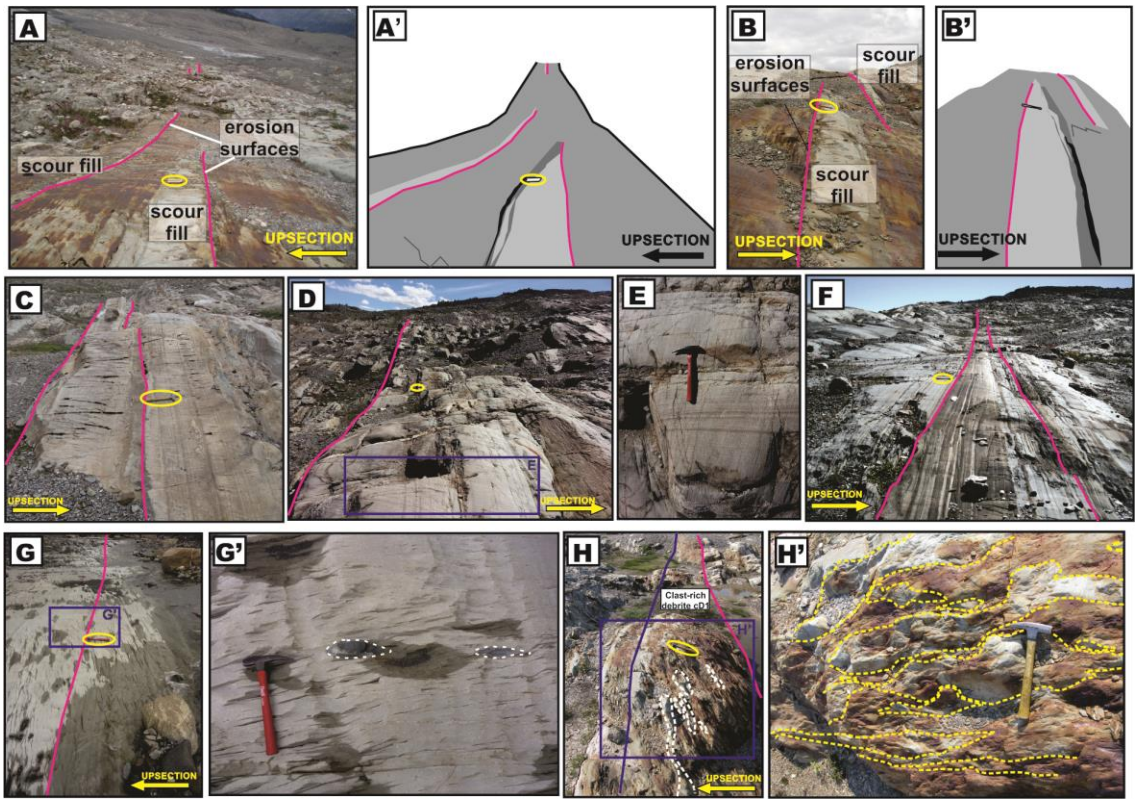

Figure 3.12. Isolated scours and their fills. Scour bases and tops are highlighted with fuchsia lines. (A, B-A',B') Two isolated scours encased within an up to 7 m thick unit of rusty-weathered, reddish brown thin-bedded, fine-grained turbidites (TBT). Scours are erosionally-based and filled with thick-bedded, coarse-grained sandstone. The scour (in the center of the photo A,B) is capped by claystone and a rare phosphatic claystone bed. A and B with yellow notebook and hammer for scale, respectively. (11A and 11C capture the same scours but are taken from opposite directions). (C-F) Isolated scour solely filled with amalgamated beds of parallel-laminated, coarse- and very coarse-grained sandstone. In E, planar laminated strata exhibit brown-coloured carbonate cementation. Hammer for scale. (G-G') Rare isolated scour within mudstone-rich deposits. Note lineations oriented from lower right to upper left are tectonic cleavage. The fill of the scour is lithologically similar to the underlying strata, and is identified only by a horizon of isolated, well-rounded, pebble- and cobble-sized (up to 10 cm-diameter) black (phosphatic?) clasts, that locally become clustered (white dotted line in photo inset 11F). (H-H') Rare isolated scour, mantled by clast-rich debrite. This debrite is recognized by brown-stained (locally sheared) mudstone matrix and embedded boudinage-like sandstone clasts (in H', some are delineated by dashed yellow lines), reflecting disruption and stretching during initial emplacement of the debris flow. Top of the debrite is indicated by blue line.

3.5.3.2 Large scours

At the Castle Creek area, large scours are rare, including one large amalgamated scour in the KIT (Fig. 3.13-3.15), and one large isolated scour in the LIF (Fig. 3.16).

In the KIT, large amalgamated scour is up to 12.5 m thick and extend beyond the limits of the outcrop (>600 m). Unlike isolated scours (previous section 3.5.3.1), it comprises several smaller (<5 m deep) erosively-based features, in which some of their bases are locally overlain by mudstone-clast breccia (F3), or well-rounded, boulder-sized sandstone clasts (Fig. 3.14G). The smaller scours are filled mostly with thick, graded granule conglomerate and very coarse- and coarse-grained sandstone with common sub-cylindrical (<1cm wide and 10-cm long), dewatering pipes (F1 and F2a, respectively; Fig. 3.3C) at their tops. In the axial part of this laterally-extensive erosional feature, these smaller scours are amalgamated but laterally become separated by up to 0.4 m thick layers of thin-bedded turbidites (F5) with occasional interbeds of medium-bedded, medium-grained sandstone (F2).

In the LIF, a unique large isolated scour can be confidently traced for >1200 m. This large scour was scarcely, patchy and unevenly filled across its composite erosion surface. It exhibits rapid lateral variations in thickness (ranging from few cm up to <1.9 m) and facies (Figs. 3.15-3.16), including discontinuous layers and/or lenses of thin-bedded, laminated and rippled cross-laminated, medium- and fine-grained, calcareous sandstone and/or mudstone (F4a,b and/or F5a), and medium-scale dune-like cross-stratified conglomerate (F4b). , quartz-rich granule conglomerate

with variable proportion of up to 17 cm-long mudstone and carbonate clasts (F1) and mudstone-clast breccia (F3).

Large scours tend to be underlain and/or overlain by numerous small isolated scours. For instance, abruptly overlying the large amalgamated scour, an up to 19m thick lithologically-complex unit of small isolated scours is observed. These scours are typically filled with m-thick, coarse-grained sandstone (F2a), except for one scour filled with clast-rich debrite (F8b). Rarely, a horizon of dm-thick bars (Fig. 3.35, see section 3.5.8) is also locally observed within this unit. The large isolated scour is intercalated between small isolated scours, but filled mostly with up to m-thick, medium-grained calcareous sandstone (F2b and F4b).

Interpretation

Owing to significant improvements in sidescan sonar resolution and more deeply penetrating seismic techniques, deep-water scours have been increasingly recognized as common features in many modern turbidite systems, especially in the channel-lobe transition zone, or CLTZ (e.g. Wynn, 2000; Wynn et al., 2002; Duarte et al., 2010; Macdonald, 2010; Macdonald et al., 2011). In these studies, scours are reported to be fields of multiple (tens to hundreds) isolated scours, that are 5-20 m deep and 80-6000 m wide, or as broad (up to 3 km wide) zones of amalgamated scours. Scours are typically irregular- or flat-based, and exhibit a range of morphologies, from erosional lineations (or linear scours) to spoon-, crescentic-, chevron-, heel- and oval-shaped erosional features. Although high-resolution images of these features are good, core control is poor (e.g. Wynn et al., 2002).

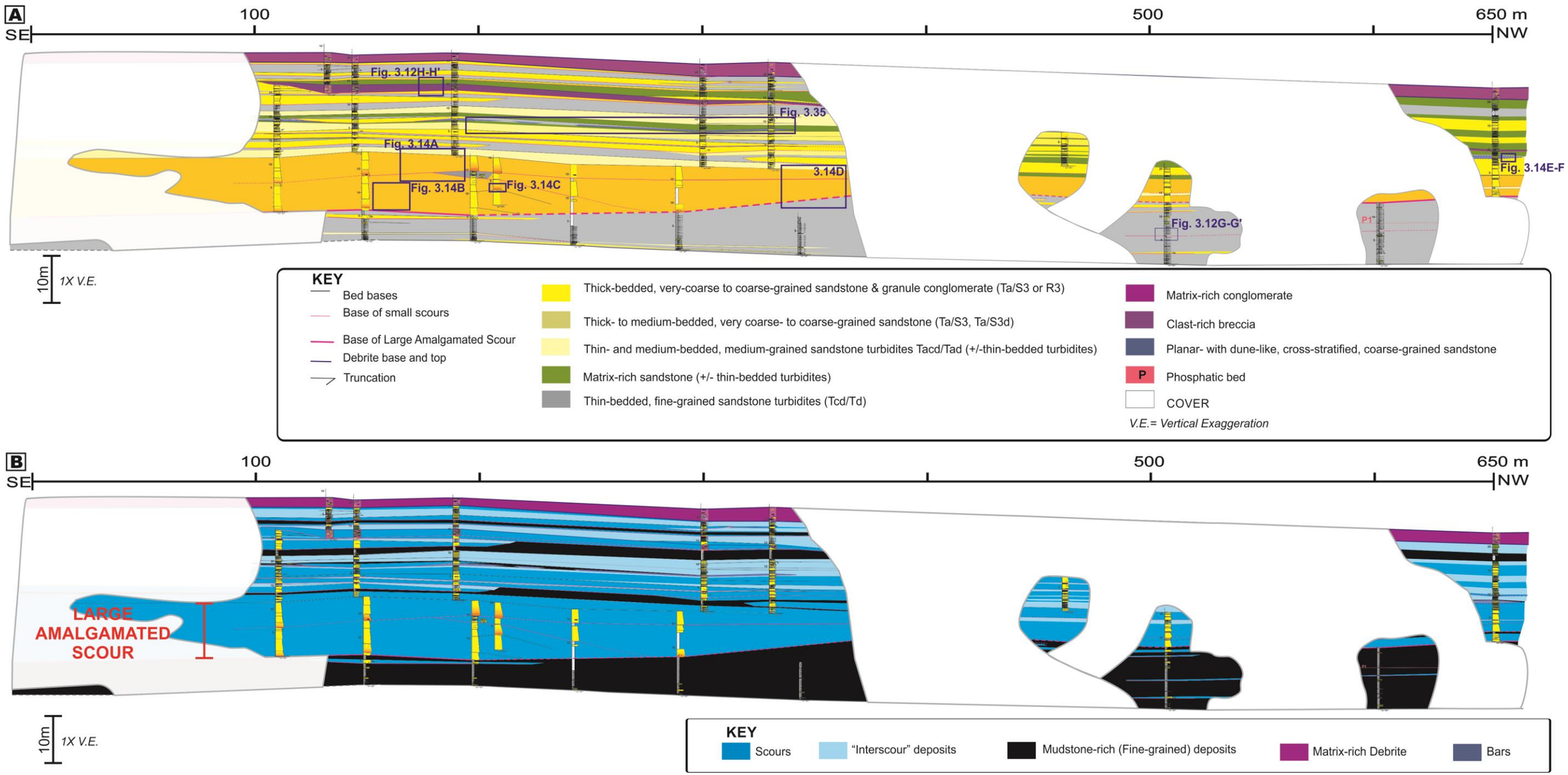

Figure 3.13. Amalgamated Scour in the KIT. Correlation panel and stratigraphic columns documenting the (A) lithofacies and (B) architecture of large and small scours and their fills. Location of these elements is shown on Fig. 3.4. Scour bases are delineated by fuchsia lines. Deeply incised into an up to 13 m thick mudstone-rich deposits, the large scour includes several small scours that become amalgamated toward the SE, and are filled with very coarse-grained sandstone and conglomerate. Above the large scour, a unit comprises numerous small scours encased between interscour deposits consisting of thin-bedded turbidites and medium-grained sandstone with variable matrix content. One scour is uniquely infilled with clast-rich debrite. At the top of the section, a matrix-rich debrite evenly blanketed the entire area. See Fig. 3.9A for legend of sedimentary logs.

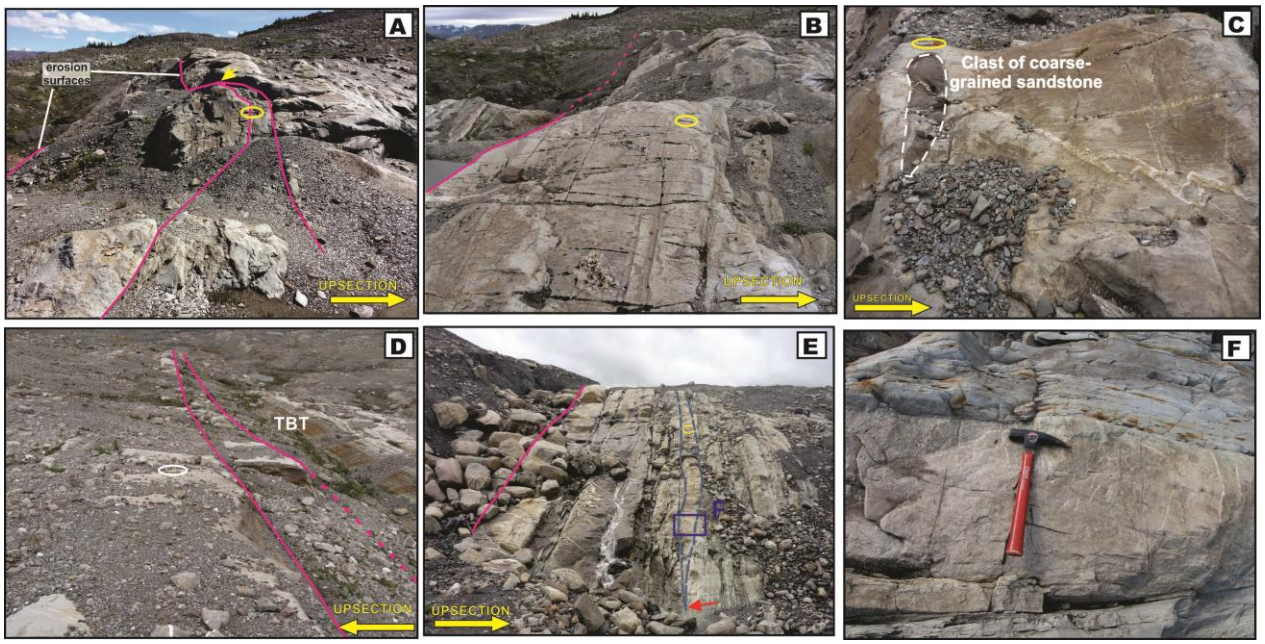

Figure 3.14. Amalgamated Scour and filling. Scour bases are marked by fuchsia lines. (A-B) The lower unit of this amalgamated scour is up to 12.5 m deep and comprises several nested erosively-based scours, that locally can be amalgamated (yellow arrow in B). Scour fills are predominantly thick-bedded, amalgamated very-coarse sandstone and granule conglomerate. Hammer for scale. (C) Rare, well-rounded, coarse-grained sandstone clasts are observed near the base of some scours (clast enclosed with white dotted line). 15 cm-long pencil marker for scale. (D) Scours tend to exhibit abrupt thinning toward their margins (hammer as scale). (E-F) Toward the NW outcrop exposures of the lower unit of the largest scour (i.e. scour margins), scour fills are still composed of thick bed of very coarse- and coarse-grained sandstone. The upper unit of scour consists of coarse grained-filled small scours intercalated with thin- to medium-beds of fine-grained turbidites, medium-grained sandstone, and matrix-rich sandstone. A horizon of hydraulic-jump bars comprising of planar- to high-angle cross-stratified sandstone (under the hammer, lightly highlighted with yellow dotted lines) is also observed within the unit. In F, the high-angle cross-stratified sandstone extends laterally over tens of meters before thinning and then pinches out (red arrow). Hammer for scale.

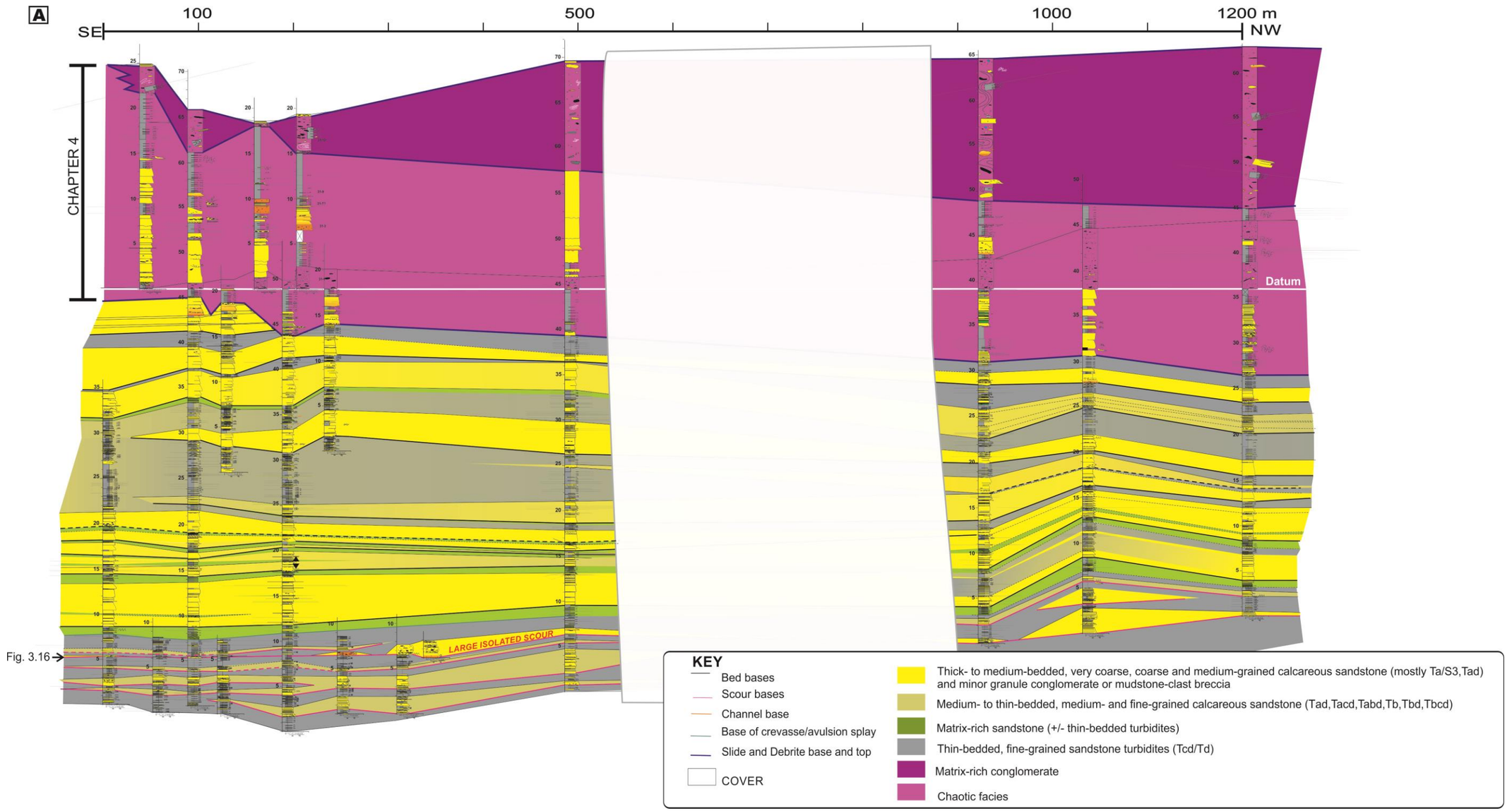

Figure 3.15. Architecture of isolated scours and vertical-stacked distributary channels in the Lowermost Isaac Formation. Interpreted correlation panel, showing the distribution of (A) lithofacies of small and large isolated scour and vertical-stacked distributary channel deposits.

Continuation of Fig. 3.15.

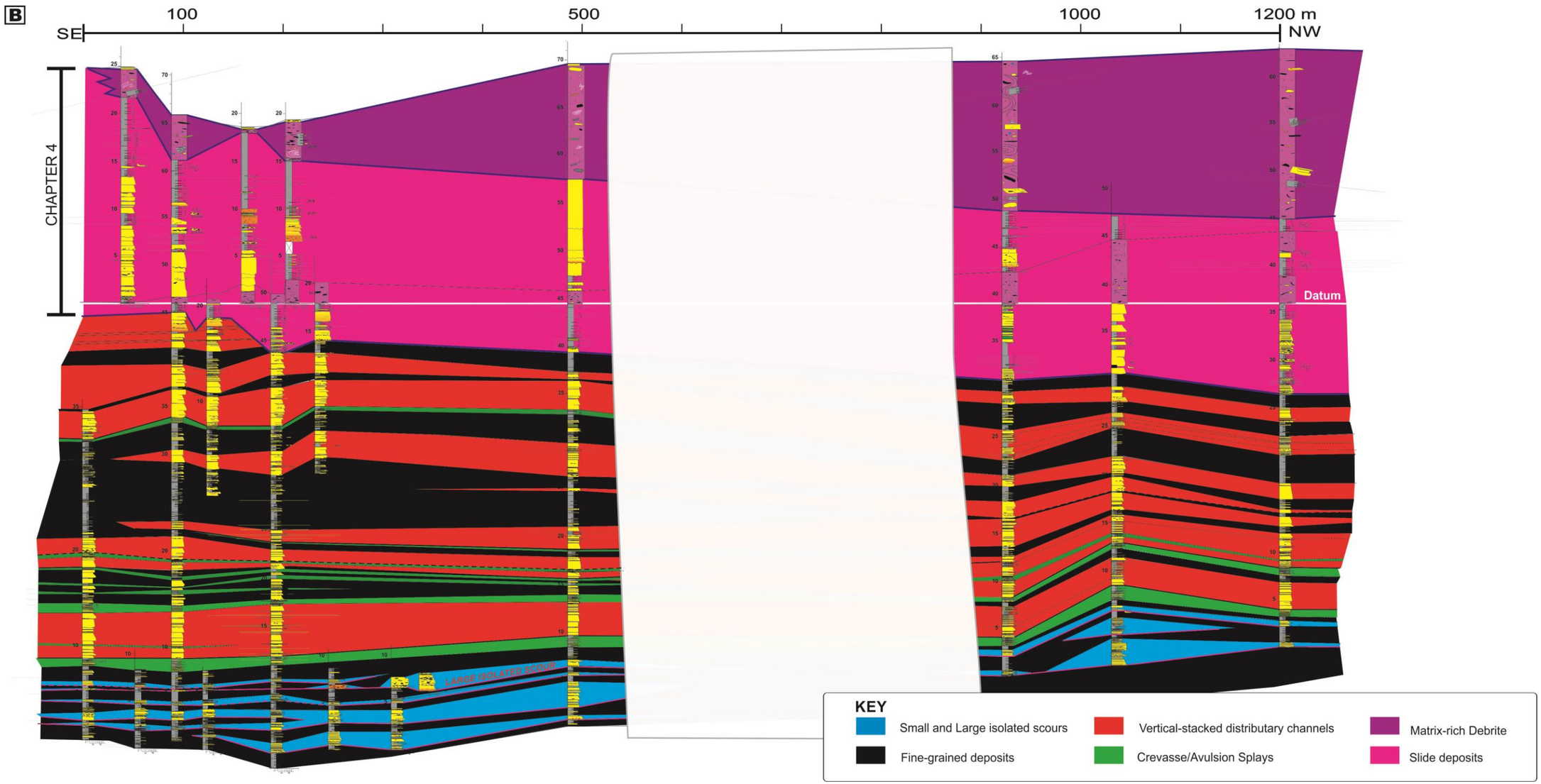

Figure 3.15 (Continued). (B) Architecture of small and large isolated scour and vertical-stacked distributary channel deposits. The top of Dm-thick unit of distributary channels is incised by Isaac mass-transport complex 1, consisting of slide and debris flow deposits.

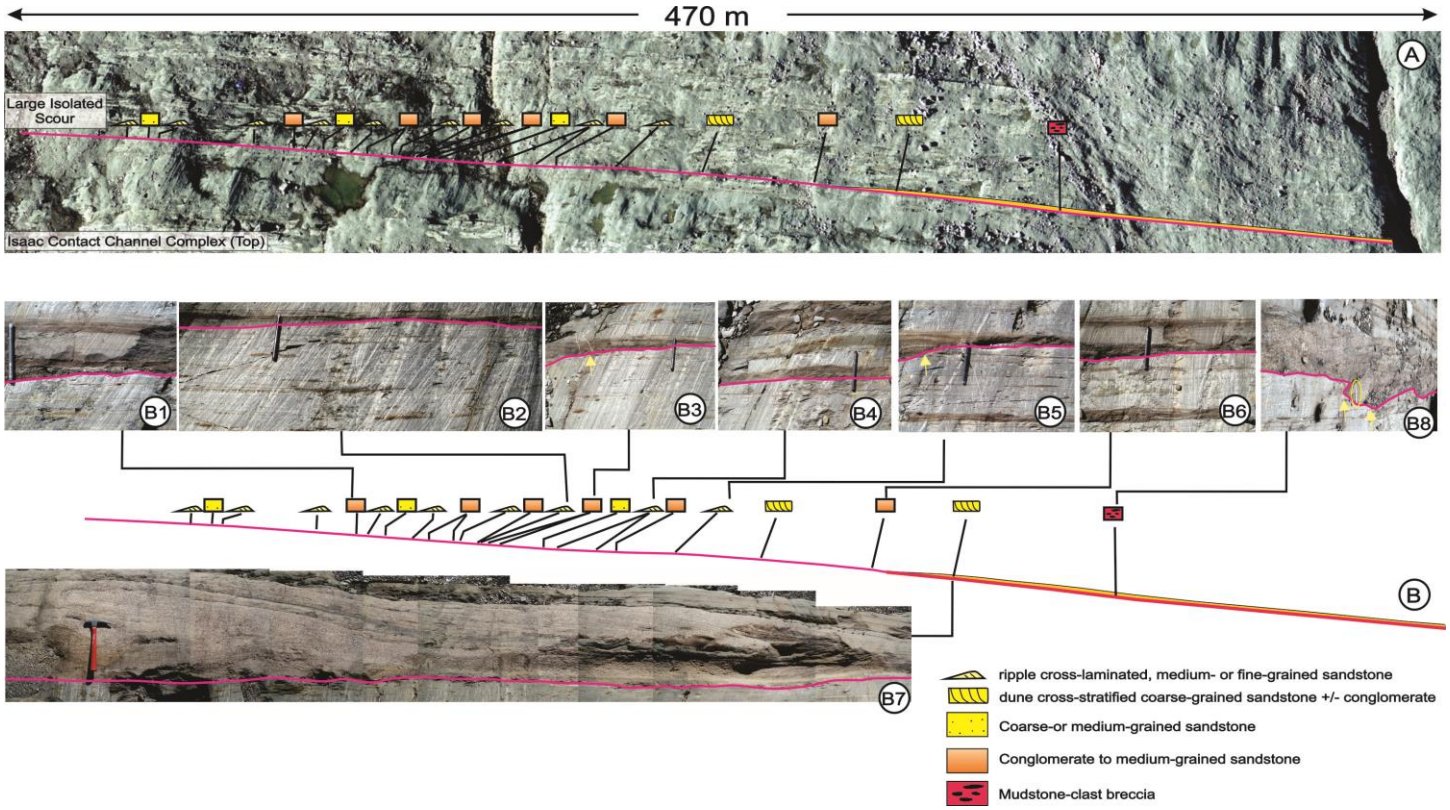

Figure 3.16. Large Isolated scour in the Lower Isaac Formation. Scour base is highlighted with fuchsia line. (A) Photomosaic of part of the scour, showing the continuity of the outcrop and impressive exposure of the scour-filling deposits across the area. This scour is encased within thin-bedded, fine-grained turbidites, consisting of intercalated, reddish brown, carbonate-cemented sandstone and grey mudstone. (B) Laterally, above the basal composite erosional surface, the scour is unevenly filled with a diverse array of facies, including coarse-grained sandstone, conglomerate, cross-laminated sandstone, cross-stratified coarse-grained sandstone or conglomerate, and mudstone-clast breccia. In photos B1-B8, yellow arrows indicate truncation. (B1-B6, pen marker for scale, B7 with hammer for scale, and B8 with 15 cm-ruler for scale, respectively).

Analogous to modern scours, scours interpreted from the ancient channel-lobe transition zone sedimentation record are small in number, including those in the Carboniferous Ross Formation of western Ireland (Chapin et al., 1994; Elliott, 2000a; Lien et al., 2003), the Albian Black Flysh of northern Spain (Vicente Bravo and Robles, 1991, 1995), and Lower Eocene Charo/Arro Canyon mouth of the southern Spanish Pyrenees (Millington and Clark, 1995), the Tertiary Piedmont basin in northwest Italy (Cazzola et al., 1983/ 1984), the Eocene-Oligocene Annot Sandstone in the French Alps (Hilton, 1995; Morris and Normark, 2000), Los Molles Formation in Neuquén basin in Argentina (Tudor, 2014), Cretaceous Tres Pasos Formation in Chile (Pemberton et al., 2016), and the Permian Ecca Group in the Karoo basin in South Africa (Hofstra et al., 2015). In these outcrops, erosional scours are generally shallower and narrower (1-5 m deep and 5-50 m wide) than the modern counterparts (Fig. 3.17), and are characterized by a scoured basal surface and a fill of amalgamated sandstone beds. Mud-draped scours are also reported (Mutti and Normark, 1991; Mutti, 1992).

The scour-and-fill elements described from the KIT and LIF are interpreted to be similar in dimensions (Fig. 3.17) and lithological make-up to those reported from many modern and ancient CLTZs (e.g. Wynn, 2000; Wynn et al., 2002; Duarte et al., 2010; Macdonald, 2010; Macdonald et al., 2011). These scours, like those in other transition zones, are interpreted to have formed immediately downflow of the terminus of slope channels as they debouched onto the proximal part of the basin floor (e.g. Mutti and Normark, 1987, 1991; Morris and Normark, 2000; Wynn et al., 2002). After exiting the channel (or canyon), turbidity currents experience an abrupt

change from confined to unconfined conditions, which coincides also with marked reduction in slope. This results in increased of turbulence and, in turn, intense seafloor erosion associated with highly unsteady and rapidly spreading wall jets (Hoyal et al., 2003; Alexander et al., 2008), and hydraulic jumps (Macdonald et al., 2011; Sumner et al., 2013). This, therefore, promotes the formation of an assortment of variously sized scours within the transition zones.

The basal erosion surface of small isolated scours are interpreted to be carved by large, turbulent eddies within the turbidity currents, that unsystematically incise the most proximal basin floor region, as soon as flow confinement decreases drastically at the channel mouth (Hoyal et al., 2003; Alexander et al., 2008). Turbidity currents may also undergo a hydraulic jump, but at different spatial locations within the CLTZ, forming additional scours as well. Based on direct observations of hydraulic jumps in active submarine density or turbidity currents, Sumner et al. (2013) proposed that the currents tend to form a region of scattered hydraulic jumps with strong vertical velocities, and the observed jumps are closely linked with the distribution of seafloor scours.

Overall, after they are created, scours become localized erosional features where the passage of one or many bypass flows occurred, until they are eventually draped and filled by a limited number of successive net depositional flows (e.g. Normark et al., 2009; Macdonald et al., 2011).

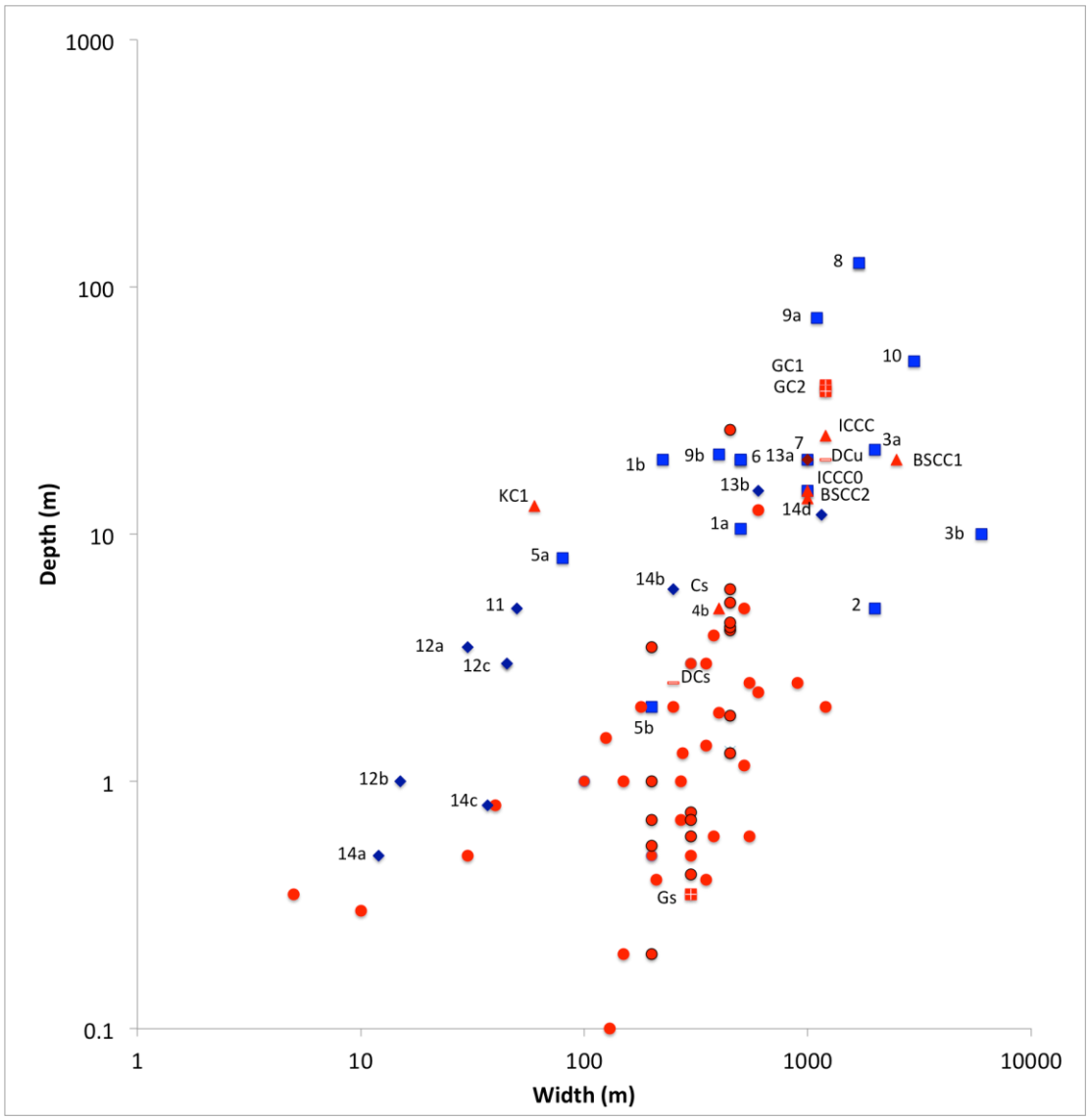

Scours in modern CLTZs (blue squares): *1- Agadir Channel Mouth* (1a- Wynn et al., 2002; 1b- Macdonald et al., 2011); *2-Umnak Channel mouth, Bering Sea* (Kenyon and Millington, 1995); *3- Setubal Canyon Mouth* (3b- Wynn et al., 2002; 3a- Macdonald et al., 2011); *4- Rhone Fan* (4b- Kenyon et al., 1995; 4a- Wynn et al., 2002); 5- Valencia channel mouth (5b-Morris et al., 1998; 5a-Wynn et al., 2002); *6- Navy Fan* (Normark et al., 1979); 7-Var Canyon Mouth (Migeon et al., 2001); *8- Makran Canyon Mouth* (Bourget et al., 2010); *9- New Jersey and Californian base of slope* (9a, 9b- Lee et al., 2002)(9a; 9b-Lee et al., 2002); *10- Horseshoe Valley* (Macdonald et al., 2011); Scours in ancient CLTZs (dark blue rhombs): *11- Albian Black Flysh* (Vicente Bravo and Robles, 1995); *12- Ross Formation, Ireland* (12a- Chapin et al., 1994; 12b- Elliott, 2000b; 12c- Macdonald et al., 2011); 13- *Karoo basin, South Africa*: 13a-Tanqua depocentre, 13b-Laingsburg depocentre (Hofstra et al., 2015); *14a-d- Tres Pasos Formation, Chile* (Pemberton et al., 2016); *Kaza-Isaac transition and Lower Isaac Formation, Canada* (this study) *Small and Large Scours*- red circles; *Channel Complexes (Cs-single channel; KC1-Kaza Channel 1, ICCC-Isaac Contact Channel Complex; ICC0-Isaac Channel Complex 0; BSCC1-Bacon Sandstone Channel Complex 1; BSCC2-Bacon Sandstone Channel Complex 2)*- red triangles; *Distributary channels (DCs- single distributary channels; DCu-units*

of stacked distributary channels) – red dash lines; *Gully-like features (Gs- single gully-like feature; GC1,GC2- Gully-like Complexes*)- red squares.

Figure 3.17. Comparison of dimensions (maximum width and depth) of deep-water scours in modern and ancient channel-lobe transition zones (CLTZs) reported. Note that dimensions in ancient examples, including those in the KIT and LIF (red circles), may be underestimated or overestimated, inasmuch as outcrop sections may not exposed the true maximum dimensions of these scours. Other channelized elements recognized in this study are also plotted, including channel complexes, distributary channels and gully-like features (represented by red triangles, red dash lines and red squares, respectively).

Macdonald et al. (2011) was able to evaluate, for first time, cores from within and outside of the same scours (i.e. intrascour vs. interscour deposits) within several modern CLTZs. Some of these scours are still completely free of sediments, but others are partly filled with thick muds, thin sands or debrites, whereas the interscour areas consist of sand-rich sediments, or of little or no depositional record. Nevertheless, analogous erosional features identified in the KIT and LIF greatly help to document the nature of scours and infilling in an ancient example.

Many small scours in the study area are typically infilled with thick-bedded, structureless very coarse- to coarse grained sandstone or occasional granule conglomerate (Figs. 3.13, 3.22, and 3.24), which are interpreted to be from deposition of rapidly collapsing, high-concentration turbidity currents, in response to the slope break and loss of confinement (e.g. Kneller and McCaffrey, 1999; Huang et al., 2009b; Cantero et al., 2012). However, some scours are instead infilled with planar-laminated sandstone beds, which are deduced to be medium- or coarse-grained lag deposits from largely bypassing flows (Figs. 3.11, 3.15, and 3.25). In a rare case of a small scour consisting of locally-clustered black clasts along its base (Fig. 3.20) and

overlying thin-bedded turbidites (cf. mud-draped scours of Mutti and Normark, 1991; Morris and Normark, 2000), it is inferred that this scour was filled from waning-depletive fine-grained turbidity flows.

Finally, a scour filled with clast-rich debrite (Fig. 3.13) is supposed to be originated from sediments of lower slope settings that were remobilized and later deposited within the scour. Based on the compositional similarity of abundant angular clasts in these clast-rich debrites and strata that make up most of the KIT, these debris-flow deposits confirm to be the product of local submarine mass movements (e.g. slide or slump) that had short run-out distances. These flows evolved and transformed rapidly into clast-prone debris flows, which in turn probably reflects a poorly consolidated, mechanically-weak parent sediment mass. Moreover, the intense remoulding of primary bedding into lensoid (boudinage-like) intraclasts and sheared matrix reflect the extensive internal shear and extension during their movement (e.g. Strachan, 2008; Tripsanas et al., 2008; Ogata, 2010).

Strata separating small scours are dominated by fine-grained turbidites, as well as medium-grained (matrix-poor) sandstone and/or matrix-rich sandstone beds (Figs. 3.11, 3.13, 3.15, 3.22, 3.24, and 3.25). They are interpreted to be deposited laterally alongside of the scours, analogous to interscour deposits of Macdonald et al. (2011). Outside the active scours, finer sediments including medium sand grains to mud tend to settle. This resulted in deposition of fine-grained turbidites and medium-grained sandstone from low- to intermediate- concentration turbidity flows. Matrix-rich sandstone beds indicate deposition from flows that experience local hydraulic jumps or that spread out along the margins of a jet flow. When the flows become

locally charged with mud, they then instantaneously collapsed laterally, and matrix-rich sandstone were progressively accumulated.

The two rare large amalgamated and isolated scours in the study area (Figs. 3.13, and 3.15) are comparable in dimensions to those large amalgamated and isolated scours described by Wynn et al. (2002) and Macdonald et al. (2011). The mentioned modern examples are interpreted to represent long-lived erosional features, that are several tens of meters deep, up to 9 km wide and preferentially occur immediately downflow of the mouth of slope channels (Wynn et al., 2002). Alternatively, the laterally-extensive erosional features here may represent erosional channels, but problematically they do not exhibit the predictable lateral change in grain size, lithofacies and bed thickness and amalgamation from axis to margin commonly recognized in deep-water channels (e.g. McHargue et al., 2011). The bases of large scours are interpreted to be composite surfaces formed by erosion and bypass of numerous large-volume turbidity flows (Fig. 3.18A). These surfaces, thus, indicate a long-term, active site of widespread erosion and bypass. For instance, some scours downstream from the Agadir canyon mouth have been active for at least >200 ka (Macdonald et al., 2011).

The large amalgamated scour in the KIT comprising of amalgamated conglomerate- and sandstone-filled small scours suggests recurring episodes of scouring and filling, and possibly coincided with high sediment volume and caliber, and sand:mud ratio (Fig. 3.18A). Common dewatering structures in strata filling these small scours resulted from deposition of rapid collapsing flows. This large amalgamated scour is then overlain by a complex succession of isolated sandstone-

filled scours surrounded into finer-grained, but still sand-rich strata indicates gradual abandonment of the scour region (Fig. 3.18B). Here, sediment volume and sand:mud ratio within the flows decrease, resulting in a more common deposition of thin-bedded turbidites and medium-grained sandstone with variable mud content. The abandonment of the scour region is interpreted to be a prolonged event, allowing the localized deposition of atypical facies or facies assemblages. The one isolated scour rarely filled with clast-rich debrite (Fig. 3.18B) here might be analogous to debris flow deposits filling scours in some modern CLTZ, which were from margin failures along modern canyon or channel mouths and were deposited within the scours during their deactivation (Macdonald et al., 2011).

The occurrence of boudinage-like clasts of sandstone embedded in this debrite supports the interpretation of a local slope instability and short distance transport. Locally (also above the large amalgamated scours), a horizon of bars was developed (Figs. 3.13, and 3.14E-F; for details about bars, see section 3.5.8). The formation of these bars tends to occur downflow of hydraulic jumps. Wynn et al. (2002) have noted possibly similar (but relatively thicker) depositional features are also formed in areas of intense erosion in modern CLTZs.

In the LIF, thin and patchy deposition of assorted facies across the laterally-extensive isolated erosional feature is interpreted to be the remnants of numerous small scours that coalesced into a broad scouring area and were developed during numerous episodes of erosion and bypass, but limited deposition. Similar facies associations have been recognized in the base-of slope bypass zone or CLTZ, as close to the mouth of Agadir mouth (Stevenson et al., 2015).

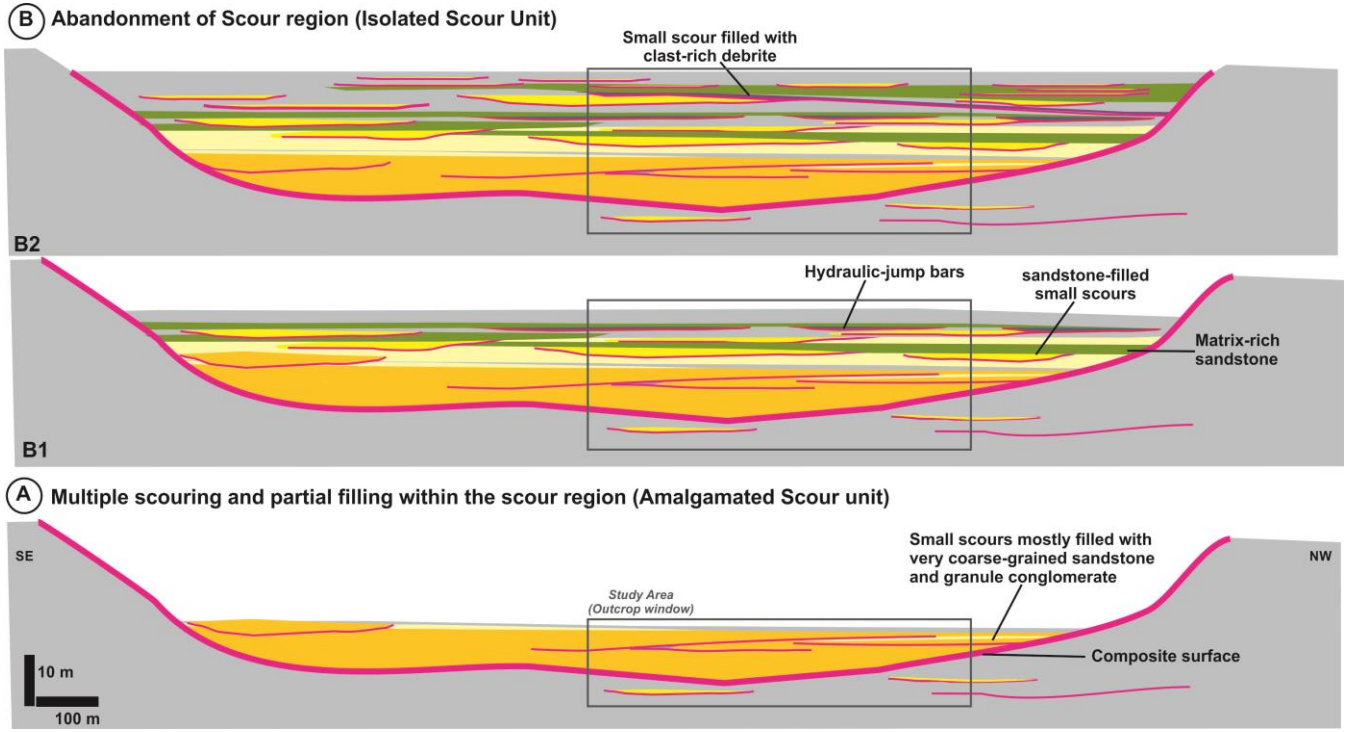

Figure 3.18. Simplified model for development of amalgamated scours in the lower KIT. (A) After the incision of a scour is initiated, numerous flows pass preferentially through this large-scale erosional region. During the most active scouring and depositional phase of the large scour region, several small scours were formed, and some even become amalgamated locally. Each small scour is demarcated by a basal erosional surface and filled with coarser strata (including very coarse-grained sandstone and granule conglomerate). (B1) During the abandonment phase of the large scour region, small scours become more intercalated with fine-grained deposits and/or matrix-rich sandstone beds. Locally, bars were also established. (B2) The scour region becomes considerably starved of coarse-sediments for extended periods. Scours filled with coarse-grained sandstone become significantly smaller, and deposition of finer sediments (fine-grained deposits and matrix-rich sandstone beds) becomes increasingly more common. Rarely, thin mass-transport deposits were filling a small scour.

Continuation of Fig. 3.18.

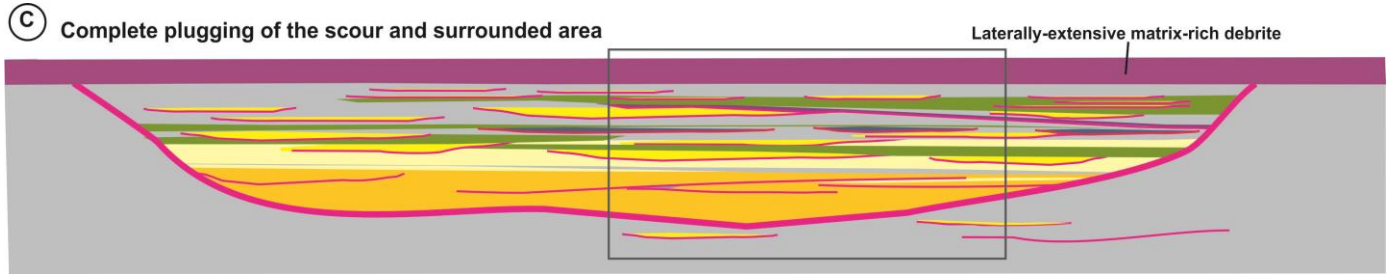

Figure 3.18. (Continued) (C) A major phase of mass-wasting deposition took place, plugging evenly the remaining scour relief.

3.5.4 Distributary channels

Distributary channels are observed at various stratigraphic levels within the KIT and LIF (Fig. 3.4). Where present, they overlie sandstone-rich splays or mudstone-rich deposits (see sections 3.5.5 and 3.5.6, respectively). It is not uncommon for these channels to be locally separated by debrites, scours or bars (sections 3.5.1, 3.5.3 or 3.5.8). Compared to channels or scours (sections 3.5.2 and 3.5.3), distributary channels are more shallowly incised and thinner. They typically exhibit little change in facies vertically, except near their tops, but they do have well-defined lateral variation in facies and bed de-amalgamation from axis to margins. Based on differences in stacking pattern, erosional basal surfaces, facies distribution, and channel geometry and margin terminations, two end-member kinds of distributary channels have been recognized: nested and vertically-stacked.

3.5.4.1 Nested distributary channels

Nested distributary channels are observed exclusively within the KIT (Figs. 3.19-3.23). These are composite features made up of multiple smaller-scale channels, each of the order of <2-3 m deep (some as little as <1 m) and up to 300 m wide (Fig. 3.19A). Channels are erosionally-based, and filled in their lower part by one to a few dm- to m-thick, amalgamated beds of structureless, coarse- and very coarse- grained sandstone and granule conglomerate, which are equivalent to Ta/S3 and R3 divisions (F2a and F1 respectively, Figs. 3.20A-B). Some beds are capped by ripple or dune-cross-stratified sandstone (Tc or F4b), and rarely by a discontinuous mudstone layer (Td). These thick, coarse-grained strata typically extend for tens to hundreds of

meters beyond the edge of the scoured base of the channel, giving the feature a wing-like geometry (Figs. 3.21A-A',B-C). Thereafter, beds tend to gradually fine, thin, and become less amalgamated, passing laterally into medium- to thin-bedded, medium- to fine-grained Tabcd/Tacd/Tbcd turbidites (F2b and F4- F5). In some cases, coarse-grained strata terminate abruptly because of scouring by overlying beds (Figs. 3.21D-D'). The upper part of the fill abruptly overlies the lower part and consists of medium- to thin-bedded, medium- to fine-grained sandstone Tbcd/Tcd turbidites (F2b and F4, and F5; Figs. 3.21B-B') that gradually thin and fine upward and laterally.

Individual erosively-based channels juxtapose vertically and laterally offset, and build up units that are up to 5-6 m thick and extend for more than 600 m laterally (Figs. 3.19B, 3.22A). In the lower part of the unit, composite channels are mostly amalgamated, but stratigraphically upward become less amalgamated and shallower. Moreover, these channels form a nested stacking pattern that in some cases appears to be compensational, although the two-dimensionality of the outcrops might make this interpretation equivocal.

A stack of nested channels is then abruptly overlain (i.e. the upper part of the unit) by an up to 3 m-thick succession of thin- and medium-bedded, medium- and fine-grained Tacd/Tbcd and Tcd turbidites (F2b-F4b, and F5). Medium-grained turbidites fine and thin over less than a hundred of meters laterally into thin-bedded fine-grained Tcd turbidites. Less commonly, dm-thick, lenticular beds of coarse-grained sandstone (Ta, F2a) are also intercalated within the succession. Discontinuous, coarse-grained, dune cross-stratified sandstone are also observed locally. Units are separated by an up to 2 m thick succession of thin-bedded, fine-

grained Tcd/Td turbidites (F5) that is traceable for at least 600 m laterally. Multiple units then stack to build up stratal elements that are up to 35 m-thick and more than 1200 m wide, and here are termed a sheet (Fig. 3.19C, 3.21F).

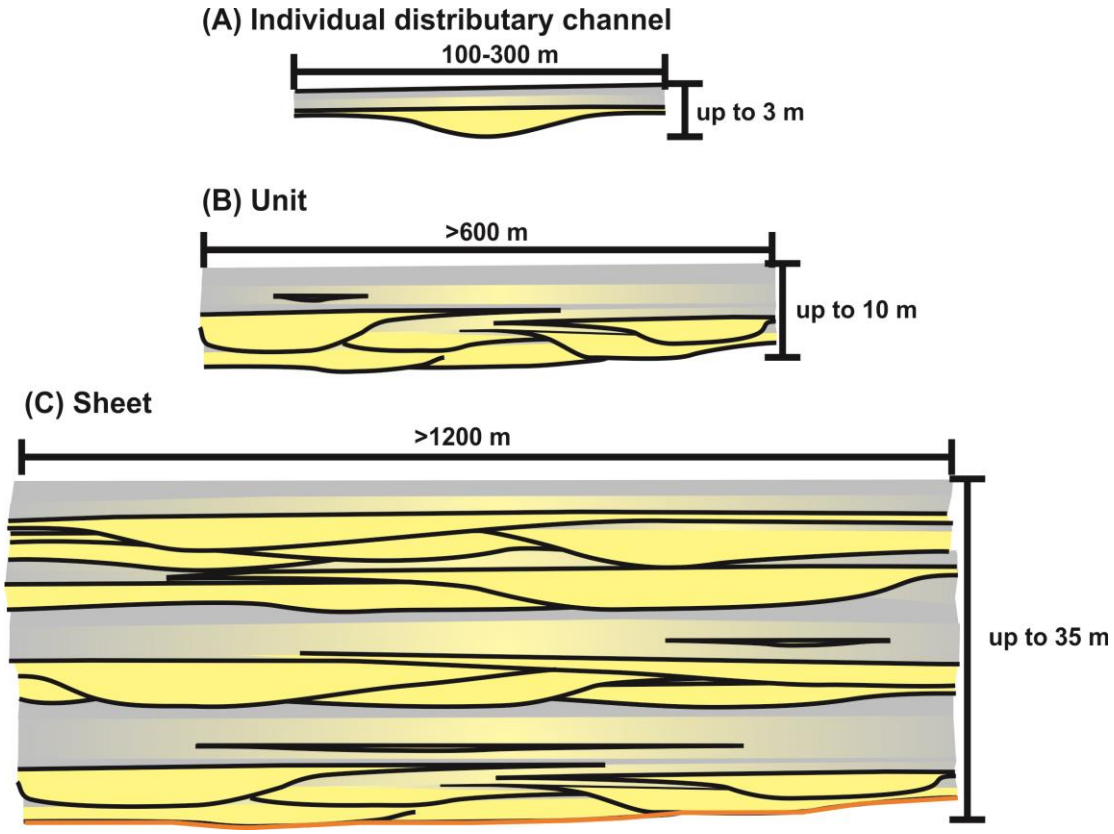

Figure 3.19. Idealized hierarchical classification scheme applied here to nested distributary channels. (A) A single type 1 channel is the lowest hierarchical order, which at its base is marked by a shallow scour overlain by a thin sandstone-dominated fill. Strata extend beyond the basal scour and gives the channel a wing-like geometry. Further laterally strata transition over a few tens of meters into thin-bedded turbidites. (B) A unit comprises multiple vertically and laterally stacked type 1 channels. In the lower part of the unit, channels are highly amalgamated. This, then, is abruptly overlain by a succession of medium- and fine-grained turbidites with local lenticular coarse-grained sandstone beds in the upper part of the unit. Units, in turn, are typically separated by an up to few meter-thick succession of thin-bedded, fine-grained turbidites. (C) A sheet is the highest hierarchical order and comprises multiple vertically-stacked units.

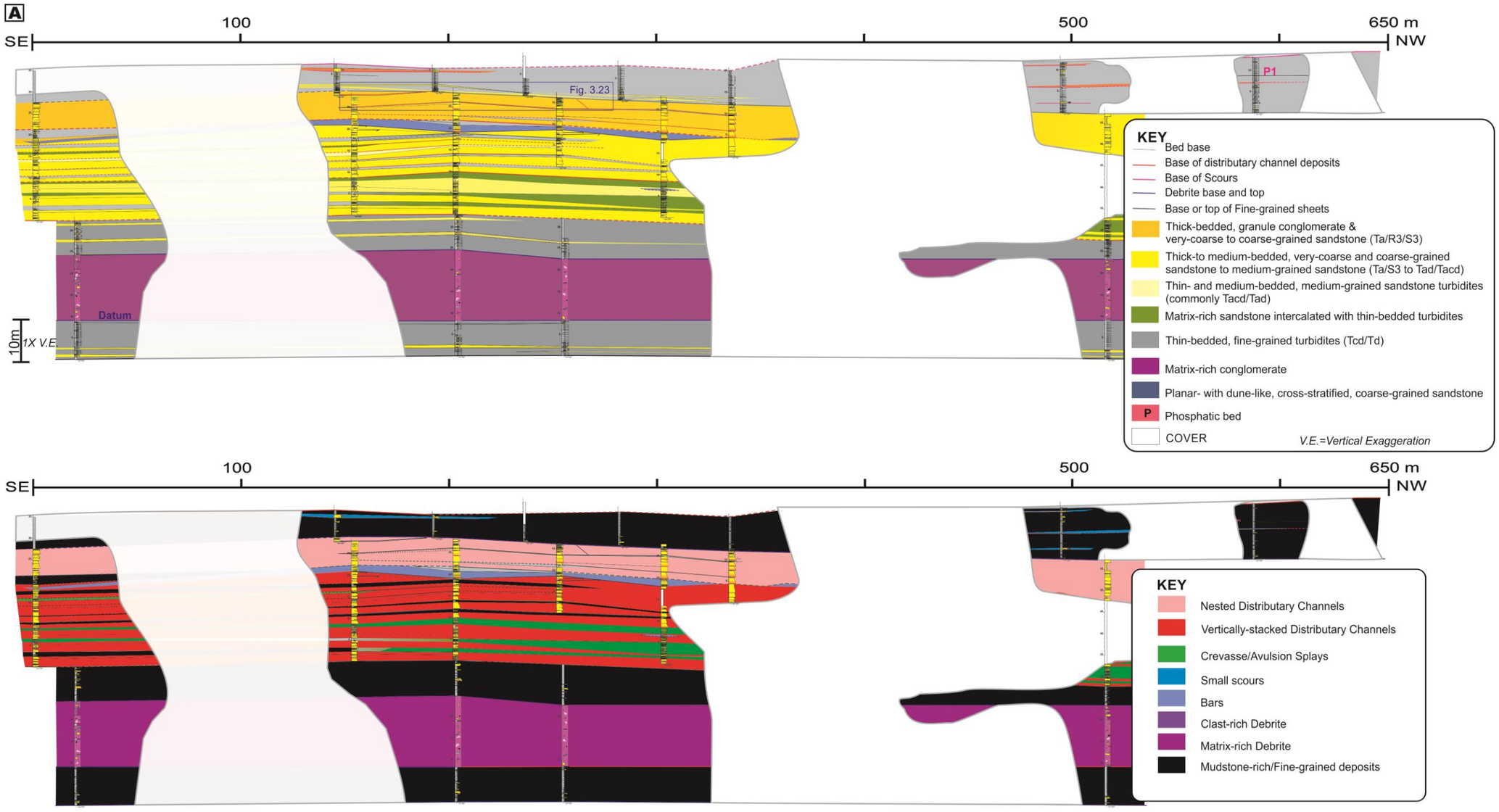

Figure 3.20. Nested and vertically-stacked distributary channels in the lower KIT. Cross-section panel with sedimentary logs illustrating (A) facies distribution and (B) architecture of both types of distributary channels. Vertically-stacked channels overlie fine-grained deposits, and are then directly overlain by a horizon of bars and nested distributary channels (see details in Fig. 3.36 and 3.23). See Fig. 3.9A for legend of sedimentary logs.

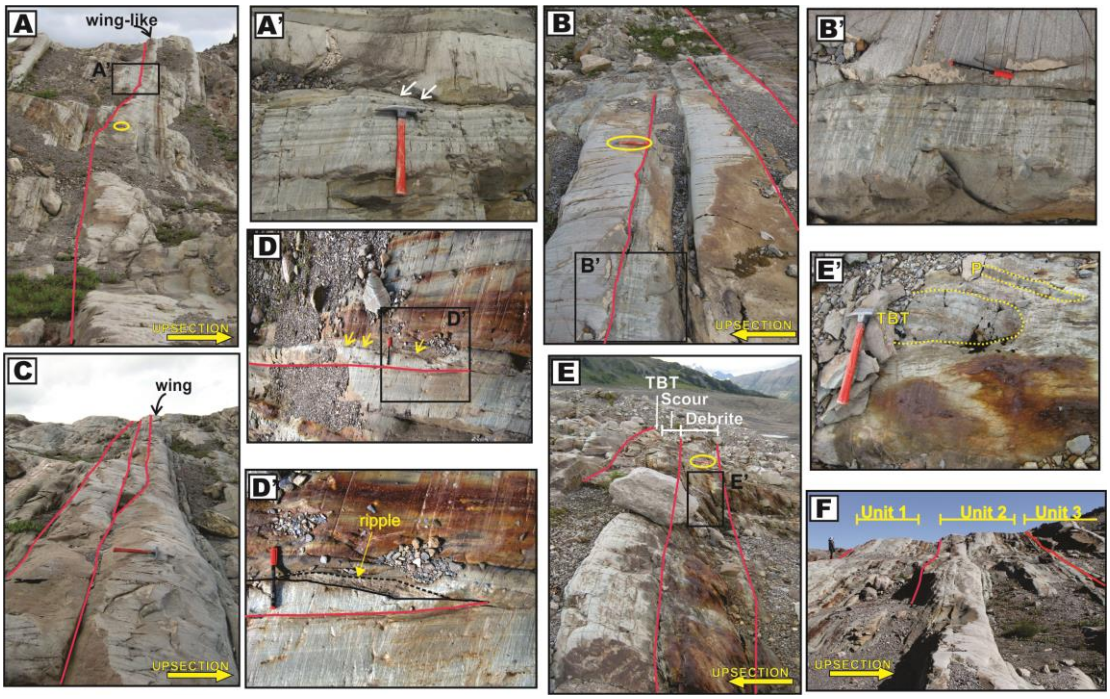

Figure 3.21. Representative photographs of nested distributary channels in the KIT. Red lines mark the scoured basal surface of individual channels. (A, A') A single, erosionally-based, low-relief channel filled with a thick, amalgamated, coarse-grained sandstone bed. This bed extends beyond of the edge of the basal surface, forming a wing-like geometry. A': Inset of A shows the truncation of underlying strata (indicated by white arrows). (B, B') The lower part of a unit consisting of three amalgamated channels, each filled with thick-bedded, structureless coarse-grained sandstone. B': Inset of B, at the top of one of channels, structureless and parallel-laminated medium-grained sandstone and mudstone are observed. (C). Three nested channels in which the uppermost channel exhibits a wing-like geometry. (D, D') Away from the channel axis, coarse-grained sandstone bed thin laterally, and they may be eroded by the overlying bed (ripple cross-laminated sandstone indicated by yellow arrow). (E, E') Scours and matrix-rich debrite are locally separating. E': Inset of E, the debrite with well-rounded clasts of thin-bedded turbidites and phosphatic beds (TBT and P, respectively). (F) Three vertically-stacked units comprising part of a sheet. Each unit is divided into a lower, amalgamated, coarser-grained sandstone-rich part sharply overlain by a less-amalgamated sandstone-rich upper part. Units are separated by dm- to m-thick succession of thin-bedded, fine-grained turbidites.

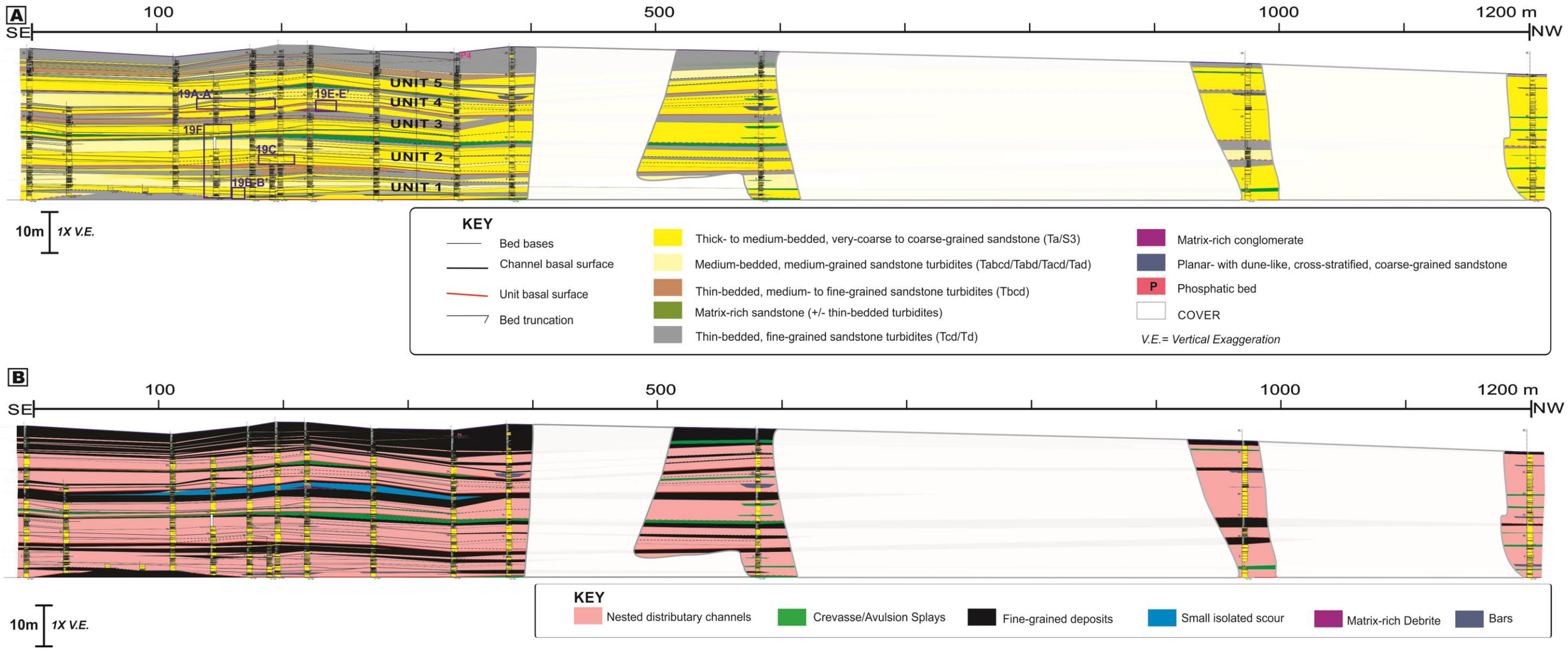

Figure 3.22. Nested distributary channels in the KIT. Schematic cross-section with sedimentary logs illustrating (A) facies distribution and (B) architecture of five depositional units comprised mostly by multiple nested distributary channels and variably continuous, thin-bedded fine-grained deposits. Local crevasse/avulsion splay deposits, scours and matrix-rich debrites are also present. Units stack vertically to form a thick "channelized" sheet.

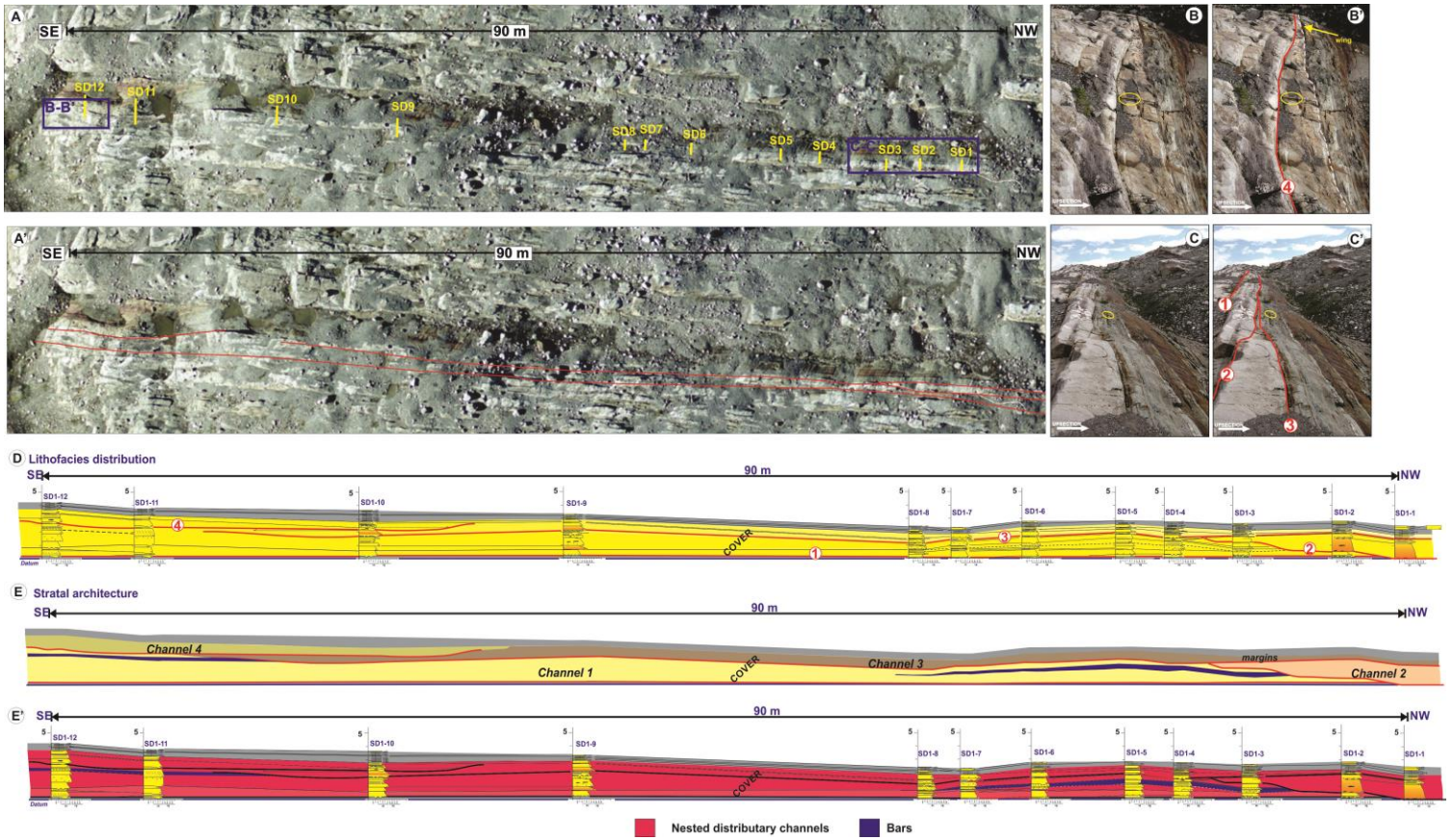

Figure 3.23. Vertical and lateral changes along a unit composed of four nested distributary channels in the KIT. (A) Aerial photograph showing location of measured stratigraphic logs. (A') Basal channel scours are indicated by red lines (B, B'; C, C') Photos and corresponding line drawings (in both hammer for scale) of the channel bases. In B, B' a coarse-grained bed thins dramatically (yellow arrow) toward the channel margin. (D) Correlation panel illustrating internal facies distribution in the channel fills. (E, E') Stratal architecture of the four nested distributary channels.

3.5.4.2 Vertically-stacked sandstone-rich shallow channelforms

At the Castle Creek study area, vertically-stacked distributary channels were previously recognized in the Upper Kaza Group by Rocheleau (2011) and Terlaky (2014). They are also common in the KIT and LIF (see Figs. 3.4, 3.15, 3.24-3.25). Channel bases are scoured with up to 4-5 m relief over 300-500 m laterally and filled by one or much more commonly several upward-fining beds. In the axis of the channel, strata consist mostly of thick-bedded, amalgamated, coarse- and very coarse-grained sandstone beds with local mudstone intraclasts, here termed F2a, or similarly Ta or S3 in the classification schemes of Bouma (1962) and Lowe (1982), respectively. Beds are capped by normally-graded, medium- to fine-grained Tb or Tc sandstone.

Laterally, strata change over <20 m into medium-grained, Tabcd/Tabd/Tacd turbidites (F2b, F4), and then, over an additional very short distance (<1 m) grade into thin-bedded, fine-grained Tbcd or Tcd turbidites (F5; see Figs. 3.26-27). In addition to the lateral facies change, some coarse-grained (Ta) beds in the channel axis become increasingly laterally more intercalated with thin-bedded Tcd turbidites and/or Tabcd/Tacd turbidites (F5a and/or F2a), that similarly thin and fine laterally. At their top, channel fills are commonly overlain by a several/few dm (up to <2 m)-thick unit of thin-bedded Tcd turbidites intercalated with uncommon medium- to thin-bedded Ta/Tb/Tbc turbidites. In the LIF, vertically-stacked sandstone-rich shallow channelforms are typically filled with calcareous or carbonate-cemented sandstone beds.

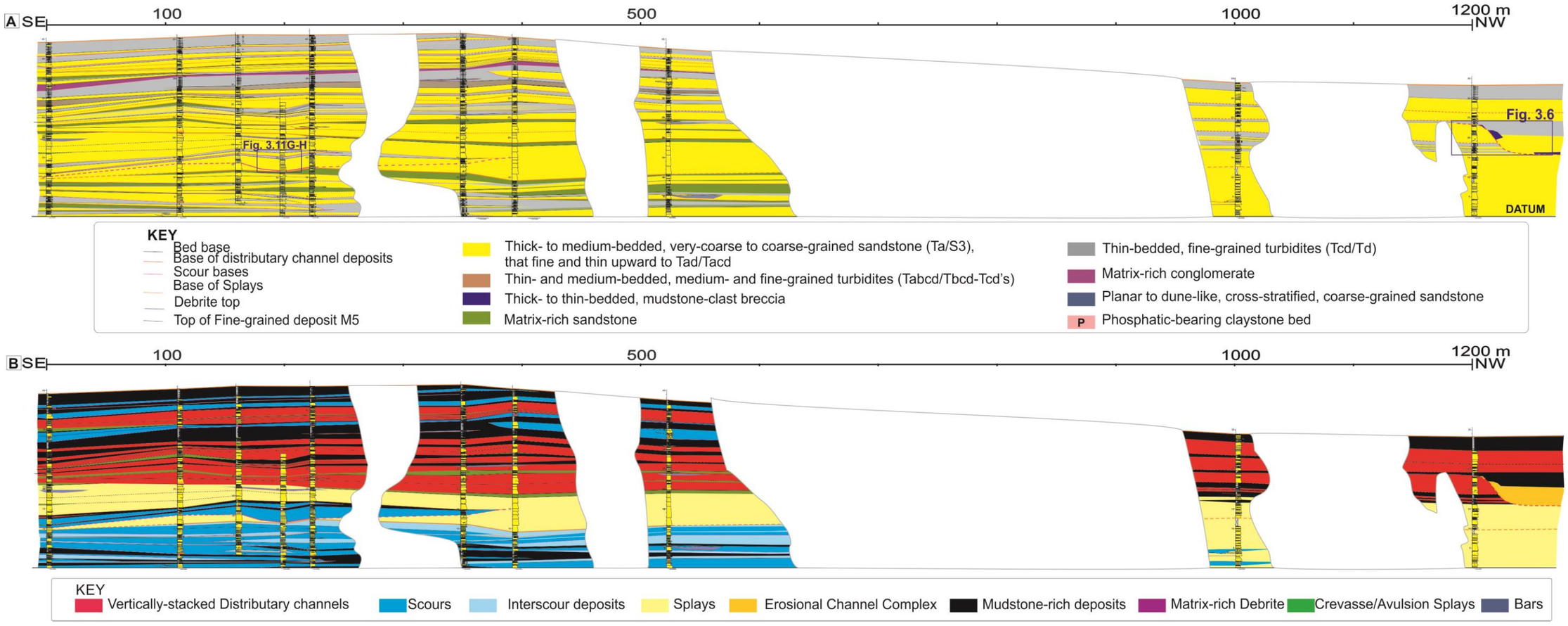

Figure 3.24. Vertically-stacked distributary channels in the upper part of KIT. A thick unit consisting of several vertically-stacked distributary channels overlies splays, both forming proximal lobe deposits. Locally, they are dissected by shallow small scours (on the SE outcrops), and exceptionally by a deep erosional channel complex (on the NW outcrops). See Fig. 3.9A for legend of sedimentary logs.

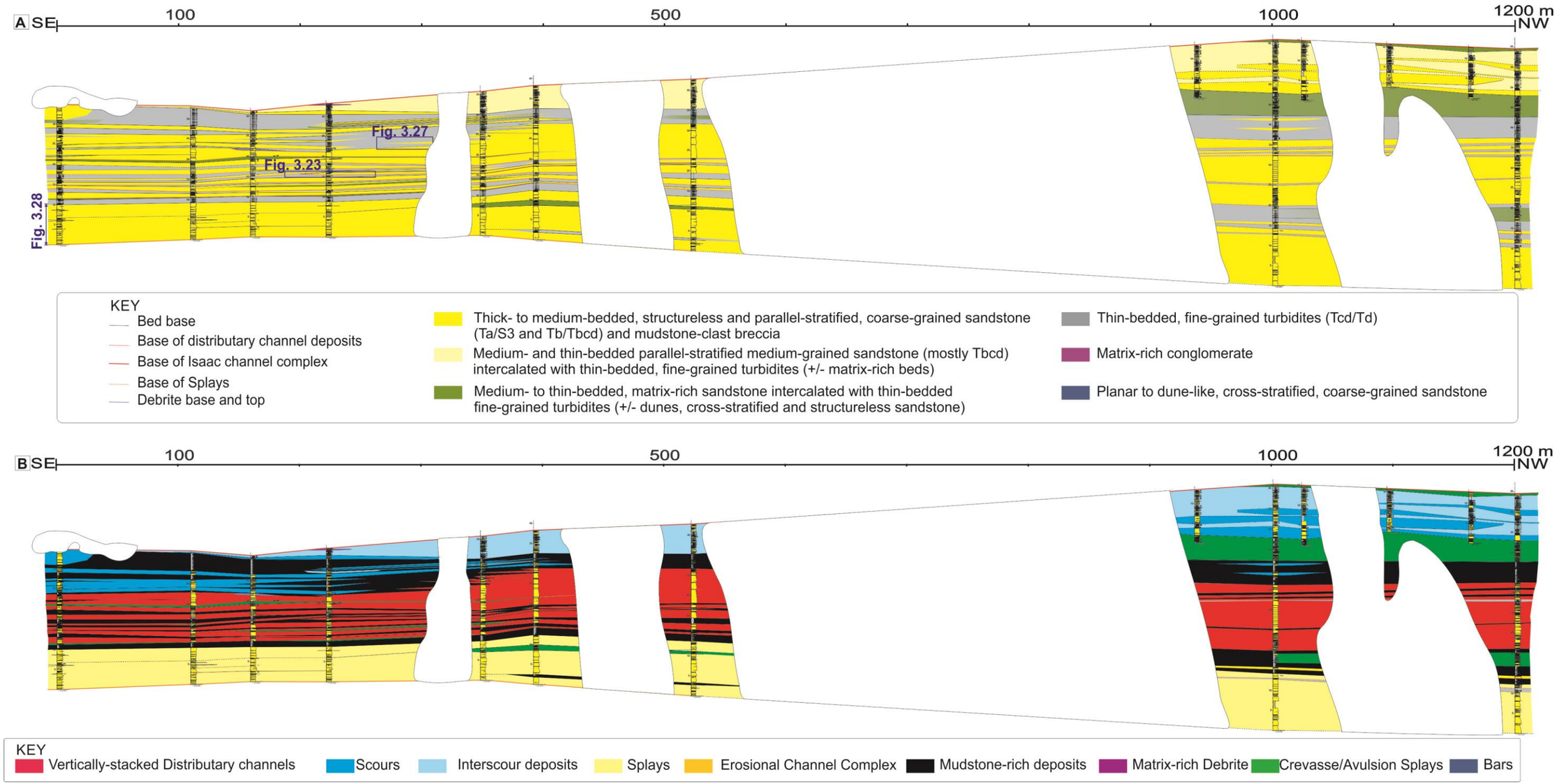

Figure 3.25. Vertically-stacked distributary channels in the KIT. A unit comprises by numerous vertically-stacked distributary channels, that overlies a splay. These channels are mostly superimposed by small scours and interscour deposits, which are then eroded by the leveed channel deposits of Isaac Contact Channel.

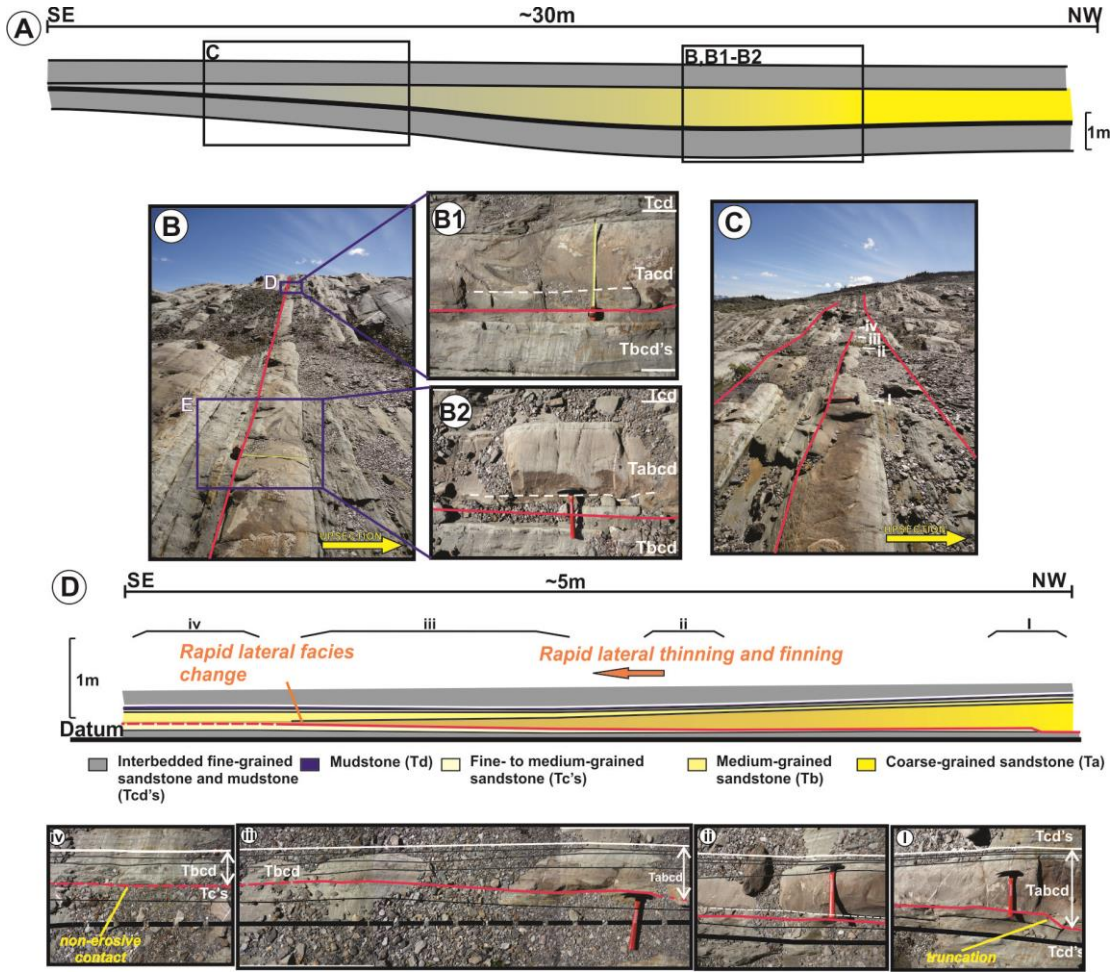

Figure 3.26. Lateral changes of vertically-stacked distributary channels in the KIT. (A-C) Overall lateral thinning and fining trends across the margin of type 2 distributary channels occurring over less than 30 meters (hammer as scale). (D) Schematic, cross-sectional diagram and corresponding photographs along one margin (from left to right). Thick-bedded, coarse- and medium-grained Tabcd/Tacd turbidites (base and top of one bedset are outlined by red and white lines respectively) thin appreciably, fine (up to upper fine-grained sandstone), and are progressively intercalated with thin-bedded fine-grained turbidites (Tcd's). Local flame structures and mudstone clasts are common at the bed bases. Laterally, turbidites either pinches out abruptly (especially their coarser parts), and/or grade into thin-bedded Tacd/Tcd with common multiple sets of ripples. The thinner beds also thin away from the channel.

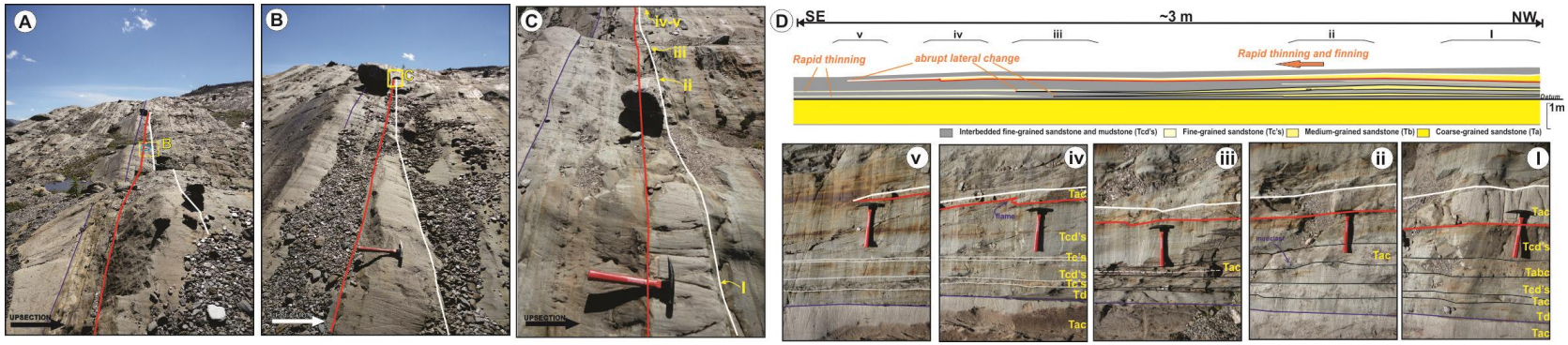

Figure 3.27. Lateral changes across a vertically-stacked distributary channels in the KIT. Channel bases are highlighted by red lines. (A-C) Vertically-stacked distributary channels are filled by one (or few) thick, highly-amalgamated beds of coarse- and/or medium-grained sandstone (50-cm marked, measured tape as scale in A-B, hammer as scale in C). See amalgamation surfaces as white dashed lines in close-up photos B1-B2. Away from the channel axis, thick coarse-grained strata corresponding to graded Tabcd turbidites thin out rapid (from B1 to B2), and then grades laterally into Tbcd (in C). (D) Schematic, cross-sectional diagram and corresponding photographs along one margin showing dramatic lateral variation in facies and thickness over less than 5 meters. (see i-iv, from left to right). Laterally, graded Tabcd turbidite bedset (top is white line) suddenly fine from coarse-grained to upper fine-grained sandstone. Local cm-scale scouring and truncation are observed along the channel base (see i). Laterally, the turbidite bedset also thin out considerably (in iv, decreasing 60-70% in thickness), then pass clearly into adjacent overbank strata as Tbcd, which are non-erosional based and laterally continuous.

In contrast to nested distributary channels (previous section 3.5.4.1), vertically-stacked distributary channels, at least as observed in a two-dimensional outcrop, generally show negligible to less erosion between successive channels and stack vertically to form decametre-thick (up to 16 m thick) units.

Interpretation

In the KIT and LIF, distributary channels filled with sandstone-rich strata that exhibit dramatic lateral facies changes are interpreted to be distributary channel fills. They formed downflow of an active feeder channel and represent efficient pathways for transport sediment to more distal splays. These channels are interpreted to be analogous to modern distributive systems documented from basin floor settings, like the Amazon (Damuth et al., 1983; Damuth and Flood, 1984; Flood and Damuth, 1987), offshore eastern Kalimantan, Indonesia (Posamentier and Kolla, 2003; Saller et al., 2008), offshore California (Normark et al., 1979; Maier et al., 2012), or local instraslope basins in the Gulf of Mexico (Prather et al., 1998; Posamentier and Walker, 2006). However, all these examples are interpreted from seismic images and as a consequence little is known about the composite lithofacies and their distribution within these elements.

In the study area, two kinds of sandstone-filled distributary channels, specifically nested and vertically-stacked distributary channels are recognized and interpreted to have been formed in different locations in a deep-water distributive channel system (Fig. 3.28- 3.29).

Nested distributary channels are interpreted to occur in the weakly-confined, upflow part of the distributary network (Fig. 3.29B). Here the scoured bases of nested

distributary channels indicate they were initiated by strong bypassing flows that incised older sand-rich channel deposits. These channels are typically filled by a small number of thick, coarse-grained sandstone beds. These coarse-grained beds tend to extend beyond the edge of the scoured base of the channel and exhibit a consistent lateral change in facies, which suggest that the axial parts of the flows were not fully confined to the low-relief channel conduits but were able to spill overs and change laterally, allowing deposition of coarse- and medium-grained sand outside the channel, forming wing-like margins. Comparable wing-like channel-margin geometries have been described from distributary channel deposits in the Annot Sandstone, France (Etienne et al., 2013), Ross Formation, Ireland (e.g. Chapin et al., 1994; Macdonald et al., 2011), and Cingoz Formation, Turkey (Kostrewa, 2004), and according to Mohrig and Buttles (2007) are suggestive of high aggradation conditions. Sensu lato, nested distributary channels are similar to overfilled channels of McHargue et al. (2011), except that they were not able to develop thick sandy overbanks because of their short life duration.

Nested distributary channels build up units that are bound by a composite, basal erosional surface formed by the incision and fill of numerous smaller channels across a broad area (see, for example, Sylvester et al., 2011). The units are commonly composed of two parts. The lower part consists of amalgamated channel fills that are interpreted to reflect high sediment discharge close to the feeder channel mouth. Here, voluminous and localized input of sediment from an upflow feeder channel spread rapidly over a wide area causing distributary channels to form simultaneously. Moreover, the nested but disorganized stacking of these channels, suggests that

channels were able to move freely laterally, and at the same time scour into previously deposited channel fills. It is envisioned that individual channels formed active, shallow, sediment-transport conduits that once partly or completely filled were promptly deactivated and avulsed. Similar tendency for frequent avulsion and abandonment of channels within distributary systems have been illustrated in laboratory experiments (e.g. Fernandez et al., 2014) and predictive models (e.g. McHargue et al., 2011). The basal, sand-rich part of the unit is then sharply overlain by a succession of thin- and medium-bedded, fine- and medium-grained turbidites interpreted to represent deposition on the margin of an adjacent nested-channel unit (cf. Prélat et al., 2009). Alternatively, it indicates an abrupt reduction of sediment supply and caliber to the system. Separating the units, laterally-extensive succession of thin-bedded turbidites indicate a temporary shut-down of local sediment transport conditions.

In contrast, vertically-stacked distributary channels are interpreted to have developed in a more unconfined part of the distributary network, downflow of nested distributary channels and immediately upflow of splays (Fig. 3.29). The basal surfaces of vertical-stacked channels reveal that these bases were formed by high-energy bypassing flows, but that may have preferentially followed pre-existing negative topography. Vertically-stacked channels were later filled by few coarse-grained, high-concentration sandy flows, resulting in coarse-grained channel-fill strata (Fig. 3.29C). The lateral facies change to finer, thinner turbidites in vertically-stacked distributary channels suggests that even with minor channel relief the high-concentration, coarse-grained part of individual flows was mostly confined to the

channel axis, and transitioned rapidly laterally into a finer, lower energy flow margin (e.g. Mohrig and Buttles, 2007; Terlaky, 2014). Downstream of vertically-stacked distributary channels, it is interpreted that most of the sediment bypassed and feed into sandstone-rich splays (e.g. Normark et al., 1979; Normark and Piper, 1985; Saller et al., 2008; Terlaky, 2014). Recent experiments on a small-scale subaqueous fan over a platform with a preset slope break by Fernandez et al. (2014) recreated similar morphological patterns, in which weakly-sinuous distributary channels are effusively formed on the middle part of the fan (upstream of the break), whereas lobated features developed on the lower fan (downdip of the break).

Based on classifications used for distributary channels (see Fig. 3.30), nested distributary channels build-up larger stratal elements called sheets, which are interpreted to be similar in geometry and dimensions to features termed (weakly-confined) distributary channel lobe complexes from seismic images of the Gulf of Mexico and offshore West Africa (Beaubouef and S.J. Friedmann, 2000; Sprague et al., 2002), channelized sheets (Pyrcz et al., 2006), or deposits of the transition from proximal to medial fan described from Skoorteenberg and Ross formations (Sullivan et al., 2000; 2004) with channels that are 8-13 m thick, up to 1000 m wide and have aspect ratios ranging from 100:1 to 1000:1 (Fig. 3.27). On the other hand, units of vertically-stacked distributary channels could be comparable to features termed (unconfined) distributary channel lobe complexes or medial fan deposits (Sullivan et al., 2000; Sullivan et al., 2004).

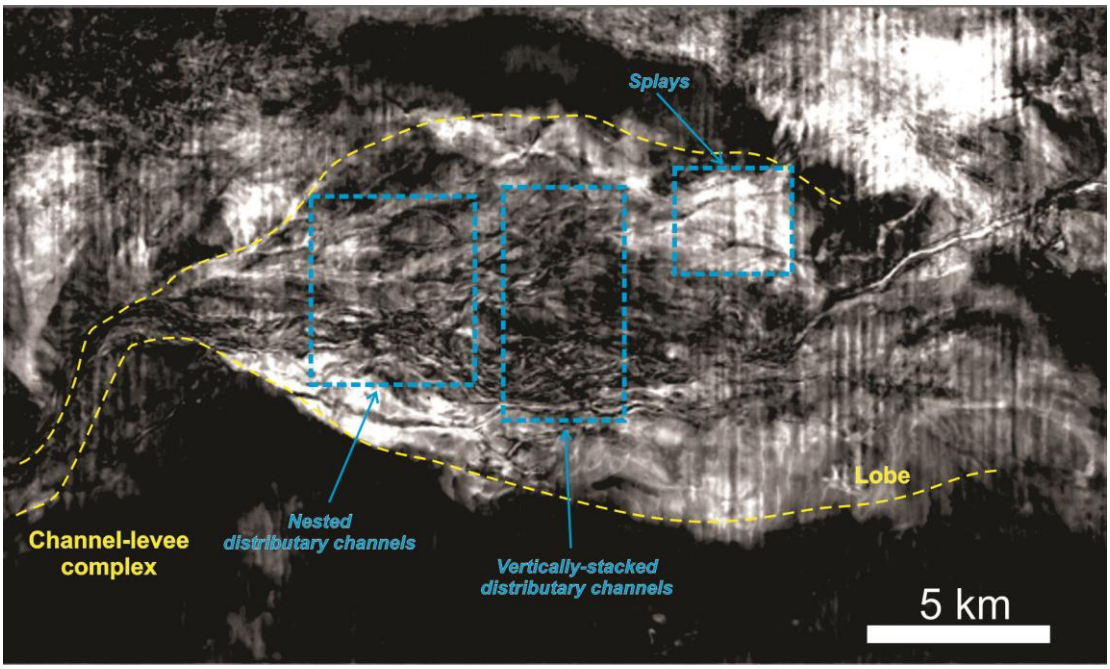

Figure 3.28. Horizon seismic slice image of distributary channel-dominated lobe deposits from De Soto Canyon area of the Gulf of Mexico. (Posamentier and Kolla, 2003, fig. 10C, p. 374; Posamentier and Walker, 2006, fig. 118, p. 476), illustrating the transition from channel-levee complex to lobe deposits (or frontal-splay deposits of Posamentier and Kolla, 2003). This lobe includes a complex network of distributary channels and splays. It is interpreted here that nested and vertically-stacked distributary channels dominate the proximal and medial parts of the network, respectively, and splays occur at the distal end of the lobe.

3.5.5 Splays

In the KIT at Castle Creek, few splay deposits crop out as sharp-based, sandstone-rich sheet-like stratal elements that extend laterally across and beyond the width of the outcrop (>1200 m, Figs. 3.4, 3.11, 3.24-3.25). They abruptly overlie scours or mudstone-rich deposits (sections 3.5.3 or 3.5.6, respectively), and commonly are overlain by vertically-stacked distributary channels or mudstone-rich deposits (sections 3.5.4.2 or 3.5.6 respectively). Rarely, splays are locally overlain by bars (section 3.5.8).

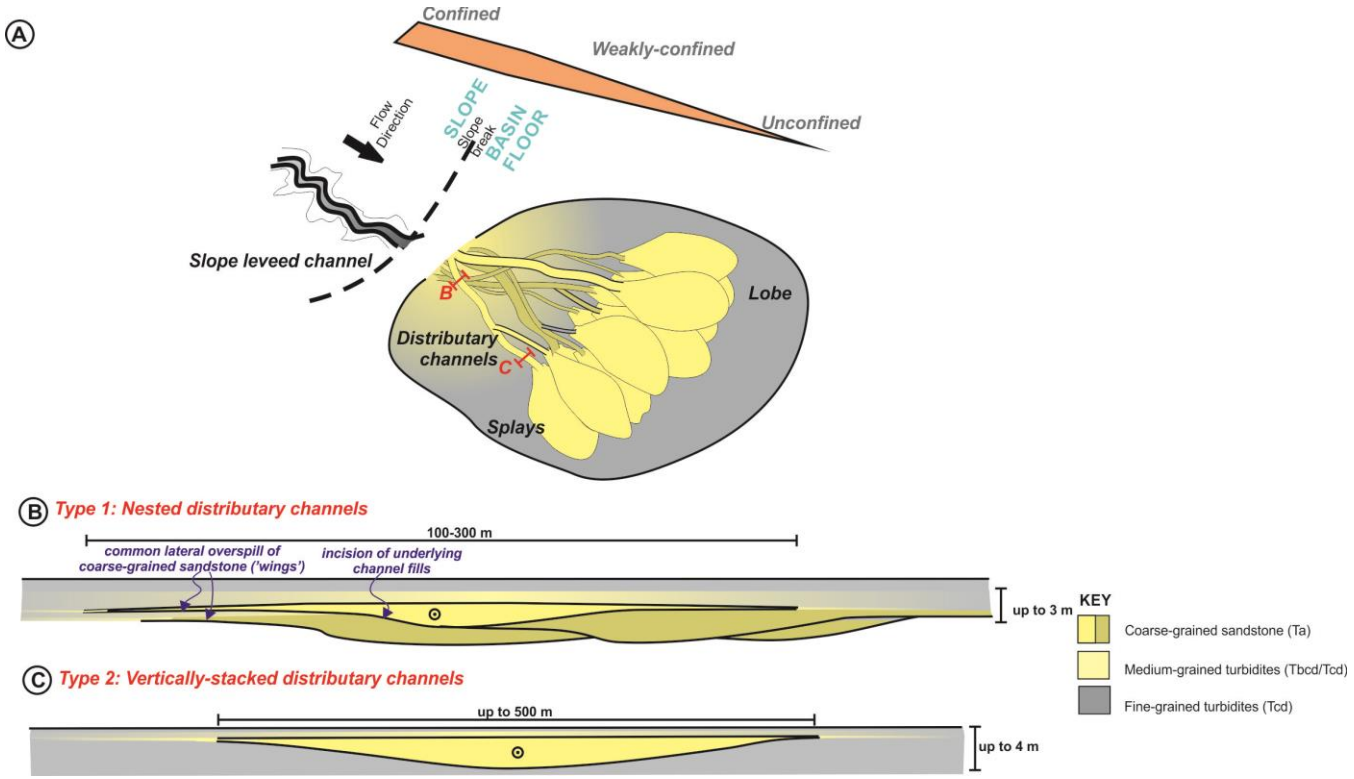

Figure 3.29. Simplified model of distributary channels. (A) Classification scheme of two different types of deep-water distributary channels based on outcrop observations and interpretations from the KIT study area. (B) Nested distributary channels begin with significant erosion and then in their axial part deposition of amalgamated, sand-rich strata. Laterally, extensive lateral overspill of these flows deposited similarly coarse but better stratified deposits that still further laterally (for few hundred of meters) transition into fine-grained, thin-bedded turbidites. Nested distributary channels are interpreted to have formed in the most proximal part of the distributive network. Vertically-stacked distributary channels, on the other hand, show negligible incision into older channel fills and have slightly thicker sand-rich channel fills with lateral overspill of medium- and fine-grained sediments. These channels are interpreted to have developed within the more medial part of the distributive network, and then further downflow transitioned directly into sand-rich splays.

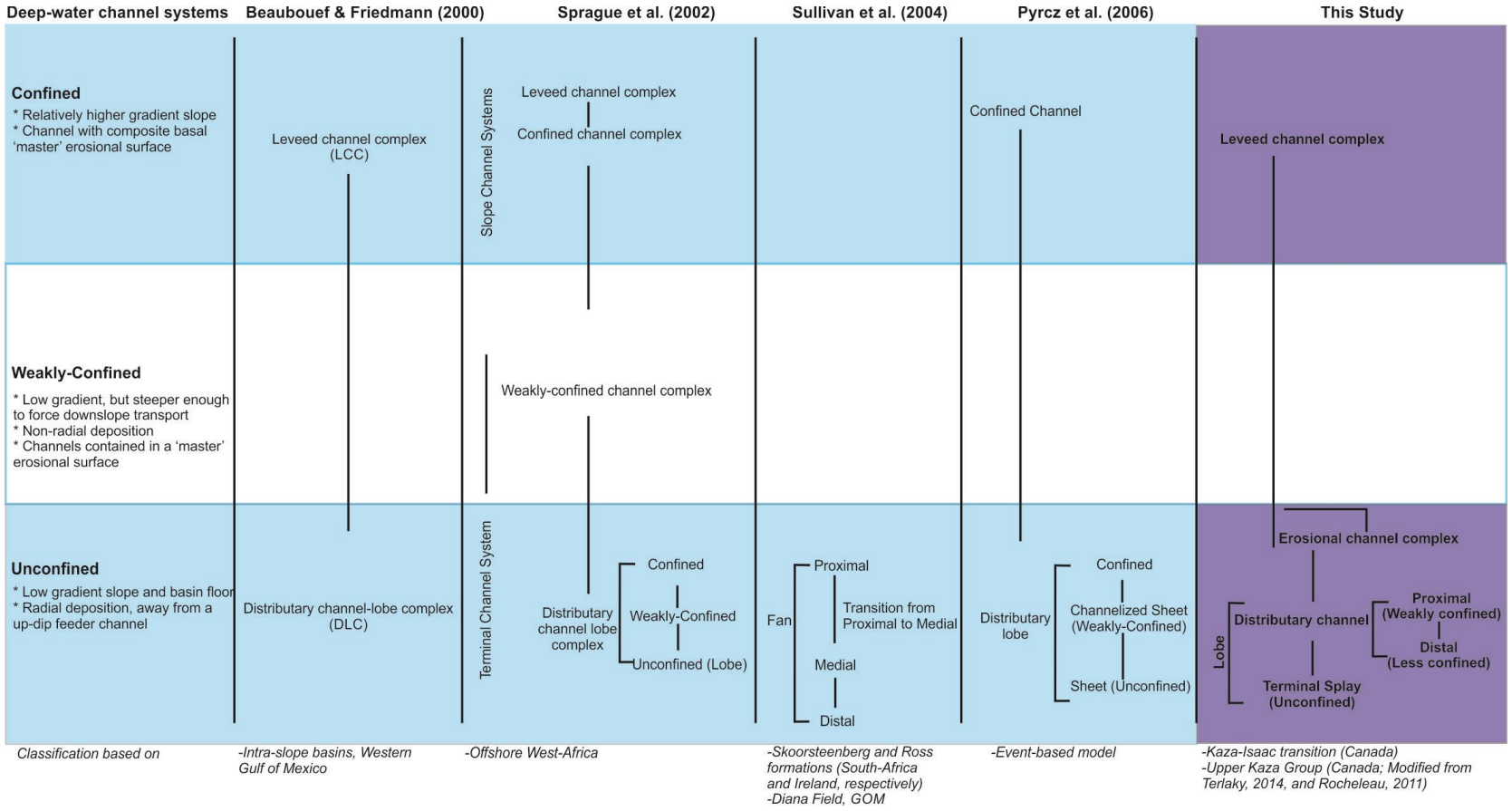

Figure 3.30. A literature compilation of the classification and terminology used for the description, interpretation and analysis of deep-water channel systems, including classification proposed in this study.

In general, splays have sharp, planar bases typically marked by an abrupt increase in grain size. Shallow scour bases (tens of cm to dm, rarely 2-5 m, deep over few meters laterally) are common. Splays are 1.5-4 m thick and dominated by amalgamated, tabular to quasi-tabular, up to 2.1 m thick, coarse- to very coarse-grained Ta/S3 sandstone (F2a) beds. Local medium-to thin-bedded, medium-grained sandstone (F2b), thinly-bedded, fine-grained Tcd or Td turbidites (F5), or medium-scale cross-stratified sandstone (F4b) occur at the tops of some splays. Mudstone-clast breccia (F3) is rare. Loading, flame and injection structures are common along bedding contacts. Internally, splays exhibit negligible vertical changes in lithofacies and bed thickness pattern, although some show subtle fining- and thinning-upward trends in their uppermost part. In some splays, thickly bedded, coarse-grained sandstone become interstratified with thin bedded, fine-grained Tcd and Td turbidites (F5) over several hundreds of meters laterally.

Splays stack vertically and form units that range from 9 to 14 m thick. Units show little vertical or lateral changes in lithofacies, but that become more evident at the km- scale. For instance, in one unit comprising three sandstone sheets (Fig. 3.31A), the high sandstone content drastically decrease from 89-100% to 70% over a lateral distance of >1 km, in which amalgamated, thick (>1 m) beds of very-coarse grained Ta sandstone (Fig. 3.31B) become slightly finer and thinner (predominantly medium- and thick-bedded (but <1 m) coarse- and medium-grained sandstone), as well as increasingly more intercalated with thin-bedded, fine-grained Tcd and Td turbidites (Fig. Fig. 3.31D).

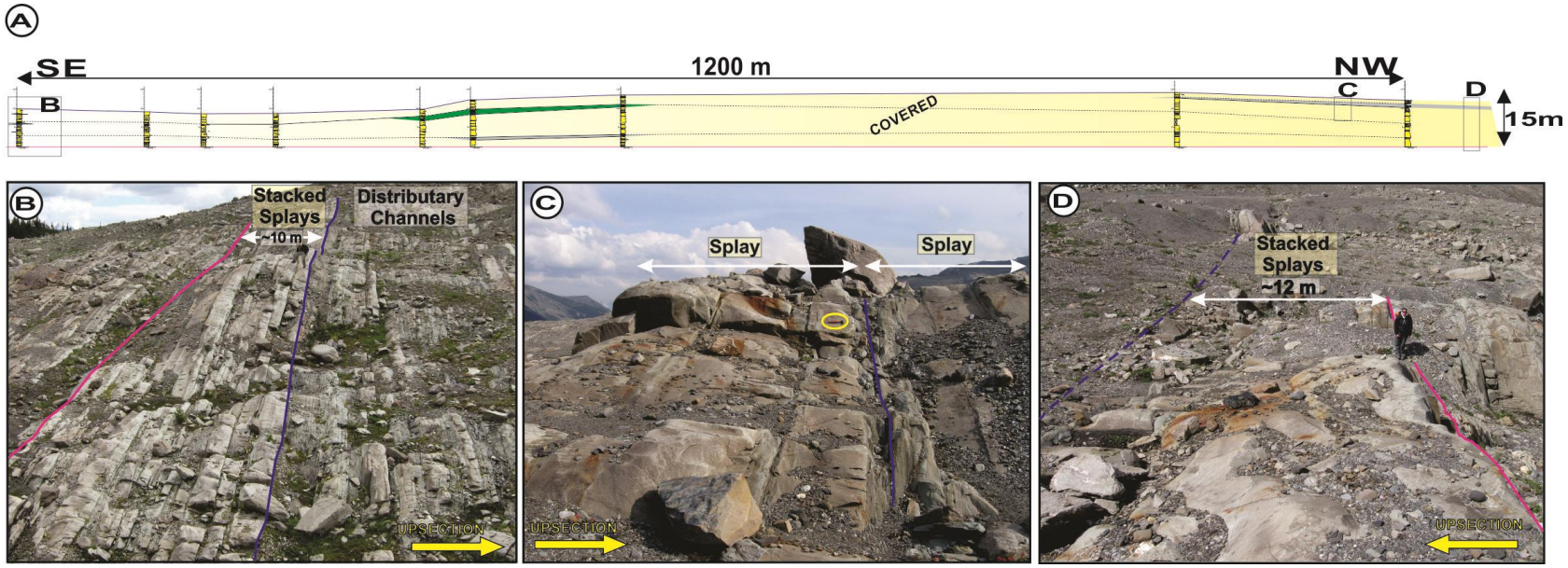

Figure 3.31. Splay deposits in the KIT. (A) Correlation line diagram showing a laterally-continuous (>1.2 km), up to 14 m thick sheet-like unit consisting of at least three stacked splay deposits – the base of each identified by a sharp grain-size break. Base and top contacts of the unit are marked in A, B and D by fuchsia and dark blue lines, respectively. In C, the base of one of the component terminal splays is indicated by a cyan line. (B) Sandstone-rich splays are composed mostly of amalgamated, very thick-bedded Ta/S3 beds. (C) Some splays are capped by thin-bedded turbidites (hammer for scale). (D) Thick amalgamated strata in the splays become slightly finer, thinner and more de-amalgamated, since the proportion of mudstone interbeds increases laterally toward the SE end of the outcrop. These splay deposits are overlain by vertically-stacked distributary channels.

Interpretation

Splays, consisting principally of laterally-continuous, coarse-grained sandstone-rich strata, indicate deposition from decelerating, high concentration sand-rich turbidity currents. Specifically, these strata resulted from the lateral merging of the high-density cores of flows (Alexander et al., 2008; Terlaky, 2014) emanating from the downflow terminus of the vertically-stacked distributary channel network. Thin-bedded, fine-grained turbidites observed at the tops of some splays is interpreted to indicate deposition along the local deactivation of that splay.

Sandstone sheet-like units have high sandstone content (near 100%) for several hundreds to >1 km, indicating that the lateral margin of a broader splay element. In the Upper Kaza Group, amalgamated splays forming laterally-extensive sheets have been documented and interpreted to represent the distal part of depositional lobes (Rocheleau, 2011; Terlaky, 2014). Sandstone-rich splay elements in the KIT are similarly interpreted, and also are of comparable thickness and width to sheet-like splays identified on shallowly-buried basin-floor lobes of offshore East Kalimatan, Indonesia (average 9.5 m thick and 985 m wide) documented by Saller et al. (2008).

3.5.6 Mudstone-rich deposits

Rusty orange/brown- and green- weathering, silty mudstone-rich, layered sheets typically separate thick sandstone-rich stratal elements in the KIT and LIF (Fig. 3.4). Units range from a few dm to tens of meters thick, and extend laterally over several hundreds of meters. In general, mudstone deposits have sharp, flat bases

and tops, although some are deeply incised by overlying sandstone-rich elements. Locally, they are intercalated with matrix-rich debrites, or punctuated by small scours. On the basis of their sand/mud ratio and lithological composition, two kinds of mudstone-rich deposits are recognized: type 1 (muddier) and 2 (sandier).

3.5.6.1 Type 1 mudstone-rich deposits

Type 1 mudstone-rich deposits are up to 12 m thick and typically extend across the entire outcrops for hundreds meters (>450 m) to several kilometers. Type 1 mudstone-rich fine-grained deposits are, consisting predominantly of thin-bedded, fine-grained Tcd or Td turbidites (F5) with low sand:mud ratio <0.3 (Fig. 3.32A). Some units show well-developed upward-fining and -thinning trends. At the Castle Creek, rare single thin (1-2 cm) interbeds of phosphatic-rich claystone (F6) occur in these mudstone-rich deposits in the KIT (e.g. M3-M6 in Fig. 3.4). Phosphatic beds (Figs. 3.32B-D-D') can be traced for up to hundreds of meters laterally, before being either locally eroded or covered by surface debris. In comparison to the major and trace geochemistry of "average" mudrocks from the uppermost Kaza strata, samples from these phosphatic beds have the highest P_2O_5% contents (ranging 13.4-15.3%, whereas the average mudstone in the Kaza is approximately 0.09%, see Table in Appendix D). They also contain high proportions of CaO, Sr, and Y (Table in Geochemistry Appendix D). Figs. 3.32D-D' and 3.32G'G' illustrates petrographic contrast between phosphatic and mudstone beds.

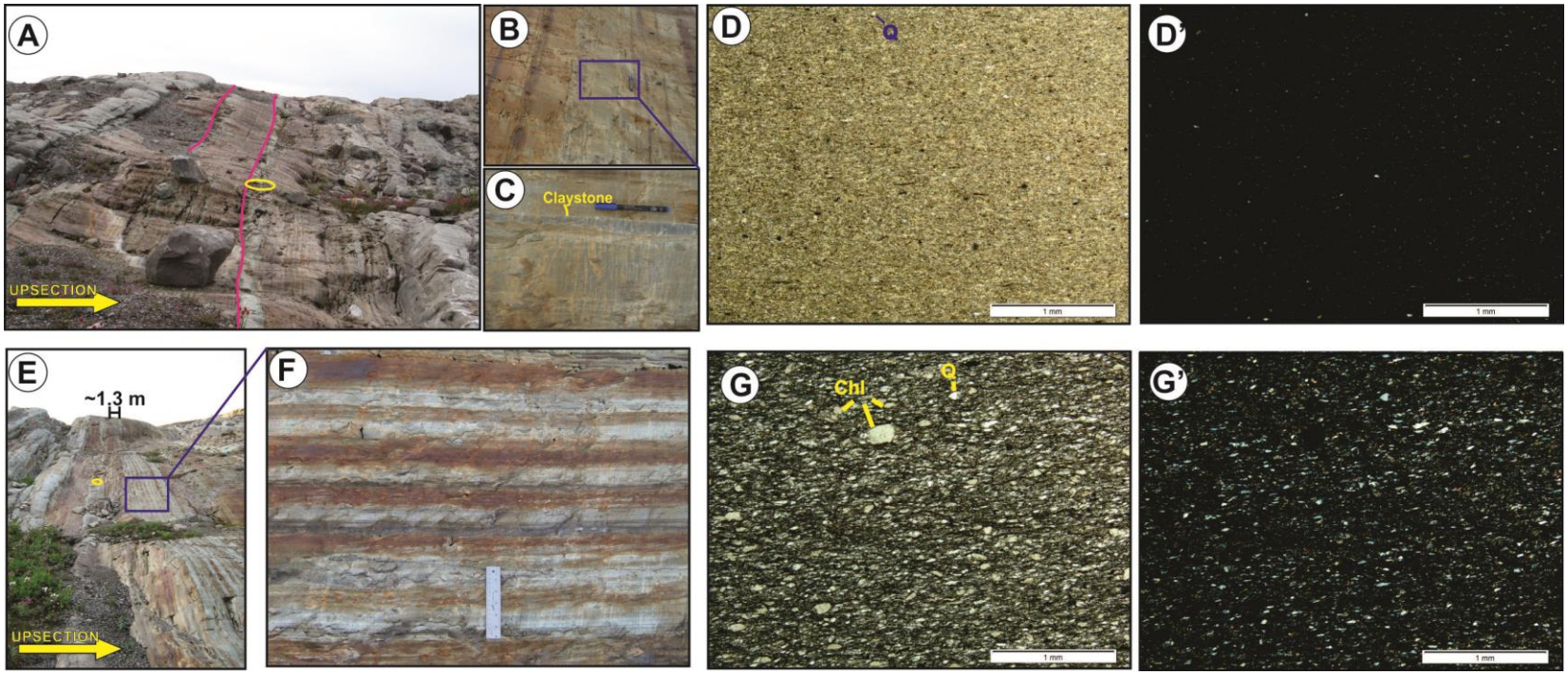

Figure 3.32. Mudstone-rich deposits in the KIT. (A) A variably rusty-weathered mudstone-dominated fine-grained sheet, that is locally incised by shallow isolated scours (scour bases highlighted by fuchsia bold lines). (B-C) Detail of mudstone-dominated fine-grained sheets, including (C) medium-gray, well-cemented, phosphatic claystone bed. (D-E) Sandstone-dominated fine-grained sheet, composed of intercalated Tb/bc and Tcd sandstones. (F) Plane-light and cross-polarized photomicrographs of a phosphatic-bearing claystone bed, showing light-coloured, homogeneous matrix of clay minerals and calcareous mud, with traces of fine-silt quartz grains. (G-G') Plane-light and cross-polarized photomicrographs of a mudstone, showing distinctive dark-brown admixture of recrystallized clay minerals, muscovite, chlorite porphyroblasts (Chl), and dispersed silt quartz grains (Q).

3.5.6.2 Type 2 mudstone-rich deposits

Type 2 mudstone-rich deposits vary laterally and vertically in terms of thickness and lithofacies make up, and are appreciably sandier than their type 1 (mudstone-dominated) counterparts (sand:mud ratios 0.3-0.6). Extending laterally for a few tens to several hundreds of meters, they are commonly up to 5 m thick. Type 2 fine-grained deposits consist of fine-grained facies (F5) but interbedded with common to abundant, thin to thick sandstone beds of F2, F4, and F7 (Figs. 3.32E-F). Generally, type 2 fine-grained deposits transition laterally into type 1-fine-grained deposits, in which sandstone beds become less abundant, thinner and finer over very short distances (e.g. <20 m). It is also common that they grade laterally into sandstone-rich elements, such as sheets and shallow channelforms.

Interpretation

Most type 1 mudstone-rich deposits in the KIT and LIF abruptly overlie sandstone-rich elements, such as splays and/or distributary channels, which comprise depositional lobes. The predominance of silty mudstone beds in type 1 mudstone-rich deposits indicates the deposition to a less energetic, more tranquil area (such as peripheral fringes of lobes of Mutti (1977) reached only by dilute turbidity currents. Alternatively, deposition of few type 1 mudstone-rich deposits seems to be related to a significant decreased in sediment supply and caliber in the system. The occurrence of thin phosphatic-bearing claystone interbeds within several type 1 mudstone-rich deposits suggest discrete deposition during strong upwelling events, possibly associated to an increased oceanic paleoproductivity in more proximal shelf and

upper slope settings, which was commonly happened during the Cryogenian period (Planavsky et al., 2010).

In contrast, type 2- mudstone-rich sheets are interpreted to represent fine-grained strata deposited in the proximal inter- or intra-lobe areas. High or low proportion of sandstone beds is indicative of the lateral or downstream distance (proximal or distal) to the axis of the depositional lobes (e.g. Rocheleau, 2011; Terlaky, 2014).

Like in the upper Kaza Group, mudstone-rich units of the KIT and LIF show no systematic vertical lithological nor mineralogical change. This differs from some ancient turbidite systems wherein mudstone-rich intervals are directly linked to major variations in sediment supply related to relative sea level change, and hence used to separate and/or hierarchically architectural elements within lobe systems (e.g. Hodgson et al., 2006; Flint et al., 2011; Prélat and Hodgson, 2013; Van der Merwe et al., 2014).

Notably also, is the presence of phosphatic beds, although rare, in the KIT. The occurrence of phosphatic beds in both shallow- and deep-marine strata are generally attributed to periods of sediment starvation that coincide with maximum transgression – forming an important stratal horizon termed a condensed horizon (Vail et al., 1984; Loutit, 1988; Kidwell, 1991). However, like thin-bedded turbidites, the sediment caliber and style of sedimentation above and below the phosphate bed show no evidence of change. This, then, suggests the phosphate beds might not have stratigraphic significance here, but instead probably represents a brief episode of elevated phosphate production in the (upflow) sediment staging area.

3.5.7 Crevasse/avulsion splays

Crevasse/avulsion splays are common throughout the KIT and LIF exposed at Castle Creek. They are sharply overlain by a variety of other stratal elements, including distributary channels, splays, or slope channel (sections 3.5.4, 3.5.5, and 3.5.2.2, respectively). Strata form sharp-based, sheet- and wedge- like units that range from 0.1 to 6 m thick (rarely up to 9 m thick); however most matrix-rich sandstone sheets that underlie distributary channels and splays are generally up to 1-1.5 m thick and less than 300-600 m wide.

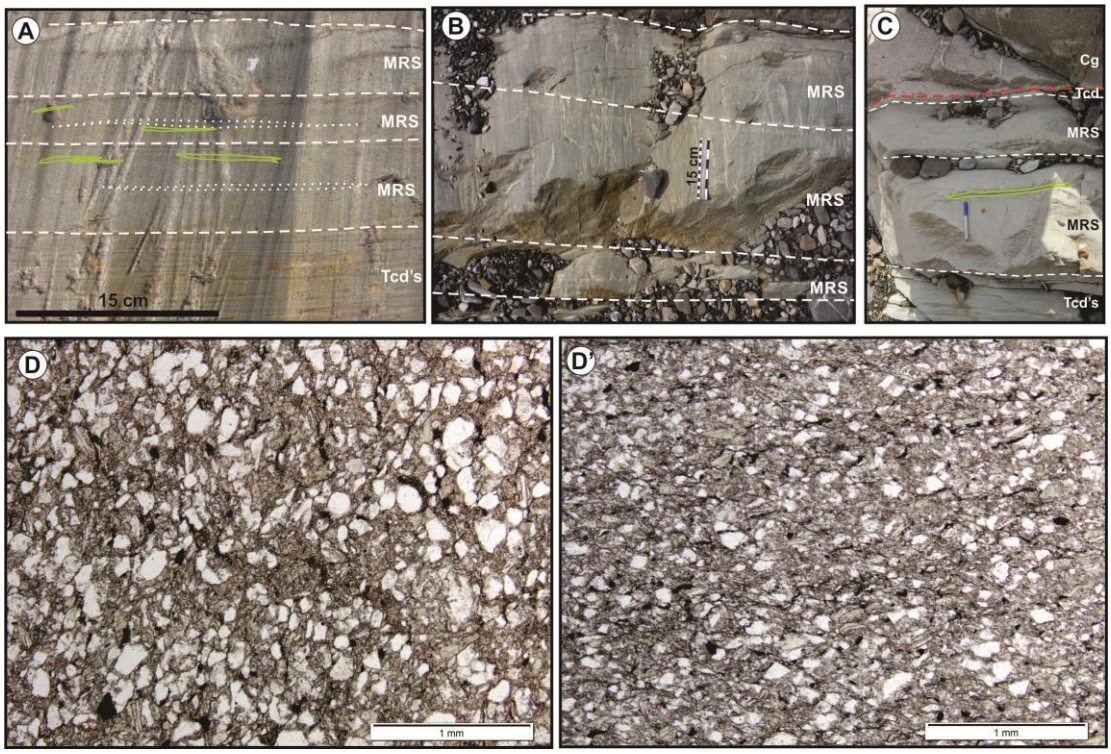

Figure 3.33. Crevasse/avulsion splay deposits in the KIT. (A-C) Sharp-based, matrix-rich sandstone (MRS) beds (F7) are typical facies of crevasse/avulsion splay deposits. White dashed lines delineate bed contacts. MRS beds are generally capped by cm-thick, graded silty mudstone of F5. Elongated mudstone clasts and/or chips (enclosed in dashed green line in A and C) are common in beds. Thicker MRS beds are partly amalgamated (see amalgamation surfaces indicated by white dotted lines in A). In C, MRS beds are erosively overlain by pebble conglomerate (Cg) beds of a leveed channel complex, Isaac Channel 1. (D-D') Plane-light photomicrographs of two matrix-rich

sandstones. Note the abundant (>40%) fine-grained matrix, which is composed mostly of recrystallized mica, chlorite and silt-sized quartz grains.

Characteristically, they consist of a few to several thin to medium beds of matrix-rich (15-50%), medium- and/or coarse-grained sandstone intercalated with fine-grained turbidites (F7 and F5, Figs. 3.33A-D,D'). Some matrix-rich (muddy) sandstone beds contain a few to abundant, dispersed, cm- to m-long mudstone clasts and/or chips (Figs. 3.33A,C). Laterally, matrix-rich beds pass rapidly into fine-grained, heterolithic strata (F5).

Interpretation

In the KIT and LIF, matrix-rich sandstone sheet-like deposits are interpreted to be crevasse/avulsion splays and represent the abrupt onset of local sand-rich sedimentation, which ultimately culminates in thick, coarse-grained sandstone-rich elements, including sandstone-rich splays and/or distributary channels (see Rocheleau, 2011; Terlaky and Arnott, 2014).

Some crevasse/avulsion splays have similar lithofacies characteristics and distribution to those recognized throughout the Upper Kaza Group by Terlaky and Arnott (2014), which are common in proximal basin-floor fan setting and are interpreted to be related to an upflow avulsion. Downflow of an avulsion node, unconfined plane-wall jet flows rapidly expanded and locally possibly also underwent a hydraulic jump. Intense scouring of the seabed charged the flow with fine-grained sediment (i.e. mostly mud and silt), resulting an abrupt change in flow rheology and subsequent deposition of distinctively matrix-rich strata (F7). Additionally, the

observed lateral change in grain size is interpreted to reflect a dramatic segregation of grain size, wherein coarser sand remained confined to the flow axis, but medium and finer sand, in addition to common mud clasts, were preferentially diverted to the margins of the flow.

3.5.8 Bars

Bars are commonly observed in distributary channels in the KIT, and less commonly occur in scours and splays (for more details of these elements, see sections 3.5.3-3.5.5). Typically, bars occur as localized, up to 1 meter-thick, composite lenticular or wedge-shaped features that are discontinuously distributed laterally along discrete bedding horizons for over hundreds of meters. The bases of bars are erosional and generally form <0.5-1 m deep, bowl- or spoon-like depressions that gradually deepen in the downflow direction (Figs. 3.34A-C). In most places, bars include similar grain size to the underlying strata, which generally is a coarse-grained sandstone (Ta) bed; however some bars abruptly overlie medium-grained sandstone, mudstone, or conglomerate.

At their upflow ends, bars are typically composed of planar-laminated coarse-grained sandstone and very-coarse grained sandstone with common dispersed coarser (up to granules) grains, which then passes abruptly laterally (downflow) into high-angle (20-30^{o}), medium-scale dune-like cross-stratified, coarse- and medium-grained sandstone (facies F4c, Figs. 3.34-3.36). Planar strata exhibit a gentle dip in the downflow direction. Individual laminae of planar and cross-stratified structures are

generally 0.2 to 1 cm thick, and normally graded. Mudstone clasts, although rare, are oriented with their long axis parallel to the stratification.

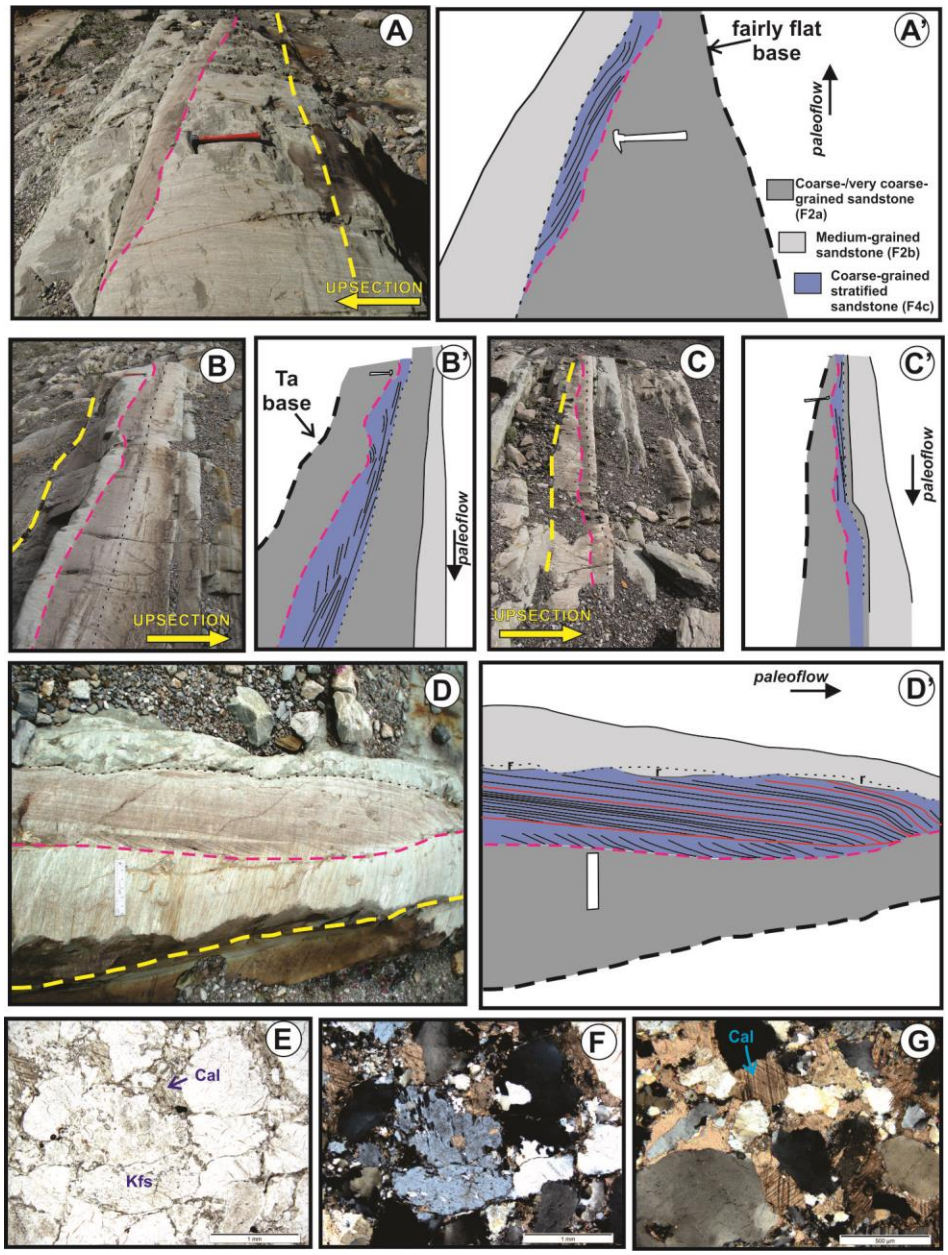

Figure 3.34. Bar deposits in the KIT. Photos (A-C) and line drawings (A'-C') showing typical internal geometry and sedimentary structures of bar deposits. (A-A') dm-deep scour infilled with gently-dipping parallel strata. (B-B') Spoon-shaped scours infilled by two cross-stratified sets. The lower set consists of upflow (backset?) dipping cross-stratification, which is extensively calcite cemented (red-brown). It is overlain by a planar laminated set. (C-C') Irregular erosional basal surface of laterally-extensive,

planar-laminated sandstone. (D-D') Scour infilled by several (>5) sets of gently-inclined parallel-lamination that pass downstream into high-angle dune-like, cross-stratified sandstone. Inter-set contacts are generally difficult to discern, but locally are sharp. Bedforms aggrade vertically, as well as accrete continuously in the downflow direction. They are topped by rippled cross-laminated, medium-grained sandstone (denoted with the letter r). (E-G) Photomicrographs in plane (E) and cross-polarized (F,G) light of facies F4c, respectively. (E-F) Pore-filling calcite cement (Cal) replacing feldspar grains (Kfs) in the planar-laminated sandstone of F4c. (G) Pervasive pore-filling calcite cement (Cal) in the associated high-angle, cross-stratified sandstone. Note the open packing of the framework grains suggesting early cementation.

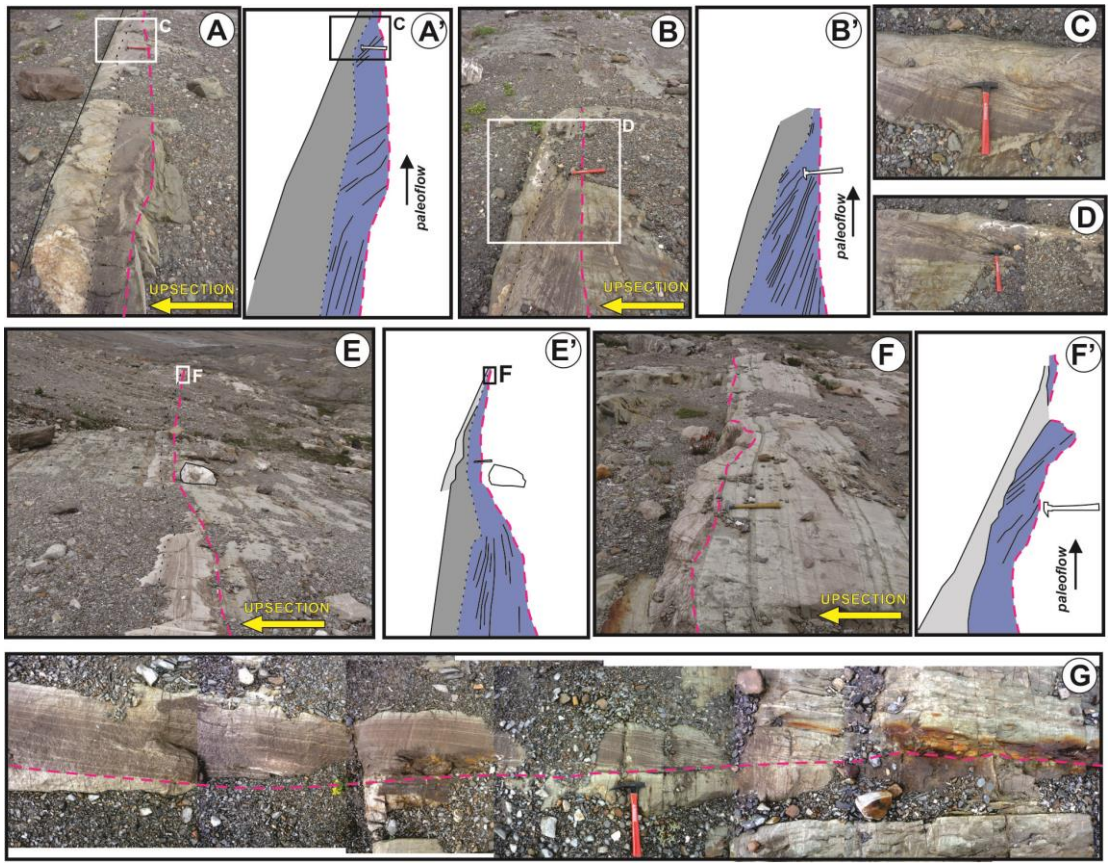

Figure 3.35. A horizon of bar deposits in the KIT. Photos (A-G) and line drawings (A'-G') illustrating the internal geometry and sedimentary structures of laterally-discontinuous bars. Photos 3.35A-G were taken along the same depositional horizon over a distance of about 100 m from SE to NW). Bar deposits occur as localized wedged-shaped features consisting of generally gently-dipping planar-laminated sandstone (e.g. bottom of 3.35A-A',E-E') that transitions abruptly downflow into high-angle, dune-like cross-stratification (e.g. top of 3.35A-A',B-B'-D-D',F-F'-G-G').

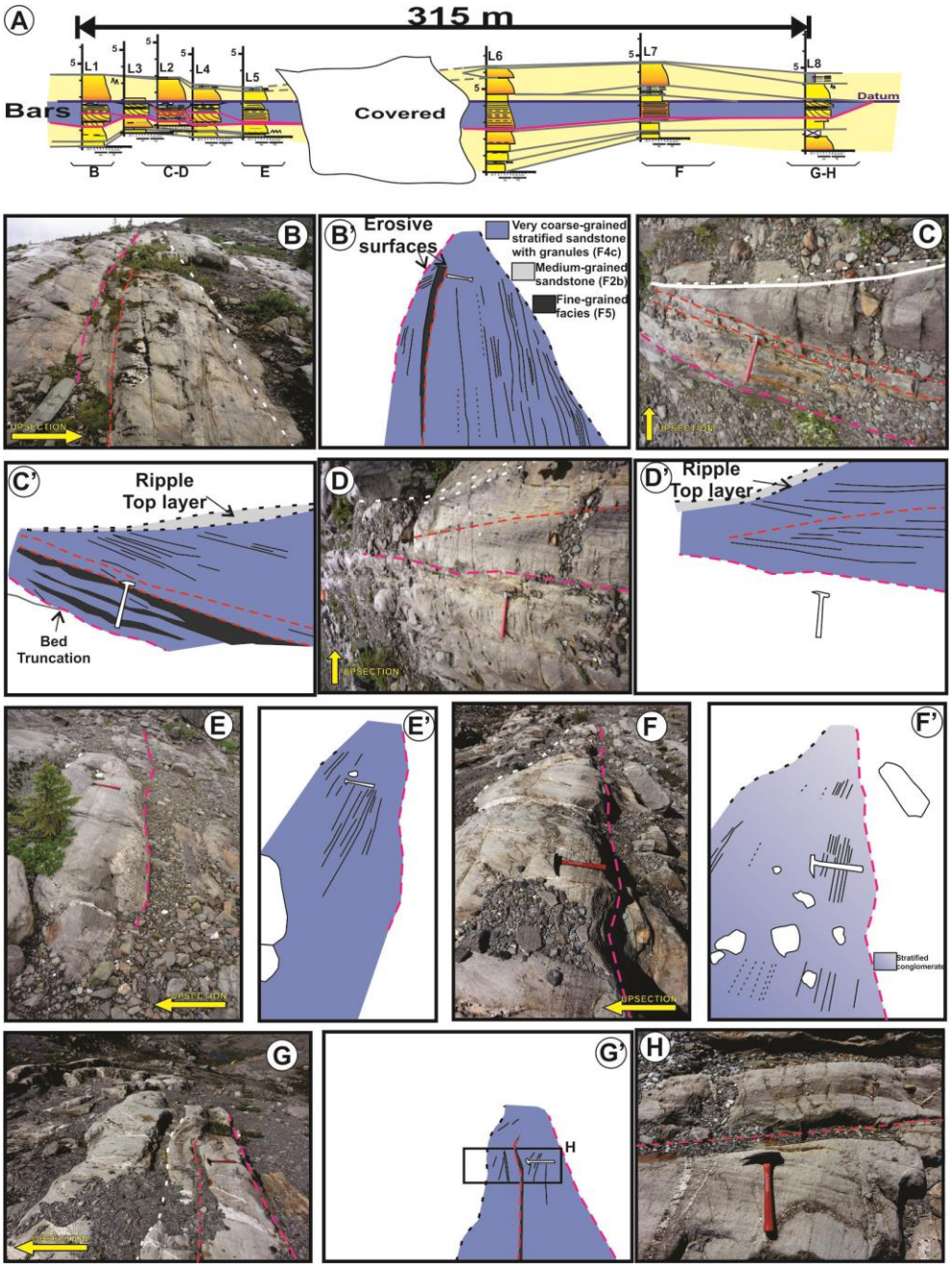

Figure 3.36. Lateral facies changes in a horizon of bar deposits in the KIT. (A) Stratigraphic correlation of measured logs showing the rapid vertical and lateral facies changes along a horizon of unit bars that can be traced laterally for several hundred of meters from SE to NW. Photos (B-G) and line drawings (B'-G') illustrate the distribution of sedimentary structures within the bars. The bases of the bars are intensively scoured, and abruptly overlain by very coarse-grained planar and high-angle cross-stratified sandstone. Local low-angle internal erosion surfaces separate individual cross- and/or planar stratified sets (see red lines in 3.36B-B',D-D',G-G'). Locally, fine-grained facies are observed at the top of some beds (e.g. 3.36B-C, G-H).

Characteristically, strata are well sorted, and exhibit a distinctive reddish brown-stripping related to a widespread (up to 40%) ferroan-calcite sparry cement (Figs. 3.34E-G). Most bars exhibit a crude upward fining from coarser- to medium-grained sandstone, and are commonly overlain by up to 3 cm single set-thick ripple cross-stratified fine-grained sandstone (F4b, Figs. 3.34D-D', 3.35C-D), or rarely mudstone layer (F5, Figs. 3.34E-G, 3.35G-H). Nonetheless, some bars display internal erosion surfaces and grain-size changes (Fig. 3.36).

Interpretation

Erosional-based, lenticular beds of planar-laminated sandstone changing abruptly downflow into high-angle, dune-like cross-stratified sandstone (F4c) in the KIT are interpreted to be bars formed immediately downflow of submerged hydraulic jumps (see experimental work on hydraulic-jump unit bars by Macdonald et al. (2009); (2013). According to these authors, hydraulic-jump unit bars comprise a gently upstream-dipping laminated sand that through a small massive sand deposit, pass abruptly downflow into a coarse-grained cross-set that at its downflow end rapidly fines and thins.

The erosive base of the bars was most likely formed downstream of the toe of the initial jump, where high vorticity, erosion and reworking occurred (e.g. Alexander et al., 2001). Most parallel- and cross-stratified beds of F4c are similar in grain size to the underlying strata, suggesting that sediment was sourced, at least in part, from the reworking of the underlying substrate (i.e. coarse-grained Ta sandstone). The parallel-laminated sandstone part of the bar represents its upflow side, which then passes abruptly into cross-stratified sandstone deposited on the downflow accreting side of

the bar. During the formation of unit bars, parallel- and associated cross-stratified sandstone are considered to be generated from initially sand-rich, high-energy supercritical flows (e.g. Alexander and Fielding, 1997; Spinewine et al., 2009), but these flows evolve through successive, stationary hydraulic jumps, like submarine cyclic steps (cf. Parker and Izumi, 2000; Fildani et al., 2006; Kostic and Parker, 2006; Spinewine et al., 2009; Cartigny et al., 2011; Kostic, 2011; Lang and Winsemann, 2013).

The common upward-fining trend observed within the bars is interpreted to suggest an overall waning and depletion of the depositional flows. At the top of the bars, ripple cross-laminated sandstone and/or mudstone layer mark the final waning phase, when flow energy and competence had decreased considerably. Bar deposits that internally show lateral and/or vertical grain-size breaks are interpreted to reflect fluctuating flow conditions during their (downstream or upstream) migration most likely related to unsteady flow conditions, bed topography or fluctuating discharge (e.g. Lang and Winsemann, 2013).

The high intra-granular volume in planar- and cross-stratified sandstone- filled with pervasive coarse-crystalline ferroan calcite cement, suggesting early (shallow burial) cementation. This is further corroborated by highly depleted carbon isotope signatures ranging from -21.42 to -16.41‰ obtained from these beds (Al-Mufti, 2013), which suggest the influence of (near sea-bed) sulphur-reducing bacterial activity on pore fluid chemistry.

Some bars in the KIT might be analogous to some depositional features that have been increasingly recognized in the modern and ancient CLTZ (Normark et al.,

1979; Vicente Bravo and Robles, 1995; Wynn, 2000; Wynn et al., 2002; Bain and Hubbard, 2016; Pemberton et al., 2016; Postma et al., 2016), yet they are comparatively smaller than many of these features.

3.6 Architectural organization

In the Castle Creek study area, detailed correlation and stratigraphic analyses through the Kaza-Isaac transition interval (KIT) and lowermost part of the overlying Isaac Formation (LIF) reveal three vertically stacked architectural assemblages (Fig. 3.4C), which stratigraphically upward are: (1) *lower KIT* (76 m thick) overlies several decametre-thick mudstone-rich and debris-flow deposits, and is composed of a siliciclastic-rich succession dominated by stacked distributary channel fills and mudstone-rich deposits that are overlain by large amalgamated and small isolated scours, which are then capped by a thick, laterally-extensive debrite, (2) *upper KIT* (178 m thick) of alternating isolated scours and basin-floor elements (namely sandstone-rich distributary channels and splays, and mudstone-rich deposits) capped by the first leveed channel, slide and mudstone-rich deposits formed at the base of the slope, and (3) *LIF* (45 m thick) of small and large isolated scours overlain by shallow distributary channels. Compared to the entire underlying sedimentary pile strata, this uppermost architectural assemblage has a distinctive reddish orange- to brownish red-weathering colour related to pervasive ferroan calcite cement.

These trends are also observed at the Mount Quanstrom study area (see Appendix G), 20 km from Castle Creek, suggesting that they are regional sedimentation patterns.

3.7 Discussion

3.7.1 Stratigraphic evolution of a CLTZ through the KIT and LIF

Although previous studies have reported the occurrence of ancient CLTZ-related deposits (e.g. Pickering, 1983; Vicente Bravo and Robles, 1991; Drinkwater and Pickering, 2001; Cornamusini, 2004; Kostrewa, 2004; Thomas, 2011; Etienne et al., 2013; Gordon, 2014; Morris et al., 2014; Pyles et al., 2014; Van der Merwe et al., 2014; Hofstra et al., 2015), this is the first to describe their characteristics and development through time. The following section integrates the observations and interpretations of the general stratal architecture of the KIT and overlying LIF (as shown in Fig. 3.4), which then provides the basis for interpreting the (external and internal) factors that controlled the formative depositional processes and ultimately the resulting stratigraphic architecture. Specifically, the succession records the effects of relative sea level changes and its influence on sediment supply and ultimately the style and pattern of sedimentation in the deep-water system. Additionally, changes in slope-basin physiography (according to the location of the CLTZ) can be established. The following is a model that describes the evolution of the CLTZ in the KIT and overlying LIF, summarized in Fig. 3.37.

Stage 1: Fine-grained, quiescent sedimentation

The basal part of the KIT is composed of the thickest, laterally-continuous, sheet-like, mudstone-rich (type 1) deposits (e.g. M1 and M2 in Fig. 3.4) in the Upper Kaza Group, consisting mostly of thin-bedded, fine-grained turbidites, and is interpreted to recording a long period of slow, quiescent sedimentation.

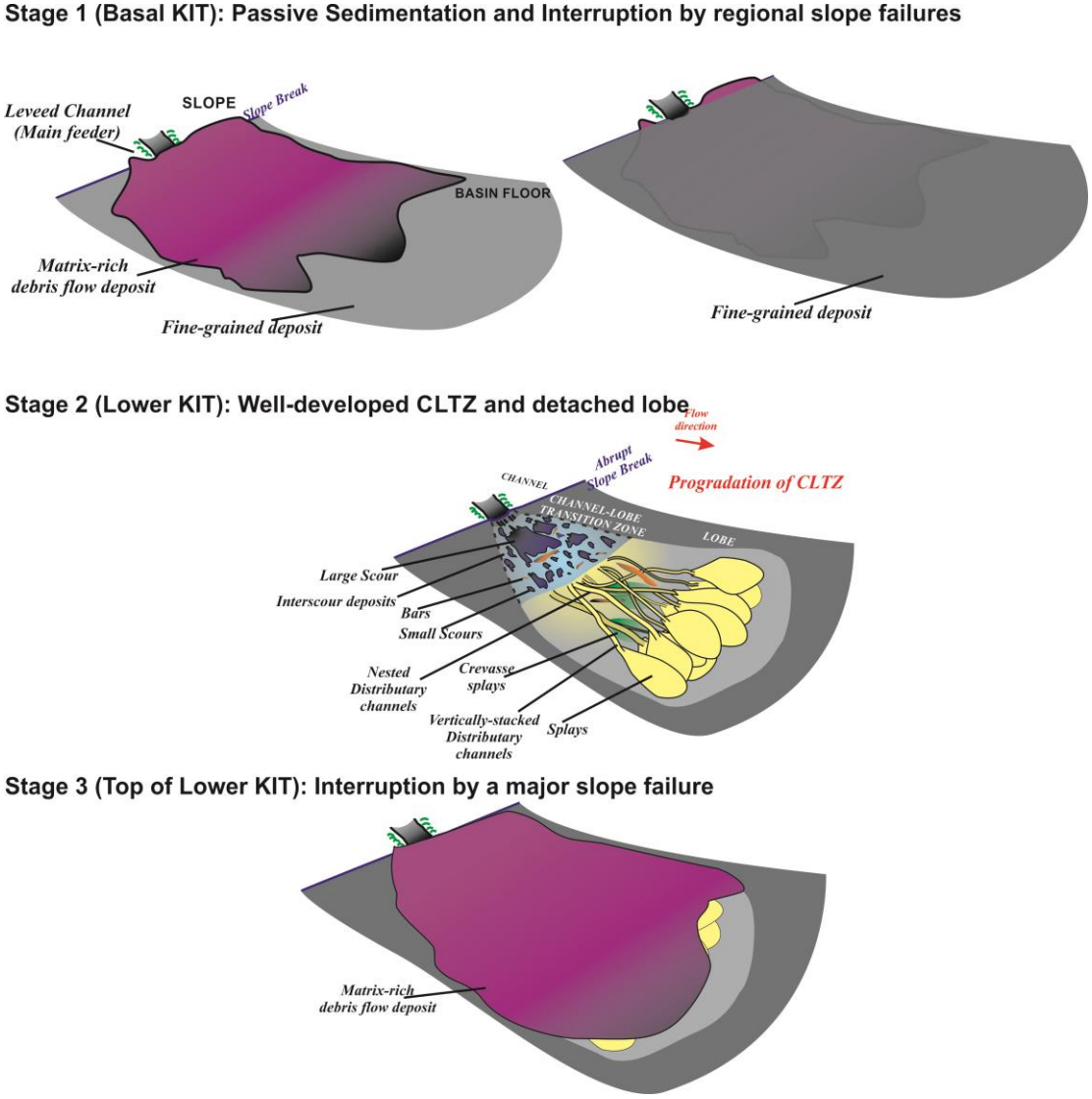

Figure 3.37. Conceptual diagram illustrating the evolution of CLTZ in the KIT and LIF. See text for explanation. Stratigraphic levels of the architectural assemblages at each stage are shown in Fig. 3.4C.

Continuation of Fig. 3.37.

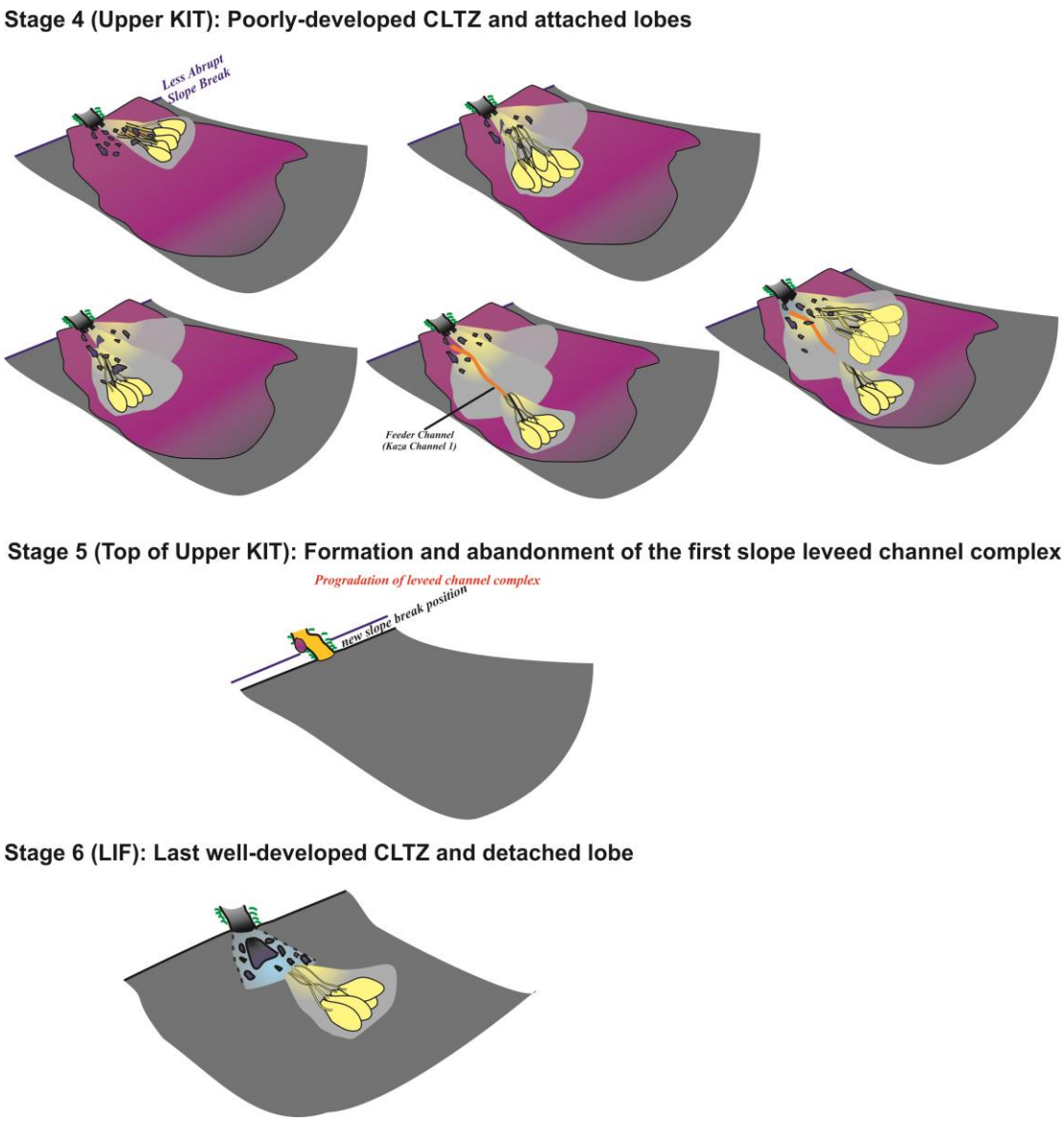

This quiescent period was interrupted at least once by the deposition of a decametre-thick, areally-extensive, mud-rich, matrix-supported, debris-flow deposit (e.g. D1 in Fig. 3.4) that contains abundant meter-scale clasts of mudstone and sandstone sourced from upslope areas. The fine-grained nature of the basal part of the KIT might imply a long-term reduction of sand supply into the local sedimentary system, which most probably coincided with highstand conditions, as sand-prone sediments were sequestered in continental and marginal marine environments and mostly mud-prone sediments were delivered to the more distal parts of the basin (e.g. Posamentier and Kolla, 2003; Maslin et al., 2004; Moscardelli et al., 2006), or alternatively the abrupt shift of an active depocentre.

Stage 2: Well-developed CLTZ

Abruptly overlying the fine-grained strata package at the base of the KIT is a several decametre-thick, sandstone-rich, proximal-lobe succession (see Fig. 3.4), indicating the reactivation of a sand-rich, high-energy transport system, most likely related to the onset of falling relative sea level (Posamentier and Kolla, 2003; Posamentier and Walker, 2006).

The proximal-lobe succession consists of vertically-stacked distributary channels overlain by nested distributary channels filled with coarser-grained strata than the vertically-stacked channels. This upward change suggests an increase in sediment supply and the development of a distributive channel network in the proximal part of a depositional lobe where channels are more confined laterally and re-occupation and/or reworking of previous channels is common (Sullivan et al., 2004). Nested distributary channel deposits are then overlain by a several-meter-thick

succession of mudstone-rich (type 1) deposits (e.g. M3 in Fig. 3.4) dissected locally by uncommon isolated small scours. This succession is interpreted to indicate the deactivation of the local transport system and hence abandonment of the (underlying) lobe.

Mudstone-rich deposits are then deeply incised by a decametre-deep, amalgamated scour comprising numerous small scours filled mostly with sandstone-rich amalgamated strata, and which upward become more intercalated with fine-grained strata. This large scour is interpreted to be formed within a well-defined CLTZ (sensu Wynn et al., 2002) that separates the main leveed channel/canyon from the downflow distributary channel-dominated proximal part of depositional lobes (the detached lobes of Wynn et al. (2002)). This CLTZ suggests the development of a well-defined base-of-slope break, and over which highly mobile sediment gravity flows scoured as they bypassed into more distal parts of the depositional system (Wynn et al., 2002). Such well-developed CLTZs have been reported to be associated with highly-efficient deep-water systems characterized by sand-rich flows, but with considerable mud content (sensu Mutti and Normark, 1987, 1991; Wynn, 2000; Wynn et al., 2002). The stacking of CLTZ-related scour deposits above proximal lobe deposits in the Lower KIT is interpreted to record a basinward advance of the CLTZ related to progradation of the basin-floor fan.

Stage 3: Major episode of slope instability

The well-developed CLTZ is then abruptly overlain by a several meter-thick, laterally-continuous, matrix-rich debrite (e.g. D2 in Fig. 3.4) related to a major submarine slope failure. Significantly, the architecture of strata immediately above

D2 differs from those that it sharply overlies (see next). This, then, suggests that emplacement of debrite D2 not only indicates an interruption in local sedimentation, but more profoundly, preceded or coincided with a systemic change in the style of sedimentation or a shift in the depocentre.

Stage 4: Poorly-developed CLTZ

Mud-rich debrite D2 is overlain by several stacked sandstone-rich proximal lobe deposits of the Upper KIT. Strata include distributary channels, fine-grained deposits and uncommon splays, all of which are dissected locally by small isolated scours (i.e. lower part of Upper KIT). This stratal assemblage suggests that deposition took place immediately downflow of the mouth of the leveed or erosional feeder channel, developing at this time attached lobes of Wynn et al. (2002). This, therefore, suggests that the CLTZ was poorly developed or even absent, which quite possibly relates to a reduction in the abruptness of the base-of-slope break, caused by emplacement of the debrite D2 (see above). Alternatively, the change may have been caused by a change in sediment supply (e.g. Millington and Clark, 1995; Wynn et al., 2002), although there is little textural or mineralogical evidence to substantiate this.

The absence or poor development of a CLTZ is typically considered to be indicative of low-efficiency systems dominated by low volume, sand-rich flows with low mud content (Mutti and Normark, 1987, 1991; Wynn et al., 2002). However, above and below the debrite D2, sediment caliber changes little, but the proportion of sandstone increases substantially. In addition, the architectural elements and their stacking patterns change abruptly, becoming dominated by proximal basin-floor

elements, mostly nested and vertically-stacked distributary channels, fine-grained sheets, and rarely splays, which locally are incised by isolated scours.

Compared to proximal basin-floor elements reported from the underlying Upper Kaza Group by Terlaky et al. (2016), stratal elements in the Upper KIT, although similar in dimensions and lithology, contain more abundant isolated scours, nested and vertically-stacked distributary channels, fine-grained deposits, and significantly fewer splays.

Stage 5: Formation and abandonment of a base-of-slope leveed channel complex

Scours and proximal lobe deposits are then overlain sharply by the Isaac Contact Channel Complex (ICCC in Fig 3.3), which represents the first slope levee-channel complex in the sedimentary pile at Castle Creek (i.e. upper part of stratal assemblage 2), and is used to mark the base of the lithostratigraphic Isaac Formation. Significantly, ICCC coincides with a dramatic increase in the average grain size from generally upper medium-lower coarse sand to upper coarse-very coarse sand, in addition to abundant granules and lesser fine pebbles. This change is interpreted to be the result of allogenic factors, specifically changes of relative sea level and its influence of the make up of sediment made available in the sediment staging area. The abrupt superposition of levee-channel deposits above proximal lobe deposits and CLTZ-related elements is interpreted to record the progradation of the leveed channel system.

ICCC consists of coarse-grained sandstone-rich channel fills that interfinger obliquely upward into thin-bedded, fine-grained (inner-bend) levee deposits. The

stratal composition and architecture of ICCC is similar to that described in Isaac Channel 2 and Isaac Units 14 and 21 (e.g. Arnott, 2007; Dumouchel, 2015), which exhibit well-developed lateral accretion deposits and are interpreted to represent the lateral migration of deep-water sinuous channels. The anomalously coarser-grained infill nature and the occurrence of some carbonate clasts in the laterally accreting channels, like ICCC, are interpreted to be formed during the transgressive or early highstand system tract (Navarro, 2006; Arnott et al., 2009; Arnott et al., 2012). At this time, medium and fine sand became sequestered in landward-migrating barrier-island complexes, whereas coarse-grained sediment became stranded on the shelf as relict or palimpsestic sediment and thereby the primary source of sand for basinward-flowing turbidity currents. This resulted in highly-stratified flows, in which the sand-rich basal portion of the flows was confined to the channel conduit (see Arnott, 2007 for full discussion of flow processes). Eventually, coarse-grained siliciclastic input diminished and was replaced, at least locally, by deposition of a decametre-thick succession of thin-bedded, fine-grained turbidites.

Stage 6: Final well-developed CLTZ

The succession of thin-bedded, fine-grained turbidites that marks the top of the KIT is then erosively overlain by an up to 45 m thick stratal interval of the LIF. This interval consists typically of carbonate-cemented, sandstone-rich, isolated scours and distributary channel fills (i.e. stratal assemblage 3). The suite of numerous small and rare large isolated scours is interpreted to be formed across the last well-developed CLTZ recorded in the Windermere stratigraphy at Castle Creek. These scours are comparable in dimensions and geometry to those scours documented from

many modern CLTZs (see extensive reviews of Wynn et al., 2002; Macdonald et al., 2011). The re-establishment of a well-developed CLTZ region suggests a steepening of the slope break at the base of slope and/or highly-efficient, sand-rich flows were supplied again into the system. Also, the pervasive early-marine carbonate cement indicates a major change in sediment supply to the Isaac slope system. Specifically, the dominant supply of siliciclastic sediment was the first time being supplemented with major contribution carbonate detritus sourced from a now extant shallow-water carbonate production zone. Later (i.e. diagenetic) dissolution of the resedimented carbonate would have been enhanced the precipitation of carbonate cement in these strata. Such carbonate-cemented strata are interpreted to be deposited during or after the rise of relative sea level.

3.7.2 Comparison of CLTZ in the KIT and LIF, and other modern and ancient examples

Owing to high-quality seafloor mapping and seismic imaging of the CLTZ in numerous modern deep-water turbidite systems, including Agadir and Lisbon basins, Unkman fan, Rhone fan, Valencia fan, and Navy fan, it has become well know that CLTZs typically comprise a myriad of erosional and depositional features, including scours of various dimensions (up to several tens of meters deep and up to nine kilometers wide), wave sediments or mounds, and coarse-grained sediment patches (e.g. O'Connell et al., 1991; Kenyon and Millington, 1995; Kenyon et al., 1995; Palanques et al., 1995; Morris et al., 1998; Wynn et al., 2002; Bonnel et al., 2005; Duarte et al., 2010; Macdonald et al., 2011). Similarly, in the stratigraphic succession

studied here, the CLTZ is characterized by small and laterally-extensive isolated and amalgamated scours that are comparable in dimensions to some of those reported in modern systems (see Fig. 3.17).

Small isolated scours described here are similar in size to many scours documented from the ancient rock record, which tend to be few meters to tens of meters deep and up to few hundreds of meters wide (e.g. Pickering, 1983; Vicente Bravo and Robles, 1991, 1995; Drinkwater and Pickering, 2001; Cornamusini, 2004; Kostrewa, 2004; Thomas, 2011; Gordon, 2014; Tudor, 2014; this study). However, a few laterally-extensive scours in the KIT and LIF, which are of the order of up to several decametres deep and >600-1200 meters wide, are comparable to the giant scours (few tens of meters deep by >1000 meters wide) interpreted within Fan 3 and A5 unit of the Karoo basin (Hofstra et al., 2015), for example, and also documented from many modern systems noted above.

The succession containing erosional surfaces and deposits associated with the CLTZ in the KIT and LIF exhibits a wide variety of facies and architectural elements. Similar diversity has been observed in a small number of other ancient examples of CLTZs, such as in Miocene Cingoz Formation of Adana Basin, southern Turkey (Kostrewa, 2004), in La Jardinera outcrops of Los Molles Formation, Argentina (Tudor, 2014) and in the Tres Pasos Formation, Chile (Pemberton et al., 2016). However, unlike these other studies, this study is the first to fully document a continuous stratigraphic section that grades upward from basin-floor deposits to channelized slope deposits, illustrating how CLTZ-related scours are variably dispersed throughout the succession.

Except for scours and nested distributary channels, most basin-floor lobe elements described in this study have been also previously documented in strata of the underlying Upper Kaza Group (Rocheleau, 2011; Terlaky, 2014; Terlaky and Arnott, 2014; Terlaky et al., 2016), and in large part are equivalent in description and dimension to elements previously reported in some seismic studies (Posamentier and Kolla, 2003; Posamentier and Walker, 2006; Jegou et al., 2008; Saller et al., 2008). The stacking of the three architectural assemblages identified in this study reflect the development or absence of a well-defined CLTZ, and when slope channels were detached or attached to their corresponding sandstone-rich proximal lobes (sensu Wynn et al., 2002). Similar stacking patterns have been directly or indirectly recognized in modern channel-lobe systems, including offshore Nigeria (Pirmez et al., 2000), offshore Indonesia (Posamentier and Kolla, 2003; Posamentier and Walker, 2006), basin 4 of Brazos-Trinity intraslope system in the Gulf of Mexico (Beaubouef et al., 2003), and in ancient channel-lobe systems in the units C-F of the Fort Brown Formation in the Karoo basin (Van der Merwe et al., 2014), in the Ross Formation at the Bridges of Ross, Ireland by (Pyles et al., 2014), and in the Guaso 1 turbidite system, Spain (Gordon, 2014). However, the scale and location of the CLTZ in these ancient systems were inferred based on paleogeographic and isopach thickness maps.

3.7.3 Reservoir potential associated to the CLTZs

The succession cropping out between basin-floor sheet-like elements of the Upper Kaza Group and channelized deposits in the overlying Isaac Formation represents an excellent analogue for deep-water turbidite reservoirs of channel-lobe systems and channel-lobe transition zones (CLTZ). Unique to the CLTZ is the ubiquitous occurrence of scours of various dimensions. However, the role that these erosional features play in the CLTZ hydrocarbon reservoir system is generally poorly understood – details that are essential for constructing reliable and realistic reservoir models.

In this study, the architectural assemblages that make up well-developed CLTZs (i.e. in the lower KIT and LIF) suggest that when channel-lobe systems are detached from an upflow channelized system (sensu Wynn et al., 2002), strata are generally mud-prone and incised locally by a variety of typically small, isolated scours (generally sandstone filled and up to 2.7 m thick and up to 500 m, rarely 1200 m wide). The large amalgamated and isolated scours may be locally important, but only if they are filled mainly with sand and have erosional contact with adjacent sandstone-rich elements (e.g. distributary channels), thereby increasing overall reservoir volume and horizontal and vertical connectivity.

In contrast, instances where the CLTZ is absent or only poorly developed (e.g. in the upper KIT), the stratigraphic record is comparatively more diverse and complex, but more importantly, is thicker (at least >1.5-2.3 times) and more sandstone rich. Under these conditions, isolated scours are common and intercalated locally with sandstone-rich, proximal lobe elements (mostly distributary channels and less common splay deposits), and rare erosional and leveed channel deposits.

Individually, these generally decametre-thick, sandstone-rich stratal units would represent good to excellent reservoirs, which may be connected horizontally and vertically by common, albeit thin, sandstone-rich scour fills.

3.8 Conclusions

The slope-basin transition typically includes the channel-lobe transition zone (CLTZ), which in deep-water turbidite systems separates slope channels from more basinward depositional lobes. Although the quality and resolution of seafloor and seismic images from many modern CLTZs have improved, the lithological details, stratal element distribution and stratigraphic evolution across the zone remain poorly known. Among ancient deep-water CLTZ analogues, the unique occurrence of strata sandwiched between the sandstone-rich, sheet-like, basin-floor deposits (Upper Kaza Group) and leveed slope channel complexes (Isaac Formation, the lower Cariboo Group) at the Castle Creek area provide, for first time, new insights into facies and stratal architecture that allow the spatial and temporal development of a CLTZ:

- In an idealized downstream transect, the studied interval comprises a slope leveed channel complex, CLTZ-related scours and proximal basin-floor elements including proximal and distal distributary channels, fine-grained sheets, and few splays. Additionally, mass-transport deposits (debrites and slide deposits), erosional channel, crevasse splays and bars are also recognized.

- Compared to underlying basin floor-dominated and overlying slope-dominated successions, the most unique elements recognized here are scours and less common nested distributary channels.
- Scour elements occur everywhere throughout study area and typically show little vertical or lateral lithological change. Based on their dimension, two types of scours have been identified: small (typically few decimeter to few meters deep, and tens to several hundreds of meters wide) and large (few to tens of meters deep, and few kilometers wide). They are mostly filled by a single or several thick- to medium-bedded, structureless or planar-laminated, very coarse- to coarse-grained sandstone beds, mudstone-clast breccia, and rarely granule conglomerate or clast-rich debrite.
- Small scours typically occur as common, isolated features that incise dm- to m-thick succession of thin-bedded, fine-grained turbidites and/or matrix-rich sandstone beds. Large scours are rare, and occur as isolated or amalgamated elements, but similarly comprise several smaller erosively-based scours that coalesce to form larger features over broad areas. Overall, scours are interpreted to have been formed downflow of the mouth of main slope channels, and are consistent in dimension and origin to erosional features documented from CLTZ areas in many modern turbidite systems.
- Stratigraphically upward, three distinctive architectural assemblages have been identified, depending on the occurrence, distribution and stacking patterns of the scours and proximal basin-floor elements. They indicate the development of

either a well- or poorly-defined CLTZ, which is associated, respectively, with detached and attached channel-lobe systems.

- Detached channel-lobe systems with well-developed CLTZ occurred in the lower Kaza-Isaac transition and lower Isaac Formation, and are characterized by large and small scours that incised into mudstone-rich deposits and are disconnected from adjacent distributary channel-dominated proximal lobes. The reservoir potential in these systems are generally poor.
- An attached channel-lobe system with a poorly-developed or absent CLTZ is recognized only in the upper Kaza-Isaac transition interval. It is comprises numerous small scours variably intercalated with various proximal basin-floor elements, which are then overlain by leveed channel, slide and fine-grained deposits. Individually, many of sandstone rich stratal elements in this system have excellent to good reservoir potential.
- The stratigraphic evolution of the CLTZ in the Kaza-Isaac transition interval and Isaac Formation is linked to important changes of relative sea level, that are predicted and linked with major variations in sediment supply (sediment volume and size), and sedimentation style. Additionally, changes in the angularity in the base-of-slope break are interpreted to have had a major impact in the presence or absence of the CLTZ.

3.9 References

Al-Mufti, O., 2013, Dune or Dune-Like Cross-Stratification in Deep-Marine Sandstones of the Neoproterozoic Windermere Supergroup, Cariboo

Mountains, British Columbia, Canada: Unpublished B.Sc. thesis thesis, University of Ottawa, 59 p.

Alexander, J., J. S. Bridge, R. J. Cheel, and S. F. Leclair, 2001, Bedforms and associated sedimentary structures formed under supercritical water flows over aggrading sand beds: Sedimentology, v. 48, p. 133-152.

Alexander, J., and C. Fielding, 1997, Gravel antidunes in the tropical Burdekin River, Queensland, Australia: Sedimentology, v. 44, p. 327-337.

Alexander, J., S. J. Mclelland, T. E. Gray, C. E. Vincent, M. R. Leeder, and S. Ellett, 2008, Laboratory sustained turbidity currents form elongate ridges at channel mouths: Sedimentology, v. 55, p. 845-868.

Allen, J. R. L., 1991, The Bouma division A and the possible duration of turbidity currents: Journal of Sedimentary Petrology, v. 61, p. 291-295.

Álvaro, J. J., G. A. Shields-Zhou, P. Ahlberg, S. Jensen, and T. Palacios, 2016, Ediacaran–Cambrian phosphorites from the western margins of Gondwana and Baltica: Sedimentology, v. 63, p. 350-377.

Arnott, R. W. C., 2007, Stratal architecture and origin of lateral accretion deposits (LADs) and conterminuous inner-bank levee deposits in a base-of-slope sinuous channel, lower Isaac Formation (Neoproterozoic), East-Central British Columbia, Canada: Marine and Petroleum Geology, v. 24, p. 515-528.

Arnott, R. W. C., and B. M. Hand, 1989, Bedforms, primary structures, and grain fabric in the presence of suspended sediment rain: Journal of Sedimentary Petrology, v. 59, p. 1062-1069.

Arnott, R. W. C., Z. Khan, and L. Navarro, 2009, Stratal Architecture of Highly Confined and Poorly Confined Deep-Marine Sinuous Channel Systems - from Outcrop Perspective, AAPG Annual Convention and Exhibition. Abstracts.: Denver, Colorado.

Arnott, R. W. C., L. Navarro, and Z. Khan, 2012, Temporal Evolution of Continental Slope Channels-A Matter of Sediment Volume and Grain Size Distribution, AAPG Annual Convention and Exhibition. Abstracts., Long Beach, California.

Arnott, R. W. C., K. Wallace, and J. Laurin, 2011, Stratal architecture and temporal evolution of a passive margin mass-transport deposit, Neoproterozoic Isaac

Formation, Cariboo Mountains, British Columbia, Canada, *in* R. C. Shipp, P. Weimer, and H. W. Posamentier, eds., Mass-Transport Deposits in Deepwater Settings, v. SEPM Special Publication, SEPM, p. 221-234.

Bain, H. A., and S. M. Hubbard, 2016, Stratigraphic evolution of a long-lived submarine channel system in the Late Cretaceous Nanaimo Group, British Columbia, Canada: Sedimentary Geology, v. 337, p. 113-132.

Beaubouef, R., V. Abreu, and J. Van Wagoner, 2003, Basin 4 of the Brazos-Trinity slope system, western Gulf of Mexico: The terminal portion of a late Pleistocene lowstand systems tract: Shelf margin deltas and linked down slope petroleum systems: Global significance and future exploration potential: Proceedings of the 23rd Annual Research Conference, Gulf Coast Section SEPM Foundation, p. 45-66.

Beaubouef, R. T., and S.J. Friedmann, 2000, High Resolution Seismic/Sequence Stratigraphic Framework for the Evolutionf Pleistocene Intra-Slope Basins, Western Gulf of Mexico: Depositional Models and Reservoir Analogs, Deep-Water Reservoirs of the World, GCSSEPM Foundation 20th Annual Research Conference.

Bonnel, C., B. Dennielou, L. Droz, T. Mulder, and S. Berné, 2005, Architecture and depositional pattern of the Rhône Neofan and recent gravity activity in the Gulf of Lions (western Mediterranean): Marine and Petroleum Geology, v. 22, p. 827-843.

Bouma, A. H., 1962, Sedimentology of some Flysch Deposits. A graphic approach to facies interpretation: Amsterdam, Elsevier.

Bourget, J., S. Zaragosi, T. Mulder, J. L. Schneider, T. Garlan, A. Van Toer, V. Mas, and N. Ellouz-Zimmermann, 2010, Hyperpycnal-fed turbidite lobe architecture and recent sedimentary processes: A case study from the Al Batha turbidite system, Oman margin: Sedimentary Geology, v. 229, p. 144-159.

Campbell, R., 1973, Structural cross-section and tectonic model of the southeastern Canadian Cordillera: Canadian Journal of Earth Sciences, v. 10, p. 1607-1620.

Campbell, R. B., F. G. Young, and E. W. Mountjoy, 1973, Geology of McBride Map-area, British Columbia (93H), Department of Energy, Mines and Resources, 104 p.

Cantero, M. I., A. Cantelli, C. Pirmez, S. Balachandar, D. Mohrig, T. A. Hickson, T. Yeh, H. Naruse, and G. Parker, 2012, Emplacement of massive turbidites linked to extinction of turbulence in turbidity currents: Nature Geoscience, v. 5, p. 42-45.

Cartigny, M. J. B., G. Postma, J. H. van den Berg, and D. R. Mastbergen, 2011, A comparative study of sediment waves and cyclic steps based on geometries, internal structures and numerical modeling: Marine Geology, v. 280, p. 40-56.

Cazzola, C., E. Mutti, and B. Vigna, 1983/ 1984, The Cengio Submarine Turbidite System of the Tertiary Piedmont Basin, Northwestern Italy: Geo-Marine Letters, v. 3, p. 173-177.

Chapin, M. A., P. Davies, J. L. Gibson, and H. S. Pettingill, 1994, Reservoir architecture of turbidite sheet sandstones in laterally extensive outcrops, Ross Formation, Western Ireland, Submarine Fans and Turbidite Systems, GCSSEPM Foundation 15th Annual Research Conference, p. 53-68.

Cornamusini, G., 2004, Sand-rich turbidite system of the Late Oligocene Northern Apennines foredeep: physical stratigraphy and architecture of the 'Macigno costiero' (coastal Tuscany, Italy), *in* S. A. Lomas, and P. Joseph, eds., Confined Turbidite Systems: London, United Kingdom, v. 222, Geological Society of London, Spec. Publ., p. 261-283.

Dalla Valle, G., and F. Gamberi, 2010, Erosional sculpting of the Caprera confined deep-sea fan as a result of distal basin-spilling processes (eastern Sardinian margin, Tyrrhenian Sea): Marine Geology, v. 268, p. 55-66.

Damuth, J. E., and R. D. Flood, 1984, Morphology, sedimentation processes, and growth pattern on the Amazon deep-sea fan: Geo-Marine Letters, v. 3, p. 109-117.

Damuth, J. E., V. Kolla, R. D. Flood, R. O. Kowsmann, M. C. Monteiro, M. A. Gorini, J. J. C. Palma, and R. H. Belderson, 1983, Distributary channel meandering and bifucation patterns on Amazon deep-sea fan as reveled by long-range side-scan sonar (GLORIA): Geology, v. 11, p. 470-473.

Deptuck, M. E., Z. Sylvester, C. Pirmez, and C. O'Byrne, 2007, Migration–aggradation history and 3-D seismic geomorphology of submarine channels in the Pleistocene Benin-major Canyon, western Niger Delta slope: Marine and Petroleum Geology, v. 24, p. 406-433.

Drinkwater, N. J., and K. T. Pickering, 2001, Architectural elements in a high-continuity sand-prone turbidite system, late Precambrian Kongsfjord Formation, northern Norway: Application to hydrocarbon reservoir characterization: AAPG Bulletin, v. 85, p. 1731–1757.

Duarte, J. C., P. Terrinha, F. M. Rosas, V. Valadares, L. M. Pinheiro, L. Matias, V. Magalhães, and C. Roque, 2010, Crescent-shaped morphotectonic features in the Gulf of Cadiz (offshore SW Iberia): Marine Geology, v. 271, p. 236-249.

Dumouchel, I. G., 2015, Stratigraphic Architecture and Depositional History of laterally-accreted channel fills in the Lower Isaac Formation, Windermere Supergroup, British Columbia, Canada, University of Ottawa, Ottawa, 108 p.

Elliott, T., 2000a, Depositional architecture of a sand-rich, channelised turbidite system: the Upper Carboniferous Ross sandstone formation, Western Ireland, *in* P. Weimer, R. M. Slatt, J. Coleman, N. C. Rosen, H. Nelson, A. H. Bouma, M. J. Styzen, and D. T. Lawrence, eds., Deep-water reservoirs of the World, GCSSEPM Foundation 20th Annual Research Conference, p. 342-364.

Elliott, T., 2000b, Megaflute erosion surfaces and the initiation of turbidite channels: Geology, p. 119-122.

Etienne, S., T. Mulder, P. Razin, M. Bez, G. Désaubliaux, R. Joussiaume, and E. Tournadour, 2013, Proximal to distal turbiditic sheet-sand heterogeneities: Characteristics of associated internal channels. Examples from the Trois Evêchés area, Eocene-Oligocene Annot Sandstones (Grès d'Annot), SE France: Marine and Petroleum Geology, v. 41, p. 117-133.

Fernandez, R. L., A. Cantelli, C. Pirmez, C. Sequeiros, and G. Parker, 2014, Growth patterns of subaqueous depositional channel lobe systems developed over a basement with a downdip break in slope: Laboratory Experiments: Journal of Sedimentary Research, v. 84, p. 168-182.

Fildani, A., N. W.R., S. Kostic, and G. Parker, 2006, Channel formation by flow stripping: large-scale scour features along the Monterey East Channel and their relation to sediment waves: Sedimentology, v. 53, p. 1265-1287.

Flint, S., D. Hodgson, A. Sprague, R. Brunt, W. Van der Merwe, J. Figueiredo, A. Prélat, D. Box, C. Di Celma, and J. Kavanagh, 2011, Depositional architecture and sequence stratigraphy of the Karoo basin floor to shelf edge succession, Laingsburg depocentre, South Africa: Marine and Petroleum Geology, v. 28, p. 658-674.

Flood, R. D., and J. E. Damuth, 1987, Quantitative characteristic of sinous distributary channels on the Amazon Deep-Sea Fan: GSA Bulletin, v. 98, p. 728-738.

Follmi, K. B., 1996, The phosphorus cycle, phosphogenesis and marine phosphate-rich deposits: Earth-Science Reviews, v. 40, p. 55-124.

Gamberi, F., and M. Rovere, 2011, Architecture of a modern transient slope fan (Villafranca fan, Gioia basin–Southeastern Tyrrhenian Sea): Sedimentary Geology, v. 236, p. 211-225.

Gervais, A., B. Savoye, T. Mulder, and E. Gonthier, 2006, Sandy modern turbidite lobes: A new insight from high resolution seismic data: Marine and Petroleum Geology, v. 23, p. 485-502.

Gordon, G. S., 2014, Stratigraphic evolution and architectural analysis of structurally confined submarine fans: A tripartite outcrop-based study: Unpublished PhD Thesis thesis, Golden, Colorado, 196 p.

Hilton, V. C., 1995, Sandstone architecture and facies from the Annot Basin of the SW Alpine foreland basin, SE France, *in* K. T. Pickering, R. N. Hiscott, N. H. Kenyon, F. Ricci Lucchi, and R. D. A. Smith, eds., Atlas of Deep Water Environments: Architectural style in turbidite systems: London, Chapman & Hall, p. 227-235.

Hiscott, R. N., 1994, Loss of capacity, not competence, as the fundamental process governing turbidity currents: Journal of Sedimentary Research, v. 64, p. 209-214.

Hodgson, D. M., S. S. Flint, D. Hodgetts, N. J. Drinkwater, E. P. Johannessen, and S. M. Luthi, 2006, Stratigraphic Evolution of Fine-Grained Submarine Fan Systems, Tanqua Depocenter, Karoo Basin, South Africa: Journal of Sedimentary Research, v. 76, p. 20-40.

Hofstra, M., D. M. Hodgson, J. Peakall, and S. S. Flint, 2015, Giant scour-fills in ancient channel-lobe transition zones: Formative processes and depositional architecture: Sedimentary Geology, v. 329, p. 98-114.

Hoyal, D. C. J. D., J. C. Van Wagoner, N. L. Adair, M. Deffenbaugh, D. Li, T. Sun, C. Huh, and D. E. Giffin, 2003, Sedimentation from jets: a depositional model for clastic deposits of all scales and environments, Online-Journal; AAPG/Data- pages, Inc., 1444 South Boulder, Tulsa, OK, 74119, USA.

Huang, H., J. Imran, C. Pirmez, Q. Zhang, and G. Chen, 2009a, The critical densimetric Froude number of subaqueous gravity currents can be non- unity or non-existent: Journal of Sedimentary Research, v. 79, p. 479-485.

Huang, H., J. Imran, C. Pirmez, Q. Zhang, and G. Chen, 2009b, The critical densimetric Froude number of subaqueous gravity currents can be non-unity or non-existent: Journal of Sedimentary Research, v. 79, p. 479-485.

Jegou, I., B. Savoye, C. Pirmez, and L. Droz, 2008, Channel-mouth lobe complex of the recent Amazon Fan: The missing piece: Marine Geology, v. 252, p. 62–77.

Kenyon, N. H., and J. Millington, 1995, Contrasting deep-sea depositional systems in the Bering Sea., *in* K. T. Pickering, R. N. Hiscott, N. H. Kenyon, F. Ricci Lucchi, and R. D. A. Smith, eds., Atlas of deep water environments: Architectural style in turbidite
systems: London, Chapman and Hall, p. 196-202.

Kenyon, N. H., J. Millington, L. Droz, and M. K. Ivanov, 1995, Scour holes in a channel-lobe transition zone on the Rhone Cone., *in* K. T. Pickering, H. R. N., K. N. H., R. L. F., and S. R.D.A., eds., Atlas of deep water environments: Architectural style in turbidite systems: London, Chapman and Hall, p. 212-215.

Khan, Z. A., and R. W. C. Arnott, 2011, Stratal attributes and evolution of asymmetric inner- and outer-bend levee deposits associated with an ancient deep-water channel-levee complex within the Isaac Formation, southern Canada: Marine and Petroleum Geology, v. 28, p. 824-842.

Kidwell, S., 1991, Condensed deposits in siliciclastic sequences: expected and observed features: Cycles and events in stratigraphy, p. 682-695.

Kneller, B., and W. D. McCaffrey, 1999, Depositional effects of flow non-uniformity and stratification within turbidity currents approaching a bounding slope: deflection, reflection, and facies variation: Journal of Sedimentary Research, v. 20, p. 980-991.

Kolla, V., H. W. Posamentier, and L. J. Wood, 2007, Deep-water and fluvial sinuous channels-Characteristics, similarities and dissimilarities, and modes of formation: Marine and Petroleum Geology, v. 24, p. 388-405.

Kostic, S., 2011, Modeling of submarine cyclic steps: Controls on their formation, migration, and architecture: Geosphere, v. 7, p. 294-304.

Kostic, S., and G. Parker, 2006, The response of turbidity currents to a canyon-fan transition: Internal hydraulic jumps and depositional signatures: Journal of Hydraulic Research, v. 44, p. 631-653.

Kostrewa, R., 2004, Internal architecture, geometry and reservoir characterisation of depositional lobes in outcrop and subsurface: examples from S-Turkey and the North Sea.: Unpublished Ph.D. thesis, Eberhard Karls University of Tübingen, 177 p.

Lang, J., and J. Winsemann, 2013, Lateral and vertical facies relationships of bedforms deposited by aggrading supercritical flows: From cyclic steps to humpback dunes: Sedimentary Geology, p. 36-54.

Leclair, S., and R. W. C. Arnott, 2005, Parallel lamination formed by high-density turbidity currents: Journal of Sedimentary Research, v. 75, p. 1-5.

Lee, S. E., P. J. Talling, G. G. J. Ernst, and A. J. Hogg, 2002, Occurrence and origin of submarine plunge pools at the base of the US continental slope: Marine Geology, v. 185, p. 363-377.

Lien, T., R. G. Walker, and O. J. Martinsen, 2003, Turbidites in the Upper Carboniferous Ross Formation, western Ireland: reconstruction of a channel and spillover system: Sedimentology, v. 50, p. 113-148.

Loutit, T. S., 1988, Condensed sections: the key to age determination and correlation of continental margin sequences, *in* C. K. Wilgus, B. S. Hastings, C. S. C. Kendall, H. W. Posamentier, C. A. Ross, and J. C. V. Wagoner, eds., Sea level changes: an integrated approach, v. vol. 42, SEPM Special Publication, p. 183-213.

Lowe, D. R., 1982, Sediment gravity flows: II. Depositional models with special reference to the deposits of high-density turbidity currents: Journal of Sedimentary Petrology, v. 52, p. 279-297.

Lowe, D. R., and R. D. LoPiccolo, 1974, The characteristics and origins of dish and pillar structures: Journal of Sedimentary Petrology, v. 44, p. 484-501.

Macauley, R. V., and S. M. Hubbard, 2013, Slope channel sedimentary processes and stratigraphic stacking, Cretaceous Tres Pasos Formation slope system, Chilean Patagonia: Marine and Petroleum Geology, v. 41, p. 146-162.

Macdonald, H., 2010, Flutes, megaflutes and erosional bedforms: a reappraisal of their dynamics, University of Leeds, 254 p.

Macdonald, H., R. B. Wynn, V. A. I. Huvenne, J. Peakall, D. G. Masson, P. P. E. Weaver, and S. D. McPhail, 2011, New insights into the morphology, fill, and remarkable longevity (>0.2 m.y.) of modern deep-water erosional scours along the northeast Atlantic margin: Geosphere, v. 7, p. 845-867.

Macdonald, R. G., 2012, Flow and sediment transport at hydraulic jumps: PhD thesis, University of East Anglia, 254 p.

Macdonald, R. G., J. Alexander, J. C. Bacon, and M. J. Cooker, 2009, Flow patterns, sedimentation and deposit architecture under a hydraulic jump on a non-eroding bed: defining hydraulic-jump unit bars: Sedimentology, v. 56, p. 1346-1367.

Macdonald, R. G., J. Alexander, J. C. Bacon, and M. J. Cooker, 2013, Variations in the architecture of hydraulic-jump bar complexes on non-eroding beds: Sedimentology, v. 60, p. 1291-1312.

Maier, K. L., A. Fildani, T. R. McHargue, C. K. Paul, S. A. Graham, and D. W. Caress, 2012, Punctuated deep-water channel migration: High-resolution subsurface data from the Lucia Chica Channel System, offshore California, U.S.A.: Journal of Sedimentary Research, v. 82, p. 1-8.

Maslin, M., M. Owen, S. Day, and D. Long, 2004, Linking continental-slope failures and climate change: Testing the clathrate gun hypothesis: Geology, v. 32, p. 53-56.

Mayall, M., E. Jones, and M. Casey, 2006, Turbidite channel reservoirs-key elements in facies prediction and effective development: Marine and Petroleum Geology, v. 23, p. 821-841.

McHargue, T., M. J. Pyrcz, M. D. Sullivan, J. D. Clark, A. Fildani, B. W. Romans, J. A. Covault, M. Levy, H. W. Posamentier, and N. J. Drinkwater, 2011, Architecture of turbidite channel systems on the continental slope: Patterns and predictions: Marine and Petroleum Geology, v. 28, p. 728-743.

Meyer, L., 2004, Internal architecture of an ancient deep-water, passive margin, basin-floor fan system, Upper Kaza Group, Windermere Supergroup, Castle Creek, British Columbia: M.Sc. Thesis thesis, Univeristy of Calgary, Calgary, Alberta, 175 p.

Meyer, L., and G. M. Ross, 2007, Channelized lobe and sheet sandstones of the Upper Kaza Group basin-floor turbidite system, British Columbia, Canada, *in* T. H. Nilsen, R. D. Shew, G. S. Steffens, and J. R. J. Studlick, eds., Atlas of deep-water outcrops, v. Studies in Geology 56, AAPG, p. 22.

Migeon, S., B. Savoye, E. Zanella, T. Mulder, J.-C. Faugères, and O. Weber, 2001, Detailed seismic-reflection and sedimentary study of turbidite sediment waves on the Var Sedimentary Ridge (SE France): significance for sediment transport and deposition and for the mechanisms of sediment-wave construction: Marine and Petroleum Geology, v. 18, p. 179-208.

Millington, J. J., and J. D. Clark, 1995, The Charo/Arro Canyon-Mouth sheet system, south-central Pyrenees, Spain: A structurally confined influence zone of sediment dispersal: Journal of Sedimentary Research, v. 65, p. 443-454.

Mohrig, D., and J. Buttles, 2007, Deep turbidity currents in shallow channels: Geology, v. 35, p. 155-158.

Morris, E. A., D. M. Hodgson, S. S. Flint, R. L. Brunt, P. J. Butterworth, and J. Verhaeghe, 2014, Sedimentology, Stratigraphic Architecture, and Depositional Context of Submarine Frontal-Lobe Complexes: Journal of Sedimentary Research, v. 84, p. 763-780.

Morris, S. A., N. H. Kenyon, A. H. Limonov, and J. Alexander, 1998, Downstream changes of large-scale bedforms in turbidites around the Valencia channel mouth, northwest Mediterranean: implications for palaeoflow reconstruction: Sedimentology, v. 45, p. 365-377.

Morris, W. R., and W. R. Normark, 2000, Sedimentologic and geometric criteria for comparing modern and ancient sandy turbidite elements, *in* P. Weimer, R. M. Slatt, J. Coleman, N. C. Rosen, H. Nelson, A. H. Bouma, M. J. Styzen, and D. T. Lawrence, eds., Deep-water reservoirs of the world (CD-ROM), Gulf Coast Section SEPM, p. 606-623.

Moscardelli, L., L. Wood, and P. Mann, 2006, Mass-transport complexes and associated processes in the offshore area of Trinidad and Venezuela: AAPG Bulletin, v. 90, p. 1059-1088.

Mulder, T., and J. Alexander, 2001, The physical character of subaqueous density flows and their deposits: Sedimentology, v. 48, p. 269-299.

Murphy, D., and C. Rees, 1983, Structural transition and stratigraphy in the Cariboo Mountains, British Columbia: Geol. Surv. Pap. Can, p. 245-252.

Mutti, E., 1977, Distinctive thin-bedded turbidite facies and related depositional environments in the Eocene Hecho Group (South-central Pyrenees, Spain): Sedimentology, v. 24, p. 107-131.

Mutti, E., 1992, Turbidite sandstones: Milan: Agip, Istituto di geologia, Università di Parma, 275 p.

Mutti, E., and W. R. Normark, 1987, Comparing examples of modern and ancient turbidite systems: problems and concepts, *in* J. K. Leggett, and G. G. Zuffa, eds., Marine clastic sedimentology: concepts and case studies: London, Graham and Troutman, p. 1-38.

Mutti, E., and W. R. Normark, 1991, An integrated approach to the study of turbidite systems, *in* P. Weimer, and M. H. Link, eds., Seismic facies and sedimentary processes of submarine fans and turbidite systems: New York, Springer-Verlag, p. 75-106.

Navarro, L., 2006, Depositional Architecture and Evolution of deep-water base-of-slope and slope channel complexes in a passive-margin setting: Isaac Formation, Windermere Supergroup (Neoproterozoic), Southern Canadian Cordillera: M.Sc.Thesis thesis, University of Ottawa, Ottawa, 272 p.

Navarro, L., Z. Khan, and R. W. C. Arnott, 2007, Depositional architecture and evolution of a deep-marine channel-levee complex: Isaac Formation (Windermere Supergroup), Southern Canadian Cordillera., *in* T. H. Nilsen, R. D. Shew, G. S. Steffens, and J. R. J. Studlik, eds., Atlas of Deep-water Outcrops., v. CD-ROM: Tulsa, AAPG Studies in Geology 56, CD-ROM, p. 22.

Normark, W. R., C. K. Paull, D. W. Caress, W. Ussler, and R. Sliter, 2009, Fine-scale relief related to Late Holocene channel shifting within the floor of the upper Redondo Fan, offshore Southern California: Sedimentology, v. 56, p. 1690-1704.

Normark, W. R., and D. J. W. Piper, 1985, Navy Fan, Pacific Ocean, *in* A. H. Bouma, W. R. Normark, and N. E. Barnes, eds., Submarine fans and related turbidite systems: New York, Springer-Verlag, p. 87-94.

Normark, W. R., D. J. W. Piper, and G. R. Hess, 1979, Distributary channels, sand lobes, and mesotopography of Navy Submarine Fan, California Borderland, with applications to ancient fan sediments: Sedimentology, v. 26, p. 749-774.

O'Connell, S., W. B. F. Ryan, and W. R. Normark, 1991, Evolution of a fan channel on the outer Mississippi Fan: evidence from side-looking sonar, *in* P. Weimer, and M. H. Link, eds., Seismic facies and sedimentary processes of submarine fans and turbidite systems: New York, Springer-Verlag, p. 365-382.

O'Byrne, C. J., M. D. Barton, G. S. Steffens, C. Pirmez, and H. Buergisser, 2007, Architecture of a laterally migrating channel complex - Isaac Formation, Windermere Supergroup, British Columbia, Canada, *in* T. H. Nilsen, R. D. Shew, G. S. Steffens, and J. R. J. Studlick, eds., Atlas of deep-water outcrops, v. CD-ROM: Tulsa, AAPG, p. 11 p.

Ogata, K., 2010, Mass Transport Complexes in Structurally contreolled basins: The Epiligurian Specchio Unit (Northern Appeninnes, Italy): Ph.D. Thesis thesis, University of Parma, Parma, 476 p.

Palanques, A., N. H. Kenyon, B. Alonso, and A. Limonov, 1995, Erosional and depositional patterns in the Valencia Channel Mouth: an example of a modern channel-lobe transition zone: Marine Geophysical Researches, v. 17, p. 503-517.

Parker, G., and N. Izumi, 2000, Purely erosional cyclic and solitary steps created by flow over a cohesive bed: Journal of Fluid Mechanics, v. 419, p. 203-238.

Pemberton, E. A. L., S. M. Hubbard, A. Fildani, B. Romans, and S. Kostic, 2015, The Stratigraphic Expression of Submarine Channel-Lobe Transitions: An Outcrop Example from Southern Chile, EGU General Assembly 2015, Viena, Austria.

Pemberton, E. A. L., S. M. Hubbard, A. Fildani, B. Romans, and L. Stright, 2016, The stratigraphic expression of decreasing confinement along a deep-water sediment routing system: Outcrop example from southern Chile: Geosphere, v. 12, p. 114-134.

Pickering, K. T., 1983, Transitional submarine fan deposits from the late Precambrian Kongsijord Formation submarine fan, NE Finnmark, N. Norway: Sedimentology, v. 30, p. 18I-199.

Pickering, K. T., and J. Corregidor, 2005, Mass-transport Complexes (MTCs) and tectonic control on basin-floor submarine fans, Middle Eocene, South Spanish Pyrenees: Journal of Sedimentary Research, v. 75, p. 761-783.

Pirmez, C., R. T. Beaubouef, S. J. Friedmann, and D. C. Mohrig, 2000, Equilibrium profile and base level in submarine channels: examples from Late Pleistocene systems and implications for the architecture of deep-water reservoirs, *in* P. Weimer, R. M. Slatt, J. Coleman, N. C. Rosen, H. Nelson, A. H. Bouma, M. J. Styzen, and D. T. Lawrence, eds., Deep-Water Reservoirs of the World, Gulf Coast Society of the Society of Economic Paleontologists and Mineralogists Foundation, 20th Annual Research Conference, p. 782-805.

Pirmez, C., R. N. Hiscott, and J. J. D. Kronen, 1997, Sandy turbidite successions at the base of channel-levee systems of the Amazon Fan revealed by FMS logs and cores: Unraveling the facies architecture of large submarine fans, *in* R. D. Flood, D. J. W. Piper, A. Klaus, and L. C. Peterson, eds., Proceedings of the Ocean Drilling Program, Scientific Results, v. 155, p. 7-33.

Planavsky, N. J., O. J. Rouxel, A. Bekker, S. V. Lalonde, K. O. Konhauser, C. T. Reinhard, and T. W. Lyons, 2010, The evolution of the marine phosphate reservoir: Nature, v. 467, p. 1088-1090.

Posamentier, H. W., and V. Kolla, 2003, Seismic geomorphology and stratigraphy of depositional elements in deep-water settings: Journal of Sedimentary Research, v. 73, p. 367–388.

Posamentier, H. W., and R. G. Walker, 2006, Deep-water turbidites and submarine fans: SEPM Special Publication, v. 84, p. 397–520.

Postma, G., D. C. Hoyal, V. Abreu, M. J. Cartigny, T. Demko, J. J. Fedele, K. Kleverlaan, and K. H. Pederson, 2016, Morphodynamics of supercritical turbidity currents in the channel-lobe transition zone, *in* G. Lamarche, J. Mountjoy, S. Bull, T. Hubble, S. Krastel, E. Lane, A. Micallef, L. Moscardelli, C. Mueller, I. Pecher, and S. Woelz, eds., Submarine Mass Movements and their Consequences, Springer, p. 469-478.

Prather, B. E., J. R. Booth, G. S. Steffens, and P. A. Craig, 1998, Classification, lithologic calibration and stratigraphic succession of seismic facies from

intraslope basins, deep water Gulf of Mexico, USA: AAPG Bulletin, v. 82, p. 701-728.

Prélat, A., and D. M. Hodgson, 2013, The full range of turbidite bed thickness patterns in submarine lobes: controls and implications: Journal of the Geological Society, v. 170, p. 209-214.

Prélat, A., D. M. Hodgson, and S. S. Flint, 2009, Evolution, architecture and hierarchy of distributary deep-water deposits: a high-resolution outcrop investigation from the Permian Karoo Basin, South Africa: Sedimentology, v. 56, p. 2132-2154.

Pyles, D. R., and D. C. Jennette, 2009, Geometry and architectural associations of co-genetic debrite–turbidite beds in basin-margin strata, Carboniferous Ross Sandstone (Ireland): Applications to reservoirs located on the margins of structurally confined submarine fans: Marine and Petroleum Geology, v. 26, p. 1974–1996.

Pyles, D. R., L. J. Strachan, and D. C. Jennette, 2014, Lateral juxtapositions of channel and lobe elements in distributive submarine fans: Three-dimensional outcrop study of the Ross Sandstone and geometric model: Geosphere, v. 10, p. 1104-1122.

Pyrcz, M. J., M. Sullivan, N. Drinkwater, J. Clark, A. Fildani, and M. Sullivan, 2006, Event-based models as a numerical laboratory for testing sedimentological rules associated with deepwater sheets: Gulf Coast Section SEPM 26th Bob F. Perkins Research Conference, p. 923-950.

R., L. M., 1999, Sedimentology and Sedimentary Basins: From Turbulence to Tectonics: Oxford, Blackwell Science.

Rocheleau, J., 2011, Depositional architecture of a near-slope turbidite succession: Upper Kaza Group, Windermerer Supergroup, Castle Creek, British Columbia, Canada: M.Sc. thesis, University of Ottawa, Ottawa, 94 p.

Romans, B. W., S. M. Hubbard, and S. A. Graham, 2009, Stratigraphic evolution of an outcropping continental slope system, Tres Pasos Formation at Cerro Divisadero, Chile: Sedimentology, v. 56, p. 737–764.

Ross, G. M., and R. W. C. Arnott, 2007, Regional geology of the Windermere Supergroup, southern Canadian Cordillera and stratigraphic setting of the Castle Creek study area, Canada, *in* T. H. Nilsen, R. D. Shew, G. S. Steffens,

and J. R. J. Studlick, eds., Atlas of deep-water outcrops, v. 56, AAPG Studies in Geology, CD-ROM, p. 16.

Ross, G. M., and C. A. Ferguson, 2003, Geology and structure cross-sections, Eddy, British Columbia. Map 1967A, scale 1:50,000: Geol. Surv. Can.

Saller, A., K. Werner, F. Sugiaman, A. Cebastiant, R. May, D. Glenn, and C. Barker, 2008, Characteristics of Pleistocene deep-water fan lobes and their application to an upper Miocene reservoir model, offshore East Kalimantan, Indonesia: AAPG Bulletin, v. 92, p. 919–949.

Samuel, A., B. Kneller, S. Raslan, A. Sharp, and C. Parsons, 2003, Prolific deep-marine slope channels of the Nile Delta, Egypt: AAPG Bulletin, v. 87, p. 541-560.

Sawyer, D. E., P. B. Flemings, R. C. Shipp, and C. D. Winker, 2007, Seismic geomorphology, lithology, and evolution of the late Pleistocene Mars-Ursa turbidite region, Mississippi Canyon area, northern Gulf of Mexico: AAPG Bulletin, v. 91, p. 215-234.

Schwarz, E., and R. W. C. Arnott, 2007, Anatomy and evolution of a slope channel-complex set (Neoproterozoic Isaac Formation, Windermere Supergroup, southern Canadian Cordillera); implications for reservoir characterization: Journal of Sedimentary Research, v. 77, p. 89-109.

Spinewine, B., O. E. Sequeiros, M. H. Garcia, R. T. Beaubouef, T. Sun, B. Savoye, and G. Parker, 2009, Experiments on wedge-shaped deep sea sedimentary deposits in minibasins and/or channel levees emplaced by turbidity currents. Part II. Morphodynamic Evolution of the wedge amd of the associated bedforms: Journal of Sedimentary Research, v. 79, p. 608-628.

Sprague, A. R., M. D. Sullivan, K. M. Campion, G. N. Jensen, D. K. Goulding, D. K. Sickafoose, and D. C. Jennette, 2002, The physical stratigraphy of deep-water strata: a hierarchical approach to the analysis of genetically related elements for improved reservoir prediction, AAPG Annual Convention and Exhibition. Abstracts. : Houston, Texas, p. 10-13.

Stevenson, C. J., C. A.-L. Jackson, D. M. Hodgson, S. M. Hubbard, and J. T. Eggenhuisen, 2015, Deep-water sediment bypass: Journal of Sedimentary Research, v. 85, p. 1058-1081.

Strachan, L. J., 2008, Flow transformations in slumps: a case study from the Waitemata Basin, New Zealand: Sedimentology, v. 55, p. 1311-1332.

Sullivan, M. D., J. L. Foreman, D. C. Jennette, D. Stern, G. N. Jensen, and F. J. Goulding, 2004, An integrated approach to characterization and modeling of deep-water reservoirs, Diana field, western Gulf of Mexico, in Integration of outcrop and modern analogs in reservoir modeling: AAPG Memoir, v. 80, p. 215–234.

Sullivan, M. D., G. N. Jensen, F. J. Goulding, D. C. Jennette, J. L. Foreman, and D. Stern, 2000, Architectural analysis of deepwater outcrops: Implications for exploration and production of the Diana Sub-basin, western Gulf of Mexico, *in* P. Weimer, R. M. Slatt, A. H. Bouma, and D. T. Lawrence, eds., Deepwater reservoirs of the world, GCSSEPM Foundation, p. 1010-1032.

Sumner, E. J., J. Peakall, D. R. Parsons, R. B. Wynn, S. E. Darby, R. M. Dorrell, S. D. McPhail, J. Perrett, A. Webb, and D. White, 2013, First direct measurements of hydraulic jumps in an active submarine density current: Geophys. Res. Lett., v. 40, p. 1-5.

Sylvester, Z., C. Pirmez, and A. Cantelli, 2011, A model of submarine channel-levee evolution based on channel trajectories: Implications for stratigraphic architecture: Marine and Petroleum Geology, v. 28, p. 716-727.

Terlaky, V., 2014, Sedimentology, Stratigraphy, Architecture and Origin of deep-water, basin-floor deposits: Middle and Upper Kaza Group, Windermere Supergroup, B.C., Canada: Ph.D. thesis, University of Ottawa, Ottawa, 213 p.

Terlaky, V., and R. W. C. Arnott, 2014, Matrix-rich and associated matrix-poor sandstones: Avulsion splays in slope and basin-floor strata: Sedimentology, v. 61, p. 1175-1197.

Terlaky, V., J. Rocheleau, and R. W. C. Arnott, 2016, Stratal composition and stratigraphic organization of stratal elements in an ancient deep-marine basin-floor succession, Neoproterozoic Windermere Supergroup, British Columbia, Canada: Sedimentology, v. 63, p. 136-175.

Thomas, M. F. H., 2011, Sedimentology and basin context of the Numidian Flysch Formation; Sicily and Tunisia: Unpublished Ph.D. thesis, University of Manchester, Manchester, 278 p.

Tripsanas, E. K., W. R. Bryant, and D. B. Prior, 2003, Structural characteristics of cohesive gravity-flow deposits, and a sedimentological approach on their flow mechanisms, *in* J. Locat, and J. Mienert, eds., Submarine Mass Movements and their Consequences, p. 129-136.

Tripsanas, E. K., D. J. W. Piper, J. K.A, and W. R. Bryant, 2008, Submarine mass-transport facies: new perspectives on flow processes from cores on the eastern North American margin: Sedimentology, v. 55, p. 97-136.

Tudor, E. P., 2014, Facies Variability in deep-water channel-to-lobe transition zone: Jurassic Los Molles Formation, Neuquen Basin Argentina: Unpublished thesis, University of Texas, Austin, Texas, 76 p. p.

Vail, P., J. Hardenbol, and R. Todd, 1984, Jurassic unconformities, chronostratigraphy, and sea-level changes from seismic stratigraphy and biostratigraphy, M 36: Interregional Unconformities and Hydrocarbon Accumulation, v. Memoir, p. 129-144.

Van der Merwe, W. C., D. M. Hodgson, R. L. Brunt, and S. S. Flint, 2014, Depositional architecture of sand-attached and sand-detached channel-lobe transition zones on an exhumed stepped slope mapped over a 2500 km2 area: Geosphere.

Vicente Bravo, J. C., and S. Robles, 1991, Characterization of the channel-lobe transition facies association of the Black Flyshjata sequence (Upper Albian, northern Spain): Geogaceta, v. 10, p. 72-75.

Vicente Bravo, J. C., and S. Robles, 1995, Large-scale mesotopographic bedforms from the Albian Black Flysch, northern Spain: characterization, setting and comparison with recent analogues, *in* K. T. Pickering, R. N. Hiscott, N. H. Kenyon, F. R. Lucchi, and R. D. A. Smith, eds., Atlas of deep water environments: Architectural style in turbidite systems: London, Chapman and Hall, p. 216-226.

Wynn, R. B., 2000, Turbidity current processes and deposits on the Northwest African Margin: Ph.D. thesis, University of Southampton, 281 p.

Wynn, R. B., B. T. Cronin, and J. Peakall, 2007, Sinuous deep-water channels: Genesis, geometry and architecture: Marine and Petroleum Geology, v. 24, p. 341-387.

Wynn, R. B., N. H. Kenyon, D. G. Masson, D. A. V. Stow, and P. P. E. Weaver, 2002, Characterization and recognition of deep-water channel-lobe transition zones: AAPG Bulletin, v. 86, p. 1441–1462.

Chapter 4

STRATAL ARCHITECTURE AND EVOLUTION OF A SLOPE MASS-TRANSPORT COMPLEX AND OVERLYING DEEP-WATER DEPOSITS, LOWER ISAAC FORMATION, WINDERMERE SUPERGROUP, CANADA

4.1 Introduction

Due to increasing geological interest by both industry and academe and the ever-expanding and improving database of high-resolution subsurface seismic data, not only have deep-water channels and leveed channels have been extensively studied in modern and ancient slope systems over the past few decades, but also mass-transport complexes, hereafter named MTCs (e.g. Deptuck et al., 2003; Posamentier and Kolla, 2003; Moscardelli et al., 2006; Posamentier and Walker, 2006; Gamberi and Rovere, 2011; McHargue et al., 2011; Olafiranye et al., 2013; Ortiz-Karpf et al., 2015). However, in spite of numerous exceptional seismic images, key sedimentological and stratigraphic data, specifically subseismic, meter-scale characteristics, which can only be acquired from core and outcrop remain poorly understood. The limited dimensions of most exposed MTCs ~~and slope channels~~, especially in terms of their width, restricts their comparative utility with seismic images, although a number of exceptions do exist, including examples from the Ainsa basin, Spain (Pickering and Corregidor, 2005), Tres Pasos Formation in Magallanes basin, Southern Chile (Armitage et al., 2009), Temburong Formation, northwest

Borneo (Jackson and Johnson, 2009), west Texas (Amerman et al., 2007), north Taranaki basin, New Zealand (King et al., 2011), Casaglia Monte della Colonna, Italy (Lucente and Pini, 2003), and Specchio Unit, Italy (Ogata, 2010; Ogata et al., 2012).

At the Castle Creek study area in the Cariboo Mountains (southern Canadian Cordillera), at least six slope channel complexes have been recognized in the Isaac Formation, lower Cariboo Group (Navarro, 2006; Arnott, 2007; Navarro et al., 2007; O'Byrne et al., 2007; Schwarz and Arnott, 2007; Khan and Arnott, 2011; Dumouchel, 2015), but few of them are interpreted to be developed in association with MTCs (e.g. Laurin et al., 2007; Arnott et al., 2011). The first major MTC in the Isaac Formation comprises Isaac slide 2 and Isaac debrite 1, and is successively overlain by mudstone-rich deposits, sandstone-rich splay, channel deposits of Isaac channel complex 0 and ponded deposits. The latter are then capped by mudstone-rich deposits. The objective of this study is to document for first time the lithological make-up and stratigraphic architecture of these strata, and evaluate any possible influence of the MTC on deposition of the overlying strata.

4.2 Study area

This study focuses on a siliciclastic-rich interval that directly underlies the first Isaac carbonate (for detailed description and discussion, see chapters 3 and 4, respectively), which is an important regional stratigraphic marker in the deep-marine sedimentary pile of the Windermere Supergroup (Ross and Murphy, 1988; Ross and Bowring, 1990; Ross et al., 1995; Ross and Ferguson, 2003; Ross and Arnott, 2007).

The interval is part of a mudstone-prone slope succession in the Isaac Formation (lower Cariboo Group) that crops out extensively in alpine exposures in the Cariboo Mountains, particularly at the Castle Creek study area (Fig. 4.1A). Here, the interval is up to 101 m thick and extends laterally for at least 1.2 km (Fig. 4.1B-C). Despite the regional low-grade regional metamorphism and tectonic deformation that affected strata of the Cariboo Group (see Murphy, 1990; Ferguson and Simony, 1991), primary physical sedimentary textures and structures are clearly preserved.

4.3 Dataset

This research was based on fieldwork conducted mostly in the Castle Creek area. Stratigraphic sections were recorded bed-by-bed and total 653 m was measured. In addition, high-resolution aerial photomosaics (1:380-1:500) were used to trace significant surfaces that in many cases bound major lithological units. Wallace (2004) is the only sedimentological study previously conducted in the debris-flow deposit of the lower part of the studied interval, which was confined to the southeast margin of the Castle Creek glacier. The present work comprises a much larger area and includes outcrops on both sides of the glacier. Location of stratigraphic sections or logs is given in Appendix B3. Paleocurrent data were difficult to obtain in the study area, except for few from ripple cross-laminated beds. Also, eight standard thin sections were examined (see Appendix C) to determine mineralogy of framework grains, matrix and/or cement, plus three x-ray fluorescence samples to determine the elemental composition of mudstone (see Appendix D).

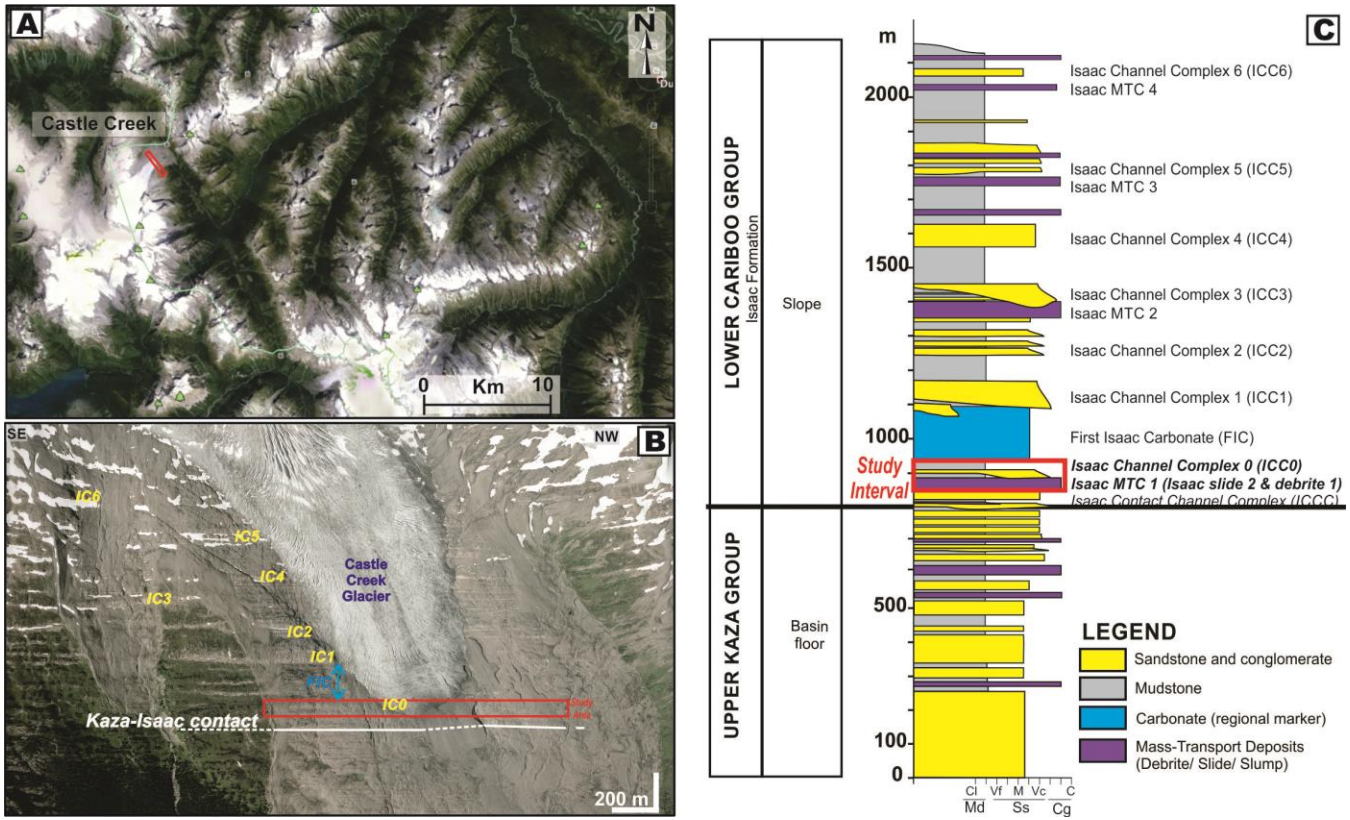

Figure 4.1. Location and stratigraphy of the Castle Creek study area in the Cariboo Mountains. (A) Satellite image from Google Earth (2014) showing the location of the Castle Creek area. (B) Location of the studied interval in the Castle Creek is indicated by red rectangle (photo from the Western Canadian Cryospheric Network and UNBC, 2008). (C) Generalized stratigraphic column for deep-water strata in the Castle Creek outcrop. Strata described here are part of the Isaac Formation (lower Cariboo Group) which at Castle Creek has been informally subdivided into six major lenticular sandstone-rich units interpreted as slope channel complexes (labeled ICC0-ICC6), and large-scale mass-transport deposits (debrites, slumps and slides, here informally named Isaac MTC 1-4) encased in a mudrock-dominated succession. Additionally, a regional marker termed the First Isaac Carbonate (FIC) also crops out.

Besides, 239 m-thick by 450 m-wide section at Mount Quanstrom, located about 20 km east of Castle Creek, was also studied. Preliminary data suggest that lithologies and stratal architectures are similar in both study areas, but certain units at Mount Quanstrom are significantly thicker, the origin of which (i.e. sedimentary or tectonic) is currently unknown and require future work (see Appendix G for description and preliminary interpretations, logs, aerial photomosaics and photographs).

4.4 Facies

Based on texture (especially grain size), framework grain mineralogy, bed thickness, and sedimentary structures, eight lithofacies were identified (Fig. 4.2A-I). Table 4.1 summarizes the characteristics of each lithofacies and its interpreted depositional origin.

4.5 Stratigraphic Architecture

In the Castle Creek study area, seven stratigraphic units separated by laterally-extensive significant surfaces are recognized (see Table 4.2 and Figs. 4.3A-C, 4.4), and in ascending stratigraphic order are described next. The lower units comprise thick slide and debris-flow deposits found in the lower Isaac Formation. These, then, are successively overlain by mudstone-rich deposits, sandstone-rich splay, channel deposits of Isaac channel complex 0 and ponded deposits, and ultimately capped by mudstone-rich deposits.

Table 4.1. Description and interpretation of lithofacies documented in this study

Lithofacies	*Grain size and composition*	*Bed thickness and contacts*	*Sedimentary Structures*	*Interpretation*	*Turbidite divisions*
F1. Clast-supported conglomerate (Fig. 4.2A,B)	Predominantly granule to medium pebble conglomerate. Quartz and feldspars clasts dispersed within a medium /coarse sandstone matrix. Some beds contain mudstone clasts. Uncommon carbonate clasts are also observed.	Beds vary from several centimeters to up to 5.5 m thick. Bed bases are sharp, loaded, undulatory, or locally erosional with relief up to <0.5 m. The tops are typically planar.	Coarse-tail, normally graded. Local basal load structures.	Differential-settling deposition from gravelly to sandy, high-concentration turbidity flows (Pirmez et al., 2004).	R3 Lowe division
F2. Sandstone (Fig. 4.2A)	Medium-, coarse- to very coarse-grained sandstone with common granules at the base of beds grading upward to fine-grained sandstone and/or mudstone. Quartzose and sub-feldspathic sandstone.	Bed thickness ranges from 0.1 to 2.8 m. Sharp or irregular erosive bases. Loaded bases are also common. Planar tops.	Typically, normally-graded. Some beds are overlain by (planar-or cross-) laminated fine-grained sandstone and/or mudstone caps. Load and flame structures are common.	Gradual deposition from sandy high-to moderate-concentration turbidity flows (Lowe, 1982; Mulder and Alexander, 2001).	S3 Lowe or Ta Bouma divisions (most common) Tad, Tacd, Tabd, Tabcd Tb, Tbd, or Tbcd Bouma turbidites(less common)
F3. Mudstone-clast breccia (Fig. 4.2C)	Abundant, up to 45 cm-long (boulder size), tabular to elongated, silty mudstone clasts embedded in a poorly-sorted matrix with dispersed medium sand grains to fine pebbles. Some clasts are structureless, laminated or interstratified with fine-sandstone.	Beds are up to 1.1 m thick. Typically, sharp to scoured or erosive bases.	Structureless and ungraded.	Deposition from very high-concentration to transitional flows between sandy-hyperconcentrated and cohesive debris flows (Lowe, 1982; Mulder and Alexander, 2001) with abundant mudstone clasts derived from local or upflow scouring of the muddy substrate.	F3 Mutti facies

F4. Cross-stratified sandstone (Fig. 4.2D,G)	Medium- and coarse-grained sandstone. Coarser beds also contain dispersed granules and pebbles. Mudstone clasts are uncommon.	Beds are up to 0.35 m thick. Bed bases are sharp or erosive.	Typical single set, medium-scale (dune) cross-stratification.	Deposition from similarly low- to moderate- concentration but higher speed sandy turbidity currents.	F6 Mutti facies
F5. Sandstone-mudstone couplets (Fig. 4.2E,F)	F5a. Very fine- and fine-grained sandstone, sharply capped by mudstone.	Sandstone-mudstone couplets are 1 to 10 cm thick. Sandstone beds vary from 0.1 to 8 cm (most common 2-3 cm) and have sharp bases and tops. Mudstone interbeds with sharp bases and tops and vary from 0.1 to 7 cm thick.	Sandstone are structureless, but predominantly parallel laminated and/or small-scale cross-laminated. Single and multiple (up to three or four) sets cross-lamination are common. Local isolated (starved) ripple formsets are observed locally.	Deposition from waning fine-grained, low-concentration turbidity flows.	Upper divisions of Bouma sequence: Tcd,Tcde, Tbcd, Td.
	F5b. Fine- and medium-grained sandstone with distinctively-thick mudstone caps.	Sandstone-mudstone couplets are up to 90 cm thick, but commonly 2 to 20 cm. Sandstone beds are up to 55 cm (commonly 0.5 to 12 cm) and have sharp bases, but diffuse tops. Some coarser interbeds. Mudstone beds are up to 35 cm thick (average 1-9 cm), represent at least 30-50% of the bed thickness and have diffuse to sharp bases.	Sandstone are structureless or sharply laminated that upward become faintly parallel- to wavy- and/or cross-laminated. Some beds contain multiple sets of ripples. Beds diffusely grade to mudstone, showing a murky or dirty appearance . Mudstone are structureless or faintly laminated. Most beds show normal grading.	Deposition from deceleration of a high-concentration flow that interacted with a topographic obstruction. This locally generated an increased in the mud content within the suspension cloud, transforming the flow into a lower transitional plug regime (Baas et al., 2011; Baas et al., 2013), which is divided by a lower sand-rich portion (turbulent zone) and a upper mud-rich portion that behave as fluid mud (rigid plug).	-
F6. Matrix-rich sandstone (Fig. 4.2G)	Moderated sorted, medium-grained sandstone to siltstone, with abundant mud matrix. Typically, they are capped by mudstone. Local F5 interbeds are observed.	Beds are up to 0.6 m thick with sharp bases and top. They are commonly capped by up to 5 cm-thick mudstone.	Structureless or normally-graded beds. Laterally, they thin and fine, and tend to transition into F5.	Deposition from moderate-concentration turbidity currents downflow of a area of rapid flow expansion	-
F7. Matrix-supported conglomerate	Muddy matrix-supported conglomerate composed of sub-angular, sub-rounded to	Beds range from 0.09 to 18 m thick. Basal contacts are sharp	Structureless and ungraded. However, one F6 show an upward	Deposition from submarine (cohesive) debris flows	F1 Mutti facies

(Fig. 4.2H)	rounded, up to boulder-size clasts or blocks of mudstone, interstratified fine-grained sandstone and mudstone, carbonated-cemented sandstone and/or minor carbonates. Internally, some clasts are undeformed, folded, and/or partially fragmented. Rafted sandstone clasts are also observed. Some clasts are aligned parallel to basal contact, but others are randomly oriented. Matrix is poorly-sorted, admixture of clay to granule quartz grains. Some F6 are overlain by discontinuous lenses of cross-stratified or parallel-laminated sandstone (F4 or F2).	and planar, locally erosional.	decrease in gravel size and abundance, and also local folding of the matrix.	generated by upslope instability, collapse and erosion (sensu Mulder and Alexander, 2001; Talling et al., 2012).	
F8. Chaotic facies (Fig. 4.2I)	Common large (tens to hundreds of meters long, and up to decametre-thick) blocks of undisturbed and deformed mudstone, interbedded fine-grained sandstone and mudstone, and coarse-grained sandstone. Shear surfaces or zones are widespread. Deformation (including brecciation, folding, contortion and/or local fragmentation) is observed. Few matrix-rich horizons (F6-like beds) are observed across the shear zones.	Up to 26 m thick, with flat to locally scoured basal surface.	Chaotic arrangement.	Deposition by submarine slide. Internal shearing within the sediment pile during movement. Large blocks are interpreted to be sandstone-rich or mudstone-rich strata that became disaggregated by extension, compression, and/or shearing during movement.	

Turbidite divisions from (Middleton and Hampton, 1973), Bouma (1962), and Lowe (1982)

Table 4.2. Summarized characteristics of stratal architecture elements documented in this study

Stratal Element	*Thickness and width (m)*	*Contacts and/or Geometry*	*Facies*	*Vertical and/or lateral trends, and/or Stacking patterns*
Slide deposits (i.e. Isaac slide 2)	Up to 26 m and >1200 m	Irregular basal surface with ramp-and-flat geometry	Blocks of F8 bounded by numerous shear zones, including some fine-grained matrix-dominated horizons	None
Debris-flow deposits (i.e. Isaac Debrite 1)	Up to 18 m and >1200 m	Irregular, erosive base. Channel-like geometry that pinches and swells laterally toward the SE, until it pinches abruptly out	F7. At the top of debrite, lenses of F1, F2 and F4	Better sorting toward the upper part
Mudstone-rich deposits (i.e. Above Isaac Debrite 1 and Blanketing the study area)	14-25 m and >1200 m	Sharp base. Sheet-like element	F5a. Local interbeds of F2	Locally, fining- and thinning- upward stratal successions
Sandstone-rich splay	Up to 10 m and > 400 m	Sharp, erosive base. Sheet-like element, but it thins and pinches laterally toward the SE	Lower part (up to 6 m thick):F2, minor F1 and F3 Upper part (up to 4 m thick): F5a, F6 and discontinuous beds of F4	Upward changes in facies and grain size, and decreasing in bed amalgamation
Erosional Channel Complex (i.e. Isaac Channel Complex 0)	>15 m and >1500 m	Erosional basal surface. Channelforms that pinch toward the NW	Mostly F1, F2 and F3. Minor F5a and F4 are more common toward the top	-Upward and lateral changes in grain size, facies and bed thickness and amalgamation -Vertically-stacked, laterally-offset channels
Ponded deposits	Up to 17 m and >400 m	Sharp base. Sheet-like elements	-Subunits or packages (3-4 m thick): F5b. Basal lenses of coarse-grained beds, but medium- and fine-grained beds predominate	- Clear lateral fining and thinning-trends, but occasional fining- and thinning- upward succession - Vertically-stacked subunits

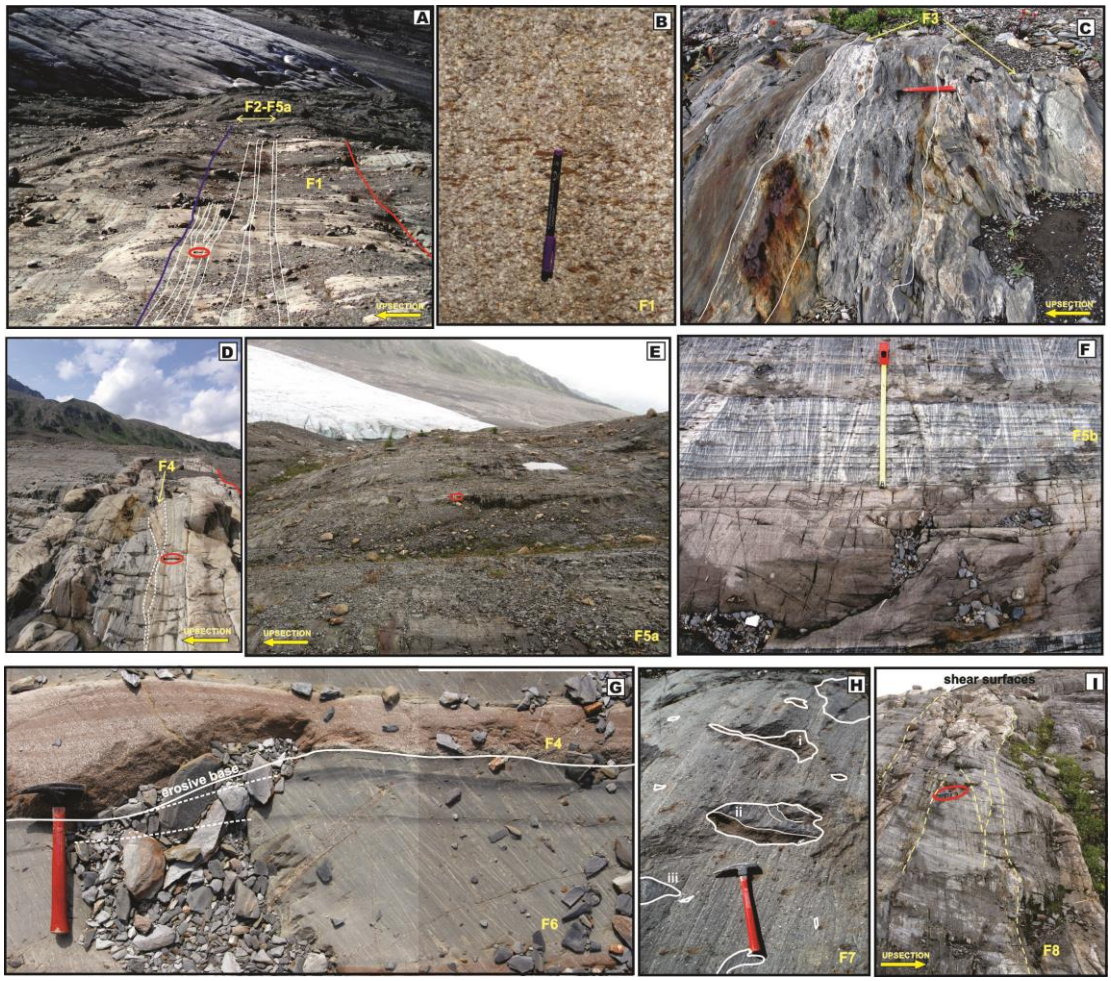

Figure 4.2. Field photographs illustrating the characteristics of lithofacies in the study area. Yellow arrows in some photos indicate stratigraphic tops. Erosive surfaces of stratal elements are indicated by red lines and bed contacts by white lines. (A) Typical thick- and medium-bedded, sharp-based, light pink-coloured, conglomerate and coarse-grained sandstone of F1 and F2, respectively. They are interpreted to be R3 or Ta/Tad/Tacd/'s turbidites that are the principal component in channel fills. Intercalated, light-greyish thin-bedded Tcd's turbidites of F5 are also observed. Hammer for scale. (B) Close-up of a F1 bed. Note abundant granule- and fine pebble-sized clasts of white quartz and feldspar and some brown/orange-coloured carbonate, surrounded by a matrix of medium/coarse-grained sand. 14 cm-long pen for scale. (C) Mudstone-clast breccia of F3 locally interstratified with coarse-grained beds. Hammer for scale. (D) A horizon of medium-scale, cross-stratified coarse-grained sandstone of F4. (E) A decameter-thick succession of thin-bedded, grey or greenish grey-coloured, fine-grained Tbcd/Tcd's turbidites of F5a. Hammer for scale. (F) Pink- to light yellow or white-coloured, sandstone beds capped with thick, dark greyish mudstone of F5b. 0.5m-long measuring tape for scale. (G) Thin- and medium-bedded, matrix-rich sandstone capped by mudstone. Matrix-rich beds are erosively overlain by planar-stratified coarse-grained sandstone of F4. Hammer for scale. (H) Detail of matrix-

supported conglomerate of F7. Note pebble and large-sized clasts of brown-coloured carbonate-cemented sandstone and grey-coloured mudstone, embedded in a mud-rich matrix with dispersed up to granule/pebbles quartz. Some clasts exhibit convolute bedding (i), and effects of disruption and disaggregation (ii and iii). (I) Irregularly-arranged and commonly lensoid-shaped stratal blocks in slide deposits of F8. Note truncation surfaces, interpreted as shear planes that bound the stratal blocks. Hammer for scale.

4.5.1 Isaac slide 2

Isaac slide 2 is up to 26 m thick and >1200 m wide (Figs. 4.3-4.4). The basal surface of the unit is irregular, and resembles a ramp-and-flat geometry (e.g. Bull et al., 2009), in which some segments (ramps) cross-cut bedding in the underlying, undisturbed carbonate-cemented sandstone-rich strata (see chapter 3), whereas adjacent segments (flats) are oriented parallel to bedding (Fig. 4.5A,B). This unit is lithologically complex and consists mostly of chaotic facies (F8) with numerous meter-scale clasts and decametre-scale blocks of fine-grained turbidites (commonly Tcd/Td's) and carbonate-cemented, very coarse/coarse-grained sandstone- and conglomerate-rich strata, commonly bounded by décollement or shear surfaces (Figs. 4.2I, 4.5C-F). Brecciation is observed locally along the margins of clasts and internally they exhibit varying levels of deformation. In the lower part of the slide, outsized coherent blocks predominate. Locally, some blocks are separated by a few centimetre- to meter-thick, horizons consisting of up to boulder-sized clasts of mudstone and minor carbonate-cemented sandstone embedded in a poorly-sorted fine-grained matrix (F6-like beds; Figs. 4.5C-D).

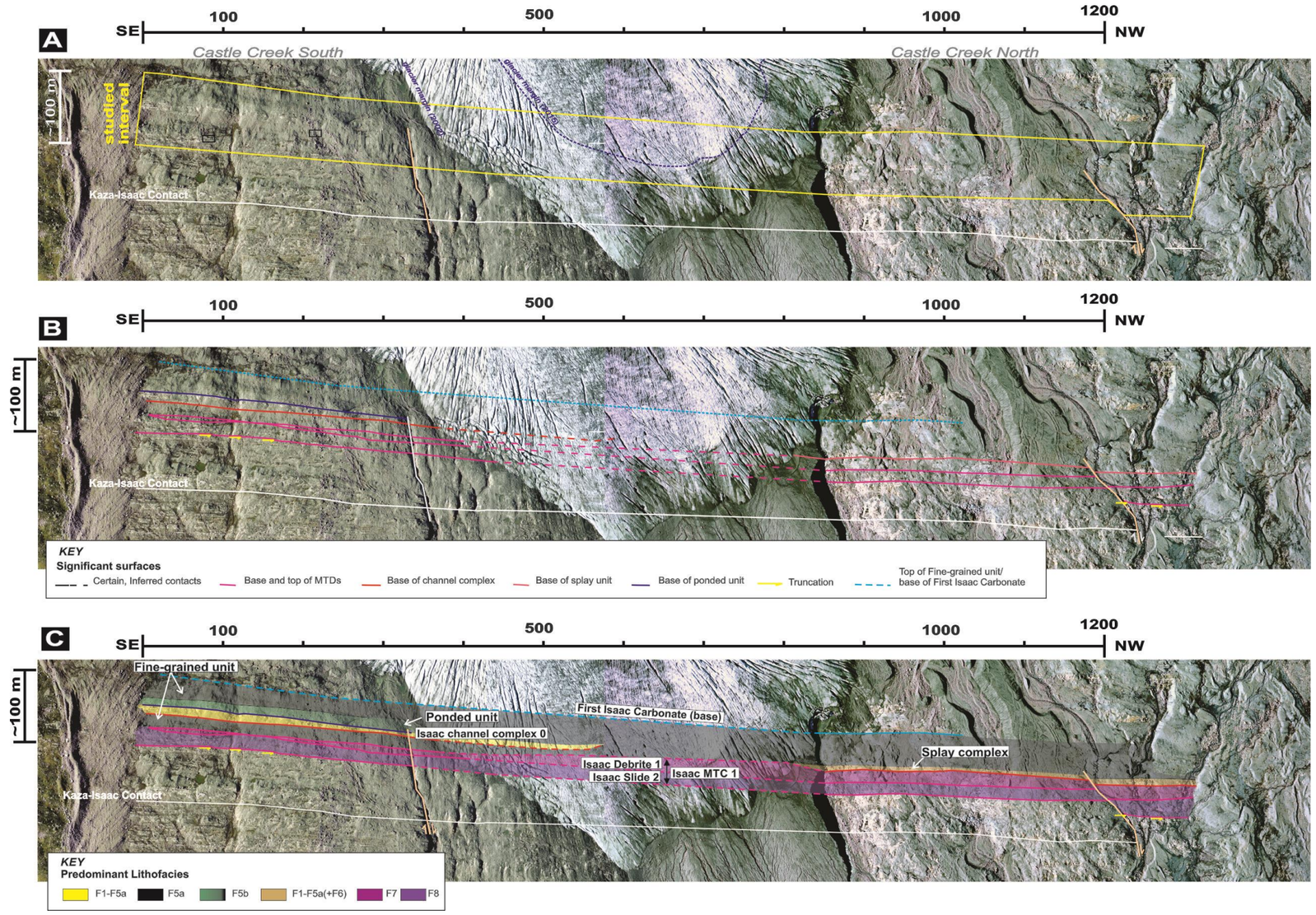

Figure 4.3. (A) Uninterpreted airphoto and (B,C) Interpreted airphotos of seven stratal units identified in the studied interval of the lowermost Isaac Formation, Castle Creek study area, including their corresponding facies distribution. These units are bounded by surfaces that can be traced laterally for several hundreds of meters on both sides of the glacier. The two lowermost units are interpreted to be slide and debris-flow deposits, which together make up Isaac MTC 1. In the Castle Creek south area, Isaac MTC 1 is overlain by fine-grained deposits, channel deposits of Isaac channel complex 0 and ponded deposits. In the Castle Creek north area, on the other hand, Isaac MTC 1 is overlain by a sandstone-rich splay unit. The entire study area is draped by fine-grained deposits.

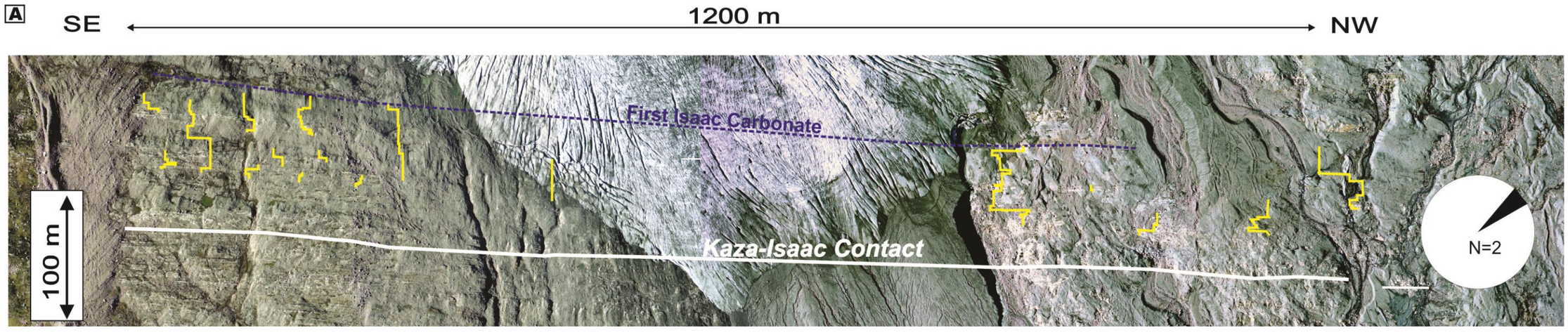

Figure 4.4. Detailed stratigraphic correlation over the seven main stratal units identified at Castle Creek (A) Location of Stratigraphic logs (also see Appendix B) and general paleocurrent diagram.

Continuation of Fig. 4.4.

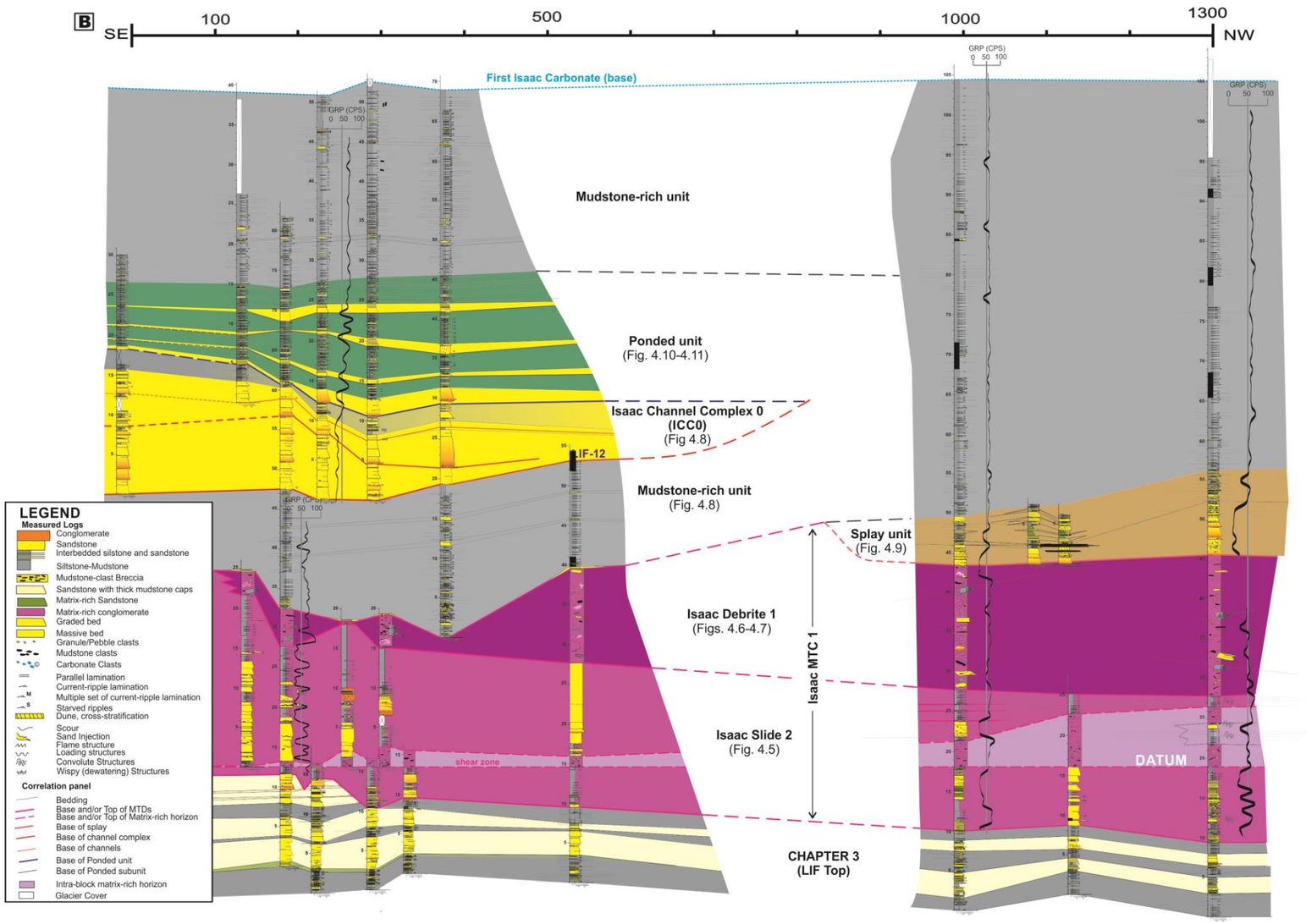

Fig. 4.4 (Continued) (B) Stratigraphic Architecture. Note that close to the base of Isaac slide 2 is a matrix-rich, mostly horizontal shear zone that can be traced across the study area. For correlation purposes, the base of this horizon is used as the stratigraphic datum.

The matrix is composed of abundant mud with rare to common dispersed sand-sized quartz grains. These matrix-dominated horizons can be traced laterally for just a few meters or thousand of meters. The most prominent (i.e. thickest and the most laterally-continuous) horizon extends across the study area (>1200 m) and is up to 8 m thick in the NW end of outcrop, but it thins abruptly to 10 cm toward the SE (Fig. 4.4). In contrast to the lower part of the slide, the upper part is generally composed of undeformed, thin-bedded, fine-grained turbidites (Fig. 4.4).

Due to its thickness and lateral extent, Isaac slide 2 is interpreted to be linked to a large-scale submarine mass failure that originated upslope. The matrix-rich horizons in the lower part of the slide are interpreted to be the result of localized shearing, fragmentation and mixing of poorly-lithified strata associated with local internal disaggregation of the slide mass during movement. These matrix-rich horizons may act to enhance the mobility of the moving mass by forming overpressure horizons that facilitate the transport of adjacent, more coherent parts of the slide (Ogata, 2010; Ogata et al., 2012; Pini et al., 2012; Ogata et al., 2014). Similar matrix-rich horizons have been documented in the Brazilian offshore (Mutti et al., 2006) and New Zealand offshore (Mountjoy and Micallef, 2012; Ogata et al., 2014) and in outcrops of the Spanish Pyrenees and Northern Italian Apennines where they were termed blocky flows by Mutti et al. (2006); Ogata (2010); and Ogata et al. (2012). The intricate juxtaposition of undeformed and deformed blocks (cf. translated and remnant blocks of Bull et al., 2009) implies that the slide mass, especially in its lower part, was variably deformed during movement and emplacement.

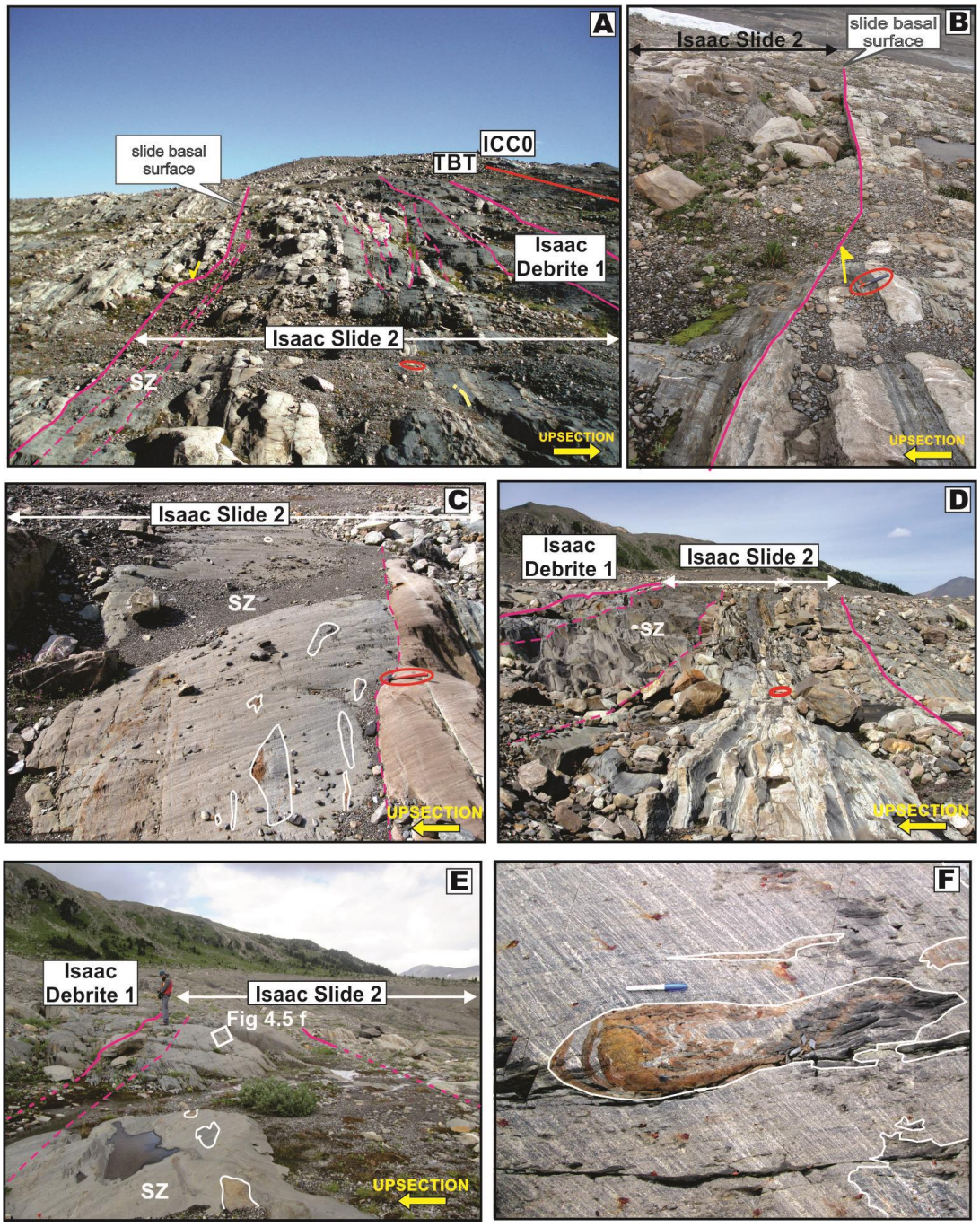

Figure 4.5. Photographs of the Isaac slide 2. (A-B) The basal and upper surfaces of MTDs (i.e. slide and debrite) are marked by bold fuchsia lines. Shear surfaces are marked by fuchsia dashed lines. The base of the ICC0 is delineated by a red line. In most photos a hammer is scale. In photo A, Isaac slide 2 is directly overlain by Isaac debrite 1, which then is overlain by thin-bedded, fine-grained turbidites (TBT) and sandstone-filled channel deposits of Isaac channel complex 0. Note the basal surface of the slide is mostly apparently flat and horizontal, but locally truncates the underlying

strata along apparent low-angle (<20º) ramps (truncation lines are highlighted by yellow arrows). (C-F) Within the lower part of the slide is a laterally-continuous matrix-rich horizon that occurs along a shear zone (SZ). The horizon becomes considerably thinner toward the SE (see photos A and C-E). This horizon contains common sandstone and/or mudstone intraclasts (enclosed in white lines) that are interpreted to be the remnants of strata that otherwise had been partly or completely disintegrated during movement. In photo F, close up of a plastically deformed intraclast that also shows partial fragmentation (14-cm marker for scale). Note typical glacial striations (from upper left to lower right) on the surface of these rocks.

Finer-grained, better-stratified strata in the uppermost part of the deposit are considered to reflect transport in the upper, low-strain part of the slide, which lead to better preservation of primary layering (e.g. Trincardi and Normark, 1989). Alternatively, some of these undeformed strata may have been deposited after slide emplacement.

The thickness and areal extent of the Isaac slide 2 is comparable to large (km)-scale slides observed on modern continental slopes (ranging in thickness from 45 to 250 m), for instance in the eastern Gulf of Mexico (e.g. Posamentier and Walker, 2006) and offshore Venezuela and Trinidad (Moscardelli et al., 2006). Since the full dimensions of the slide exceed those of the study area, it is possible that it might compare to giant slides (i.e. hundreds of kilometre wide), like the Brunei Slide (Gee et al., 2007) and Storegga Slide (Canals et al., 2004).

4.5.2 Isaac debrite 1

Isaac debrite 1 extends across the width of the study area (>1200 m). It exhibits an irregular, erosive base, and has a channel-like geometry that pinches and swells laterally (see Figs. 4.3, 4.4 and 4.6A-C). It is up to 18 m thick in the NW, but then thins unevenly toward the SE, where it then pinches out abruptly. Near its pinch

out, sediment has been injected locally into the sand-rich parts of thin-bedded turbidites at the top of the Isaac slide 2 (see previous section 4.5.1; Figs. 4.4 and 4.6A).

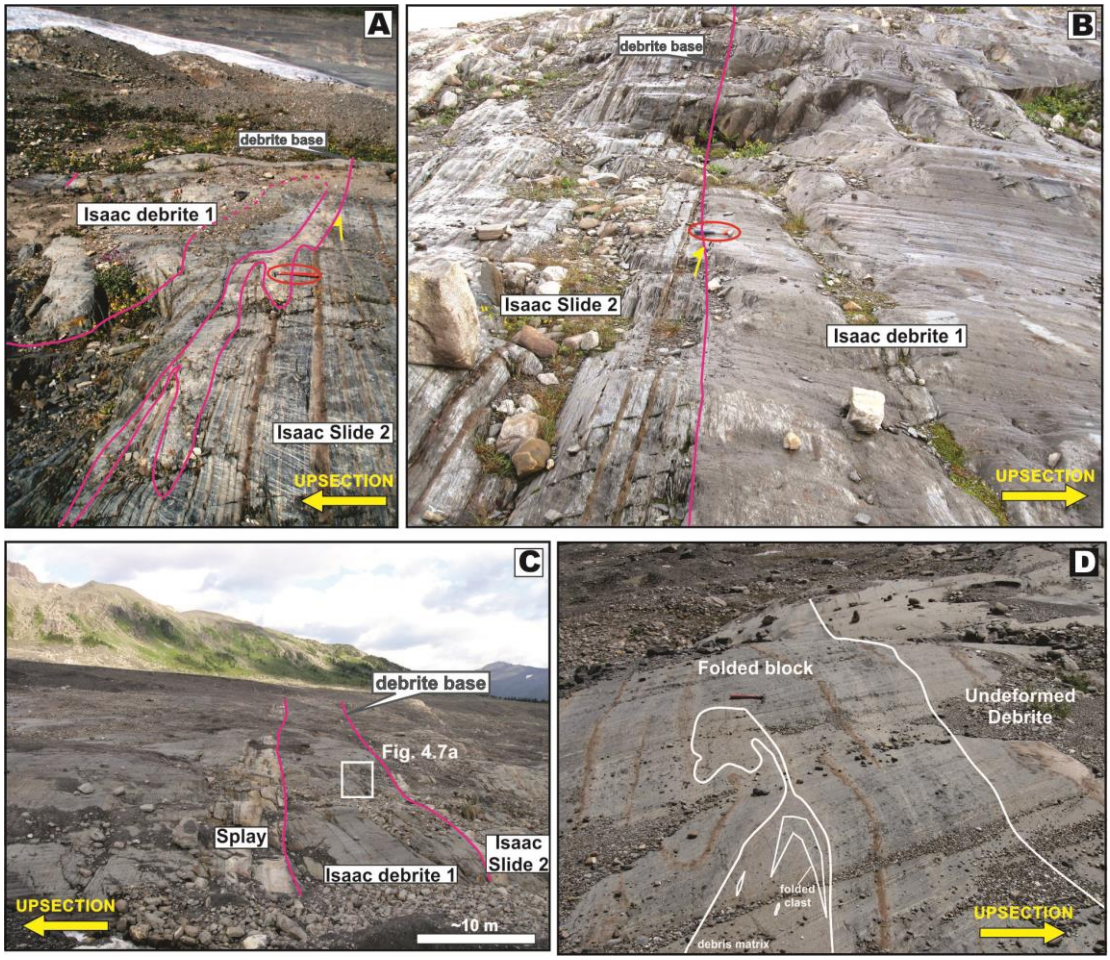

Figure 4.6. Photographs of Isaac debrite 1. The basal and upper surfaces of the debrite are highlighted by bold fuchsia lines. (A-B) Isaac debrite 1 is a matrix (mud)-rich debrite that locally truncates underlying fine-grained turbidites of Isaac slide 2 (truncation is indicated by yellow arrows). In photo A, the debrite thins and pinches out abruptly along its SE margin, wherein several debris injections intrude the sand-rich parts of thin sandstone beds at the top of Isaac slide 2. (C-D) On the opposite (NW) side of the glacier, however, the debrite thickens significantly. In photo D, a close up showing a large folded block (its top is delineated by white bold line) within the middle part of the debrite. Note the debris matrix is injected into the hinge zone of the folded block and also contains folded clasts of mudstone. The folding and deformation of some clasts or blocks might have been produced during the downslope transport of the debris

flow. In contrast, the upper part of the debrite (at right of the photo) is less deformed and contains fewer clasts.

Isaac debrite 1 consists of poorly-sorted, matrix-supported conglomerate (F7) with abundant dispersed sand- to pebble-size quartz grains (Fig. 4.2H). Additionally, common chaotically-arranged, decimetre- to meter-scale, subangular to rounded clasts and/or stratified blocks of undeformed, folded and/or distorted mudstone, sandstone, thinly interstratified fine-grained sandstone-mudstone, carbonate-cemented sandstone, and rare limestone fragments are dispersed in a matrix of structureless, silty mudstone (Fig. 4.6D and 4.7A-F). Notably also, the size of clasts varies laterally, with the largest clasts preferentially concentrated toward the NW (Figs. 4.7A-E). The top of the debrite is distinctively better sorted with less mud matrix, and is overlain by a laterally-discontinuous lens consisting of conglomerate, and parallel- and cross-laminated sandstone (F1, F2 and F4).

Isaac debrite 1 is interpreted to be the deposit of a major (km-wide/long) submarine debris flow, which earlier was termed the Lower debris flow deposit, or LDF, by Wallace (2004). The size, roundness and diverse (but siliciclastic-rich) composition of the blocks/clasts suggest the remobilization of sediments sourced from upper slope areas, although the small number of micritic carbonate clasts might have been sourced from shelf areas. The deformed and disaggregated character of the clasts and matrix is interpreted to be the result of the dynamic internal character (including disparate areas of compression and extension) within the moving debris flow.

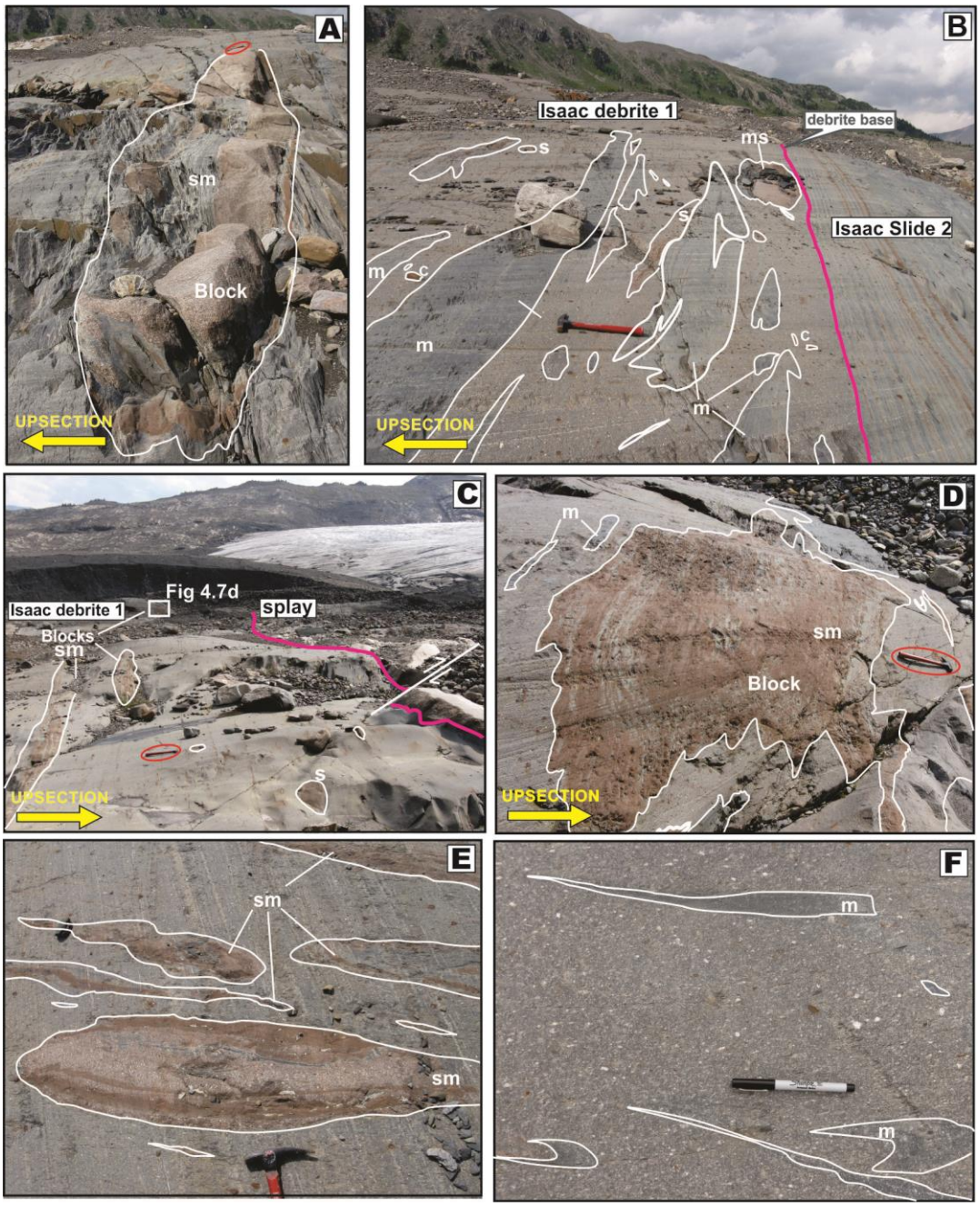

Figure 4.7. Detail photographs of grain framework and matrix of Isaac Debrite 1. (A-E) The debrite includes up to meter-sized intraclasts or larger blocks of grey mudstone (m), pink to brown, carbonate-cemented medium- to very coarse-grained sandstone (s), interbedded sandstone and mudstone (sm) and some orange to brown carbonates (c). Intraclasts and blocks tend to be aligned sub-parallel to the base of the debrite. In photo D, a close up of an angular block with oddly ragged margins of a brownish carbonate-cemented sandstone with thin interlayers of grey mudstone. Note how the surrounding debris matrix intrudes into the block. (F) Detail of characteristic matrix of F7 strata,

which consists of massive silty mudstone with abundant, dispersed white quartz sand, granules and pebbles. Visually, it resembles a starry night sky. Note some grey elongated and folded mudstone clasts that are enclosed in white bold lines and surrounded by matrix.

Common parallel- and/or cross-laminated sandstone, that directly overlie the debrite, suggest that during movement the entrainment and mixing of seawater along the top of the debris flow generated a dilute, moderate- to high-speed, low-concentration turbidity current. This overriding current reworked the top of the debris flow either during its movement and/or following deposition (Mulder and Alexander, 2001), which caused fine-grained sediment to be winnowed and coarser sediment to be concentrated, and hence better sorted. In addition, this current formed the traction structures (plane bed and/or cross-lamination) that caps the debrite.

The uneven geometry and dramatic lateral changes in thickness of the Isaac debrite 1, in conjunction to its abrupt depositional pinch-out onto the underlying slide deposits, suggests that its geometry was most likely controlled by topography along the top of the underlying slide (i.e. Isaac slide 2).

4.5.3 Mudstone-rich deposits

On the SE side of the glacier, a decameter-thick (14-19 m) mudstone-rich unit overlies Isaac slide 2 and part of Isaac debrite 1, and it is locally eroded by Isaac channel complex 0 (Figs. 4.3, 4.4 and 4.8A,E). It consists of a succession of laterally-continuous, thin-bedded, fine-grained turbidites (F5a) composed mostly of upper Bouma division Tcd's. Locally, few lens-shaped interbeds of coarse-grained sandstone (F2), up to 60 cm-thick, are also observed. These coarse-grained beds

(commonly Tacd and Tbc) thin and fine laterally over several hundreds of meters (Fig. 4.8F).

Above both Isaac slide 2 and part of Isaac debrite 1, fine-grained deposits are interpreted to be the result of low-concentration turbidity currents that were preferentially routed through the topographic irregularities formed along the tops of mass-transport deposits. These strata are significantly thicker in the SE part of the study area, which then suggests an area of lower topography compared to the NW area. Notably, Isaac debrite 1 is appreciably thicker in the NW area compared to the SE, and therefore most probably represented a topographic high at the time of deposition.

4.5.4 Sandstone-rich splay

On the NW side of the glacier, a sandstone-rich unit directly overlies Isaac debrite 1 (Figs. 4.3 and 4.4). It is about 10 m thick, but over 400 m laterally thins to 6 m toward the SE before being covered by the glacier (Figs. 4.9A-B). Based on upward changes in facies and bed amalgamation, it can be divided in two parts: a lower part that is 3-6 m-thick and consists mostly of highly-amalgamated, thick-bedded, structureless, very-coarse and coarse-grained sandstone (basal F2) and less common granule conglomerate (F1) and mudstone-clast breccia (F3) with common erosive bases (Figs. 4.9C-E, 4.2C). The upper part is 3-4 m-thick and heterolithic, composed predominantly of thin-bedded Tcd turbidites (F5a) intercalated with laterally-discontinuous, thick-bedded, parallel- and cross-stratified, very coarse- and coarse- grained sandstone (F4; Figs. 4.2G, 4.9F). Loaded bases and flame structures

are observed locally. Coarser-grained beds thin and pinch out laterally over a few hundreds of meters laterally. Some thin- and thick-bedded, matrix-rich sandstone with thin mudstone caps (F6) are also present (Fig. 4.2G), but they rapidly thin and grade laterally into thin-bedded, fine-grained turbidites (F5a).

The sandstone-rich unit is interpreted to be a splay developed from sandy unconfined flows that were preferentially diverted and deposited in a topographic low in the uneven upper topographic surface of Isaac debrite 1. This splay unit is assumed to be fed by an unexposed channel. The amalgamated, coarse-grained strata in the lower part of the splay resulted from deposition of high-concentration turbidity flows that transported copious coarse sand- and gravel-sized quartz and minor carbonate particles. Deposition was most likely caused by either an abrupt change (reduction) in the local slope or a loss of upflow confinement, which then caused the flows to rapidly expand and decelerate. Mudstone clasts in discontinuous breccia beds were likely sourced locally. Thin-bedded fine-grained turbidites in the upper part of the splay indicates a change to low energy deposition by diluted flows, which irregularly was interrupted by sandier, more concentrated, but laterally more restricted sandstone that deposited lens of coarse-grained F4 strata. Local matrix-rich sandstones are interpreted to be deposition downstream of hydraulic jumps. Deposition of the fine-grained upper unit is interpreted to indicate the smoothing of the debrite-related topography, which then allowed flows to bypass the area and transport sediment further downslope.

At the Castle Creek study area, splays overlying mass-transport complexes in the Isaac slope system have been previously interpreted (Navarro et al., 2007; Arnott

et al., 2011; Khan, 2012). Moreover, comparable localized sand-prone slope deposits that are tens of square kilometers in area, up to several tens of meters thick with evidences of erosion, channelization and/or bypass have been also reported in the Gulf of Mexico and offshore Nigeria, and have been termed splays (Posamentier and Kolla, 2003; Posamentier and Walker, 2006), aprons (Prather et al., 1998a), and transient fans (Adeogba et al., 2005).

4.5.5 Isaac channel complex 0

Isaac channel complex 0 (ICC0) is the last and thickest coarse-grained, siliciclastic-rich stratal package below mixed (carbonate-siliciclastic) strata of the first Isaac carbonate (see chapter 5). ICC0 is confined to the SE side of the glacier, and here erosionally overlies the fine-grained unit described in section 4.5.3. ICC0 is 15 m thick, but thins laterally over 600 m to 10 m thick toward the NW before being covered by the glacier (Figs. 4.3 and 4.4). Nevertheless, toward the SE, it can be traced on the available airphotos for least 1.5-2 km (Figs. 4.8A-B; also see Fig. 3.17). Due to the paucity of paleocurrent data and oblique cut of the outcrop belt, the entire width of the channel complex cannot be appraised.

Coarse-grained strata (mostly F1, F2 and F3) of ICC0 with characteristically high sandstone:mudstone ratio (0.8-1.00) are interpreted to represent deposits of a slope channel complex. In the study area, ICC0 consists of at least two vertical-stacked, laterally-offset channel units, which here are informally named C1 and C2.

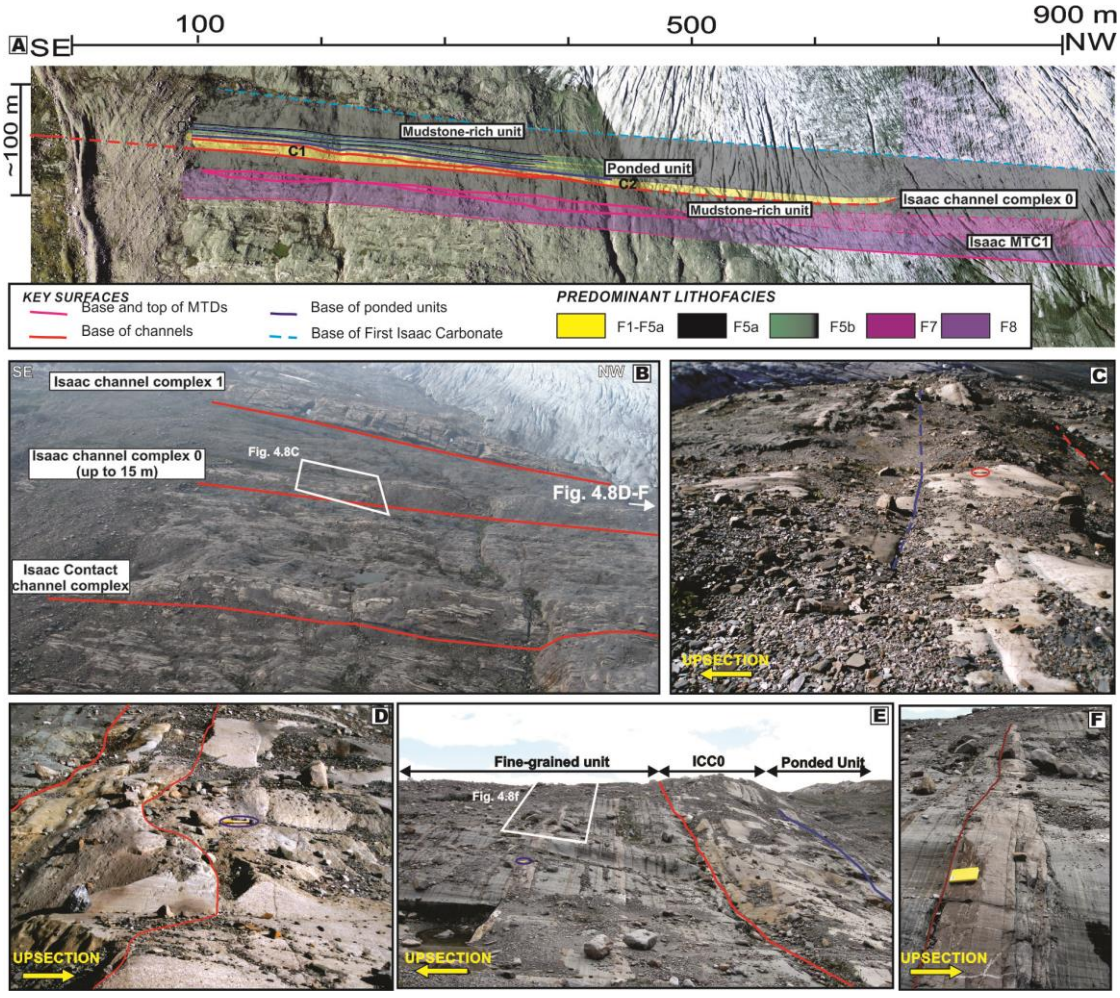

Figure 4.8. Architectural stacking pattern of mass-transport, fine-grained, channel and ponded deposits in Castle Creek south. (A) Interpreted airphoto (see text for details). (B) Panoramic view showing the three lowermost channel complexes in the Isaac Formation at Castle Creek – the base of each channel complex is highlighted by a red line. Isaac channel complex 0, or ICC0, erosionally bounded and comprises two channel units. (C-D) Erosionally-based, highly-amalgamated, very coarse-grained sandstone and pebble conglomerate (F1 and F2) make up most of the channel fill. (E-F) Outcrop photograph of fine-grained unit that underlies ICC0 and is composed predominantly of fine-grained turbidites (F5a) with uncommon interbeds of coarse-grained sandstone (photo F).

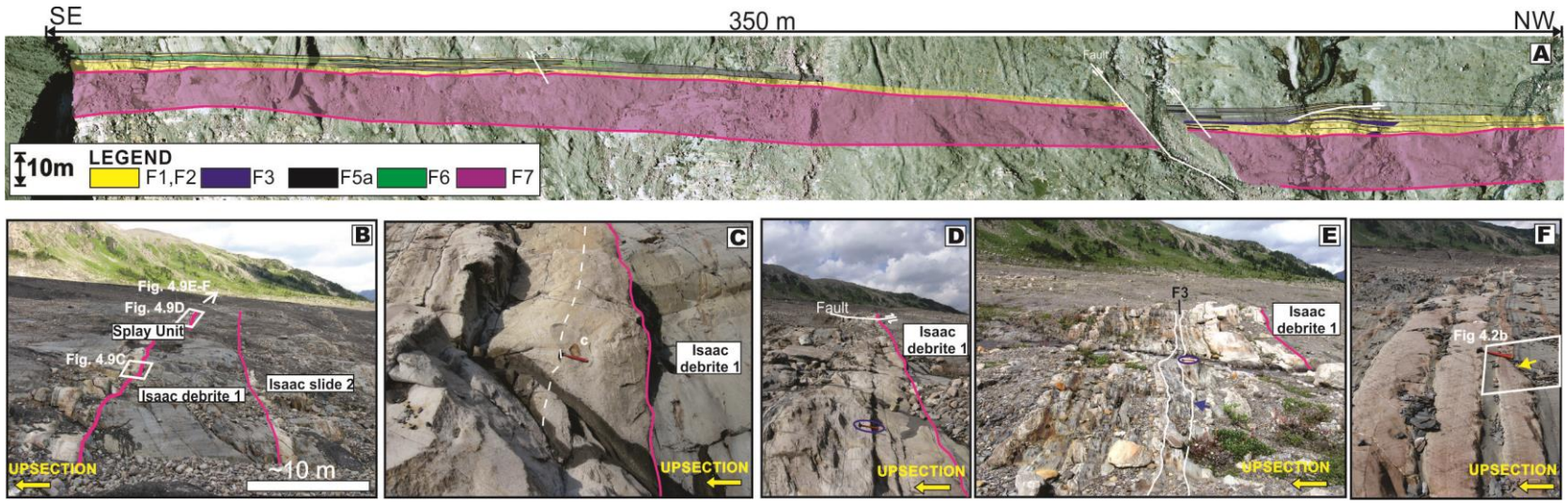

Figure 4.9. Sandstone-rich splay deposits in Castle Creek north. (A) Interpreted airphoto (see text for details). (B) Panoramic outcrop view indicating sandstone-rich splay that directly overlie Isaac debrite 1. (C-D) The lower part of the splay is amalgamated and composed predominantly of quartz-rich siliciclastic coarse-grained strata (F1, F2 and/or F4) with rare carbonate clasts (photo C). Amalgamation surface is marked by white dashed line. (E) Mudstone-clast breccia (F3) are less common. (F) The upper part of the splay consists of planar-or cross-laminated coarse-grained sandstone (F4), that are intercalated with fine-grained turbidites (F5a) and occasional matrix-rich sandstone (F6). Blue and yellow arrows in photos E and F indicate localized cm-scale scours at the base of these beds.

Each channel unit consists of several (2 or more) channel fills. C1 is up to 10 m, but thickens toward the SE (Fig. 4.8A). Component channels of C1 are highly amalgamated and hence difficult to differentiate, and are filled mostly with amalgamated, thick-bedded, clast-supported, granule to pebble conglomerate and very coarse- to coarse-grained sandstone (F1 and F2, respectively; Figs. F2A, 4.8C-E). C2 is up to 8 m thick, and near the SE glacier margin scours deeply into C1. Similar to C1, channel deposits of C2 consist of thick graded beds of subfeldspathic sandstone and conglomerate (F2 and F1), but dispersed carbonate granules and pebbles are more common (Fig. 4.2B). Moreover, these channels show better developed upward and lateral changes in grain size, facies, and bed thickness. At their tops, cross-bedded sandstone (F4) and sandstone-mudstone couplets (F5a) are also more common.

Overall, coarse-grained strata of ICC0 are interpreted to be siliciclastic-rich channel fills deposited by gravelly and sandy siliciclastic-rich, high-concentration turbidity currents. In C2, the upward and lateral fining and thinning of channel-filling strata most probably reflect the progressive reduction in sediment concentration, and hence flow speed stratigraphically upward and toward the margins of an undersized channelized flows (Gardner et al., 2003). The lateral offset of channel units may suggest channel migration. ICC0 is interpreted to be a major deep-water channel formed on the lower slope, although it is smaller than those channels that overlie deep-marine mass-transport complexes in the Gulf of Mexico (Beaubouef and S.J. Friedmann, 2000; Posamentier and Kolla, 2003; Posamentier and Walker, 2006), Amazon (Pirmez et al., 1997), offshore Venezuela-Trinidad (Moscardelli et al., 2006), and Indus and Niger Delta (Deptuck et al., 2007).

4.5.6 Ponded deposits

In Castle Creek South, ICC0 is sharply overlain by an up to 17 m-thick stratal unit that differs noticeably from other strata in the study area. It comprises four vertically-stacked packages, or subunits; each is about 3-5 m thick and can be traced laterally for at least 400 m (Figs. 4.3, 4.10A).

Each subunit consists mostly of laterally-extensive, thin- to medium-bedded (commonly 0.02-0.2 m), medium- to fine-grained sandstone that commonly grade diffusely upward into thick mudstone (F5b), commonly without sharp break in grain size. Although significantly less common, thicker and coarser interbeds (generally up to 0.9 m, up to lower coarse sand sizes) are also observed.

However, at the base of the subunits, the thickest and coarsest beds (i.e. up to 2.7 m thick), generally amalgamated, coarse- to very coarse-grained sandstone and/or rarely granule conglomerate (Figs. 4.10B-C) with erosional bases and/or localized load, flame and sandstone injection structures consistently occur.

Characteristically, the lower sandstone parts of F5b beds are up to 0.55 m thick (but normally ranging from 0.005 to 0.12 m) and consists of structureless or sharply laminated sandstone, becoming upward faintly planar-, wavy- and/or cross-laminated sandstone with a darker or dirty appearance (Figs. 4.2F, 4.10D). Some sandstone interbeds contain multiple ripple cross-laminated sets with common interlaminated mudstone (Fig. 4.10E). Discontinuous, dune cross-stratification and mudstone clasts occur rarely in coarser beds. Notably, the uppermost mudstone part of these beds, which is faintly laminated and/or structureless, is 0.01-0.09 m thick (up

to 0.35 m), and represents >30-50% of the bed thickness. Paleocurrent data were difficult to obtain on the glacially-polished outcrop face in the study area, but measurements from a small number of ripple cross-laminated beds suggest a general paleoflow toward the Northeast.

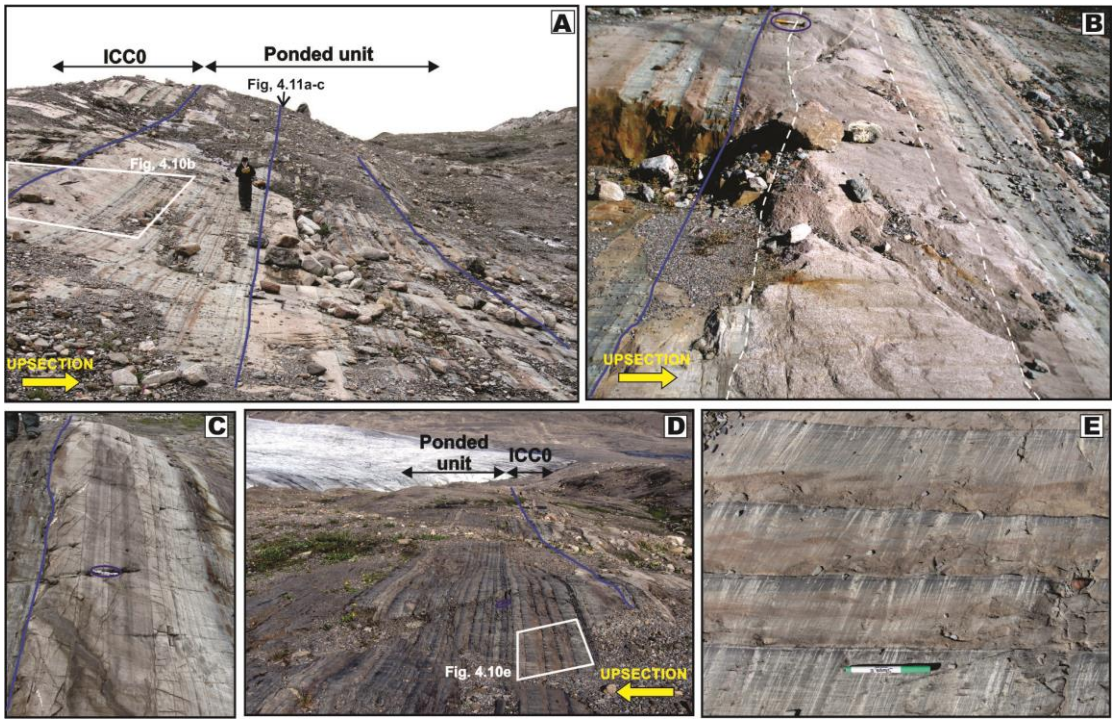

Figure 4.10. Ponded deposits sharply overlying ICC0 in Castle Creek south. (A) Outcrop view of several (>3) subunits or packages that stack to form a decameter-thick ponded unit –base of each subunit is indicated by a blue line. (B-C) The thickest and coarsest-grained strata (up to granule conglomerate) occur at the base of each subunit. Strata are either structureless (in photo B) and/or planar-laminated (in photo C). In B, hammer for scale and in C an 16-cm long ruler. Amalgamation surfaces are indicated with dashed white lines. (D) Most of a ponded subunit's thickness consist of medium-or fine-grained sandstone that diffusely-grade upward into thick mudstone (F5b). In D, a 15-cm long ruler for scale. (E) Close up of some F5b beds that exhibit upward changes in colour, grain size and sedimentary structure. Brownish pink, cross-laminated (several ripple sets) to wavy-laminated, medium-grained sandstone grade upward to yellowish, beige or light-grey, faintly-laminated or structureless, very fine-grained sandstone or siltstone, which then are capped by dark grey structureless mudstone. In E, a 14cm-long marker for scale.

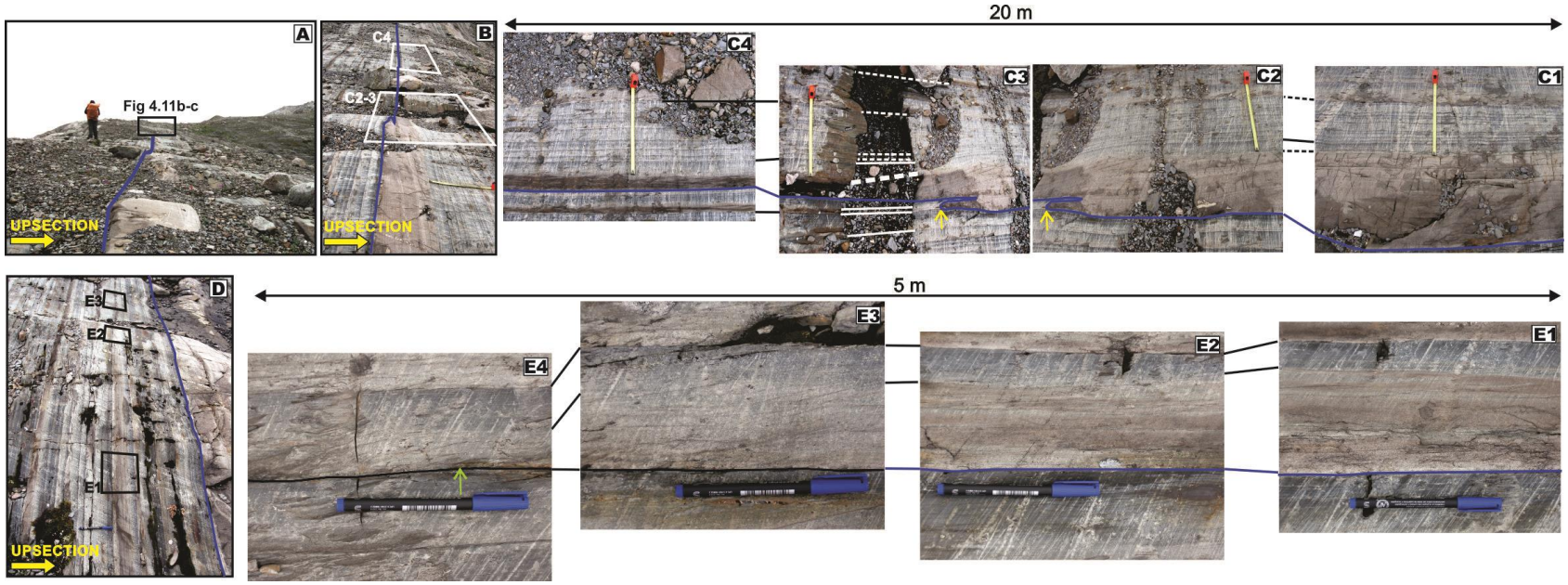

Figure 4.11. Lateral fining- and thinning-trends of ponded deposits. (A-C) Close up of one of the thickest, coarsest-grained sandstone beds at the base of a subunit. Over tens of meters, thick-bedded, structureless very coarse-grained sandstone (photos A, C1) grade laterally into planar-laminated, coarse-grained sandstone (see photos B, C2-C3). Further laterally it fines and thins into planar-laminated, medium-grained sandstone (see photo C4). Yellow arrows in C2 and C3 indicate the same local sand injection. In photos C1-C4, 50 cm-long division of a measuring tape. (D-E4) Close up of medium/fine-grained F5b strata within a subunit. Pinkish coloured, planar to wavy-laminated, medium-grained sandstone that grades diffusely upward into a grey mudstone cap (photos E1-E2). The bed then grades laterally into a light-pink to white coloured, faintly-laminated, fine-grained sandstone with mudstone cap (photo E3). Still further laterally, it thins and fines laterally to become coarse siltstone with mudstone cap (photo E4). Green arrow in photo E4 indicates the abrupt pinch out of the fine-grained sandstone.

Distinctively, beds that made up this stratal unit exhibit a gradual textural and compositional change upward, which is accompanied by an upward change in colour reflecting an upward decrease in ferroan carbonate cement. Medium- or coarser-grained strata are reddish brown to light pink owing to iron oxidation of the moderate to low amount of carbonate cement (see Appendix Petrography), whereas finer-grained sandstone and siltstone are lighter in colour (white, light beige to light yellowish grey) and mudstone is grey. The analysis of sand:mud ratios, or more accurately sand:silt:clay ratios, in the finer-grained portions of the beds was beyond the scope of this work; however controlled sampling and petrographic examinations are suggested for further studies.

Over tens or a few hundreds of meters, thick- and medium-bedded, medium- and coarse-grained strata generally fine and thin laterally toward the SE, grading into parallel- and/or cross-laminated, medium- to fine-grained sandstone capped by mudstone (Figs. 4.11A-C4). Some fine-grained strata show similar trends, as they thin and fine laterally into mudstone (Figs. 4.11D-E4).

Within each subunit, multiple sequences fine and thin upward, with a concomitant decrease in sand content. The ponded unit is not found to the NW.

Laterally-extensive, intercalated fine- and medium-grained diffusely-graded sandstone capped by a thick mudstone that makes up at least 30% of the bed thickness are interpreted to represent deposition that was influenced by at least partial topographical confinement or constriction (e.g. Pickering and Hiscott, 1985; Haughton, 1994; 2001), possibly formed downstream by deposition of an (unexposed) mass-transport deposit, such as debrite (e.g. Gee et al., 2001). Besides

this MTD proposed herein, another possible mechanism able to create some topographic alteration in the seafloor morphology is related to loading and early post-depositional processes that reactivated differential intra-block movements across the underlying Isaac slide 2 and caused significant changes in its already-uneven anatomy (e.g. Alves, 2010; Ogata et al., 2014; Kneller et al., 2016).

The beds described above form four subunits with a consistent upward-fining and -thinning motif. This suggests that each subunit represents an individual sedimentation unit related to a single turbidity current that evolved spatially and/or temporally. Initially, a large-volume, sand/gravel-rich, high-concentration turbidity flow with low to moderate mud content passed across the study area resulting in erosion and deposition of the thickest, coarsest-grained at the base of the subunit. Further downflow, the flow encountered a topographical obstruction that caused it to become partially ponded. This resulted in an upstream backwater effect that formed a progressively thickening, upflow-migrating suspension cloud, similar to what was observed in recent experiments of Patacci et al. (2015). The concentration of mud within the cloud became sufficiently high to form a mobile fluid-mud layer on top of an aggrading basal sandy layer. Deposition of most F5b strata occurred under these conditions, similar to what Baas et al. (2011) termed lower transitional plug regime, which consists of a lower turbulent zone overlain abruptly by a progressively thickening rigid plug. The common occurrence of planar or wavy lamination, and locally ripple cross-stratification, in the lower sand-rich part of beds, in conjunction to an upward increasing of mud at the top of F5b beds, indicates a period of traction transport prior to en-masse deposition of the fluid mud layer (mudstone cap).

Vertically-stacked ponded beds have previously described from the ancient sedimentary record, and are mostly associated to closed/semi-closed depressions (e.g. Lucchi and Valmori, 1980; Hiscott and Pickering, 1984; Pickering and Hiscott, 1985; Marjanac, 1990; Muzzi Magalhaes and Tinterri, 2010). However, unlike these strata, ponded beds described here do not exhibit divergent or reversal paleocurrent directions, and also build up a stack of discrete sandstone-mudstone couplets that progressively fine and thin upward.

Ponded deposits, comprising stacked sandstone and mudstone couplets, have recently been recognized in the Isaac Formation between Isaac channel complexes 4 and 5 (Terlaky, 2015; personal communication). Here, unlike this study, it can be clearly shown that a mass-transport deposit immediately preceded the onset of ponded bed deposition. As a consequence now, more detailed fieldwork and petrographic study is needed to fully constrain the variety of characteristics of ponded deposits. Such work will help to comprehensively reconstruct the flow properties and depositional evolution of individual ponded beds and the collective subunit packages. The present study, therefore, should be considered as a first attempt.

Ponded or contained deposits have been widely reported in the ancient record from the slope or basin floor of small structurally-confined basins like the Sorbas and Tabernas basins, Spain (Lucchi and Valmori, 1980; Pickering and Hiscott, 1985; Haughton, 1994; 2001; Sinclair and Tomasso, 2002; Amy et al., 2007; Muzzi Magalhaes and Tinterri, 2010; Southern et al., 2015; Marini et al., 2016), Castagnola Formation, Italy (Marini et al., 2016), but also larger foredeep and foreland basins like the Marnoso Arenacea (Lucchi and Valmori, 1980; Sinclair and Tomasso, 2002;

Amy et al., 2007; Muzzi Magalhaes and Tinterri, 2010; Southern et al., 2015; Marini et al., 2016), Annot Sandstone (Sinclair and Tomasso, 2002; Amy et al., 2007; Southern et al., 2015), Cloridorme Formation, Quebec (Pickering and Hiscott, 1985), Tres Pasos Formation, Chile , and Hecho Group (Remacha et al., 2005). They have been also documented in intraslope mini-basins of the Gulf of Mexico (Behrens, 1984; Prather et al., 1998b; Prather, 2003; Smith, 2004; Prather et al., 2012b), on the slope offshore Nigeria (Prather et al., 2012a), on lows or valleys across the flanks of mid-Atlantic ridge (van Andel and Komar, 1969) and in the Mediterranean basin (Blanpied and Stanley, 1981; Stanley, 1981).

4.5.7 Mudstone-rich drape deposits

A mudstone-rich stratal unit uniformly drapes ponded deposits, and then is overlain by carbonate- and mixed (siliciclastic-carbonate)- and carbonate-dominated strata of the First Isaac Carbonate (Figs. 4.3 and 4.4). It is up to 25 m-thick, and extends across the study area (>1200 m), and consists of interbedded fine-grained sandstone with mudstone Tcd/Td's with sharp contacts (F5a; Fig. 4.2E). Uncommon interbeds of medium- and thick-bedded, medium-grained and coarse-grained sandstone (F2) are locally observed. Up to decameter-thick, upward fining- and thinning-sequences are occasionally observed.

Typically, mudstone rocks in this unit (and in Isaac Formation, in general) are grey to greenish grey, however some mudstone interbeds are slightly darker (medium grey). Preliminary lithogeochemical (major, trace, and rare-earth-element) analyses from samples of both mudstones are consistently similar (see Geochemical Appendix

5), but darker grey mudstone has relatively higher TOC concentrations (0.4% compared to 0.04%). Note that TOC values in average thin-bedded turbidites in the Isaac Formation are <0.1% (Navarro, 2006; Davis, 2011).

Thin-bedded, fine-grained strata of this unit are interpreted to be deposited from low-concentration, siliciclastic mud-rich turbidity currents that extensively blanketed the entire study area. Similar mudstone-rich drape or blanket deposits have been recorded on the top of some ponded deposits of the Gulf of Mexico (Prather et al., 1998a). Deposition of the fine-grained unit coincides with a general change in sediment supply and composition within the Isaac slope system from siliciclastics to mixed (siliciclastic and carbonates) and carbonate. Local occurrence of high-TOC mudstone indicates that some flows were enriched in organic matter, which probably originated from much shallower parts of the slope or shelf, and then was transported downslope by fine-grained, turbidity currents.

4.6 Discussion

4.6.1 Stratigraphic evolution of Isaac MTC 1 and overlying deposits

The detailed sedimentology and architecture of the Isaac MTC 1 and overlying deposits allow the establishment of the following evolutionary model (Fig. 4.12) that can be related to major changes in sediment supply, caliber and composition in response to change of relative sea level. Most importantly, this model illustrates how the depositional characteristics of some deep-water deposits are controlled by the evolving topography formed on the top of the large-scale MTC.

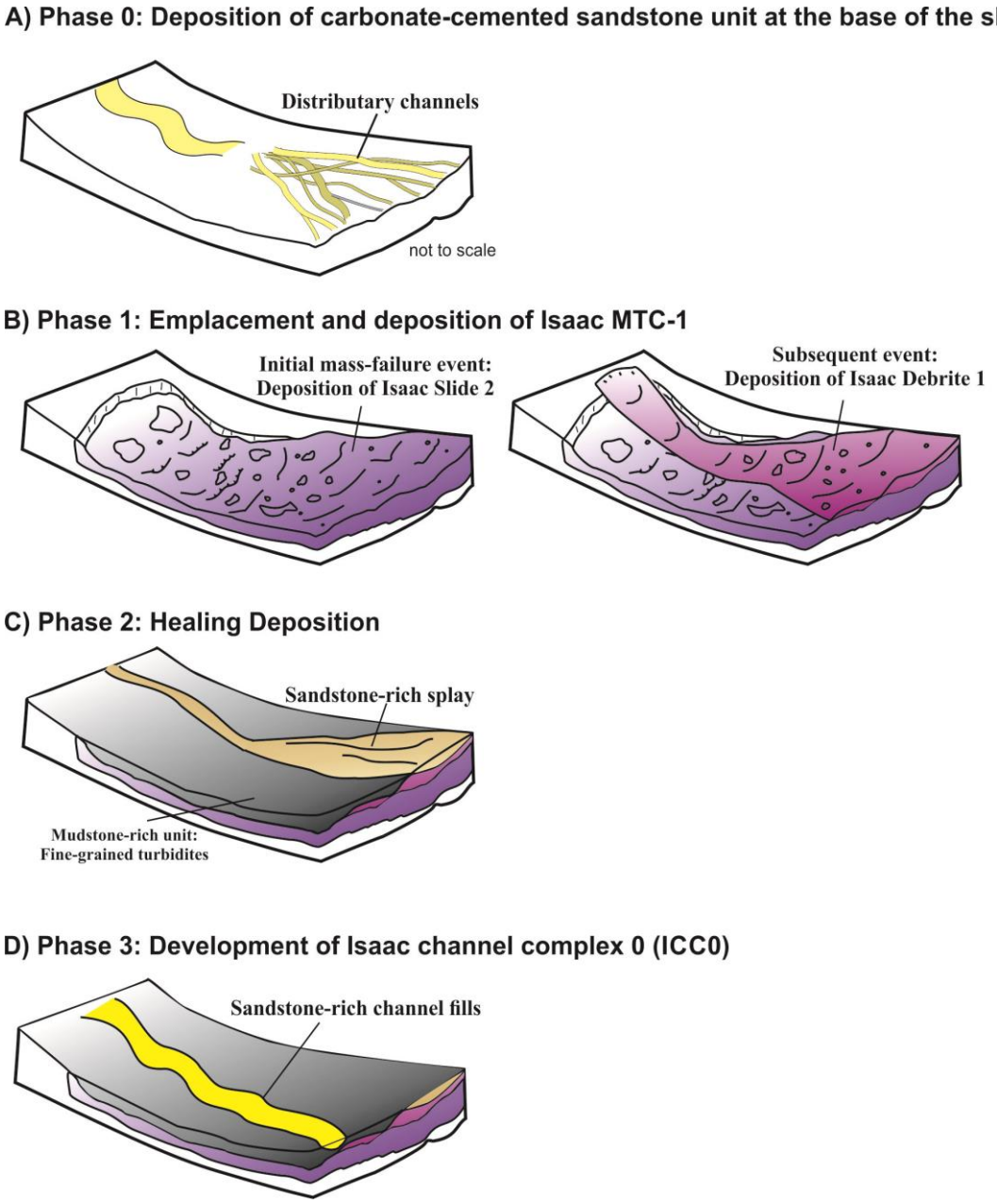

Figure 4.12. Depositional model of Isaac MTC 1 and overlying deposits in the studied section. See text for discussion.

Continuation of Fig. 4.12.

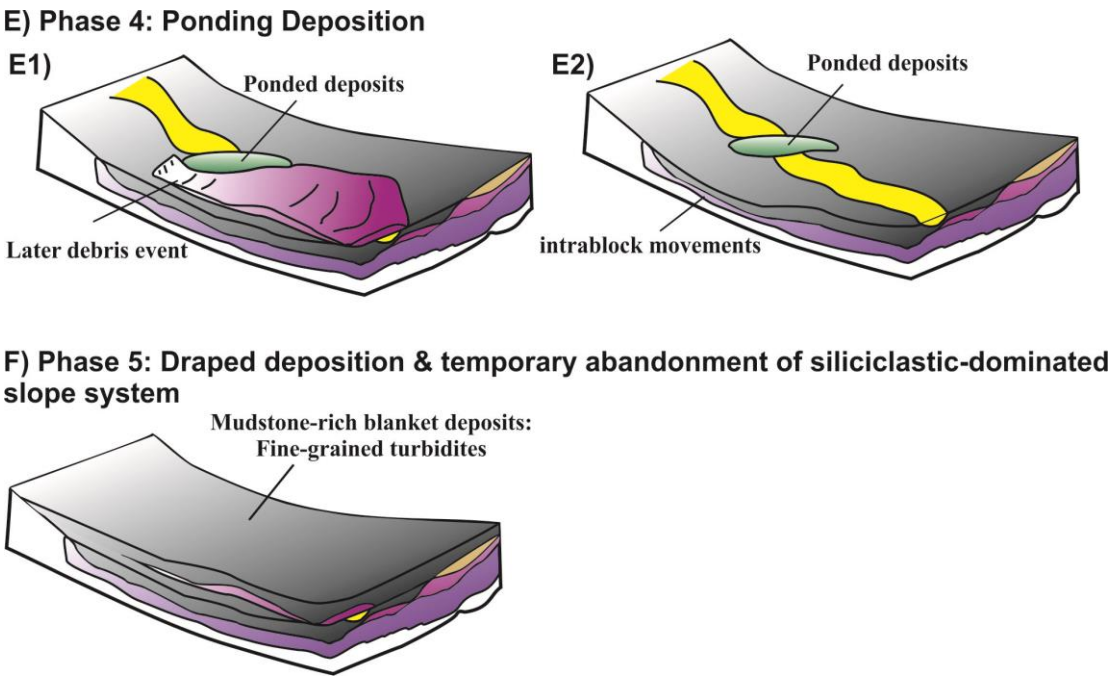

Phase 0: Deposition of carbonate-cemented sandstone-rich unit

Prior to the deposition of Isaac MTC 1, an up to 38 m thick stratal unit consisting of reddish- to brownish-weathering coloured, carbonate-cemented sandstone formed a succession of stacked scours and distributary channel deposits (see chapter 3, Fig 4.12a). These strata mark for the first time widespread submarine carbonate cementation on the Isaac slope system, which in turn suggests a major change in sediment provenance. Now, in addition to the dominant siliciclastic sediment source, a significant supply of carbonate ions was also being delivered into the slope system. The carbonate was most probably being sourced from the dissolution of unstable shallow-water carbonate grains that were eroded from a coeval carbonate platform and then resedimented downslope. Carbonate cementation was promoted on the lower slope by conditions of high carbonate saturation, normal to elevated alkalinity, variable seawater temperature and locally elevated nutrient levels (van Der Kooij et al., 2010). Carbonate-cemented, sandstone-rich strata are interpreted here to be accumulated during or after a rapid rise in relative sea level that initiated at least locally shallow-water carbonate production. Significantly, early cementation of near-surface slope sediments would have steepened the slope, which later by have been out of graded with transport conditions (Hedberg, 1970; Ross et al., 1994).

Phase 1: Emplacement and deposition of MTC

Out-of-grade slope conditions are indicated by Isaac Slide 2 and Isaac debrite 1, which collectively comprise the first extensive mass-transport complex (informally termed Isaac MTC 1) in the Isaac slope system (Fig. 4.12b).

The uneven seafloor topography created along the top of Isaac slide 2 appears to have controlled the emplacement of Isaac debrite 1. Specifically, the 'pinch-and-swell' geometry of the debrite (i.e. lateral thinning and pinch out in the SE and drastic thickening toward the NW) suggests that the debrite infilled the irregular topography across the top of the slide. However, like the slide, the top of the debrite was irregular, thereby forming a new topographically irregular seafloor.

Large-scale slope collapses indicated by Isaac MTC 1 are interpreted to be related to a phase of heightened slope instability caused by conditions of falling relative sea level. The composition of blocks and clasts in the MTC, in addition to the overlying sediment pile (see next), indicates a return of predominantly siliciclastic sediment supply. The scattered carbonate clasts in the debrite are probably eroded remnants of a now deactivated upper-slope and/or carbonate shelf.

Phase 2: Healing deposition

This phase relates to a progressive muting of newly-created seafloor topography across the upper surface of the Isaac MTC 1 (Fig 4.12c). Initially, the irregularity on the top of the MTC influenced the transport pathways of later currents. Widespread deposition of thin-bedded, fine-grained turbidites that overlie most of the MTC suggests that most bathymetric lows became moderately filled and healed by waning, fine-grained turbidity flows. Specifically, the axial sand-rich parts of turbidity currents were preferentially routed through a topographically low area located on the north side of the glacier. Here a sandstone-rich splay unit was built up. This splay is inferred to be fed by a (unexposed) channel found up-dip. The fine-grained margins of these flows, in addition to the preferential preservation of fine-

grained strata occurred everywhere else, which in outcrop represents the south side of the glacier.

The healing phase is interpreted to signal the cessation of (gravitational) slope instability during the terminal phase of relative sea level fall and the early to mid part of the lowstand (e.g. Posamentier and Walker, 2006). Moreover, it signals the resumption of mostly siliciclastic sediment to the Isaac continental slope.

Phase 3: Channel incision, bypass and filling

The architecture of Isaac channel complex 0 (ICC0), which consists of two vertically-stacked, laterally-offset channel units (informally named C1 and C2) records multiple (at least two major) incisional and infill episodes (Fig 4.12d). The basal surface of each channel unit marks the incisional episode when significant erosion and bypass occurred and transferred most of the transported coarse-grained siliciclastic-rich sediment further basinward (Stevenson et al., 2015). Subsequent episodes of channel fill probably coincided with changes in the made up of the transport sediment, and an increase in sediment volume and/or caliber that resulted in local (?) net deposition and channel backfill. Channels fills of C1 and C2 are composed of thick-bedded, amalgamated, quartz-feldspathic, coarse- and very coarse-grained, sandstone and granule conglomerate. These sediments are interpreted to reflect lowstand reactivation of the hinterland sediment source, and therefore full bypass of the older highstand continental shelf.

Phase 4: Ponded deposition

ICC0 is sharply overlain by a decameter-thick ponded unit. This unit consists mostly of medium- and fine-grained strata that distinctively grade sharply or diffusely

into thick mudstone caps (Fig 4.12e). The bipartite nature of these beds, but more specifically the thick mudstone caps, is interpreted to indicate deposition from sediment suspensions with anomalously high volume of silt and clay. The abnormal abundance of fine sediment is believed to be an artifact of flow confinement (sensu Pickering and Hiscott, 1985; Muzzi Magalhaes and Tinterri, 2010), specifically partial downflow confinement. This confinement is thought to be the product of topography formed by an unexposed mass-transport deposit (i.e. Fig. 4.12E1), or alternatively by post-emplacement intra-block movements and differential compaction across the underlying Isaac Slide 2 (i.e. Fig. 4.12E2). The ponded deposition was coincident with the onset of a protracted relative sea-level rise, and a commensurate decrease in the sand:mud ratio of the throughgoing turbidity currents (e.g. Posamentier and Kolla, 2003).

Phase 5: Drape deposition

With the ongoing rise of relative sea level, the area became draped with thin-bedded, mudstone-rich fine-grained turbidites (Fig 4.12f). Eventually, the rising of relative sea level culminated in the onset of deposition of first Isaac carbonate or FIC (see Chapter 5 for detailed information of its facies, architectural constituents and depositional evolution).

4.6.2 Comparison of MTC and overlying deposits with ancient and modern analogues

Similar to other MTCs reported from the ancient rock record (Pickering and Corregidor, 2005; Amerman et al., 2007; Armitage et al., 2009; Jackson and Johnson,

2009; Ogata, 2010; Arnott et al., 2011) and also imaged in seismic (Posamentier and Kolla, 2003; Moscardelli et al., 2006; Posamentier and Walker, 2006; Moscardelli and Wood, 2007), the upper surface of Isaac MTC 1 is interpreted to have been irregular and as a consequence influenced the location of younger sediment-transport pathways and related spatial patterns of depositions (e.g. Moscardelli et al., 2006; Posamentier and Walker, 2006; Jackson and Johnson, 2009).

Based on seismic data, the lateral extent of some MTD is of the order of tens of kilometers with local relief of several tens up to hundreds of meters (Prather et al., 1998a; Brami et al., 2000; Deptuck et al., 2003; Posamentier and Kolla, 2003; Moscardelli et al., 2006; Posamentier and Walker, 2006; Moscardelli and Wood, 2007; Gamberi et al., 2010, 2011; Alves, 2015). As a consequence of this irregularity, deep-water deposits that overlie MTCs typically exhibit lenticular geometries, pinch-out margins, and variable lateral and vertical thickness patterns. Additionally, some ancient examples illustrate that even more subtle, subseismic-scale (i.e. meter to several meters) relief variations influence the depositional patterns of overlying strata (Jackson and Johnson, 2009). Isaac MTC 1 is estimated to extend laterally for at least 1.2 km with relief of several meters or more. This topography controlled the location of the fine-grained turbidite and sandstone-rich splay. Due to outcrop limitations, the relationship between the location and formation of ICC0 and the topography of the underlying the MTC is unclear.

A second example of MTD-controlled sedimentation is the occurrence of the ponded strata succession above ICC0. Here it is argued that partial topographic confinement, which was possibly formed by the surface topography of an unexposed

MTD, which provided the requisite topographical relief needed to increase local mud concentration.

4.6.3 Reservoir Implications

Understanding the type, dimensions, contacts, lithological distribution, depositional relationships and architectural styles of MTCs and their related overlying deposits are valuable on the interpretation of prospective hydrocarbon reservoirs.

The reservoir potential of Isaac MTC 1 varies stratigraphically upward. In the lower part of the MTC, Isaac slide 2 comprises a series of decametre-scale blocks of stratified and poorly-stratified sandstone- and/or mudstone-rich packages. Depending on the lithological distribution, quantity and allocation of shear planes, and preservation of primary stratal textures in the slide blocks, the potential of this slide would be considered moderate to poor. Nevertheless, blocks composed of undeformed to moderately-deformed sandstone-rich strata might be viable reservoir targets, possibly comparable to some slides that have been proven to be prolific hydrocarbon reservoirs in South Texas (Gamboa et al., 2010), Gulf of Mexico (Ogiesoba and Hammes, 2012), and offshore Nigeria (Edwards, 2000; Posamentier and Walker, 2006). Additionally, post-depositional normal faults, fractures and chasms have been recognized within modern and ancient MTCs and/or related turbidites, most notably those rich in carbonate (Clayton et al., 1998; Apotria et al., 2004). The importance of these features is that they are able to focus fluid flow and generate good reservoirs and mineralization (Jackson and Johnson, 2009; Alves, 2015). The paucity of these features in Isaac Slide 2 is probably a reflection of its

siliciclastic composition. Likewise, the debrite at the top of Isaac MTC 1 represents a very poor reservoir, due to its limited lateral continuity, variable thickness and mud-prone composition. This is typical of most debris-flow deposits, since they are characterized by poor porosity and permeability (e.g. Alves, 2015).

Ponded deposits above ICC0 would similarly have poor reservoir potential. Although the sandstone parts of these strata might be good to moderate reservoir quality, they are thin to medium bedded, but most importantly capped vertically by thick mudstone, which would prevent vertical connectivity.

In this study, the most prospective reservoir units are the sandstone- and conglomerate-rich channel fills of ICC0. Channel reservoirs associated with MTCs have been reported from the Gulf of Mexico (Amerman et al., 2007; Armitage et al., 2009; Jackson and Johnson, 2009), and offshore Brazil (Posamentier and Walker, 2006). Significant reservoirs have been recognized in sandstone-prone deposits that are trapped at the top of the MTDs (Wood et al., 2015).

4.7 Conclusions

This outcrop-based study, for first time, documents the component facies and stratigraphic architecture of the lowermost Isaac Formation in the Windermere deep-water depositional system, Cariboo Mountains. The principal observations and interpretations are as follows:

- A decametre-thick and km-wide mass-transport complex (Isaac MTC 1), which comprises slide and debris-flow deposits, was developed within the lower slope succession. The slide is characterized by an irregular basal surface

with ramp-and-flat geometry that is overlain by numerous up-to-decametre-scale blocks of lithologically-diverse and chaotically-arranged strata bounded by shear surfaces. In the lower part of the slide, matrix-rich horizons are present along some shear surfaces, indicating intense local disaggregation of the slide masses during movement. The slide is then overlain by a debrite with a channel-like geometry. The debrite pinches and swells laterally and consists of poorly-sorted, matrix-supported conglomerate with abundant up to meter-scale siliciclastic-rich clasts. Based on the stacking of slide and debris flow deposits and their individual and collective character and considerable decameter-thick and at least several km-wide dimensions of the MTC, it is interpreted to have been associated to with major episode of mass wasting.

- The irregular depositional topography on the top of Isaac MTC 1 was filled and healed by thin-bedded, fine-grained turbidites. Locally, a sandstone-rich splay was also developed as a result of deposition from sandy unconfined flows.
- The fine-grained turbidites that overlie the Isaac MTC 1 are deeply incised by Isaac channel complex 0 (ICC0), which at least in the study area became a major sand-rich transport fairway. Channels in this channel complex were filled predominantly with highly-amalgamated, thick-bedded, coarse-grained siliciclastic-rich strata with 80-100% sandstone to mudstone ratio. Due to outcrop limitations, the possible relationship between the location of ICC0 and the topography of the underlying Isaac MTC 1 is unclear.

- Ponded deposits above the ICC0 are composed mostly of sandstone-rich strata capped by thick mudstone. These strata are inferred to be the resulted of interaction by voluminous, high-concentration turbidity flows and topography along the surface of a (unexposed) mass-transport deposit found downstream. Flows became partially ponded, which caused the suspension cloud at the top of the current to thicken (inflated) and migrate upflow (similar to the backwater effect in open channel flows). This resulted in a significant increased in local mud concentration, which led to the formation of a mobile fluid-mud layer above the aggrading basal sandy layer, similar make up to the lower transitional plug flow of Baas et al. (2011). The upward thinning and fining of stacked bipartite beds (sand-rich base overlain abruptly by fluid-mud layer) is interpreted to represent deposition from single turbidity current. As such, these characteristics and interpreted origin contrast the origin and lithological make up of ponded deposits in geological literature. The latter deposits most probably reflect complete flow confinement, whereas flows here are interpreted to have been partly confined, and at depositional manifest mostly in emplacement of the multiple thick, mud-rich caps
- Deposition of fine-grained siliciclastic-rich turbidites then blanketed the entire study area. This was then succeeded by initiation of the first Isaac carbonate system.
- The depositional model of Isaac MTC 1 and overlying elements consists of six main phases: (A) Phase 0 – preceding deposition of Isaac MTC 1. The

succession consists of stacked scours and distributary channels filled with the first early (diagenetic) carbonate-cemented sandstones on the Isaac slope. Deposition coincided with a rapid rise in relative sea level. Early carbonate sediment strata caused the continental slope to be out of grade with transport conditions, resulting in widespread gravitational slope instability during Phase 1. Instability triggered the successive emplacement of large-scale slide and debris flow deposits, which together make up Isaac MTC 1. This occurred during a fall of relative sea level. (C) Phase 2 – Deposition of a thick pile of fine-grained turbidites, although locally a sandstone-rich splay was formed. This phase is interpreted to have taken place during the terminal phase of the relative sea level fall and the early to mid part of the lowstand. (D) Phase 3 – Formation and infill of Isaac channel complex 0 (ICC0). Thick-bedded, amalgamated, coarse-grained, siliciclastic-rich channel-fill strata are interpreted to reflect lowstand reactivation of the hinterland source region. (E) Phase 4 – With the resumption of a rising relative sea level, the slope became gravitationally unstable once again, and possibly emplaced an unexposed MTD. The presence of the MTD is suggested by the ponded sandstone with their distinctively thick mud caps. (F) Phase 5 – Continued relative sea level rise and deposition of thin, fine-grained turbidites that show an upward change from siliciclastics to mixed (siliciclastic-carbonate) and ultimately carbonate at the base of the First Isaac Carbonate (chapter 5).

4.8 References

Adeogba, A. A., T. R. McHargue, and S. A. Graham, 2005, Transient fan architecture and depositional controls from near-surface 3-D seismic data, Niger Delta continental slope: AAPG bulletin, v. 89, p. 627-643.

Alves, T. M., 2010, 3D Seismic examples of differential compaction in mass-transport deposits and their effect on post-failure strata: Marine Geology, v. 271, p. 212-224.

Alves, T. M., 2015, Submarine slide blocks and associated soft-sediment deformation in deep-water basins: A review: Marine and Petroleum Geology, v. 67, p. 262-285.

Amerman, R., B. Trudgill, E. P. Nelson, M. H. Gardner, P. Arbués, J. Borer, J. Clark, G. L. Ford, H. Ortner, D. Paton, P. Plink-Björklund, and D. R. Pyles, 2007, Comparison of Deep- water Mass Transport Complex Settings: West Texas; South-Central Pyrenees, Spain; Northern Calcareous Alps, Austria.

Amy, L. A., B. C. Kneller, and W. D. McCaffrey, 2007, Facies architecture of the Grès de Peïra Cava, SE France: landward stacking patterns in ponded turbiditic basins: Journal of the Geological Society, v. 164, p. 143-162.

Apotria, T., R. Lindholm, W. Metner, M. Eze, D. Gunn, J. Geslin, P. Rumelhart, F. Goulding, and S. Mitchell, 2004, Volume Interpretation of Shelf Collapse Processes and Biafra "Disturbed" Reservoirs, Eastern Niger Delta Joint Venture, AAPG International Conference, Cancun, Mexico.

Armitage, D. A., B. W. Romans, J. A. Covault, and S. A. Graham, 2009, The influence of mass-transport-deposit surface topography on the evolution of turbidite architecture: the Sierra Contreras, Tres Pasos formation (Cretaceous), southern Chile: Journal of Sedimentary Research, v. 79, p. 287-301.

Arnott, R. W. C., 2007, Stratal architecture and origin of lateral accretion deposits (LADs) and conterminuous inner-bank levee deposits in a base-of-slope sinuous channel, lower Isaac Formation (Neoproterozoic), East-Central British Columbia, Canada: Marine and Petroleum Geology, v. 24, p. 515-528.

Arnott, R. W. C., K. Wallace, and J. Laurin, 2011, Stratal architecture and temporal evolution of a passive margin mass-transport deposit, Neoproterozoic Isaac Formation, Cariboo Mountains, British Columbia, Canada, *in* R. C. Shipp, P.

Weimer, and H. W. Posamentier, eds., Mass-Transport Deposits in Deepwater Settings, v. SEPM Special Publication, SEPM, p. 221-234.

Baas, J. H., J. L. Best, and J. Peakall, 2011, Depositional processes, bedform development and hybrid bed formation in rapidly decelerated cohesive (mud–sand) sediment flows: Sedimentology, v. 58, p. 1953-1987.

Baas, J. H., A. G. Davies, and J. Malarkey, 2013, Bedform development in mixed sand–mud: The contrasting role of cohesive forces in flow and bed: Geomorphology, v. 182, p. 19-32.

Beaubouef, R. T., and S.J. Friedmann, 2000, High Resolution Seismic/Sequence Stratigraphic Framework for the Evolutionf Pleistocene Intra-Slope Basins, Western Gulf of Mexico: Depositional Models and Reservoir Analogs, Deep-Water Reservoirs of the World, GCSSEPM Foundation 20th Annual Research Conference.

Behrens, E., 1984, Unifite muds in intraslope basins, northwest gulf of Mexico: Geo-Marine Letters, v. 4, p. 227-233.

Blanpied, C., and D. J. Stanley, 1981, Uniform mud (unifite) deposition in the Hellenic Trench, eastern Mediterranean.

Bouma, A. H., 1962, Sedimentology of some Flysch Deposits. A graphic approach to facies interpretation: Amsterdam, Elsevier.

Brami, T. R., C. Pirmez, C. Archie, S. Heeralal, and K. L. Holman, 2000, Late Pleistocene deep-water stratigraphy and depositional processes, offshore Trinidad and Tobago, GSTT 2000 SPE Conference and Exhibition.

Bull, S., J. Cartwright, and M. Huuse, 2009, A review of kinematic indicators from mass-transport complexes using 3D seismic data: Marine and Petroleum Geology, v. 26, p. 1132-1151.

Canals, M., G. Lastras, R. Urgeles, J. L. Casamor, J. Mienert, A. Cattaneo, M. De Batist, H. Haflidason, Y. Imbo, J. S. Laberg, J. Locat, D. Long, O. Longva, D. G. Masson, N. Sultan, F. Trincardi, and P. Bryn, 2004, Slope failure dynamics and impacts from seafloor and shallow sub-seafloor geophysical data: case studies from the COSTA project: Marine Geology, v. 213, p. 9-72.

Clayton, C. A., M. F. Cohen, M. Anis, T. W. Cooley, M. M. Honarpour, J. P. Wallace, M. R. Chambers, A. O. Fadase, F. N. Pebdani, E. G. Odior, E. U.

Nwaeri, A. H. Membere, E. O. Ekworomadu, K. A. Miner, B. O. Ogunjana, and R. Al-Hussainy, 1998, Ubit Field Rejuvenation: A Case History of Reservoir Management of a Giant Oil Field, Offshore Nigeria, Society of Petroleum Engineers.

Davis, L., 2011, Architecture of deep-marine interchannel deposits: Isaac Formation, Windermere Supergroup (Neoproterozoic), Southern Canadian Cordillera: M.Sc. Thesis thesis, University of Ottawa, Ottawa, 174 p.

Deptuck, M. E., G. S. Steffens, M. Barton, and C. Pirmez, 2003, Architecture and evolution of upper fan channel-belts on the Niger Delta slope and in the Arabian Sea: Marine and Petroleum Geology, v. 20, p. 649-676.

Deptuck, M. E., Z. Sylvester, C. Pirmez, and C. O'Byrne, 2007, Migration–aggradation history and 3-D seismic geomorphology of submarine channels in the Pleistocene Benin-major Canyon, western Niger Delta slope: Marine and Petroleum Geology, v. 24, p. 406-433.

Dumouchel, I. G., 2015, Stratigraphic Architecture and Depositional History of laterally-accreted channel fills in the Lower Isaac Formation, Windermere Supergroup, British Columbia, Canada, University of Ottawa, Ottawa, 108 p.

Edwards, M. B., 2000, Origin and significance of retrograde failed shelf margins; tertiary northern Gulf Coast Basin.: Gulf Coast Assoc. Geol. Soc. Trans., v. 50, p. 81-93.

Ferguson, C. A., and P. S. Simony, 1991, Preliminary report on structural evolution and stratigraphic correlations, northern Cariboo Mountains, British Columbia: Current Research, v. Part A, Geological Survey of Canada, p. 103-110.

Gamberi, F., and M. Rovere, 2011, Architecture of a modern transient slope fan (Villafranca fan, Gioia basin–Southeastern Tyrrhenian Sea): Sedimentary Geology, v. 236, p. 211-225.

Gamberi, F., M. Rovere, and M. Marani, 2010, Modern Examples of Mass, AAPG Annual Convention and Exhibition, New Orleans, Louisiana.

Gamberi, F., M. Rovere, and M. Marani, 2011, Mass-transport complex evolution in a tectonically active margin (Gioia Basin, Southeastern Tyrrhenian Sea): Marine Geology, v. 279, p. 98-110.

Gamboa, D., T. Alves, J. Cartwright, and P. Terrinha, 2010, MTD distribution on a 'passive' continental margin: The Espírito Santo Basin (SE Brazil) during the Palaeogene: Marine and Petroleum Geology, v. 27, p. 1311-1324.

Gardner, M. H., J. M. Borer, J. J. Melick, N. Mavilla, M. Dechesne, and R. N. Wagerle, 2003, Stratigraphic process-response model for submarine channels and related features from studies of Permian Brushy Canyon outcrops, West Texas: Marine and Petroleum Geology, v. 20, p. 757-787.

Gee, M., H. Uy, J. Warren, C. Morley, and J. Lambiase, 2007, The Brunei slide: a giant submarine landslide on the North West Borneo Margin revealed by 3D seismic data: Marine Geology, v. 246, p. 9-23.

Gee, M. J. R., D. G. Masson, A. B. Watts, and N. C. Mitchell, 2001, Passage of debris flows and turbidity currents through a topographic constriction: seafloor erosion and deflection of flow pathways: Sedimentology, v. 48, p. 1389-1409.

Haughton, P., 2001, Contained turbidites used to track sea bed deformation and basin migration, Sorbas Basin, south-east Spain: Basin Research, v. 13, p. 117-139.

Haughton, P. D. W., 1994, Deposits of deflected and ponded turbidity currents, Sorbas Basin, Southeast Spain: Journal of Sedimentary Research, v. 64, p. 233-246.

Hedberg, H. D., 1970, Continental Margins from Viewpoint of the Petroleum Geologist: AAPG Bulletin, v. 54, p. 3-43
.

Hiscott, R. N., and K. T. Pickering, 1984, Reflected turbidity currents on an Ordovician basin floor, Canadian Appalachians: Nature, v. 311, p. 143-145.

Jackson, C. A. L., and H. D. Johnson, 2009, Sustained turbidity currents and their interaction with debrite-related topography; Labuan Island, offshore NW Borneo, Malaysia: Sedimentary Geology, v. 219, p. 77-96.

Khan, Z., 2012, Origin and architecture of deep-water levee deposits: Insight from the ancient rock record and experiments: PhD Thesis thesis, University of Ottawa, Ottawa, Ontario, 300 p.

Khan, Z. A., and R. W. C. Arnott, 2011, Stratal attributes and evolution of asymmetric inner- and outer-bend levee deposits associated with an ancient

deep-water channel-levee complex within the Isaac Formation, southern Canada: Marine and Petroleum Geology, v. 28, p. 824-842.

King, P., B. Ilg, M. Arnot, G. Browne, L. Strachan, M. Crundwell, and K. Helle, 2011, Outcrop and seismic examples of mass-transport deposits from a late Miocene deep-water succession, Taranaki Basin, New Zealand.

Kneller, B., M. Dykstra, L. Fairweather, and J. P. Milana, 2016, Mass-transport and slope accommodation: implications for turbidite sandstone reservoirs: AAPG Bulletin, v. V. 100, p. 213-235.

Laurin, J., K. Wallace, R. W. C. Arnott, and E. Schwarz, 2007, Stratigraphic anatomy and depositional history of a mass transport complex (MTC), Isaac Formation, Windermere Supergroup, Canada, *in* T. H. Nilsen, R. D. Shew, G. S. Steffens, and J. R. J. Studlick, eds., Atlas of deep-water outcrops, AAPG Studies in Geology 56, p. 119-122.

Lowe, D. R., 1982, Sediment gravity flows: II. Depositional models with special reference to the deposits of high-density turbidity currents: Journal of Sedimentary Petrology, v. 52, p. 279-297.

Lucchi, F. R., and E. Valmori, 1980, Basin-wide turbidites in a Miocene, over-supplied deep-sea plain: a geometrical analysis: Sedimentology, v. 27, p. 241-270.

Lucente, C. C., and G. A. Pini, 2003, Anatomy and emplacement mechanism of a large submarine slide within a Miocene foredeep in the northern Apennines, Italy: A field perspective: American Journal of Science, v. 303, p. 565-602.

Marini, M., M. Patacci, F. Felletti, and W. D. McCaffrey, 2016, Fill to spill stratigraphic evolution of a confined turbidite mini-basin succession, and its likely well bore expression: The Castagnola Fm, NW Italy: Marine and Petroleum Geology, v. 69, p. 94-111.

Marjanac, T., 1990, Reflected sediment gravity flows and their deposits in flysch of Middle Dalmatia, Yugoslavia: Sedimentology, v. 37, p. 921-929.

McHargue, T., M. J. Pyrcz, M. D. Sullivan, J. D. Clark, A. Fildani, B. W. Romans, J. A. Covault, M. Levy, H. W. Posamentier, and N. J. Drinkwater, 2011, Architecture of turbidite channel systems on the continental slope: Patterns and predictions: Marine and Petroleum Geology, v. 28, p. 728-743.

Middleton, G. V., and M. A. Hampton, 1973, Sediment gravity flows: mechanics of flow and deposition, *in* G. V. Middleton, and A. H. Bouma, eds., Turbidites and Deep Water Sedimentation. : Los Angeles, Short Course Notes, No 1, SEPM (Pacific Section), p. 1-38.

Moscardelli, L., and L. Wood, 2007, New classification system for mass transport complexes in offshore Trinidad: Basin Research, v. 20, p. 73-98.

Moscardelli, L., L. Wood, and P. Mann, 2006, Mass-transport complexes and associated processes in the offshore area of Trinidad and Venezuela: AAPG Bulletin, v. 90, p. 1059-1088.

Mountjoy, J., and A. Micallef, 2012, Polyphase Emplacement of a 30 km3 Blocky Debris Avalanche and Its Role in Slope-Gully Development, *in* Y. Yamada, K. Kawamura, K. Ikehara, Y. Ogawa, R. Urgeles, D. Mosher, J. Chaytor, and M. Strasser, eds., Submarine Mass Movements and Their Consequences: Advances in Natural and Technological Hazards Research, v. 31, Springer Netherlands, p. 213-222.

Mulder, T., and J. Alexander, 2001, The physical character of subaqueous density flows and their deposits: Sedimentology, v. 48, p. 269-299.

Murphy, D. C., 1990, Stratigraphy and structure, southern Rocky Mountain Trench to the headwaters of the North Thompson River, Cariboo Mountains, British Columbia.: Current Research, v. Part E, Geological Survey of Canada, p. 71-80.

Mutti, E., M. Carminatti, J. L. P. Moreira, and A. A. Grassi, 2006, Chaotic deposits: examples from the Brazilian offshore and from outcrop studies in the Spanish Pyrenees and Northern Apennines, Italy., AAPG. Annual meeting, Houston, 9–12 April.

Muzzi Magalhaes, P., and R. Tinterri, 2010, Stratigraphy and depositional setting of slurry and contained (reflected) beds in the Marnoso-arenacea Formation (Langhian-Serravallian) Northern Apennines, Italy: Sedimentology, v. 57, p. 1685-1720.

Navarro, L., 2006, Depositional Architecture and Evolution of deep-water base-of-slope and slope channel complexes in a passive-margin setting: Isaac Formation, Windermere Supergroup (Neoproterozoic), Southern Canadian Cordillera: M.Sc.Thesis thesis, University of Ottawa, Ottawa, 272 p.

Navarro, L., Z. Khan, and R. W. C. Arnott, 2007, Depositional architecture and evolution of a deep-marine channel-levee complex: Isaac Formation (Windermere Supergroup), Southern Canadian Cordillera., *in* T. H. Nilsen, R. D. Shew, G. S. Steffens, and J. R. J. Studlik, eds., Atlas of Deep-water Outcrops., v. CD-ROM: Tulsa, AAPG Studies in Geology 56, CD-ROM, p. 22.

O'Byrne, C. J., M. D. Barton, G. S. Steffens, C. Pirmez, and H. Buergisser, 2007, Architecture of a laterally migrating channel complex - Isaac Formation, Windermere Supergroup, British Columbia, Canada, *in* T. H. Nilsen, R. D. Shew, G. S. Steffens, and J. R. J. Studlick, eds., Atlas of deep-water outcrops, v. CD-ROM: Tulsa, AAPG, p. 11 p.

Ogata, K., 2010, Mass Transport Complexes in Structurally contreolled basins: The Epiligurian Specchio Unit (Northern Appeninnes, Italy): Ph.D. Thesis thesis, University of Parma, Parma, 476 p.

Ogata, K., J. J. Mountjoy, G. A. Pini, A. Festa, and R. Tinterri, 2014, Shear zone liquefaction in mass transport deposit emplacement: A multi-scale integration of seismic reflection and outcrop data: Marine Geology, v. 356, p. 50-64.

Ogata, K., R. Tinterri, G. A. Pini, and E. Mutti, 2012, The Specchio Unit (Northern Apennines, Italy): An Ancient Mass Transport Complex Originated from Near-Coastal Areas in an Intra-Slope Setting, *in* Y. Yamada, K. Kawamura, K. Ikehara, Y. Ogawa, R. Urgeles, D. Mosher, J. Chaytor, and M. Strasser, eds., Submarine mass movements and their consequences: 5th International Symposium, Springer, p. 595-605.

Ogiesoba, O., and U. Hammes, 2012, Seismic interpretation of mass-transport deposits within the upper Oligocene Frio Formation, south Texas Gulf Coast: AAPG Bulletin, v. 96, p. 845-868.

Olafiranye, K., C. A. L. Jackson, and D. M. Hodgson, 2013, The role of tectonics and mass-transport complex emplacement on upper slope stratigraphic evolution: A 3D seismic case study from offshore Angola: Marine and Petroleum Geology, v. 44, p. 196-216.

Ortiz-Karpf, A., D. M. Hodgson, and W. D. McCaffrey, 2015, The role of mass-transport complexes in controlling channel avulsion and the subsequent sediment dispersal patterns on an active margin: The Magdalena Fan, offshore Colombia: Marine and Petroleum Geology, v. 64, p. 58-75.

Patacci, M., P. D. W. Haughton, and W. D. Mccaffrey, 2015, Flow Behavior of Ponded Turbidity Currents: Journal of Sedimentary Research, v. 85, p. 885-902.

Pickering, K. T., and J. Corregidor, 2005, Mass-transport Complexes (MTCs) and tectonic control on basin-floor submarine fans, Middle Eocene, South Spanish Pyrenees: Journal of Sedimentary Research, v. 75, p. 761-783.

Pickering, K. T., and R. N. Hiscott, 1985, Contained (reflected) turbidity currents from the Middle Ordovician Cloridorme Formation, Quebec, Canada: an alternative to the antidune hypothesis: Sedimentology, v. 32, p. 373-394.

Pini, G. A., K. Ogata, A. Camerlenghi, A. Festa, C. C. Lucente, and G. Codegone, 2012, Sedimentary Mélanges and Fossil Mass- Transport Complexes: A Key for Better Understanding Submarine Mass Movements?, *in* Y. Yamada, K. Kawamura, K. Ikehara, Y. Ogawa, R. Urgeles, D. Mosher, J. Chaytor, and M. Strasser, eds., Submarine mass movements and their consequences: 5th International Symposium, v. Advances in Natural and Technological Hazards Research 31, p. 585-594.

Pirmez, C., R. N. Hiscott, and J. J. D. Kronen, 1997, Sandy turbidite successions at the base of channel-levee systems of the Amazon Fan revealed by FMS logs and cores: Unraveling the facies architecture of large submarine fans, *in* R. D. Flood, D. J. W. Piper, A. Klaus, and L. C. Peterson, eds., Proceedings of the Ocean Drilling Program, Scientific Results, v. 155, p. 7-33.

Pirmez, C., J. Marr, C. Shipp, and F. Kopp, 2004, Observations and numerical modeling of debris flows in the Na Kika Basin, Gulf of Mexico, Annual Offshore Technology Conference, Houston, Texas, p. 13.

Posamentier, H. W., and V. Kolla, 2003, Seismic geomorphology and stratigraphy of depositional elements in deep-water settings: Journal of Sedimentary Research, v. 73, p. 367–388.

Posamentier, H. W., and R. G. Walker, 2006, Deep-water turbidites and submarine fans: SEPM Special Publication, v. 84, p. 397–520.

Prather, B., C. Pirmez, Z. Sylvester, and D. Prather, 2012a, Stratigraphic response to evolving geomorphology in a submarine apron perched on the upper Niger Delta slope: Prather, BE, Deptuck, ME, Mohrig, D., Van Hoorn, B., and Wynn, R., Application of the Principles of Seismic Geomorphology to

Continental-Slope and Base-of-Slope Systems: SEPM, Special Publication, v. 99, p. 145-161.

Prather, B. E., 2003, Controls on reservoir distribution, architecture and stratigraphic trapping in slope settings: Marine and Petroleum Geology, v. 20, p. 529-545.

Prather, B. E., J. R. Booth, G. S. Steffens, and P. A. Craig, 1998a, Classification, lithologic calibration and stratigraphic succession of seismic facies from intraslope basins, deep water Gulf of Mexico, USA: AAPG Bulletin, v. 82, p. 701-728.

Prather, B. E., J. R. Booth, G. S. Steffens, and P. A. Craig, 1998b, Classification, lithologic calibration, and stratigraphic succession of seismic facies of intraslope basins, deep-water Gulf of Mexico: AAPG bulletin, v. 82, p. 701-728.

Prather, B. E., C. Pirmez, and C. D. Winker, 2012b, Stratigraphy of linked intraslope basins: Brazos–Trinity system western Gulf of Mexico: Application of the Principles of Seismic Geomorphology to Continental-Slope and Base-of-Slope Systems: Case Studies from Seafloor and Near-Seafloor Analogues: SEPM, Special Publication, v. 99, p. 83-109.

Remacha, E., L. P. Fernández, and E. Maestro, 2005, The transition between sheet-like lobe and basin-plain turbidites in the Hecho basin (south-central Pyrenees, Spain): Journal of Sedimentary Research, v. 75, p. 798-819.

Ross, G. M., and R. W. C. Arnott, 2007, Regional geology of the Windermere Supergroup, southern Canadian Cordillera and stratigraphic setting of the Castle Creek study area, Canada, *in* T. H. Nilsen, R. D. Shew, G. S. Steffens, and J. R. J. Studlick, eds., Atlas of deep-water outcrops, v. 56, AAPG Studies in Geology, CD-ROM, p. 16.

Ross, G. M., J. D. Bloch, and H. R. Krouse, 1995, Neoproterozoic strata of the southern Canada Cordillera and the isotopic evolution of seawater sulfate: Precambriam Research, v. 73, p. 71-99.

Ross, G. M., and S. A. Bowring, 1990, Detrital zircon geochronology of the Windermere Supergroup and the tectonic assembly of the southern Canadian Cordillera: The Journal of Geology, p. 879-893.

Ross, G. M., and C. A. Ferguson, 2003, Geology and structure cross-sections, Eddy, British Columbia. Map 1967A, scale 1:50,000: Geol. Surv. Can.

Ross, G. M., and D. C. Murphy, 1988, Transgressive stratigraphy, anoxia, and regional correlations within the late Precambrian Windermere grit of the southern Canadian Cordillera: Geology, v. 16, p. 139-143.

Ross, W. C., B. A. Halliwell, J. A. May, D. E. Watts, and J. P. M. Syvitski, 1994, Slope readjustment: A new model for the development of submarine fans and aprons: Geology, v. 22, p. 511-514.

Schwarz, E., and R. W. C. Arnott, 2007, Anatomy and evolution of a slope channel-complex set (Neoproterozoic Isaac Formation, Windermere Supergroup, southern Canadian Cordillera); implications for reservoir characterization: Journal of Sedimentary Research, v. 77, p. 89-109.

Sinclair, H., and M. Tomasso, 2002, Depositional evolution of confined turbidite basins: Journal of Sedimentary Research, v. 72, p. 451-456.

Smith, R., 2004, Silled sub-basins to connected tortuous corridors: sediment distribution systems on topographically complex sub-aqueous slopes: Geological Society, London, Special Publications, v. 222, p. 23-43.

Southern, S. J., M. Patacci, F. Felletti, and W. D. McCaffrey, 2015, Influence of flow containment and substrate entrainment upon sandy hybrid event beds containing a co-genetic mud-clast-rich division: Sedimentary Geology, v. 321, p. 105-122.

Stanley, D., 1981, Unifites: structureless muds of gravity-flow origin in Mediterranean basins: Geo-Marine Letters, v. 1, p. 77-83.

Stevenson, C. J., C. A.-L. Jackson, D. M. Hodgson, S. M. Hubbard, and J. T. Eggenhuisen, 2015, Deep-water sediment bypass: Journal of Sedimentary Research, v. 85, p. 1058-1081.

Talling, P. J., D. G. Masson, E. J. Sumner, and G. Malgesini, 2012, Subaqueous sediment density flows: Depositional processes and deposit types: Sedimentology, v. 59, p. 1937-2003.

Trincardi, F., and W. R. Normark, 1989, Pleistocene Suvero slide, Paola basin, southern Italy: Marine and Petroleum Geology, v. 6, p. 324-335.

van Andel, T. H., and P. D. Komar, 1969, Ponded Sediments of the Mid-Atlantic Ridge between 22° and 23° North Latitude: Geological Society of America Bulletin, v. 80, p. 1163-1190.

van Der Kooij, B., A. Immenhauser, T. Steuber, J. R. Bahamonde Rionda, and O. MerÍNo TomÉ, 2010, Controlling factors of volumetrically important marine carbonate cementation in deep slope settings: Sedimentology, v. 57, p. 1491-1525.

Wallace, K., 2004, Architecture and Sedimentology of Two Submarine Debris Flow Deposits in the Neoproterozoic Isaac Formation, East-Central British Columbia: B.Sc. Thesis thesis, University of Ottawa, Ottawa, Canada, 133 p.

Wood, L., L. Moscardelli, D. Dunlap, and S. Cardona, 2015, Healing-Phase, Top-Trapped Fills associated with Mass Transport Complexes: Controls on Turbidite deposition in Chaotic Margin Settings: Sixth Annual Deepwater and Shelf Reservoir.

Chapter 5

STRATAL ARCHITECTURE, ORIGIN AND ALLOCYCLIC CONTROL ON DEPOSITION IN SLOPE CHANNELS VERSUS GULLIES IN AN ANCIENT MIXED SILICICLASTIC-CARBONATE SLOPE SYSTEM, NEOPROTEROZOIC ISAAC FORMATION, SOUTHEASTERN CANADIAN CORDILLERA

5.1 Introduction

Deep-water slope channel deposits represent important hydrocarbon reservoirs, and over the few past decades have been exhaustively studied in both modern and ancient siliciclastic-dominated systems (e.g. Clark and Pickering, 1996; Posamentier and Kolla, 2003; Posamentier and Walker, 2006; Deptuck et al., 2007b; Kolla et al., 2007; Nilsen et al., 2007; McHargue et al., 2011). Significantly less well known, however are the processes and deposits in mixed siliciclastic-carbonates (hereafter termed as mixed) and carbonate slope systems. At the Castle Creek study area in the southern Canadian Cordillera, an up to 195 m thick, well-exposed lithologically distinctive succession of the First Isaac Carbonate, which is an important stratigraphic marker within the siliciclastic-dominated Windermere Supergroup.

This chapter aims to: (1) document the spectrum of deep-water facies and stratal elements in a mixed and carbonate unit of the First Isaac Carbonate (FIC), and in particular two distinctive kinds of channelized elements observed: channels and

gullies; (2) interpret how these channelized elements were formed; (3) examine how their contrasting architectures have been influenced by differences in sediment flux, size and mineralogical composition, which in turn are considered to be intimately related to changes in relative sea level; and finally (4) evaluate the role of slope gradient in the development of these channelized elements.

5.2 First Isaac Carbonate (FIC)

At the Castle Creek study area, the Isaac Formation is the lowermost unit in the Neoproterozoic Cariboo Group and consists of a 1300 m thick, mudstone-dominated succession with six intercalated, few to several decametre-thick, discontinuous, coarse-grained sandstone and conglomerate units (Fig. 5.1; see Chapter 1 Introduction for a more detailed discussion of regional geology and stratigraphy) that are interpreted to represent slope channel-levee complexes (e.g. Navarro, 2006; Arnott, 2007; Navarro et al., 2007; O'Byrne et al., 2007; Ross and Arnott, 2007; Schwarz and Arnott, 2007; Khan and Arnott, 2011). In the Cariboo Mountains, which include the Castle Creek study area, regional correlations are aided by the occurrence of two distinctive and mappable carbonate units in the Cariboo Mountains (e.g. Ross and Murphy, 1988; Ross, 1991; Ross and Arnott, 2007). The lower carbonate unit (focus of this study) is informally named the first (or lower) Isaac carbonate (e.g. Ross, 2003; Gammon and Arnott, 2007), and hereafter abbreviated FIC. This is the first study to provide a detailed analysis of the sedimentology, stratigraphy and stratal architecture of the FIC, and therein add to the ever-going global inventory of ancient deep-water carbonate and mixed systems.

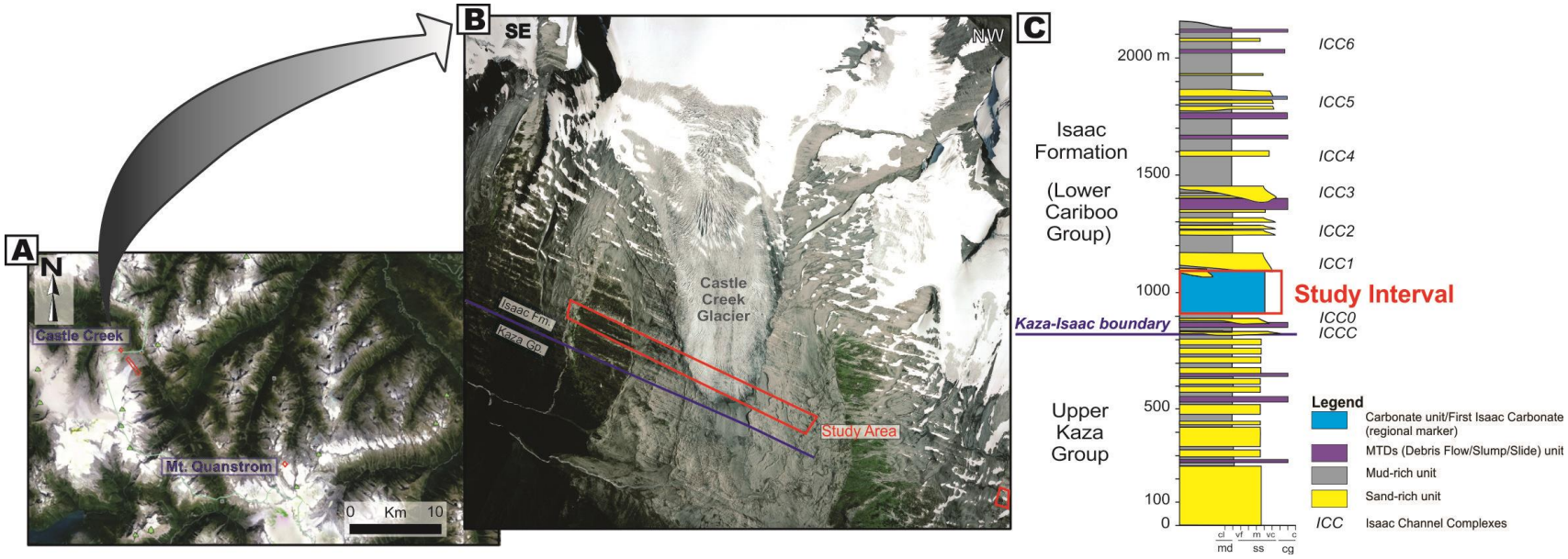

Figure 5.1. Location and stratigraphy of the first Isaac carbonate (FIC) in the study areas. (A, B) Location of the lower Isaac Formation at the Castle Creek and Mount Quanstrom areas. Red rectangle in B indicates position of the FIC, which is approximately 100 m above the contact between the Upper Kaza Group and overlying Isaac Formation. (A-satellite image from Google Earth, 2014; B-aerial photograph from Western Canadian Cryospheric Network and UNBC, 2008). (C) Nomenclature of exposed Windermere Supergroup stratigraphy, in the study area, which in the Isaac Formation consists of six major lenticular sandstone-rich units (labeled IC1-IC6), and mass-transport deposits (debrites, slumps and slides) encased in a mostly mudrock-dominated succession. The carbonate-rich FIC is indicated by the red rectangle and is the focus of this study

5.3 Methodology

This research was based on fieldwork carried out over several summers in the Castle Creek area, and in an ancillary area at Mt. Quanstrom, about 20 km east of Castle Creek (Fig. 5.1). Stratigraphic sections were analyzed in bed-by-bed detail and a total of 1055 m of stratigraphy measured. High-resolution aerial photomosaics (1:300-1:500) were used to trace beds and bedsets and correlate significant surfaces that in many cases bound major architectural elements. Paleocurrent data were difficult to obtain in the study area, except for few from a dune cross-stratified bed. Additionally, a total of 45 petrographic thin sections were studied, in addition to 4 representative samples using cathodoluminescence microscopy (see Appendix C) to help determine sediment composition and provenance, original and post-depositional fabrics, and cement generations. 6 x-ray fluorescence samples were collected, prepared and evaluated (see Appendix D).

Supplementary stable isotope data of the middle and upper part of the studied FIC strata are presented in Appendix E. The $\delta^{13}C$ and $\delta^{18}O$ bulk isotopic compositions are from 25 fine-grained carbonate samples (all results are reported using the standard ‰ notation in units of ‰ relative to the PDB standard), and $\delta^{13}C_{org}$ of organic residue are from 11 mudstone/siltstone samples that were previously analyzed but not published (G. M. Ross, unpublished data).

At Castle Creek, vertically-dipping strata crop out laterally and on opposite sides of the glacier. The studied area is approximately 195 m thick and >1.5 km wide (Fig. 5.1). Despite low-grade metamorphism, primary physical sedimentary structures

and textures are well-preserved. Locally, however, strata are variably deformed and/or faulted, and show evidence of diagenetic and metamorphic overprint (for more details of the structural framework along the Cariboo Mountains, see Murphy, 1990; Ferguson and Simony, 1991). It is important to note that a detailed analysis of the post-depositional diagenetic and metamorphic processes were beyond the scope of this study.

5.4 Facies

In the study area, ten lithofacies are identified based on grain composition, grain size, primary physical sedimentary structures, bed thickness, degree of bed amalgamation, and carbonate cementation. On the basis of their dominant siliciclastic vs. carbonate composition, these facies have been sub-divided into three groups: siliciclastic-, mixed, and carbonate-dominated. Table 5.1 summarizes the main stratal attributes of each lithofacies and their interpreted formative process; Figure 5.2 illustrates representative photographs of each facies.

Table 5.1. Summary of deep-water siliciclastic, mixed and carbonate facies in the First Isaac Carbonate

Facies	Lithology, texture and physical sedimentary structure	Bed thickness (m), geometry and contacts	Depositional Processes	Equivalent Facies	Architectural Element Association
SILICICLASTIC-DOMINATED FACIES GROUP (>75% siliciclastics)					
F1. Quartz-rich conglomerate and very coarse- and coarse-grained sandstone	White to light beige, structureless, clast-supported, granule and pebble conglomerate, and white to yellow to light orange, structureless, normal grading (but some massive), coarse-grained to very coarse-grained sandstone, with or without mudstone tops. Some sandstone beds are calcareous, exhibiting up to 25% calcite cement.	From 0.17 to 4 m. Mostly amalgamated to semi-amalgamated beds. Sharp, loaded, and erosive bases, and sharp tops.	Deposition from gravelly and sandy siliciclastic-rich, high-concentration turbidity flows.	Ta[1] or R3/S3[2]. Some beds are overlain by thin Td cap.	Slope channels
F2. Mudstone-clast breccia	Abundant, angular to subangular, from chips to boulder-sized clasts of light grey and dark grey/ black mudstone clasts in a white to yellow, poorly-sorted, coarse-grained, sand matrix with common quartz granules and pebbles. Rounded mudclasts are uncommon. In one bed, carbonate clasts are also observed.	From 0.3 to 1 m. Lenticular beds. Erosive bases and sharp tops.	Deposition from sandy siliciclastic-rich, high-concentration turbidity currents, enriched with consolidated mudstone clasts that were eroded from upflow muddy substrate	-	Slope channels
F3. Medium-grained calcareous sandstone	Yellow, white to orange, graded, rippled cross- and/or planar-laminated, medium-grained calcareous sandstone. Beds are commonly overlain by a thin mudstone cap. Locally, multiple (>4-5) sets of non-climbing ripples are observed.	From 5 cm to 1 m. Commonly tabular beds. Sharp bases and tops.	Deposition from sandy siliciclastic-rich, high- to moderate- concentration, decelerating turbidity flows	Tacd, Tad, Tc, and rare Tabcd [1]	Slope channels Overbank deposits
F4. Stratified sandstone	Typically orange to deep red, but some yellow, planar- and dune cross-stratified, medium- and coarse-grained calcareous sandstone, and uncommonly granule conglomerate.	From 3 cm to 0.4 m. Typically, lenticular beds in slope gullies, whereas tabular beds are more common in overbank deposits. Erosive bases and sharp tops.	Deposition from sandy siliciclastic-rich, high- to moderate- concentration turbidity flows under tractional conditions.	Tb, and Tbc[d][1]. Rarely S1[2]	Slope Gullies Overbank deposits
F5. Fine-grained calcareous sandstone and mudstone, and mudstone	Orange to pink, ripple cross-laminated, and occasionally parallel laminated, fine-grained calcareous sandstone, capped by light grey silty mudstone. Thicker interbeds of ripple cross-laminated sandstone consist of multiple (up to 3) sets. Single set, starved ripples are observed locally. Some intervals are composed mostly of light grey silty mudstone beds, and some are overlain by a thin layer of black claystone.	From 0.2 to 15 cm (av. 1-4 cm). Tabular beds. Sharp bases and tops.	Deposition from low-concentration, decelerating turbidity currents under traction transport conditions, followed by suspension deposition of mud	Tcd, or Td[e][1]	Mudstone-dominated (siliciclastic) deposits Overbank deposits Slope Channels Slope Gullies
F6. Carbonaceous sandstone	Intense orange to red, planar laminated, medium-grained sandstone with interlayered, sharp-based, dark-grey to black graphitic or carbonaceous bands. Cross-lamination is rare. Comparatively	From 0.29 to 0.4 m. Lenticular beds. Sharp, erosive bases and sharp tops.	Deposition from sandy low-concentration turbidity flows under tractional conditions	Tb[1]	Slope Gullies

	high TOC content (0.37%, see Appendix 5) in the study area.				
F7. Matrix-rich sandstone	Poorly-sorted, structureless, medium- and coarse-grained sandstone with mudchips	From 5 to 19 cm. Sharp bases and tops.	Deposition from high-concentration turbidity currents downflow of a area of rapid flow expansion	-	Crevasse-splay deposit
MIXED-DOMINATED FACIES GROUP (50-75% siliciclastics or carbonates)					
F8. Mixed siliciclastic-carbonate conglomerate and sandstone	Dark brown (and less commonly light brown), poorly-sorted, mostly clast-supported, structureless and mostly ungraded, mixed, conglomerate with medium- to very coarse-grained sand matrix. Carbonate clasts are granule and pebble, and rarely boulders. Coarse- to very coarse-grained, mixed sandstone. Mixed conglomerate can be categorized as petromict conglomerate (Pettijohn, 1975) or quartzose or siliciclastic calcirudites (modified from Grabau, 1904). Mixed sandstone can be classified as hybrid arenites of Zuffa (1980), or quartzose or siliciclastic calcarenites (modified from Grabau, 1904).	From 0.11 to 3.5 m. Amalgamated beds, with sharp, wavy or erosive bases, and sharp tops.	Deposition from gravelly and sandy mixed (siliciclastic-carbonate)-rich, high-density turbidity flows	Ta[1], R3 and S3[2]	Slope Channel
CARBONATE-DOMINATED FACIES GROUP (>75% carbonates)					
F9. Fine-grained calcarenite and calcilutite	Reddish brown, maroon, to orange, well-sorted, commonly parallel- and/or cross-laminated, fine-grained and very fine- calcarenites that typically grade to calcilutites. Medium-grained calcarenites are less common. Single ripple sets are common. Yellowish to dark olive to dark grey, graded (occasionally planar laminated), silt- to mud-sized calcilutites. Common calcite veins parallel to bedding or weathered surfaces. Texturally, calcarenite and calcilutites can be classified as grainstone and mudstone (Dunham, 1962), respectively; though both are largely recrystallized. Some fine-grained calcareous beds are sharply overlain by light grey, siliciclastic mudstone.	Up to 40 cm, but average 2-5 cm. Tabular beds, sharp bases and tops.	Traction followed by suspension fallout deposition from carbonate-rich, low-concentration turbidity flows. Some flows were then followed by suspension settling deposition from the diluted but siliciclastic-rich tail of the flows.	Typical calciturbidites Tde, Tbde and Tcde[1], less common Tabcde and Tacde[1]. Some tops: siliciclastic Td[1]	Calciturbidite-dominated deposits Slope Channels Slope Gullies
F10. Carbonate breccia	Reddish to yellowish brown, poorly-sorted, ungraded, disorganized, structureless, mud- or clast-supported carbonate breccia. Abundant, non-skeletal carbonate lithoclasts, as well as clasts of calciturbidites, mudstone or interbedded fine-grained calcareous sandstone and mudstone. *F10a. Mud-supported carbonate breccia*	From 0.7 to 5.25 m thick. Tabular to lenticular bed, Erosive bases and sharp or irregular tops.	Deposition from calcareous-rich muddy debris flows initiated on carbonate platform and upper slope	Calcidebrites (MTD)	Overlying or Intercalated in Calciturbidite-dominated Units Capping Slope Channels

consist of up to cobble-sized, mostly carbonate clasts embedded in a matrix of calcareous mud with common dispersed, sand- to pebble-size (up to 1.5 cm) quartz grains, and occasional siliciclastic mud.

F10b. Clast-supported carbonate breccia consist mostly of carbonate clasts of variable size (up to several decimeters-long), and elongated and with their long-axes aligned parallel to sub-parallel to the basal contact. Typically, clasts show no internal stratification, but locally are crudely layered. Isolated blocks and/or raft clasts are occasionally observed.

Turbidite division terminology from 1-Bouma (1962), and 2-Lowe (1982)

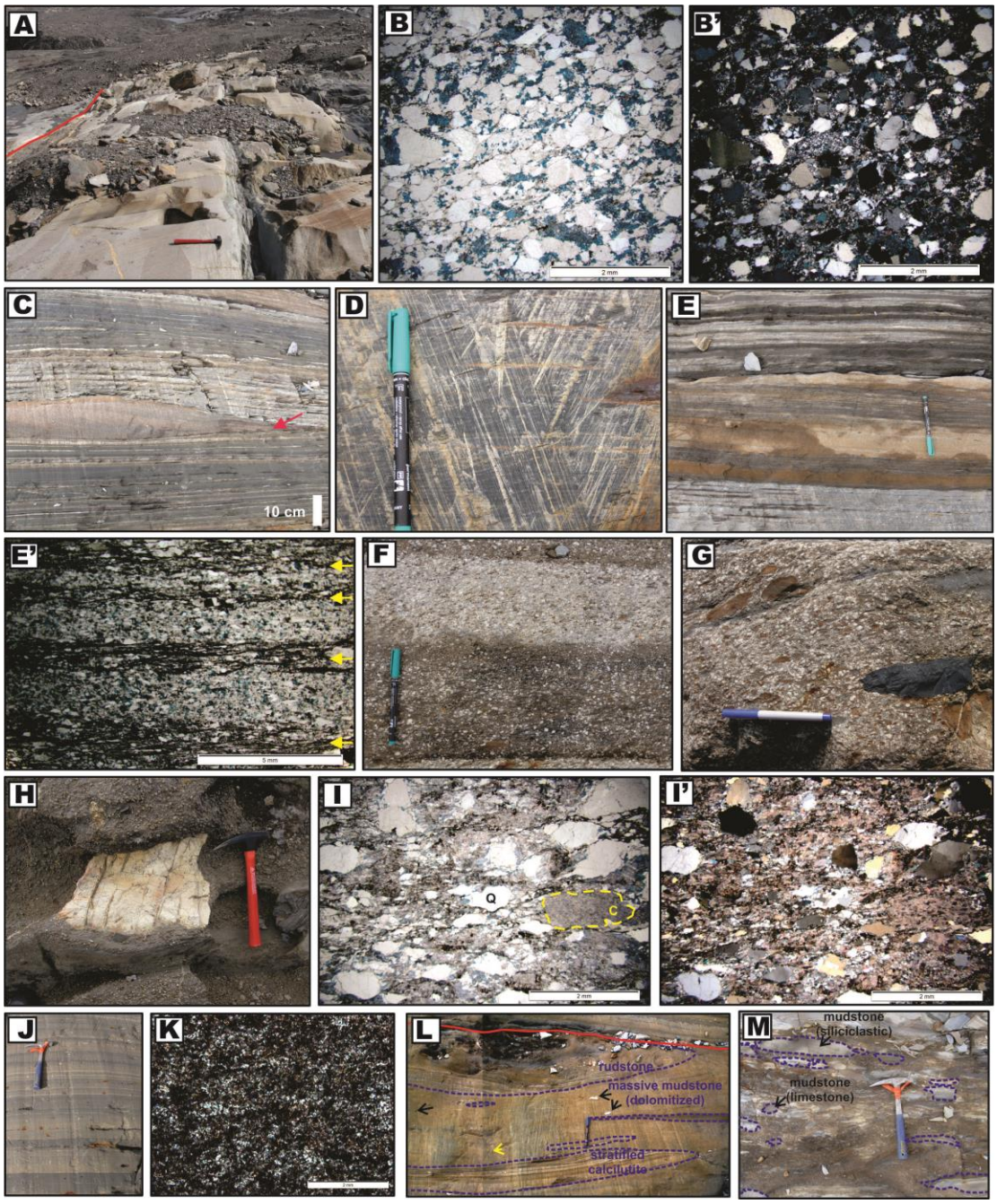

Figure 5.2. Representative photos and photomicrographs of facies of the FIC. (A) Thick-bedded, amalgamated, quartz-rich conglomerate and sandstone (F1) that fill channels in Bacon Sandstone channel complex 1 (base of channel complex is indicated by red line). (B-B', plane- and cross polarized light, respectively). Petrographically, strata of F1 are dominated by quartz grains (up to 90-100%) with pore-filling, ferroan calcite cement. (C) Orange-coloured, dune cross-stratified medium-grained sandstone (F4, indicated with red arrow) along the base of a gully. (D) Grey, thin-bedded, fine-grained sandstone to siltstone Tcd/Td turbidites (F5) that characterize fine-grained

siliciclastic deposits. (E) Medium-grained, planar-stratified sandstone with intercalated layers of dark grey/black carbonaceous-rich medium-grained sandstone (F6). Like dune cross-stratified sandstone, these occur at the base of some gullies. (E') Photomicrograph with plane polarized light showing medium-grained sand grains embedded in calcite cemented and grey/black parallel-to-bedding graphite-rich bands (indicated with yellow arrows). (F-G) Channel-fill strata of Bacon Sandstone channel 1 also consist of brown beds or layers of mixed granule and pebble conglomerate (F8) with abundant olive to orange carbonate and white quartz clasts, and minor black mudstone clasts. (H) Clasts of up to boulder-size cryptalgal laminites (light yellow) and crystalline limestone pebbles (olive) in channel fills of Bacon Sandstone channel complex 1. (I-I', plane- and cross-polarized light, respectively) Petrographically, F8 consists of carbonate (c) and quartz grains (Q) with an extensive carbonate cement (25-30%, up to 50%). (J) Light yellow-orange to olive, thin-bedded, commonly normally-graded calcilutites beds (F9), which typically occurred in fine-grained, calciturbidite units 1-3 and at the top of the gullies. (K) Photomicrograph with plane polarized light showing micritic limestone that was partially dolomitized. (L) Mud-supported carbonate breccia (F10a) with pebble- to boulder-sized clasts (white dashed outlines) of calcilutite, mudstone, rudstone, and pitted quartz granules embedded in a light orange, carbonate mudstone matrix. (M) Clast-supported carbonate breccia (F10b) consists mostly of carbonate and siliciclastic mudstone clasts (orange/brown and grey, respectively) and quartz pebbles dispersed in a yellow to orange carbonate-rich mudstone matrix.

5.5 Deep-water stratal architecture in the FIC

There is an extensive literature about architectural element analysis in modern and ancient fluvial systems (e.g. Miall, 1985, 1996) and deep-water siliciclastic systems (e.g. Mutti and Normark, 1987, 1991; Clark and Pickering, 1996), but significantly less for examples in modern or ancient carbonate or mixed slope systems.

An architectural element refers to a distinctive stratal body or assemblage of bodies that are bounded by above and below by genetically-related surfaces that formed in the same depositional setting (Pickering et al., 1989). In this way, an architectural element is distinguished based on its internal and external characteristics, including geometry, scale and facies. Based on detailed field-based

observations, six principal architectural elements are identified in the FIC at the Castle Creek study area, and include: slope channel complexes, leveed deposits, slope gullies, siliciclastic- and calciturbidite-rich fine-grained deposits, and calcidebrites (Table 5.2 and Figs. 5.3-5.4).

5.5.1 Slope channel complexes (i.e. Bacon sandstone)

In the lower part of the FIC, two channel complexes crop out and are informally termed Bacon sandstone channel complex 1 and 2 (Fig. 5.3-5.4). They form decameter-thick (14-20 m) conglomerate- and sandstone-dominated units that can be traced laterally for >1-2 km, and comprise 15% of the cross-sectional area of the FIC. Strata exhibit high sand/gravel content (90-100%) and a distinctive carbonate cement pattern (for more details see Appendix C), which in many places causes them to have a distinctive brown-white colour striping that is similar to bacon. Bacon sandstone channel complex 1 is exposed on both sides of the glacier and overlies a thick succession of laterally-continuous, fine-grained siliciclastic turbidites (Fig. 5.5). Bacon sandstone channel complex 2, on the other hand, overlies the thickest calciturbidite unit (i.e. Calciturbidite Unit 2) and is exposed on one (NW) side of glacier where it can be traced for more than several hundred meters toward the northwest (Fig. 5.6).

Each Bacon sandstone channel complex comprises three or more erosively-based, up to 5 m thick channel fills that can be traced laterally for at least 400 m (Fig. 5.7). Laterally-discontinuous, mudstone-clast breccia (F2) locally overlie channel bases.

Table 5.2. General characteristics of stratal architecture elements documented in the FIC

Stratal Element		*Thickness and width (m)*	*Contacts and/or Geometry*	*Facies*	*Vertical and/or lateral trends, and/or Stacking patterns*
Slope channel complexes (i.e. Bacon Sandstone channel complexes 1 & 2)		Complex: 14-20 m and >1000-2500 m Single: Up to 5 m thick	Erosive base. Channelforms	Mostly F1 and F8, and minor to rare F2, F4, F5 and F9. Rare F7.	- Subtle upward fining and thinning (at the top) - Lateral changes in grain size and lithofacies, grain mineralogy or composition, bed amalgamation, and carbonate cementation (i.e. brown-white pseudobeds, bands or horizons). -Vertical-stacked channels
Levee deposits		Up to 6 m and >1200 m	Sharp base. Sheet-like element	F3 and F5. Occasional F4	Lateral fining and thinning trends
Slope gully-like features (i.e. Gully complexes 1 & 2)		Single: Up to 1.5 m (but commonly dm-thick) and 100-300 m Complex: Up to 40 m thick	Erosive base. Lenticular forms, typically overlain by sheet-like drapes	Fill: F4 and F6. Drapes: F5 overlain by F9	Vertical stacked
Fine-grained deposits	Fine-grained siliciclastic turbidites	Up to 24 m and >1200 m	Sharp base and top. Sheet-like element	F5. Rare F9.	-Local fining- and thinning- upward
	Fine-grained calciturbidites (i.e. Calciturbidite Units 1, 2 & 3)	Up to 20 m and > 1200 m	Sharp base and top. Sheet-like element	F9, and occasional F5, except Calciturbidite Unit 1 also contain mostly F8, F3 and F4 interbeds	-Local fining- and thinning- upward
Calcidebrites (i.e. Calcidebrites 1, 2 & 3)		Up to 5 m and >1200 m	Sharp, erosive base. Discontinuous lenses to laterally-continuous sheets.	F10	- Intercalated or at the top of Calciturbidite Units 1, 2 & 3

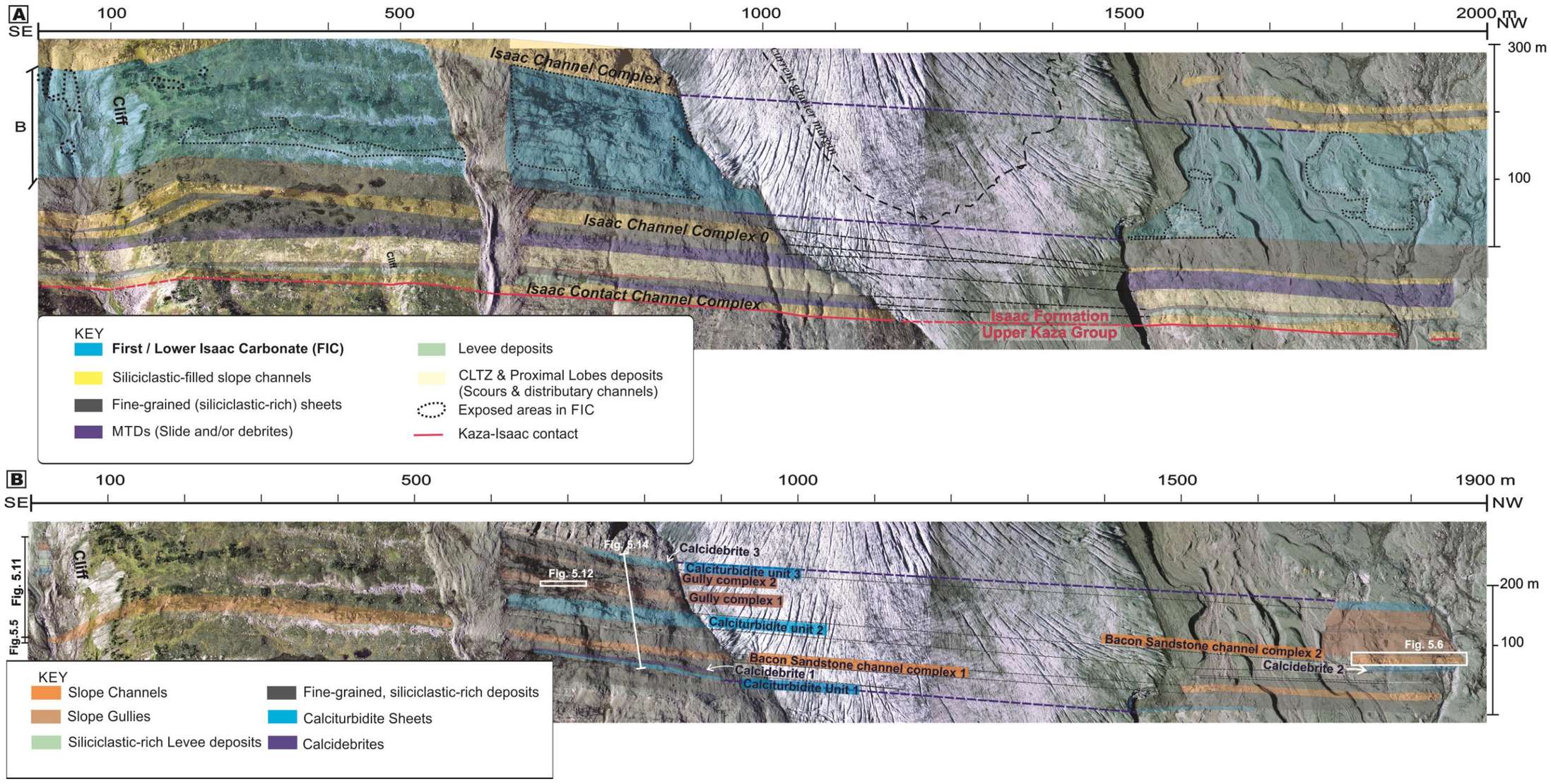

Figure 5.3. Stratal architecture of the lowermost Isaac Formation and the First Isaac Carbonate (FIC). (A) Photomosaic of the lower Isaac Formation at Castle Creek that illustrating the main architectural elements and their bounding surfaces. In the siliciclastic-dominated deep-water sedimentary pile of the Isaac Formation, the first Isaac carbonate, or FIC (coloured blue), forms a regionally distinctive stratigraphic marker. (B) Architectural elements of the FIC, including slope channels, siliciclastic-rich leveed deposits and slope gullies, separated by siliciclastic- and/or calciturbidite-rich deposits.

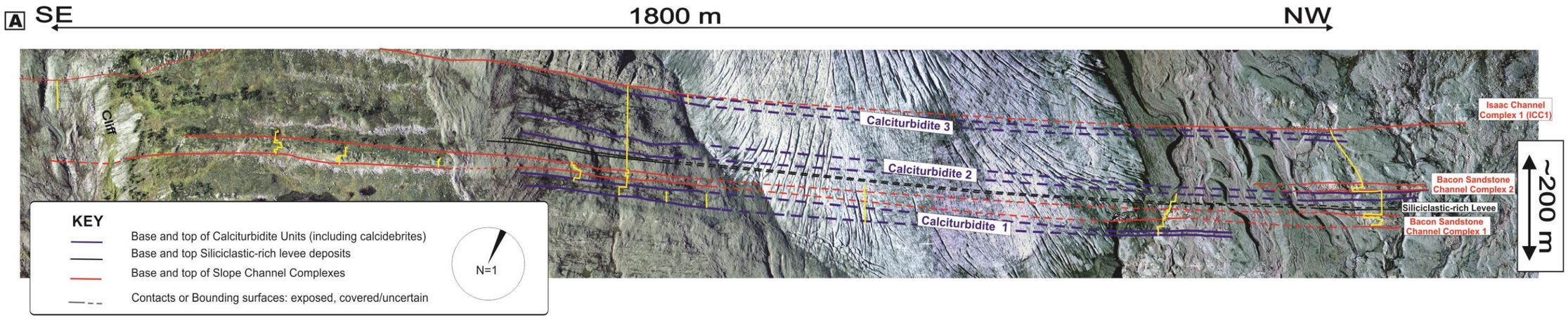

Figure 5.4. Airphotomosaic and Correlation panel of the First Isaac Carbonate (FIC) at the Castle Creek study area. (A) Section locations and bounding surfaces of main stratal elements are indicated. Paleocurrent indicators are scarce.

Continuation of Fig. 5.4.

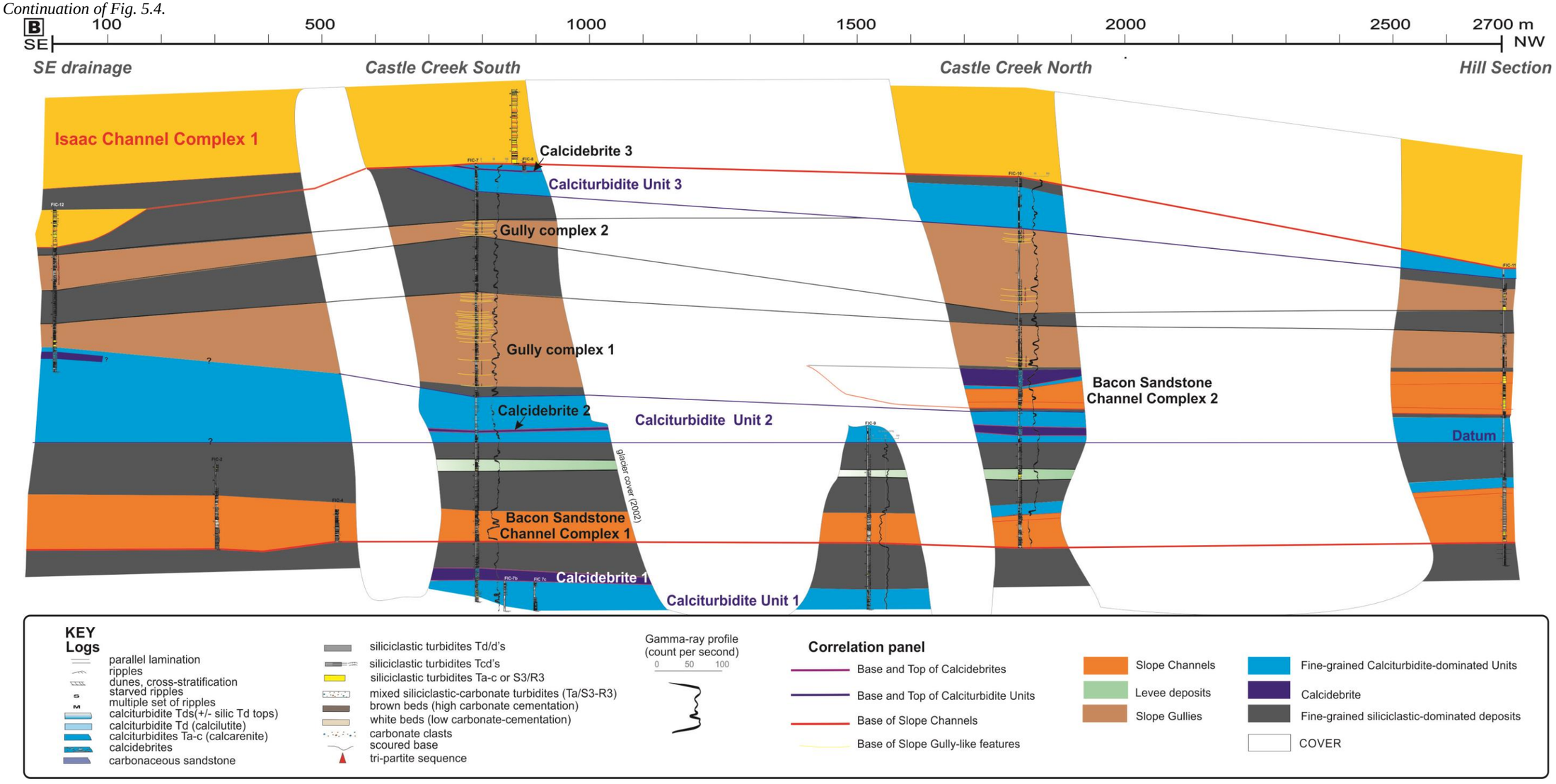

Figure 5.4 (Continued). (B) General architecture of the FIC is shown, consisting three main calciturbidite (sheet-like) units, interbedded locally with calcidebrites, and separated by thin-bedded, fine-grained siliciclastic turbidites: Calciturbidite unit 1 is the first unit and crops out above Isaac Channel 0, Calciturbidite Unit 2 is the thickest and most laterally-extensive unit, and Calciturbidite Unit 3 directly underlies Isaac Channel 1. In addition to these calciturbidite units, slope channels termed here as Bacon Sandstone channel complexes 1 and 2 are recognized in the lower FIC (respectively, above calciturbidites units 1 and 2), whereas numerous slope gullies making up gully complexes 1 and 2 are identified in the upper FIC.

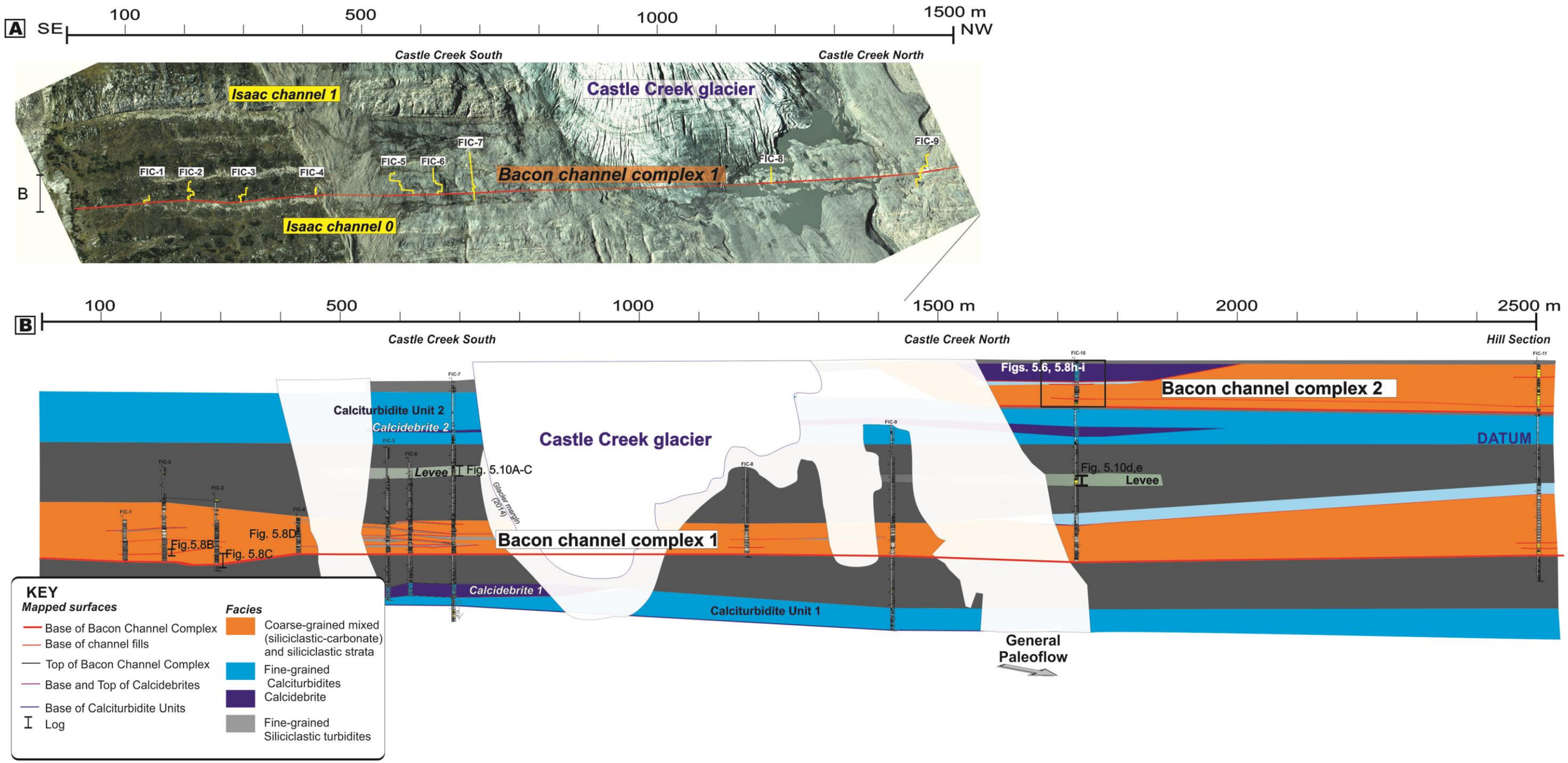

Figure 5.5. Stratigraphic cross-section of the Bacon Sandstone channel complex 1. (A) Interpreted composite airphotos of the channel. (B) Stratigraphic cross-section panel of Bacon channel complex 1 over 1.5 km laterally. This channel complex is up to 20 m thick and comprises several stacked channel fills composed mostly of siliciclastic- and mixed (siliciclastic-carbonate)-rich coarse-grained facies (F1 and F9, respectively). It then is overlain by a thick succession of thin-bedded siliciclastic turbidites (grey) that are locally interbedded with sandstone-rich levee deposits (green, mostly facies F3 and F5).

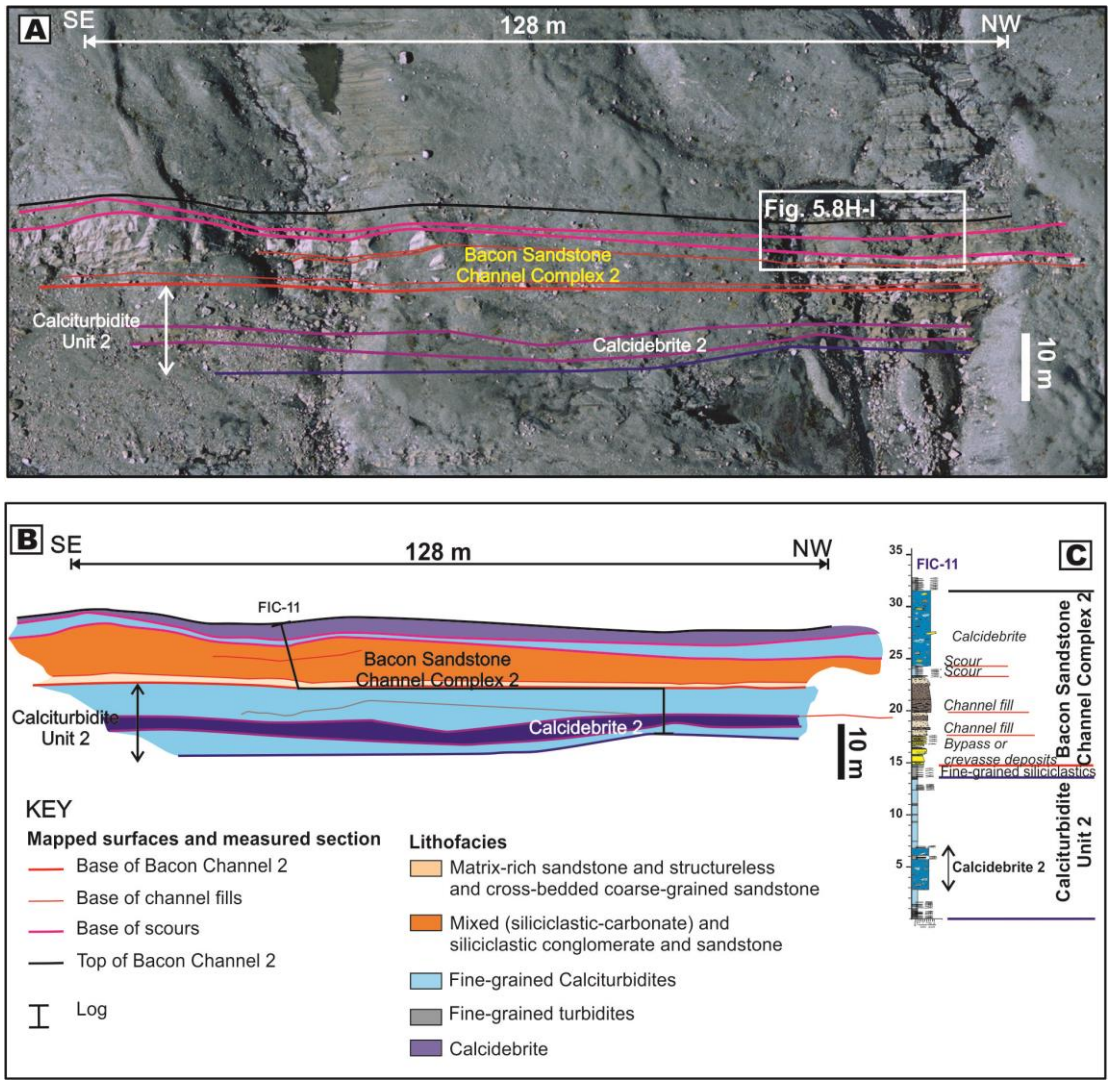

Figure 5.6. Stratigraphic cross-section of the Bacon Sandstone channel complex 2 at Castle Creek North (i.e. North side of the glacier). (A-C) Airphoto and line-drawing of this channel complex, and traced measured section (FIC-11). (D) Stratigraphic log showing its constituent architectural elements. Channels are predominantly filled by F1 and F8 strata. At the top of the complex, few scours are filled with thin-bedded, fine-grained calciturbidites and calcidebrite (F9 and F10, respectively).

Channels are mostly filled with thickly-bedded, highly-amalgamated, coarse-grained sandstone and conglomerate (F1 and F8; Figs. 5.5-5.7) composed of mixed- or quartz-rich sediment with dispersed white quartz clasts and orange-olive-brown carbonate clasts, including oolitic limestone (Fig. 5.8e), peloidal limestone (Fig.

5.8f), dolomitized limestone (Fig. 5.8g), cryptalgal laminite (Fig. 5.2h), carbonate mudstone, and recrystallized limestone. Clasts are subangular to rounded. Many of the large clasts, which range up to 0.5 cm long, are dolomitized.

Strata are typically dark brown but locally exhibit a distinctive patchy to continuous brown and white striping that is irregularly subparallel, but in places is discordant to bedding (Figs. 5.2f, 5.7, 5.8b-d). These variably coloured layers reflect differences in the amount of predominantly ferroan calcite and variably ferroan dolomite cement, wherein brown layers have up to 40% and white layers less than 15% carbonate cement. Preliminary petrographic analyses suggest a complex diagenetic history or paragenesis that includes at least seven episodes of carbonate cementation (see Appendix C2 for details); the details of which are beyond the scope of this research and require further work.

Laterally, over distances of <200 m, these amalgamated, coarse-grained strata change to a succession of interstratified thick- to thin-bedded, granule conglomerate and coarse- to medium-grained, mixed- and quartz-rich sandstone (F8 and F1, respectively), cross-stratified sandstone (F4), (siliciclastic) mudstone or sandstone-mudstone (F5) and rare fine-grained calcarenite and calcilutites (F9). Dolomitized carbonate clasts are less common. In addition to changes in lithofacies, strata also become increasingly brown and white striped and then mostly white, reflecting a lateral decrease in ferroan calcite cement and a commensurate increase in the abundance of quartz framework grains.

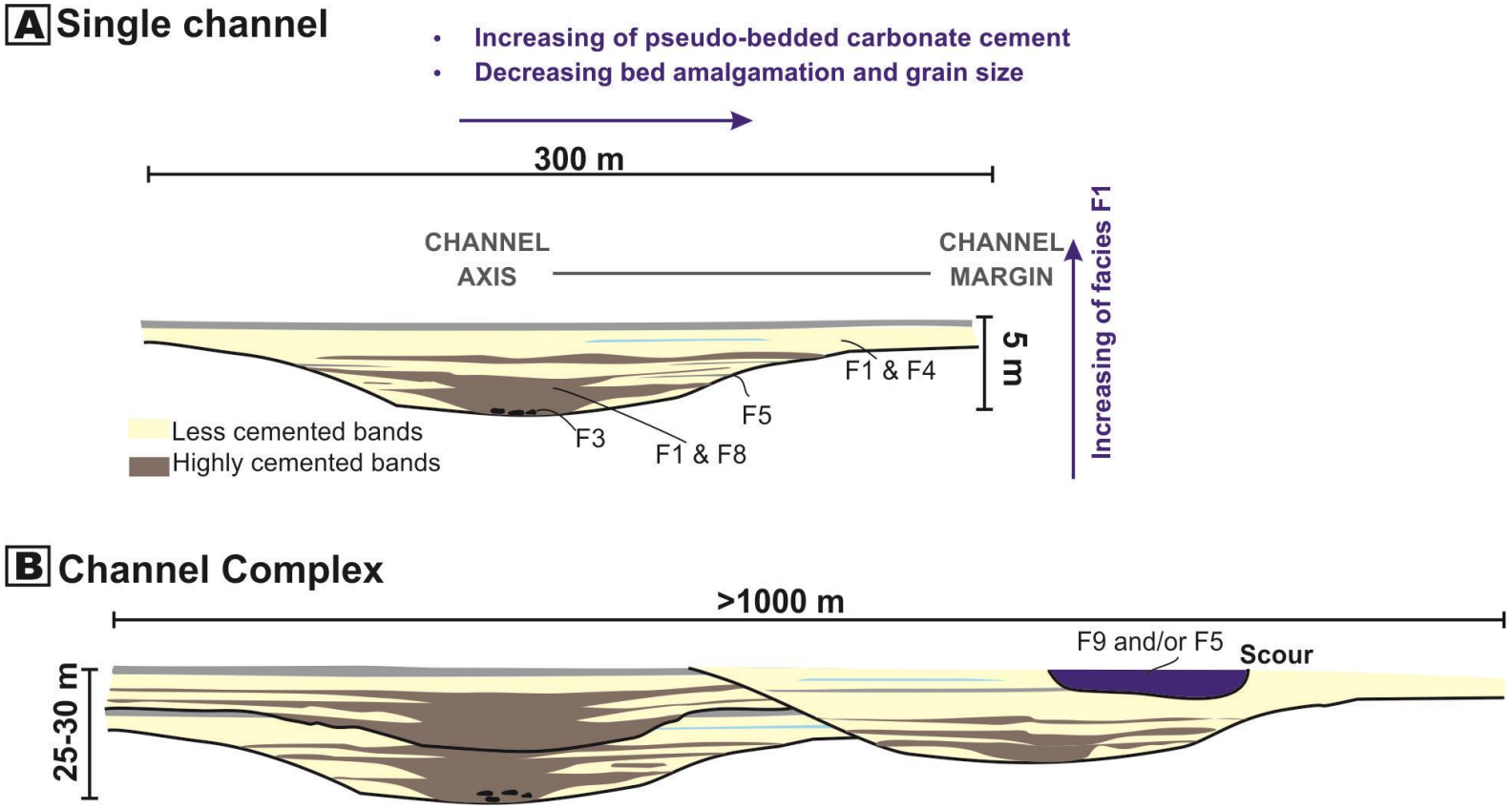

Figure 5.7. Schematic representation illustrating characteristics and hierarchical channel arrangement in Bacon Sandstone channel complexes. (A) Channel fills exhibit amalgamated to semi-amalgamated, coarse-grained F1 and F8 strata, and tend to be commonly capped by thin-bedded, fine-grained turbidites F5. At its axis, high brownish carbonate cementation typically occurred, and stripping or banded (pseudo-bedding) white/brown cementation is predominant toward the margins. (B) A channel complex is composed of several channel fills. Locally, scoured surfaces overlain by calcidebrites and fine-grained calciturbidites are present at the top of the complex.

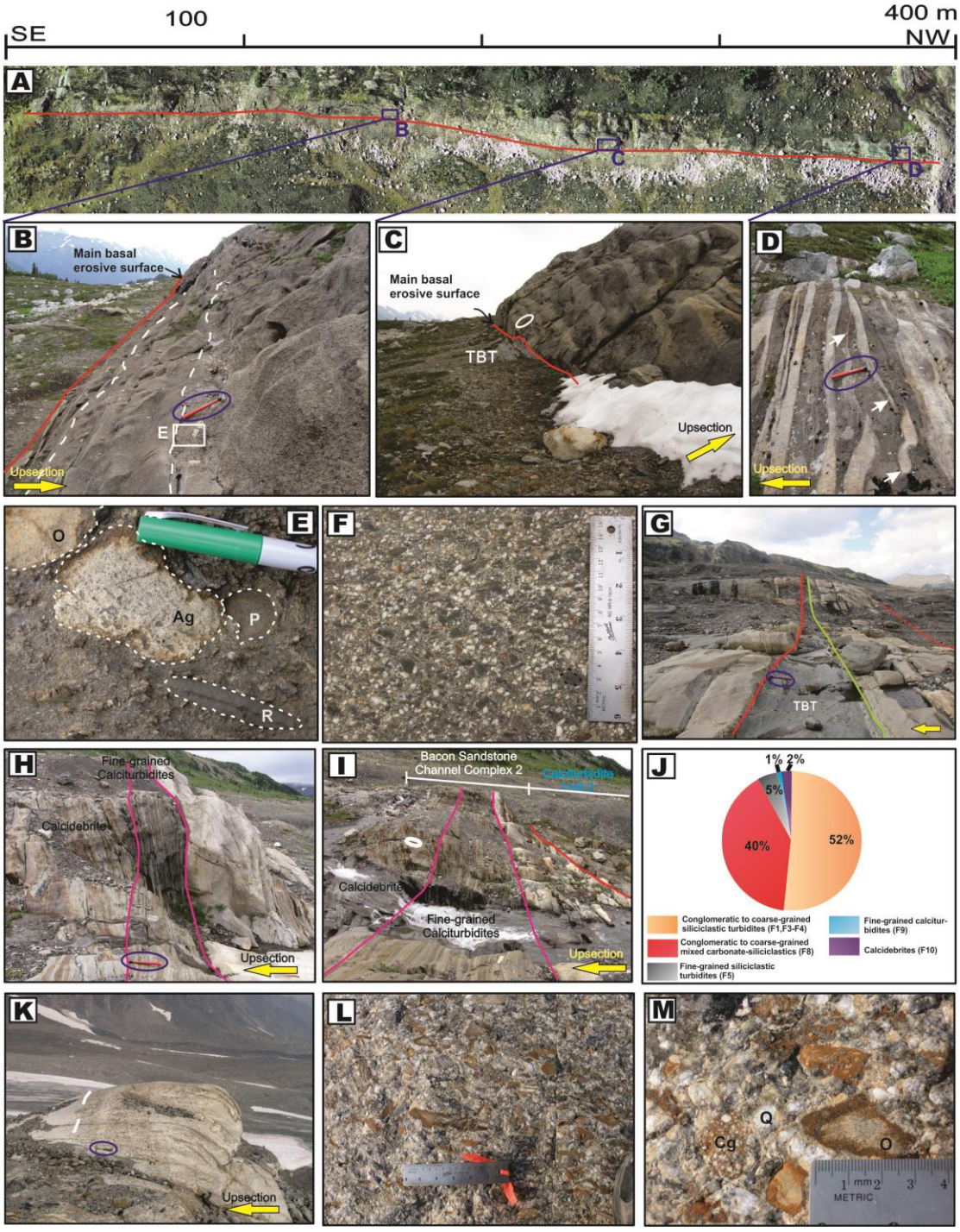

Figure 5.8. Representative photos of the Bacon Sandstone channel complexes. At Castle Creek (A-G) and Mt. Quanstrom (K-M). Channel bases are indicated by red lines. (A-B) At the axis of Bacon Sandstone Channel Complex 1, highly amalgamated coarse-grained beds of F8 with typical brownish weathering-colour, owing to a pervasive ferroan calcite cementation, are common (hammer for scale). Amalgamation surfaces are marked by white dashed lines. (C-D) Laterally away from the axis of the channels,

coarse-grained strata normally exhibit brown and white weathering-coloration strips, denoting well- and poorly-cemented layers respectively (hammer for scale). Thin white arrows in D indicate contacts between variably coloured layers that crosscut true depositional bedding (i.e. pseudo-bedding). (E-F) Close-up photos of F8 with dispersed quartz grains and abundant carbonate clasts (enclosed in white dashed lines) with variable composition, including: aggregate grains (Ag), ooidal limestone (O), peloidal limestone (P), and recrystallized carbonate mudstone (R). Light orange clasts are dolomitized. (G) At the margins of the Bacon Sandstone Channel 1, channels are separated by grey, thin-bedded, fine-grained siliciclastic turbidites or TBT (F5, at center of photo, base of TBT marked by green solid line). (H-I) At the top of Bacon Sandstone Channel Complex 2, scours are filled with fine-grained calciturbidites and calcidebrites (F9 and F10, respectively) are observed. Scour bases are delineated by magenta lines. (J) Percentage of lithofacies in the channel deposits. (K-L) Slope channels equivalent to Bacon Sandstone channel fills at Mt. Quanstrom, which are similar to those at Castle Creek, but are less weathered. Quartz (Q) and carbonate clasts are common to abundant, including some ooidal limestone (O) and calcareous conglomerate (Cg) clasts.

The top of each channel complex is marked by a sharp, generally flat surface overlain by an up to 15 m thick succession of thin-bedded, mudstone-rich siliciclastic turbidites. Locally, however, the surface is incised by a local meter-scale erosional features overlain by an up to 8 m thick, laterally discontinuous unit of interstratified thin-bedded, medium- and fine-grained calciturbidites and fine-grained siliciclastic turbidites (F9 and F5). Observed also are uncommon calcidebrites (F10) with isolated clasts of coarse-grained calcareous sandstone and calcilutites, and deformed, interstratified calciturbidites and siliciclastic turbidites.

At the Mt. Quanstrom study area, only one Bacon Sandstone channel complex is partly exposed (Fig. 5.6). It is up to 27 m thick, and can be followed for about 100 m laterally. Channel fills are lithologically similar to those observed in Castle Creek, consisting mostly of thick beds of pebble- to granule conglomerate with abundant quartz and carbonate clasts (F1 and F8).

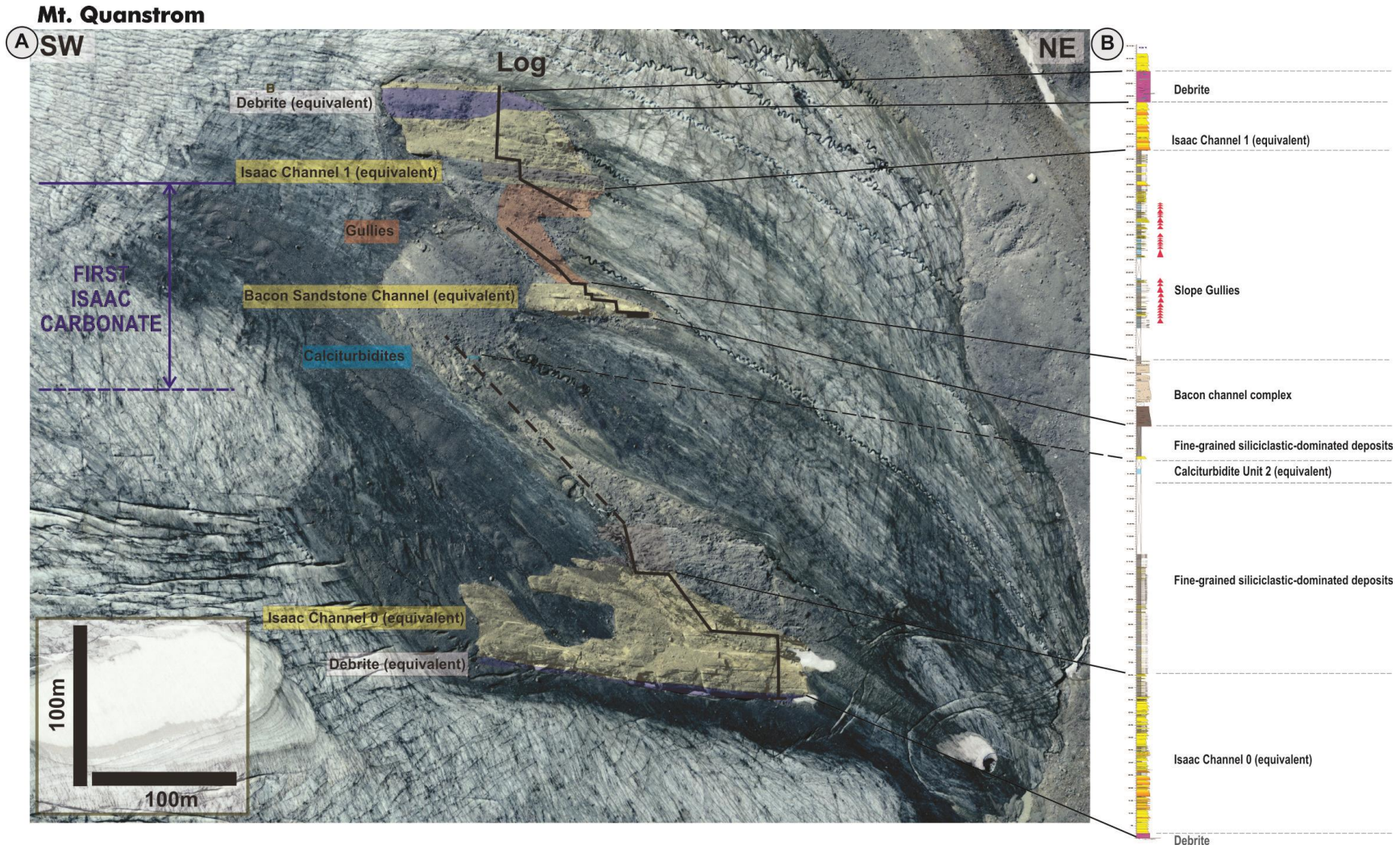

Figure 5.9. Stratal elements and facies of the First Isaac Carbonate (FIC) at Mount Quanstrom area. (A) Airphoto showing distribution and stacking of stratal elements. (B) Stratigraphic log of the FIC, which like at Castle Creek, is sandwiched between siliciclastic-dominated channelized strata (comparable to Isaac Channels 1 and 0).

Furthermore, coarse-grained strata are more commonly intercalated with up to 2 m thick of mudstone units (F5). Based on its stratigraphic position, this channel complex is probably equivalent to Bacon Sandstone channel complex 2 in the Castle Creek study area.

Interpretation

The base of both Bacon Sandstone channel complexes is a composite (i.e. stratigraphic) surface formed collectively of the bases of its component channels (see, for example, Sylvester et al., 2011). Following an episode of bypass, channels were filled in their axial part by high-concentration, mixed- and siliciclastic-rich, sandy and gravelly turbidites (F8 and F1, respectively). Abundant carbonate clasts (see above) and the pervasive (brown coloured) carbonate cement suggest that sediment was being sourced from an active shallow-water carbonate platform.

Over a few 100s of meters laterally these strata thin and become increasingly interstratified with a variety of other lithofacies (e.g. F3, F4, F5, and rarely F9) suggesting deposition from the lower-concentrated part of the flows along the channel margin. Channel fills are then capped by a succession of fine-grained siliciclastic turbidites suggesting temporary deactivation of the transport system. These fine-grained units, however, are generally absent in the axial part of the channel complex where successive channels are amalgamated, but are much better developed, most likely due to preservation, in the channel margin areas (see Fig. 5.6).

In addition to the lateral changes in lithofacies from channel axis to margins, the lateral change in stratal colouration reflects spatial changes in framework-grain

mineralogy. Coarser-grained particles, including many large dolomitized carbonate clasts, preferentially accumulated in the axial parts of the channels. In contrast, finer-grained sediment, in this case dominated by quartz, was selectively fractionated toward the lower energy margins of the flow and hence accumulated along the margins of the channel. This mineral fractionation is interpreted to be principally due to differences in grain size, since effects of differences in grain density were probably negligible.

The well-preserved roundness of many carbonate clasts and extensive carbonate cementation observed in Bacon sandstone strata suggest widespread early submarine cementation (van Der Kooij et al., 2010); but cemented pseudo-beds or bands might have been formed and/or enhanced during later, burial diagenesis (Flugel, 2010).

The small-scale erosional features observed locally at the top of the channel complexes are interpreted to be scours formed by erosive bypass flows. These scours were then filled or draped by fine-grained, carbonate- and siliciclastic-rich turbidites. Localized calcidebrites within the upper scour fills were most likely associated with local instabilities and sediment failures along their margins.

These scour deposits, or where absent, the top of Bacon Sandstone channel complexes 1 and 2, are then overlain by a thick succession of thin-bedded, fine-grained siliciclastic turbidites that were formed by dilute, low-concentration turbidity flows marking the deactivation of the local transport system.

In spite of the absence of skeletal (carbonate) debris in the calcareous strata of the FIC in the (Neoproterozoic) Windermere Supergroup, Bacon sandstone channel

complexes show architectural and sedimentological similarities in terms of channel dimensions and vertical and lateral trends of channel-fill lithofacies (i.e. bed amalgamation and grain size) to other mixed and/or carbonate slope channel complexes described from the ancient (e.g. see extensive review in Payros and Pujalte, 2008) and modern deep-marine sedimentary record (e.g. Mulder et al., 2012a; Mulder et al., 2012b; Jo, 2013; Mulder et al., 2014). For more details and comparison, see section 5.6.3 and Table 5.3.

5.5.2 Levee deposits

Above Bacon Sandstone channel complex 1 is an up to 6 m-thick, laterally-continuous (>1.2 Km) succession of intercalated medium- to thick-bedded, medium- and coarse-grained calcareous sandstone (F2) and thin-bedded, fine-grained siliciclastic-rich sandstone turbidites of F5 (representing <1% of the FIC; Figs. 5.3 and 5.10). F2 sandstones are structureless, planar-laminated, or significantly, consist of multiple-set ripple cross-lamination. In addition, coarser, thicker F2 beds fine and thin and change into F5 strata over less than a few hundreds of meters laterally (Fig. 5.10).

Interpretation

The laterally-continuous intercalated medium- and coarse-grained calcareous sandstones and fine-grained siliciclastic-rich sandstone turbidites that crop out above Bacon Sandstone channel complex 1 are interpreted to be the levee of an unexposed slope channel.

Table 5.3. General overview and comparison of channel and leveed channel complexes reported in ancient and modern carbonate and mixed slope systems

Case study area and Age	Slope system and Tectonic Setting	Dimensions and Geometry	Description		Long-term evolution	References
			Facies	Other features		
Great Bahamas Bank (toe of the slope). Modern.	Pure carbonate environment in a sub-tropical, low-latitude setting. Intraplatform basins (Graben-and-horst paleotopography formed in rift basin during the Cretaceous-Early Jurassic.).	*Channel Complex*: 6 m deep and up to 2-km wide (Mulder et al., 2014). *Channel system*: Up to 30 m-thick and 2 km-wide (Jo, 2013). *Levees:* Up to 20 m thick, and up to 2-4-km-wide, bird-wing, wedged- or mustache-shaped, asymmetrical topographic structures.	*Channel complex:* filled with four sedimentary units dominated by high-amplitude discontinuous chaotic facies (interpreted as mass-transport deposits), high-amplitude continuous planar reflections (interpreted as coarse-grained turbidites), low-amplitude discontinuous sub-horizontal reflections (interpreted as medium- to finer-grained turbidites), and sediment waves (interpreted as antidunes) consisting mainly of moderately bioturbated, foraminiferal wackestone and mudstone. The topmost filling is entirely composed of hemipelagic oozes. *Levees:* Variable-amplitude, continuous reflectors, interpreted as layered fine-grained turbidites with local sandy deposits. At the top of the levees, rough undulating structures interpreted as sediment waves.	-	Tectonic influenced. Progradation.	Mulder et al. (2012a); Jo (2013); Mulder et al. (2014)
Azagador Member, SW flank of Vera basin and E of Sorba basin, Almería, southern Spain. Miocene (Upper Tortonian).	Mixed system (including redeposited temperate carbonates). Narrow platform. Foreland basin	*Channel:* Up to 20 m thick, and tens to hundreds of meters wide. *Levees:* Tens of meters wide.	*Channels:* Thick-bedded, amalgamated, lensoidal, coarse-grained calciturbidites (calcarenites and up to pebble-sized calcirudites) and mixed, bioclastic (mostly coralline algae, bivalves and bryozoans). Mixed facies with variable (up to 20%) siliciclastic content. Local lateral accretion features. Cut-and-fill structures. Fining-upward packages. Lateral grain-size change from pebble to sand. *Levees:* Amalgamated, thin-bedded, laterally persistent, coarse-grained calciturbidites (calcirudites and calcarenites), alternating with fine- to medium-grained sandstone. Overall fining- and thinning-upward stacking pattern. Beds can be traced laterally into channel deposits.	-	Tectonic influenced.	Braga et al. (2001)
Porto Torres sub-basin, Sardinia, Italy. Miocene (Burdigalian–Serravallian).	Mixed slope system. Rift basin	*Sassari Channel*: up to 4 km and 300 m thick, composed of up to 6 partly nested, vertically-stacked channel units. *Levees:* 50 m thick and 500 m wide; *inner levee* 100–150 m wide with strata sloping 35° towards the channel axis and *back-levee* 350–400 m wide with strata dipping 8–12° outwards. Asymmetrical channel and levee geometry.	*Channel-axis deposits*: Thick-bedded structureless and cross-stratified, up to boulder- to coarse-grained sandstone calciturbidites (bioclastic rudstone and floatstone with subordinate grainstone/packstone containing abundant red algae both as branching forms and rhodoliths, bivalves (pectinids and ostreids), echinoids, benthic and planktonic foraminifers), and mixed sandstone and silty sandstone. Local megabreccia beds. *Channel-margin deposits:* Lateral bars as sigmoidal clinostratified units (Up to 20 m high with 30° steep foresets) of coarse-grained mixed sandstone and pebbly sandstone, that drape/onlap the channel margin. Local up to cobble-sized conglomerate, fine rhodalgal rudstone/floatstone and coarse grainstone. Multiple Erosive surfaces. Common lensing and wedging stratal geometries. Upward mixed sandstone rapidly pass to quartz rich, poorly-	Early widespread cementation. Mixed sandstone normally exhibits buff poorly-cemented (quartz rich), and patchy to continuously well-cemented strata. Reddish/brownish crusts of intense and extensive bioturbation commonly occur	General shallowing-upward sequence.	Vigorito et al. (2006)

			cemented sandstone, that in turn become more siliciclastic into quartz-feldspathic sandstone. Laterally from channel axis to margin, fining and thinning lateral trend, and more alternation of carbonate and siliciclastic silty/sandy deposits. *Inner levee deposits*: mainly of fine- to pebbly, rhodolith-rich rudstone and floatstone and rare grainstone/packstone. *Outer back-levee deposits*: mainly of fine rhodalgal rudstone/floatstone and/or coarse grainstone and subordinate silty packstone. Local intraclasts-rich layers. These back levee rapidly pinches out into marly deposits.	in the well-cemented intervals (locally forming hardgrounds).		
Isili Basin, Sardinia, Italy. Oligo-Miocene (Aquitanian-Burdigalian).	Mixed slope system. Rift basin	*Isili Channel*: Two channel levee complexes (60-100 m thick and up to 1 km wide), consisting of up to 9 nested, erosive-based, channel units (individually, up to 10 m thick, and up to several tens of meters wide). *Levees:* Mound-shaped units, up to 10 m thick and 40–80 m wide, commonly developed on the (preferentially, right-hand) edges of individual channel units. Asymmetrical channel geometry.	*Channel axis deposits*: Structureless and cross- or parallel-stratified, very coarse-grained high-density calciturbidites (bioclastic rudstone, fine floastone, and coarse-grainstone/packstone rich in rhodoliths, bivalves, branching red algae fragments and serpulids, and minor bryozoans, echinoids). Channels are capped by thin-bedded, locally parallel- to ripple cross-laminated sandy/silty turbidites, followed by hemipelagic marls, which intercalated locally with sandy turbidite layers. Local mixed pebbly breccias (calcidebrites). *Channel-margin (right-hand) deposits*: Steeply-inclined, sigmoidal clinoforms of very coarse-grained calciturbidites (including rhodolith-, serpulid- and branching red algae-rich floatstones/rudstones and grainstones), interpreted as lateral-accretion bars. Local collapse megabreccias. Multiple erosion surfaces. Individual channels show crude fining- and thinning-upward. From channel axis to margin, strata show distinct wedging geometry, and lateral fining trend. *Levee:* Coarse-grained calciturbidites (not explicitly described). Laterally, some of the beds extend continuously into the adjacent channel margins for several tens to hundreds of meters and are correlatable with the upper portion of the channel-axis units.	Multiple patchy to continuous reddish early hardgrounds, and local intense bioturbation.	Progradation.	Vigorito et al. (2005)
Base-of-slope deposits of Anotz Formation, Navarre, W Pyrenees, Spain. Lower-Middle Eocene.	Mixed slope system. Foreland basin	*Channel complex*: up to 100 m thick, 500 m wide (up to 1 km), consisting of nested erosive-based units (individually 10 m thick and >50 m wide). *Levees:* 100 m thick, and ~1 km wide.	*Channel deposits*: Thick-bedded, amalgamated clast-supported debrites, and conglomeratic-, stratified and graded calciturbidites, that are capped by alternations of thin-bedded calciturbidites and hemipelagic marls. Total calciclastic content: 90%. Local bed onlap the channel base. Crude thinning- and fining-upward sequences. *Levees*: Hemipelagic muddy limestone with intercalations of thin-bedded calciturbidites, commonly slumped. Total calciclastic content: 25%.	-	Progradation with lateral shift along depositional strike due to tectonic influence.	Payros et al. (2007)
Napier Formation, Canning Basin, Western Australia. Upper Devonian.	Mixed fore-reef slope. Intracratonic basin	Channel fills: up to 6 m thick and 100 m wide, typically <30-50 m wide.	*Channel fills*: Thick-bedded, coarse-grained breccias and quartzo-feldspathic sandstone alternating with intervals of thinly-bedded limestone (packstone, grainstone and rudstone of notably brachiopods, crinoids, gastropods, nautiloids and ammonoids).	Brecciation, calcite veining and pervasive cementation and dolomitization.	Progradation?	George et al. (1997)

Base-of-slope deposits of the Monte Corvo and Fonte-Gelata and Venacquaro formations, Gran Sasso d'Italia, central Italy. Late Cretaceous to Eocene.	Carbonate slope. Foredeep basin	*Channel complex*: up to 220 m thick, and total width: up to 6 km. *Calciturbidite-filled channels*: tens to >100 m wide, *calcidebrite-filled channels*: 100-200 m wide. *Left-hand levee:* few meters thick; *Right- hand levee:* 70 m thick and more than 2 km wide. *Whole system*: ~20 km long.	*Channel fills*: Thick-bedded, amalgamated, fine- to medium-grained calciturbidites (packstone and grainstone with mainly skeletal fragments and minor lithoclasts), intercalated with thin (up to 5 cm-thick) mudstone layers. At the upper part, channel filled with up to 15 m-thick, clast-supported intraclastic breccia and megabreccia (calcidebrites) containing a large variety of platform- and slope-derived lithoclasts and minor skeletal fragments. Laterally, beds become thinner *Levees:* Mostly pelagic limestone, with minor amounts of calciturbidites (more abundant in the right-hand levee).	-	Progradation.	van Konijnenburg (1999); Payros and Pujalte (2008)
Fans of the C Member of Macqam Fm., Sumeini Group, Oman. Early to Middle Triassic.	Distally steepened carbonate slope. Passive-margin basin	*Channel complexes:* around 25 m thick, and <1 km wide. *Levees:* Not exposed (inferred by the author).	*Channel fills:* Thick-bedded, lenticular, calcirudites (interpreted here as calcidebrites) with tabular clasts of limestone and oolitic calciturbidites, and thinner beds of oolitic calcarenites that also contain bivalves, peloids, gastropods, ostracods and brachiopods. Cut-and-fill. Fining- and thinning-up sequences. Lateral facies change from calcirudites to calcarenites.	Localized dolomitization layers or bands.	Southern fans: aggradation. Northern fans: retrogradation.	Watts (1988)
Bacon Sandstone Channels, FIC, Windermere Supergroup. Neoproterozoic.	Mixed slope system. Passive-margin basin	*Channel complexes*: up to 20 m thick and >1.5 m wide. Individual channels: up to 5 m deep and are at least 400 m wide. *Levees:* Up to 6 m thick, and >300 m wide.	*Channel-axis deposits* are thick-bedded quartz- and mixed-rich coarse-grained sandstone and conglomerate with non-skeletal carbonate clasts. Mudstone-clast breccias are locally observed at the channel bases. *Channel-margin deposits*: Thick- to thin-bedded, granule conglomerate and coarse- to medium-grained quartz-rich sandstone, cross-stratified sandstone, and (siliciclastic) mudstone or sandstone-mudstone. Fine-grained calcarenite or calcilutites are minor. Channels are capped by thin-bedded, fine-grained sandstone-mudstone. Rarely, channels are filled with thin-bedded, finer-grained calciturbidites. Calcidebrites locally occur at the top of the channel complexes. *Levees 1 (uppermost Bacon channel 1):* Thin-bedded fine-grained sandstone and mudstone. *Levees 2 (slightly above Bacon channel 1):* Unexposed related channel. Intercalation of medium- to thick-bedded, structureless, planar and (multiple sets) ripple cross-laminated, calcareous medium- and coarse-grained sandstone and mudstone and thin-bedded fine-grained turbidites. Lateral fining and thinning trends over less than a hundred of meters.	Widespread carbonate cementation. Common brown, well- and white-poorly-cemented layers	Progradation.	This study

The lateral fining and thinning of strata over distances of a few 100s of meters is consistent with interpreted levee deposits in other parts of the Castle Creek study area (Navarro, 2006; Schwarz and Arnott, 2007; Mussa-Caleca, 2008; Davis, 2011; Khan and Arnott, 2011; Khan, 2012). Moreover, the occurrence of multiple-set ripple cross-stratified sandstones is suggestive of sustained steady flow, which also is consistent with flow and depositional conditions on channel-bounding levees (e.g. Khan and Arnott, 2011).

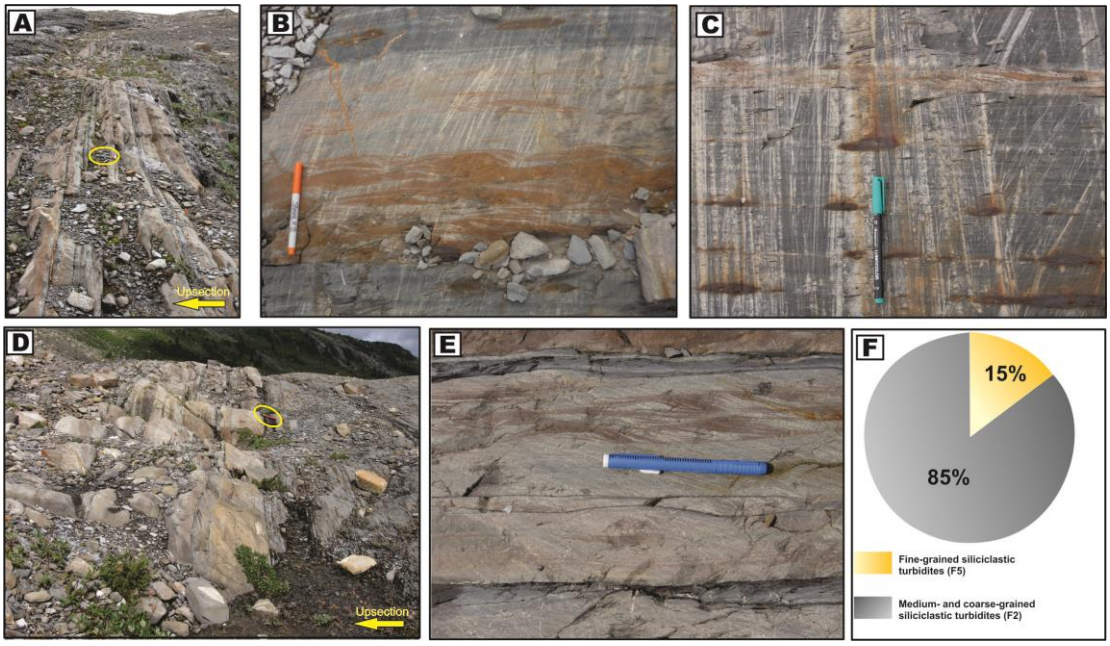

Figure 5.10. Representative photos of levee deposits at Castle Creek. (A) In the Castle Creek south study area (SE side of the glacier), levee strata exposed in the Castle Creek South consist of laterally-continuous, interstratified, thin-to medium-bedded sandstone and mudstone. Hammer for scale. (B) Common thick-bedded, cross-laminated, medium-grained calcareous sandstone consisting of multiple set, non-climbing ripples (T_c). Beds fine vertically from medium- to fine-grained sandstone. (C) A few tens of meters from (B), T_c beds fine and thin laterally. (D) Levee strata exposed in the Castle Creek north study area (NW side of the glacier). Hammer as scale. (E) Medium-bedded, medium grained sandstone T_{bc} with minor vertical fining. (F) Percentage of lithofacies in the levee deposits.

5.5.3 Slope gully-like features

In contrast to channel and levee deposits (previous sections 5.5.1 and 5.5.2), gully-like features or simply gullies are isolated, shallow (<1.5 m deep), narrow (100-300 m wide) features with low sand content (commonly <10-20%; see Figs. 5.9 and 5.10). They represent about 25% of the FIC. Due to the narrowness of the outcrop compared to the width and spacing of the gullies it is difficult to unequivocally determine if multiple gullies form along discrete stratigraphic horizons, or if they are irregularly distributed through the section. Notwithstanding, at both Castle Creek and Mt. Quanstrom individual gully fills and associated deposits stack upward (at least 6-7) to form 10-40 m thick complexes (Fig. 5.9). At the small (meter)-scale, three consistently stacked stratal units, here termed units 1, 2 and 3, are typically observed, although in some places unit 1 is absent (Fig. 5.10). Each is described next.

Typically, gullies have a low-relief basal scour that can be traced for up to 300 m laterally and filled with strata of unit 1. Unit 1 ranges up to 1.5 m thick but typically is several cm to a few dm thick, and consists of isolated lenses of reddish to orange, coarse- and medium-grained sandstone or granule conglomerate. These strata occur as laterally-discontinuous single dune cross-stratified formsets, or more commonly laterally-continuous planar-stratified sandstone (F4, Fig. 5.12c), occasionally with carbonaceous-rich laminae (F6, Fig. 5.2e). Dune cross- or parallel-stratified beds are then normally capped by a veneer of ripple cross-laminated, fine-grained sandstone and mudstone (F5, Fig. 5.12c). Beds are thicker and slightly coarser in the deepest part of the scour and then truncate laterally against its margins (Fig. 5.9).

Erosionally-based gullies are then sharply and conformably overlain by an up to 0.8 m thick sheet-like succession consisting of light yellow or beige to grey, thinly-bedded, upper-division (mostly Tcde, Tde) fine-grained siliciclastic sandstone turbidites (F5). These strata make up unit 2 and extend for hundreds of meters laterally except where truncated by scours filled with coarser-grained strata of an overlying unit 1.

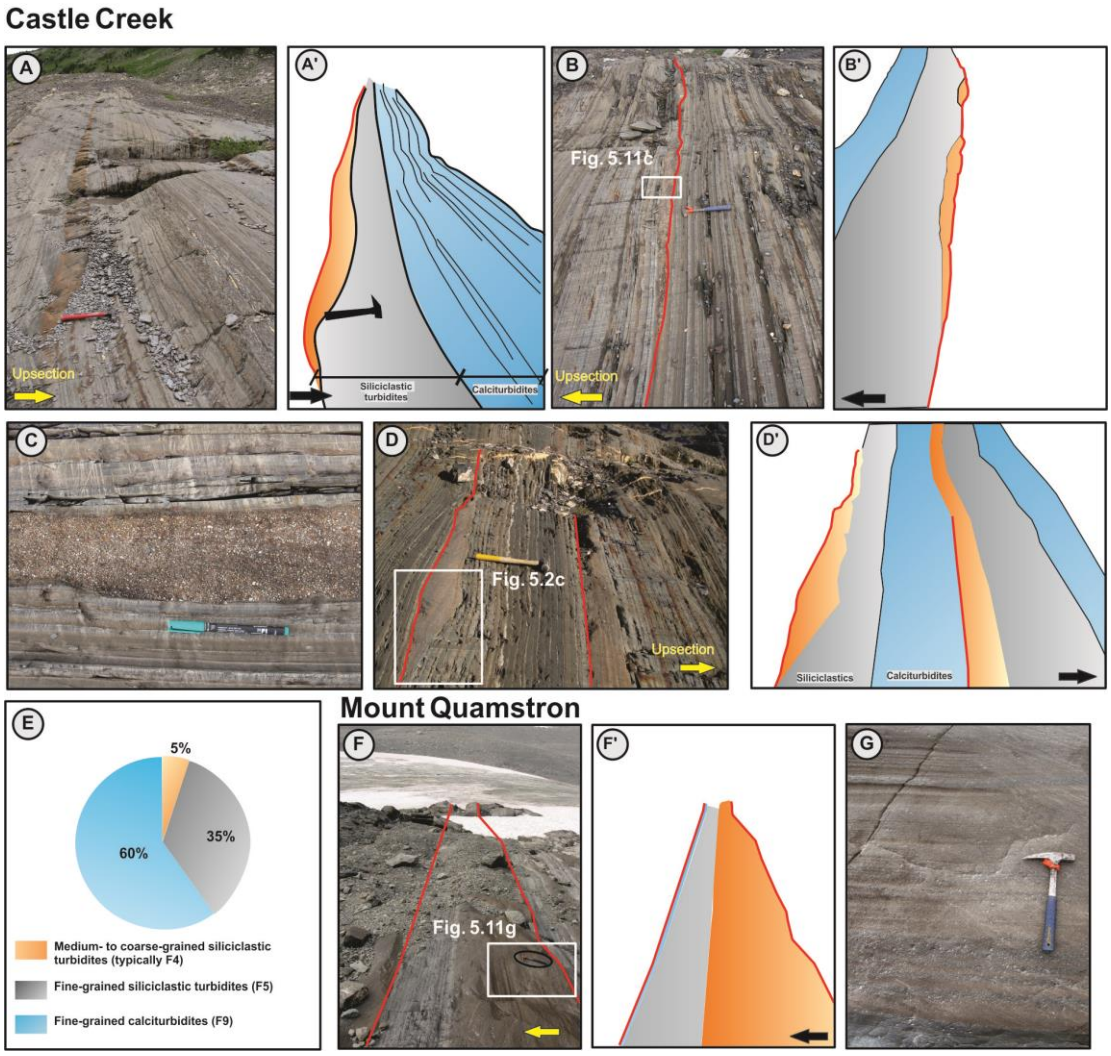

Figure 5.11. Representative facies of gullies. Photos (A-C,E-F), and corresponding line drawings (A'-C',E'-F'). The base of individual gullies is indicated by red lines. At Castle Creek, gullies are characteristically filled with isolated beds of coarse-grained

siliciclastic facies of F4 (orange), overlain sharply by laterally-continuous fine-grained siliciclastic turbidites of F5 (grey), and then draped by laterally-extensive fine-grained calciturbidites of F9 (blue). Coarse-grained beds at the base of gullies are commonly of dm-thick, planar-stratified calcareous sandstone (A), dune cross-stratified sandstone and conglomerate (B-D), or rarely, carbonaceous sandstone (see also Fig. 5.2e). (E) Percentage distribution of lithofacies in gully deposits. (F-G) At Mt. Quanstrom study, gullies are generally filled with m-thick beds of basal planar-parallel sandstone, which then are similarly overlain by fine-grained siliciclastics, capped by fine-grained calciturbidites or interbedded calci- and siliciclastic turbidites.

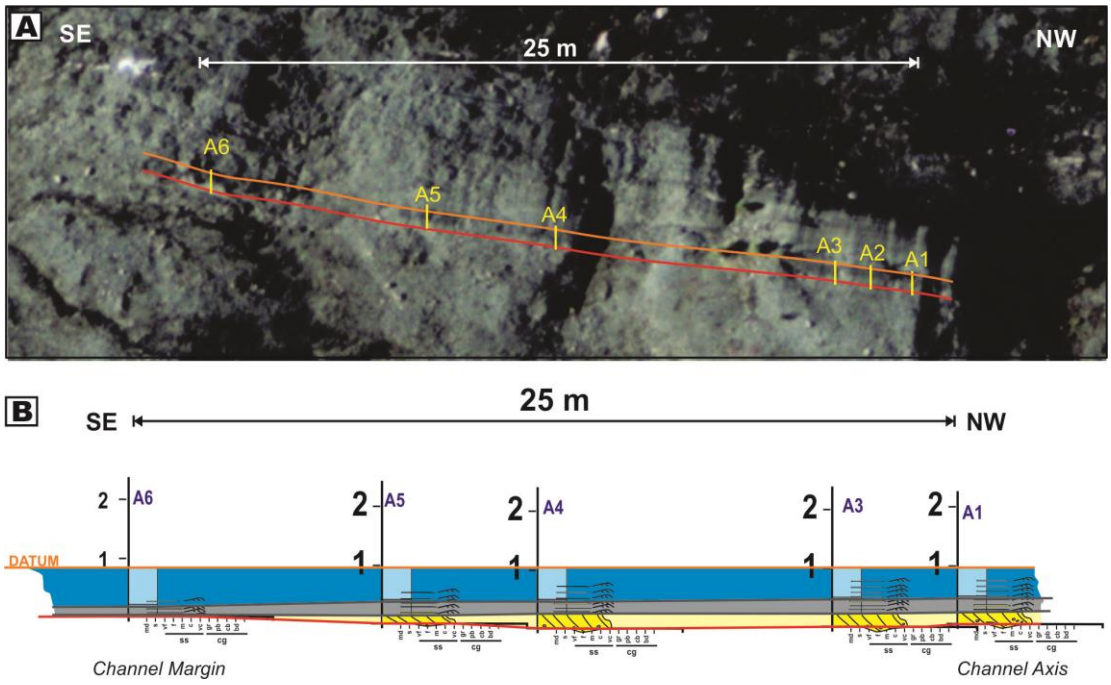

Figure 5.12. Stratigraphic correlation of a gully in the upper part of the FIC. (A) Airphoto the basal surface (red line) and (B) corresponding measured logs. A single-set dune dune cross-stratified, coarse-grained sandstone is observed. This is then overlain by a succession of thin-bedded, fine-grained, siliciclastic turbidites capped by fine-grained calciturbidites.

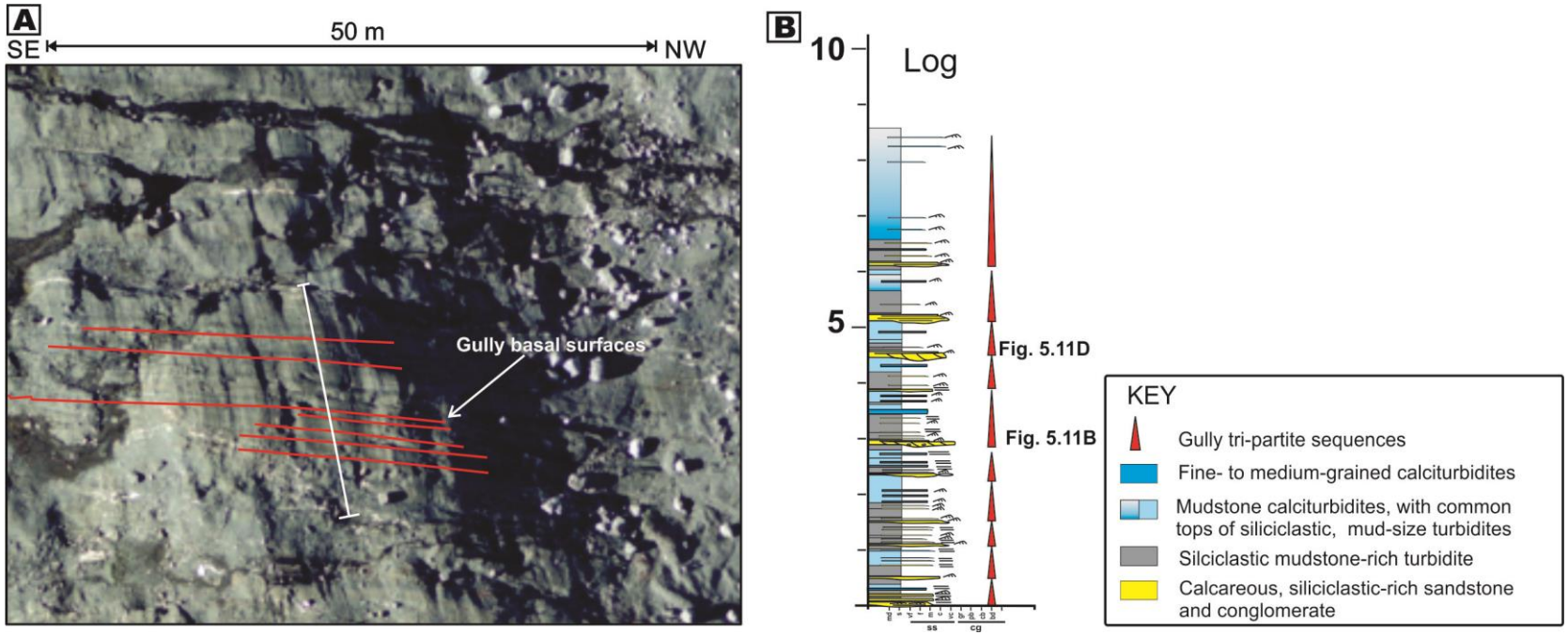

Figure 5.13. Aerial photo of a succession of stacked gully fills (A) corresponding measured stratigraphic log (B). The erosional base of each gully is indicated by red line, which then is overlain by a succession that changes upward from siliciclastic to carbonate strata.

Table 5.4. General overview and comparison of gullies reported in ancient and modern carbonate and mixed slope systems

Case study area and Age	Slope system, Tectonic Setting	Dimensions and Geometry	Facies Description	Long-term evolution	References
Western Great Bahamas Bank (middle to upper slope). Modern.	Carbonate system Intraplatform basins.	*Gullies*: small, straight, V-shaped, shallow channels, that are 0.5-2 m (up to ~10–20 m) deep and are ~200-400 m (up to 700 m) wide. They tend to be asymmetrical, form on relatively steep slopes (1.3-3º), and incised into a smooth area interpreted as mud-dominated zone (typical facies of the upper and middle slope). Some gullies are regularly spaced, generally linear and sub-parallel, and others are irregularly-shaped. Locally, series of gullies convey and terminate into a channel-levee system at the base of slope.	Gully floors are commonly covered with strings of coarse-grained sediments. High-resolution seismic profiles shows that some gullies are recently draped by continuous layers of transparent, low-amplitude reflectors (fine-grained facies?) preserving the gully morphology, whereas dissymmetric gullies are filled with relatively-high amplitude reflectors (coarse-grained facies?) overlaid by a low-amplitude transparent drape (fine-grained facies?). Additionally, cores from others gullies exhibit that they consist of carbonate foraminifer oozes (mudstone to wackestone) interbedded with thick beds of partially lithified carbonate sand (wackestone) consisting of foraminifera with a reduced carbonate mud fraction and agglomerate particles. More regular gullies show permanent aggradation due to the staking of regular sediment drape.	Tectonic influenced. Progradation.	Mulder et al. (2012a); Jo (2013); Principaud et al. (2013); Ducassou et al. (2014); Jo et al. (2014); Mulder et al. (2014)
Little Bahamas Bank, Tongue of the Ocean and Exuma Sound, Eastern Great Bahamas Bank (upper to lower slope) Modern.	Carbonate system Intraplatform basins.	*Gullies*: Up to 5 m deep and up to 35 to 100 m wide. They are well-defined, regularly-spaced, V- or U-shaped morphological features. Some large gullies/canyons are up to 50-150 m. Gullies feed into grainstone-dominated aprons at lower slope/ toe of slope.	Sand- and gravel-sized grain-dominated gullies fills (grainstone and rudstone). Some gullies are filled with elongate patches of symmetrically rippled sands. Gullies are encased within periplatform ooze.	Tectonic influenced. Progradation.	Schlager and Chermak (1979); (Mullins et al., 1984); Harwood and Towers (1988); Rankey and Doolittle (2012); Chabaud et al. (2014)
Great Barrier reef margins (upper to lower slope) Late Pleistocene to late Holocene	Mixed slope system. Passive-margin basin.	*Gullies:* Up to 60 to 300 m deep and up to 2 km wide. They include larger, straight to sinuous channels, which are morphologically similar to slope-confined submarine canyons with rectilinear pathways. Some tributary of gullies merge in the lower canyon	Core from gullies/canyons record a shift from siliciclastic- or mixed-dominated turbidites as sandy coarse-grained deposits from very fine- to medium-grained sands and local gravels, to mud-dominated calciturbidites or calcidebrites toward the top.	Progradation/ Aggradation.	Feary et al. (1993); Puga-Bernabéu et al. (2011); Webster et al. (2012); Puga-Bernabéu et al. (2013)
Clinothems on the Northwest Shelf of Australia	Mixed slope system. Foreland basin.	*Gullies:* Straight, U-shaped and evenly-spaced, that are in average, 25-110 m deep, and 150-400 m wide. Where the gradient is 3-5º, they are 100-300 m wide, and where the gradient exceeds 8º, 300-800 m wide.	They are recognized by basal erosional surface and facies heterogeneities (not described by author)	Progradation.	Fubara (2014)

Miocene		Aggrading gully systems with few asymmetrical forms. Lateral variability in geometry and stacking patterns of the gullies correlate with along-strike variations in clinoform dip. The clinoforms are relatively steep and locally associated with concave upwards updip slope failures.			
Base-of-slope deposits of Anotz Formation, Navarre, W Pyrenees, Spain. Lower-Middle Eocene.	Mixed slope system. Foreland basin.	*Gullies:* tens to hundreds of metres wide, and 10-20 m thick. In average, 300 m wide and 15 m thick. Gullied succession can be up to 100 m thick. Gullies are straight linear features. Tributary network of small gullies tend to merge downslope.	Gullies are erosive-based. Gully with multi-episodic fills: Internally-bedded, large calcarenitic bodies, composed of cross-stratified and graded calciturbidites (coarse-grained calcarenites and calcirudites), and debrites. Irregularly amalgamated and with no preferred vertical arrangement of facies. Gully with single scour-and-fill: massive calcarenitic bodies. Gullies are incised into hemipelagic marl deposits (commonly slumped), with occasional thin-bedded calciturbidites.	Progradation with lateral shift along depositional strike due to tectonic influence.	Payros et al. (2007)
Gargano Peninsula, in southern Italy Cretaceous.	Carbonate system Foreland basin.	*Gullies*: Hundreds of meters wide and up to 30 m deep. U-shaped gullies with irregular surface.	Gullies are filled with thin- to thick-bedded, massive and normally-graded bioclastic grainstone beds, that are clustered in lenticular bodies with highly biconvex in the basal part of the gullies and more tabular in the upper part.	Tectonic influence as margin retreat induced by faulting, followed by progradation of the platform	Hairabian et al. (2014)
Borne Fm., Margins of the Vercors platform, France Cretaceous (Lower Barremian)	Carbonate system Foreland basin.	*Gullies*: several hectometres wide, incised into the underlying shale-dominated deposits. Gullies are interpreted to amalgamate downslope.	Gullies are filled with few discontinuous massive debrites and tabular bioclastic calciturbidites (packstone-grainstone with bryozoans and sponge spicules) interbedded with shale.	Progradation.	(Jacquin et al., 1991)
Canning basin, Western Australia Upper Devonian (Famennian)	Carbonate system Intracratonic basin	Gullies: < 2-3 m deep, and decameters wide. They are closely-spaced.	Gullies are filled with allodapic grainstone/ rudstone. Gullies are encased in silty skeletal wackestone	Progradation.	Playton et al. (2011)
Bacon Sandstone Channels, FIC, Windermere Supergroup. Neoproterozoic	Mixed slope system. Passive-margin basin.	Gullies: up to 2 m deep and 100-300 wide Stacked nested gullies form up to Dm-thick units.	Gullies are typically erosive-based, and filled consistently with wedged shaped, coarse-grained siliciclastics, including planar stratified or single set dune cross-stratified, coarse-grained sandstone or granule conglomerate, and carbonaceous sandstone. They are overlain by fine-grained siliciclastic beds, and are then capped by fine-grained calciturbidites with occasional siliciclastic mudstone tops.	Progradation.	This study

In most places these fine-grained siliciclastic strata are overlain sharply and conformably by an up to 1 m thick sheet-like unit (Unit 3) consisting mostly of olive to greenish black calcilutite (F9) with minor fine-grained calcarenite interbeds. It is important to note that at the same stratigraphic horizon at Mt. Quanstrom strata exhibit a similar tripartite assemblage made up of units 1, 2 and 3, and then stacked to form an interval of up to 50 m thick (Figs. 5.5, and 5.12).

Interpretation

Low-relief scoured features in the FIC, here termed gullies, were previously interpreted by Gammon and Arnott (2007) to be shallow, broad channels associated with overbank-splay deposition. However, the occurrence of multiple small-scale features with a consistent vertical and lateral stratal distribution of facies, and the absence of equivalent large-scale channel systems in the study area or other localities (e.g. at Mt. Quanstrom) suggest an alternative explanation. The incision and infill of gullies is interpreted here to be the consequence of the episodic passage of relatively small volume, and hence areally restricted, siliciclastic-rich turbidity currents. In these flows coarse-grained sediment was confined to the high-energy axial part of the current. In addition, it is this part of the current that during the passage of the head and some or much of the body formed the shallow, broad basal scour. Importantly, if these scours are indeed randomly distributed and not formed along discrete stratigraphic horizons, it would suggest irregularly spaced areas of slope instability and related turbidity current activity along a laterally extensive slope – specifically a line source of sediment, which contrasts with the point source suggested for slope

channels (see above). Following the early erosive episode, the later passage of the rest of the body and/or tail of the current reworked a stranded residuum of coarse-grained sediment that had just previously accumulated on the erosion surface into planar-laminated or dune cross-stratified sandstone capped by a thin veneer of (low energy) ripple cross-stratified sandstone. These strata, and those into which the basal scour was eroded, were then draped by a several dm-thick succession of thin-bedded, fine-grained siliciclastic turbidites (Unit 2). These strata were deposited by low-concentration, low-energy, fine-grained siliciclastic-rich turbidity currents and represent the ambient transport and depositional conditions in this area of the basin. An alternative explanation for units 1 and 2 is predicated on the occurrence of multiple unit 1 scours and their fills along discrete stratigraphic horizons, which then were draped by finer-grained strata of unit 2. In this scenario, multiple laterally-adjacent gullies were formed on the sea bed by numerous erosional flows that were preferentially routed through the scours and deposited only a thin residue of coarse-grained siliciclastic sand along the evolving scour surface. This coarse-grained sediment was eventually reworked into planar- or dune cross-stratified sandstone capped by ripples, presumably by the last high-energy flow to have transited the area. This episode was then abruptly succeeded by an extended period characterized by much finer-grained, lower energy flows that deposited unit 2.

Seismic observations from modern carbonate systems, like the Great Bahamas Bank, show multiple seafloor erosional features, termed gullies, which are 400-700 m wide, 10-20 m deep and have a 400 to 1200 m lateral spacing (Mulder et al., 2012a; Mulder et al., 2012b). More recent high resolution seismic indicates that some gullies

are filled with a relatively high amplitude (possibly sandy) basal part overlain by a low-amplitude transparent (probably fine grained) drape (Principaud et al., 2013). Although seemingly similar to the erosionally-based gullies (unit 1) overlain by a drape of unit 2 and 3, it is important to note that modern gullies are 1-2 orders of magnitude deeper (for more details and comparison, see section 5.7.2 and Table 5.4). In addition, some are bordered by well-developed depositional levees (Mulder et al., 2012b), but these features are absent at Castle Creek.

Nevertheless, irrespective of the interpretation of units 1 and 2, these siliciclastic units are then overlain abruptly by a laterally-continuous unit of calcilutite-rich strata, indicating not only a decrease in energy but more profoundly a major change in sediment composition. Moreover, it indicates the cessation of siliciclastic sedimentation and the rejuvenation of an active shallow-water carbonate factory with a significant fine-grained carbonate efflux. Downslope transport of fine-grained carbonate sediment has been observed in modern carbonate environments, like the modern Bahama Banks, and termed density cascading (Wilson and Roberts, 1995). In this process density currents (i.e. hyperpycnal flows) are formed of platform-top waters made more dense by some combination of thermal, salinity and/or suspended sediment effects (Wilson and Roberts, 1992, 1995). These currents eventually penetrate downward along the slope, carrying their load of dispersed fine-grained sediment plus any sediment eroded from the seafloor, to their compensation depth, whereafter they become separated from the seafloor and deposit an extensive nepheloid drape of carbonate fine-grained sediment (Wilson and Roberts, 1995). If, however, a sufficient volume of seafloor sediment has been incorporated into the flow

the current may self-ignite, thereby enabling it to continue downslope and beyond the compensation depth.

5.5.4 Fine-grained deposits

Sheet-like, fine-grained deposits are widespread, especially in the upper part of the FIC, and volumetrically represent about 56% of this stratigraphic marker. Based on the principal mineralogy, they are classified as siliciclastic and calcareous turbidites.

5.5.4.1 Fine-grained siliciclastic turbidites

Fine-grained siliciclastic turbidites make up about 36% of the FIC (Fig. 5.14). Typically they overlie slope channels, levee deposits, slope gullies, and calciturbidite units. Units range from 3 to 25 m thick (average 11 m) and can be traced laterally over several hundreds to thousands of meters. Strata are mud-dominated, consisting mostly of thin-bedded, upper-division, red to yellow fine-grained sandstone and grey mudstone turbidites (F5, Fig. 12d), although uncommon thin, fine-grained calcarenite and calcilutite (F9) interbeds are observed locally (Fig. 5.12a-b). In some places, fine-grained siliciclastic successions fine and thin upward.

5.5.4.2 Fine-grained calcareous turbidites

Three major laterally-continuous (>1200m) successions of fine-grained calcareous turbidites, or simply calciturbidites, are identified in the FIC, representing approximately 20% of the section. These are informally named calciturbidite units 1 to 3, which are up to 8.5, 20, and 17 m thick, respectively (Figs. 5.3, 5.4, 5.14).

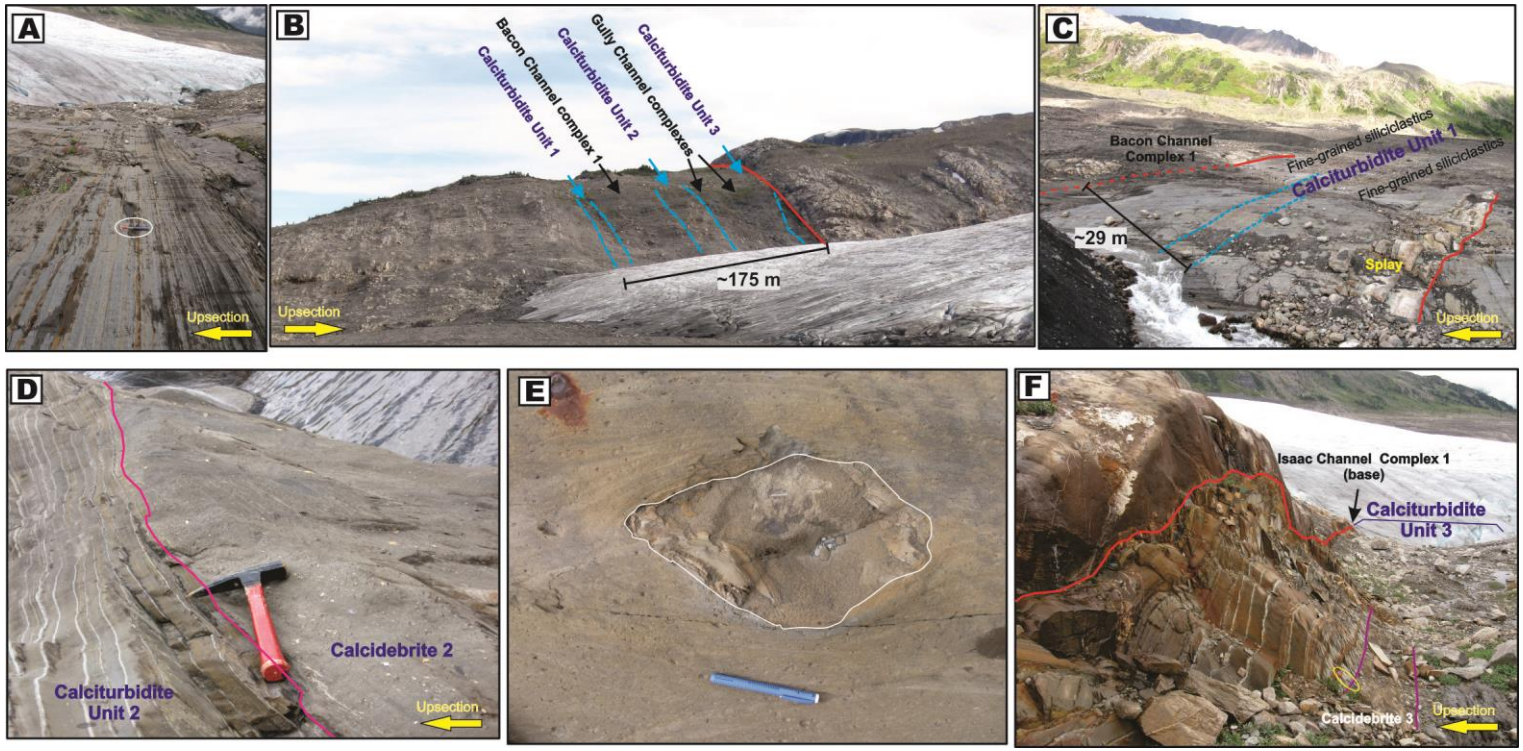

Figure 5.14. Fine-grained siliciclastic and calcareous strata and calcidebrites in the FIC. (A) Fine-grained siliciclastic-dominated deposits are composed of laterally continuous, orange and yellow, thinly-bedded, ripple cross-stratified fine-grained calcareous sandstone and grey mudstone with uncommon medium-grained sandstone are locally intercalated. (B) Photo showing the bounding surfaces that separate the three main calciturbidites units comprising the FIC in the Castle Creek south study area – see text for detailed description of each unit. (C) Basal part of the FIC at Castle Creek north, above siliciclastic strata of Isaac channel 0. (D) Irregular contact between calciturbidite unit 2 and calcidebrite 2. (E) Calcidebrite 2 consists of a matrix-rich carbonate breccia with up to boulder-sized carbonate lithoclasts (enclosed by white line). (F) Calcidebrite 3 forms an interbed within calciturbidite unit 3 and is composed of clast-rich carbonate breccia with abundant (some contorted and disrupted) clasts of orange, carbonate mudstone, light grey siliciclastic mudstone (below hammer) and white quartz pebbles.

In the earlier work of Ross (1991); and Ross et al. (1995), strata comprising calciturbidites units 2 and 3 plus associated siliciclastics were collectively termed the Lower or First Isaac Carbonate (FIC), the lowermost regional marker of the Isaac Formation in the Cariboo Mountains. In this study, however, the FIC is interpreted to also include strata extending to the base of calciturbidite unit 1. Lithologically, calciturbidite units 1-3 consist predominantly of thin- and medium-bedded (up to 0.39 m thick), reddish brown to orange, fine-grained calcarenites and dark olive to dark grey, calcilutites with occasional siliciclastic mudstone tops (F9). Strata contain minor (<3%) quartz grains and lack micritic intraclasts, peloids or ooids. Locally, these strata fine and thin upward. Medium-grained siliciclastic sandstone and calcarenite interbeds (F3/F4 and F9, respectively) are uncommon. Calciturbidite unit 1 comprises sandier strata, whereas calciturbidite unit 3 includes thicker calcilutite beds. Microscopically, calciturbidites exhibit evidence of extensive recrystallization and/or dolomitization. Additionally, up to 2 m-thick intervals of thin-bedded, mudstone-rich siliciclastic turbidites (F5) are also present. Characteristically, calciturbidite units are capped or intercalated by discontinuous up to few m thick calcidebrites (see next section 5.5.5).

Standard (bulk) isotopic analyses of calcilutites and mudrocks from the FIC are presented in Fig. 5.15 (results are relative to PBD), and include a section from calciturbidite units 2 to 3; note the absence of data from calciturbidite unit 1 (unpublished data of G.M. Ross; see Appendix 6).

The calcilutites are characterized by $\delta^{13}C_{carb}$ values that vary from -3.2 to 3.8‰ (average 1.7‰). Values are consistently positive, except in the uppermost part

of the FIC (calciturbidite unit 3) where they become negative. Organic matter residue in mudrocks of the FIC is characterized by highly negative $\delta^{13}C_{org}$ values (-14.3 to -25.9‰) with the most negative values (-25.9‰) measured in calciturbidite unit 3. Both negative $\delta^{13}C_{carb}$ and $\delta^{13}C_{org}$ shifts occur beneath the base of Isaac Channel 1, which coincides also with a major change from carbonate- to siliciclastic-dominated strata in the Isaac Formation.

In contrast to the stratigraphic variation observed in the $\delta^{13}C$ data, the $\delta^{18}O_{carb}$ data are uniformly negative with a narrow range of values (-15.8±0.8‰). Both are interpreted to be artifacts of isotopic re-equilibration and homogenization caused by low-grade regional metamorphism (e.g. Derry, 2010). Similar homogenization of oxygen isotopic system has been recognized in the Old Fort Point Formation, the lowermost and most areally extensive regional marker in the Windermere Supergroup in the Southern Canadian Cordillera (Smith, 2009). Hence, $\delta^{18}O$ isotopes are not discussed any further.

At Mt. Quanstrom, only one partly exposed calciturbidite-rich unit is observed (Fig. 5.9). It is about 2 m thick and composed mostly of thin beds of dark grey to black calcilutites. Based on its stratigraphic position and the dominance of calcilutites, it is correlated with calciturbidite unit 2 in the Castle Creek study area.

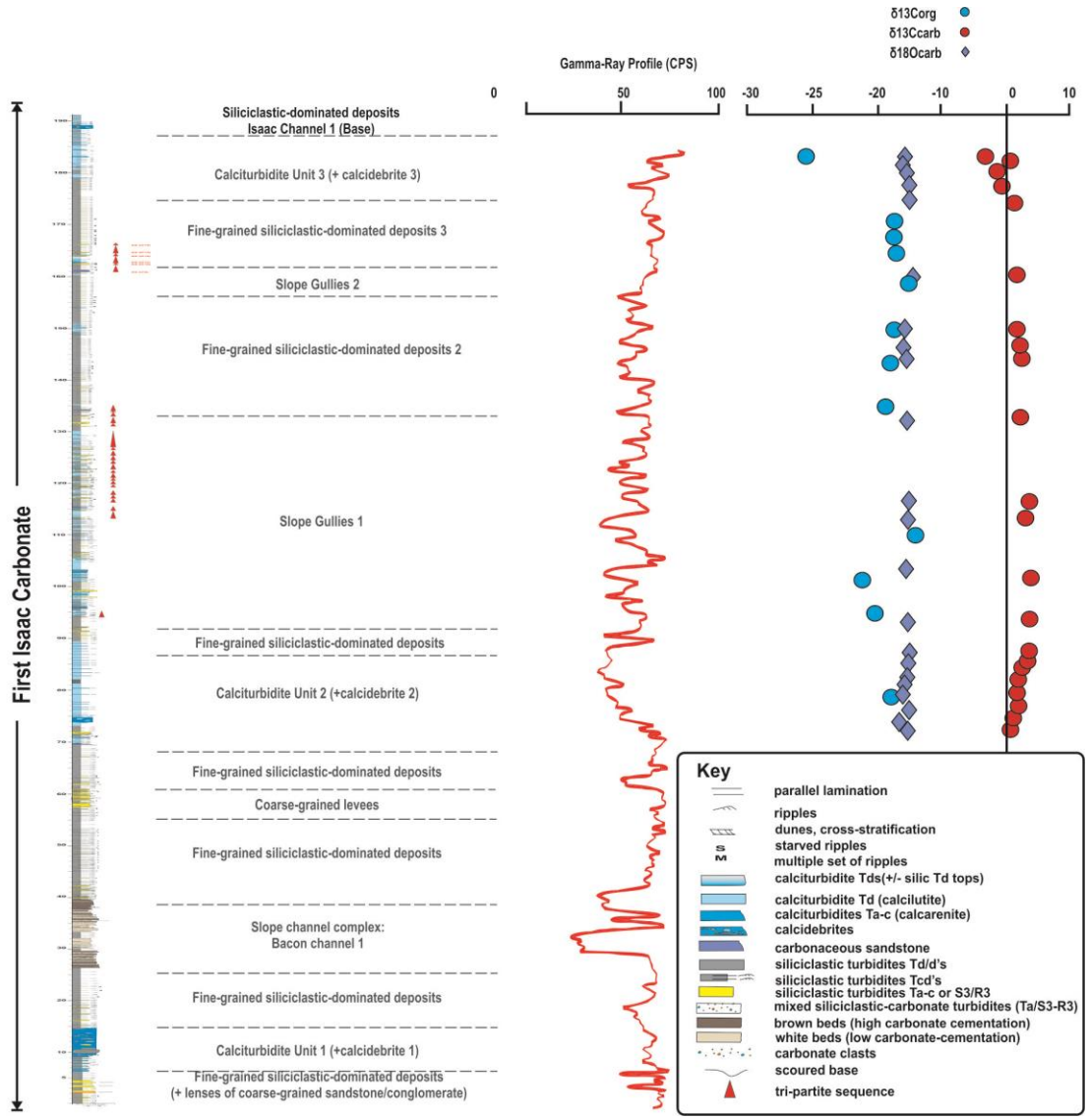

Figure 5.15. Generalized stratigraphic section and $\delta^{13}C$ and $\delta^{18}O$ profiles through most the First Isaac Carbonate in Castle Creek south study area. Results are relative to PBD. Red and blue circles indicate $\delta^{13}C_{carb}$ and $\delta^{13}C_{org}$, respectively, and blue diamonds indicate $\delta^{18}O_{carb}$ (from unpublished data of G.M. Ross, 2003; see Appendix 6). Gamma-ray profile measured in count per seconds (cps, see Appendix 7 for data).

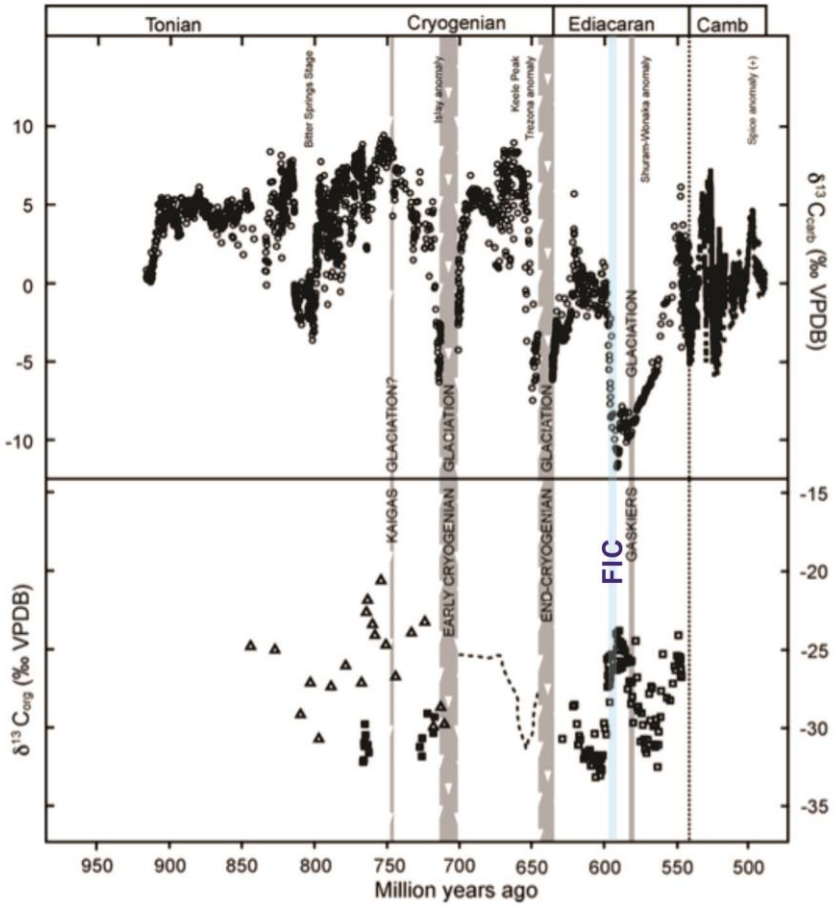

Figure 5.16. The FIC (highlighted in blue) plotted on the global compilation of $\delta^{13}C$ data from Neoproterozoic (Cryogenian) marine carbonates (from Halverson et al., 2010). Note the three major negative anomalies that straddle major global glaciations: Sturtian or early Cryogenian glaciation (approximately 720-680 Ma), Marinoan or end-Cryogenian glaciation (approximately 650-635) and Gaskiers glaciation (approximately 580-570 Ma). Although poorly chronologically constrained, the FIC may precede a smaller-scale glacial event that post-dated the Marinoan glaciation, but preceded the Gaskiers glaciation.

Interpretation

Fine-grained siliciclastic turbidites represent deposition of continentally-derived fine-grained detritus on the continental slope by low-concentration turbidity currents. The intercalated occurrence of these thick siliciclastic mudstone-rich units within the FIC is interpreted to indicate protracted periods of sustained low physical energy.

Fine-grained calciturbidite units, on the other hand, were deposited principally by low-concentration, calcareous-rich, fine-grained turbidity currents. Sediment was sourced from a coeval carbonate platform and then resedimented downslope. The thickness and areally widespread distribution of these strata suggest high carbonate sediment production and downslope export, and is consistent with conditions possibly associated to highstand shedding (Mullins et al., 1984; e.g. Droxler and Schlager, 1985; Schlager et al., 1994) and highstand bundling (e.g. Droxler and Schlager, 1985; Andresen et al., 2003; Jorry et al., 2008). However, due to extensive recrystallization and local dolomitization, determining the origin of carbonate mud is problematic. Nevertheless, there are only three possible carbonate mud sources during the Neoproterozoic: (1) direct chemical or abiotic precipitation from seawater (Grotzinger, 1989, 1990), (2) microbially-mediated precipitation (Shields, 2005), or (3) erosion and disintegration of partially-lithified microbial mats (Petrov, 2001; Bailey et al., 2009). Muddy carbonate platforms were common during the Late Proterozoic (Kah and Knoll, 1996; Sherman, 2000), which in part is thought to be related to the appearance and growth of calcified cyanobacteria (Riding, 2006, 2011;

Lenton et al., 2014). Blooms of planktonic cyanobacteria would have induced direct precipitation of carbonate mud in the water column, termed whitings in modern carbonate setting (Sherman, 2000; Shields, 2005), which then was made available for later resedimentation downslope onto the slope, possibly by processes like density cascading (sensu Wilson and Roberts, 1992, 1995).

The $\delta^{13}C$ isotopic signatures through the middle and upper FIC (Fig. 5.14) are considered to reflect primary sedimentary conditions, as argued also by Ross (2003). During much of Neoproterozoic (Knoll et al., 1986; Kaufman and Knoll, 1995; Shields and Veizer, 2002; Halverson et al., 2005; Halverson et al., 2010) like much of the FIC (>0.6‰), $\delta^{13}C_{carb}$ from marine carbonates was positive (Fig. 5.16). This suggests a long-term episode of increased rates of organic carbon burial (Hayes et al., 1999; Kump and Arthur, 1999), which quite possibly also promoted oxygenation of the Earth's atmosphere (Marais et al., 1992; Canfield, 2005; Kennedy et al., 2006; Lenton et al., 2014). Negative isotopic signatures in the Neoproterozoic (Cryogenian), on the other hand, represent temporary, comparatively, short-lived events, which commonly have been explained in two ways: the first model involves a stratified Cryogenian ocean with upwelling of anoxic, isotopically depleted, alkaline deep waters (Grotzinger and Knoll, 1995; Kaufman and Knoll, 1995); and a second that relies on the partial oxidation of an vast oceanic reservoir of reactive dissolved organic carbon (Rothman et al., 2003; Swanson-Hysell et al., 2010). Furthermore, it has been shown that negative carbon-isotope excursions correlate with major glacial events (e.g. Kennedy et al., 1998; James et al., 2001; Halverson et al., 2005; Fairchild

and Kennedy, 2007; Halverson et al., 2010; Hoffman and Halverson, 2011; Johnston et al., 2012). Accordingly, the negative $\delta^{13}C_{carb}$ values (<-0.5‰) at the top of the FIC are interpreted to reflect deposition prior to a major glacial event.

The age of the FIC is unknown, and bracketed only by the underlying Old Fort Point Formation, which has been dated at 607.8 ± 4.7 Ma (Kendall et al., 2004), and the overlying Neoproterozoic Hamill Group (569.6 ± 5.3 Ma; Colpron et al., 2002). Accordingly, the FIC is interpreted to have preceded a glacial event that post-dated the well-known Marinoan glaciation and pre-dated the Gaskiers glaciation (see Fig. 5.15-5.16). Significantly, the FIC is overlain directly by Isaac channel 1, which signals the return of a long-term dominance of siliciclastic sedimentation (Navarro, 2006). The base of this channel complex has been interpreted to mark a major sequence boundary formed during a major fall of relative sea level (Navarro, 2006). A similar trend has been noted in the late Cryogenian cap-carbonate-like strata of the Rainstorm Member of the Johnnie Formation in the Death Valley (USA). Here, a negative $\delta^{13}C$ isotopic excursion is overlain by a major sequence boundary that marks by the base of an incised valley (Corsetti and Kaufman, 2003), interpreted to be coincident with a glacio-eustatic lowstand (Christie-Blick et al., 1989).

5.5.5 Calcidebrites

Although uncommon (<3% of the FIC), calcidebrites, here numbered 1 to 3, are on top or intercalated with calciturbidite-dominated units 1 to 3 (described in section 5.5.4.2; Figs. 5.11, 5.12c-d). Typically, calcidebrites are lenticular with sharp

basal and top contacts, up to 5 m thick, and can be traced laterally for several hundreds (e.g. calcidebrite 1 and 3) to thousands of meters (e.g. calcidebrite 2). Strata consist typically of matrix- or clast-supported conglomerate (F10) with a poorly-sorted, orange to greyish orange matrix of carbonate mud or mixed (carbonate-siliciclastic) mud. Dispersed white quartz sand, granules and pebbles are common. Clasts are gravel-sized, undeformed to moderately deformed, and composed of a diverse assemblage of lithologies, including calcilutites and siliciclastic mudstone and minor fine-grained calcarenite, and sandstone. Notably, calcidebrite 2 is a mud-dominated conglomerate with abundant clasts of massive calcilutites, but also fragments of dolomitized cryptalgal laminites, oolitic limestone, and carbonate aggregates (Figs. 5.2k-l, 5.12 e-h). At the Mt. Quanstrom study area, calcidebrites were not observed.

Interpretation

Calcidebrites in the FIC are interpreted to be the result of deposition from carbonate-rich debris flows most likely associated with episodic slope failure events. Based on lithologies of the clasts embedded in the calcidebrites, a close correlation with specific source areas on a carbonate platform or upper slope can be inferred (e.g. Reijmer, 1998; Reijmer et al., 2015). The presence of cryptalgal laminite and ooidal carbonate clasts in calcidebrite 2 strongly suggests sourcing from a well-established carbonate platform, specifically an upflow platform interior. Nevertheless, abundant calcilutite and (siliciclastic) mudstone clasts and carbonate/mixed mud matrix in all calcidebrites indicate that the principal source was probably from a carbonate

platform margin and/or upper slope areas, where fine-grained sediments dominated. Following the slope failure, these clasts became mixed into a fine-grained sediments as the sediment mass evolved into a more fluidal debris flow.

The scarcity of calcidebrites in the FIC suggests that overall the slope was relatively stable. This might be as a result of a pervasive early-diagenetic carbonate cementation that stabilized the slope (e.g. Grammer et al., 1993). Calcidebrites of the FIC are comparatively fewer and smaller than those of modern examples (including carbonate megabreccias) and associated mass-transport deposits – for example calcidebrites on the Bahamas banks are tens to few hundreds of meters thick and at least tens of kilometers in width and length (Principaud et al., 2013; Jo et al., 2015; Tournadour et al., 2015), and show a short distance transport from their upslope source area (e.g. Cook et al., 1972; de Graciansky and Chenet, 1979; Crevello and Schlager, 1980; Reijmer, 1998; Reijmer et al., 2012b; Reijmer et al., 2015).

5.6 Discussion

At Castle Creek the FIC forms an almost 200 m-thick sequence sandwiched between siliciclastic-dominated strata of Isaac channel complexes 0 and 1 (Fig 5.1). Stratigraphically-upward, it includes three deep-water carbonate-rich stratal units termed here calciturbidite units 1 to 3, variously separated by thick siliciclastic-rich fine-grained deposits, decametre-thick slope channel complexes filled with mixed- and siliciclastic-rich grain-dominated strata (i.e. Bacon channel complexes 1 and 2), and gullies filled with a consistent vertical succession of siliciclastic- and

calciturbidite-rich strata (i.e. Gully complexes 1 and 2). Locally, minor levee deposits and calcidebrites also occur. A correlative sequence of the FIC was also identified at the Mount Quanstrom study area (Fig 5.9), where slope channel and gully complexes with similar lithological and architectural attributes crop out and support the likelihood of a strong regional control on the distribution and evolution of the FIC.

5.6.1 Stratigraphic framework of the FIC within the Isaac Formation

At the large-scale, the FIC overlies an up to 30 m thick succession of fine-grained siliciclastic turbidites with a small number of intercalated lenses of conglomerate and sandstone. This fine-grained siliciclastic-rich interval, in turn, overlies Isaac channel complex 0 (ICC0), which is composed mostly of thick amalgamated to semi-amalgamated, subfeldspathic-rich conglomerate and sandstone strata (for more details see Chapter 4). ICC0 is interpreted to represent deposition during a major sea-level fall, followed by deposition of fine-grained deposits marking the beginning of a long-term eustatic rise.

Associated also with rising sea level was a dramatic change from deep-water siliciclastic to carbonate deposition, suggesting the initiation, growth and progradation of a extensive shallow-marine carbonate production zone from which carbonate-rich sediments were increasingly remobilized downslope and transported farther basinward (Schlager et al., 1994). Overall, the FIC is inferred to have developed during a long-term, possibly 3rd order rise of relative sea level (Fig. 5.17;

Navarro, 2006; Ross and Arnott, 2007) that quite possibly was related to a protracted period of deglaciation.

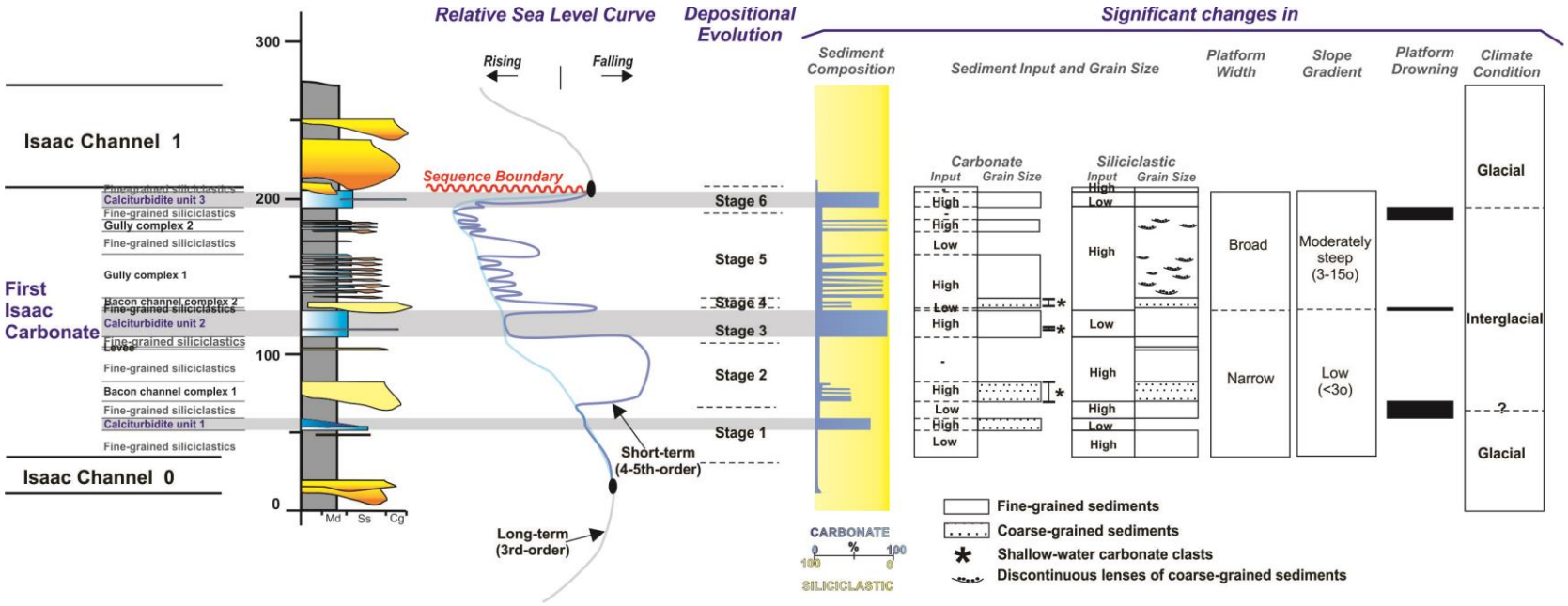

Figure 5.17. Evolutionary model illustrating the combined of long- and short-term changes in relative sea level and a suite of physical and chemical conditions on the stratigraphic development of the FIC.

Development of calciturbidite units 1, 2 and 3 in the FIC record three discrete episodes of voluminous production and export of carbonate sediment onto an otherwise siliciclastic-dominated continental slope. The stratal make-up of calciturbidite unit 1 and 2 is consistent with highstand-shedding sedimentation patterns, like those reported from modern Bahamian and Caribbean carbonate systems and in Papua New Guinean mixed slope system, where sea level rise has flooded the platforms and as a consequence dramatically increased carbonate production and downslope remobilization of carbonate-rich sediment (Haak and Schlager, 1989; Tcherepanov et al., 2008; Jorry et al., 2010; Reijmer et al., 2012a; Reijmer et al., 2012b; Reijmer et al., 2015). Calciturbidite unit 3, however, is inferred to be formed after a relative sea level was falling, which caused part of the carbonate platform to re-enter optimal production conditions with significant amount of fine-grained carbonate sediment exported to the slope. A similar trend has been recently documented in mixed carbonate-siliciclastic system along the Great Barrier Reef margin and adjacent Queensland Trough and Plateau (Harper et al., 2015).

The carbonate-rich succession of the FIC is then erosively overlain by the more than 100 m-thick Isaac slope channel complex 1 or IC1 (for details on the dimensions, facies distribution and architecture of IC1 see Navarro, 2006; Anthony, 2010; Dumouchel, 2012), which marked the cessation of carbonate sedimentation and resumption of voluminous siliciclastic deposition onto the Windermere continental slope and further basinward. The base of IC1, therefore, is interpreted to represent a possible 3rd-order sequence boundary associated with a major fall in relative sea level

(Fig. 5.17), most probably related to the resumption of glacial conditions (Navarro, 2006).

5.6.2 Major factors controlling the deposition and evolution of the FIC and coeval carbonate platform

Mixed carbonate-siliciclastic turbidite systems record the complex interaction between external (allogenic) and internal (autogenic) forces that govern the input and distribution of carbonate and terrigenous sediments supplied to the slope and more distal basin settings. Stratigraphic analysis of the FIC has helped to elucidate the evolution of a mixed slope system, and also to identify possible factors that controlled its development. Changes in facies, geometry and distribution of stratal elements are interpreted to be controlled by differences in input variables, namely sediment flux, size and mineralogical composition, which in turn are thought to be largely linked to allogenic controls, such as eustasy and climate (e.g. Catuneanu et al., 2011). In addition to dynamic allogenic signals, changes in slope gradient also profoundly influenced deposition of the FIC.

In the absence of absolute age control for the Neoproterozoic FIC, sedimentation rates and duration of inferred sea-level changes cannot be accurately assessed. Adding to this uncertainty is the fact that accumulation rates based on the ancient sedimentary record are invariably lower than those reported from modern carbonate systems (Sadler, 1981). Furthermore, the incomplete nature of ancient sedimentary record makes comparing rates of accumulation and estimating rates of

carbonate growth/accumulation under different climatic and eustatic regimes to those observed rates in modern depositional settings problematic (Kemp and Sadler, 2014). Also, estimated carbonate accumulation rates from ancient rock record tend to primarily reflect long-term changes in accommodation space rather than short-term changes in mostly local processes or sea level (Kemp and Sadler, 2014).

Despite these limitations, the large- and small-scale stratal architecture and sediment composition of resedimented deposits of the FIC still provide invaluable spatial and temporal changes in the production and export of sediments from the adjacent coeval carbonate platform system to this mixed slope system, which is interpreted to be influenced by two orders of relative sea level changes: long-term (probably 3rd-order) and short-term (possibly 4th- or 5th-order). The interaction between these allogenic drivers is considered to have significantly modulated the stratigraphic development of the FIC. Overall carbonate sediment production tends to be mostly controlled by the long-term evolution and accommodation on the platform, whereas major changes in carbonate production and export potential, and changes in source platform areas and related sediment types are largely influenced by shorter sea-level variations (e.g. Rusciadelli et al., 2009).

The following is an evolutionary model that describes the temporal development of the FIC (see also Figs. 5.17-5.19). This model comprises six main stages of carbonate platform development, and related depositional/erosional episodes in the FIC slope system, wherein channels and gullies were developed.

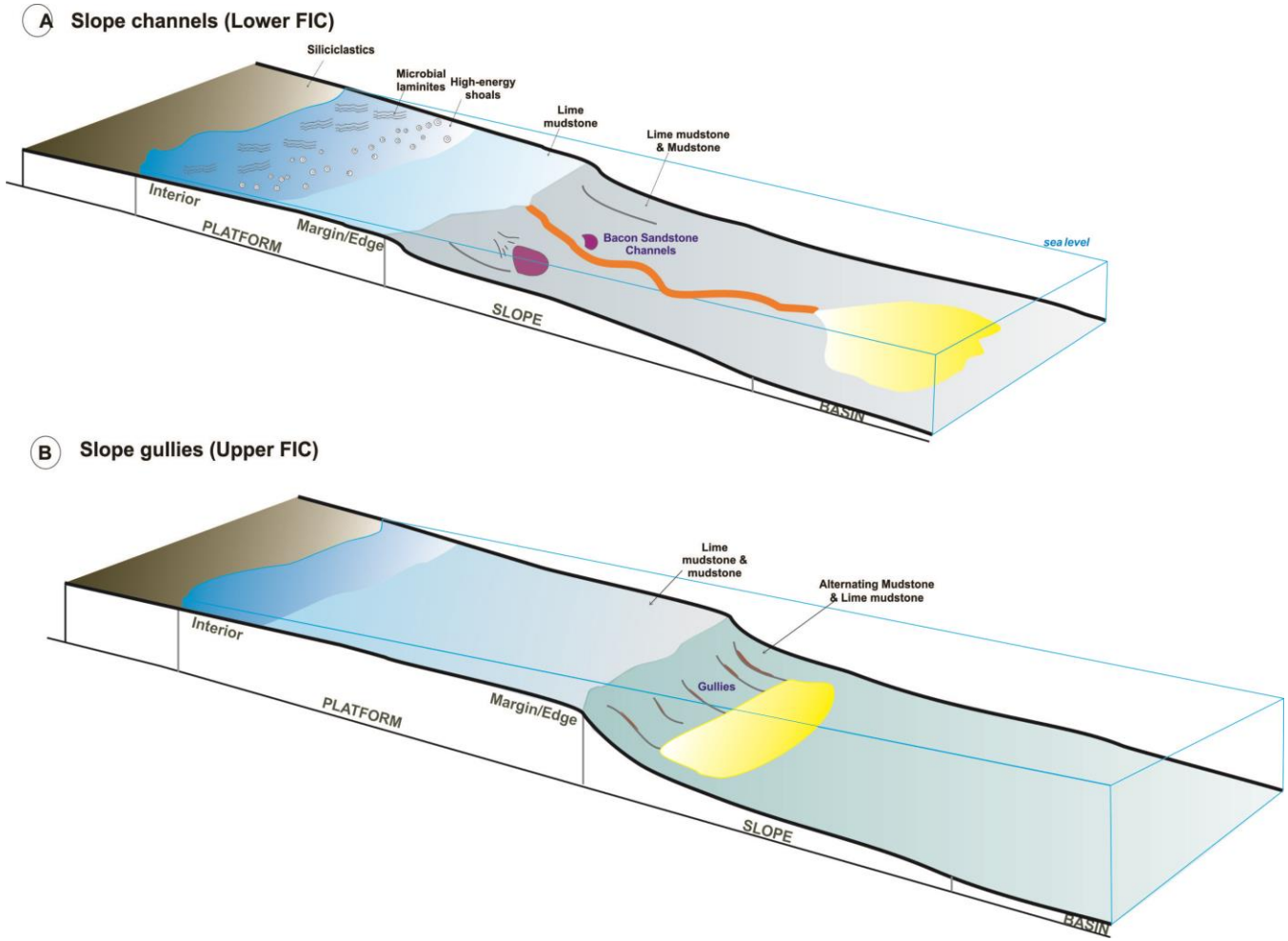

Figure 5.18. Schematic of two end-member channelized features developed in the lower and upper parts of the FIC. See text for details.

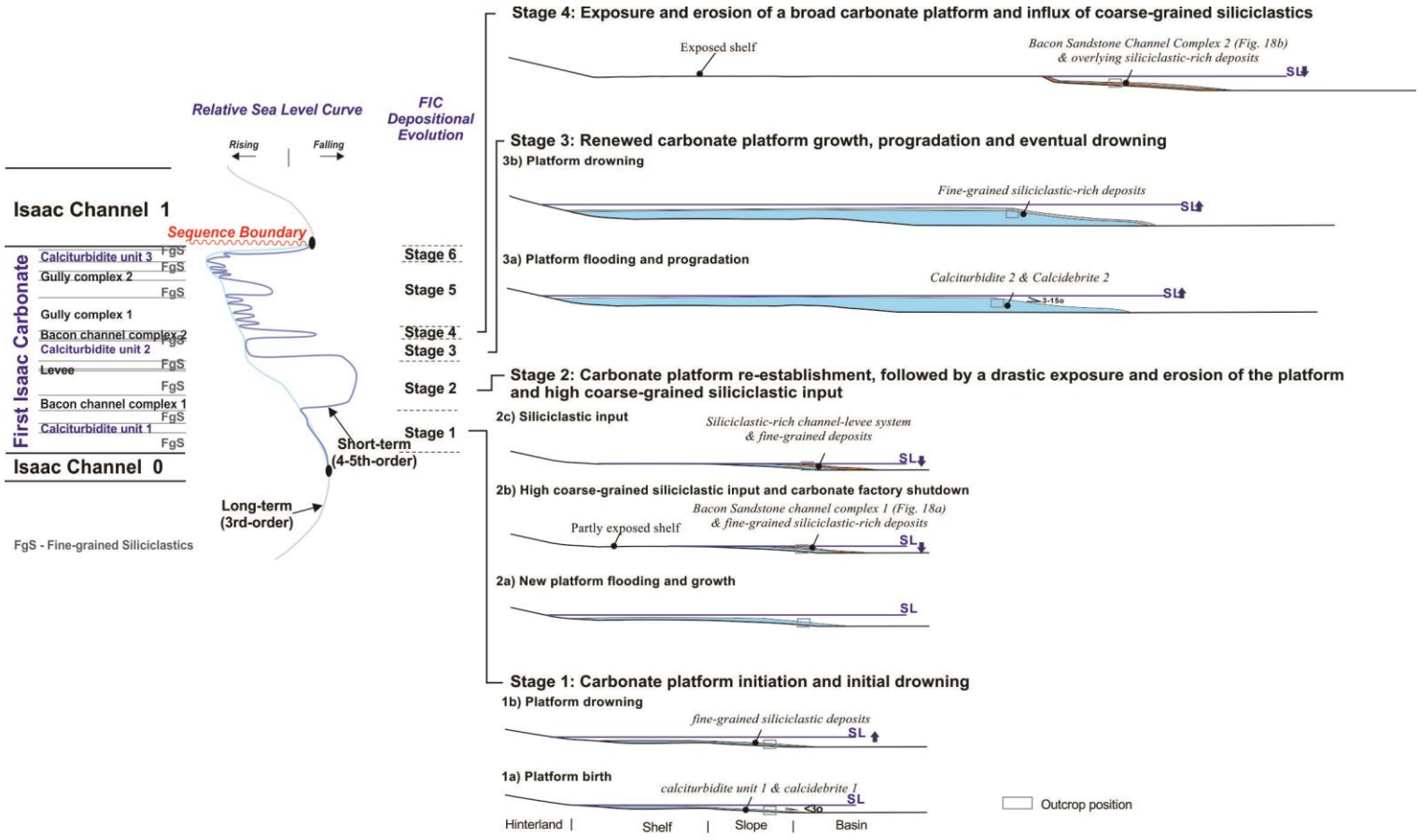

298

Figure 5.19. Evolutionary stages of carbonate-platform development and deactivation and associated slope sedimentation during the FIC. See text for details.

Continuation Fig. 5.19

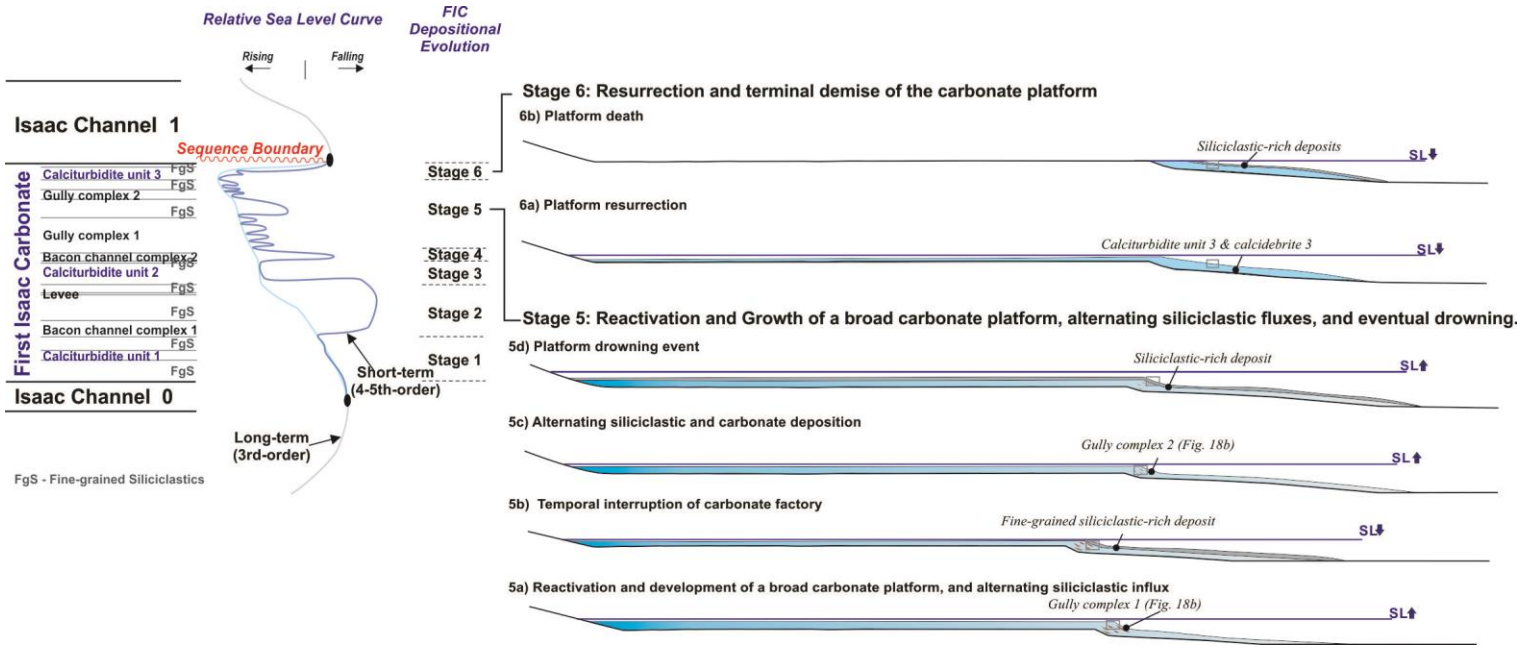

Stage 1: *Initial establishment and then drowning of carbonate platform*

Following the deposition and abandonment of Isaac Channel 0, an incipient carbonate platform was developed at the beginning of a long-term (3rd-order) relative sea level rise. The platform was connected to a low-angle continental slope inherited from the earlier siliciclastic-dominated system, which based on modern siliciclastic deep-water systems was probably of the order of 1-3^{o} (e.g. Posamentier and Kolla, 2003; Deptuck et al., 2007a). Initially, fine-grained siliciclastic-rich sediments were principally supplied to the slope. However, as sea level continued to rise shelf accommodation space increased substantially, which then resulted in the inception of a carbonate platform, and in addition of a carbonate component to the existing sediment supply. The intense red and orange sandstone turbidites with high carbonate-siliciclastic content (up to 70:30) of calciturbidite unit 1 corresponds to this initial export of mixed material onto the Windermere continental slope. Similar to many modern mixed and carbonate systems, rising relative sea level may have coincided with terminal glacial or the transition from glacial to interglacial conditions, when abnormally high insolation triggered the melting of glacial ice sheets (e.g. Jorry et al., 2010).

As sea level continued to rise the growth, particularly upward, of the platform was unable to keep pace and eventually became drowned (e.g. Kim et al., 2012). Drowning and associated cessation of the carbonate production was initially accompanied by a collapse of the margin and deposition of calcidebrite 1, followed thereafter by deposition of a decameter-thick succession of mostly fine-grained siliciclastic turbidites.

Stage 2: *Carbonate platform re-establishment followed by exposure and erosion, and high coarse-grained siliciclastic input*

Despite the long-term trend of rising relative sea level, the platform became reactivated during a brief, but high amplitude fall of relative sea level. Reduced water depth re-established optimal conditions for carbonate growth, which in turn reinitiated the platform and carbonate sediment production. At this time, the platform consisted of microbial mats (photic zone) and ooidal sands on the platform interior (shallow water areas) and calcareous muds on the platform margin and slope. Eventually, relative sea level fell so far that the platform became subaerially exposed and eroded. A high flux of coarse-grained siliciclastic sediment commonly mixed with eroded coarse-grained carbonate fragments, including cryptalgal microbialites, ooidal, peloidal, and micritic clasts, was transported downslope through the channels that make up Bacon sandstone channel complex 1 (Fig. 5.18a).

As the sea level continued to fall, siliciclastic input became dominant and a decameter-thick succession of fine-grained turbidites and a siliciclastic channel-levee system developed. Sand-rich levee strata crop out locally in the study area, and are interpreted to be related to the overspill of siliciclastic flows, flowing basinward through siliciclastic slope leveed channels (e.g. Khan and Arnott, 2011). Following the abandonment of the local channel-levee system, an up to 11-m thick unit of thin-bedded siliciclastic turbidites was deposited.

Stage 3: *Renewed carbonate platform growth, progradation and temporary drowning*

Stage 2 was terminated by a major rise of the relative sea level and the re-establishment of a robust carbonate platform and the deposition of calciturbidite unit 2, the thickest (up to 20 m) carbonate-rich unit in the FIC. The considerable thickness of calciturbidite unit 2 suggests sustained maintenance of a robust carbonate platform, and in turn a good balance between the relative sea level rise and growth space and carbonate productivity (Jones and Desrochers, 1992). In addition, the positive carbon isotopic values in calciturbidite unit 2 is consistent with patterns related to voluminous carbonate shedding, possibly associated with interglacial conditions (sensu Droxler and Schlager, 1985).

The dominance of mud-dominated carbonate strata in calciturbidite unit 2 is interpreted to reflect a well-developed and prograding carbonate platform with an expansive platform-top mud factory that sourced a voluminous supply of fine-grained carbonate sediment to the slope (e.g. Playton et al., 2011). These carbonate-rich slope sediments were then most likely affected by extensive early (marine) cementation and lithification (van Der Kooij et al., 2010), which in turn resulted in a steepening of the continental slope (Davies, 1977; Schlager and Camber, 1986). Moreover, the paucity of calcidebrites might also indicate early lithification that stabilized the slope and inhibited cohesive mass movements (e.g. Schlager and Camber, 1986). Considering that in modern carbonate and mixed systems platform-margin failures are common on slopes greater than >20^{o} (e.g. Playton et al., 2011), it is estimated that the slope gradient here was moderately steep, >3^{o}, but <20^{o}. Calciturbidite unit 2 is then

overlain by an up to 4.5 m-thick succession of thin-bedded siliciclastic turbidites, which is interpreted to indicate the temporary drowning of the platform by the ongoing rise of relative sea level and a return to fine-grained siliciclastic sedimentation.

Stage 4: *Exposure and erosion of a broad carbonate platform and influx of coarse-grained siliciclastics*

The major rise of relative sea level that deposited calciturbidite unit 2, and ultimately its cap of fine-grained turbidites, was terminated by a high-amplitude fall of relative sea level. This event caused the carbonate platform to not only be exposed and eroded, but siliciclastic sediments, especially sand and gravel, to be reintroduced and resedimented onto the slope. Under these conditions, Bacon Sandstone channel complex 2 was formed (Fig. 5.18a), at this time with channels filled with quartz sand and gravel, and abundant ooidal and micritic carbonate clasts eroded from the interior and outer/margin of the exposed platform.

Stage 5: *Reactivation and growth of a broad carbonate platform, alternating with episodes of siliciclastic input followed by drowning*

This stage is marked by a return to rising of relative sea level and the development of a new and broad carbonate platform that transitioned basinward to a moderately steep continental slope, inherited from Stage 3. Although the platform was growing, expanding and prograding, the carbonate production was periodically interrupted by siliciclastic input. The m-scale alternation of mud-rich carbonate sediments, produced on the platform top and margin, and fine-grained siliciclastic sediments, sourced from the hinterland, are interpreted to reflect short-term

oscillations of relative sea level. It is these changes that resulted in the rhythmic alternation of optimal carbonate and sub-optimal conditions for carbonate growth, and ultimately deposition of fine-grained calci- and silici- clastic turbidites, respectively. Locally intercalated with the fine-grained siliciclastic turbidites are cm- to dm-thick, coarse- and medium-grained siliciclastic sandstone with rare granules confined to shallow, erosionally-based gullies (Fig. 5.18b). The coarse sediment that mantles the base of the gullies is interpreted to represent coarse palimpsest shelf sediment that later was resedimented downslope, and whose movement was facilitated by the steepness of the slope related to sea-floor early diagenesis and lithification formed during stage 3. This, then, is similar to modern systems where submarine gullies preferentially form in mud-dominated slope systems with gradients of at least 3^{o}, but $<10\text{-}15^{o}$ (e.g. Spinelli and Field, 2001; Micallef and Mountjoy, 2011; Mulder et al., 2012a; Principaud et al., 2013).

Gully complex 1 is then overlain by a 25-thick interval of thin-bedded siliciclastic turbidites interpreted to be related to a fall of relative sea level, which temporarily terminated carbonate production. These strata indicate that the supply of sediment to the slope was dominated by fine-grained siliciclastics. At the same time, some coarser-grained (mostly sand) sediment was also being supplied but became stranded on the shelf. Falling relative sea level was then followed by a rise that reactivated the carbonate platform and carbonate production. Similar to gully complex 1, gully complex 2 consists of m-thick calciturbidite units intercalated with fine-grained siliciclastic turbidites interbedded with thin, coarse-grained gully fills. Accordingly, gully complex 2, like gully complex 1, is interpreted to reflect rhythmic

changes of relative sea level and commensurate changes in the mineralogy of sediment supply and its patterns of transport and deposition. Gully complex 2, in turn, is overlain by an up to 12-m thick succession of thin-bedded siliciclastic turbidites, which in this case is interpreted to reflect a prolonged drowning of the broad carbonate platform and cessation of carbonate production (e.g. Schlager and Camber, 1986; Webster et al., 2004; Schlager, 2005; Catuneanu, 2006; Tcherepanov et al., 2010), and therein comparable to drowning deposits reported in mixed systems of the Gulf of Papua and Great Barrier Reef (e.g. Webster et al., 2004; Tcherepanov et al., 2010).

Stage 6: *Rejuvenation and then terminal demise of the carbonate platform*

Following deposition of the thick unit of fine-grained siliciclastic strata at the top of the Stage 5, a long-term fall of relative sea level began. The local occurrence of calcidebrite 3 is suggestive of slope instability, which commonly is associated with conditions of falling relative sea level in both modern carbonate systems (e.g. Reijmer, 1998; Reijmer et al., 2012b; Reijmer et al., 2015) and siliciclastic slope systems (e.g. Ross et al., 1994). As water depth decreased and eventually entered the optimal range for carbonate production, the carbonate platform was rejuvenated and resulted in the deposition of the thick- to medium-bedded, mostly calcilutites that built up calciturbidite unit 3. Importantly, negative carbon isotope values in calciturbidite unit 3 might insinuate that this fall of relative sea level and associated rejuvenation of the carbonate platform and sediment production may be a consequence of the onset of glacial conditions following a long-term interglacial period. Calciturbidite unit 3 is possibly analogue to an unique slope carbonate

interval deposited in the mixed carbonate-siliciclastic system along the central Great Barrier Reef margin during the falling of a relative sea level (Harper et al., 2015).

Deposition of an up to 5 m thick interval of fine-grained siliciclastic turbidites that overlie calciturbidite 3 marked the final demise of the carbonate platform and the long-term return of siliciclastic sedimentation, which culminated in deposition of Isaac Channel 1 (Navarro, 2006).

5.6.3 Comparison with slope channels and gullies from other mixed and carbonate systems

The facies distribution and stratal architecture observed in the Neoproterozoic FIC reveal an intricate coexistence and interaction of deep-water carbonate and siliciclastic deposits; however, the absence of a good modern deep-water mixed slope system analogue is problematic. Nevertheless, a number of key stratal elements described here, such as slope channels and small gullies, have been recognized in other modern and ancient carbonate and mixed slope systems (also known as calciclastic slope systems by Payros and Pujalte, 2008), and therein help to constrain the interpretations made here.

Calciclastic slope channel complexes, like the Bacon sandstone channel complexes, are generally smaller than those in siliciclastic systems. However it is important to note that most of the calciclastic examples have been described from the ancient sedimentary record (for an extensive review of calciclastic submarine channels and fans, see Payros and Pujalte, 2008), and only recently have leveed channels been documented from a modern deep-water carbonate system (Mulder et

al., 2012a; Mulder et al., 2014). Also most of these channel complexes, irrespective of the tectonic setting, were formed during the long-term progradation of a carbonate platform.

In comparison to modern and ancient Phanerozoic calciclastic examples, which are composed mostly of carbonate skeletal grains, Neoproterozoic Bacon channel complexes are characterized by mixed detrital assemblage of non-skeletal carbonate and siliciclastic grains. Notwithstanding differences in sediment composition, the channel dimensions, grain size range, bed amalgamation, vertical and lateral facies distribution, and even cementation style in the FIC are consistent with these younger examples (Table 5.3). Typically, most calciclastic channel complexes are a few decameters deep and tens to hundreds of meters wide (Watts, 1988; van Konijnenburg, 1999; Braga et al., 2001; Vigorito et al., 2005, 2006; Payros et al., 2007; Mulder et al., 2014). Similar to Bacon sandstone channel complexes, most ancient complexes are erosional (Price, 1977; Cook and Egbert, 1981; Wright and Wilson, 1984; Lehmann et al., 1995; Bernecker, 1997; Gallagher et al., 2001; Brett and Baird, 2002; Wallace et al., 2002; Savary and Ferry, 2004), with lesser levee bounded channel complexes (Watts, 1988; van Konijnenburg, 1999; Braga et al., 2001; Vigorito et al., 2005, 2006; Payros et al., 2007; Mulder et al., 2014). Channel complexes comprise multiple channel fills composed mostly of thick- to thin-bedded, structureless, coarse-grained sandstone to pebble conglomerate with common to abundant carbonate clasts. Minor calcidebrite, slumps or fine-grained deposits are also present (Price, 1977; Cook and Egbert, 1981; Wright and Wilson, 1984; Jacquin et al., 1991; Lehmann et al., 1995; Brett and Baird, 2002). Individual

channel fills exhibit upward-fining and -thinning trends, and are capped by thin-bedded turbidites (e.g. Watts, 1988; George et al., 1997; Braga et al., 2001; Vigorito et al., 2005, 2006; Payros et al., 2007; Payros and Pujalte, 2008, and references therein). Similar fining and thinning trends also occur laterally from channel axis to margin (e.g. Watts, 1988; George et al., 1997; Vigorito et al., 2005, 2006), and only a small number of examples are interpreted to have lateral-accretion deposits (Braga et al., 2001; Vigorito et al., 2006). In addition to the Bacon Sandstone channel complexes, other ancient examples (e.g. Watts, 1988; George et al., 1997; Vigorito et al., 2005, 2006) exhibit widespread, patchy to continuous "layered" cementation in the coarse-grained channel deposits, suggesting that this might be characteristic of coarse-grained calciclastic channel fills.

On modern carbonate mud-dominated continental slopes, like the Bahamian banks, submarine gullies are well developed and extend for several hundreds kilometers down-dip (Table 5.4; Mullins et al., 1984; Mullins and Cook, 1986; Harwood and Towers, 1988; Mulder et al., 2012a; Rankey and Doolittle, 2012; Jo, 2013; Principaud et al., 2013; Chabaud et al., 2014; Mulder et al., 2014; Principaud et al., 2015). Although common in many modern systems, similar features have only been reported rarely from the ancient record (e.g. Jacquin et al., 1991; Payros et al., 2007; Playton et al., 2011; this study; Fubara, 2014; Hairabian et al., 2014). The gullies of the FIC are much smaller (<2 m deep and hundreds meters wide) compared to those documented from the Bahamian banks, which are of the order of <10 to 30 m deep and 400-750 wide (Mulder et al., 2012a; Principaud et al., 2013; Principaud et

al., 2015; Tournadour et al., 2015); however some gullies from the southwestern edge of the Great Bahamas Bank range from 0.5 to 2 m deep (Jo, 2013).

Most modern and ancient submarine gullies in calciclastic systems are linear features that incise adjacent carbonate mudstone or carbonate ooze. However, some gullies recently imaged on high-resolution seismic from the Great Bahamas Bank are interpreted to be aggradational, and are encased within fine-grained levees that are 20 m thick and 2 km wide (Mulder et al., 2012a). Typically, the gullies are characterized by a simple scour filled with a basal layer of coarse-grained calciturbidites or turbidites, draped with carbonate mud-dominated deposits. Calcidebrites are locally observed within some gully fills (e.g. Jacquin et al., 1991; Payros et al., 2007).

Submarine gullies in modern carbonate and mixed slope systems, such as in the Bahamas, feed broad depositional aprons in the lower slope and/or basin-floor areas (e.g. Schlager and Chermak, 1979; Schlager and Ginsburg, 1981; Mullins et al., 1984; Mullins and Cook, 1986; Playton et al., 2011; Rankey and Doolittle, 2012); but in a few examples (Payros et al., 2007; Mulder et al., 2012a), some number of adjacent gullies coalesce to form a single channel that terminates basinward in a depositional lobe system. However, based on their thinness and discontinuous distribution, gullies in the FIC are interpreted to be ephemeral features that conducted low volume, coarse-sediment-transporting turbidity currents further downslope.

5.6.4 Reservoir implications

Currently, several notable examples of hydrocarbon reservoirs hosted in carbonate and mixed slope deposits have been recognized, including the Cretaceous

Poza Rica field in the Gulf of Mexico (Enos, 1977), Carboniferous Tengiz and Korolev fields in Kazakhstan (Weber et al., 2003; Francis, 2004; Harris et al., 2000), the Wolfcampian slope and basinal carbonates within the Permian Basin of west Texas and New Mexico (Dutton et al., 2005), the Cretaceous Campos and Santos basins in Brazil (Bruhn et al., 2003), and the Eocene Zella, Gialo and Sahl fields in Sirte basin, Libya (Baaske et al., 2008). However, subsurface characterization, modelling and prediction of these reservoirs is challenging due to poor seismic resolution, high vertical and lateral facies variability, and lack of information about internal stratal geometry and continuity. The FIC, therefore, provides the opportunity to analyze contrasting facies and architecture of slope channel and gullied features, and accordingly, their reservoir characteristics and potential.

Lithologically, channel-fill strata of Bacon Sandstone channel complexes exhibit excellent horizontal and vertical stratal connectivity, especially in the axis of channels. Channels are filled mostly with stacked, highly amalgamated, coarse-grained sandstone and conglomerate (F1 and F8). At the top of some fills, fine-grained turbidites and calciturbidites, and uncommon calcidebrites would only represent local baffles to fluid flow, affecting most significantly, but still only locally, vertical connectivity. However, in the absence of secondary dissolution, extensive early and late diagenetic carbonate cementation within channel filling strata would significantly reduce effective porosity. Cementation is particularly intense in strata along channel margins (more bi-colour, bacon-like layers or pseudo-beds), which potentially form representing additional intrastratal seals and/or diagenetic compartmentalization.

Slope gully-fill deposits of the FIC, on the other hand, consist mostly of medium- and coarse-grained siliciclastic strata (F2 or F4), draped by laterally-continuous siliciclastic and calciclastic fine-grained facies (F5 and F9, respectively). Although probably having good reservoir quality, these gully deposits form isolated, thin, lenticular bodies encased in non-reservoir thin-bedded turbidites and calciturbidites, and therefore would have limited reservoir volume. In contrast, more areally extensive calciturbidite units consist mostly of highly-cemented calcareous mudstone-rich beds that could potentially host oil and/or gas, but only where were densely fractured or leached forming secondary porosity.

5.7 Conclusions

This outcrop-based study is the first to described in detail facies, architecture and stratigraphic evolution of mixed carbonate-siliciclastic slope deposits of the First Isaac Carbonate (FIC), a major regional stratigraphic marker within the siliciclastic-dominated Windermere turbidite system. Also, it illustrates how rhythmic changes in sea level controlled the production, distribution and accumulation of carbonate sediments and how these strata are complexly intercalated with siliciclastic sediments sourced from the hinterland. Additionally, it illustrates how temporal changes in the gradient of the continental slope influenced sediment transport processes, and accordingly, slope morphology and stratal architecture.

Within the FIC, two types of deep-water slope channels are recognized: channels and gullies. Slope channels are up to 20 m thick and >2 km wide, composite

features consisting of amalgamated smaller channels filled predominantly with thick-bedded, quartz-rich sandstone and conglomerate, as well as mixed carbonate-siliciclastic sandstone and conglomerate with common shallow-water carbonate clasts and particular carbonate cementation. In contrast, gullies are isolated, <300 m wide and up to 2 m thick features filled with medium-bedded, planar or (single set) dune cross-stratified coarse-grained sandstone, and consistently overlain by fine-grained siliciclastic turbidites overlain by calciturbidites. Gullies stack to form up to Dm-thick units. In addition to differences in strata composition, channels and gullies are interpreted to result from systematic temporal changes in sediment supply and composition. Slope channels were formed during episodes of substantially lowered relative sea level when high input of point-sourced coarse-grained siliciclastic and carbonate sediments were delivered directly to a low-angle (previously inherent siliciclastic) slope. Gullies, on the other hand, were formed from a line source and also during an extended period of oscillating relative sea level evidenced by the repetitive alternation of fine-grained siliciclastic and carbonate sediments dominated strata. Moreover the common intercalation of coarse-grained siliciclastic sand-rich gully fills, albeit thin and areally restricted, suggest a steeper slope condition that quite possibly was a developed then during episodes of early diagenetic cementation of carbonate-rich continental slope deposits.

5.8 References

Andresen, N., R. J.J.G, and D. A.W., 2003, Timing and distribution of calciturbidites around a deeply submerged carbonate platform in a seismically active setting

(Pedro Bank, Northern Nicaragua Rise, Caribbean Sea). Int. J. Earth Sci. Geol. Rundsch., v. 92, p. 573-592.

Anthony, D., 2010, Isaac Channel 1 – siliciclastic lowstand channel deposits following highstand carbonate production.: BSc Thesis thesis, University of Ottawa.

Arnott, R. W. C., 2007, Stratal architecture and origin of lateral accretion deposits (LADs) and conterminuous inner-bank levee deposits in a base-of-slope sinuous channel, lower Isaac Formation (Neoproterozoic), East-Central British Columbia, Canada: Marine and Petroleum Geology, v. 24, p. 515-528.

Baaske, U. P., J. V. Itterbeeck, H. Griffiths, P. Tricker, M. Mugheiry, and P. Burgess, 2008, The Eocene Carbonate System(s) of the Sirte Basin, Libya: Implications of Regional-Scale Observations: AAPG International Conference and Exhibition. Abstract.

Bailey, J. V., V. J. Orphan, S. B. Joye, and F. A. Corsetti, 2009, Chemotrophic microbial mats and their potential for preservation in the rock record: Astrobiology, v. 9, p. 843-859.

Bernecker, T., 1997, Mid-late Tertiary deep-water temperate carbonate deposition, offshore Gippsland Basin, southeastern Australia, *in* N. P. James, and J. A. D. Clarke, eds., Cool-water Carbonates, SEPM Spec. Publ., p. 221-236.

Bouma, A. H., 1962, Sedimentology of some Flysch Deposits. A graphic approach to facies interpretation: Amsterdam, Elsevier.

Braga, J. C., J. M. Martin, and J. L. Wood, 2001, Submarine lobes and feeder channels of redeposited, temperate carbonate and mixed siliciclastic-carbonate platform deposits (Vera Basin, Almería, southern Spain): Sedimentology, v. 48, p. 99-116.

Brett, C. E., and G. C. Baird, 2002, Revised stratigraphy of the Trenton Group in its type area, central New York State: sedimentology and tectonics of a Middle Ordovician shelf-to-basin succession: Physics and Chemistry of the Earth, Parts A/B/C, v. 27, p. 231-263.

Bruhn, C. H. L., J. A. T. Gomes, C. D. L. Jr., and P. R. S. Johann, 2003, Campos Basin: Reservoir Characterization and Management – Historical Overview and Future Challenges, Offshore Technology Conference, Houston, p. 1-14.

Canfield, D. E., 2005, THE EARLY HISTORY OF ATMOSPHERIC OXYGEN: Homage to Robert M. Garrels: Annual Review of Earth and Planetary Sciences, v. 33, p. 1-36.

Catuneanu, O., 2006, Principles of Sequence Stratigraphy: Amsterdam, Elsevier 375 p.

Catuneanu, O., W. E. Galloway, C. G. S. C. Kendall, A. D. Miall, H. W. Posamentier, A. Strasser, and M. E. Tucker, 2011, Sequence Stratigraphy: Methodology and Nomenclature: Newsletters on Stratigraphy, v. 44, p. 173-245.

Chabaud, L., E. Ducassou, T. Mulder, and J. Giraudeau, 2014, Isotope Stratigraphy and Biostratigraphy of a Modern Carbonate System: The Northern Bahamas Slope Over the Late Quaternary, *in* R. Rocha, J. Pais, J. C. Kullberg, and S. Finney, eds., STRATI 2013: Springer Geology, Springer International Publishing, p. 1287-1291.

Christie-Blick, N., M. Levy, J. F. Mount, P. W. Signor, and P. K. Link, 1989, Stratigraphic and tectonic framework of upper Proterozoic and Cambrian rocks in the western United States: Late Proterozoic and Cambrian Tectonics, Sedimentation, and Record of Metazoan Radiation in the Western United States: Pocatello, Idaho, to Reno, Nevada 20-29 July, 1989, p. 7-21.

Clark, J. D., and K. T. Pickering, 1996, Architectural elements and growth patterns of submarine channels: application to hydrocarbon exploration: AAPG Bulletin, v. 80, p. 194-221.

Colpron, M., J. M. Logan, and J. K. Mortensen, 2002, U-Pb zircon age constraint for late Neoproterozoic rifting and initiation of the lower Paleozoic passive margin of western Laurentia: Canadian Journal of Earth Sciences, v. 39, p. 133-143.

Cook, H. E., and R. M. Egbert, 1981, Carbonate Submarine Fan Facies Along a Paleozoic Prograding Continental Margin, Western United States: ABSTRACT: AAPG Bulletin, v. 65, p. 913-913.

Cook, H. E., P. N. McDaniel, E. W. Mountjoy, and L. C. Pray, 1972, Allochthonous carbonate debris flows at the Devonian bank (‘reef') margins, Alberta, Canada: Bull. Can. Petrol. Geol., v. 20, p. 439-497.

Corsetti, F. A., and A. J. Kaufman, 2003, Stratigraphic investigations of carbon isotope anomalies and Neoproterozoic ice ages in Death Valley, California: Geological Society of America Bulletin, v. 115, p. 916-932.

Crevello, P. D., and W. Schlager, 1980, Carbonate debris sheets and turbidites, Exuma Sound, Bahamas: Journal of Sedimentary Petrology, v. 50, p. 1121-1148.

Davies, G. R., 1977, Turbidites Debris Sheets and Truncation Structures in Upper Paleozoic Deep-Water Carbonates of the Sverdrup Basin, Arctic Archipelago: Deep-water Carbonate Environments, v. No. 25, Soc. Econ. Paleontoloists Mineralogists Spec. Pub. , 221-247 p.

Davis, L., 2011, Architecture of deep-marine interchannel deposits: Isaac Formation, Windermere Supergroup (Neoproterozoic), Southern Canadian Cordillera: M.Sc. Thesis thesis, University of Ottawa, Ottawa, 174 p.

de Graciansky, P. C., and P. Y. Chenet, 1979, Sedimentological study of cores 138 to 56 (Upper Hauterivian to Middle Cenomanian): An attempt at reconstruction of paleoenvironments, Init. Repts. DSDP, v. 47 (Part 2): Washington, DC (U.S. Govt. Printing Office), p. 403-418.

Deptuck, M. E., D. J. W. Piper, B. Savoye, and A. Gervais, 2007a, Dimensions and architecture of late Pleistocene submarine lobes off the northern margin of East Corsica: Sedimentology, p. 1-32.

Deptuck, M. E., Z. Sylvester, C. Pirmez, and C. O'Byrne, 2007b, Migration–aggradation history and 3-D seismic geomorphology of submarine channels in the Pleistocene Benin-major Canyon, western Niger Delta slope: Marine and Petroleum Geology, v. 24, p. 406-433.

Derry, L. A., 2010, A burial diagenesis origin for the Ediacaran Shuram–Wonoka carbon isotope anomaly: Earth and Planetary Science Letters, v. 294, p. 152-162.

Droxler, A. W., and W. Schlager, 1985, Glacial versus interglacial sedimentation rates and turbidite frequency in the Bahamas.: Geology, v. 13, p. 799-802.

Ducassou, E., L. Chabaud, M. l. Principaud, S. Schmidt, and T. Mulder, 2014, Early marine lithification on the western slopes of Great Bahama Bank, Bahamas: EGU General Assembly 2014.

Dumouchel, I. G., 2012, Effects of relative sea-level change on the stratigraphic architecture of a passive margin deep-marine channel fill complex, Windermere Supergroup, British Columbia, Canada.: BSc Thesis thesis, University of Ottawa, 59 p.

Dunham, R., 1962, Classification of carbonate rocks according to depositional texture, *in* W. E. Ham, ed., Classification of Carbonate Rocks, v. Memoir 1, American Association of Petroleum Geologists, p. 108-121.

Dutton, S. P., E. M. Kim, R. F. Broadhead, W. D. Raatz, C. L. Breton, S. C. Ruppel, and C. Kerans, 2005, Play analysis and leading-edge oil-reservoir development methods in the Permian basin: Increased recovery through advanced technologies: AAPG Bulletin, v. 89, p. 553-576.

Enos, P., 1977, Tamabra Limestone of the Poza Rica trend, Cretaceous, Mexico, *in* H. E. Cook, and P. Enos, eds., Deep water carbonate environments, v. 25: SEPM Special Publication, p. 273-314.

Fairchild, I. J., and M. J. Kennedy, 2007, Neoproterozoic glaciation in the Earth System: Journal of the Geological Society, v. 164, p. 895-921.

Feary, D. A., P. A. Symonds, P. J. Davies, C. J. Pigram, and R. D. Jarrard, 1993, Geometry of Pleistocene facies on the Great Barrier Reef outer shelf and upper slope—seismic stratigraphy of Sites 819, 820, and 821: JA McKenzie, PJ Davies, A. Palmer-Julson, et al., Proceedings of the Ocean Drilling Program, scientific results: College Station, Texas (Ocean Drilling Program), v. 133, p. 327-351.

Ferguson, C. A., and P. S. Simony, 1991, Preliminary report on structural evolution and stratigraphic correlations, northern Cariboo Mountains, British Columbia: Current Research, v. Part A, Geological Survey of Canada, p. 103-110.

Flugel, E., 2010, Microfacies of carbonate rocks: analysis, interpretation and application, Springer, 984 p.

Francis, B. P., Weber, L.J., Batchel, S., Harris, P.M., Fisher, D., and Kenter, J.A.M., 2004, Prediction and mapping of deep-water slope carbonate reservoirs using seismic data, Tengiz Field, western Kazakhstan: AAPG Annual Meeting Abstracts.

Fubara, A. E., 2014, Miocene Depositional Architecture in the Mixed Clastic-Carbonate Rankin Platform: Implications for Clinoform Development and

Morphodynamic Diversity: AAPG Annual Convention and Exhibition, Houston, TX.

Gallagher, S., A. Smith, K. Jonasson, M. Wallace, G. Holdgate, J. Daniels, and D. Taylor, 2001, The Miocene palaeoenvironmental and palaeoceanographic evolution of the Gippsland Basin, Southeast Australia: a record of Southern Ocean change: Palaeogeography, Palaeoclimatology, Palaeoecology, v. 172, p. 53-80.

Gammon, P. R., and R. W. C. Arnott, 2007, Source control over calciturbidite facies distributions in the Lower Isaac Carbonate, Windermere Supergroup, Canada, AAPG Annual Convention and Exhibition. Abstracts.: Long Beach, California, AAPG Search and Discover Article #90063.

George, A. D., P. E. Playford, C. M. Powell, and P. M. Tornatora, 1997, Lithofacies and sequence development on an Upper Devonian mixed carbonate-siliciclastic fore-reef slope, Canning Basin, Western Australia: Sedimentology, v. 44, p. 843-867.

Grabau, A. W., 1904, On the classification of sedimentary rocks: American Geologist, v. 33, p. 228-247.

Grammer, G. M., R. N. Ginsburg, and P. M. Harris, 1993, Timing of Deposition, Diagenesis, and Failure of Steep Carbonate Slopes in Response to a High-Amplitude/High-Frequency Fluctuation in Sea Level, Tongue of the Ocean, Bahamas: Chapter 4.

Grotzinger, J. P., 1989, Facies and Evolution of Precambrian Carbonate Depositional Systems, Controls on Carbonate Platforms and Basin Development, v. 44, SEPM Society for Sedimentary Geology, p. 79-106.

Grotzinger, J. P., 1990, Geochemical model for Proterozoic stromatolite decline: American Journal of Science, v. 290, p. 80-103.

Grotzinger, J. P., and A. H. Knoll, 1995, Anomalous carbonate precipitates: is the Precambrian the key to the Permian?: Palaios, p. 578-596.

Haak, A., and W. Schlager, 1989, Compositional variations in calciturbidites due to sea-level fluctuations, late Quaternary, Bahamas: Geologische Rundschau, v. 78, p. 477-486.

Hairabian, A., J. Borgomano, J.-P. Masse, and S. Nardon, 2014, 3-D stratigraphic architecture, sedimentary processes and controlling factors of Cretaceous deep-water resedimented carbonates (Gargano Peninsula, SE Italy): Sedimentary Geology.

Halverson, G. P., P. F. Hoffman, D. P. Schrag, A. C. Maloof, and A. H. N. Rice, 2005, Toward a Neoproterozoic composite carbon-isotope record: Geological Society of America Bulletin, v. 117, p. 1181-1207.

Halverson, G. P., B. P. Wade, M. T. Hurtgen, and K. M. Barovich, 2010, Neoproterozoic chemostratigraphy: Precambrian Research, v. 182, p. 337-350.

Harper, B. B., Á. Puga-Bernabéu, A. W. Droxler, J. M. Webster, E. Gischler, M. Tiwari, T. Lado-Insua, A. L. Thomas, S. Morgan, L. Jovane, and U. Röhl, 2015, Mixed Carbonate–Siliciclastic Sedimentation Along the Great Barrier Reef Upper Slope: A Challenge To the Reciprocal Sedimentation Model: Journal of Sedimentary Research, v. 85, p. 1019-1036.

Harris, P. M., R. A. Garber, and M. E. Clark, 2000, Geologic framework for Korolev Field, Kazakhstan: A Carboniferous isolated carbonate platform, AAPG Annual Meeting Abstracts., New Orleans.

Harwood, G. M., and P. A. Towers, 1988, Seismic sedimentologic interpretation of a carbonate slope, north margin of Little Bahama Bank, *in* J. A. Austin, Jr., W. Schlager, and e. al, eds., Proceedings of the Ocean Drilling Program, Scientific results, Volume 101, v. Volume 101: College Station, Texas, Ocean Drilling Program, p. 263-277.

Hayes, J. M., H. Strauss, and A. J. Kaufman, 1999, The abundance of 13C in marine organic matter and isotopic fractionation in the global biogeochemical cycle of carbon during the past 800 Ma: Chemical Geology, v. 161, p. 103-125.

Hoffman, P. F., and G. P. Halverson, 2011, Chapter 36 Neoproterozoic glacial record in the Mackenzie Mountains, northern Canadian Cordillera: Geological Society, London, Memoirs, v. 36, p. 397-412.

Jacquin, T., A. Arnaud-Vanneau, H. Arnaud, C. Ravenne, and P. R. Vail, 1991, Systems tracts and depositional sequences in a carbonate setting: a study of continuous outcrops from platform to basin at the scale of seismic lines: Marine and Petroleum Geology, v. 8, p. 122-139.

James, N. P., G. M. Narbonne, and T. K. Kyser, 2001, Late Neoproterozoic cap carbonates: Mackenzie Mountains, northwestern Canada: precipitation and global glacial meltdown: Canadian Journal of Earth Sciences, v. 38, p. 1229-1262.

Jo, A., 2013, Carbonate slope morphology and sedimentary processes along Southwestern Great Bahama Bank: M.Sc. Thesis thesis, University of Miami, Florida, 102 p.

Jo, A., G. P. Eberli, and M. Grasmueck, 2014, Margin Collapse and Slope Failure along Southwestern Great Bahama Bank: Sedimentary Geology.

Jo, A., G. P. Eberli, and M. Grasmueck, 2015, Margin collapse and slope failure along southwestern Great Bahama Bank: Sedimentary Geology, v. 317, p. 43-52.

Johnston, D. T., F. A. Macdonald, B. C. Gill, P. F. Hoffman, and D. P. Schrag, 2012, Uncovering the Neoproterozoic carbon cycle: Nature, v. 483, p. 320-323.

Jones, B., and A. Desrochers, 1992, Shallow platform carbonates: Facies models; Response to Sea Level Change: Geological Association of Canada, p. 277-301.

Jorry, S. J., A. W. Droxler, and J. M. Francis, 2010, Deepwater carbonate deposition in response to re-flooding of carbonate bank and atoll-tops at glacial terminations: Quaternary Science Reviews, v. 29, p. 2010-2026.

Jorry, S. J., A. W. Droxler, G. Mallarino, G. R. Dickens, S. J. Bentley, L. Beaufort, L. C. Peterson, and B. N. Opdyke, 2008, Bundled turbidite deposition in the central Pandora Trough (Gulf of Papua) since Last Glacial Maximum: Linking sediment nature and accumulation to sea level fluctuations at millennial timescale: Journal of Geophysical Research: Earth Surface, v. 113, p. F01S19.

Kah, L. C., and A. H. Knoll, 1996, Microbenthic distribution of Proterozoic tidal flats: environmental and taphonomic considerations: Geology, v. 24, p. 79-82.

Kaufman, A. J., and A. H. Knoll, 1995, Neoproterozoic variations in the C-isotopic composition of seawater: stratigraphic and biogeochemical implications: Precambrian Research, v. 73, p. 27-49.

Kemp, D. B., and P. M. Sadler, 2014, Climatic and eustatic signals in a global compilation of shallow marine carbonate accumulation rates: Sedimentology, v. 61, p. 1286-1297.

Kendall, B. S., R. A. Creaser, G. M. Ross, and D. Selby, 2004, Constraints on the timing of Marinoan "Snowball Earth" glaciation by 187 Re–187Os dating of a Neoproterozoic, post-glacial black shale in Western Canada: Earth and Planetary Science Letters, v. 222, p. 729-740.

Kennedy, M., M. Droser, L. M. Mayer, D. Pevear, and D. Mrofka, 2006, Late Precambrian Oxygenation; Inception of the Clay Mineral Factory: Science, v. 311, p. 1446-1449.

Kennedy, M. J., B. Runnegar, A. R. Prave, K.-H. Hoffmann, and M. A. Arthur, 1998, Two or four Neoproterozoic glaciations?: Geology, v. 26, p. 1059-1063.

Khan, Z., 2012, Origin and architecture of deep-water levee deposits: Insight from the ancient rock record and experiments: PhD Thesis thesis, University of Ottawa, Ottawa, Ontario, 300 p.

Khan, Z. A., and R. W. C. Arnott, 2011, Stratal attributes and evolution of asymmetric inner- and outer-bend levee deposits associated with an ancient deep-water channel-levee complex within the Isaac Formation, southern Canada: Marine and Petroleum Geology, v. 28, p. 824-842.

Kim, W., B. W. Fouke, A. L. Petter, T. M. Quinn, C. Kerans, and F. Taylor, 2012, Sea-level rise, depth-dependent carbonate sedimentation and the paradox of drowned platforms: Sedimentology, v. 59, p. 1677-1694.

Knoll, A., J. Hayes, A. Kaufman, K. Swett, and I. Lambert, 1986, Secular variation in carbon isotope ratios from Upper Proterozoic successions of Svalbard and East Greenland.

Kolla, V., H. W. Posamentier, and L. J. Wood, 2007, Deep-water and fluvial sinuous channels-Characteristics, similarities and dissimilarities, and modes of formation: Marine and Petroleum Geology, v. 24, p. 388-405.

Kump, L. R., and M. A. Arthur, 1999, Interpreting carbon-isotope excursions: carbonates and organic matter: Chemical Geology, v. 161, p. 181-198.

Lehmann, D., C. E. Brett, R. Cole, and G. Baird, 1995, Distal sedimentation in a peripheral foreland basin: Ordovician black shales and associated flysch of the

western Taconic foreland, New York State and Ontario: Geological Society of America Bulletin, v. 107, p. 708-724.

Lenton, T. M., R. A. Boyle, S. W. Poulton, G. A. Shields-Zhou, and N. J. Butterfield, 2014, Co-evolution of eukaryotes and ocean oxygenation in the Neoproterozoic era: Nature Geosci, v. 7, p. 257-265.

Lowe, D. R., 1982, Sediment gravity flows: II. Depositional models with special reference to the deposits of high-density turbidity currents: Journal of Sedimentary Petrology, v. 52, p. 279-297.

Marais, D. J. D., H. Strauss, R. E. Summons, and J. M. Hayes, 1992, Carbon isotope evidence for the stepwise oxidation of the Proterozoic environment: Nature, v. 359, p. 605-609.

McHargue, T., M. J. Pyrcz, M. D. Sullivan, J. D. Clark, A. Fildani, B. W. Romans, J. A. Covault, M. Levy, H. W. Posamentier, and N. J. Drinkwater, 2011, Architecture of turbidite channel systems on the continental slope: Patterns and predictions: Marine and Petroleum Geology, v. 28, p. 728-743.

Miall, A. D., 1985, Architectural-element analysis: A new method of facies analysis applied to fluvial deposits: Earth-Science Reviews, v. 22, p. 261-308.

Miall, A. D., 1996, Methods of Architectural-Element Analysis. Sedimentary Facies, Basin Analysis, and Petroleum Geology, *in* A. D. Miall, ed., The Geology of Fluvial Deposits, Springer Berlin Heidelberg, p. 75-98.

Micallef, A., and J. J. Mountjoy, 2011, A topographic signature of a hydrodynamic origin for submarine gullies: Geology, v. 39, p. 115-118.

Mulder, T., E. Ducassou, G. P. Eberli, V. Hanquiez, E. Gonthier, P. Kindler, M. Principaud, F. Fournier, P. Léonide, I. Billeaud, B. Marsset, J. J. G. Reijmer, C. Bondu, R. Joussiaume, and M. Pakiades, 2012a, New insights into the morphology and sedimentary processes along the western slope of Great Bahama Bank: Geology, v. 40, p. 603-606.

Mulder, T., E. Ducassou, H. Gillet, V. Hanquiez, M. Principaud, L. Chabaud, G. P. Eberli, P. Kindler, I. Billeaud, E. Gonthier, F. Fournier, P. Léonide, and J. Borgomano, 2014, First Discovery of Channel–Levee Complexes In A Modern Deep-Water Carbonate Slope Environment: Journal of Sedimentary Research, v. 84, p. 1139-1146.

Mulder, T., E. Ducassou, H. Gillet, V. Hanquiez, E. Tournadour, J. Combes, G. P. Eberli, P. Kindler, E. Gonthier, G. Conesa, C. Robin, R. Sianipar, J. J. G. Reijmer, and A. François, 2012b, Canyon morphology on a modern carbonate slope of the Bahamas: Evidence of regional tectonic tilting: Geology.

Mullins, H. T., and H. E. Cook, 1986, Carbonate apron models: Alternatives to the submarine fan model for paleoenvironmental analysis and hydrocarbon exploration: Sedimentary Geology, v. 48, p. 37-79.

Mullins, H. T., K. C. Heath, H. M. Van Buren, and C. R. Newton, 1984, Anatomy of a modern open-ocean carbonate slope: northern Little Bahama Bank: Sedimentology, v. 31, p. 141-168.

Murphy, D. C., 1990, Stratigraphy and structure, southern Rocky Mountain Trench to the headwaters of the North Thompson River, Cariboo Mountains, British Columbia.: Current Research, v. Part E, Geological Survey of Canada, p. 71-80.

Mussa-Caleca, M., 2008, Architecture and depositional history of a Neoproterozoic deep-water slope channel complex in a passive margin setting: Isaac Formation, Windermere Supergroup, southern Canadian Cordillera.: M.Sc. Thesis thesis, University of Ottawa, Ottawa, Ontario.

Mutti, E., and W. R. Normark, 1987, Comparing examples of modern and ancient turbidite systems: problems and concepts, *in* J. K. Leggett, and G. G. Zuffa, eds., Marine clastic sedimentology: concepts and case studies: London, Graham and Troutman, p. 1-38.

Mutti, E., and W. R. Normark, 1991, An integrated approach to the study of turbidite systems, *in* P. Weimer, and M. H. Link, eds., Seismic facies and sedimentary processes of submarine fans and turbidite systems: New York, Springer-Verlag, p. 75-106.

Navarro, L., 2006, Depositional Architecture and Evolution of deep-water base-of-slope and slope channel complexes in a passive-margin setting: Isaac Formation, Windermere Supergroup (Neoproterozoic), Southern Canadian Cordillera: M.Sc.Thesis thesis, University of Ottawa, Ottawa, 272 p.

Navarro, L., Z. Khan, and R. W. C. Arnott, 2007, Depositional architecture and evolution of a deep-marine channel-levee complex: Isaac Formation (Windermere Supergroup), Southern Canadian Cordillera., *in* T. H. Nilsen, R. D. Shew, G. S. Steffens, and J. R. J. Studlik, eds., Atlas of Deep-water

Outcrops., v. CD-ROM: Tulsa, AAPG Studies in Geology 56, CD-ROM, p. 22.

Nilsen, T. H., R. D. Shew, G. S. Steffens, and J. R. J. Studlick, 2007, Atlas of Deep-Water Outcrops, American Association of Petroleum Geologists, 519 p.

O'Byrne, C. J., M. D. Barton, G. S. Steffens, C. Pirmez, and H. Buergisser, 2007, Architecture of a laterally migrating channel complex - Isaac Formation, Windermere Supergroup, British Columbia, Canada, *in* T. H. Nilsen, R. D. Shew, G. S. Steffens, and J. R. J. Studlick, eds., Atlas of deep-water outcrops, v. CD-ROM: Tulsa, AAPG, p. 11 p.

Payros, A., and V. Pujalte, 2008, Calciclastic submarine fans: An integrated overview: Earth-Science Reviews, v. 86, p. 203-246.

Payros, A., V. Pujalte, and X. Orue-Etxebarria, 2007, A point-sourced calciclastic submarine fan complex (Eocene Anotz Formation, western Pyrenees): facies architecture, evolution and controlling factors: Sedimentology, v. 54, p. 137-168.

Petrov, P. Y., 2001, Microbial Mats As a Source of Carbonate Sediments in the Late Precambrian: Evidence from the Linok Formation, the Middle Riphean of the Turukhansk Uplift, Siberia: Lithology and Mineral Resources, v. 36, p. 164-186.

Pettijohn, E. J., 1975, Sedimentary Rocks: New York, Harper & Row.

Pickering, K. T., R. Hiscott, and F. J. Hein, 1989, Deep-marine Environments: Clastic Sedimentation and Tectonics: London, Unwin Hyman.

Playton, T. E., X. Janson, and C. Kerans, 2011, Carbonate slopes and margins, *in* N. P. James, and R. W. Dalrymple, eds., Facies models 4, The Geological Association of Canada, p. 449-476.

Posamentier, H. W., and V. Kolla, 2003, Seismic geomorphology and stratigraphy of depositional elements in deep-water settings: Journal of Sedimentary Research, v. 73, p. 367–388.

Posamentier, H. W., and R. G. Walker, 2006, Deep-water turbidites and submarine fans: SEPM Special Publication, v. 84, p. 397–520.

Price, I., 1977, Deposition and derivation of clastic carbonates on a Mesozoic continental margin, Othris, Greece: Sedimentology, v. 24, p. 529-546.

Principaud, M., T. Mulder, H. Gillet, and J. Borgomano, 2015, Large-scale carbonate submarine mass-wasting along the northwestern slope of the Great Bahama Bank (Bahamas): Morphology, architecture, and mechanisms: Sedimentary Geology, v. 317, p. 27-42.

Principaud, M. l., T. Mulder, J. Borgomano, E. Ducassou, V. Hanquiez, H. Gillet, V. Marieu, and P. Sorriaux, 2013, Carbonate slope gully system on the Westside Great Bahama Bank: EGU General Assembly 2013.

Puga-Bernabéu, Á., J. M. Webster, R. J. Beaman, and V. Guilbaud, 2011, Morphology and controls on the evolution of a mixed carbonate–siliciclastic submarine canyon system, Great Barrier Reef margin, north-eastern Australia: Marine Geology, v. 289, p. 100-116.

Puga-Bernabéu, Á., J. M. Webster, R. J. Beaman, and V. Guilbaud, 2013, Variation in canyon morphology on the Great Barrier Reef margin, north-eastern Australia: The influence of slope and barrier reefs: Geomorphology, v. 191, p. 35-50.

Rankey, E. C., and D. F. Doolittle, 2012, Geomorphology of carbonate platform-marginal uppermost slopes: Insights from a Holocene analogue, Little Bahama Bank, Bahamas: Sedimentology, v. 59, p. 2146-2171.

Reijmer, J. G., P. Palmieri, and R. Groen, 2012a, Compositional variations in calciturbidites and calcidebrites in response to sea-level fluctuations (Exuma Sound, Bahamas): Facies, v. 58, p. 493-507.

Reijmer, J. J. G., 1998, Compositional variations during phases of progradation and retrogradation of a Triassic carbonate platform (Picco di Vallandro/Dürrenstein, dolomites, Italy): Geologische Rundschau, v. 87, p. 436-448.

Reijmer, J. J. G., P. Palmieri, and R. Groen, 2012b, Compositional variations in calciturbidites and calcidebrites in response to sea-level fluctuations (Exuma Sound, Bahamas): Facies, v. 58, p. 493–507.

Reijmer, J. J. G., P. Palmieri, R. Groen, and M. Floquet, 2015, Calciturbidites and calcidebrites: Sea-level variations or tectonic processes?: Sedimentary Geology, v. 317, p. 53-70.

Riding, R., 2006, Cyanobacterial calcification, carbon dioxide concentrating mechanisms, and Proterozoic–Cambrian changes in atmospheric composition: Geobiology, v. 4, p. 299-316.

Riding, R., 2011, Calcified cyanobacteria, Encyclopedia of Geobiology, Springer, p. 211-223.

Ross, G. M., 1991, Tectonic setting of the Windermere Supergroup revisited: Geology, v. 19, p. 1125-1128.

Ross, G. M., 2003, Slope Carbonate deposition in the Neoproterozoic Windermere turbidite system (Western Canada) significance in basin analysis, Slope Conference, Submarine Slope Systems: processes, products and predictions. Abstracts.: Liverpool, p. 71.

Ross, G. M., and R. W. C. Arnott, 2007, Regional geology of the Windermere Supergroup, southern Canadian Cordillera and stratigraphic setting of the Castle Creek study area, Canada, *in* T. H. Nilsen, R. D. Shew, G. S. Steffens, and J. R. J. Studlick, eds., Atlas of deep-water outcrops, v. 56, AAPG Studies in Geology, CD-ROM, p. 16.

Ross, G. M., J. D. Bloch, and H. R. Krouse, 1995, Neoproterozoic strata of the southern Canada Cordillera and the isotopic evolution of seawater sulfate: Precambriam Research, v. 73, p. 71-99.

Ross, G. M., and D. C. Murphy, 1988, Transgressive stratigraphy, anoxia, and regional correlations within the late Precambrian Windermere grit of the southern Canadian Cordillera: Geology, v. 16, p. 139-143.

Ross, W. C., B. A. Halliwell, J. A. May, D. E. Watts, and J. P. M. Syvitski, 1994, Slope readjustment: A new model for the development of submarine fans and aprons: Geology, v. 22, p. 511-514.

Rothman, D. H., J. M. Hayes, and R. E. Summons, 2003, Dynamics of the Neoproterozoic carbon cycle: Proceedings of the National Academy of Sciences, v. 100, p. 8124-8129.

Rusciadelli, G., B. D'Argenio, S. Di Simone, V. Ferreri, A. Randisi, and C. Ricci, 2009, Carbonate-platform production and export potential recorded in upper Jurassic base-of-slope deposits (Central Apennines, Italy): External Controls on Deep-Water Depositional Systems, p. 279-301.

Sadler, P. M., 1981, Sediment Accumulation Rates and the Completeness of Stratigraphic Sections: The Journal of Geology, v. 89, p. 569-584.

Savary, B., and S. Ferry, 2004, Geometry and petrophysical parameters of a calcarenitic turbidite lobe (Barremian-Aptian, Pas-de-la-Cluse, France): Sedimentary Geology, v. 168, p. 281-304.

Schlager, W., 2005, Carbonate Sedimentology and Sequence Stratigraphy, SEPM Society for Sedimentary Geology, 169 p.

Schlager, W., and O. Camber, 1986, Submarine slope angles, drowning unconformities, and self-erosion of limestone escarpments: Geology, v. 14, p. 762-765.

Schlager, W., and A. Chermak, 1979, Modern sediment facies of platform-basin transition, Tongue of the Ocean, Bahamas, *in* L. A. Doyle, and O. H. Pilkey, eds., Geology of Continental slopes, v. 27, SEPM Spec. Publ., p. 193-208.

Schlager, W., and R. N. Ginsburg, 1981, Bahama carbonate platforms -the deep and the past., *in* M. B. Cita, and W. B. F. Ryan, eds., Carbonate Platforms of the Passive-Type Continental Margins, Present and Past., v. 44: Mar. Geol., p. 1-24.

Schlager, W., J. J. G. Reijmer, and A. Droxler, 1994, Highstand Shedding of Carbonate Platforms: Journal of Sedimentary Research, Section B: Stratigraphy and Global Studies, v. Vol. 64B, p. 270-281.

Schwarz, E., and R. W. C. Arnott, 2007, Anatomy and evolution of a slope channel-complex set (Neoproterozoic Isaac Formation, Windermere Supergroup, southern Canadian Cordillera); implications for reservoir characterization: Journal of Sedimentary Research, v. 77, p. 89-109.

Sherman, A. G., 2000, Sedimentology of a late Mesoproterozoic muddy carbonate ramp, northern Baffin Island, Arctic Canada.

Shields, G., and J. Veizer, 2002, Precambrian marine carbonate isotope database: Version 1.1: Geochemistry, Geophysics, Geosystems, v. 3, p. 1 of 12-12 of 12.

Shields, G. A., 2005, Neoproterozoic cap carbonates: a critical appraisal of existing models and the plumeworld hypothesis: Terra Nova, v. 17, p. 299-310.

Smith, M. D., 2009, Stratigraphic and Geochemical Evolution of the Old Fort Point Formation, Southern Canadian Cordillera: The deep-marine perspective of Ediacaran Post-Glacial Environmental Change: PhD Thesis thesis, University of Ottawa, Ottawa, 430 p.

Spinelli, G. A., and M. E. Field, 2001, Evolution of continental slope gullies on the northern California margin: Journal of Sedimentary Research, v. 71, p. 237-245.

Swanson-Hysell, N. L., C. V. Rose, C. C. Calmet, G. P. Halverson, M. T. Hurtgen, and A. C. Maloof, 2010, Cryogenian Glaciation and the Onset of Carbon-Isotope Decoupling: Science, v. 328, p. 608-611.

Sylvester, Z., C. Pirmez, and A. Cantelli, 2011, A model of submarine channel-levee evolution based on channel trajectories: Implications for stratigraphic architecture: Marine and Petroleum Geology, v. 28, p. 716-727.

Tcherepanov, E. N., A. W. Droxler, P. Lapointe, G. R. Dickens, S. J. Bentley, L. Beaufort, L. C. Peterson, J. Daniell, and B. N. Opdyke, 2008, Neogene evolution of the mixed carbonate-siliciclastic system in the Gulf of Papua, Papua New Guinea: Journal of Geophysical Research: Earth Surface, v. 113, p. F01S21.

Tcherepanov, E. N., A. W. Droxler, P. Lapointe, K. Mohn, and O. A. Larsen, 2010, Siliciclastic influx and burial of the Cenozoic carbonate system in the Gulf of Papua: Marine and Petroleum Geology, v. 27, p. 533-554.

Tournadour, E., T. Mulder, J. Borgomano, V. Hanquiez, E. Ducassou, and H. Gillet, 2015, Origin and architecture of a Mass Transport Complex on the northwest slope of Little Bahama Bank (Bahamas): Relations between off-bank transport, bottom current sedimentation and submarine landslides: Sedimentary Geology, v. 317, p. 9-26.

van Der Kooij, B., A. Immenhauser, T. Steuber, J. R. Bahamonde Rionda, and O. MerÍNo TomÉ, 2010, Controlling factors of volumetrically important marine carbonate cementation in deep slope settings: Sedimentology, v. 57, p. 1491-1525.

van Konijnenburg, J.-H., 1999, Stratigraphic architecture of a Lower Cretaceous-Lower Tertiary carbonate base-of-slope succession: Gran Sasso d'Italia (central Apennines, Italy), *in* P. M. Harris, A. H. Saller, and J. A. Simo, eds.,

Advances in Carbonate Sequence Stratigraphy: Application to Reservoirs, Outcrops and Models., v. 63: SEPM Spec. Publ., p. 291-315.

Vigorito, M., M. Murru, and L. Simone, 2005, Anatomy of a submarine channel system and related fan in a foramol/rhodalgal carbonate sedimentary setting: a case history from the Miocene syn-rift Sardinia Basin, Italy: Sedimentary Geology, v. 174, p. 1-30.

Vigorito, M., M. Murru, and L. Simone, 2006, Architectural patterns in a multistorey mixed carbonate–siliciclastic submarine channel, Porto Torres Basin, Miocene, Sardinia, Italy: Sedimentary Geology, v. 186, p. 213-236.

Wallace, M. W., G. R. Holdgate, J. Daniels, S. J. Gallagher, and A. Smith, 2002, Sonic velocity, submarine canyons, and burial diagenesis in oligocene-holocene cool-water carbonates, gippsland basin, southeast australia: AAPG bulletin, v. 86, p. 1593-1607.

Watts, K. F., 1988, Triassic carbonate submarine fans along the Arabian platform margin, Sumeini Group, Oman: Sedimentology, v. 35, p. 43-71.

Weber, L. J., B. P. Francis, P. M. Harris, and M. E. Clark, 2003, Stratigraphy, lithofacies,and reservoir distribution; Tengiz Field, Kazakhstan., AAPG Annual Meeting Abstracts, Salt Lake City, Utah.

Webster, J. M., R. J. Beaman, Á. Puga-Bernabéu, D. Ludman, W. Renema, R. A. J. Wust, N. P. J. George, P. J. Reimer, G. E. Jacobsen, and P. Moss, 2012, Late Pleistocene history of turbidite sedimentation in a submarine canyon off the northern Great Barrier Reef, Australia: Palaeogeography, Palaeoclimatology, Palaeoecology, v. 331-332, p. 75-89.

Webster, J. M., L. Wallace, E. Silver, B. Applegate, D. Potts, J. C. Braga, K. Riker-Coleman, and C. Gallup, 2004, Drowned carbonate platforms in the Huon Gulf, Papua New Guinea: Geochemistry, Geophysics, Geosystems, v. 5.

Wilson, P. A., and H. H. Roberts, 1992, Carbonate-periplatform sedimentation by density flows: a mechanism for rapid off-bank and vertical transport of shallow-water fines: Geology, v. 20, p. 713-716.

Wilson, P. A., and H. H. Roberts, 1995, Density cascading: off-shelf sediment transport, evidence and implications, Bahama Banks: Journal of Sedimentary Research, v. 65.

Wright, V. P., and R. Wilson, 1984, A carbonate submarine-fan sequence from the Jurassic of Portugal: Journal of Sedimentary Research, v. 54, p. 394-412.

Zuffa, G. G., 1980, Hybrid arenites: their composition and classification.: Journal of Sedimentary Petrology, v. 50, p. 21-29.

Chapter 6

CONCLUSIONS

6.1 Thesis Summary

Strata in the study area record the conformable change from the sheetlike basin floor strata of the upper Kaza Group (UKG) to leveed channel complexes in the Isaac Formation (IF), lower Cariboo Group. The occurrence and areal distribution of individual stratal elements (dm up to several meters in vertical scale) that make up the Kaza-Isaac transition, or simply KIT, and overlying IF were likely controlled by autogenic processes, whereas large-scale changes (several Dm to Hm in vertical scale) including key changes in mineralogy and stratal element stacking patterns are interpreted to be related to major changes in sediment supply, most probably linked to long-term (3^{rd} order) changes of relative sea level. The sequential development of the KIT and overlying IF is summarized next and illustrated in Fig. 6.1:

(i) Decameter-thick, laterally-extensive, fine-grained strata at the base of the study area (see base of lower KIT in chapter 3) recorded a protracted episode of slow, quiescent sedimentation with reduced sand input. Deposition was interrupted by the emplacement of a Dm-thick, areally-extensive, matrix-rich debrite related to a major mass-wasting event. Both fine-grained and debris-flow deposits are interpreted to be developed during highstand conditions when coarse-grained siliciclastic sediment was preferentially retained in continental and marginal marine environments and mostly mud-prone sediments delivered to the basin.

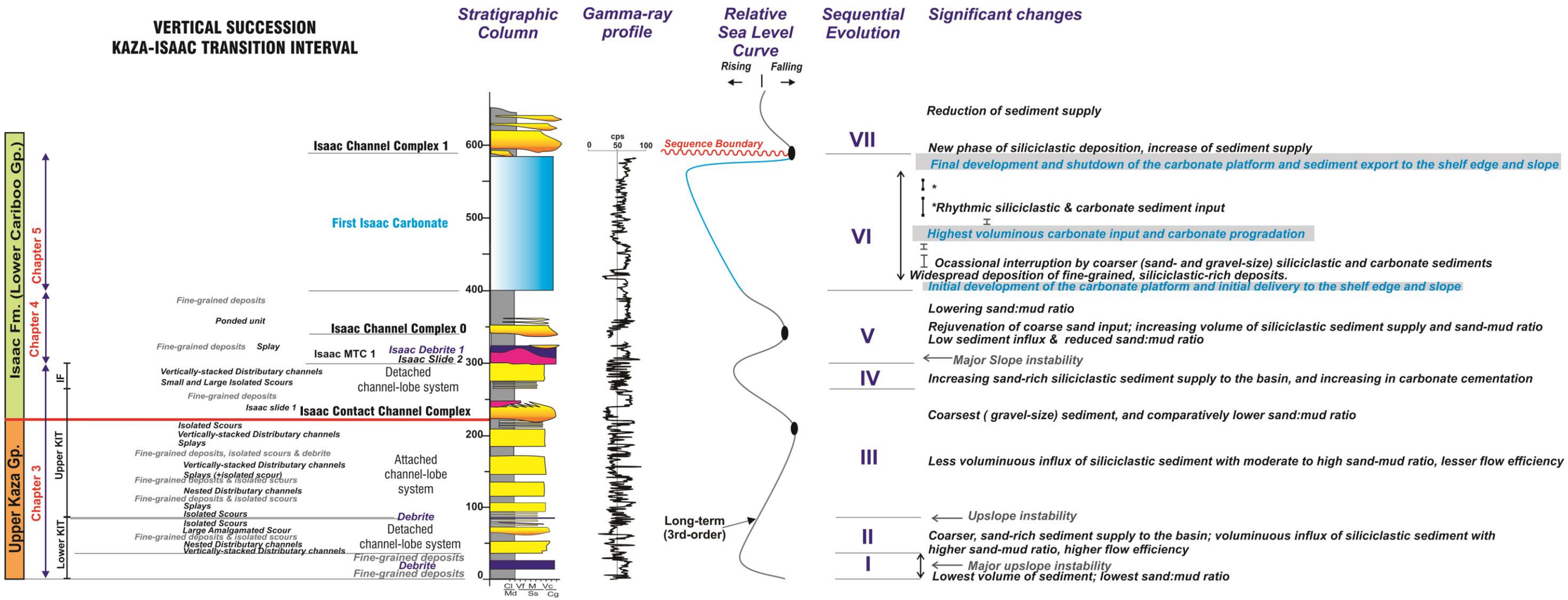

Figure 6.1. Generalized log of studied deep-water sequence between the Upper Kaza Group and the Isaac Formation. This sequence recorded major variations in sediment source (linked to mineralogical composition) and supply (sediment volume and size), which are intrinsically related to long-term changes in relative sea level. These variations controlled the overall sedimentation style and pattern in the system. See text for detailed explanation.

(ii) During the subsequent fall of relative sea level, coarse-grained sand-rich sediment became increasingly supplied to the system, and formed a detached channel-lobe system consisting of rare large amalgamated and small isolated scours, which are dispersed within a well-developed channel-lobe transition zone or CLTZ (i.e. broad intermediate area between upstream slope channel and downstream proximal lobes), and overlain distributary channel-dominated lobe (see lower KIT in chapter 3). This succession is then sharply overlain by a laterally-continuous, matrix-rich debrite that may locally caused a reduction in the abruptness of the base-of-slope break.

(iii) Following the emplacement of the debrite, incoming flows became significantly more sand-rich, and hence had lower transport efficiency. This related in the formation of an attached channel-lobe system, wherein the proximal lobes were welded to a poorly-developed or absent CLTZ. Here, small isolated scours locally dissecting distributary channels, fine-grained deposits and/or uncommon splays (see upper KIT in chapter 3). This is interpreted to take place during the latter stages of falling relative sea level and the subsequent lowstand.

Sharply incising the attached channel-lobe system in the first slope levee-channel complex in the Isaac Formation - Isaac Contact Channel Complex or ICCC (see top of upper KIT in chapter 3). Significantly, the ICCC consists of upper coarse- and very coarse-grained sandstone with common fine gravel clasts, which contrast the more typical upper medium- to lower coarse-grained sandstone that makes up most of the coarse-grained strata in the UKG and IF. Also, unlike most channel fills in the IF, which are aggradationally filled, ICCC exhibits well developed lateral accretion deposits related to extensive lateral channel migration. The stark change in grain size and channel-migration behaviour is interpreted to be a consequence of conditions related to a rise of relative sea level. Specifically, transgression resulted in the selective removal (and landward transport) of medium and fine sand from the local sediment supply, leaving a residuum of coarse-grained mixed with easily

transported fine-grained detritus. It is this unique sediment supply, one enriched in fine- and coarse-grained sediment that resulted in the development of laterally-accreting slope leveed channel complex ICCC. Locally, a minor slide incised the channel complex. Eventually, coarse-grained siliciclastic input became depleted and deposition of thin-bedded, fine-grained turbidites dominated.

(iv) The continued rise of relative sea level and the eventual onset of highstand conditions were marked by the activation of a shallow-water carbonate platform, and accordingly the development of a mixed siliciclastic carbonate system. At this time, a detached channel-lobe system comprising numerous small and a rare large isolated scours overlain by distributary channels developed and was sourced with a mixture of siliciclastic and previously-formed carbonate sediments (see LIF in chapter 3). The re-initiation of a well-developed CLTZ region might be a consequence of early submarine carbonate cementation, which in turn steepened the continental slope break, and accordingly increased flow efficiency.

(v) During the subsequent fall of relative sea level and the demise of the shallow-water carbonate factory and return to siliciclastic sediment, the now oversteepened continental slope underwent a period of widespread mass wasting and deposition of mass-transport complex Isaac MTC 1, including slide and debris flow deposits (see Isaac Slide 2 and Isaac debrite 1, chapter 4). The gradual return of gravitational stability on the slope and the healing of seafloor topography along the top of Isaac MTC 1 was marked by widespread deposition of thin-bedded, fine-grained turbidites (see chapter 4), except for localized areas where some sand-rich parts of turbidity currents became preferentially routed and deposited to form a sandstone-rich splay (see chapter 4).

With the establishment of lowstand conditions, and the reactivation of the sand-rich hinterland sediment source directly into the deep marine, Isaac channel complex 0 (ICC0)

was formed (see chapter 4). ICC0 is capped by the ponded unit (see chapter 4), which is interpreted to be associated with partial flow confinement related to topography formed by an unexposed mass-transport deposit. The whole succession is then buried by a thick draped of fine-grained turbidites (see chapter 4).

(vi) The preceding events mark the beginning of a long-term (3^{rd}-order) eustatic rise that culminated in the development of the first Isaac carbonate or FIC (see chapter 5). At the small-scale, key stratal architecture and sediment composition of resedimented deposits of the FIC also indicate variations in the sediment production and export from a coeval carbonate platform system to a mixed slope system, but influenced by short-term (possibly 4^{th}- or 5^{th}-order).

(vii) The top of the FIC is then erosively overlain by Isaac slope channel complex 1 or ICC1. ICC1 indicates the termination of carbonate production during a major lowstand, and the return of voluminous siliciclastic deposition onto the Laurentian continental slope and further basinward.

6.2 Thesis Conclusions and Contributions

The word transition comes from the Latin transitio or transitus, which means “go across or cross over”, and symbolically summarizes the essence of this work. Submarine channel systems and related fans are ubiquitous geomorphic features on continental margins and basin-floor areas respectively, and represent significant repositories of clastic sediments that in some cases contain important hydrocarbon reserves. Over the past decades, they have been intensively studied in both modern and ancient systems. However, significantly less attention has been paid to the slope to basin floor transition, and as a result many important issues remain unresolved. This dissertation, therefore, is a detailed descriptive account of

strata that between the sheetlike basin-floor strata of the Neoproterozoic UKG and leveed channel deposits of the IF at Castle Creek and Mount Quanstrom. At Castle Creek, which is the principal study area, the stratigraphic succession is well exposed over an area of 600 m thick by >1200 m wide; it is here that strata were described in bed-by-bed detail and correlated laterally.

Chapter 3, therefore, is a detailed description of the lithological make-up of the slope-basin floor transition, or what commonly is termed the channel-lobe transition zone (CLTZ). Unlike previously-deposited basin-floor deposits of the upper Kaza Group and leveed-channel strata in the overlying Isaac Formation, the studied interval between the Kaza-Isaac transition and lowermost Isaac Formation comprises a uniquely heterogeneous assemblage of stratal elements that include small- and large-scale scours, nested and vertical-stacked distributary channels, splays, erosional feeder channel, leveed channel complex, fine-grained sheets, mass-transport deposits, crevasse splays and hydraulic-jump unit bars. Of particular note is the unique occurrence of scours that range from centimeter- to kilometer-scale and nested distributary channels. The distribution and arrangement of these and the other stratal elements are interpreted to form two end-member depositional systems: detached and attached channel-lobe systems. Detached and attached channel-lobe systems are those with a well-developed (bypass-dominated) CLTZ, which typically consists of small scours and rare large scours that incised into mudstone-rich deposits and are disconnected from adjacent distributary channel-dominated proximal lobes. Attached channel-lobe systems, on the other hand, are characterized by a poorly-developed or absent (deposition-dominated) CLTZ and builds up a unit that is thicker (almost >2X times), more sandstone rich, and more architecturally diverse than in detached systems. Specially, it includes numerous small scours intercalated within a thick package of proximal basin-floor elements consisting mostly distributary channels and fine-grained turbidites, and less common splay deposits and rare

erosional and leveed channel. The vertical and lateral stacking of these systems then forms the basis of a discussion of the temporal and spatial evolution of an ancient CLTZ and how changes in sediment supply, likely caused by changes of relative sea level, but also basin physiography, controlled its development.

Chapter 4 is a detailed description of a succession of the lower Isaac Formation. This succession, which includes a km-scale, mass-transport complex Isaac MTC 1 (including slide and debris-flow deposits), sandstone-rich channel fill and fine-grained deposits, marks the transition from siliciclastic-dominated to mixed- and then carbonate-dominated deposition in the Isaac lower slope system. The general distribution of lithofacies and stratal elements allows establishing of a depositional continuum that is interpreted to be controlled by variations in sediment supply, caliber and composition in response of major changes of relative sea level.

Chapter 5 documents the lithological make-up and stratigraphic architecture of the first Isaac carbonate (FIC), which is an important regional marker within the siliciclastic-dominated Windermere turbidite system. The FIC is a unique Neoproterozoic succession of mixed carbonate-siliciclastic slope deposits that consists of three distinct calciturbidites units separated by siliciclastic- and/or mixed-rich channel deposits, siliciclastic- and carbonate-rich gully deposits, and siliciclastic-rich fine-grained deposits. At the large- and small-scale, abrupt changes in facies, grain composition and architectural styles in the FIC are interpreted to be consequence of long- and short-term changes in relative sea level that controlled episodes of carbonate production and export of carbonate into an otherwise siliciclastic dominated sedimentary system. Additionally, temporal changes in the gradient of the continental slope and possibly also climate could have also temporarily influenced sediment transport processes and ultimately the depositional record.

6.3 Recommendations for Future Research

This investigation is the first to study, at least in bed-by-bed detail, the lithological make up and related depositional processes that moulded the stratigraphic pile between the slope and basin floor deposits in the Windermere turbidite system. During the course of that work, a number of new areas for future research were identified:

Chapter 3

- A detailed documentation and comparison of matrix-rich sandstone strata associated to different stratal elements (i.e. scours, avulsion splays and distributary channels) would be useful.
- In addition to the data presented here, a more detailed characterization of the laterally-continuous horizons mantled with discontinuous bar deposits would provide much needed insight into these enigmatic structures. One possible origin for these dune-like bedforms might include stationary hydraulic jumps associated with submarine cyclic steps. Particularly interest is explaining how and why.

Chapter 4

- This thesis documents km-scale, mass-transport complex Isaac MTC 1 that comprises two stacked mass wasting deposits: Isaac slide 1 and Isaac debrite 1. Observations in this study recognized a wide variety of internal shear surfaces and deformation structures within the slide. A more in-depth structural analysis of the slide blocks could help differentiate primary from secondary (i.e. tectonic) deformation structures and therein provide a better insight into the internal kinematic indicators of block displacement within the slide movement.
- Detailed investigation of the lateral and vertical changes in the lithology and petrography above Isaac channel complex 0 should be conducted. The objective of

that study would be to determine the origin of these diffusely-graded sandstone and mudstone beds, and their apparent repetitive vertical and lateral trends. Such study would require a combined sedimentological and statistical analysis that addresses changes in features, like: bed thickness, bed type, net-to-gross, grain size, proportion and thickness ratio of sandstone/siltstone to mud caps, siltstone vs. mudstone content, etc. Specifically, are these strata the result of a single or multiple turbidity currents, and is the apparent systematic stacking of these strata a consequence of an evolving current, or a succession of separate transport events. Also, why are these strata diffusely graded, and why are they only locally developed?

Chapter 5

- Despite the considerable advance made in this thesis by describing the general stratigraphic framework of facies and stratal units that comprises the FIC, a number of unresolved issues remain, including (i) the origin of the characteristic carbonate cement-poor and carbonate cement-rich, which, respectively are the light and dark layers in the Bacon sandstone channel-fill strata, and (ii) the physical and chemical origin of the tripartite lithologies that make up gully complexes. Could these repetitively stacked units be actually linked to short-term "cyclical" changes in the composition of sediment being made available in the sedimentary staging area – Milankovitch cycles?
- An in-depth study focusing on the microfacies and isotope geochemistry of carbonate rocks within the FIC, and in calciturbidite units 1, 2 and 3, is indispensable. Carbon isotopes, for instance, could help provide important data for

constructing a $\delta^{13}C$ chemostratigraphy framework for deep-water strata of the Windermere Supergroup, but more profoundly aid in the reconstruction of seawater composition and its relationship and implications for late Neoproterozoic glaciation, and possibly also the rise of metazoan life.

APPENDICES

APPENDIX A: Samples

SUPPLEMENTAL ELECTRONIC MATERIAL

Appendix A comprises the tabulated data from both Castle Creek and Mount Quanstrom study areas. These data include GPS points, grain size, interpreted facies and weathering colour. This appendix also includes an aerial photograph showing location of most samples in Castle Creek South.

File name	Description
A1_Samples_DATA.PDF	Spreadsheets
A2_Samples_plotted_aerialphoto_CCSouth.PDF	Airphoto documenting location of samples in Castle Creek South

APPENDIX B: Castle Creek field data

SUPPLEMENTAL ELECTRONIC MATERIAL

Appendix B includes aerial photographs showing location of measured stratigraphic logs in the Castle Creek study area. Additionally, tabulated data of paleocurrent measurements are provided.

File name	Description
B1_LowerKIT_measured_sections.PDF	Aerial photograph documenting location of stratigraphic logs (chapter 3)
B2_UpperKIT_UKG_measured_sections.PDF	Aerial photograph documenting location of stratigraphic logs (chapter 3)
B3_UpperKIT_ICCC-LIF_measured_sections.PDF	Aerial photograph documenting location of stratigraphic logs (chapter 3)
B4_ IsaacMTC1_&_ICC0_measured_sections.PDF	Aerial photograph documenting location of stratigraphic logs (chapter 4)
B5_ FIC_measured_sections.PDF	Aerial photograph documenting location of stratigraphic logs (chapter 5)
B6_Paleocurrents.PDF	Spreadsheet

APPENDIX C: Petrography

SUPPLEMENTAL ELECTRONIC MATERIAL

Appendix C includes textural, compositional and microstructural analysis of thin-section samples of mudstone, sandstone, conglomerate and carbonate from the both study area. For sample location see Appendix A. Visual estimates of mineral abundances and constituents were made using the charts of Terry and Chilingar (1955) and Scholle and Ulmer-Scholle (2003). Cathodoluminescence (CL) petrography conducted for some selected samples are also provided.

File name	Description
C1_Petrography_DATA.PDF	Spreadsheets
C2_Carbonate_Cement_Phases_FIC.PDF	Spreadsheets documenting multiple generation of carbonate cements identified in the carbonate rocks of the First Isaac Carbonate, including general petrographic characteristics and cathodoluminescence patterns
C3_Photomicrographs.PDF	Collection of photomicrographs from thin section petrography and cathodoluminescence petrography

APPENDIX D: Geochemistry

SUPPLEMENTAL ELECTRONIC MATERIAL

Appendix D comprises the complete geochemical results of fine-grained meta-sedimentary rocks from the Castle Creek and Mount Quanstrom study areas. These data include average concentration, range (maximum and minimum) and standard deviation values for major, selected trace and rare-earth elements of the Upper Kaza Group (UKG) and Isaac Formation (IF) from analyzed samples. Pearson correlation coefficient (r) was calculated to test the quality of linearity between different elements and identify correlations of high statistical significance. Geochemical graphs through the Kaza-Isaac stratal interval are provided. Additionally, TOC content is also included. For Sample location, see Appendix B.

File name	Description
D1_Geochemistry_CastleCreek_DATA.PDF	Spreadsheets
D2_Geochemistry_MountQuanstrom_DATA.PDF	Spreadsheets
D3_Geochemistry_Correlation_Coefficients.PDF	Spreadsheets
D4_Geochemistry_Graphics.PDF	Graphs showing major and minor elements in the UKG and IF. Graph showing phosphate content of phosphatic beds vs. mudstone in the UKG.
D5_TOC_DATA.PDF	Spreadsheets

APPENDIX E: Carbonate Isotope data

SUPPLEMENTAL ELECTRONIC MATERIAL

Appendix E includes the tabulated data of the stable isotope results of ^{18}O and ^{13}C from samples of the First Isaac carbonate in the Castle Creek study area (compared to PBD standard). Samples are from unpublished data by G. M. Ross

File name	Description
E_Carbonate_isotope_FIC_DATA.PDF	Spreadsheet

APPENDIX F: Gamma Rays

SUPPLEMENTAL ELECTRONIC MATERIAL

Appendix F contains high-resolution spectral gamma-ray profiles taken along stratigraphic sections at the Castle Creek outcrops using a portable gamma-ray scintillometer. Measurements were taken every 75 cm.

File name	Description
F_GammaRayProfiles_DATA.PDF	Spreadsheets

APPENDIX G: Mount Quanstrom field data

SUPPLEMENTAL ELECTRONIC MATERIAL

Appendix G comprises the field data obtained from the Mount Quanstrom study area. These data include uninterpreted and interpreted aerial photographs, measured stratigraphic sections, and correlation panels.

File name	Description
G1_Quanstrom_KIT&LIF_Airphotomosaic.PDF	Uninterpreted and interpreted airphoto mosaic documenting stratal architecture between the KIT and LIF (equivalent to chapter 3).
G2_Quanstrom_ KIT&LIF_Correlation.PDF	Drafted sections and correlation panel (equivalent to chapter 3).
G3_Quanstrom_ IsaacSlideQ1&LIF_Aerial_photograph.PDF	Uninterpreted and interpreted aerial photographs documenting stratal architecture of Isaac Slide Q1 and overlying elements (equivalent to chapter 4).
G4_Quanstrom_ IsaacSlideQ1&overlying_elements_Log.PDF	Stratigraphic log-base (equivalent to chapter 4)
G5_Quanstrom_ IsaacDebriteQ1&overlying_elements _Log.PDF	Stratigraphic log-top (equivalent to chapter 4)

References

Scholle, P. A., and D. S. Ulmer-Scholle, 2003, A Color Guide to the Petrography of Carbonate Rocks: Grains, Textures, Porosity, Diagenesis, AAPG Memoir 77, v. 77, AAPG.

Terry, R., and G. Chilingar, 1955, Comparison charts for visual estimation of percentage composition: Journal of Sediment Petrology, v. 25, p. 229-234.

Appendix A: Sample database

Table A.1. Sample location taken and examined from Castle Creek study area, Cariboo Mountains, British Columbia

Note: UTM coordinates in grid system NAD27. UTM Zone is 10U

Stratigraphic Unit	Sample #	Elevation (m)	Easting	Northing	Grain Size	Turbidite Facies	Weathering colour
UKG	KI-1	1883	0672223	5881330	medium sand	Tb	Green with reddish/brownish
UKG	KI-2	1881	0672217	5881338	silt	Td, structureless	Green
UKG	KI-3	1885	0672216	5881334	coarse Lower sand	Ta	Green
UKG	KI-4	1885	0672209	5881336	silt	Td, laminated	Brown
UKG	KI-5	1885	0672192	5881337	medium Upper-coarse Lower sand	Tc, dune	Brown
UKG	KI-6	1886	0672196	5881333	silt	Td, laminated	Green
UKG	KI-7	1876	0672169	5881368	silt	Td (laminated + structureless)	Brown & Green
UKG	KI-8	1888	0672197	5881320	very coarse Upper sand	Ta	Green
UKG	KI-9	1887	0672170	5881342	coarse Lower sand	Tb	Pinkish-Green
UKG	KI-10	1887	0672207	5881279	medium Upper sand	Tb, base	Green
UKG	KI-11	1887	0672208	5881280	medium Lower-fine Upper sand	Tb, top	Green
UKG	KI-12	1889	0672175	5881332	medium Upper-coarse Lower sand	Tb	Reddish/Brownish
UKG	KI-13	1885	0672185	5881291	very coarse Upper sand	Mudstone-clast breccia	Green
UKG	KI-14	1894-1893	0672168	5881280	silt	Td, laminated	Light/dark brown
UKG	KI-15	1894	0672127	5881317	coarse Upper-very coarse Lower sand	Ta	Green
UKG	KI-16	1891	0672123	5881324	medium Lower sand	Ta	Brown
UKG	KI-17	1891	0672123	5881321	coarse Upper sand	Ta, base	Brown
UKG	KI-18	1898	0672184	5881238	medium Upper sand	Ta, top	Green
UKG	KI-19	1905	0672173	5881241	coarse Upper sand	Ta	Green
UKG	KI-20	1901	0672161	5881250	coarse Upper sand	Tb	Brown
UKG	KI-21	1892	0672155	5881251	silt	Td	Green
UKG	KI-22	1898	0672163	5881243	very coarse sand	Ta	Brown
UKG	KI-23	1902	0672155	5881240	coarse Lower sand	Ta	Brown
IF	KI-24	1902	0672144	5881220	pebble conglomerate	Ta	Pink

IF	KI-25	2264	0672338	5881356	medium Upper-coarse Lower sand	Tb	White, Pink
IF	KI-26	1971	0672178	5881314	coarse Upper sand	Ta	Green
IF	KI-27	1897	0672077	5881269	medium Lower sand	Tb	Brown
IF	KI-28	1897	0672077	5881273	fine sand	Tcd (Tc=ripples)	Brown
IF	KI-29	1897	0672057	5881315	silt	Td, laminated	Green
IF	KI-30	1887	0672061	5881292	silt	Td, laminated	Gray
IF	KI-31	1893	0672077	5881256	silt	Td, laminated	Gray
IF	KI-32	1896	0672085	5881255	silt	Td	Green
IF	KI-33	1896	0672115	5881196	silt/ very fine sand	Td	Orange
IF	KI-34	1894	0672038	5881293	pebble conglomerate	Ta	Orange
UKG	KI-35	1879	0672173	5881400	coarse Lower sand	Ta, base	Green
	KI-36	2204	0674208	5882061	medium Upper sand	Ta, heavily carbonate cemented	Brown
	KI-37	2209	0674170	5882055	silt	Td	
	KI-38	2208	0674219	5882070	silt	Td	
	KI-39	2204	0674209	5882113	silt/ very fine sand	Tcde	
	KI-40	2234	0674245	5882038	very coarse Upper sand	Ta	
IF	KI-41	1196	0672439	5880965	conglomerate	Ta	Brown
IF	KI-42	1900	0672146	5881215	medium Upper sand	Tb	Green
IF	KI-43	1898	0672137	5881207	medium Upper sand	Ta	Green
IF	KI-44	1909	0672104	5881185	medium Upper sand	Ta, base	Brown
IF	KI-45	1909	0672104	5881185	medium Upper sand	Ta, top	Green
IF	KI-46a,b	1915	0672107	5881169	medium Upper/coarse Lower sand	Tb(d)c	Brown
IF	KI-47	1912	0672101	5881155	coarse Lower sand	Tb	Orange/Brown
IF	KI-48a,b	1911	0672101	5881156	medium Lower sand-silt	Tad	Green
IF	KI-49	1916	0672098	5881185	coarse Lower sand	Ta	Brown
	KI-50	1891	0672050	5881287	coarse Upper sand	Tc2	Brown
IF	KI-51	1908	0672056	5881136	very coarse Lower sand	Ta	Brown
IF	KI-52	1909	0672051	5881133	very coarse Lower sand	Ta	White
IF	KI-53	1904	0672016	5881217	medium sand-silt	Tcd	Brown/dark gray
IF	KI-54	1889	0671937	5881309	medium Upper/coarse Lower sand	Ta (b?)	Brown
IF	KI-55	1888	0671929	5881309	conglomerate	Ta	Orange
IF	KI-56	1889	0671935	5881281	coarse Lower/ medium Upper sand	Ta	Brown
IF	KI-57	1905	0671976	5881207	medium Lower sand	Tb, base	Pink/ Brown
FIC	KI-58	1908	0671989	5881105	medium Lower sand	Tac	Orange
FIC	KI-59	1908	0671992	5881105	medium Lower sand	Tb	Orange

FIC	KI-60	1909	0671991	5881109	medium Lower sand	Tac	Orange
FIC	KI-61	1909	0671991	5881109	silt/medium Lower sand	Tdc	Gray/Orange
FIC	KI-62	1909	0671974	5881114	conglomerate	Ta	Brown
FIC	KI-63	1909	0671977	5881118	very coarse Upper sand	Ta	White
FIC	KI-64	1911	0671974	5881109	mud	Td	Gray
FIC	KI-65	1912	0671975	5881105	coarse Upper sand	Ta	Orange
FIC	KI-66	1911	0671967	5881107	very coarse Upper sand	Ta	Orange/Brown
FIC	KI-67	1914	0671969	5881108	coarse Upper sand	Ta	White to pink
FIC	KI-68	1912	0671979	5881099	coarse Upper sand	Ta	Orange/pink Brown
FIC	KI-69	1913	0671977	5881099	coarse Upper sand	Ta	Orange
FIC	KI-70	1916	0671982	5881087	medium Lower/ silt	Tcd	Orange/ Gray
FIC	KI-71	1916	0671976	5881089	medium Lower sand	Tab	Orange
FIC	KI-72	1913	0671955	5881085	coarse Upper sand	Tab	Orange
FIC	KI-73	1915	0671965	5881059	medium Lower sand-silt	Tcd,Tc	Gray/Orange
FIC	KI-74	1910	0671930	5881061	calcilutite	Td	Olive
FIC	KI-75	1906	0671929	5881084	calcilutite	Td	Olive
FIC	KI-76	1909	0671921	5881078	calcilutite	Td	Dark Olive
FIC	KI-77	1909	0671919	5881068	calcarenite-calcilutite	Tbd	Orange/ Dark Olive
FIC	KI-78	1905	0671900	5881047	calcilutite	Td	Darker Olive
FIC	KI-79	1904	0671893	5881048	coarse Upper sand	Tc2	Orange
FIC	KI-80	1905	0671911	5881044	calcilutite	Td	Dark Olive
FIC	KI-81	1899	0671895	5881040	calcilutite	Td	Dark Olive
FIC	KI-82	1904	0671893	5881052	fine sand-mud	Tcd	Brownish Gray
FIC	KI-83	1904	0671893	5881063	mud	Td	Brownish Gray
FIC	KI-84	1909	0671889	5881054	sand	Ta	Orange
FIC	KI-85	1909	0671889	5881054	calcilutite	Td	Dark Olive
FIC	KI-86	1907	0671896	5881031	coarse-medium sand	Tb	Orange/ Dark Gray
FIC	KI-87	1905	0671893	5881027	mud-calcarenite	Td,Tc	Gray/ Dark Olive
FIC	KI-88	1904	0671876	5881021	coarse Upper sand	Tb	Orange
FIC	KI-89	1903	0671875	5881019	coarse Upper sand	Tc	Orange
FIC	KI-90	1902	0671853	5881007	calcilutite	Td	Olive
FIC	KI-91	1902	0671853	5881007	medium Lower sand	Ta	Orange
FIC	KI-92	1902	0671853	5881010	medium Lower sand	Tb	Orange/ Dark Olive
FIC	KI-93	1901	0671849	5881009	medium Lower sand	Tba	Orange
FIC	KI-94	1904	0671858	5881006	calcilutite	Td	Orange
FIC	KI-95	1903	0671848	5881019	calcilutite	Td	Orange
FIC	KI-96	1907	0671851	5881008	calcilutite	Td	Orange
IF	KI-97	1922	0672157	5881095	medium Lower sand	Tbd	Orange/ Brown

IF	KI-98	1916	0672090	5661161	silt	Shear Zone (middle)	
IF	KI-99	1903	0672106	5881148	medium Lower sand	Tdc	Green
FIC	KI-100	1974	0672178	5880790	very coarse Upper sand	Ta	White
FIC	KI-101	1980	0672294	5880622	conglomerate	Ta	Dark Brown
UKG	KI-102a	1900	0672175	5881406	silty mud	Td (non weathered)	beige/light brown
UKG	KI-102b				very fine sand-mud	Tcd	red/brown
UKG	KI-103	1884	0672132	5881330	silty mud	Td (non weathered)	beige/light brown
UKG	KI-104	1900	0672175	5881406	medium sand	Tab	green
UKG	KI-105a	1884	0672185	5881352	medium sand	Ta	green
UKG	KI-105b	1884	0672185	5881353	medium sand	Ta	green
UKG	KI-105c	1884	0672177	5881364	medium sand	Tab	green
UKG	KI-106a	1884	0672187	5881349	coarse sand	Ta	green
UKG	KI-106b	1884	0672186	5881348	coarse sand	Ta	green
UKG	KI-106c	1884	0672186	5881348	coarse sand	Ta	green
UKG	KI-107a	1888	0672207	5881319	medium sand	Ta	green
UKG	KI-107b	1889	0672209	5881315	medium sand	Ta	green
UKG	KI-107b	1889	0672209	5881315	medium sand	Ta	green
IF	KI-108				very coarse sand	Ta	reddish/brown
IF	KI-109				very coarse sand	Tb	reddish/brown
IF	KI-110a				conglomerate	Ta	Reddish/Pink
IF	KI-110b				conglomerate	Ta	Pink
IF	KI-110c				conglomerate	Ta	Pink
FIC	KI-111a				sand	Ta	light brown/ white
FIC	KI-111b				sand	Ta	light brown/ white
UKG	KI-112				phosphatic bed		grey
UKG	KI-113	1877	0672078	5881410	sand	Tb	green
UKG	KI-114	1877	0672078	5881410	sand	Tb	green (non weathering stained)
		1891	0672114	5881323			
		1891	0672114	5881323			
UKG	KI-115	1867	0672281	5881382	medium Lower sand	Ta	green
UKG	KI-116	1867	0672272	5881380	coarse Lower sand	Ta (base)	green
UKG	KI-117	1872	0672265	5881367	coarse Lower sand	Tb (middle)	green
UKG	KI-118	1873	0672231	5881421	medium Upper/coarse Lower sand	Ta (top)	green
UKG	KI-119	1877	0672243	5881388	granule conglomerate	Ta (base)	greenish
UKG	KI-120	1871	0672260	5881365	medium Lower sand	Ta (top)	green
UKG	KI-121	1878	0672271	5881355	coarse Upper/very coarse Upper sand	Tc2 (base)	reddish
UKG	KI-122	1878	0672234	5881368	medium Upper sand	Ta (top)	green (full with pipes)

UKG	KI-123	1880	0672251	5881360	very coarse Lower sand	Ta (middle)	green
UKG	KI-124	1878	0672238	5881367	coarse Upper sand	Ta (top)	green
UKG	KI-125A	1877	0672228	5881374	medium Upper sand	Ta (base)	green
UKG	KI-125B	1877	0672228	5881374	medium Upper sand	Ta (middle)	reddish
UKG	KI-125C	1877	0672228	5881374	medium Upper sand	Ta (top)	green
UKG	KI-126	1879	0672226	5881376	coarse Upper sand	Tc2	reddish
UKG	KI-127	1880	0672233	5881344	medium Lower sand	Tb	green
UKG	KI-128	1884	0067222	5881360	fine Upper sand	Ta	green
UKG	KI-129	1884	0672222	5881360	mud with granule	Debrite	green
UKG	KI-130	1873	0672216	5881354	medium Upper sand	Tb	reddish
UKG	KI-131	1882	0672210	5881359	medium Upper /coarse Lower sand	Ta	green
UKG	KI-132	1885	0672214	5881357	medium Upper sand	Ta	reddish
UKG	KI-133	1879	0672202	5881358	muddy sandstone	matrix-rich sandstone (middle)	green
UKG	KI-134A	1878	0672198	5881372	medium Lower sand	Ta (base)	green
UKG	KI-134B	1878	0672198	5881372	medium Lower sand	Ta (middle)	green
UKG	KI-135	1882	0672199	5881352	coarse sand	Ta (middle)	green
UKG	KI-136	1880	0672197	5881349	coarse Upper sand	Tc2 (base)	reddish
UKG	KI-137	1880	0672195	5881356	coarse sand	Ta (base)	green
IF	KI-138	1913	0672019	5881118	mud	Td	grey
IF	KI-139	1913	0672014	5881116	mud	Td	green
UKG	KI-140	013		0671776	muddy sand	matrix-rich sandstone	green
UKG	KI-141	014		0671755	phosphatic bed	-	grey
UKG	KI-142a	015		0671214	sand	green	green
UKG	KI-142b	016		0671072	muddy sand	matrix-rich sandstone	green
UKG	KI-142c	017		0670967	mud	green	green
UKG	KI-143	018		0670967	muddy sand-medium sand	matrix-rich sandstone	green
FIC	KI-144	019		0670940	carbonaceous sand	Tb	pink
UKG	KI-145	020		0672276	muddy sand-mud	Matrix-rich sandstone-Td	green

Notation: UKG-Upper Kaza Group; IF- Lower Isaac Formation, Cariboo Group; and FIC-First Isaac Carbonate, Lower Isaac Formation.

Table A.2. Sample location from Mount Quanstrom study area, Cariboo Mountains, British Columbia

Note: UTM coordinates in grid system NAD27. UTM Zone is 10U

Stratigraphic Unit	Sample #	Elevation (m)	Easting	Northing	Grain Size	Turbidite & others facies	Weathering colour
UKG	Q1	2155	0689711	5871653	mud	Td	green to rusty orange
UKG	Q2	2160	0689676	5871577	mud	Td	green to rusty orange
UKG	Q3	2155	0689627	5871581	mud	Td	green
UKG	Q4	2148	0689612	5871515	medium Upper/coarse lower sand	Ta	green
UKG	Q5	2169	0689512	5871483	mud	Td	grey
UKG	Q6	2177	0689482	5871695	mud	Td	grey
UKG	Q7	2171	0689528	5871460	mud	Td	grey
IF	Q8	2254	0689095	587145	mud	Td	grey
FIC	Q9	2273	0689039	5871029	calcilutite	Td cal	dark grey
IF	Q10	2320	0688975	5870868	mud	Td	grey
IF	Control points	1810	0671610	5882120			
IF	Control points	2016	0689377	5871466			
IF	Control points	2167	0689519	5871524			
IF	Q11	2157	0689615	5817539	mud	Td	green
IF	Q12	2156	0689620	5871514	muddy sand	matrix-rich sandstone	green
IF	Q13	2159	0689557	5871577	fU sand, mud	Tcd	grey

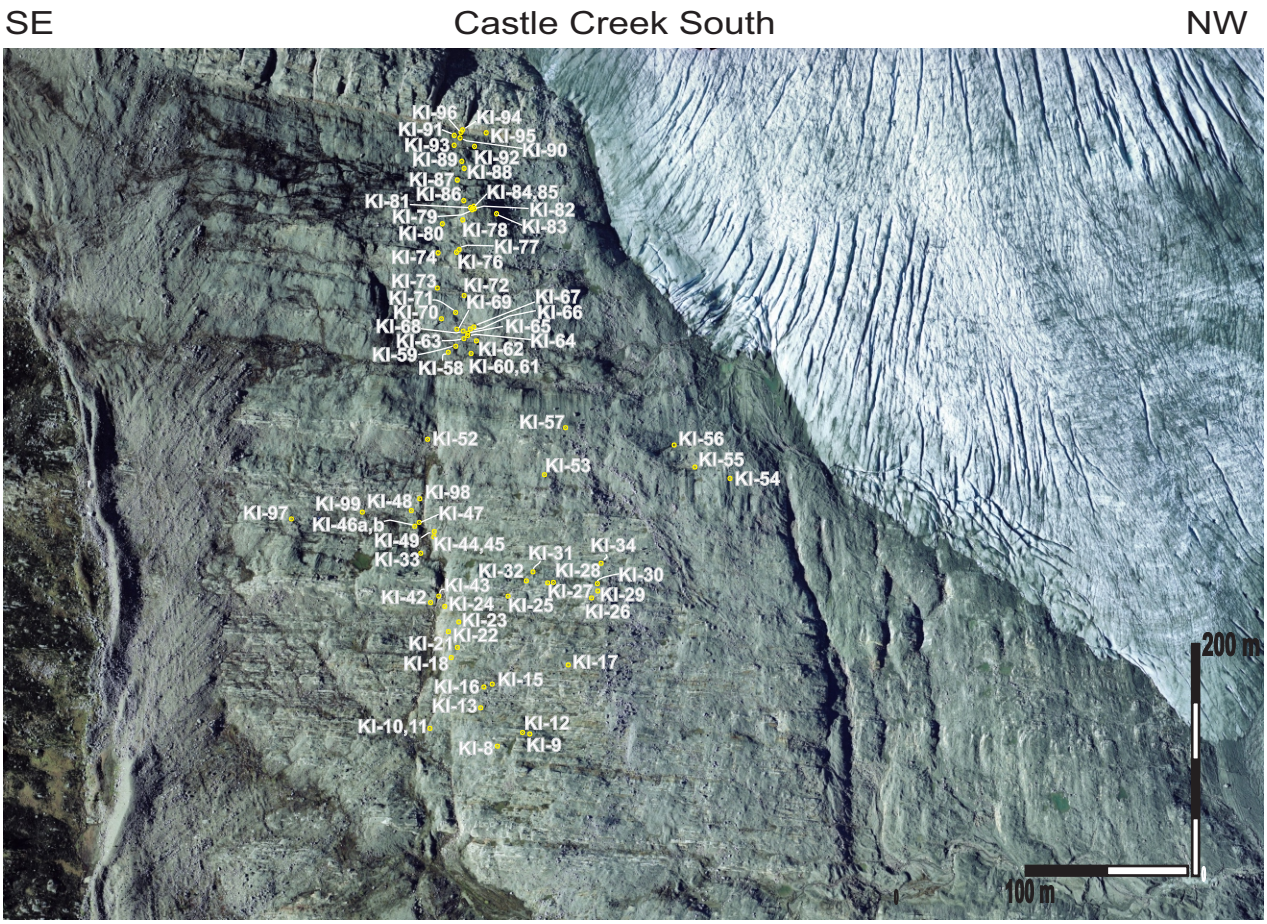

Figure A.1. Aerial photograph with location of samples in the Castle Creek South study area. For sample info, see Table A.1.

Appendix B: Castle Creek field data

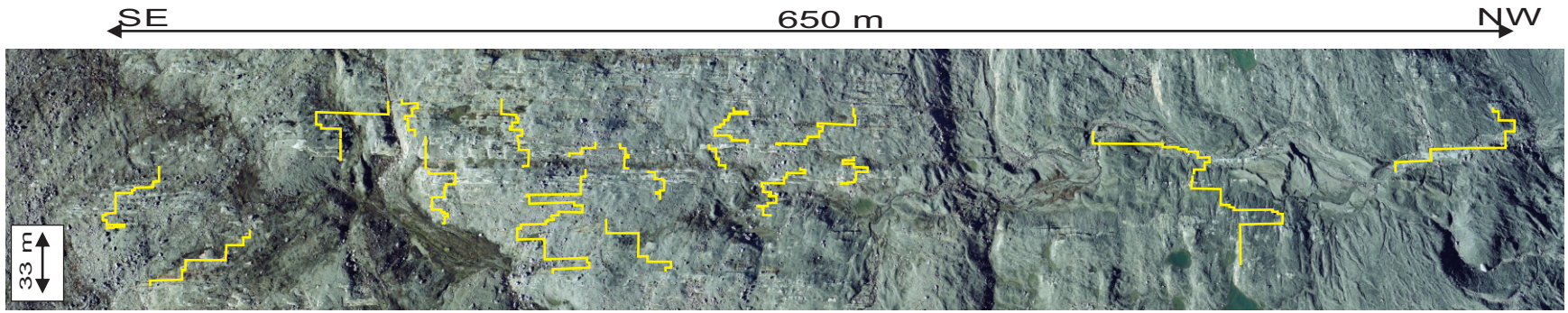

Figure B.1. Aerial photograph of the Castle Creek study area showing location of measured sedimentary logs in the lower Kaza-Isaac transition (KIT). Stratigraphy up is towards the top.

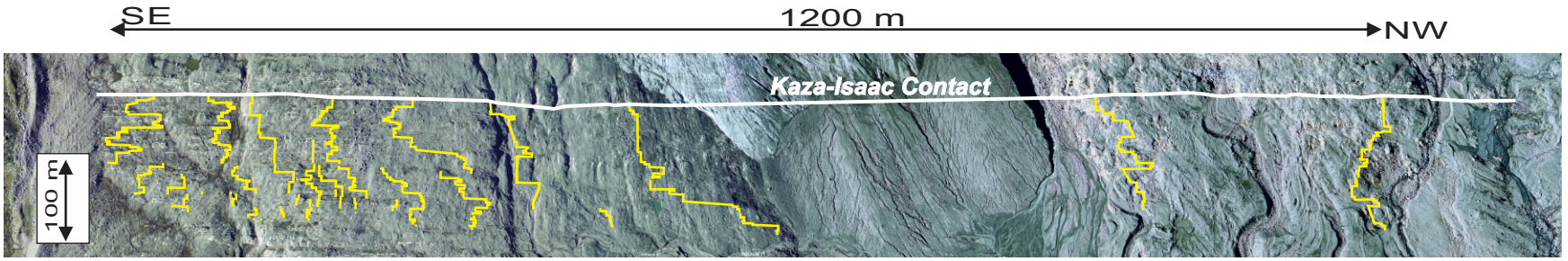

Figure B.2. Aerial photograph of the Castle Creek study area showing the location of measured sedimentary logs in the upper Kaza-Isaac transition (KIT). Stratigraphy up is towards the top.

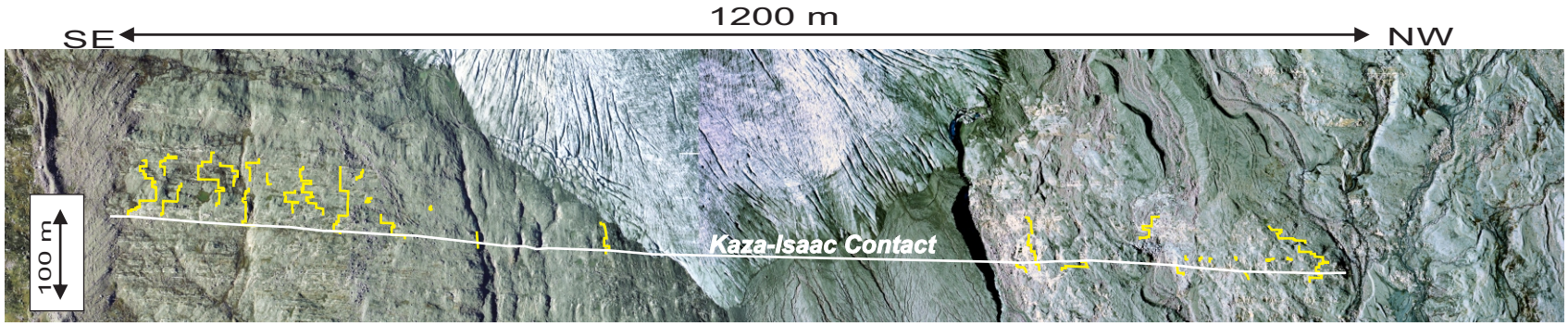

Figure B.3. Aerial photograph of the Castle Creek study area with location of measured sedimentary logs in Isaac contact channel complex (uppermost Kaza-Isaac transition) and overlying LIF . Stratigraphy up is towards the top.

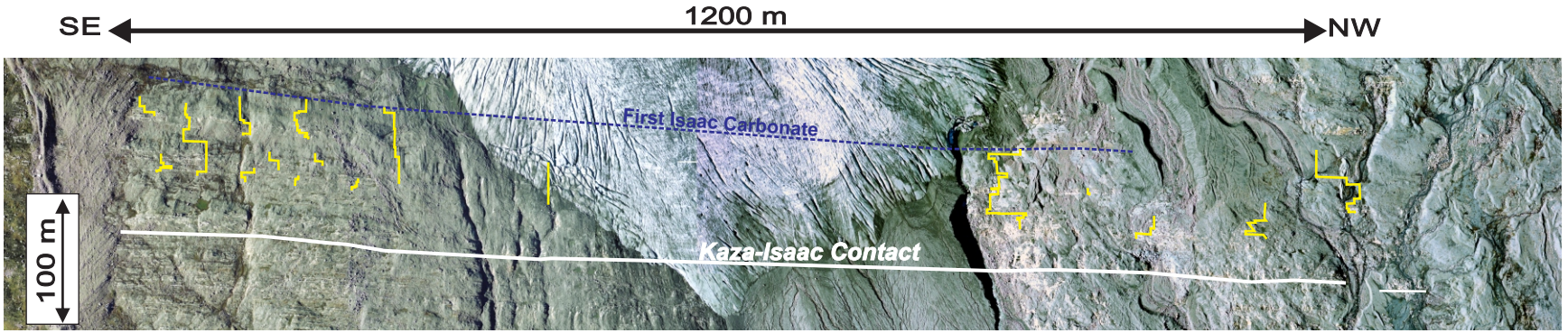

Figure B.4. Aerial photograph of the Castle Creek study area showing location of measured stratigraphic section between Isaac Mass-transport complex 1 and overlying stratal elements, including Isaac channel complex 0. Stratigraphy up is towards the top.

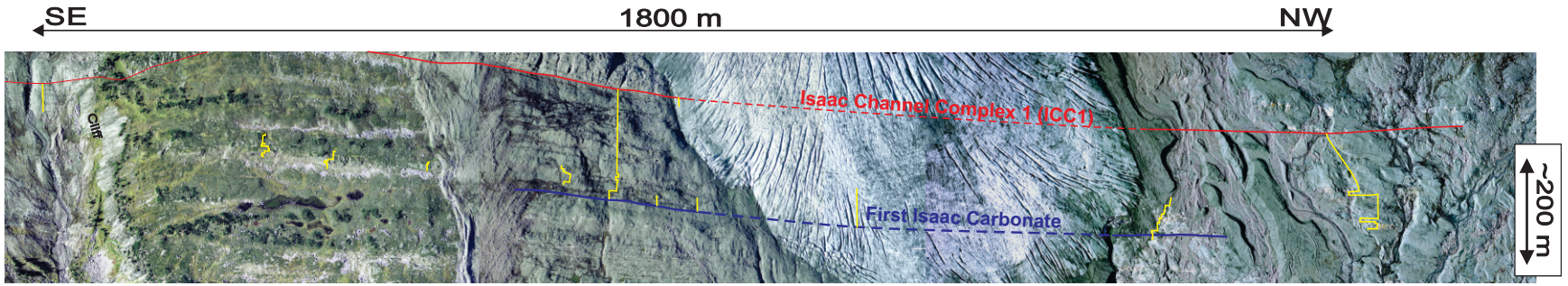

Figure B.5. Aerial photograph of the Castle Creek study area showing location of measured stratigraphic section in the First or Lower Isaac Carbonate, a major regional marker of the Windermere Supergroup. It is erosively overlain by Isaac Channel Complex 1. Stratigraphy up is

Appendix B: Castle Creek field data

Table B.1. List of Paleocurrent measurements from Castle Creek study area, Cariboo Mountains, British Columbia

Chapter	Stratigraphic Unit	Sedimentary Structure	(Drct.°)
3	UKG	Dune or dune-like bedform	020
	UKG	Dune or dune-like bedform	030
	UKG	Dune or dune-like bedform	020
	UKG	Dune or dune-like bedform	010
	UKG	Dune or dune-like bedform	033
	UKG	Ripple	017
	UKG	Dune or dune-like bedform	026
	UKG	Dune or dune-like bedform	040
	UKG	Ripple	042
	UKG	Ripple	026
	UKG	Ripple	038
	UKG	Ripple	034
	UKG	Dune	140
	UKG	Dune or dune-like bedform	028
	UKG	Dune or dune-like bedform	208
	LIF	Dune	325
	LIF	Dune	023
	LIF	Dune	139
	LIF	Dune	145
4	LIF	Ripple	055
	LIF	Ripple	042
5	FIC	Dune	027

Notation: UKG-Upper Kaza Group; LIF- Lower Isaac Formation, Cariboo Group; FIC=First Isaac Carbonate

Appendix C1: Petrography

Table C.1. Petrography analyses of rock samples from Upper Kaza Group and Isaac Formation, including First Isaac Carbonate, from both Castle Creek and Mount Quanstrom study area, Cariboo Mountains, British Columbia. For sample location, see Appendix A.

		Siliciclastic composition										Carbonate Composition						
Sample ID	**Sorting (*)**	**Quartz**	**Feldspar**	**Rock Fragment**	**Recrystallized fine-grained matrix of white muscovite, sericite, chlorite & quartz**	**Recrystallized medium- to coarse-grained matrix of quartz, and minor white mica & chlorite**	**Muscovite**	**Chlorite**	**Pyrite**	**Zircon**	**Tourmaline**	**Intraclast**	**Peloids**	**Microspar****	**Pseudospar****	**Spar or Metaspar****	**Dolomite****	**Comments**
2	w	5	-	-	85	-	-	10	-	-	-	-	-	-	-	-	-	
3	p	58	8	-	18	12		Tz	-	-	Tz	-	-	-	-	3	1	Alteration of feldspar. Vein filled with calcite. Some feldspar grains show brittle deformation.
4	p	17	-	-	70	-	-	10	3	-	-	-	-	-	-	-	-	Slaty cleavage. Sand-size quartz grains.
6	P	70	3		21	-	Tz	-	2	Tz	-	-	-	-	-	4	-	Altered feldspar into calcite. Alignment of chlorite/ muscovite.
7	p	11	-	-	88	-	-	9	2	Tz	-	-	-	-	-	-	-	Alignment of chlorite/ muscovite to the foliation.

8	vp	38	5	-	-	40	3	Tz	-	-	-	-	-	-	-	12	3	Alteration of feldspar into clay minerals and/or calcite. Ghosts of grains that are dolomitized.
9	p	35	4	-	19	38	5	1	Tz	Tz	-	-	-	-	-	Tz	Tz	
10	m-p	75	4	-	11	-	-	10	-	Tz	-	-	-	-	-	-		Alignment of chlorite/ muscovite to the foliation.
11	m	74	3	-	15	-	-	8	-	Tz	-	-	-	-	-	-	-	Upward decrease of quartz content in the recrystallized matrix.
13	vp	27	8	1	40	23	-	1	-	-	Tz	-	-	-	-	-	-	Rare fragment of mudstone, that is deformed. Alteration of feldspar into clay minerals.
15	p	74	7	-	-	19	Tz	-	Tz	-	Tz	-	-	-	-	-	Tz	Alteration of feldspar into clay minerals.
16	w	69	6	-	Tz	15	-	-	1	-	-	-	-	-	-	9	-	Porphyroblasts of muscovite.
17	w	75	5	-	-	14	-	-	Tz	-	-	-	-	-	-	6	-	Altered feldspars (some into calcite). Common quartz subgrains.
18	p	75	4	-	Tz	20	-	1	-	-	-	-	-	-	-	-	-	Alteration of feldspar.
19	p	74	5	-	-	20	Tz	1	Tz	-	-	-	-	-	-	-	-	
20	p	62	6	-	-	27	-	-	-	Tz	Tz	-	-	-	-	3	2	Alteration of feldspar into clay minerals and/or calcite.
22	p	59	3	-	-	15	Tz	-	Tz	Tz	-	-	-	-	-	13	10	Brown-reddish ferroan microdolomite/ ankerite. Alteration of feldspar. Subgrain formation and dynamic recrystallization.
23	p	67	4	-	-	26	2	-	Tz	-	-	-	-	-	-	-	1	Dark brown ferroan dolomite. Quartz subgrain formation and dynamic recrystallization.
24	p	40	1	-	-	51***	-	-	-	-	-	-	-	-	-	5	3	** Sand-sized matrix of quartz and feldspar grains (5%). Subgrain formation and dynamic recrystallization.
25	p	55	5	-	18	11	2	1	-	-	-	-	-	-	-	-	4	Alteration of feldspar to clay minerals.
26	p	48	3	-	-	47	-	2	Tz	-	-	-	-	-	-	-	-	Extensive subgrain formation and

																		dynamic recrystallization.
27	m-p	59	1	-	-	-	-	10	Tz	Tz	-	-	-	-	-	30	-	Metaspar with twinning. Large clumps of pyrite. Layer of fine mica. Slaty cleavage. Sand-size quartz grains.
28	m-p	18	-	-	60	-	-	-	1	-	-	-	-	-	-	10	-	Layer containing heavy minerals
29	w	7	-	-	85	-	-	8	-	-	-	-	-	-	-	-	-	Silt-size quartz grains. Porphyroblasts of chlorite and quartz. Slaty cleavage.
30	w	7	-	-	78	-	-	15	-	-	-	-	-	-	-	-	-	Silt-size quartz grains. Porphyroblasts of chlorite.
31	w	20	-	-	68	-	-	12	-	-	-	-	-	-	-	-	-	Silt-size quartz grains. Porphyroblasts of chlorite. Well-developed slaty cleavage. Microvein filled with quartz. Pyrite crystals.
33	p	6	-	-	71	-	-	3	-	-	-	-	-	-	20	-	-	Silt-size quartz grains. Slaty cleavage.
34a	vp	36	5			39***	Tz	-	-	-	-	-	-	-	-	20	-	***Sand-sized matrix of quartz and feldspar grains (10%). Alteration of feldspar into clay minerals and/or calcite. Mostly, Blue stain (ferroan calcite) with patches of pink stain (non-ferroan calcite)
34b	vp	33	3	-	-	35***	-	-	-	-		-	-	-	-	16	13	*** Sand-sized matrix of quartz and feldspar grains (5%). Mostly blue stain (ferroan calcite).
35	p	31	5	-	64	-	-	10	Tz	Tz	-	-	-	-	-	-	-	Alteration of feldspar into clay minerals. Porphyroblasts of intergrowth chlorite/muscovite.
40	p	26	Tz	-	-	20	-	-	2	-	-	-	-	-	-	35	17	Most blue staining (ferroan calcite), and some patches of pink staining (non-ferroan calcite). Few Microveins filled with pink, non-ferroan calcite. Layers of clay minerals. Local ferroan microdolomite.
41	p	41	3	-	-	45***	-	-	-	-	-	-	-	-	-	2	9	*** Sand-sized matrix of quartz and feldspar grains (10%). Alteration of feldspar. Local ferroan microdolomite.

42	m-p	65	5	-	-	24	-	-	-	-	-	-	-	-	-	-	6	Brown/reddish ferroan dolomite. Quartz subgrain formation and dynamic recrystallization.
43	p	60	7	-	-	30	-	-	Tz	-	-	-	-	-	-	3	-	Alteration of feldspar to clay minerals. Microvein filled with calcite. Subgrain formation and dynamic recrystallization.
46		23	-	-	41	-	12	-	1	-	-	-	-	-	-	15	-	Calcite shows single and multiple twinning. Chlorite/Muscovite are aligned to the foliation.
47	m-p	46	3	-	-	5	5	-	-	-	-	-	-	-	-	39	-	Pyrite crystals. Aligned muscovite grains to the foliation.
48	m-p	68	Tz	-	15	-	-	14	3	-	-	-	-	-	-	-	-	Rhombohedric pyrite.
49	p	54	3	-	-	-	5	-	Tz	-	-	-	-	-	-	33	-	Intergrowth chlorite/muscovite are aligned to the foliation. Quartz subgrains and dynamic recrystallization. Clean Calcite with common twinning.
50	m	45	4	-	-	5	5		-	Tz	Tz					37	-	Some feldspar are . Calcite crystals show twinning. Microdolomite.
51	vp	38	1	Tz	-	35	-	1	-	-	-	-	-	-	-	15	10	Large calcite crystals. Chlorite porphyroblasts. Most quartz particles are monocrystalline, and rare truly polycrystalline. Rare mudstone fragment.
52	p	40	3	-	-	47	-	5	-	-	-	-	-	-	-	2	3	Chlorite porphyroblasts.
53	w	3	-	-	79	-	-	10	-	-	-	-	-	3	-	-	5	Chlorite porphyroblasts. Layers of ferroan microdolomite/ankerite. Layers of microspar.
54	p	35	5	-	-	31	-	-	Tz	-	-	-	-	-	-	29	-	Large pyrite crystals. Common alteration of feldspar, forming pseudomatrix as patches of fine muscovite. Deformed feldspar.
55	m-p	38	-	-	-	54	-	2	-	-	-	-	-	-	-	3	3	Alteration of feldspar, locally forming pseudomatrix. Some altered feldspars appear to be replaced by

																		microdolomite. Metaspar consists of inequigranular, coarsely crystalline calcite with twinning. Chlorite porphyroblasts. Besides the large framework clasts and recrystallized matrix, common sand-sized quartz grains are dispersed as matrix (8%)
56	p	61	-	-	-	17	-	-	-	-	-	-	-	-	17	5	-	Blue staining in calcite (ferroan calcite). Vein filled with calcite.
57	p	54	2	-	-	20	-	-	-	Tz	-	-	-	-	-	-	24	Alteration of feldspar, locally forming pseudomatrix.
58	w	6	-	-	10	-	10	5	Tz	-	-	-	3	-	81	-	3	Pseudospar formed by recrystallization of matrix. Blue staining (Fe-calcite). Pyritized micritic intraclasts (frambroidal pyrite?). Muscovite porphyroblasts. Large cubic pyrite. Well-developed foliation. Microdolomite
59	w	5	-	Tz	15	-	-	1	Tz	-	-	-	-	-	71	-	-	Rare fragment of mudstone. Chlorite/ muscovite porphyroblasts. Muscovite-dominated bands. Large pyrite
60	w	9	-	-	-	10	-	-	Tz	-	-	-	-	2	88	3		Rare large pyrite crystals. Bands or patches of minute pyrite. Inequigranular, coarsely crystalline calcite. Layer of pyritized intraclast and heavy minerals. At the top, layers of muscovite and dolomites.
61	w	3	-	-	87	-	-	10	-	-	-	-	-	-	-	-	-	Chlorite porphyroblasts. At the top, a layer of microspar with traces of quartz
62		10	-	Tz	-	15	-	-	Tz	-	-	5	-	-	45	20		Large particles (coarse sand to granules). Elongated and fibrous, clean metaspar. One clast contains phosphatic grains that are surrounded by equigranular calcite with common twinning. One clast consists of microspar. Spar consisting of inequigranular coarse-grained crystalline calcite (dirty and clean).

																			Rare mudstone fragment. Recrystallized siliciclastic matrix consist mostly of silt-size quartz and muscovite
63	w	12	-	-		83	-	-	Tz	-	-	-	-	-		10	5	Large pyrite. Metaspar consists of clean, large crystals with twinning. Some calcite crystals are stained with blue (Fe-calcite), but others are light pink (non-Fe calcite). Recrystallized siliciclastic matrix is composed mostly of silt-size quartz and white mica or muscovite
64	p	7	-	-	80	-	-	10	Tz	-	-	-	-	-	-	-	2	Large pyrite. Chlorite porphyroblasts. Interlayer of dolomite crystals. Quartz grains are from silt to sand
65	w	10	-	-	-	30	-	-	-	-	-	-	-	-	10	38	12	Well-developed foliation. Spar consisting of inequigranular coarse-grained crystalline calcite (dirty and clean). Some calcite are stained with blue (Fe-calcite), but others are light pink (non-Fe calcite)
66	p	21	-	Tz	-	44	-	-	-	-	-	-	-	-	15	10	10	Brown/reddish iron-rich ferroan microdolomite/ ankerite?. Rare mudstone fragment.
67	m	35	-	-	-	46	-	-	-	Tz	Tz	-	-	-	8	14	7	Aggregates of euhedral pyrite. Medium- and coarse-grained crystalline calcite (clean and turbid). Microdolomite
68	m	28	-	-	-	35	-	-	-	-	-	-	-	-	15		22	Fractures or veins filled with calcite. Medium- and coarse-grained crystalline calcite (clean and turbid). Microdolomite
69	p	26	-	-	-	10										39	25	-
70	m-p	10	-	-	78	-	-	-	-	-	-	-	-	3	-	-	10	Feldspar and chlorite porphyroblasts. Large pyrite crystals. Ferroan microdolomite/ankerite. Veins filled

																		with calcite. Quartz grains are from silt to sand.
71	w	15	-	-	-	-	-	-	Tz	-	-	-	4		81	-	-	Microvein filled by quartz. Inequigranular, coarsely crystalline calcite. Dirty calcite crystals are stained or mottled with blue (Fe-calcite). Peloid are pyritized. Large pyrite crystals.
72	p	24	-	-	-	68	-	-	Tz	Tz	-	-	-		18	-	-	Quartz grains are from silt to sand. Large pyrite crystals. Seams/compaction bands
73	m	13	-	-	-	-	10	-	Tz	-	-	-	-	-	87	-	-	Inequigranular, coarsely crystalline calcite (clean and turbid). Bands/layers of chlorite/muscovite intergrowth. Layers of minute pyrite. Rarely large pyrite crystals.
74	w	Tz	-	-	-	-	-	-	-	-	-	-	Tz	-	100	-	-	Poor fabric preservation. Pseudospar/spar are the result from recrystallization of matrix & grains. Micas aligned along the foliation. Possible ghosts of grains exhibit dark borders.
75	w	Tz	-	-	50	-	-	-	-	-	-	-	-	50	-	-	-	Patches of brown/ yellowish brown ferroan microdolomite/ankerite.
76	w	3	-	-	-	-	-	Tz	-	-	-	-	-	77	-	20	-	Silt quartz grains. Calcite veins filled with non-ferroan calcite. Large cubic pyrite with pressure shadows. Vein filled with calcite and minute pyrite crystals.
77	w	10	-	-	50	-	-	-	-	-	-	-	-	40	-	-	-	Large cubic pyrite with pressure shadows. Ferroan microdolomite/ankerite. Layer of coarse-grained quart grains. Microveins filled with clean calcite.
78	w	3	-	-	-	-	-	-	-	-	-	-	-	97	-	-	-	Most stained was washed out. Veins filled with calcite and quartz. Interlayer of siliciclastic siltstone.
79	w	20	-	-	-	-	-	-	-	-	-	-	10	-	-	70	-	Patches of pyrite microcrystals with

																		dark borders. Peloids or intraclasts that show patchy recrystallization. Local silicification. Metaspar consists of inequigranular, coarsely crystalline calcite with twinning. Some twins are bent. Poor fabric preservation. Clean and turbid calcite.
80	w	Tz	-	-	-	-	-	-	-	-	-	-	-	98	-	1	3	Microveins filled with calcite. Inequigranular recrystallized calcite. Light brown ferroan microdolomite.
81b	w	Tz	-	-	-	-	-	-	-	-	-	-	-	58	-	2	40	Microspar result from recrystallization of the matrix. Mottled, brown ferroan microdolomite. Bands of microdolomite.
81a	w	Tz	-	-	-	-	-	-	-	-	-	-	-	55	-	5	40	Microveins filled with calcite, pyrite and silicates. Bands of recrystallized calcite and microdolomite. Mottled, brown ferroan microdolomite.
82	w	1	-	-	85	-	-	1	-	-	-	-	-	12	-	3	3	Microveins filled with calcite, pyrite and silicates. Chlorite porphyroblasts.
83	w	Tz	-	-	85	-	-	-	-	-	-	-	10	-	-	-	5	Brown ferroan microdolomite. Microspar consists of recrystallized ferroan calcite, and shows blue-staining indicating Fe-calcite content.
84	w	1	-	-	45	-	-	-	-	-	-	-	-	30	-	3	21	Horizontal seams filled with calcite. Brown ferroan microdolomite Microspar formed by recrystallization of the matrix. Microspar exhibits blue-staining indicating Fe-calcite content.
85b	w	Tz	-	-	-	-	-	-	-	-	-	-	-	100	-	-	-	Vein filled with calcite and quartz. Clustered pyrite crystals.
85a	m	25	-	-	40	-	-	-	-	-	-	-	-	-	30	-	5	Intercalated layers or bands of recrystallized siliciclastic matrix of mica-chlorite-quartz-graphite with slaty cleavage, and layer of pseudospar with non-graphite. Large pyrite crystals. Brown ferroan microdolomite/ankerite.

86	p	30	-	-	73	-	-	7	-	-	Tz	-	-	-	20	-	-	Interlayers of graphite. Slaty cleavage. Large pyrite crystals.
90	w	Tz	-	-	-	-	-	-	-	-	-	-	3	-	-	-	5	Brownish ferroan dolomite/ankerite. Peloid grains are pyritized. Large pyrite crystals. Fabric entirely obliterated by recrystallization. Difficult to discriminate matrix vs. grains. Vein filled by calcite. Metamorphic muscovite.
91	w	1	-	-	-	-	-	2	1	-	-	-	-	30	70	-	-	Large pyrite crystals. Pyritized peloids, some are aligned following the foliation. Fabric preservation is poor. Horizontal seams filled with calcite. Large crystals with pressure shadows.
92	w	3	-	-	-	-	Tz	-	3	-	-	-	5	25	66	-	-	Peloids that are pyritized (biogenic pyrite?). Microveins filled with non-ferroan calcite. Large pyrite crystals with pressure shadows. Peloids that are pyritized (biogenic pyrite?). Aggregate of large muscovite. Quartz grains are corroded by calcite. Fabric preservation is poor.
93	w	3	-	-	-	-	-	Tz	1	-	-	Tz	5	40	52	-	-	Patches of microspar. Aggregates of quartz. Interlayer of mudstone.
94	-	Tz	-	-	-	-	-	-	-	-	-	Tz	3	-	97	-	-	Micritic intraclast. Pseudospar formed from the recrystallization of matrix. Matrix might be also dolomitized. Silicification of grains. Medium crystalline calcite (clean). Peloids that are pyritized (biogenic pyrite?).
95	w	-	-	-	-	-	-	-	-	-	-	-	3	97	-	-	-	Microspar formed from the recrystallization of matrix. Matrix might be also dolomitized. Local silicification. Light blue staining (ferroan calcite). Layer or patches of peloids that are pyritized (biogenic pyrite?).
96	w	3	-	-	67	-	-	-	-	-	-	-	-	30				Microveins and lenses filled with

																		calcite. Large pyrite. Abundant ferroan calcite.
97	m	45	3	-	-	5	-	5	7	Tz	-	-	-	-	-	35	Tz	Mostly blue stain (ferroan calcite). Some layers of pyritized grains and heavy minerals.
98	vp	10	-	-	84	-	-	5	-	-	-	-	-	-	-	-	1	Sample from shear zone. Quartz grains are from silt to coarse sand. Chlorite porphyroblasts. Common seams and pressure shadows.
99	w	70	3	-	18	-	-	5	1	-	-	-	-	-	-	1	2	Chlorite porphyroblasts. Large pyrite crystals. Alteration of feldspar.
100	p	25	-	-	-	30	-	-	-	-	-	-	-	-	7	40	3	Metaspar consists of inequigranular, coarsely crystalline calcite with twinning. Some twin lamellas are noticeably bent. Reddish to brownish Fe-microdolomite/ankerite.
101	m	10	-	-	-	15	-	-	-	-	-	-	-	-	37	30	5	Metaspar consists of inequigranular, coarsely crystalline calcite with common twinning. Patches of reddish brown Fe-microdolomite/ankerite. Calcitic clasts. Some elongated metamorphic? calcite crystals. Clean and turbid calcite.
105b	p	59	3	-	-	28	1	-	-	Tz	-	-	-	-	-	6	3	Some feldspar are altered and/or deformed.
106a	vp	46	8	-	10	25	1	-	-	Tz	-	-	-	-	-	7	3	Alteration of feldspar into clay minerals. Layers of clay minerals. Some feldspar are broken.
107b	m	54	5	-	-	27	-	-		-	Tz	-	-	-	-	3	1	Alteration of feldspar into clay minerals and/or calcite. Some feldspars are also deformed.
108	m	37	5	-	-	10	-	4	3	Tz	Tz	-	-	-	-	41	-	Pyritized grains. Altered feldspar.
110b	p	39	3	-		39***	-	-	Tz	Tz	-	-	-	-	-	15	5	*** Sand-sized matrix of quartz and feldspar grains (16%). Alteration of feldspar. Local ferroan microdolomite.
111a	w	15	-	-	-	19	-	1	Tz	-	-	5	-	-	44	15	1	Chlorite porphyroblasts. Intraclasts are

																			phosphatized. Metaspar consists of clean, large crystals with marked twinning (some multiple twinning) and some inclusions. Large pyrite
112	w	Tz	-	-	100	-	-	-	-	-	-	-	-	-	-	-	-	-	Matrix contains abundant phosphate, fine muscovite, clay minerals and microspar.
113	vp	18	1	-	60	-	-	20	Tz	Tz	-	-	-	-	-	-	-	-	Porphyroblasts of chlorite.
115	p	48	8	-	37	5	-	-	Tz	-	-	-	-	-	-	2	-	-	Alteration of feldspar into clay minerals and/or calcite.
117	p	53	7	-	32	8	-	-	Tz	-	-	-	-	-	-	-	-	-	Brittle deformation and alteration of feldspars. Perthite texture of plagioclase.
122	p	70	9	-	14	7	-	-	-	-	-	-	-	-	-	-	-	-	Alteration of feldspar into clay minerals. Some feldspar grains are broken.
125b	p	56	4	-	-	26	Tz	-	Tz	-	-	-	-	-	-	14	-	-	Microveins filled with calcite. Some feldspar grains are broken.
126	p	44	6	Tz	-	28	-	-	-	Tz					22				Rare fragment of fine-grained sandstone. Some feldspar grains are deformed and/or broken. Alteration of feldspar into clay minerals and calcite.
127	p	19	2	-	61	-	-	17	-	-	-	-	-	-	-	1	-	-	Alteration of feldspar into clay minerals.
130	m	70	3	-	-	17	Tz	2	Tz	Tz	Tz	-	-	-	-	8	-	-	Alteration of feldspar into calcite
131	p	65	5	-	14	11	2	3	Tz	-	-	-	-	-	-	-	-	-	Alteration of feldspar.
133	p	32	-	-	52	-	-	15	-	-	-	-	-	-	-	-	-	-	Pyritized grains.
134b	p	60	4	-	-	31	Tz	-	Tz	-	Tz	-	-	-	-	5	Tz		
136	p	44	5	-	-	17	Tz	1	Tz	-	-	-	-	-	33	-	-	-	Brittle deformation and alteration of feldspars.
140	vp	15	1	-	71	-	-	13	-	-	-	-	-	-	-	-	-	-	
141	w	1	-	-	99	-	-	-	-	-	-	-	-	-	-	-	-	-	Matrix contains abundant phosphate, fine muscovite, clay minerals and

																			microspar.
142	p	29	Tz		54	-	-	15	2	-	-	-	-	-	-	-	-	Alteration of feldspar to clay minerals.
143	p	26	Tz	-	62	-	-	12	3	-	-	-	-	-	-	-	-	Alteration of feldspar to clay minerals. Minute and large pyrite crystals.
144	p	20	5	-	75	-	-	15	-	-	-	-						Quartz grains are from silt to granules. Locally, some feldspar grains are altered into fine muscovite, forming pseudomatrix.
145	vp	15	-	-	65	-	20	-	Tz	-	-	-	-	-	-	-	-	Aggregates of quartz
Q1	p	13	-	-	84	-	-	3	-	-	-	-	-	-	-	-	-	Crenulation cleavage.
Q4	p	55	2	-	28	5	-	-	15	-	-	-	-	-	-	-	-	
Q8	w	2	-	-	98	-	-	-	-	-	-	-	-	-	-	-	-	Quartz porphyroblasts. Seams. Undulatory cleavage. Recrystallized matrix also contains microspar.
Q9	w	5	-	-	40	-	-	-	Tz	-	-	-	-	55	-	-	-	Crenulation cleavage. Upward decrease of calcite content. Large muscovite-rich and calcite-rich layers or bands.

Notation: (*) Sorting: vp= very poorly sorted; p= poorly sorted, m=moderately poorly sorted, w= well sorted.

(**) Crystal size: Microspar= <30 μm; Pseudospar= >30 μm; Spar and Metaspar= >50 μm; Microdolomite/ankerite= <20 μm

Appendix C2: Petrography

Table C.2. Petrographic characteristics of carbonate cements identified from samples of the First Isaac Carbonate, at Castle Creek study area, Cariboo Mountains, British Columbia.

Carbonate cement phases	General characteristics (*)	Cathodoluminescence patterns	Relative timing of cementation
C1	Microspar, mostly without pyrite. Dirty, cloudy or turbid iron-rich calcite.	Dull orange CL	Early diagenesis
C2	Medium to coarse calcite pseudospar and/or spar, without pyrite. Alteration of C1. Dirty, cloudy or turbid calcite. Variable iron content, including C2a: Iron-poor, and C2b: Iron-rich. Observed also in some calcitic clasts.	Dull to less dull orange CL	Early to late diagenesis Clasts: Detrital
C3	Medium to coarse calcite pseudospar and/or spar. Alteration of C1. Commonly associated with angular to rounded, pyritized or pyritic grains or peloids that are disseminated and occasionally clustered. Some pyrites are frambroidal. Possibly, pyrite has a biogenic origin?. Dirty, cloudy or turbid calcite. Observed also in some calcitic clasts.	Dull orange CL	Early to late diagenesis Clasts: Detrital
C4	Coarse and poikilotopic spar and metaspar (>50-100 μm crystal size). Clear calcite.	Less dull orange CL	Metamorphism
C5	Fibrous or elongated calcite along pressure shadows or veins. Clear calcite. Common alteration to microdolomite.	Less dull orange CL	Metamorphism
C6	Micro to pseudospar. Partial replacement of D1. Mn-rich?	Bright orange CL	Metamorphism
D1	Anhedral to subhedral dolomicrospar (<20 μm in crystal size), possibly low iron content but Mn-rich. Typical alteration to ferroan microdolomite or ankerite. Variable iron content, including D1a: Iron-poor, and D1b: Iron-rich. Observed also in some dolomitic clasts.	Bright yellowish orange CL (altered) Bright/dull yellowish orange CL (unaltered, zoned)	Late Diagenesis Metamorphism Clasts: Detrital

(*) Crystal size: Microspar= <30 μm; Pseudospar= >30 μm; Spar and Metaspar= >50 μm; Microdolomite/ankerite= <20 μm

Appendix C3. Photomicrophotographs

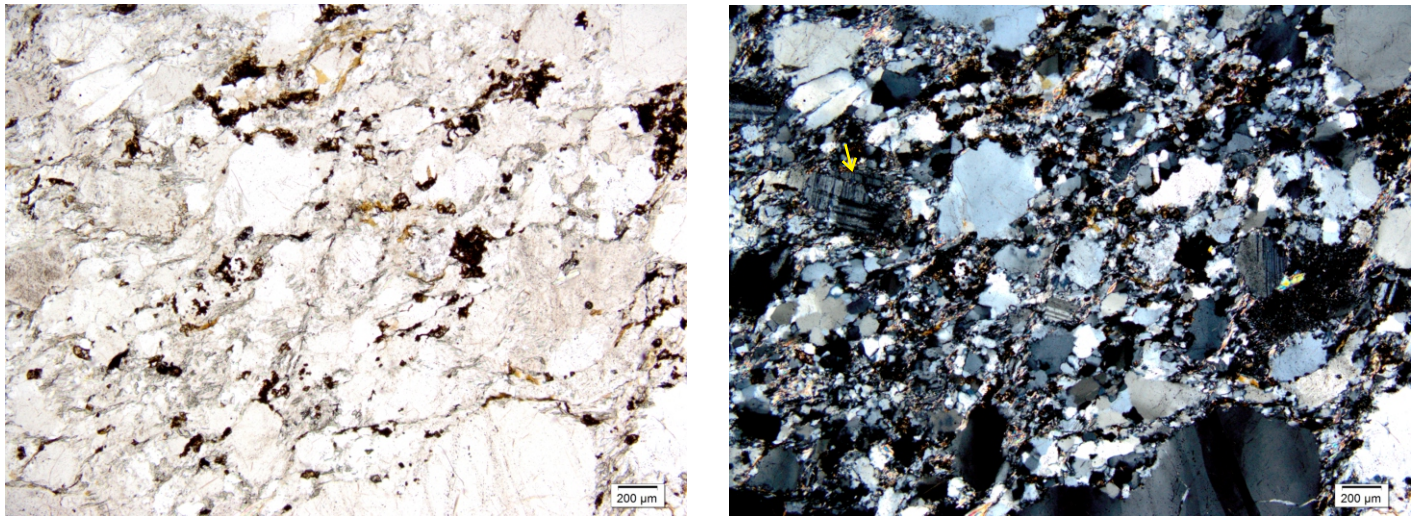

Figure C.1. Poorly sorted subfeldspathic sandstone. Feldspar grains commonly exhibit brittle deformation (arrow). Partial recrystallization with gradual transition between subgrains and new grains of quartz. Left photo, plane-polarized light. Right photo, same view under crossed

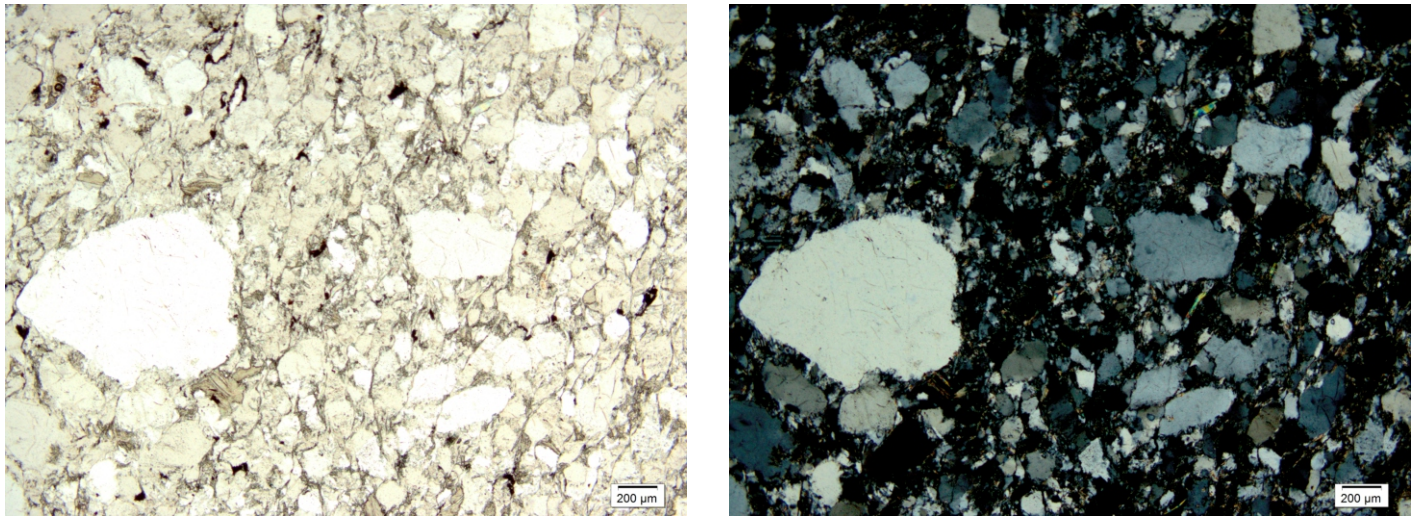

Figure C.2. Poorly sorted sandstone. Local bulging recrystallization. Left photo, plane-polarized light. Right photo, same view under crossed

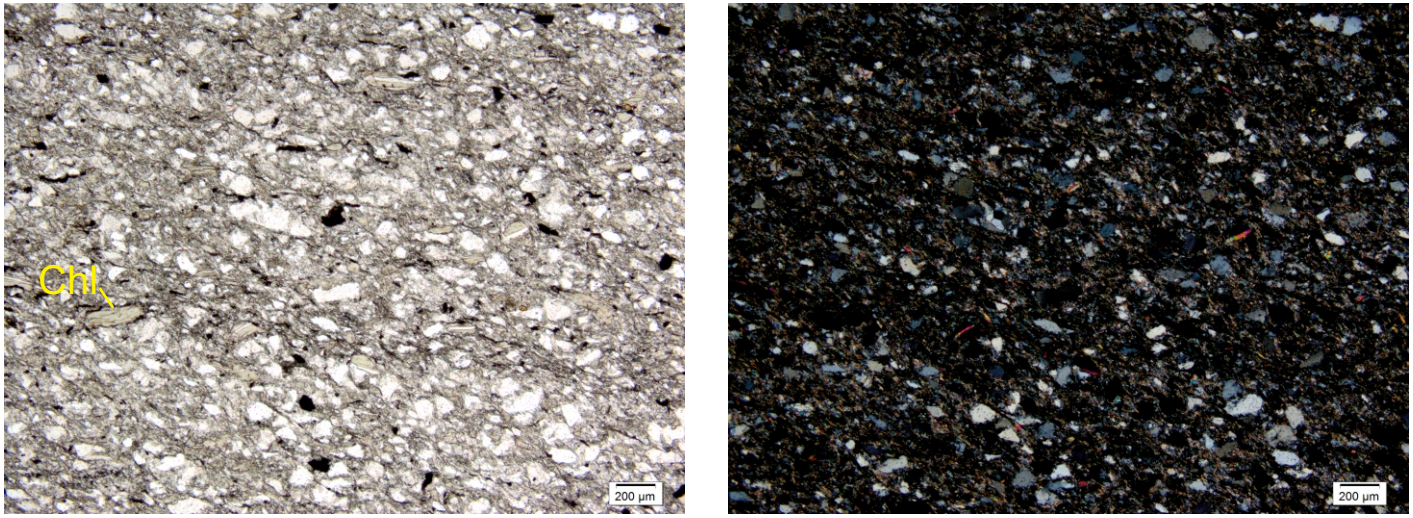

Figure C.3. Poorly-sorted matrix-rich sandstone. Silt- and sand-size quartz grains and porphyroblasts of chlorite embedded in a recrystallized matrix containing muscovite, and chlorite. Left photo, plane-polarized light. Right photo, same view under crossed polars.

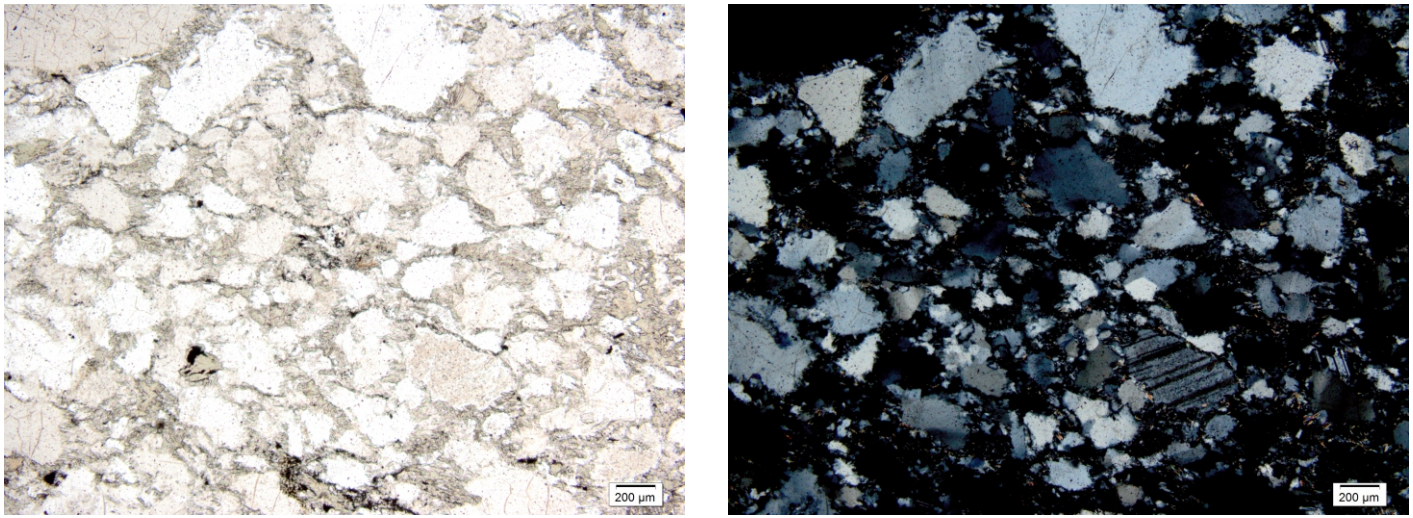

Figure C.4. Clean sandstone. Quartz and feldspar sand-size grains surrounded by fine mica, and quartz grains that result from the recrystallization, probably mainly by subgrain rotation. Left photo, plane-polarized light. Right photo, same view under crossed polars.

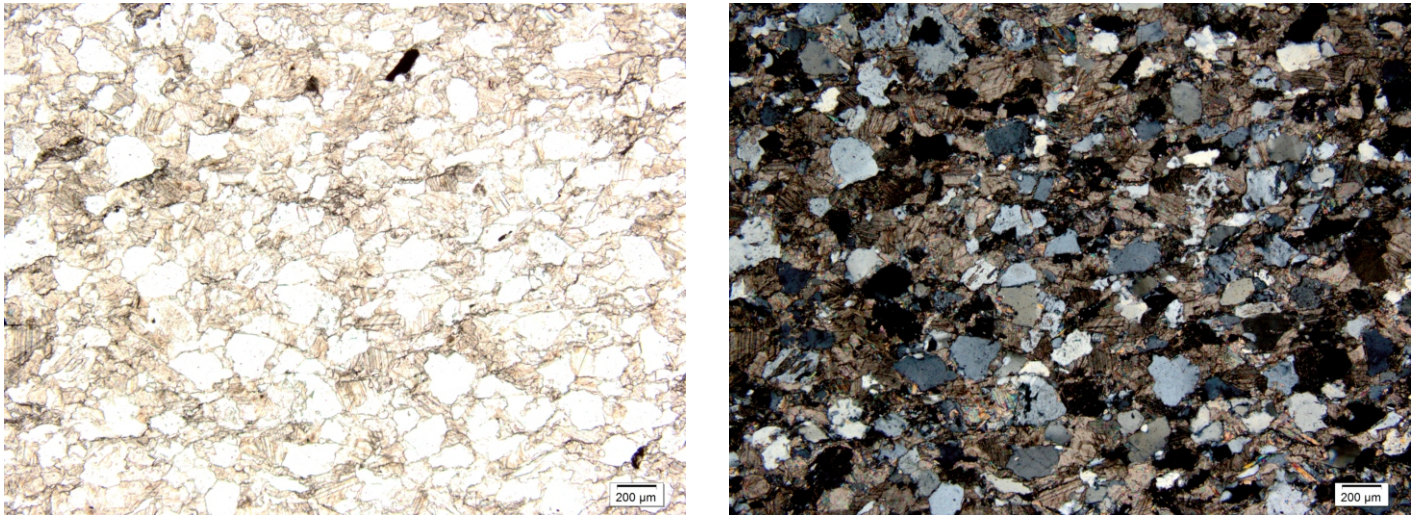

Figure C.5. Calcareous sandstone. Quartz grains are floating in a pervasive calcite cement, that show cloudy and clean crystals. Single and multiple twinning. Left photo, plane-polarized light. Right photo, same view under crossed polars.

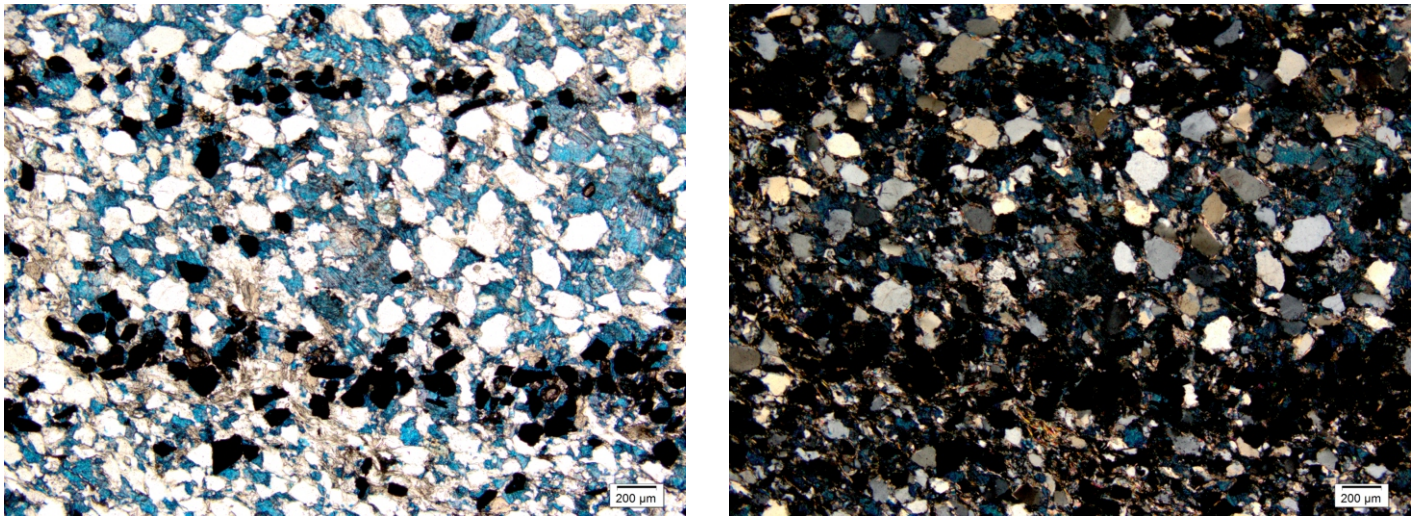

Figure C.6. Calcareous sandstone. Pervasive ferroan calcite cement (blue staining). Interlayers of black grains o peloids that are pyritized. Left photo, plane-polarized light. Right photo, same view under crossed polars.

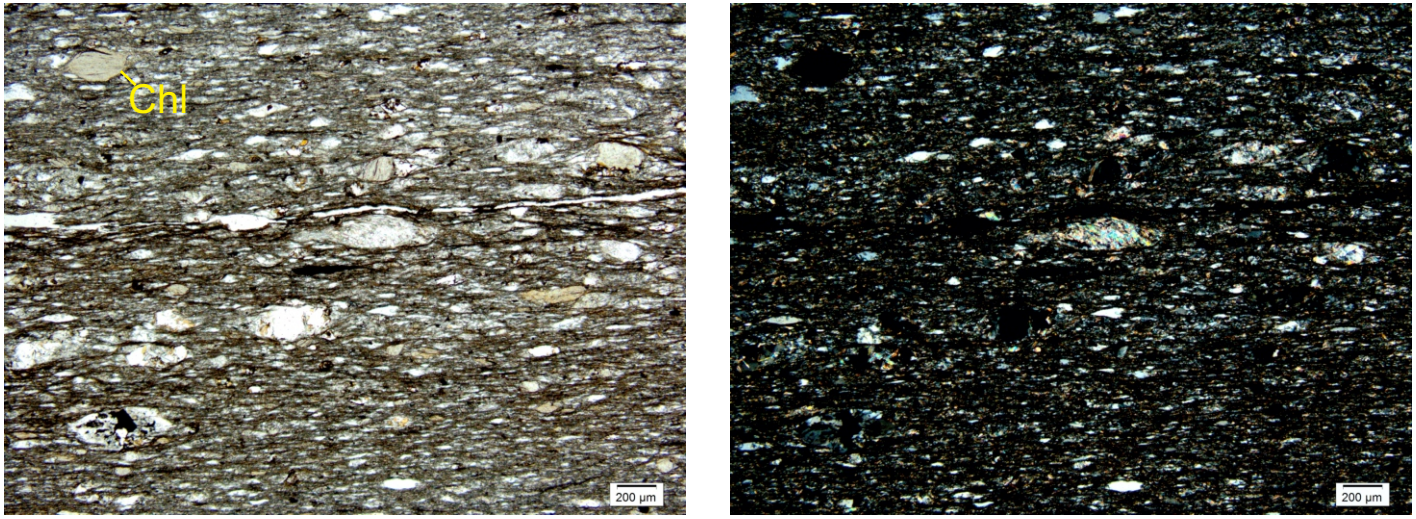

Figure C.7. Fine-grained horizon along a shear zone. Fine-grained matrix surrounding quartz grains and lenticular aggregates of chlorite (pale green) showing the elongated deformation and recrystallization. Left photo, plane-polarized light. Right photo, same view under crossed

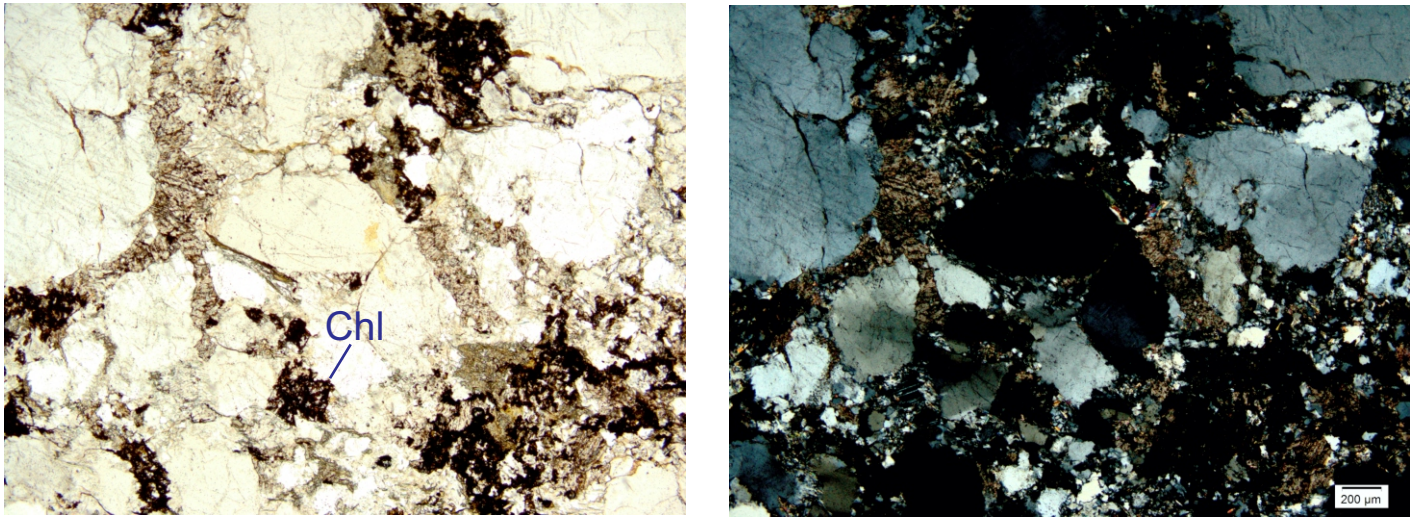

Figure C.8. Poorly sorted conglomerate. Quartz grains are surrounded by turbid calcite spar. Local replacement of brown ferroan microdolomite or ankerite. Left photo, plane-polarized light. Right photo, same view under crossed polars.

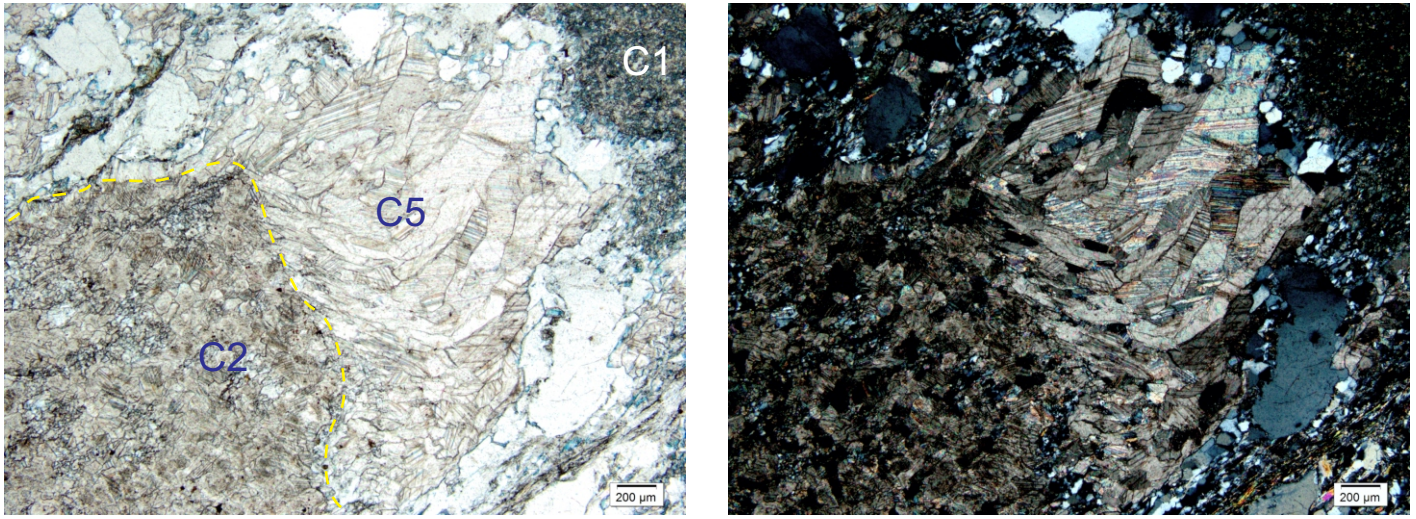

Figure C.9. Brown layer from the Bacon sandstone, First Isaac Carbonate. Ghost or relict of large carbonate grain (turbid spar C2) that is locally fringed by elongated fibrous clean calcite (C5). Locally, ferroan microspar (C1) is also observed. For general information of carbonate cement phases, see Appendix C2. Left photo, plane-polarized light. Right photo, same view under crossed polars.

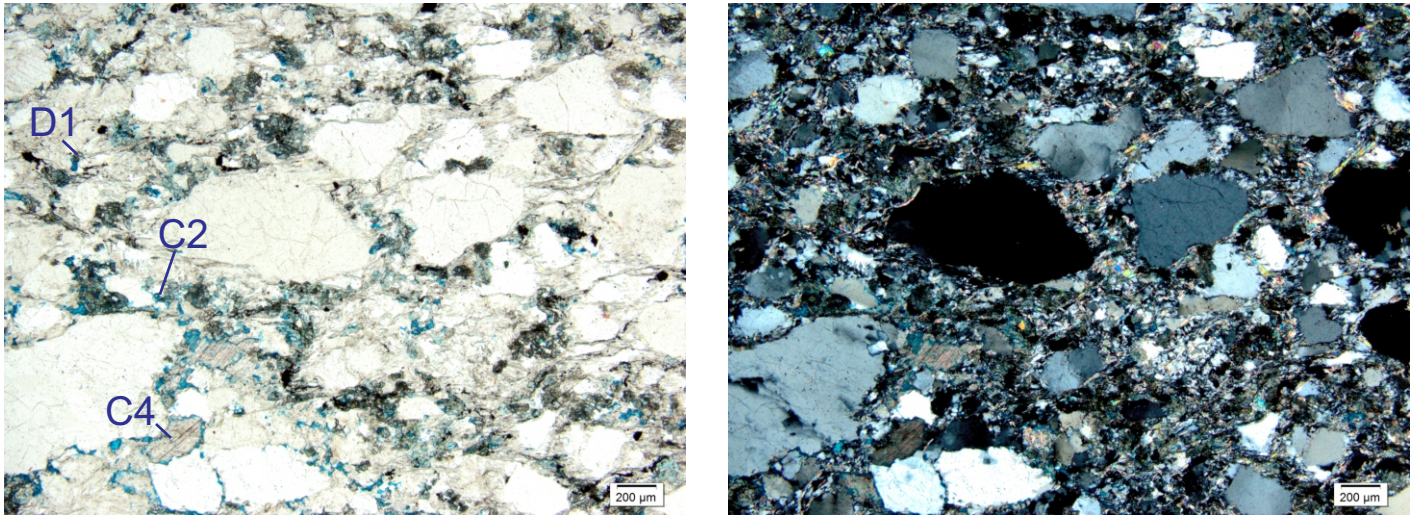

Figure C.10. White layer from the Bacon sandstone, First Isaac Carbonate. Common medium-grained recrystallized matrix of quartz and white mica. Low proportion of turbid calcite pseudospar or spar (C2), clean calcite spar (C4), and microdolomite (D1). For general information of carbonate cement phases, see Appendix C2. Left photo, plane-polarized light. Right photo, same view under crossed polars.

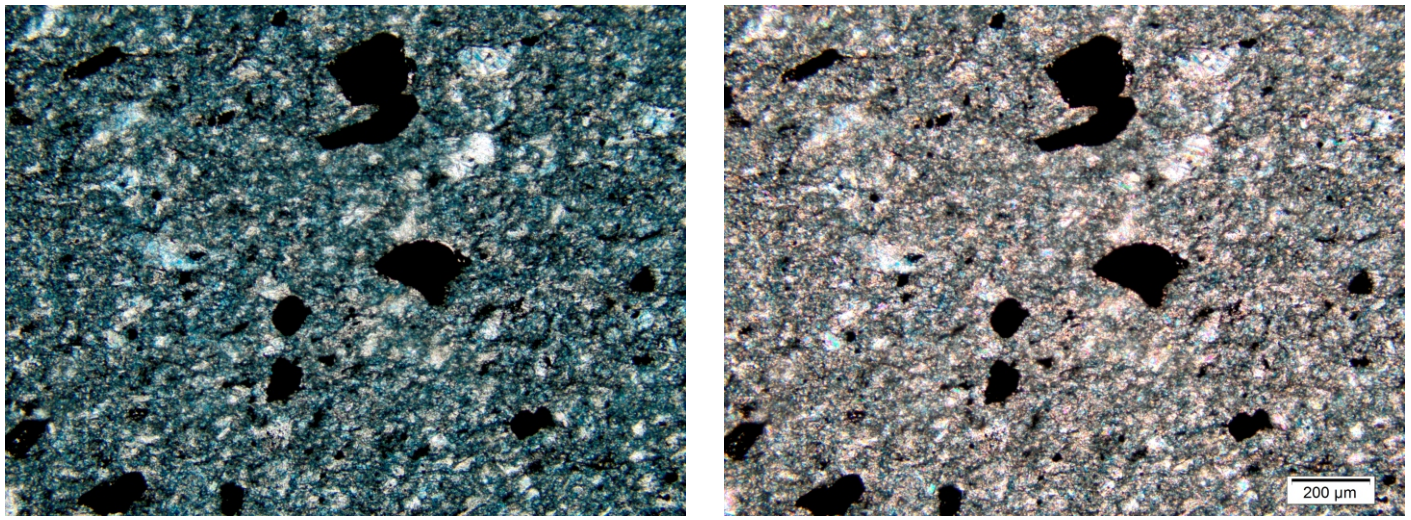

Figure C.11. Calcarenite, First Isaac Carbonate. Pervasive dirty ferroan pseudospar (C3). The high recrystallization in the rock have obliterated most original textures and constituents. Black peloidal grains are pyritized. Dispersed microdolomites are also observed locally. For general information of carbonate cement phases, see Appendix C2. Left photo, plane-polarized light. Right photo, same view under

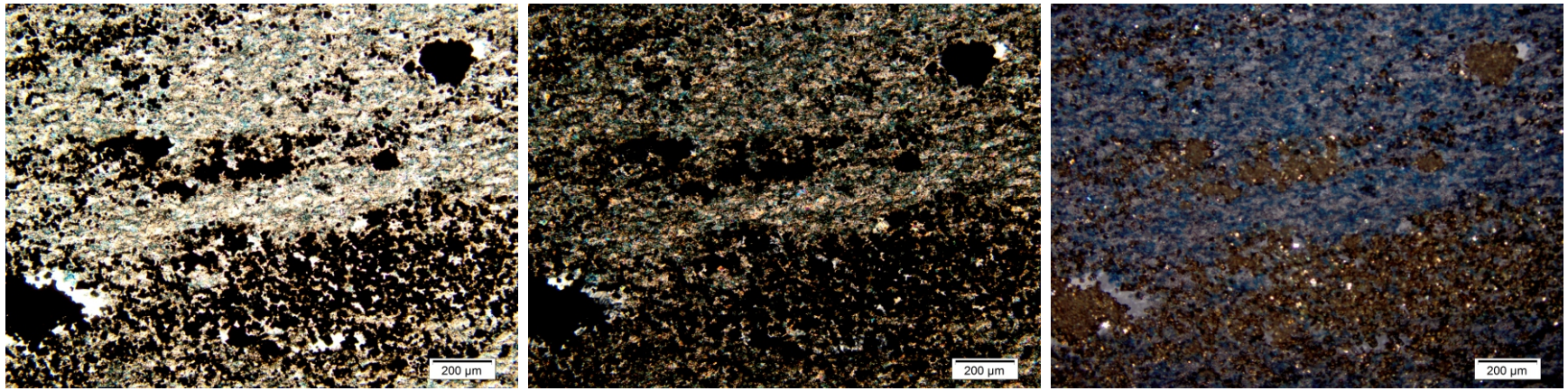

Figure C.12. Calcarenite, First Isaac Carbonate. Abundant spar (C3), with layers and patches of black peloidal grains that are pyritized (on the right, characteristic metallic yellow of pyrite under reflected light). Left photo, plane-polarized light. For general information of carbonate cement phases, see Appendix C2. Center photo, same view under crossed polar, Right photo, same view under reflected light.

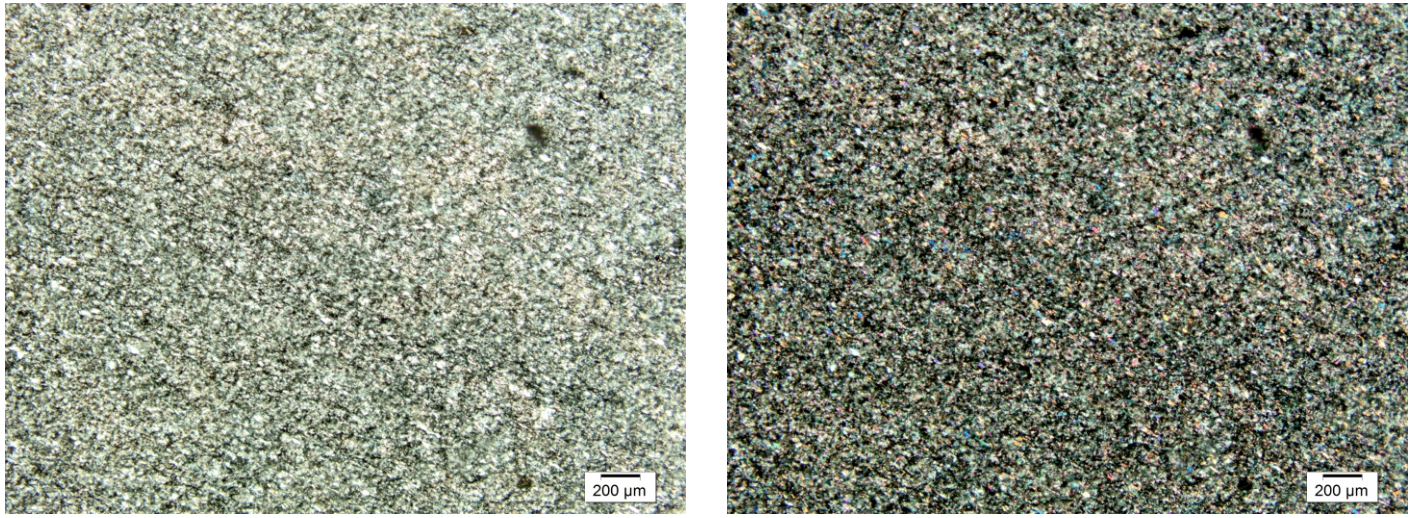

Figure C.13. Calcilutite, First Isaac Carbonate. Pervasive dirty ferroan microspar (C1). For general information of carbonate cement phases, see Appendix C2. Left photo, plane-polarized light. Right photo, same view under crossed polars.

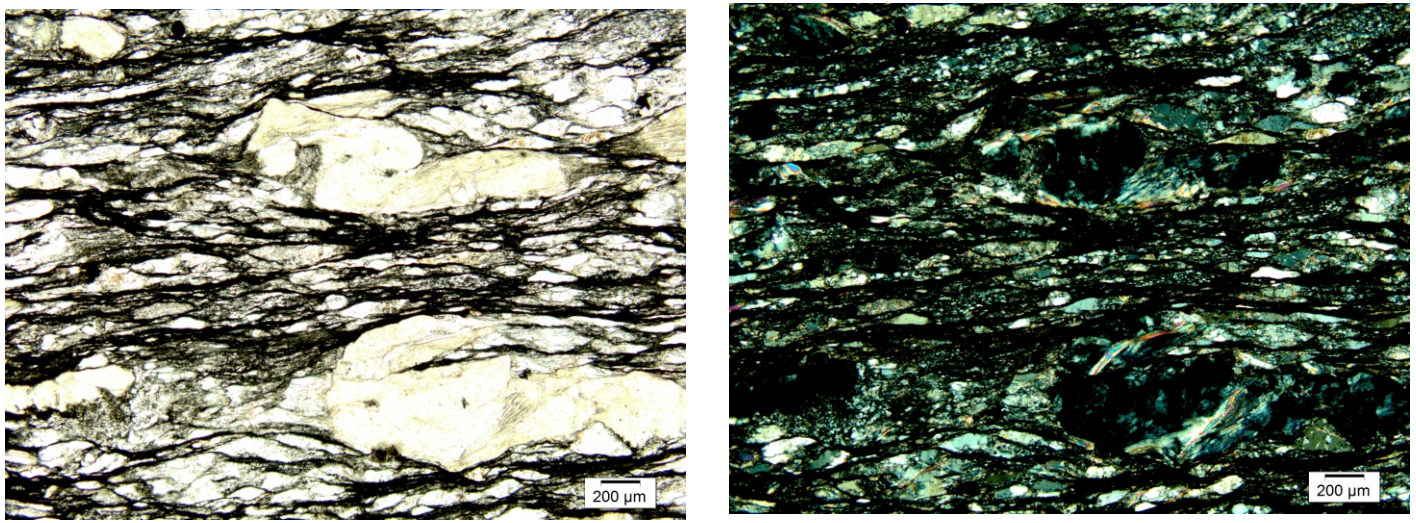

Figure C.14. Carbonaceous sandstone. Abundant recrystallized matrix of thin mica, chlorite, and black graphite anatomizing around grains of quartz and porphyroblasts of chlorite. Typical slaty cleavage. Left photo, plane-polarized light. Right photo, same view under crossed polar.

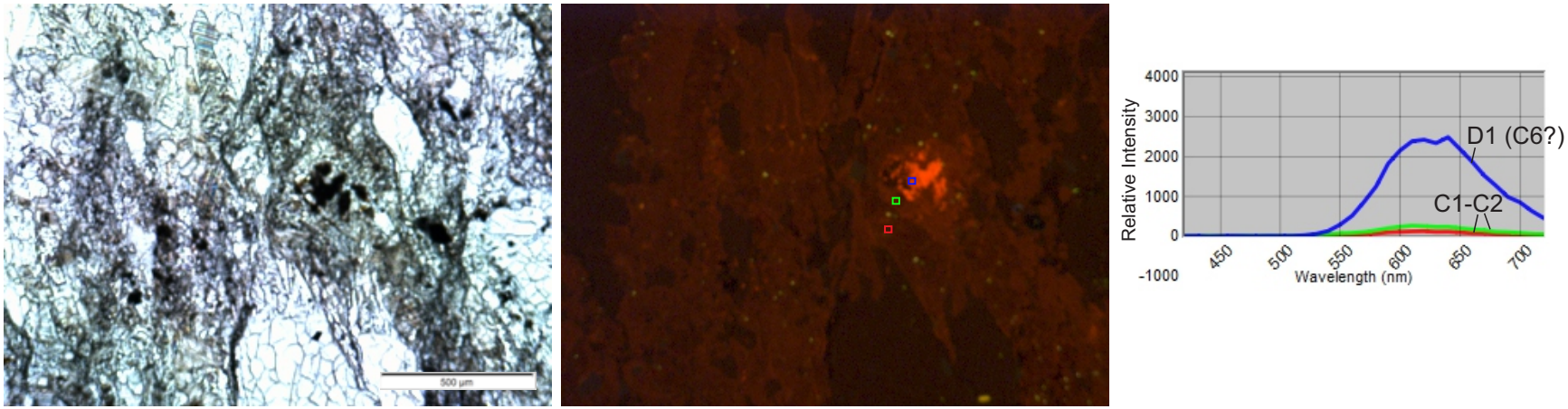

Figure C.15. Carbonate cements under cathodoluminicence microscope, First Isaac Carbonate. Pervasive dirty ferroan spar with dull orange CL (red, green squares). Locally, brown ferroan microdolomites seem to be replaced by less-ferroan calcite (C6) with bright yellowish orange CL (blue square). For general information of carbonate cement phases, see Appendix C2. Left photo, plane-polarized light. Center photo, same view under CL. Right photo, CL-spectra.

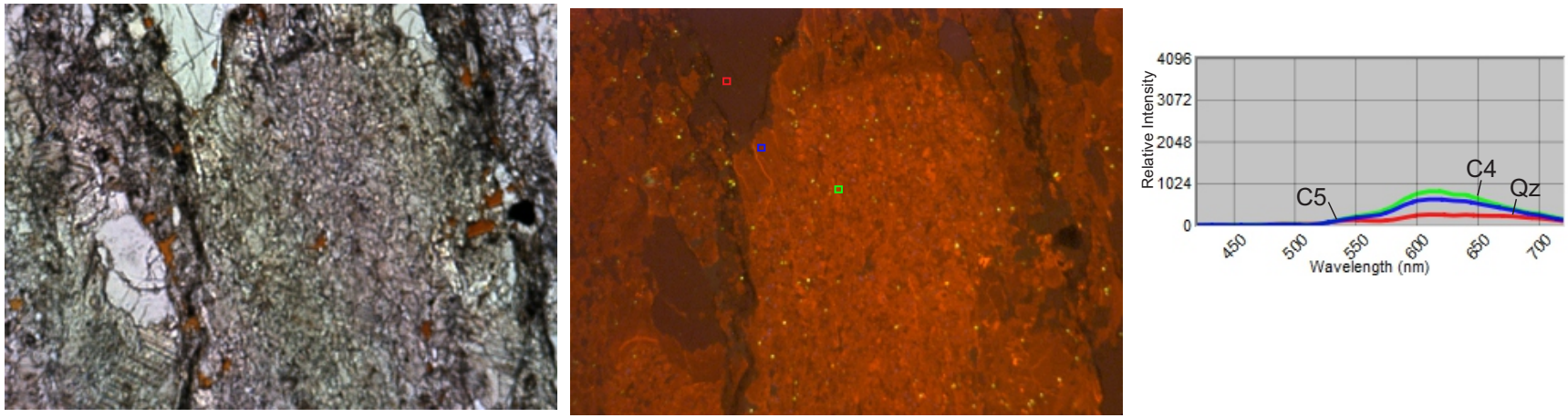

Figure C.16. Carbonate cements under cathodoluminicence microscope, First Isaac Carbonate. A ghost of a carbonate clast with less dull orange CL (green square), fringed by elongated calcite with less dull orange CL (blue square). Quartz grains exhibit dark brown CL (red square). For general information of carbonate cement phases, see Appendix C2. Left photo, plane-polarized light. Center photo, same view under CL. Right photo, CL-spectra.

Appendix D: Geochemical data

Table D.1. Major, trace and rare-earth elements of fine-grained sedimentary rocks of the Upper Kaza Group at the Castle Creek study area.

Sample Name	SiO2 (%)	Al2O3 (%)	CaO (%)	K2O (%)	MgO (%)	MnO (%)	Na2O (%)	P2O5 (%)	Fe2O3 (T) (%)	TiO2 (%)	Zn (ppm)	Ba (ppm)	Co (ppm)	Ga (ppm)	La (ppm)	Ni (ppm)	Pb (ppm)	Rb (ppm)	Sr (ppm)	Th (ppm)	U (ppm)	V (ppm)	Y (ppm)	Zr (ppm)	Nb (ppm)	Cr (ppm)	Ce (ppm)	Nd (ppm)
KI-142c	47.36	25.68	0.23	5.343	3.52	0.06	0.47	0.137	10.977	1.096	128	1307	44	29	96	55	21	186	88	38	12	172	43	186	19	218	199	77
KI-21	50.84	24.79	0.15	5.731	2.44	0.04	0.59	0.073	7.924	1.242	70	1488	32	25	94	30	37	202	78	63	30	155	30	380	18	250	183	59
KI-14	56.62	22.57	0.14	5.225	2.63	0.03	0.62	0.073	7.033	0.796	92	1091	18	20	56	37	26	186	77	35	13	110	34	165	15	150	128	51
KI-141	37.93	14.33	17.45	3.254	2.07	0.04	0.29	13.403	5.538	0.480	65	879	14	10	150	26	2	102	1148	9	4	75	299	185	16	76	258	146
KI-7	53.27	19.36	0.16	3.684	3.77	0.08	0.65	0.073	11.071	1.031	133	992	29	18	35	67	35	138	78	33	15	131	27	198	17	228	111	37
KI-112	32.29	12.95	19.75	2.066	3.11	0.06	0.26	15.285	9.044	0.361	118	569	16	8	81	54	23	63	2038	0	0	64	199	171	12	61	125	83
KI-2	44.11	25.27	0.17	5.580	4.00	0.06	0.42	0.091	11.689	1.348	130	1769	35	32	88	72	28	203	95	34	12	182	36	178	22	291	132	48
KI-133	56.59	16.79	0.16	1.929	4.63	0.09	1.12	0.066	13.583	1.049	156	601	35	14	37	76	11	75	54	26	10	110	23	182	15	231	70	29
KI-140	52.31	21.89	0.18	4.548	3.48	0.07	0.53	0.083	10.132	1.065	111	1264	36	23	67	58	17	165	72	29	13	150	31	160	17	236	84	32
												1769.0							2038.0									
Maximum	56.62	25.68	19.75	5.73	4.63	0.09	1.12	15.29	13.58	1.35	156.00	0	44.00	32.00	150.00	76.00	37.00	203.00	0	63.00	30.00	182.00	299.00	380.00	22.00	291.00	258.00	146.00
Minimum	32.29	12.95	0.14	1.93	2.07	0.03	0.26	0.07	5.54	0.36	65.00	569.00	14.00	8.00	35.00	26.00	2.00	63.00	54.00	0.00	0.00	64.00	23.00	160.00	12.00	61.00	70.00	29.00
Standard Deviation	**8.41**	**4.80**	**8.15**	**1.48**	**0.81**	**0.02**	**0.25**	**6.31**	**2.52**	**0.33**	**30.34**	**396.70**	**10.43**	**8.24**	**35.37**	**18.13**	**11.14**	**54.63**	**704.46**	**17.89**	**8.27**	**41.27**	**99.06**	**68.28**	**2.82**	**79.81**	**59.65**	**36.50**
												1106.6																
Average	**47.92**	**20.40**	**4.27**	**4.15**	**3.29**	**0.06**	**0.55**	**3.25**	**9.67**	**0.94**	**111.44**	**7**	**28.78**	**19.89**	**78.22**	**52.78**	**22.22**	**146.67**	**414.22**	**29.67**	**12.11**	**127.67**	**80.22**	**200.56**	**16.78**	**193.44**	**143.33**	**62.44**

Table D.2. Major, trace and rare-earth elements of fine-grained sedimentary rocks of the Isaac Formation at the Castle Creek study area.

Sample Name	SiO2 (%)	Al2O3 (%)	CaO (%)	K2O (%)	MgO (%)	MnO (%)	Na2O (%)	P2O5 (%)	Fe2O3 (T) (%)	TiO2 (%)	Zn (ppm)	Ba (ppm)	Co (ppm)	Ga (ppm)	La (ppm)	Ni (ppm)	Pb (ppm)	Rb (ppm)	Sr (ppm)	Th (ppm)	U (ppm)	V (ppm)	Y (ppm)	Zr (ppm)	Nb (ppm)	Cr (ppm)	Ce (ppm)	Nd (ppm)
KI-144	66.93	17.08	0.12	3.289	1.34	0.01	0.98	0.058	5.067	0.770	79	716	17	12	47	14	55	117	104	29	8	111	18	262	12	181	101	37
KI-83	51.92	23.67	3.13	3.460	2.00	0.02	1.50	0.04	5.603	0.780	89	578	9	17	67	19	15	137	699	28	14	112	8	160	15	169	103	35
KI-82	41.90	14.21	15.45	2.204	1.93	0.06	0.85	0.045	7.058	0.380	64	363	57	12	101	33	41	83	619	17	3	62	18	108	7	98	174	65
KI-70	45.47	14.70	8.34	2.370	3.45	0.34	0.61	0.031	9.922	0.767	69	374	28	4	29	39	34	92	196	33	16	88	13	193	12	157	42	8
KI-64	59.03	18.57	0.13	2.342	2.77	0.02	0.68	0.045	10.120	1.110	128	374	29	15	46	55	34	92	165	48	21	116	25	422	13	225	81	30
KI-61	53.66	22.40	0.57	3.198	2.57	0.05	1.08	0.071	8.684	0.975	114	535	19	14	65	59	34	122	229	44	17	110	29	178	17	210	124	55
KI-139	55.43	24.63	0.17	3.666	2.29	0.05	1.31	0.076	7.575	0.772	105	658	22	19	86	44	14	136	262	27	9	110	26	144	15	148	110	45
KI-138	53.21	21.62	1.05	3.069	2.63	0.11	1.03	0.071	9.238	0.975	106	521	54	19	68	80	50	116	228	33	10	116	26	258	15	193	129	37
KI-53	51.24	21.38	3.89	3.721	2.69	0.09	0.78	2.105	8.232	0.797	116	643	22	16	87	45	20	134	211	27	14	105	27	186	14	160	161	59
KI-31	53.62	23.86	0.17	4.601	2.92	0.05	0.95	0.081	7.973	0.903	104	782	28	20	57	47	42	165	156	35	13	108	30	189	15	173	95	31
Maximum	***66.93***	***24.63***	***15.45***	***4.60***	***3.45***	***0.34***	***1.50***	***2.11***	***10.12***	***1.11***	***128.00***	***782.00***	***57.00***	***20.00***	***101.00***	***80.00***	***55.00***	***165.00***	***699.00***	***48.00***	***21.00***	***116.00***	***30.00***	***422.00***	***17.00***	***225.00***	***174.00***	***65.00***
Minimum	***41.90***	***14.21***	***0.12***	***2.20***	***1.34***	***0.01***	***0.61***	***0.03***	***5.07***	***0.38***	***64.00***	***363.00***	***9.00***	***4.00***	***29.00***	***14.00***	***14.00***	***83.00***	***104.00***	***17.00***	***3.00***	***62.00***	***8.00***	***108.00***	***7.00***	***98.00***	***42.00***	***8.00***
Standard Deviation	**6.84**	**3.83**	**5.01**	**0.74**	**0.59**	**0.10**	**0.27**	**0.65**	**1.69**	**0.20**	**21.25**	**149.17**	**15.46**	**4.73**	**21.80**	**19.21**	**14.01**	**25.23**	**201.94**	**8.89**	**5.15**	**16.70**	**7.36**	**87.90**	**2.76**	**35.28**	**38.06**	**16.61**
Average	**53.24**	**20.21**	**3.30**	**3.19**	**2.46**	**0.08**	**0.98**	**0.26**	**7.95**	**0.82**	**97.40**	**554.40**	**28.50**	**14.80**	**65.30**	**43.50**	**33.90**	**119.40**	**286.90**	**32.10**	**12.50**	**103.80**	**22.00**	**210.00**	**13.50**	**171.40**	**112.00**	**40.20**

Table D.3. Major, trace and rare-earth elements of fine-grained sedimentary rocks of the Uppermost Kaza Group at the Mount Quanstrom study area.

Sample Name	SiO2 (%)	Al2O 3 (%)	CaO (%)	K2O (%)	MgO (%)	MnO (%)	Na2O (%)	P2O5 (%)	Fe2O 3(T) (%)	TiO2 (%)	Zn (ppm)	Ba (ppm)	Co (ppm)	Ga (ppm)	La (ppm)	Ni (ppm)	Pb (ppm)	Rb (ppm)	Sr (ppm)	Th (ppm)	U (ppm)	V (ppm)	Y (ppm)	Zr (ppm)	Nb (ppm)	Cr (ppm)	Ce (ppm)	Nd (ppm)
Q-3	53.82	22.97	0.17	5.038	2.79	0.07	0.68	0.066	7.614	0.878	88	1122	21	20	44	22	23	185	138	32	12	110	22	183	15	174	85	26
Q-1	56.51	21.34	0.20	4.513	3.00	0.07	0.57	0.096	8.330	0.809	89	1012	23	18	130	30	25	161	112	35	13	96	33	157	14	154	229	83
Maximum	**56.51**	**22.97**	**0.20**	**5.04**	**3.00**	**0.07**	**0.68**	**0.10**	**8.33**	**0.88**	**89.00**	**1122.00**	**23.00**	**20.00**	**130.00**	**30.00**	**25.00**	**185.00**	**138.00**	**35.00**	**13.00**	**110.00**	**33.00**	**183.00**	**15.00**	**174.00**	**229.00**	**83.00**
Minimum	**53.82**	**21.34**	**0.17**	**4.51**	**2.79**	**0.07**	**0.57**	**0.07**	**7.61**	**0.81**	**88.00**	**1012.00**	**21.00**	**18.00**	**44.00**	**22.00**	**23.00**	**161.00**	**112.00**	**32.00**	**12.00**	**96.00**	**22.00**	**157.00**	**14.00**	**154.00**	**85.00**	**26.00**
Standard Deviation	**1.90**	**1.15**	**0.02**	**0.37**	**0.15**	**0.00**	**0.08**	**0.02**	**0.51**	**0.05**	**0.71**	**77.78**	**1.41**	**1.41**	**60.81**	**5.66**	**1.41**	**16.97**	**18.38**	**2.12**	**0.71**	**9.90**	**7.78**	**18.38**	**0.71**	**14.14**	**101.82**	**40.31**
Average	**55.17**	**22.16**	**0.19**	**4.78**	**2.90**	**0.07**	**0.63**	**0.08**	**7.97**	**0.84**	**88.50**	**1067.00**	**22.00**	**19.00**	**87.00**	**26.00**	**24.00**	**173.00**	**125.00**	**33.50**	**12.50**	**103.00**	**27.50**	**170.00**	**14.50**	**164.00**	**157.00**	**54.50**

Table D.4. Major, trace and rare-earth elements of fine-grained sedimentary rocks of the lower Isaac Formation at the Mount Quanstrom study area.

Sample Name	SiO2 (%)	Al2O 3 (%)	CaO (%)	K2O (%)	MgO (%)	MnO (%)	Na2O (%)	P2O5 (%)	Fe2O 3(T) (%)	TiO2 (%)	Zn (ppm)	Ba (ppm)	Co (ppm)	Ga (ppm)	La (ppm)	Ni (ppm)	Pb (ppm)	Rb (ppm)	Sr (ppm)	Th (ppm)	U (ppm)	V (ppm	Y (ppm)	Zr (ppm)	Nb (ppm)	Cr (ppm)	Ce (ppm)	Nd (ppm)
Q-10	45.78	29.46	0.13	6.121	2.33	0.01	1.28	0.049	7.805	1.068	97	1302	35	22	88	64	95	214	262	43	16	165	35	156	19	223	156	67
Q-6	56.19	21.14	0.22	4.455	2.98	0.08	0.57	0.08	8.529	0.914	95	883	27	22	74	21	10	159	96	30	9	141	25	156	16	185	161	54
Q-5	53.12	22.96	0.18	4.850	3.15	0.07	0.84	0.063	8.590	0.917	100	1044	34	19	50	37	43	181	119	39	17	128	23	169	14	178	127	49
Maximum	**56.19**	**29.46**	**0.22**	**6.12**	**3.15**	**0.08**	**1.28**	**0.08**	**8.59**	**1.07**	**100.00**	**1302.00**	**35.00**	**22.00**	**88.00**	**64.00**	**95.00**	**214.00**	**262.00**	**43.00**	**17.00**	**165.00**	**35.00**	**169.00**	**19.00**	**223.00**	**161.00**	**67.00**
Minimum	**45.78**	**21.14**	**0.13**	**4.46**	**2.33**	**0.01**	**0.57**	**0.05**	**7.81**	**0.91**	**95.00**	**883.00**	**27.00**	**19.00**	**50.00**	**21.00**	**10.00**	**159.00**	**96.00**	**30.00**	**9.00**	**128.00**	**23.00**	**156.00**	**14.00**	**178.00**	**127.00**	**49.00**
Standard Deviation	**5.35**	**4.37**	**0.05**	**0.87**	**0.43**	**0.04**	**0.36**	**0.02**	**0.44**	**0.09**	**2.52**	**211.36**	**4.36**	**1.73**	**19.22**	**21.73**	**42.85**	**27.68**	**89.94**	**6.66**	**4.36**	**18.77**	**6.43**	**7.51**	**2.52**	**24.21**	**18.36**	**9.29**
Average	**51.70**	**24.52**	**0.18**	**5.14**	**2.82**	**0.05**	**0.90**	**0.06**	**8.31**	**0.97**	**97.33**	**1076.33**	**32.00**	**21.00**	**70.67**	**40.67**	**49.33**	**184.67**	**159.00**	**37.33**	**14.00**	**144.67**	**27.67**	**160.33**	**16.33**	**195.33**	**148.00**	**56.67**

Table D.5. Correlation coefficient (r) between major and selected trace elements for samples (n=11) of fine-grained sedimentary rocks of the Upper Kaza Group at both Castle Creek and Mount Quanstrom study areas.

	SiO2	Al2O3	CaO	K2O	MgO	MnO	Na2O	P2O5	Fe2O3(T)	TiO2	Zn	Ba	Co	Ga	La	Ni	Pb	Rb	Sr	Th	U	V	Y	Zr	Nb	Cr	Ce	Nd
SiO2	1.00	0.50	-0.87	0.33	0.24	0.29	0.78	-0.87	0.20	0.51	0.09	0.14	0.30	0.32	-0.46	-0.02	0.27	0.42	-0.87	0.63	0.56	0.28	-0.81	0.03	0.04	0.51	-0.31	-0.63
Al2O3	0.50	1.00	-0.80	0.93	0.06	-0.11	0.11	-0.80	0.12	0.79	-0.05	0.87	0.60	0.95	-0.10	-0.06	0.54	0.95	-0.78	0.84	0.70	0.84	-0.73	0.29	0.68	0.72	-0.02	-0.43
CaO	-0.87	-0.80	1.00	-0.60	-0.40	-0.30	-0.62	1.00	-0.41	-0.83	-0.24	-0.53	-0.63	-0.72	0.45	-0.18	-0.46	-0.69	0.97	-0.80	-0.69	-0.69	0.95	-0.14	-0.46	-0.82	0.33	0.72
K2O	0.33	0.93	-0.60	1.00	-0.28	-0.40	-0.17	-0.60	-0.23	0.59	-0.37	0.90	0.32	0.85	0.12	-0.33	0.51	0.99	-0.60	0.75	0.65	0.69	-0.49	0.32	0.62	0.49	0.19	-0.18
MgO	0.24	0.06	-0.40	-0.28	1.00	0.81	0.54	-0.39	0.98	0.49	0.96	-0.04	0.65	0.23	-0.54	0.91	0.03	-0.19	-0.31	-0.02	-0.09	0.38	-0.49	-0.30	0.26	0.58	-0.59	-0.58
MnO	0.29	-0.11	-0.30	-0.40	0.81	1.00	0.52	-0.30	0.76	0.23	0.74	-0.26	0.39	-0.04	-0.49	0.60	-0.04	-0.30	-0.21	-0.15	-0.19	0.07	-0.41	-0.40	-0.08	0.34	-0.57	-0.55
Na2O	0.78	0.11	-0.62	-0.17	0.54	0.52	1.00	-0.62	0.50	0.41	0.42	-0.21	0.33	0.02	-0.63	0.28	0.01	-0.06	-0.61	0.35	0.32	0.10	-0.63	0.06	-0.09	0.45	-0.53	-0.65
P2O5	-0.87	-0.80	1.00	-0.60	-0.39	-0.30	-0.62	1.00	-0.41	-0.83	-0.24	-0.53	-0.63	-0.72	0.44	-0.18	-0.46	-0.69	0.97	-0.80	-0.69	-0.69	0.95	-0.14	-0.46	-0.82	0.33	0.72
Fe2O3(T)	0.20	0.12	-0.41	-0.23	0.98	0.76	0.50	-0.41	1.00	0.56	0.94	0.03	0.75	0.30	-0.51	0.92	0.10	-0.14	-0.32	0.08	0.02	0.48	-0.50	-0.15	0.34	0.64	-0.53	-0.57
TiO2	0.51	0.79	-0.83	0.59	0.49	0.23	0.41	-0.83	0.56	1.00	0.33	0.75	0.83	0.86	-0.31	0.40	0.46	0.66	-0.82	0.79	0.72	0.92	-0.77	0.38	0.80	0.99	-0.26	-0.60
Zn	0.09	-0.05	-0.24	-0.37	0.96	0.74	0.42	-0.24	0.94	0.33	1.00	-0.16	0.57	0.13	-0.57	0.93	0.02	-0.29	-0.14	-0.16	-0.24	0.29	-0.36	-0.37	0.17	0.42	-0.58	-0.51
Ba	0.14	0.87	-0.53	0.90	-0.04	-0.26	-0.21	-0.53	0.03	0.75	-0.16	1.00	0.49	0.92	0.13	-0.02	0.46	0.90	-0.55	0.68	0.60	0.85	-0.43	0.35	0.86	0.68	0.11	-0.20
Co	0.30	0.60	-0.63	0.32	0.65	0.39	0.33	-0.63	0.75	0.83	0.57	0.49	1.00	0.72	-0.23	0.59	0.20	0.37	-0.60	0.52	0.43	0.86	-0.61	0.18	0.67	0.84	-0.21	-0.45
Ga	0.32	0.95	-0.72	0.85	0.23	-0.04	0.02	-0.72	0.30	0.86	0.13	0.92	0.72	1.00	-0.07	0.19	0.47	0.87	-0.70	0.72	0.59	0.95	-0.65	0.23	0.85	0.81	-0.04	-0.39
La	-0.46	-0.10	0.45	0.12	-0.54	-0.49	-0.63	0.44	-0.51	-0.31	-0.57	0.13	-0.23	-0.07	1.00	-0.46	-0.32	0.01	0.33	-0.13	-0.13	-0.17	0.59	0.07	0.07	-0.38	0.92	0.88
Ni	-0.02	-0.06	-0.18	-0.33	0.91	0.60	0.28	-0.18	0.92	0.40	0.93	-0.02	0.59	0.19	-0.46	1.00	0.04	-0.26	-0.11	-0.13	-0.16	0.39	-0.27	-0.25	0.34	0.50	-0.52	-0.42
Pb	0.27	0.54	-0.46	0.51	0.03	-0.04	0.01	-0.46	0.10	0.46	0.02	0.46	0.20	0.47	-0.32	0.04	1.00	0.54	-0.32	0.64	0.65	0.43	-0.59	0.47	0.24	0.44	-0.17	-0.46
Rb	0.42	0.95	-0.69	0.99	-0.19	-0.30	-0.06	-0.69	-0.14	0.66	-0.29	0.90	0.37	0.87	0.01	-0.26	0.54	1.00	-0.69	0.79	0.68	0.73	-0.59	0.30	0.63	0.58	0.09	-0.30
Sr	-0.87	-0.78	0.97	-0.60	-0.31	-0.21	-0.61	0.97	-0.32	-0.82	-0.14	-0.55	-0.60	-0.70	0.33	-0.11	-0.32	-0.69	1.00	-0.79	-0.69	-0.68	0.84	-0.15	-0.52	-0.80	0.20	0.59
Th	0.63	0.84	-0.80	0.75	-0.02	-0.15	0.35	-0.80	0.08	0.79	-0.16	0.68	0.52	0.72	-0.13	-0.13	0.64	0.79	-0.79	1.00	0.96	0.69	-0.73	0.66	0.51	0.72	0.03	-0.42
U	0.56	0.70	-0.69	0.65	-0.09	-0.19	0.32	-0.69	0.02	0.72	-0.24	0.60	0.43	0.59	-0.13	-0.16	0.65	0.68	-0.69	0.96	1.00	0.60	-0.63	0.78	0.43	0.66	0.02	-0.39
V	0.28	0.84	-0.69	0.69	0.38	0.07	0.10	-0.69	0.48	0.92	0.29	0.85	0.86	0.95	-0.17	0.39	0.43	0.73	-0.68	0.69	0.60	1.00	-0.63	0.30	0.90	0.90	-0.14	-0.44
Y	-0.81	-0.73	0.95	-0.49	-0.49	-0.41	-0.63	0.95	-0.50	-0.77	-0.36	-0.43	-0.61	-0.65	0.59	-0.27	-0.59	-0.59	0.84	-0.73	-0.63	-0.63	1.00	-0.12	-0.31	-0.77	0.50	0.85
Zr	0.03	0.29	-0.14	0.32	-0.30	-0.40	0.06	-0.14	-0.15	0.38	-0.37	0.35	0.18	0.23	0.07	-0.25	0.47	0.30	-0.15	0.66	0.78	0.30	-0.12	1.00	0.26	0.31	0.18	-0.02
Nb	0.04	0.68	-0.46	0.62	0.26	-0.08	-0.09	-0.46	0.34	0.80	0.17	0.86	0.67	0.85	0.07	0.34	0.24	0.63	-0.52	0.51	0.43	0.90	-0.31	0.26	1.00	0.77	0.07	-0.15
Cr	0.51	0.72	-0.82	0.49	0.58	0.34	0.45	-0.82	0.64	0.99	0.42	0.68	0.84	0.81	-0.38	0.50	0.44	0.58	-0.80	0.72	0.66	0.90	-0.77	0.31	0.77	1.00	-0.36	-0.66
Ce	-0.31	-0.02	0.33	0.19	-0.59	-0.57	-0.53	0.33	-0.53	-0.26	-0.58	0.11	-0.21	-0.04	0.92	-0.52	-0.17	0.09	0.20	0.03	0.02	-0.14	0.50	0.18	0.07	-0.36	1.00	0.87
Nd	-0.63	-0.43	0.72	-0.18	-0.58	-0.55	-0.65	0.72	-0.57	-0.60	-0.51	-0.20	-0.45	-0.39	0.88	-0.42	-0.46	-0.30	0.59	-0.42	-0.39	-0.44	0.85	-0.02	-0.15	-0.66	0.87	1.00

Table D.6. Correlation coefficient (r) between major and selected trace elements for samples (n=13) of fine-grained meta-sedimentary rocks of the Isaac Formation at both Castle Creek and Mount Quanstrom study areas.

	SiO2	Al2O3	CaO	K2O	MgO	MnO	Na2O	P2O5	Fe2O3(T)	TiO2	Zn	Ba	Co	Ga	La	Ni	Pb	Rb	Sr	Th	U	V	Y	Zr	Nb	Cr	Ce	Nd
SiO2	1.00	0.00	-0.68	-0.02	-0.29	-0.40	-0.02	-0.07	-0.24	0.36	0.37	0.03	-0.49	0.15	-0.40	-0.26	-0.17	-0.03	-0.51	0.22	0.06	0.25	0.03	0.56	0.15	0.41	-0.26	-0.23
Al2O3	0.00	1.00	-0.66	0.83	0.03	-0.47	0.62	0.02	-0.08	0.57	0.50	0.74	-0.23	0.80	0.32	0.35	0.26	0.85	-0.07	0.39	0.30	0.77	0.58	-0.22	0.87	0.49	0.26	0.37
CaO	-0.68	-0.66	1.00	-0.54	-0.09	0.40	-0.23	0.07	-0.05	-0.83	-0.68	-0.52	0.46	-0.59	0.27	-0.20	-0.08	-0.56	0.60	-0.62	-0.45	-0.77	-0.48	-0.36	-0.78	-0.78	0.14	0.06
K2O	-0.02	0.83	-0.54	1.00	0.11	-0.34	0.29	0.03	-0.14	0.43	0.19	0.97	-0.13	0.74	0.23	0.08	0.42	0.99	-0.28	0.28	0.16	0.81	0.56	-0.36	0.71	0.37	0.37	0.43
MgO	-0.29	0.03	-0.09	0.11	1.00	0.62	-0.55	0.08	0.85	0.38	0.27	0.03	0.11	-0.01	-0.38	0.32	-0.20	0.13	-0.44	0.39	0.52	0.12	0.20	0.06	0.22	0.18	-0.26	-0.32
MnO	-0.40	-0.47	0.40	-0.34	0.62	1.00	-0.48	0.03	0.52	-0.17	-0.38	-0.35	0.15	-0.63	-0.44	0.06	-0.15	-0.34	-0.16	-0.11	0.09	-0.34	-0.33	-0.09	-0.23	-0.26	-0.47	-0.57
Na2O	-0.02	0.62	-0.23	0.29	-0.55	-0.48	1.00	-0.19	-0.58	0.02	0.04	0.23	-0.27	0.33	0.35	0.10	0.18	0.32	0.52	-0.04	-0.06	0.21	-0.02	-0.29	0.40	0.07	0.06	0.19
P2O5	-0.07	0.02	0.07	0.03	0.08	0.03	-0.19	1.00	0.04	-0.09	0.32	-0.03	-0.16	0.00	0.30	0.04	-0.24	0.01	-0.09	-0.22	0.06	-0.09	0.17	-0.05	0.00	-0.15	0.34	0.28
Fe2O3(T)	-0.24	-0.08	-0.05	-0.14	0.85	0.52	-0.58	0.04	1.00	0.47	0.42	-0.18	0.34	-0.08	-0.29	0.62	-0.05	-0.13	-0.45	0.52	0.52	0.07	0.35	0.36	0.14	0.32	-0.21	-0.24
TiO2	0.36	0.57	-0.83	0.43	0.38	-0.17	0.02	-0.09	0.47	1.00	0.74	0.40	-0.22	0.44	-0.35	0.52	0.27	0.45	-0.57	0.89	0.74	0.78	0.55	0.54	0.78	0.96	-0.20	-0.12
Zn	0.37	0.50	-0.68	0.19	0.27	-0.38	0.04	0.32	0.42	0.74	1.00	0.10	-0.21	0.49	0.01	0.53	-0.13	0.21	-0.39	0.62	0.58	0.42	0.61	0.50	0.56	0.64	0.03	0.11
Ba	0.03	0.74	-0.52	0.97	0.03	-0.35	0.23	-0.03	-0.18	0.40	0.10	1.00	-0.09	0.68	0.19	0.01	0.49	0.96	-0.32	0.27	0.12	0.82	0.51	-0.32	0.62	0.37	0.38	0.46
Co	-0.49	-0.23	0.46	-0.13	0.11	0.15	-0.27	-0.16	0.34	-0.22	-0.21	-0.09	1.00	0.04	0.31	0.46	0.38	-0.15	0.09	-0.17	-0.37	-0.21	0.21	-0.05	-0.38	-0.26	0.38	0.24
Ga	0.15	0.80	-0.59	0.74	-0.01	-0.63	0.33	0.00	-0.08	0.44	0.49	0.68	0.04	1.00	0.46	0.22	0.10	0.75	-0.12	0.17	-0.02	0.70	0.60	-0.14	0.63	0.34	0.53	0.51
La	-0.40	0.32	0.27	0.23	-0.38	-0.44	0.35	0.30	-0.29	-0.35	0.01	0.19	0.31	0.46	1.00	0.12	0.01	0.20	0.46	-0.46	-0.52	0.01	0.33	-0.54	0.03	-0.35	0.85	0.83
Ni	-0.26	0.35	-0.20	0.08	0.32	0.06	0.10	0.04	0.62	0.52	0.53	0.01	0.46	0.22	0.12	1.00	0.42	0.08	-0.19	0.51	0.35	0.21	0.65	0.26	0.38	0.44	0.05	0.08
Pb	-0.17	0.26	-0.08	0.42	-0.20	-0.15	0.18	-0.24	-0.05	0.27	-0.13	0.49	0.38	0.10	0.01	0.42	1.00	0.38	-0.14	0.37	0.11	0.37	0.41	0.08	0.19	0.37	0.11	0.21
Rb	-0.03	0.85	-0.56	0.99	0.13	-0.34	0.32	0.01	-0.13	0.45	0.21	0.96	-0.15	0.75	0.20	0.08	0.38	1.00	-0.24	0.30	0.21	0.81	0.52	-0.36	0.73	0.38	0.33	0.41
Sr	-0.51	-0.07	0.60	-0.28	-0.44	-0.16	0.52	-0.09	-0.45	-0.57	-0.39	-0.32	0.09	-0.12	0.46	-0.19	-0.14	-0.24	1.00	-0.49	-0.30	-0.42	-0.52	-0.39	-0.32	-0.49	0.19	0.18
Th	0.22	0.39	-0.62	0.28	0.39	-0.11	-0.04	-0.22	0.52	0.89	0.62	0.27	-0.17	0.17	-0.46	0.51	0.37	0.30	-0.49	1.00	0.86	0.58	0.48	0.55	0.59	0.90	-0.32	-0.15
U	0.06	0.30	-0.45	0.16	0.52	0.09	-0.06	0.06	0.52	0.74	0.58	0.12	-0.37	-0.02	-0.52	0.35	0.11	0.21	-0.30	0.86	1.00	0.39	0.19	0.48	0.47	0.70	-0.45	-0.29
V	0.25	0.77	-0.77	0.81	0.12	-0.34	0.21	-0.09	0.07	0.78	0.42	0.82	-0.21	0.70	0.01	0.21	0.37	0.81	-0.42	0.58	0.39	1.00	0.53	0.09	0.84	0.76	0.19	0.26
Y	0.03	0.58	-0.48	0.56	0.20	-0.33	-0.02	0.17	0.35	0.55	0.61	0.51	0.21	0.60	0.33	0.65	0.41	0.52	-0.52	0.48	0.19	0.53	1.00	0.06	0.56	0.48	0.40	0.49
Zr	0.56	-0.22	-0.36	-0.36	0.06	-0.09	-0.29	-0.05	0.36	0.54	0.50	-0.32	-0.05	-0.14	-0.54	0.26	0.08	-0.36	-0.39	0.55	0.48	0.09	0.06	1.00	-0.04	0.57	-0.46	-0.46
Nb	0.15	0.87	-0.78	0.71	0.22	-0.23	0.40	0.00	0.14	0.78	0.56	0.62	-0.38	0.63	0.03	0.38	0.19	0.73	-0.32	0.59	0.47	0.84	0.56	-0.04	1.00	0.73	0.07	0.16
Cr	0.41	0.49	-0.78	0.37	0.18	-0.26	0.07	-0.15	0.32	0.96	0.64	0.37	-0.26	0.34	-0.35	0.44	0.37	0.38	-0.49	0.90	0.70	0.76	0.48	0.57	0.73	1.00	-0.17	-0.06
Ce	-0.26	0.26	0.14	0.37	-0.26	-0.47	0.06	0.34	-0.21	-0.20	0.03	0.38	0.38	0.53	0.85	0.05	0.11	0.33	0.19	-0.32	-0.45	0.19	0.40	-0.46	0.07	-0.17	1.00	0.94
Nd	-0.23	0.37	0.06	0.43	-0.32	-0.57	0.19	0.28	-0.24	-0.12	0.11	0.46	0.24	0.51	0.83	0.08	0.21	0.41	0.18	-0.15	-0.29	0.26	0.49	-0.46	0.16	-0.06	0.94	1.00

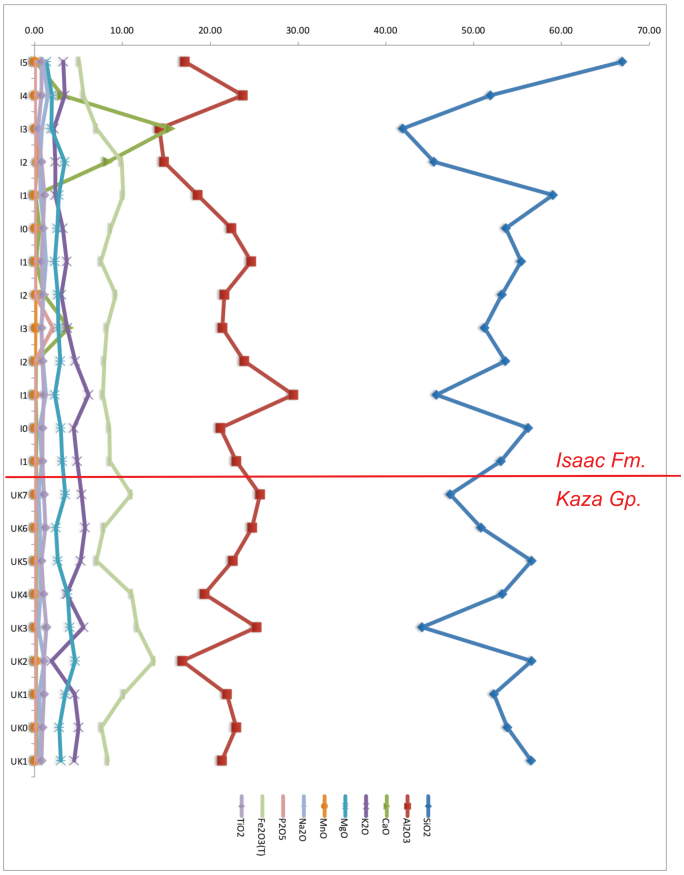

Figure D.1. Major element diagram (in wt%) from sedimentary rocks throughout the studied interval between Uppermost Kaza Group and Isaac Formation at the Castle Creek study area. See Appendix B for sample location.

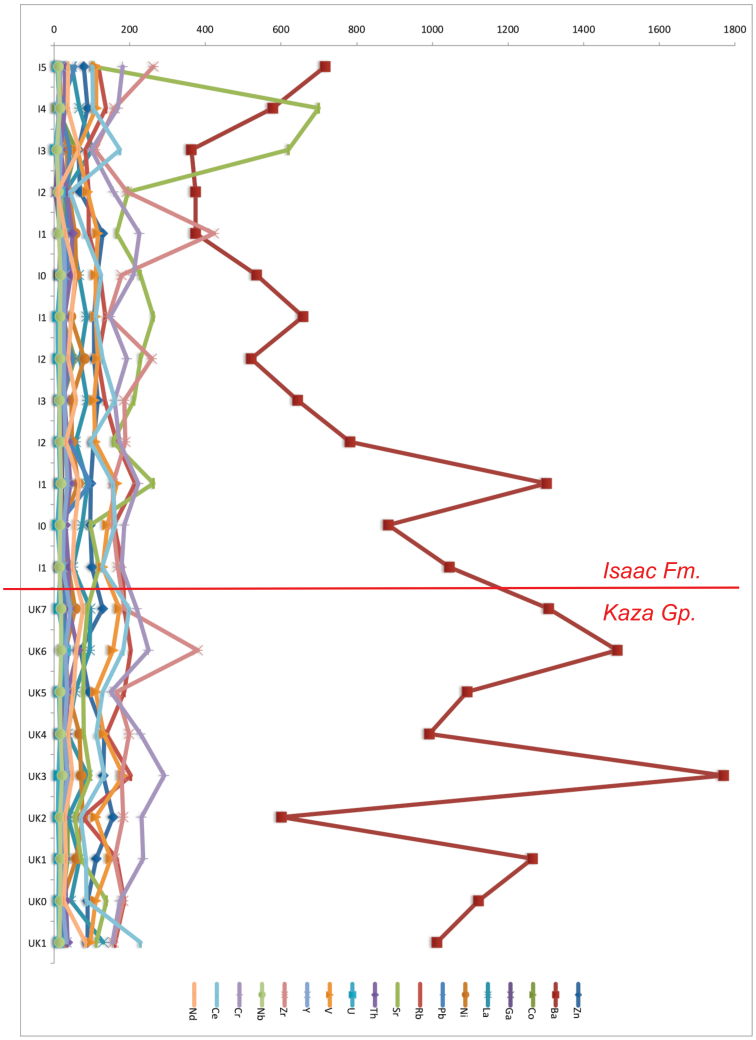

Figure D.2. Minor element diagram (in ppm) from sedimentary rocks throughout the studied interval between Uppermost Kaza Group and Isaac Formation at the Castle Creek study area. See Appendix B for sample location.

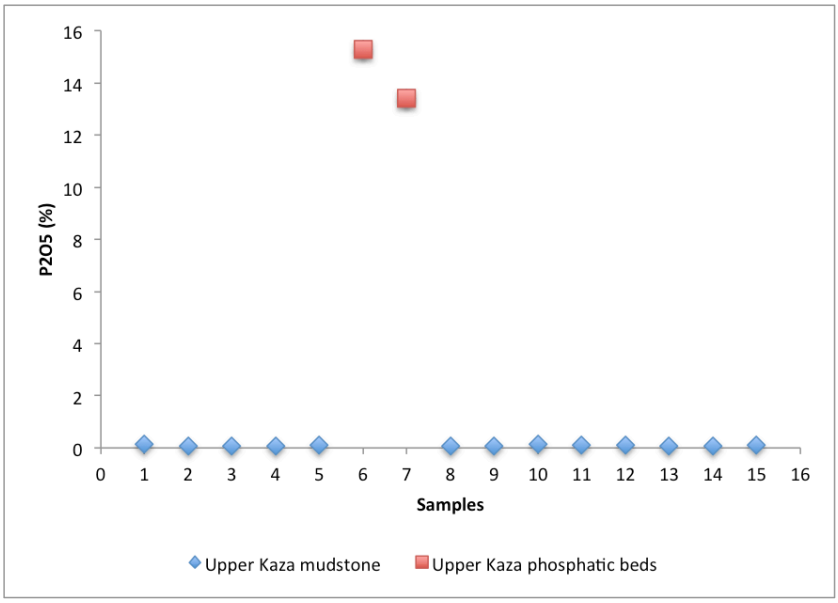

Figure D.3. Phosphate content (in weight percent) from phosphatic beds vs. mudstone of the Uppermost Kaza Group at the Castle Creek study area.

Table D.7. Total organic carbon content (in weight percent) from fine-grained sedimentary rocks of the Upper Kaza Group and Isaac Formation at the Castle Creek study area. See Appendix B for sample location

Stratigraphic Unit	Sample	TOC (wt%)
Upper Kaza Group	KI-2	0.00
	KI-7	0.002
	KI-14	0.003
	KI-21	0.003
	KI-53	0.379
	KI-112	0.003
	KI-133	0.002
	KI-140	0.001
	KI-141	0.001
Isaac Formation	KI-31	0.004
	KI-61	0.19
	KI-64	0.003
	KI-138	0.44
	KI-139	0.004
	KI-144	0.37

Appendix E: Carbonate $\delta^{13}C$ and $\delta^{18}O$ isotope data of the First Isaac Carbonate

Table E.1. Carbon and oxygen isotope composition of carbonates and shale from the FIC. This is illustrated in Fig. 5.15 (Samples are from unpublished data by G. M. Ross)

Unit	Stratal Element	Sample Name	Description	$\delta^{13}C_{org}$	$\delta^{13}C_{carb}$	$\delta^{18}O_{carb}$
FIC	Calciturbidite Unit 2	RAR-R071-B	limestone		0.6	-15.3
FIC	Calciturbidite Unit 2	RAR-R071-C	shale	-18.0		
FIC	Calciturbidite Unit 2	RAR-R071-D	limestone		1.2	-16.6
FIC	Calciturbidite Unit 2	RAR-R071-E	limestone		2.0	-15.2
FIC	Calciturbidite Unit 2	RAR-R071-F	limestone		1.7	-16.2
FIC	Calciturbidite Unit 2	RAR-R071-G	vein		2.0	-15.8
FIC	Calciturbidite Unit 2	RAR-R071-H	limestone		2.4	-15.5
FIC	Calciturbidite Unit 2	RAR-R071-I	limestone		3.3	-15.2
FIC	Calciturbidite Unit 2	RAR-R071-J	limestone		3.5	-15.1
FIC	Calciturbidite Unit 2	RAR-R071-K	shale	-20.4		
FIC	Calciturbidite Unit 2	RAR-R071-L	limestone		3.5	-15.3
FIC	Gullies 1	RAR-R071-M	shale	-22.3		
FIC	Gullies 1	RAR-R071-N	shale	-14.3		
FIC	Gullies 1	RAR-R071-O	limestone		3.8	-15.4
FIC	Gullies 1	RAR-R071-P	shale	-18.8		
FIC	Gullies 1	RAR-R071-Q	limestone		3.2	-15.2
FIC	Gullies 1	RAR-R071-R	limestone		3.7	-15.2
FIC	Fine-grained siliciclastics	RAR-R071-S	shale	-18.1		
FIC	Fine-grained siliciclastics	RAR-R071-T	limestone		2.3	-15.3
FIC	Fine-grained siliciclastics	RAR-R071-U	limestone		2.5	-15.4
FIC	Fine-grained siliciclastics	RAR-R071-V	shale	-17.6		
FIC	Gullies 2	RAR-R071-W	limestone		2.2	-16.0
FIC	Gullies 2	RAR-R071-X	limestone		1.8	-15.8
FIC	Gullies 2	RAR-R071-Y	shale	-15.3		
FIC	Gullies 2	RAR-R071-Z	limestone		1.7	-15.2
FIC	Fine-grained siliciclastics	RAR-R071-AA	shale	-17.3		
FIC	Fine-grained siliciclastics	RAR-R071-BB	shale	-17.6		
FIC	Fine-grained siliciclastics	RAR-R071-CC	shale	-17.6		
FIC	Calciturbidite Unit 3	RAR-R071-DD	limestone		1.4	-15.1
FIC	Calciturbidite Unit 3	RAR-R071-EE	limestone		-0.5	-15.2

FIC	Calciturbidite Unit 3	RAR-R071-FF	limestone		-1.2	-15.6
FIC	Calciturbidite Unit 3	RAR-R071-GG	limestone		0.7	-16.1
FIC	Calciturbidite Unit 3	RAR-R071-HH	limestone		-3.2	-15.7
FIC	Calciturbidite Unit 3	RAR-R071-II	shale	-25.9		

Appendix F: Gamma Ray profiles and data

Table F.1. Gamma-ray data recorded for Section KI1, Castle Creek South

#	Meters	Stratal element	Readings 1	Readings 2	Readings 3	Average
1	0.75	**Sandstone Unit 4**	43.3	42.7	44.3	**43.4**
2	1.5		35	36.2	36.1	**35.8**
3	2.25		42.2	51.8	47	**47**
4	3		36.1	32.1	32.3	**33.5**
5	3.75		49.9	44.9	45.6	**46.8**
6	4.5		30.9	33.4	29	**31.1**
7	5.25		62.6	66.4	64.9	**64.6**
8	6		40.5	40.6	43.1	**41.4**
9	6.75		43.4	36.6	39.3	**39.8**
10	7.5		40.3	32.8	36.8	**36.6**
11	8.25		64.4	57.9	61.7	**61.3**
12	9	**Mudstone**	62.3	65.1	64.5	**64**
13	9.75		81	70.7	73.4	**75**
14	10.5		61.4	68.1	70.7	**66.7**
15	11.25		69.6	70.8	69.3	**69.9**
16	12		73.2	71.1	77.5	**73.9**
17	12.75		76.6	75	76.2	**75.9**
18	13.5		73.8	72.6	79.1	**75.2**
19	14.25		79.9	79.8	85.3	**81.7**
20	15	**Sandstone Unit 5**	62.7	60.1	60	**60.9**
21	15.75		39.7	43.4	44.2	**42.4**
22	16.5		53.9	55.5	57.7	**55.7**
23	17.25		49.5	50.8	45.2	**48.5**
24	18		37.2	39.7	37.2	**38**
25	18.75		67.7	71.4	67.1	**68.7**
26	19.5		55	47.1	45.8	**49.3**
27	20.25		50.6	55.4	53	**53**
28	21		54.6	59.2	58.1	**57.3**
29	21.75		40.8	33.3	31.9	**35.3**
30	22.5		36	36.4	46.4	**39.6**
31	23.25		34.5	34.7	32.7	**34**
32	24		40.5	44.3	43.6	**42.8**
33	24.75		62.8	71.8	64.1	**66.2**
34	25.5		52	53.3	55.8	**53.7**
35	26.25		50.4	51	49.8	**50.4**
36	27		43.2	50.1	47.4	**46.9**
37	27.75		57.1	56.7	61.6	**58.5**
38	28.5		33.3	38.6	38.8	**36.9**
39	29.25		42.1	43	39.6	**41.6**
40	30		36.7	37.8	33.3	**35.9**
41	30.75		44.1	41.3	38.5	**41.3**
42	31.5		54	54.7	58.6	**55.8**

43	32.25		66.5	71.1	68.2	**68.6**
44	33		76.9	75.3	75.8	**76**
45	33.75		41.3	45.8	41.5	**42.9**
46	34.5		39.7	36.8	38.3	**38.3**
47	35.25		75.2	75.4	71.4	**74**
48	36		58	45.8	51.9	**51.9**
49	36.75		76.7	71.1	75	**74.3**
50	37.5		54.6	53.7	49.6	**52.6**
51	38.25		43.8	42.7	39.5	**42**
52	39		41.9	39	37.6	**39.5**
53	39.75		60	61.3	59.8	**60.4**
54	40.5		50.8	49.3	52.1	**50.7**
55	41.25		40.9	39.5	39.2	**39.9**
56	42		37.1	35	36.2	**36.1**
57	42.75		46.5	49.1	51.2	**48.9**
58	43.5	**Mudstone**	68.2	64.9	67	**66.7**
59	44.25		65.1	67.6	59.6	**64.1**
60	45		65.7	58.5	61.1	**61.8**
61	45.75		73.1	78.9	74.1	**75.4**
62	46.5		79	65.2	64.5	**69.6**
63	47.25		68.6	67.8	66.1	**67.5**
64	48		76.1	76.7	74.3	**75.7**
65	48.75		74.1	72.7	71.3	**72.7**
66	49.5	**Sandstone Unit 6**	27.9	31.3	32.6	**30.6**
67	50.25		70.1	67	72.1	**69.7**
68	51		54.1	58.2	63.8	**58.7**
69	51.75		55.1	40.7	42.1	**46**
70	52.5		59.5	54.2	54.7	**56.1**
71	53.25		43	41.8	40.2	**41.7**
72	54		0	0	0	
73	54.75		37.7	37.5	36.4	**37.2**
74	55.5		46.5	49.8	48.8	**48.4**
75	56.25		31.1	34.5	32.6	**32.7**
76	57		48.3	44.5	44.3	**45.7**
77	57.75		46.8	46.1	44.6	**45.8**
78	58.5		42.9	41.3	46	**43.4**
79	59.25		44.8	38.6	37.6	**40.3**
80	60		42	35.8	42.6	**40.1**
81	60.75		33.8	37.1	35	**35.3**
82	61.5		37.3	38	39.5	**38.3**
83	62.25		43.4	44.6	43.6	**43.9**
84	63		30.8	26.7	30.2	**29.2**
85	63.75		38.3	38.1	38	**38.1**
86	64.5		90.7	94.4	90.7	**91.9**
87	65.25		42.1	38.9	39.4	**40.1**
88	66		40.9	37.1	39	**39**
89	66.75		41.6	43.4	40.9	**42**
90	67.5		49	43.3	42.2	**44.8**

91	68.25		40.6	40.1	39.8	**40.2**
92	69		36.3	39.8	42.2	**39.4**
93	69.75		36.9	34.7	37.4	**36.3**
94	70.5		37.4	39.4	40.5	**39.1**
95	71.25		40.7	41.4	42.3	**41.5**
96	72		37.5	34.5	37.2	**36.4**
97	72.75		41.1	46.1	41.1	**42.8**
98	73.5		49.7	47.5	47	**48.1**
99	74.25		53.6	54.2	55.3	**54.4**
100	75		41.4	44.3	41.5	**42.4**
101	75.75		35.6	31.7	31.4	**32.9**
102	76.5		37.7	40.1	39.7	**39.2**
103	77.25		40.5	38.5	35.2	**38.1**
104	78		35.7	38.5	36.1	**36.8**
105	78.75		75.4	70.3	66.7	**70.8**
106	79.5		41.1	43.1	45.8	**43.3**
107	80.25		31.2	33	35.4	**33.2**
108	81		76	69.3	73.3	**72.9**
109	81.75		37	40.9	42.2	**40**
110	82.5	**Mudstone**	62.8	67.6	62.3	**64.2**
111	83.25		77.3	68.8	73.3	**73.1**
112	84		67.5	66.3	62.9	**65.6**
113	84.75		69.1	68.9	67.5	**68.5**
114	85.5		61.5	64.2	59.9	**61.9**
115	86.25	**Sandstone Unit 7**	49.8	55.9	53.3	**53**
116	87		37	36	39.9	**37.6**
117	87.75		49.1	47.4	46.7	**47.7**
118	88.5		31.1	34.2	32.1	**32.5**
119	89.25		54.7	55.1	56.5	**55.4**
120	90		40.3	42.3	44.5	**42.4**
121	90.75		32.8	34.2	31.5	**32.8**
122	91.5		43.7	47.1	48.3	**46.4**
123	92.25	**Mudstone**	70.6	66.6	65	**67.4**
124	93		58	63.3	63.1	**61.5**
125	93.75		70.6	65.2	70.7	**68.8**
126	94.5		75.5	81.1	77.2	**77.9**
127	95.25		69.7	68.8	64.2	**67.6**
128	96	**Sandstone**	36.6	32.4	35.5	**34.8**
129	96.75		40	40.4	38.5	**39.6**
130	97.5		38.5	35.9	41.3	**38.6**
131	98.25		45.3	45	39	**43.1**
132	99		37.8	39.5	38.4	**38.6**
134	99.75		44	42.5	43.9	**43.5**
135	100.5		40.5	38	36	**38.2**
136	101.25		50.9	57.5	56.9	**55.1**
137	102		57	61.7	64	**60.9**
138	102.75		43.2	38.7	39.5	**40.5**
139	103.5		35.6	34.7	37.9	**36.1**

140	104.25		40.3	41.8	43.5	**41.9**
141	105		41.5	41.3	42.2	**41.7**
142	105.75		67.1	79.8	78.3	**75.1**
143	106.5		41.5	44	43.2	**42.9**
144	107.25		47.8	45.3	47	**46.7**
145	108		37.1	44.1	42.3	**41.2**
146	108.75		46.4	48.1	42.2	**45.6**
147	109.5		45.3	46.7	50.3	**47.4**
148	110.25		37.3	30.9	34	**34.1**
149	111		56.6	53.7	58.3	**56.2**
150	111.75		71.4	70.5	74.8	**72.2**
151	112.5		72.9	77.2	82.1	**77.4**
152	113.25		58	56.6	56.7	**57.1**
153	114		35.4	37.9	41.2	**38.2**
154	114.75		55.5	52.8	53.1	**53.8**
155	115.5		54	57.6	51.1	**54.2**
156	116.25		45.3	50.4	44.8	**46.8**
157	117		31.8	33.4	34.2	**33.1**
158	117.75		31.9	32.9	33.8	**32.9**
159	118.5		30.8	30	33.6	**31.5**
160	119.25		33.3	36.9	36.1	**35.4**
161	120		36.9	40.1	38.9	**38.6**
162	120.75		37.3	30.7	34.6	**34.2**
163	121.5		55.6	53.1	51.1	**53.3**
164	122.25		50	52.8	48.2	**50.3**
165	123		70.2	73.4	71.4	**71.7**
166	123.75		57.1	55.8	56.2	**56.4**
167	124.5		40	38.1	44.4	**40.8**
168	125.25	**Mudstone**	79.1	77.8	82.1	**79.7**
169	126		75.2	75.1	79.8	**76.7**
170	126.75		81.6	76.3	74.8	**77.6**
171	127.5		80.5	76.7	80.7	**79.3**
172	128.25		73.9	75.1	77.9	**75.6**
173	129	**Base of Isaac Contact Channel Complex**	42.7	41.7	40.6	**41.7**
174	129.75		30	32.1	31.5	**31.2**
175	130.5		34.1	33.9	30.3	**32.8**
176	131.25		31.6	27.6	27.9	**29**
177	132		34.9	30.2	30.5	**31.9**
178	132.75		29.6	25.3	26.7	**27.2**
179	133.5		27.1	24	24.8	**25.3**
180	134.25		43.6	52.5	54.8	**50.3**
181	135		30.8	30.1	29.4	**30.1**
182	135.75		34.8	39.5	41.2	**38.5**
183	136.5		41.8	42.1	39	**41**
184	137.25		30.1	29.4	30.2	**29.9**
185	138		36	33.2	34.3	**34.5**
186	138.75		32.7	35.7	33.5	**34**

187	139.5		32.9	36.5	36.4	**35.3**
188	140.25		32.6	27.4	29	**29.7**
189	141		36.9	36.5	37.3	**36.9**
190	141.75		21	25.7	29.1	**25.3**
191	142.5		31.9	32	32.6	**32.2**
192	143.25		36.7	34	37.1	**35.9**
193	144		28.3	31.6	32.5	**30.8**
194	144.75		30.8	33.8	33.5	**32.7**
195	145.5		32.8	33	33.5	**33.1**
196	146.25		28.9	29.1	29.3	**29.1**
197	147		33	33.4	34.1	**33.5**
198	147.75		30.1	30.7	33.9	**31.6**
199	148.5	**Top of Isaac Contact Channel**	47	42.7	44.9	**44.9**
180	149.25		73.5	70.8	67.2	**70.5**
181	150		69.7	68.2	71.6	**69.8**
182	150.75		62.1	62.3	64.7	**63**
183	151.5		70.9	75.6	70.2	**72.2**
184	152.25		75.6	78	74	**75.9**
185	153		73.5	74.5	74	**74**
186	153.75		77	73.1	72	**74**
187	154.5		70.2	70.9	73.2	**71.4**
188	155.25		76.6	74.8	70	**73.8**
189	156		70.9	73.4	71.4	**71.9**
190	156.75		72.1	68.7	76.6	**72.5**
191	157.5		74	81	71.9	**75.6**
192	158.25		68.8	63.7	63.4	**65.3**
193	159		69.7	71.2	70.8	**70.6**
194	159.75		71.6	72.2	73	**72.3**
195	160.5		71.1	79.4	77	**75.8**
196	161.25		74.3	71.2	72.9	**72.8**
197	162		73.2	71.5	75	**73.2**
198	162.75		71.6	74.4	70.6	**72.2**
199	163.5		74.9	74.8	73.5	**74.4**
200	164.25		74.3	72	73.1	**73.1**
201	165		70.5	72.4	64.1	**69**
202	165.75	**Calcareous Sandstone Unit 1**	52.5	55	58.8	**55.4**
203	166.5		53.1	51.1	50.7	**51.6**
204	167.25		52.5	48.3	50	**50.3**
205	168		57.7	56.6	61.5	**58.6**
206	168.75		55.9	52.1	53.4	**53.8**
207	169.5		46.9	50.5	48.9	**48.8**
208	170.25		76.2	71.5	76	**74.6**
209	171		63.6	68.6	69	**67.1**
210	171.75		64.4	66.1	68.3	**66.3**
211	172.5		57.2	60	58.9	**58.7**
212	173.25		37.4	38.9	34.3	**36.9**
213	174		46.9	53.9	47.4	**49.4**

214	174.75		48.8	44.7	39.4	**44.3**
215	175.5		50.2	45.3	47.9	**47.8**
216	176.25		40.1	37.3	38.4	**38.6**
217	177		38.5	42.1	37.8	**39.5**
218	177.75		54.1	54.8	55.3	**54.7**
219	178.5		46	45.8	44.5	**45.4**
220	179.25		63.4	74.1	66.5	**68**
221	180		38.2	40.5	39.4	**39.4**
222	180.75		66.3	64.7	65.4	**65.5**
223	181.5		47.7	42.6	45.9	**45.4**
224	182.25		64.3	63.1	56.9	**61.4**
225	183		40.7	35.8	34.5	**37**
226	183.75		31.7	34.9	37.2	**34.6**
227	184.5		62.6	64.6	69.2	**65.5**
228	185.25		42.9	40.2	37.9	**40.3**
229	186		57.4	64.1	58.4	**60**
230	186.75		56.5	55.5	55.3	**55.8**
231	187.5		64.1	61.3	66.2	**63.9**
232	188.25		71.1	69.6	71.3	**70.7**
233	189		64.1	59.1	65.7	**63**
234	189.75		73.3	75.6	72.2	**73.7**
235	190.5		69.9	77.2	70.7	**72.6**
236	191.25		32	32.4	29.5	**31.3**
237	192		68.9	66.3	68.3	**67.8**
238	192.75		55.6	57.6	51.8	**55**
239	193.5		75	67.8	67.6	**70.1**

Isaac Slide 2

Table F.2. Gamma-ray data recorded for Section LI-3, Castle Creek

#	Meters	Stratal element	Readings 1	Readings 2	Readings 3	Average	Lithology
1	0.75	**Isaac slide 2**	71.1	69.6	71.3	**70.7**	
2	1.5		64.1	59.1	65.7	**63**	
3	2.25		73.3	75.6	72.2	**73.7**	
4	3		69.9	77.2	70.7	**72.6**	
5	3.75		32	32.4	29.5	**31.3**	
6	4.5		68.9	66.3	68.3	**67.8**	
7	5.25		55.6	57.6	51.8	**55**	
8	6		75	67.8	67.6	**70.1**	
9	6.75		34.1	38.1	31.9	**34.7**	
10	7.5		36.6	35	36.3	**36**	
11	8.25		67.3	66.1	66.7	**66.7**	
12	9		61.3	66.3	61.1	**62.9**	
13	9.75		57.3	53.5	55.7	**55.5**	
14	10.5		74.2	66.2	71.1	**70.5**	
15	11.25		44.5	44.3	43	**43.9**	
16	12		31.9	30.6	30.9	**31.1**	
17	12.75		37.3	35.1	34.3	**35.6**	
18	13.5		33.4	30.8	32.9	**32.4**	
19	14.25		64.8	62.6	70.7	**66**	
20	15		31.9	32	30.3	**31.4**	
21	15.75		37.4	36.4	38.1	**37.3**	
22	16.5		46.9	43.6	42.8	**44.4**	
23	17.25		44.1	44.8	39.3	**42.7**	
24	18		73	74.8	71.2	**73**	
25	18.75		35.7	29.1	32.8	**32.5**	
26	19.5		39	37	38.5	**38.2**	
27	20.25		34.1	33.6	32.2	**33.3**	
28	21		58.9	49.7	56.1	**54.9**	
29	21.75		31.2	32.3	32.8	**32.1**	
30	22.5		70.3	73.3	68.6	**70.7**	
31	23.25		66.4	72.8	69.8	**69.7**	
32	24		45	41.9	42.1	**43**	
33	24.75		35.3	35	34	**34.8**	
34	25.5		34.2	31.3	34.6	**33.4**	
35	26.25		43	39.8	44.9	**42.6**	
36	27		38.1	39.4	36.3	**37.9**	
37	27.75		84.3	91.6	89.6	**88.5**	
38	28.5		82.3	86.5	88.9	**85.9**	
39	29.25		75.1	71	83	**76.4**	
40	30		46.9	39.8	42.9	**43.2**	
41	30.75		69.3	69	72	**70.1**	
42	31.5		67.3	64.4	71.9	**67.9**	
43	32.25		70.2	69	66.3	**68.5**	
44	33		60	60.3	59.6	**60**	
45	33.75		71.3	70	71.2	**70.8**	

46	34.5		72.8	70.7	68.7	**70.7**	
47	35.25		71.4	65.5	68.1	**68.3**	
48	36		63.4	61.8	70	**65.1**	
49	36.75		71.6	72.7	72.2	**72.2**	
50	37.5		67.3	70.3	67.4	**68.3**	
51	38.25		72.5	67.4	73.5	**71.1**	
52	39		64.5	68.8	66.9	**66.7**	
53	39.75	**Isaac Debrite 1 base**	70.5	65.9	68.1	**68.2**	Mud-rich debrite
54	40.5		65.7	60.8	60	**62.2**	Mud-rich debrite
55	41.25		57.9	59.8	55	**57.6**	Mud-rich debrite
56	42		58.3	56	59.7	**58**	Mud-rich debrite
57	42.75		54.6	63	63.1	**60.2**	Mud-rich debrite
58	43.5		54.7	49.4	46.5	**50.2**	Mud-rich debrite
59	44.25	**Isaac Debrite 1 top**	55.1	59.2	58.1	**57.5**	Mud-rich debrite
60	45	**Fine-grained unit**	65.2	64.7	67.5	**65.8**	
61	45.75		67	63	67.8	**65.9**	
62	46.5		66.8	73.2	75.9	**72**	
63	47.25		41.5	37.5	37	**38.7**	
64	48		55.4	54	57	**55.5**	
65	48.75		65.3	63.4	71.3	**66.7**	
66	49.5		61.1	59.8	58.6	**59.8**	
67	50.25		67.7	69.2	67.4	**68.1**	
68	51		69.3	62.5	67.9	**66.6**	
69	51.75		62.2	66.3	65.1	**64.5**	
70	52.5		61.8	63.2	64.4	**63.1**	
71	53.25		-	-	-	**-**	
72	54		-	-	-	**-**	
73	54.75		-	-	-	**-**	
74	55.5		-	-	-	**-**	
75	56.25		-	-	-	**-**	
76	57		-	-	-	**-**	
77	57.75		-	-	-	**-**	
78	58.5		-	-	-	**-**	
79	59.25		-	-	-	**-**	

Table F.3. Gamma-ray data recorded for Section LI-5, Castle Creek

#	Meters	Stratal element	Readings 1	Readings 2	Readings 3	Average	Lithology
1	0.75	**Base of Isaac Channel Complex 0**	34.3	36	32.3	**34.2**	
2	1.5		34.1	36.4	34	**34.8**	
3	2.25		36.3	37.5	37.1	**37**	
4	3		39.2	36.1	39.3	**38.2**	
5	3.75		39	38.7	37.4	**38.4**	
6	4.5		34.4	31.1	34.9	**33.5**	
7	5.25		42.6	39.6	39.9	**40.7**	
8	6		43.2	43.4	37.2	**41.3**	
9	6.75		37.2	38.5	35.5	**37.1**	
10	7.5		45.5	38.7	38.6	**40.9**	
11	8.25		34.7	39.1	37.1	**37**	
12	9		39.5	43.1	39.5	**40.7**	
13	9.75		31.6	32.9	30.6	**31.7**	
14	10.5		29.8	31.8	34.6	**32.1**	
15	11.25		37.7	36.2	35.5	**36.5**	
16	12		45.6	48.5	44.8	**46.3**	
17	12.75		51.6	49.8	51	**50.8**	
18	13.5		47.1	59.8	56.4	**54.4**	
19	14.25		47.5	32.4	30	**36.6**	
20	15	**Top of Isaac Channel 0**	36.3	33.4	36.8	**35.5**	Sandstone
21	15.75		69	67.1	66.2	**67.4**	Interbedded Mudstone & sandstone
22	16.5		56.8	59.9	58.9	**58.5**	Interbedded Mudstone & sandstone
23	17.25		42.5	41.1	39.6	**41.1**	Interbedded Mudstone & sandstone
24	18		55.8	55.6	61.1	**57.5**	Interbedded Mudstone & sandstone
25	18.75		61.8	60.6	63	**61.8**	Interbedded Mudstone & sandstone
26	19.5		51.5	52.5	52	**52**	Interbedded Mudstone & sandstone
27	20.25		65.6	60.3	56.8	**60.9**	Interbedded Mudstone & sandstone
28	21		69.2	71.7	72.5	**71.1**	Interbedded Mudstone & sandstone
29	21.75		56.2	55.8	63	**58.3**	Interbedded Mudstone & sandstone
30	22.5		41.2	41	37	**39.7**	Sandstone
31	23.25		74	74.9	75	**74.6**	Interbedded Mudstone & sandstone
32	24		54.5	55	54.5	**54.7**	Sandstone
33	24.75		81.2	78.1	78.9	**79.4**	Interbedded Mudstone & sandstone
34	25.5		46.6	42	45	**44.5**	Sandstone
35	26.25		63.2	66.9	67.4	**65.8**	Interbedded Mudstone & sandstone
36	27		63.4	62.6	60.4	**62.1**	Interbedded Mudstone & sandstone
37	27.75		63.6	71.5	64.1	**66.4**	Interbedded Mudstone & sandstone
38	28.5		62.8	66.4	63.2	**64.1**	Interbedded Mudstone & sandstone
39	29.25		73.9	73.8	69.5	**72.4**	Interbedded Mudstone & sandstone
40	30		69.3	74.4	70.1	**71.3**	Interbedded Mudstone & sandstone
41	30.75		70.2	71.2	72.9	**71.4**	Interbedded Mudstone & sandstone
42	31.5		64	64.9	66.9	**65.3**	Interbedded Mudstone & sandstone
43	32.25		67.8	71.7	73.8	**71.1**	Interbedded Mudstone & sandstone
44	33		68.3	70.1	68	**68.8**	Interbedded Mudstone & sandstone

45	33.75	63.7	64.5	62.7	**63.6**	Interbedded Mudstone & sandstone
46	34.5	64.8	68.8	63.7	**65.8**	Interbedded Mudstone & sandstone
47	35.25	71.8	71.5	72.6	**72**	Interbedded Mudstone & sandstone
48	36	67.1	69.6	71.1	**69.3**	Interbedded Mudstone & sandstone
49	36.75	68.5	62.1	70	**66.9**	Interbedded Mudstone & sandstone
50	37.5	67.9	65.6	64.8	**66.1**	Interbedded Mudstone & sandstone
51	38.25	66.6	63.8	69.7	**66.7**	Interbedded Mudstone & sandstone
52	39	66.9	69.7	66.9	**67.8**	Interbedded Mudstone & sandstone
53	39.75	67.1	68.8	68.3	**68.1**	Interbedded Mudstone & sandstone
54	40.5	67.7	61.7	62.9	**64.1**	Interbedded Mudstone & sandstone
55	41.25	63.8	68.5	72	**68.1**	Interbedded Mudstone & sandstone
56	42	70	69.7	64.2	**68**	Interbedded Mudstone & sandstone
57	42.75	70.2	68.9	66.3	**68.5**	Interbedded Mudstone & sandstone
58	43.5	67.4	69	71	**69.1**	Interbedded Mudstone & sandstone
59	44.25	72	72.7	68.9	**71.2**	Interbedded Mudstone & sandstone
60	45	63.5	62	61.9	**62.5**	Interbedded Mudstone & sandstone
61	45.75	71.7	67.6	72.5	**70.6**	Interbedded Mudstone & sandstone
62	46.5	71.3	72.3	68.5	**70.7**	Interbedded Mudstone & sandstone
63	47.25	65.3	67.8	63	**65.4**	Interbedded Mudstone & sandstone
64	48	71.1	67.3	70.4	**69.6**	Interbedded Mudstone & sandstone
65	48.75	69.1	72.3	66.2	**69.2**	Interbedded Mudstone & sandstone

Table F.4. Gamma-ray data recorded for Section LI-13, Castle Creek

#	Meters	Stratal element	Readings 1	Readings 2	Readings 3	Average	Lithology
1	0.75	**Isaac Slide 2**	36.1	39.9	37	**37.7**	Sandstone
2	1.5		43.5	42.2	40.4	**42.0**	Sandstone
3	2.25		33.5	36	32.6	**34.0**	Sandstone
4	3		29.1	30.7	32	**30.6**	Sandstone
5	3.75		29.9	28.1	28.7	**28.9**	Sandstone
6	4.5		30.7	35.7	31	**32.5**	Sandstone
7	5.25		54.9	52.8	53.6	**53.8**	Sandstone
8	6	**12 cm above Shear zone base**	56	54.1	53.8	**54.6**	Sandy mudstone (shear zone)
9	6.75		52.1	55.7	56.2	**54.7**	Sandy mudstone
10	7.5		59.5	62.6	55.5	**59.2**	Sandy mudstone
11	8.25		57.8	58.4	64.7	**60.3**	Sandy mudstone
12	9		73.5	70	76.6	**73.4**	Sandy mudstone
13	9.75		29.1	29.3	30.8	**29.7**	Pebble conglomerate
14	10.5		29.5	26.5	29.1	**28.4**	Very coarse sandstone
15	11.25		25.8	28.7	26.7	**27.1**	Very coarse sandstone
16	12		63	58	60.3	**60.4**	Mudstone
17	12.75		55.9	55.6	51.3	**54.3**	Interbedded Mudstone & sandstone
18	13.5		59.4	58.8	55.3	**57.8**	Interbedded Mudstone & sandstone
19	14.25		58.7	64.5	59.8	**61.0**	Interbedded Mudstone & sandstone
20	15		63.5	61	66.1	**63.5**	Interbedded Mudstone & sandstone
21	15.75	**Isaac Debrite 1 base**	60.4	61.5	64	**62.0**	Mudstone
22	16.5		48.6	51.7	47.3	**49.2**	Mud-rich debrite
23	17.25		45.5	50.9	46.9	**47.8**	Mud-rich debrite
24	18		51.9	56.3	54.5	**54.2**	Mud-rich debrite
25	18.75		48.2	50.4	51.4	**50.0**	Mud-rich debrite
26	19.5		56.6	60.2	58.6	**58.5**	Mud-rich debrite
27	20.25		59.7	57.5	53	**56.7**	Mud-rich debrite
28	21		60.3	61.1	59.9	**60.4**	Mud-rich debrite
29	21.75		67.2	61.1	64.6	**64.3**	Mud-rich debrite
30	22.5		62.2	58	63.3	**61.2**	Mud-rich debrite
31	23.25		56.4	57	54.1	**55.8**	Mud-rich debrite
32	24		63.8	61.8	61.2	**62.3**	Mud-rich debrite
33	24.75		59.9	58.4	58.6	**59.0**	Mud-rich debrite
34	25.5		42.1	46.9	43.1	**44.0**	Mud-rich debrite
35	26.25		52.7	56.7	57.37	**55.6**	Mud-rich debrite
36	27		59.4	64.4	61.8	**61.9**	Mud-rich debrite
37	27.75		58.9	59.6	58.2	**58.9**	Mud-rich debrite
38	28.5		60.6	64.1	59.5	**61.4**	Mud-rich debrite
39	29.25	**Isaac Debrite 1 top**	68.3	65.8	66.9	**67.0**	Mud-rich debrite
40	30	**Sandstone-rich Splay**	26.9	24.6	23.7	**25.1**	Granule conglomerate
41	30.75		29.7	29.6	30.8	**30.0**	Sandstone
42	31.5		29.5	26.4	24.8	**26.9**	Sandstone
43	32.25		29.4	31.2	31	**30.5**	Sandstone
44	33		43.4	45.5	45.2	**44.7**	Sandstone

45	33.75		59	58.3	59.4	**58.9**	Interbedded Mudstone & sandstone
46	34.5		43.7	37.7	41.8	**41.1**	Sandstone interbedded with mudstone
47	35.25		40.5	38	37.1	**38.5**	Sandstone
48	36	**Fine-grained deposits**	57.1	61.8	57.5	**58.8**	Interbedded Mudstone & sandstone
49	36.75		52.4	53.1	54.4	**53.3**	Interbedded Mudstone & sandstone
50	37.5		54.5	54	53.3	**53.9**	Sandstone interbedded with mudstone
51	38.25		55.1	56.4	56.6	**56.0**	Sandstone interbedded with mudstone
52	39		57.9	58.8	55.9	**57.5**	Sandstone interbedded with mudstone
53	39.75		53.1	51.8	55.1	**53.3**	Interbedded Mudstone & sandstone
54	40.5		57.4	52.7	54.4	**54.8**	Sandstone interbedded with mudstone
55	41.25		61.5	59.4	61.3	**60.7**	Sandstone interbedded with mudstone
56	42		56	54.4	57.4	**55.9**	Sandstone interbedded with mudstone
57	42.75		65.8	65.6	63.2	**64.9**	Sandstone interbedded with mudstone
58	43.5		50.7	52.1	54.9	**52.6**	Sandstone interbedded with mudstone
59	44.25		59.1	54.4	56.6	**56.7**	Interbedded Mudstone & sandstone
60	45		53.6	64.7	57.7	**58.7**	Interbedded Mudstone & sandstone
61	45.75		59.3	59.4	58.2	**59.0**	Interbedded Mudstone & sandstone
62	46.5		60.7	61.8	59.9	**60.8**	Sandstone interbedded with mudstone
63	47.25		58.3	55.5	59.2	**57.7**	Interbedded Mudstone & sandstone
64	48		55.9	54.7	63.9	**58.2**	Sandstone interbedded with mudstone
65	48.75		57.1	54	56.5	**55.9**	Sandstone interbedded with mudstone
66	49.5		54.1	55.1	58.1	**55.8**	Sandstone interbedded with mudstone
67	50.25		60.1	61.9	59	**60.3**	Sandstone interbedded with mudstone
68	51		57.5	53.5	57.6	**56.2**	Sandstone interbedded with mudstone
69	51.75		57.3	58.5	56.7	**57.5**	Interbedded Mudstone & sandstone
70	52.5		54.5	51.7	52.3	**52.8**	Sandstone interbedded with mudstone
71	53.25		53.1	54.9	55.9	**54.6**	Sandstone interbedded with mudstone
72	54		58.7	54.7	60.9	**58.1**	Sandstone interbedded with mudstone
73	54.75		50.5	53.3	50.1	**51.3**	Sandstone interbedded with mudstone
74	55.5		50.4	56.5	62.3	**56.4**	Interbedded Mudstone & sandstone
75	56.25		58.1	57.1	58.5	**57.9**	Interbedded Mudstone & sandstone
76	57		55.3	54	51.9	**53.7**	Interbedded Mudstone & sandstone
77	57.75		57.6	58.3	56.7	**57.5**	Interbedded Mudstone & sandstone
78	58.5		62.1	62.8	60.6	**61.8**	Interbedded Mudstone & sandstone
79	59.25		60.7	58.7	60.1	**59.8**	Interbedded Mudstone & sandstone
80	60		58.6	56.7	55.4	**56.9**	Interbedded Mudstone & sandstone
81	60.75		57	58	59.2	**58.1**	Interbedded Mudstone & sandstone
82	61.5		61.6	56.1	58.3	**58.7**	Interbedded Mudstone & sandstone
83	62.25		56.9	53.7	59.2	**56.6**	Interbedded Mudstone & sandstone
84	63		59.3	53.4	62.3	**58.3**	Interbedded Mudstone & sandstone
85	63.75		63.3	56	56.4	**58.6**	Interbedded Mudstone & sandstone
86	64.5		57.7	59.2	56.6	**57.8**	Interbedded Mudstone & sandstone
87	65.25		55.2	57.9	6.3	**39.8**	Interbedded Mudstone & sandstone
88	66		61.6	62.2	62.4	**62.1**	Interbedded Mudstone & sandstone
89	66.75		61.6	57.1	53.8	**57.5**	Interbedded Mudstone & sandstone
90	67.5		56.6	58.6	55.6	**56.9**	Interbedded Mudstone & sandstone
91	68.25		58.7	63.2	57.1	**59.7**	Interbedded Mudstone & sandstone
92	69		57	59.2	57.4	**57.9**	Interbedded Mudstone & sandstone

93	69.75	55.4	63.8	59	**59.4**	Interbedded Mudstone & sandstone
94	70.5	56.6	58.5	55.6	**56.9**	Interbedded Mudstone & sandstone
95	71.25	57.9	58.7	57.5	**58.0**	Interbedded Mudstone & sandstone
96	72	54	54.2	55.5	**54.6**	Interbedded Mudstone & sandstone
97	72.75	58.3	57.4	51.9	**55.9**	Interbedded Mudstone & sandstone
98	73.5	57.4	59.4	57.7	**58.2**	Interbedded Mudstone & sandstone
99	74.25	39.7	40.8	41.2	**40.6**	Sandstone
100	75	54.3	57.7	53.3	**55.1**	Interbedded Mudstone & sandstone
101	75.75	55.9	58.6	57.5	**57.3**	Interbedded Mudstone & sandstone
102	76.5	56	62.6	55.2	**57.9**	Interbedded Mudstone & sandstone
103	77.25	57.2	58.3	59.1	**58.2**	Interbedded Mudstone & sandstone
104	78	58.4	55.4	58.8	**57.5**	Interbedded Mudstone & sandstone
105	78.75	57.4	54.9	59.4	**57.2**	Interbedded Mudstone & sandstone
106	79.5	56	58.1	56.3	**56.8**	Interbedded Mudstone & sandstone
107	80.25	57.4	57.9	56.7	**57.3**	Interbedded Mudstone & sandstone
108	81	60	58.9	56.8	**58.6**	Interbedded Mudstone & sandstone
109	81.75	54.9	51.3	54.1	**53.4**	Interbedded Mudstone & sandstone
110	82.5	62.3	55.9	5.1	**41.1**	Interbedded Mudstone & sandstone
111	83.25	60.7	58.9	58.1	**59.2**	Interbedded Mudstone & sandstone
112	84	52.8	54.4	56.8	**54.7**	Interbedded Mudstone & sandstone
113	84.75	56	56.8	52.7	**55.2**	Interbedded Mudstone & sandstone
114	85.5	56.7	58.3	55.2	**56.7**	Interbedded Mudstone & sandstone
115	86.25	58.1	57.8	56.5	**57.5**	Interbedded Mudstone & sandstone
116	87	54.5	54.4	55.2	**54.7**	Interbedded Mudstone & sandstone
117	87.75	57.7	52	57	**55.6**	Interbedded Mudstone & sandstone
118	88.5	57.3	60	62.1	**59.8**	Interbedded Mudstone & sandstone
119	89.25	60.3	57.5	54.3	**57.4**	Interbedded Mudstone & sandstone
120	90	59.1	57.6	51.8	**56.2**	Interbedded Mudstone & sandstone
121	90.75	57.3	58.7	55.3	**57.1**	Interbedded Mudstone & sandstone
122	91.5	54.3	53	54.7	**54.0**	Calciturbidites
123	92.25	54.1	55.5	53.2	**54.3**	Calciturbidites
124	93	57.2	54.8	53.8	**55.3**	Calciturbidites

Table F.5. Gamma-ray data recorded for Section LI-16, Castle Creek

#	Meters	Stratal element	Readings 1	Readings 2	Readings 3	Average	Lithology
1	0.75	**Isaac Slide 2**	34.3	32.9	32	**33.1**	Sandstone
2	1.5		55.4	54.2	56.7	**55.4**	Mudstone interbedded with sandstone
3	2.25		58.3	59.9	60.2	**59.5**	Mudstone interbedded with sandstone
4	3		38	35.7	40.6	**38.1**	Sandstone
5	3.75		63.5	65.7	67.4	**65.5**	Mudstone interbedded with sandstone
6	4.5		35.9	33.5	33.9	**34.4**	Sandstone
7	5.25		61.9	58.1	58.5	**59.5**	Mudstone
8	6		29	29.1	30.7	**29.6**	Sandstone
9	6.75		34.7	32.6	33	**33.4**	Sandstone
10	7.5		32.3	37	34.4	**34.6**	Sandstone
11	8.25		60.8	53	56.5	**56.8**	Mudstone interbedded with sandstone
12	9		47	49.8	49.6	**48.8**	Sandy Mudstone
13	9.75		53.7	53.6	55.7	**54.3**	Sandy Mudstone
14	10.5		48.9	47.4	46	**47.4**	Sandy Mudstone
15	11.25		50.7	53.3	54.4	**52.8**	Sandy Mudstone
16	12		51	49.9	53.5	**51.5**	Sandy Mudstone
17	12.75		35.3	33.7	33	**34.0**	Sandstone
18	13.5		59.8	61.2	59.8	**60.3**	Mudstone
19	14.25		59.6	57.7	57.3	**58.2**	Mudstone
20	15		56	54.3	58.8	**56.4**	Mudstone
21	15.75		61.3	57.6	62.5	**60.5**	Mudstone
22	16.5	**Isaac Debrite 1 base**	63.5	66.7	63.9	**64.7**	Mud-rich debrite
23	17.25		50	48.5	49.4	**49.3**	Mud-rich debrite
24	18		59.9	65.1	61.5	**62.2**	Mud-rich debrite
25	18.75		54.2	48.5	45.4	**49.4**	Mud-rich debrite
26	19.5		54	55.7	54.3	**54.7**	Mud-rich debrite
27	20.25		51.9	52.2	53	**52.4**	Mud-rich debrite
28	21		52.2	52.5	51.5	**52.1**	Mud-rich debrite
29	21.75		42.2	42.4	42.3	**42.3**	Mud-rich debrite
30	22.5		49.6	49.3	49.1	**49.3**	Mud-rich debrite
31	23.25		49.2	50.4	51.2	**50.3**	Mud-rich debrite
32	24		51.9	55	54.5	**53.8**	Mud-rich debrite
33	24.75		4.7	46.9	49.1	**33.6**	Mud-rich debrite
34	25.5		48.2	47.4	42.7	**46.1**	Mud-rich debrite
35	26.25		53	44.8	47.3	**48.4**	Mud-rich debrite
36	27		46.6	45.8	50.6	**47.7**	Mud-rich debrite
37	27.75		-	-	-	-	COVERED
38	28.5		-	-	-	-	COVERED
39	29.25		-	-	-	-	COVERED
40	30		-	-	-	-	COVERED
41	30.75		-	-	-	-	COVERED
42	31.5		-	-	-	-	COVERED
43	32.25		-	-	-	-	COVERED
44	33		-	-	-	-	COVERED

45	33.75		-	-	-	-	COVERED
46	34.5	**Isaac Debrite 1 top**	-	-	-	-	COVERED
47	35.25	**Sandstone-rich splay**	32.1	30.9	35.2	**32.7**	Pebble conglomerate
48	36		17.1	19.1	17.2	**17.8**	Very coarse sandstone
49	36.75		26.2	25.8	26.3	**26.1**	Very coarse sandstone
50	37.5		17.9	18.6	20.9	**19.1**	Granule conglomerate
51	38.25		20.7	20.2	20.9	**20.6**	Very coarse sandstone
52	39		20.9	20.5	22.3	**21.2**	Very coarse sandstone
53	39.75		23.9	21.5	26.1	**23.8**	Coarse sandstone
54	40.5		49.6	46.5	44.5	**46.9**	Mudstone-clast breccia
55	41.25		52.3	49.5	53.1	**51.6**	Mudstone-clast breccia
56	42		55.6	54.9	54.3	**54.9**	Mudstone interbedded with sandstone
57	42.75		33.9	36.7	35.1	**35.2**	Sandstone
58	43.5	**Fine-grained deposits**	51.7	51.9	52.7	**52.1**	Mudstone interbedded with sandstone
59	44.25		52.6	52.8	50.9	**52.1**	Mudstone interbedded with sandstone
60	45		54	60.2	58	**57.4**	Mudstone interbedded with sandstone
61	45.75		54.1	55	51.1	**53.4**	Mudstone interbedded with sandstone
62	46.5		48	52.6	55.1	**51.9**	Mudstone interbedded with sandstone
63	47.25		54.6	53.4	53	**53.7**	Sandstone interbedded with mudstone
64	48		58.7	55	48.6	**54.1**	Mudstone interbedded with sandstone
65	48.75		55.8	58.1	57.1	**57.0**	Sandstone interbedded with mudstone
66	49.5		65.5	69.2	66.3	**67.0**	Mudstone interbedded with sandstone
67	50.25		59	60.9	55.9	**58.6**	Mudstone interbedded with sandstone
68	51		57.4	59.6	53.7	**56.9**	Mudstone interbedded with sandstone
69	51.75		54.8	58.2	57.8	**56.9**	Mudstone interbedded with sandstone
70	52.5		59.4	54.9	57.4	**57.2**	Mudstone interbedded with sandstone
71	53.25		58.5	55.5	53.8	**55.9**	Mudstone interbedded with sandstone
72	54		59.8	61.9	59.7	**60.5**	Mudstone interbedded with sandstone
73	54.75		56.7	53.2	56.9	**55.6**	Mudstone interbedded with sandstone
74	55.5		58.7	59.3	58.2	**58.7**	Mudstone interbedded with sandstone
75	56.25		59.4	59.5	61.1	**60.0**	Mudstone interbedded with sandstone
76	57		56.9	55	59.6	**57.2**	Mudstone interbedded with sandstone
77	57.75		60.2	58	61.5	**59.9**	Mudstone interbedded with sandstone
78	58.5		63.8	54.4	63	**60.4**	Mudstone interbedded with sandstone
79	59.25		58.6	57.1	58.3	**58.0**	Mudstone interbedded with sandstone
80	60		53.4	52.1	55.4	**53.6**	Mudstone interbedded with sandstone
81	60.75		57.1	56.5	54.1	**55.9**	Mudstone interbedded with sandstone
82	61.5		58.5	57.5	55.4	**57.1**	Mudstone interbedded with sandstone
83	62.25		63.6	59.3	59.6	**60.8**	Mudstone interbedded with sandstone
84	63		62.7	60.2	60.1	**61.0**	Mudstone interbedded with sandstone
85	63.75		62.7	62.5	60.1	**61.8**	Mudstone interbedded with sandstone
86	64.5		63.5	67	67.7	**66.1**	Mudstone interbedded with sandstone
87	65.25		57.8	57.8	56.3	**57.3**	Mudstone interbedded with sandstone
88	66		59.7	56.1	58	**57.9**	Mudstone interbedded with sandstone
89	66.75		63.6	60.2	58.8	**60.9**	Mudstone interbedded with sandstone
90	67.5		56.4	57.7	59.4	**57.8**	Mudstone interbedded with sandstone
91	68.25		58.2	56.7	66.1	**60.3**	Mudstone interbedded with sandstone
92	69		59.3	63.6	61.3	**61.4**	Mudstone interbedded with sandstone

93	69.75	60.9	56.3	56.2	**57.8**	Mudstone interbedded with sandstone
94	70.5	62.2	58.9	59.9	**60.3**	Mudstone interbedded with sandstone
95	71.25	61.7	60.2	55	**59.0**	Mudstone interbedded with sandstone
96	72	62.2	60.3	61.7	**61.4**	Mudstone interbedded with sandstone
97	72.75	57.1	56.6	55	**56.2**	Mudstone interbedded with sandstone
98	73.5	61.8	57.3	57.4	**58.8**	Mudstone interbedded with sandstone
99	74.25	55	53.2	55.5	**54.6**	Mudstone interbedded with sandstone
100	75	56.2	56	51.1	**54.4**	Mudstone interbedded with sandstone
101	75.75	56	57.8	56.9	**56.9**	Mudstone interbedded with sandstone
102	76.5	52.4	56.4	55.5	**54.8**	Mudstone interbedded with sandstone
103	77.25	57.6	57.5	53.7	**56.3**	Mudstone interbedded with sandstone
104	78	59.1	54.9	57.2	**57.1**	Mudstone interbedded with sandstone
105	78.75	58.1	57.9	52.3	**56.1**	Mudstone interbedded with sandstone
106	79.5	61.2	59	62.7	**61.0**	Mudstone interbedded with sandstone
107	80.25	58.5	54.1	55.2	**55.9**	Mudstone interbedded with sandstone

Table F.6. Gamma-ray data measured for stratigraphic section FIC 7, Castle Creek South

#	Meters	Unit	Stratal Element	Reading 1	Reading 2	Reading 3	Average
1	0.75	**FIC**		65.3	70.4	67.6	**67.8**
2	1.5	**FIC**		74.4	70.8	67.3	**70.8**
3	2.25	**FIC**		74.6	64.9	64.4	**68**
4	3	**FIC**		72.6	71.8	70.9	**71.8**
5	3.75	**FIC**		52	50.4	53.6	**52**
6	4.5	**FIC**		71.3	70.2	69.2	**70.2**
7	5.25	**FIC**		67	66.1	64	**65.7**
8	6	**FIC**		69.7	71.8	70.1	**70.5**
9	6.75	**FIC**		46.4	47.8	49.3	**47.8**
10	7.5	**FIC**		71.6	75.8	71.4	**72.9**
11	8.25	**FIC**		69.5	68.7	64.3	**67.5**
12	9	**FIC**		63.2	66.9	68.6	**66.2**
13	9.75	**FIC**		66.9	60.4	52.3	**59.9**
14	10.5	**FIC**		65.1	63.6	62.2	**63.6**
15	11.25	**FIC**		63.8	63.3	64.6	**63.9**
16	12	**FIC**		61	63.8	59.3	**61.4**
17	12.75	**FIC**		58.4	60.7	62.9	**60.7**
18	13.5	**FIC**		65.8	62.4	67	**65.1**
19	14.25	**FIC**		63.9	65.3	64.9	**64.7**
20	15	**FIC**		66.3	67.1	67.6	**67**
21	15.75	**FIC**		67.4	63.1	67.6	**66**
22	16.5	**FIC**		61.8	63.4	65	**63.4**
23	17.25	**FIC**		63.6	56.4	60.3	**60.1**
24	18	**FIC**		58.6	61.4	62.2	**60.7**
25	18.75	**FIC**		56.9	58.2	61.5	**58.9**
26	19.5	**FIC**		56.2	57.6	61.8	**58.5**
27	20.25	**FIC**		54.3	52.1	59.8	**55.4**
28	21	**FIC**		57.7	57.9	56.3	**57.3**
29	21.75	**FIC**		54.8	55.1	56	**55.3**
30	22.5	**FIC**	**Calcidebrite 1**	54.4	47.7	48.3	**50.1**
31	23.25	**FIC**		55.6	53.3	57.1	**55.3**
32	24	**FIC**	**Fine-grained siliciclastics**	60.2	62.5	62.8	**61.8**
33	24.75	**FIC**		67.2	60	65.4	**64.2**
34	25.5	**FIC**		66.6	66.2	67.1	**66.6**
35	26.25	**FIC**		66.7	64.7	66.2	**65.9**
36	27	**FIC**		63.9	63.5	61.2	**62.9**
37	27.75	**FIC**		61.9	59.3	59	**60.1**
38	28.5	**FIC**		64.4	69.4	67	**66.9**
39	29.25	**FIC**		68.2	64.7	67.2	**66.7**
40	30	**FIC**		67.7	66.4	68.1	**67.4**
41	30.75	**FIC**		66.9	65.5	67.2	**66.5**

42	31.5	**FIC**		64	62.5	68.4	**65**
43	32.25	**FIC**		69.4	61.1	64.1	**64.9**
44	33	**FIC**		61.6	64.9	64.3	**63.6**
45	33.75	**FIC**		61.3	66	64.2	**63.8**
46	34.5	**FIC**		62	62.7	60.1	**61.6**
47	35.25	**FIC**	**Bacon Sandstone Channel Complex 1-base**	28.5	30.2	26	**28.2**
48	36	**FIC**		31.2	27.6	31.1	**30**
49	36.75	**FIC**		26.9	25	26.3	**26.1**
50	37.5	**FIC**		29.7	26.8	28.3	**28.3**
51	38.25	**FIC**		22.2	21.4	24.6	**22.7**
52	39	**FIC**		30.1	28.3	26	**28.1**
53	39.75	**FIC**		40.6	41.7	43.9	**42.1**
54	40.5	**FIC**		68.8	74.5	68.6	**70.6**
55	41.25	**FIC**		64.9	64.6	68.5	**66**
56	42	**FIC**		45.4	40.1	44.7	**43.4**
57	42.75	**FIC**		65.4	69.8	70.8	**68.7**
58	43.5	**FIC**		62.8	50	53.8	**55.5**
59	44.25	**FIC**		47.5	43.3	40.3	**43.7**
60	45	**FIC**		39.5	37.6	39.7	**38.9**
61	45.75	**FIC**		41.7	43.4	43.9	**43**
62	46.5	**FIC**		41.2	39.7	40.3	**40.4**
63	47.25	**FIC**		33.6	39	38.1	**36.9**
64	48	**FIC**		43.3	50.5	49.9	**47.9**
65	48.75	**FIC**		61.1	57.8	59.8	**59.6**
66	49.5	**FIC**		64.1	63.7	64.6	**64.1**
67	50.25	**FIC**		58.8	61.5	61.9	**60.7**
68	51	**FIC**		60.8	63.3	62.7	**62.3**
69	51.75	**FIC**	**Fine-grained siliciclastics**	66.3	66.8	61.9	**65**
70	52.5	**FIC**		57.9	60.9	64.5	**61.1**
71	53.25	**FIC**		70.3	67	61.7	**66.3**
72	54	**FIC**		63.4	64.4	66	**64.6**
73	54.75	**FIC**		64.1	68.9	64.2	**65.7**
74	55.5	**FIC**		67.7	62.7	60.6	**63.7**
75	56.25	**FIC**		68.3	69.8	68.7	**68.9**
76	57	**FIC**		64.3	64.9	63.3	**64.2**
77	57.75	**FIC**		64	60.6	61.5	**62**
78	58.5	**FIC**		67.3	62.4	63.7	**64.5**
79	59.25	**FIC**		65.9	68.2	66.2	**66.8**
80	60	**FIC**		63	68.7	64.7	**65.5**
81	60.75	**FIC**		70.6	73.4	72.7	**72.2**
82	61.5	**FIC**		63.2	69.7	61.8	**64.9**
83	62.25	**FIC**		73.2	66.1	75.3	**71.5**
84	63	**FIC**		71	66.2	66.6	**67.9**
85	63.75	**FIC**		65.7	66.9	64.6	**65.7**
86	64.5	**FIC**		67.3	68.2	69.7	**68.4**
87	65.25	**FIC**		66.3	62.1	62.5	**63.6**
88	66	**FIC**		67.6	70.3	70.6	**69.5**

89	66.75	**FIC**		70.8	74.3	71.3	**72.1**
90	67.5	**FIC**		71.9	68.3	69.7	**70**
91	68.25	**FIC**	**Levee deposits**	71.4	73.9	66.5	**70.6**
92	69	**FIC**		68.1	70.7	73	**70.6**
93	69.75	**FIC**		68.5	66.7	63.2	**66.1**
94	70.5	**FIC**		51.2	56.3	46.3	**51.3**
95	71.25	**FIC**		54.4	51	50.3	**51.9**
96	72	**FIC**		50.6	50.7	46.2	**49.2**
97	72.75	**FIC**		63.3	61	68.8	**64.4**
98	73.5	**FIC**		64.7	65.9	64.4	**65**
99	74.25	**FIC**		74.8	72.6	71.8	**73.1**
100	75	**FIC**		64.6	66	59.6	**63.4**
101	75.75	**FIC**		64.9	67.1	64.4	**65.5**
102	76.5	**FIC**		62.2	65.8	66.2	**64.7**
103	77.25	**FIC**		69.4	66.6	65.6	**67.2**
104	78	**FIC**		63	64.7	70.3	**66**
105	78.75	**FIC**		67.2	68	72.2	**69.1**
106	79.5	**FIC**	**Calciturbidite Unit 2 - base**	66.5	73.2	72.2	**70.6**
107	80.25	**FIC**		71.4	74.6	70.5	**72.2**
108	81	**FIC**		67.3	55.8	64.7	**62.6**
109	81.75	**FIC**		71.3	71.5	64.9	**69.2**
110	82.5	**FIC**		54.3	65.4	54.7	**58.1**
111	83.25	**FIC**		66.3	65.7	65.1	**65.7**
112	84	**FIC**	**Calcidebrite 2**	51.6	50.2	46.1	**49.3**
113	84.75	**FIC**		51.1	48	46.9	**48.7**
114	85.5	**FIC**		51.6	50.2	49.4	**50.4**
115	86.25	**FIC**		53.3	52	59.7	**55**
116	87	**FIC**		47.9	45.3	47.6	**46.9**
117	87.75	**FIC**		48.4	47.1	48.4	**48**
118	88.5	**FIC**		46.6	44.4	46.9	**46**
119	89.25	**FIC**		43.7	44.6	39.8	**42.7**
120	90	**FIC**		40.5	44	42.9	**42.5**
121	90.75	**FIC**		43.6	41.4	40.1	**41.7**
122	91.5	**FIC**		50.6	49.4	52.6	**50.9**
123	92.25	**FIC**		47.4	49.1	43.7	**46.7**
124	93	**FIC**		43.9	43.5	36.3	**41.2**
125	93.75	**FIC**		40.9	41	40.7	**40.9**
126	94.5	**FIC**		38.9	36.8	36.9	**37.5**
127	95.25	**FIC**		40.8	42.6	42	**41.8**
128	96	**FIC**		41.3	46.1	42.7	**43.4**
129	96.75	**FIC**		43	47	43.9	**44.6**
130	97.5	**FIC**		40.6	42.6	44.9	**42.7**
131	98.25	**FIC**		42.8	42	42.6	**42.5**
132	99	**FIC**		39.3	42.4	42.7	**41.5**
133	99.75	**FIC**	**Calciturbidite Unit 2 - top**	41	42.8	50.7	**44.8**
134	100.5	**FIC**		61.6	59.9	61.9	**61.1**
135	101.25	**FIC**		65.6	64.1	67	**65.6**
136	102	**FIC**		49.5	36.6	35.2	**40.4**

137	102.75	**FIC**	**Gully Complexes 1 & 2 & Fine-grained siliciclastics**	41.8	62.5	61.7	**55.3**
138	103.5	**FIC**		54.2	65.2	57.8	**59.1**
139	104.25	**FIC**		59.2	56.6	63.4	**59.7**
140	105	**FIC**		56.5	62.1	58.1	**58.9**
141	105.75	**FIC**		57.8	63.8	65.3	**62.3**
142	106.5	**FIC**		64.3	63.4	59.6	**62.4**
143	107.25	**FIC**		62.3	50.9	45.6	**52.9**
144	108	**FIC**		54.2	49.2	50.1	**51.2**
145	108.75	**FIC**		48.8	50	51.3	**50**
146	109.5	**FIC**		53.9	65.9	61.4	**60.4**
147	110.25	**FIC**		41	43.8	40.2	**41.7**
148	111	**FIC**		52	49.1	51.2	**50.8**
149	111.75	**FIC**		52.6	48.9	50.8	**50.8**
150	112.5	**FIC**		49.3	60	52.9	**54.1**
151	113.25	**FIC**		58.5	57.4	59.4	**58.4**
152	114	**FIC**		54.5	50.1	43.8	**49.5**
153	114.75	**FIC**		40.4	42.8	39.2	**40.8**
154	115.5	**FIC**		44.2	39.7	40.4	**41.4**
155	116.25	**FIC**		48.7	47.1	45.9	**47.2**
156	117	**FIC**		63.9	67.6	70.7	**67.4**
157	117.75	**FIC**		63.1	67.1	58.2	**62.8**
158	118.5	**FIC**		69.4	75.5	72.5	**72.5**
159	119.25	**FIC**		64.5	64.2	58.1	**62.3**
160	120	**FIC**		58.2	61.8	69.9	**63.3**
161	120.75	**FIC**		61.9	56.3	56.8	**58.3**
162	121.5	**FIC**		53.5	52.5	55.5	**53.8**
163	122.25	**FIC**		50.1	42.8	46.4	**46.4**
164	123	**FIC**		49	59.5	62.7	**57.1**
165	123.75	**FIC**		62.5	54	51.9	**56.1**
166	124.5	**FIC**		51.6	58.2	52	**53.9**
167	125.25	**FIC**		43.4	38.9	33.7	**38.7**
168	126	**FIC**		36.1	43.8	38.6	**39.5**
169	126.75	**FIC**		44.1	41	42.7	**42.6**
170	127.5	**FIC**		43.7	55.5	53	**50.7**
171	128.25	**FIC**		57.2	66.2	67.3	**63.6**
172	129	**FIC**		65.4	62.1	60.2	**62.6**
173	129.75	**FIC**		57.4	60.2	58.5	**58.7**
174	130.5	**FIC**		60.7	55.9	57.5	**58**
175	131.25	**FIC**		54.3	46.2	49.5	**50**
176	132	**FIC**		52.3	49.2	49.4	**50.3**
177	132.75	**FIC**		58.9	62.9	67.2	**63**
178	133.5	**FIC**		61.6	54.1	56	**57.2**
179	134.25	**FIC**		50.2	47.8	47.7	**48.6**
180	135	**FIC**		47.3	51.3	52	**50.2**
181	135.75	**FIC**		66.6	63.2	57.8	**62.5**
182	136.5	**FIC**		66.1	49.9	52.7	**56.2**
183	137.25	**FIC**		46.5	40.2	40.8	**42.5**

184	138	**FIC**	47.5	58.9	55.7	**54**
185	138.75	**FIC**	53.9	46.9	44.4	**48.4**
186	139.5	**FIC**	52.3	59.1	63	**58.1**
187	140.25	**FIC**	59	66.5	62.9	**62.8**
188	141	**FIC**	62.6	61.2	57.7	**60.5**
189	141.75	**FIC**	60.1	60.7	64	**61.6**
190	142.5	**FIC**	59	55.6	53.9	**56.2**
191	143.25	**FIC**	51.9	50.3	49.9	**50.7**
192	144	**FIC**	57.3	70.8	64.9	**64.3**
193	144.75	**FIC**	63.8	58.7	65.7	**62.7**
194	145.5	**FIC**	64.7	58.4	56.4	**59.8**
195	146.25	**FIC**	59.1	65.2	70.7	**65**
196	147	**FIC**	60.7	61.5	67.9	**63.4**
197	147.75	**FIC**	68.3	64.3	59.6	**64.1**
198	148.5	**FIC**	61.8	63.2	63.8	**62.9**
199	149.25	**FIC**	56.9	42.4	44.1	**47.8**
200	150	**FIC**	48.9	56.6	56.3	**53.9**
201	150.75	**FIC**	58.2	62.1	59.4	**59.9**
202	151.5	**FIC**	66.4	64.3	64.6	**65.1**
203	152.25	**FIC**	65.2	62.9	62	**63.4**
204	153	**FIC**	64.3	63.9	64.5	**64.2**
205	153.75	**FIC**	57.8	55.6	60	**57.8**
206	154.5	**FIC**	66	62.7	56.1	**61.6**
207	155.25	**FIC**	63.5	67.8	66.7	**66**
208	156	**FIC**	65.4	66.8	67.1	**66.4**
209	156.75	**FIC**	50	46.6	50	**48.9**
210	157.5	**FIC**	48.1	55.5	57.8	**53.8**
211	158.25	**FIC**	51.6	53	54.7	**53.1**
212	159	**FIC**	54.3	51.2	51.7	**52.4**
213	159.75	**FIC**	48.9	48.8	45.5	**47.7**
214	160.5	**FIC**	49.1	58.4	56	**54.5**
215	161.25	**FIC**	54.3	57.4	61.1	**57.6**
216	162	**FIC**	57.2	55.5	58.5	**57.1**
217	162.75	**FIC**	63.3	62.4	64.1	**63.3**
218	163.5	**FIC**	62	55.1	51.1	**56.1**
219	164.25	**FIC**	46.8	47.4	50.9	**48.4**
220	165	**FIC**	47.4	55.2	54.9	**52.5**
221	165.75	**FIC**	57.4	56.5	56.6	**56.8**
222	166.5	**FIC**	57.9	59.8	57.9	**58.5**
223	167.25	**FIC**	60.3	67.3	70.5	**66**
224	168	**FIC**	60.9	62.5	61.3	**61.6**
225	168.75	**FIC**	55.7	52	50.8	**52.8**
226	169.5	**FIC**	58.3	54.5	53.3	**55.4**
227	170.25	**FIC**	56.4	53.3	55.8	**55.2**
228	171	**FIC**	54.6	54.3	51.4	**53.4**
229	171.75	**FIC**	52.3	69.1	65.5	**62.3**
230	172.5	**FIC**	60.2	54.7	58	**57.6**
231	173.25	**FIC**	53.3	49.5	54.4	**51.4**

232	174	**FIC**		50.2	48.1	46	**48.1**
233	174.75	**FIC**		52.3	64.3	63.6	**60.1**
234	175.5	**FIC**		55.2	63.1	59.7	**59.3**
235	176.25	**FIC**		63.4	57.3	61.1	**60.6**
236	177	**FIC**		57.6	60.3	63.8	**60.6**
237	177.75	**FIC**		62.9	60.7	62.2	**61.9**
238	178.5	**FIC**		62.7	63.2	65.7	**63.9**
239	179.25	**FIC**		66.1	69.2	69.7	**68.3**
240	180	**FIC**		67.7	66.4	64.7	**66.3**
241	180.75	**FIC**		65.9	66.4	70.2	**67.5**
242	181.5	**FIC**		69	66.1	70.8	**68.6**
243	182.25	**FIC**		70.5	61.7	62.9	**65**
244	183	**FIC**		65	64.7	66.6	**65.4**
245	183.75	**FIC**		65	66.7	63.5	**65.1**
246	184.5	**FIC**		60.7	69.8	66.5	**65.7**
247	185.25	**FIC**		60.3	63.2	65.3	**62.9**
248	186	**FIC**		64.4	73.3	70.8	**69.5**
249	186.75	**FIC**		68.9	71.3	72.7	**71**
250	187.5	**FIC**		73.9	73.6	68.1	**71.9**
251	188.25	**FIC**		67.1	71.8	66.2	**68.4**
252	189	**FIC**		65	66.4	65.8	**65.7**
253	189.75	**FIC**		65.2	62.4	62.6	**63.4**
254	190.5	**FIC**		67.1	68.2	73.8	**69.7**
255	191.25	**FIC**		64.3	57.3	60.5	**60.7**
256	192	**FIC**		56	59.1	65.7	**60.3**
257	192.75	**FIC**		62.4	61.7	63.5	**62.5**
258	193.5	**FIC**		61	65.5	62.1	**62.9**
259	194.25	**FIC**	**Calciturbidite Unit 3**	66.6	66.3	64.6	**65.8**
260	195	**FIC**		68.7	63.3	64.8	**65.6**
261	195.75	**FIC**		61.5	69.4	68.9	**66.6**
262	196.5	**FIC**		71.6	65.5	60.9	**66**
263	197.25	**FIC**		50,7	52.9	53.3	**53.1**
264	198	**FIC**		55.9	71.5	60.2	**62.5**
265	198.75	**FIC**		66.4	69.1	68.9	**68.1**
266	199.5	**FIC**		70	76.5	76.4	**74.3**
267	200.25	**FIC**		64	73.5	70.4	**69.3**
268	201	**FIC**		67.7	60.6	66.9	**65.1**
269	201.75	**FIC**	**Calcidebrite 3**	67.3	73.6	71.8	**70.9**
270	202.5	**FIC**		62.8	62.5	62.1	**62.5**
271	203.25	**FIC**		65.5	71.3	74.7	**70.5**
272	204	**FIC**		76.3	82.7	86.3	**81.8**
273	204.75	**FIC**		82.9	72.8	81.1	**78.9**
274	205.5	**-**	**Isaac Channel Complex 1-base**	-	-	-	**-**

Table F.7. Gamma-ray data measured for Section FIC 9, Castle Creek North

#	Meters	Unit	Stratal Element	Reading 1	Reading 2	Reading 3	Average	Lithology
1	0.75	**FIC**	**Calciturbidite Unit 1**	50.9	58.4	50.3	**53.2**	Calciturbidite
2	1.5	**FIC**		51.7	52	51.3	**51.7**	Calciturbidite
3	2.25	**FIC**		54.8	57.7	49.5	**54.0**	Calciturbidite
4	3	**FIC**		51.6	53.7	50	**51.8**	Calciturbidite
5	3.75	**FIC**		47.8	46	51.7	**48.5**	Calciturbidite
6	4.5	**FIC**		44.9	46	45.1	**45.3**	Calciturbidite
7	5.25	**FIC**		46.2	49.9	45.2	**47.1**	Calciturbidite
8	6	**FIC**		52.6	53.1	55.1	**53.6**	Calciturbidite
9	6.75	**FIC**		53.1	49.1	51.6	**51.3**	Calciturbidite
10	7.5	**FIC**	**Fine-grained Siliciclastic deposits**	54.2	55.1	55.3	**54.9**	Interbedded Mudstone & sandstone
11	8.25	**FIC**		53.6	59.6	59.2	**57.5**	Interbedded Mudstone & sandstone
12	9	**FIC**		58.2	51	55.3	**54.8**	Interbedded Mudstone & sandstone
13	9.75	**FIC**		52	59.4	52.7	**54.7**	Interbedded Mudstone & sandstone
14	10.5	**FIC**		55.7	61.1	58.1	**58.3**	Interbedded Mudstone & sandstone
15	11.25	**FIC**		55	54.4	58.2	**55.9**	Interbedded Mudstone & sandstone
16	12	**FIC**		54.3	55.8	55.2	**55.1**	Interbedded Mudstone & sandstone
17	12.75	**FIC**		56.6	59.9	59.2	**58.6**	Interbedded Mudstone & sandstone
18	13.5	**FIC**		57.1	53	52.1	**54.1**	Interbedded Mudstone & sandstone
19	14.25	**FIC**		55.9	56	59	**57.0**	Interbedded Mudstone & sandstone
20	15	**FIC**		53	49.6	56.1	**52.9**	Interbedded Mudstone & sandstone
21	15.75	**FIC**		57.3	55	58.1	**56.8**	Interbedded Mudstone & sandstone
22	16.5	**FIC**		58.7	60	59.9	**59.5**	Interbedded Mudstone & sandstone
23	17.25	**FIC**		66.8	64	61.3	**64.0**	Interbedded Mudstone & sandstone
24	18	**FIC**		55.4	58.7	58.2	**57.4**	Interbedded Mudstone & sandstone
25	18.75	**FIC**		55.9	59.4	57.3	**57.5**	Interbedded Mudstone & sandstone
26	19.5	**FIC**		62.9	58.6	59.8	**60.4**	Interbedded Mudstone & sandstone
27	20.25	**FIC**		56.8	58.4	60.6	**58.6**	Interbedded Mudstone & sandstone
28	21	**FIC**		60.4	62.7	59.2	**60.8**	Interbedded Mudstone & sandstone
29	21.75	**FIC**		57.4	60	57.7	**58.4**	Interbedded Mudstone & sandstone
30	22.5	**FIC**		62.2	64.3	60.8	**62.4**	Interbedded Mudstone & sandstone
31	23.25	**FIC**		61.3	63.4	61.6	**62.1**	Interbedded Mudstone & sandstone
32	24	**FIC**		57.1	62.8	56.1	**58.7**	Interbedded Mudstone & sandstone
33	24.75	**FIC**		57.7	57.9	58	**57.9**	Interbedded Mudstone & sandstone
34	25.5	**FIC**		59.3	63.5	60.4	**61.1**	Interbedded Mudstone & sandstone
35	26.25	**FIC**	**Bacon Sandstone Channel Complex 1**	60	59.5	58.7	**59.4**	Interbedded Mudstone & sandstone
36	27	**FIC**		36.5	37.3	40.7	**38.2**	Conglomerate
37	27.75	**FIC**		29.1	27.5	27.1	**27.9**	Sandstone
38	28.5	**FIC**		26.1	23.8	23.5	**24.5**	Sandstone
39	29.25	**FIC**		28.9	27	26.5	**27.5**	Sandstone
40	30	**FIC**		35.2	34	33.1	**34.1**	Sandstone
41	30.75	**FIC**		28.5	26.9	31.9	**29.1**	Conglomerate/sandstone
42	31.5	**FIC**		32.6	31.4	32	**32.0**	Conglomerate
43	32.25	**FIC**		27.1	26.4	27.7	**27.1**	Conglomerate

44	33	**FIC**		26	26.7	27.9	**26.9**	Conglomerate
45	33.75	**FIC**		28.8	28.5	28.9	**28.7**	Conglomerate
46	34.5	**FIC**		31.4	30.3	31.2	**31.0**	Conglomerate
47	35.25	**FIC**		24.9	23.3	27.2	**25.1**	Conglomerate
48	36	**FIC**		29	29.9	27.6	**28.8**	Conglomerate
49	36.75	**FIC**		35.5	36.2	35.5	**35.7**	Sandstone
50	37.5	**FIC**		29.6	31.3	32.9	**31.3**	Conglomerate
51	38.25	**FIC**		34.6	30	33.8	**32.8**	Conglomerate
52	39	**FIC**		24.8	28.9	27.2	**27.0**	Conglomerate
53	39.75	**FIC**		32.4	33.9	36.3	**34.2**	Sandstone
54	40.5	**FIC**	**Fine-grained Siliciclastic deposits**	50.9	52.4	44.6	**49.3**	Interbedded Sandstone & mudstone
55	41.25	**FIC**		54.7	5.7	48.5	**36.3**	Interbedded Sandstone & mudstone
56	42	**FIC**		51.2	54.7	54	**53.3**	Interbedded Sandstone & mudstone
57	42.75	**FIC**		46.1	47.2	48	**47.1**	Sandstone
58	43.5	**FIC**		63.1	63.1	63.8	**63.3**	Interbedded Mudstone & sandstone
59	44.25	**FIC**		61.8	62.4	61.6	**61.9**	Interbedded Mudstone & sandstone
60	45	**FIC**		62.3	60.3	68.3	**63.6**	Interbedded Mudstone & sandstone
61	45.75	**FIC**		63.1	62.3	59.7	**61.7**	Interbedded Sandstone & mudstone
62	46.5	**FIC**		56.9	54.8	55	**55.6**	Interbedded Sandstone & mudstone
63	47.25	**FIC**		58.9	59.8	56.9	**58.5**	Interbedded Sandstone & mudstone
64	48	**FIC**		56.7	58.8	57.5	**57.7**	Interbedded Sandstone & mudstone
65	48.75	**FIC**		56.8	57.4	58.6	**57.6**	Interbedded Sandstone & mudstone
66	49.5	**FIC**		57.5	61.9	61	**60.1**	Interbedded Sandstone & mudstone
67	50.25	**FIC**		57.7	61.2	57.1	**58.7**	Interbedded Mudstone & sandstone
68	51	**FIC**		57.3	65.3	56	**59.5**	Interbedded Mudstone & sandstone
69	51.75	**FIC**		59.7	60.5	56.9	**59.0**	Interbedded Sandstone & mudstone
70	52.5	**FIC**		55.6	57.2	57.7	**56.8**	Interbedded Sandstone & mudstone
71	53.25	**FIC**		52.7	53.9	58.5	**55.0**	Interbedded Sandstone & mudstone
72	54	**FIC**		50.5	52.2	52.7	**51.8**	Interbedded Sandstone & mudstone
73	54.75	**FIC**		56.5	53.7	56.7	**55.6**	Interbedded Sandstone & mudstone
74	55.5	**FIC**		58.3	60.6	54	**57.6**	Interbedded Sandstone & mudstone
75	56.25	**FIC**		52.4	54.4	50.3	**52.4**	Interbedded Mudstone & sandstone
76	57	**FIC**		60.2	56.2	60	**58.8**	Interbedded Mudstone & sandstone
77	57.75	**FIC**		54.7	56.9	54.2	**55.3**	Interbedded Mudstone & sandstone
78	58.5	**FIC**		63.1	60.4	60.9	**61.5**	Interbedded Mudstone & sandstone
79	59.25	**FIC**		60.1	60.4	58.4	**59.6**	Interbedded Mudstone & sandstone
80	60	**FIC**		-	-	-	**-**	COVERED
81	60.75	**FIC**		-	-	-	**-**	COVERED
82	61.5	**FIC**		-	-	-	**-**	COVERED
83	62.25	**FIC**		59.2	60.8	57	**59.0**	Interbedded Mudstone & sandstone
84	63	**FIC**		61.1	56.8	55.9	**57.9**	Conglomerate
85	63.75	**FIC**		47.5	52.4	51.8	**50.6**	Sandstone
86	64.5	**FIC**		38.6	35.9	36.1	**36.9**	Interbedded Mudstone & sandstone
87	65.25	**FIC**		51.9	52.5	53	**52.5**	Interbedded Mudstone & sandstone
88	66	**FIC**		41.1	51.3	52.8	**48.4**	Interbedded Mudstone & sandstone
89	66.75	**FIC**		54.7	57.2	53.9	**55.3**	Interbedded Mudstone & sandstone
90	67.5	**FIC**		60.6	63.8	5.6	**43.3**	Interbedded Mudstone & sandstone

91	68.25	**FIC**		59	60.6	54.1	**57.9**	Interbedded Mudstone & sandstone
92	69	**FIC**		56.2	52.6	55.7	**54.8**	Interbedded Mudstone & sandstone
93	69.75	**FIC**		48.9	46.6	52.6	**49.4**	Interbedded Mudstone & sandstone
94	70.5	**FIC**	**Calciturbidite Unit 2**	47.1	45.4	47.6	**46.7**	Calciturbidite
95	71.25	**FIC**		50.1	49	43.7	**47.6**	Calciturbidite

Table F.8. Gamma-ray data recorded for Section FIC 10, Castle Creek North

#	Meters	Unit	Stratal Element	Reading 1	Reading 2	Reading 3	Average	Lithology
1	0.75	**FIC**	**Bacon Sandstone channel complex 1-base**	34.5	31.5	29	31.7	Conglomerate
2	1.5	**FIC**		32.6	32	33.2	32.6	Sandstone
3	2.25	**FIC**		29.9	31.2	32.4	31.2	Sandstone
4	3	**FIC**		37.6	37.2	35	36.6	Sandstone
5	3.75	**FIC**		29.7	32.6	33.1	31.8	Conglomerate
6	4.5	**FIC**		25.4	25.5	28.3	26.4	Conglomerate
7	5.25	**FIC**		28.1	22.3	25	25.1	Conglomerate
8	6	**FIC**		24.3	24.7	25	24.7	Sandstone
9	6.75	**FIC**		20.9	25.8	24.6	23.8	Conglomerate
10	7.5	**FIC**		27.8	27.2	29.1	28.0	Conglomerate
11	8.25	**FIC**		24.8	23.7	21.6	23.4	Conglomerate
12	9	**FIC**		20.8	20.2	21	20.7	Conglomerate
13	9.75	**FIC**		23.8	19.8	20.7	21.4	Conglomerate
14	10.5	**FIC**		22.5	22.9	22	22.5	Conglomerate
15	11.25	**FIC**		22.8	21.1	22.1	22	Sandstone
16	12	**FIC**		20.9	23	20.6	21.5	Conglomerate
17	12.75	**FIC**		x	x	x		covered
18	13.5	**FIC**		26.9	27.3	26.4	26.9	Conglomerate
19	14.25	**FIC**		38.3	30.1	34	34.1	Conglomerate
20	15	**FIC**		23.6	22	23.9	23.2	Conglomerate
21	15.75	**FIC**		47.5	53.5	53.3	51.4	Interbedded sandstone & mudstone
22	16.5	**FIC**		52.8	50.2	51.1	51.4	Interbedded Mudstone & sandstone
23	17.25	**FIC**		43.6	50.1	47.1	46.9	Calciturbidites
24	18	**FIC**		44.4	49.7	50.1	48.1	Calciturbidites
25	18.75	**FIC**		42.4	44.8	47.9	45.0	Calciturbidites
26	19.5	**FIC**		51.5	48.6	50.7	50.3	Calciturbidites
27	20.25	**FIC**		49	50.3	52.7	50.7	Calciturbidites
28	21	**FIC**		54.5	51.4	52.2	52.7	Calciturbidites with mudstone tops
29	21.75	**FIC**		53.2	51.4	55.1	53.2	Calciturbidites with mudstone tops
30	22.5	**FIC**		58.4	46.9	49.8	51.7	Calciturbidites with mudstone tops
31	23.25	**FIC**		56.3	60.3	56	57.5	Calciturbidites with mudstone tops
32	24	**FIC**		57.3	58.4	57	57.6	Calciturbidites with mudstone tops
33	24.75	**FIC**		58.4	59.3	56.9	58.2	Interbedded Mudstone & sandstone
34	25.5	**FIC**		-	-	-	-	COVERED
35	26.25	**FIC**		67.9	62.9	61.8	64.2	Interbedded Mudstone & sandstone
36	27	**FIC**		62.2	60.3	62.4	61.6	Interbedded Mudstone & sandstone
37	27.75	**FIC**		55.6	57.9	59.4	57.6	Interbedded Mudstone & sandstone
38	28.5	**FIC**		58.8	60.9	59.3	59.7	Interbedded Mudstone & sandstone
39	29.25	**FIC**		55.2	55.1	54.8	55.0	Interbedded Mudstone & sandstone
40	30	**FIC**		58.6	61.1	56.5	58.7	Interbedded Mudstone & sandstone
41	30.75	**FIC**		62.2	58.1	57.1	59.1	Interbedded Mudstone & sandstone
42	31.5	**FIC**	**Levee deposits**	43.7	43.6	44.3	43.9	Sandstone
43	32.25	**FIC**		43.7	44.7	44.3	44.2	Sandstone
44	33	**FIC**		42.8	41.6	46.6	43.7	Interbedded sandstone & mudstone

45	33.75	**FIC**		41.9	45.9	40	42.6	Sandstone
46	34.5	**FIC**		46.9	53.1	49.8	49.9	Sandstone
47	35.25	**FIC**		60.2	57.7	57.9	58.6	Interbedded Mudstone & sandstone
48	36	**FIC**		54.6	59.8	56.5	57.0	Interbedded Mudstone & sandstone
49	36.75	**FIC**		58.9	57	55.5	57.1	Interbedded Mudstone & sandstone
50	37.5	**FIC**		57.3	56.2	60.6	58.0	Interbedded Mudstone & sandstone
51	38.25	**FIC**		63.5	59.6	61.6	61.6	Interbedded Mudstone & sandstone
52	39	**FIC**		60.4	59.2	58.8	59.5	Interbedded Mudstone & sandstone
53	39.75	**FIC**		64.8	62.3	63.9	63.7	Interbedded Mudstone & sandstone
54	40.5	**FIC**		58.9	56.6	58.8	58.1	Interbedded Mudstone & sandstone
55	41.25	**FIC**		59.1	58.2	63.3	60.2	Interbedded Mudstone & sandstone
56	42	**FIC**		58.7	56.9	61.1	58.9	Interbedded Mudstone & sandstone
57	42.75	**FIC**		59.7	58.5	57.4	58.5	Interbedded Mudstone & sandstone
58	43.5	**FIC**		56	59.5	54.7	56.7	Interbedded Mudstone & sandstone
59	44.25	**FIC**		65.4	64	61.1	63.5	Interbedded Mudstone & sandstone
60	45	**FIC**		62.6	69.6	65.2	65.8	Interbedded Mudstone & sandstone
61	45.75	**FIC**		67.9	66.2	63.7	65.9	Interbedded Mudstone & sandstone
62	46.5	**FIC**		60.4	60.4	57.2	59.3	Interbedded Mudstone & sandstone
63	47.25	**FIC**		61.8	58.5	61.2	60.5	Interbedded Mudstone & sandstone
64	48	**FIC**	**Calciturbidite Unit 2 base**	46	48.3	44.8	46.4	Calciturbidites
65	48.75	**FIC**		40.7	41.7	41.8	41.4	Calciturbidites
66	49.5	**FIC**		40.7	37.5	41.5	39.9	Calciturbidites
67	50.25	**FIC**	**Calcidebrite 2-base**	43.5	39.2	41.8	41.5	Calcidebrite
68	51	**FIC**		52	48.4	45.8	48.7	Calcidebrite
69	51.75	**FIC**		44.3	48.9	43.9	45.7	Calcidebrite
70	52.5	**FIC**		45.6	44.9	39.1	43.2	Calcidebrite
71	53.25	**FIC**		40.6	41	44.5	42.0	Calcidebrite
72	54	**FIC**	**Calcidebrite 2-top**	53.8	53.6	53.9	53.8	Calcidebrite
73	54.75	**FIC**		40.2	42.6	38	40.3	Calciturbidites
74	55.5	**FIC**		44.1	43	41	42.7	Calciturbidites
75	56.25	**FIC**		42.6	42	41.3	42.0	Calciturbidites
76	57	**FIC**		42.2	42.5	41.2	42.0	Calciturbidites
77	57.75	**FIC**		40.8	40.2	39.2	40.1	Calciturbidites
78	58.5	**FIC**		40.8	40.2	39.2	40.1	Calciturbidites
79	59.25	**FIC**		40.2	40.3	33.6	38.0	Calciturbidites
80	60	**FIC**	**Calciturbidite Unit 2 top**	38.1	35.1	40.7	38.0	Calciturbidites
81	60.75	**FIC**		50.2	53.7	52.3	52.1	Interbedded Mudstone & sandstone
82	61.5	**FIC**	**Bacon Sandstone channel complex 2**	36.9	33.4	37.7	36	Sandstone
83	62.25	**FIC**		39.4	39	38.1	38.8	Sandstone
84	63	**FIC**		42.1	41.9	37.6	40.5	Muddy Sandstone
85	63.75	**FIC**		38.7	41.6	42.9	41.1	Sandstone
86	64.5	**FIC**		24.7	23.9	24.4	24.3	Sandstone
87	65.25	**FIC**		24	29.9	24.2	26.0	Sandstone
88	66	**FIC**		23.3	24.5	25.4	24.4	Sandstone
89	66.75	**FIC**		34.3	34.2	32.1	33.5	Mudstone-clast breccia
90	67.5	**FIC**		24.1	25.1	27.7	25.6	Conglomerate
91	68.25	**FIC**		19.2	20.1	18.6	19.3	Conglomerate

92	69	**FIC**	28.2	27	31.6	28.9	Conglomerate
93	69.75	**FIC**	35.8	36.9	39.1	37.3	Interbedded sandstone & mudstone
94	70.5	**FIC**	46.6	43.3	47.8	45.9	Calciturbidites
95	71.25	**FIC**	48.4	45.6	46.9	47.0	Sandstone
96	72	**FIC**	56	50.5	54.2	53.6	Interbedded Mudstone & sandstone
97	72.75	**FIC**	58.1	60.8	58.3	59.1	Interbedded Mudstone & sandstone
98	73.5	**FIC**	57.1	58.3	60	58.5	Interbedded Mudstone & sandstone
99	74.25	**FIC**	22.5	22.6	21.7	22.3	Sandstone
100	75	**FIC**	39.9	40.7	39.9	40.2	Sandstone
101	75.75	**FIC**	25.9	28.8	27.7	27.5	Sandstone
102	76.5	**FIC**	59.2	57.1	60	58.8	Interbedded Mudstone & sandstone
103	77.25	**FIC**	52.4	54.6	55.4	54.1	Interbedded Mudstone & sandstone
104	78	**FIC**	54.3	55.9	53.9	54.7	Mudstone
105	78.75	**FIC**	49	45.6	47.8	47.5	Interbedded Mudstone & sandstone
106	79.5	**FIC**	44.1	44.2	43.5	43.9	Sandstone
107	80.25	**FIC**	54.1	49.7	51	51.6	Calciturbidites
108	81	**FIC**	63.4	62	62.4	62.6	Interbedded Mudstone & sandstone
109	81.75	**FIC**	58.8	58	58.8	58.5	Interbedded Mudstone & sandstone
110	82.5	**FIC**	36.2	39.1	40.5	38.6	Calciturbidites
111	83.25	**FIC**	46.5	48.4	49	48.0	Calciturbidites
112	84	**FIC**	66.4	61.1	64.1	63.9	Interbedded Mudstone & sandstone
113	84.75	**FIC**	59	59.5	61.1	59.9	Interbedded Mudstone & sandstone
114	85.5	**FIC**	59.3	65.4	59.8	61.5	Interbedded Mudstone & sandstone
115	86.25	**FIC**	56.6	59.2	54.2	56.7	Interbedded Mudstone & sandstone
116	87	**FIC**	61	60.4	58.6	60	Interbedded Mudstone & sandstone
117	87.75	**FIC**	55.4	59	58.1	57.5	Interbedded Mudstone & sandstone
118	88.5	**FIC**	60.7	63.2	61	61.6	Interbedded Mudstone & sandstone
119	89.25	**FIC**	63.4	59.8	60.3	61.2	Interbedded Mudstone & sandstone
120	90	**FIC**	50.9	47.5	48.7	49.0	Interbedded Mudstone & sandstone
121	90.75	**FIC**	55.9	52.9	57.8	55.5	Interbedded Mudstone & sandstone
122	91.5	**FIC**	50.1	50.8	49.3	50.1	Interbedded Mudstone & sandstone
123	92.25	**FIC**	48.8	4.4	48.2	33.8	Calciturbidites
124	93	**FIC**	53.6	53.1	53.6	53.4	Calciturbidites
125	93.75	**FIC**	42.7	44.4	40.2	42.4	Calciturbidites
126	94.5	**FIC**	43.1	50.6	48.8	47.5	Calciturbidites
127	95.25	**FIC**	46.4	48.5	48.2	47.7	Calciturbidites
128	96	**FIC**	53.1	56.8	53.7	54.5	Interbedded Mudstone & sandstone
129	96.75	**FIC**	53	61.3	57.8	57.4	Interbedded Mudstone & sandstone
130	97.5	**FIC**	57.9	58.1	62	59.3	Interbedded Mudstone & sandstone
131	98.25	**FIC**	60.4	55.8	59.6	58.6	Interbedded Mudstone & sandstone
132	99	**FIC**	54.1	50.1	54.4	52.9	Interbedded Mudstone & sandstone
133	99.75	**FIC**	52.9	52.5	53.5	53.0	Interbedded Mudstone & sandstone
134	100.5	**FIC**	52.2	57.7	49.6	53.2	Interbedded Mudstone & sandstone
135	101.25	**FIC**	55.1	57.7	57.9	56.9	Interbedded Mudstone & sandstone
136	102	**FIC**	52.5	54.3	56.8	54.5	Interbedded Mudstone & sandstone
137	102.75	**FIC**	56.4	59.9	56.1	57.5	Interbedded Mudstone & sandstone
138	103.5	**FIC**	53.5	50.3	48.2	50.7	PARTLY-COVERED
139	104.25	**FIC**	34.3	34.2	30.5	33	Calciturbidites

140	105	**FIC**		33	30.6	31.2	31.6	Calciturbidites
141	105.75	**FIC**		54.9	53.9	52.9	53.9	Interbedded Mudstone & sandstone
142	106.5	**FIC**		59.6	60.2	61.6	60.5	Interbedded Mudstone & sandstone
143	107.25	**FIC**		58.7	57.1	59.4	58.4	Interbedded Mudstone & sandstone
144	108	**FIC**		58.9	62.7	58.1	59.9	Interbedded Mudstone & sandstone
145	108.75	**FIC**		47.8	43.4	43.1	44.8	Calciturbidites
146	109.5	**FIC**		55.9	55.6	57.8	56.4	Interbedded Mudstone & sandstone
147	110.25	**FIC**		51.4	53.7	51.2	52.1	Interbedded Mudstone & sandstone
148	111	**FIC**		53.1	53.8	53.1	53.3	Interbedded Mudstone & sandstone
149	111.75	**FIC**		57	56.6	55.7	56.4	Interbedded Mudstone & sandstone
150	112.5	**FIC**		53.2	57.1	53.9	54.7	Interbedded Mudstone & sandstone
151	113.25	**FIC**		50.9	54	50.3	51.7	Interbedded Mudstone & sandstone
152	114	**FIC**		53.3	56.8	54.7	54.9	Interbedded Mudstone & sandstone
153	114.75	**FIC**		62.2	58.1	59.8	60.0	Interbedded Mudstone & sandstone
154	115.5	**FIC**		60.6	61.6	58.9	60.4	Interbedded Mudstone & sandstone
155	116.25	**FIC**		54.6	60	59.3	58.0	Interbedded Mudstone & sandstone
156	117	**FIC**		52	53.4	58.4	54.6	Interbedded Mudstone & sandstone
157	117.75	**FIC**		-	-	-	-	COVERED
158	118.5	**FIC**		54.4	57.1	56.5	56	Sandstone
159	119.25	**FIC**		46.3	42.8	42.6	43.9	Calciturbidites
160	120	**FIC**		48	47.6	48.7	48.1	Calciturbidites
161	120.75	**FIC**		54.6	51.6	50.8	52.3	Calciturbidites
162	121.5	**FIC**		58.4	54.9	55	56.1	Calciturbidites
163	122.25	**FIC**		43.7	44.6	43.1	43.8	Calciturbidites
164	123	**FIC**		43.1	43.6	42.2	43.0	Sandstone
165	123.75	**FIC**		39.8	38.4	36	38.1	Calciturbidites
166	124.5	**FIC**	**Calciturbidite Unit 3 base**	34.1	37.5	34.9	35.5	Calciturbidites
167	125.25	**FIC**		41.6	41.9	40.5	41.3	Calciturbidites
168	126	**FIC**		40.9	41.6	42.1	41.5	Calciturbidites
169	126.75	**FIC**		47.2	51	50.3	49.5	Calciturbidites
170	127.5	**FIC**		41.6	41.7	38.4	40.6	Calciturbidites
171	128.25	**FIC**		41.4	41.4	40.5	41.1	Calciturbidites
172	129	**FIC**		41.6	38.4	37.3	39.1	Calciturbidites
173	129.75	**FIC**		41.9	42.8	39.6	41.4	Calciturbidites
174	130.5	**FIC**		46.9	50.4	46.3	47.9	Calciturbidites
175	131.25	**FIC**		43.3	42.9	39.7	42.0	Calciturbidites
176	132	**FIC**		38.1	41.9	37.6	39.2	Calciturbidites
177	132.75	**FIC**		43.4	42.9	41.9	42.7	Calciturbidites
178	133.5	**FIC**		45.9	54.8	48.7	49.8	Calciturbidites
179	134.25	**FIC**		45.3	42	44.7	44	Calciturbidites
180	135	**FIC**		58.5	56.2	58	57.6	Calciturbidites
181	135.75	**FIC**		43	45.2	45.8	44.7	Calciturbidites
182	136.5	**FIC**		43.7	43.4	43.1	43.4	Calciturbidites
183	137.25	**FIC**		33.9	36	37.8	35.9	Calciturbidites
184	138	**FIC**		41.5	40.2	45.6	42.4	Calciturbidites
185	138.75	**FIC**		40.6	42.4	44.9	42.6	Calciturbidites
186	139.5	**FIC**		45.1	39.1	43.3	42.5	Calciturbidites
187	140.25	**FIC**		46.5	46	45.3	45.9	Calciturbidites

188	141	**FIC**		41	44	44.2	43.1	Calciturbidites
189	141.75	**FIC**		41.8	42.6	40.1	41.5	Calciturbidites
190	142.5	**FIC**		39.6	38.7	40.3	39.5	Calciturbidites
191	143.25	**FIC**	**Calciturbidite Unit 3 top**	38.9	35.2	39.5	37.9	Calciturbidites
192	144	**FIC**	**Fine-grained siliciclastic deposits**	36.7	36.8	32.9	35.5	Interbedded Mudstone & sandstone
193	144.75	**FIC**		42.5	41.4	42.6	42.2	Interbedded Mudstone & sandstone
194	145.5	**FIC**		58	54.5	58	56.8	Interbedded Mudstone & sandstone
195	146.25	**FIC**		75.8	78.6	73.4	75.9	Interbedded Mudstone & sandstone
196	147	**FIC**		76.4	72.2	63.2	70.6	Interbedded Mudstone & sandstone
197	147.75	**FIC**	**Isaac channel complex 1**	73.3	79.1	78.1	76.8	Conglomerate/Sandstone
198	148.5	**FIC**		65.9	62.6	68.2	65.6	Sandstone

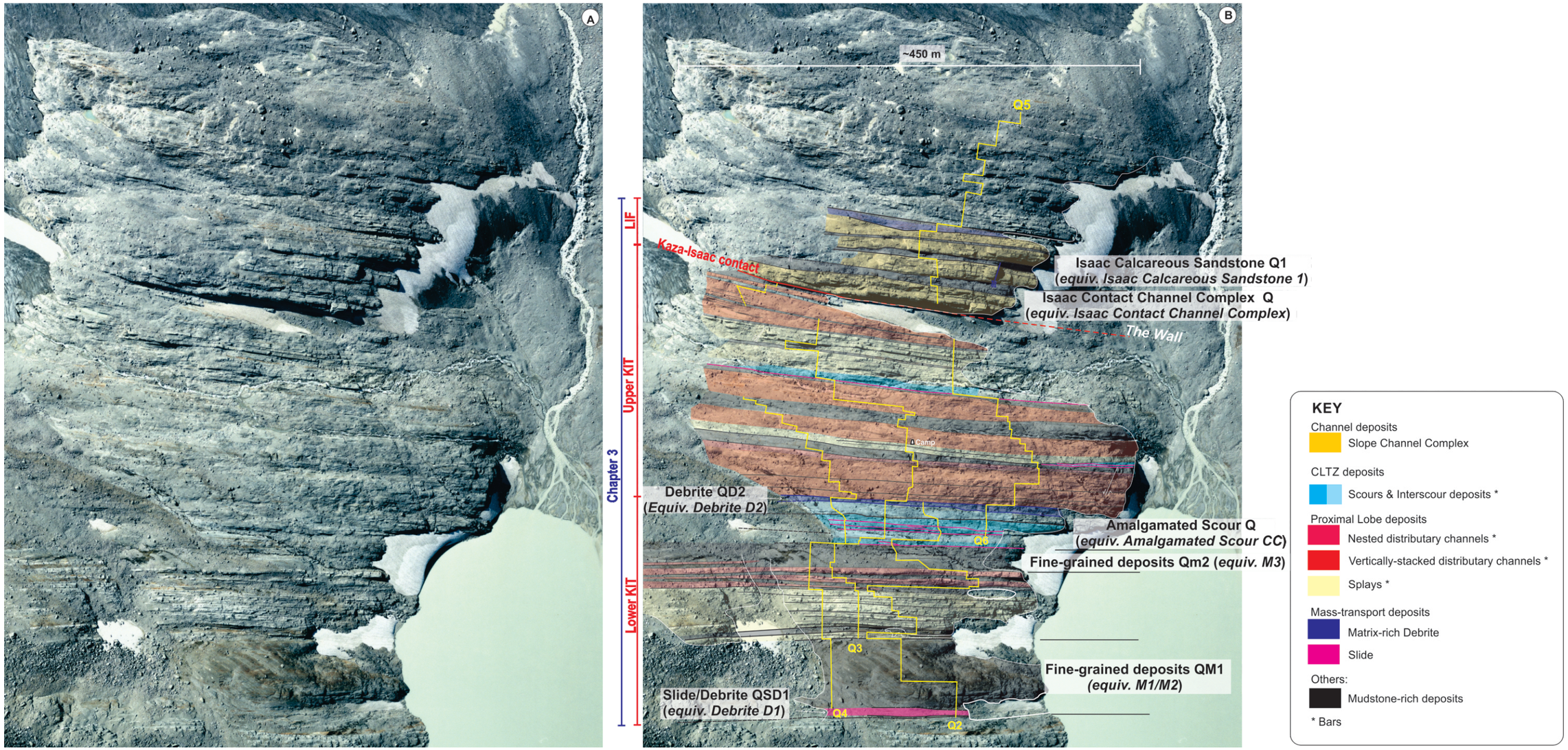

Figure G.1. (A) Uninterpreted and (B) Interpreted air photo mosaics of the Kaza-Isaac transition interval (KIT) and overlying Isaac Formation at Mount Quanstrom. In B, stratal elements are identified. Interpreted equivalent (equiv.) stratal elements from Castle Creek study area are indicated in italic letters.

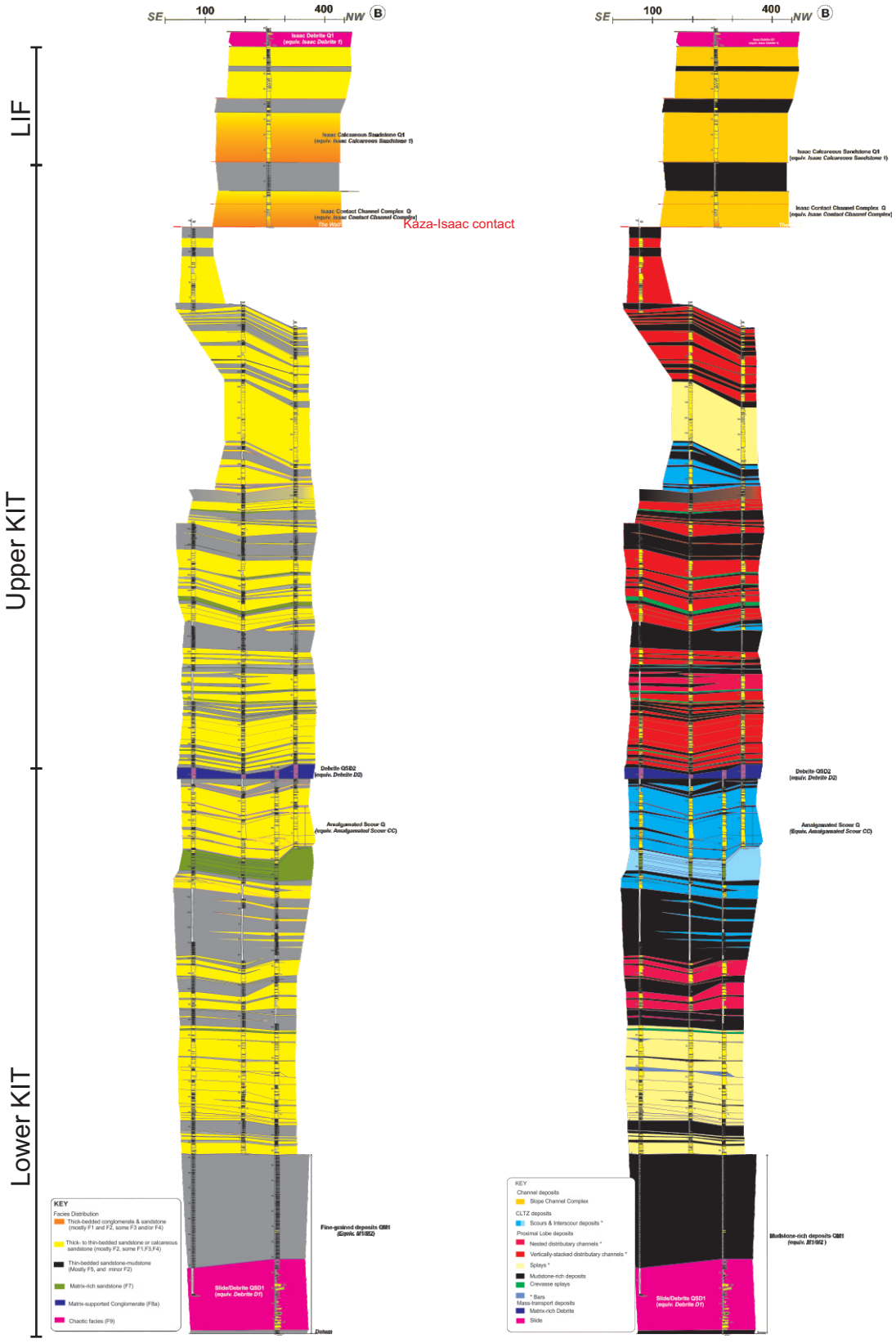

Figure G.2. Correlation panels along the Kaza-Isaac transition (KIT) and overlying lowermost Isaac Formation (LIF), showing (A) facies distribution and (B) stratal elements. For log legend, see Fig. 3.9A. Equivalent stratal elements from Castle Creek study area are indicated in italic.

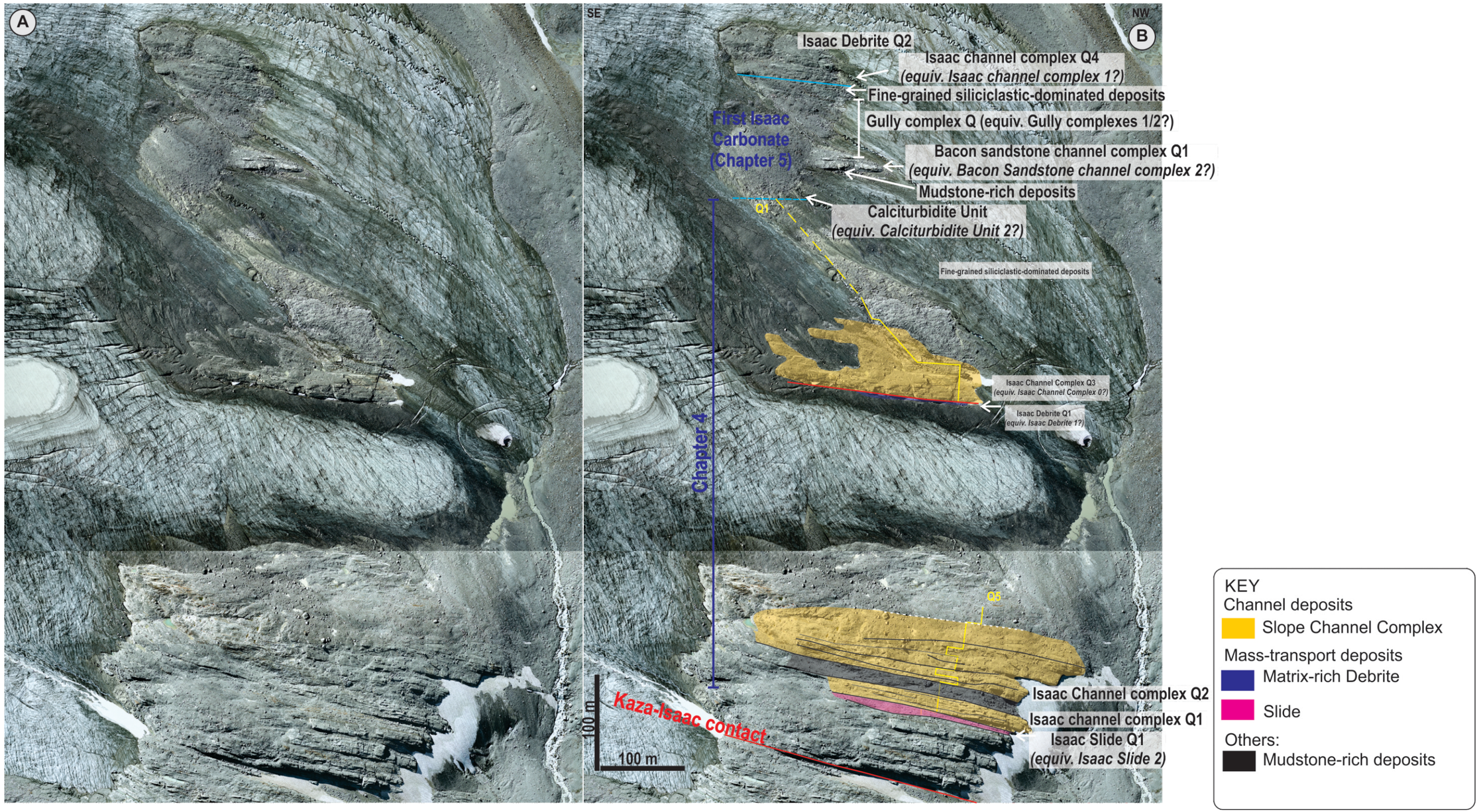

Figure G.3. (A) Uninterpreted and (B) Interpreted air photo mosaics of the Isaac Formation at Mount Quanstrom. In B, stratal elements are identified. Interpreted equivalent (equiv.) stratal elements from Castle Creek study area are indicated in italic letters.

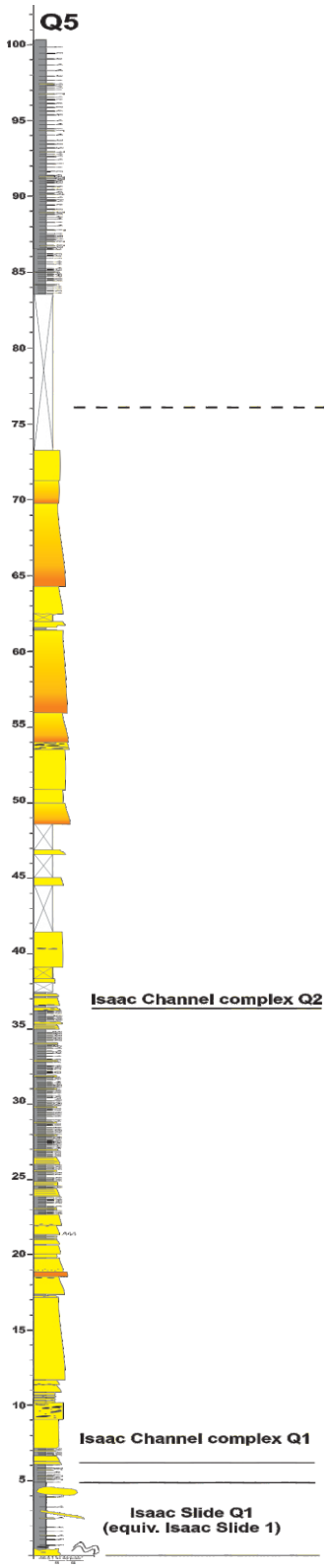

Figure G.4. Stratigraphic section Q5 (top). Located almost 60 m above the contact between the Upper Kaza Group and Isaac Formation. It includes slide deposits of Isaac slide Q1 and coarse-grained siliciclastic-rich strata of Isaac channel complexes Q1-Q2, which are separated with fine-grained siliciclastic-rich deposits.

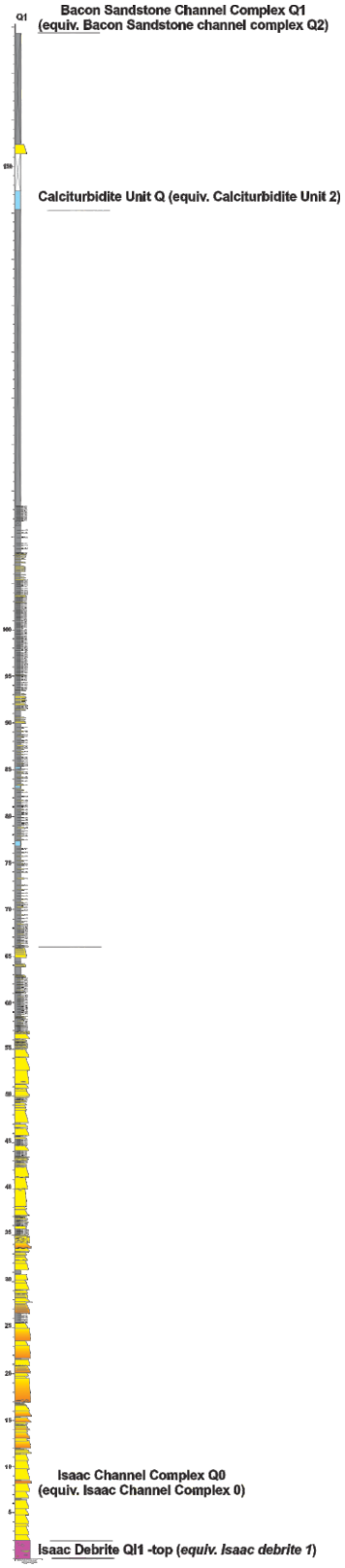

Figure G.5. Stratigraphic section Q1. Located below the First Isaac carbonate, this section includes at the base debris flow deposits of Isaac debrite Q2 and coarse-grained siliciclastic-rich strata of Isaac channel complex Q0, which are overlain by fine-grained siliciclastic-rich deposits.